

ICEFIELD RANGES RESEARCH PROJECT

SCIENTIFIC RESULTS

VOLUME 3



PUBLISHED JOINTLY BY THE
AMERICAN GEOGRAPHICAL SOCIETY
AND THE
ARCTIC INSTITUTE OF NORTH AMERICA

ICEFIELD RANGES RESEARCH PROJECT
ADVISORY COMMITTEE
(1971)

Dr. Walter A. Wood, *Chairman*
2561 North Vermont Street
Arlington, Virginia 22207

Mr. William A. Anders
6703 Wemberly Way
McLean, Virginia 22101

Dr. Henri Bader
Institute of Marine Science
University of Miami
Rickenbacker Causeway
Miami, Florida 33149

Dr. E. Lovell Becker, M.D.
435 East 70 Street, Apt. 12K
New York, New York 10021

Dr. A. C. Bryan, M.D.
Department of Anesthesia
University of Toronto
101 College Street
Toronto 2, Ontario, Canada

Dr. Ian McTaggart Cowan
Dean, Faculty of Graduate Studies
University of British Columbia
Vancouver 8, B.C., Canada

Dr. William O. Field
American Geographical Society
Broadway at 156 Street
New York, New York 10032

Dr. G. D. Garland
Department of Physics
University of Toronto
Toronto 5, Ontario, Canada

Dr. Richard P. Goldthwait
Chairman, Department of Geology
The Ohio State University
125 South Oval Drive
Columbus, Ohio 43210

Mr. George Gryc
Chief, Alaskan Mineral Resources Branch
U.S. Geological Survey
345 Middlefield Road
Menlo Park, California 94025

Mr. Trevor A. Harwood
Defence Research Board/DREO
125 Elgin Street
Ottawa 4, Ontario, Canada

Dr. Geoffrey F. Hattersley-Smith
The Crossways
Cranbrook, Kent, England

Dr. Calvin J. Heusser
Sterling Forest
P.O. Box 608
Tuxedo, New York 10987

Dr. J. Peter Johnson, Jr.
Department of Geography
Carleton University
Ottawa 1, Ontario, Canada

Dr. Melvin G. Marcus
Department of Geography
University of Michigan
Ann Arbor, Michigan 48104

Dr. John W. Marr
Department of Biology
University of Colorado
Boulder, Colorado 80302

Dr. Carlos Monge, M.D.
Apartado 821
Lima, Peru

Dr. Terris Moore
123 Brattle Street
Cambridge, Massachusetts 02138

Mr. Graham W. Rowley
245 Sylvan Road
Ottawa 2, Ontario, Canada

Dr. John S. Tener
Canadian Wildlife Service
400 Laurier Avenue, West
Ottawa 4, Ontario, Canada

Member Emeritus

Prof. Robert P. Sharp
Department of Geological Sciences
California Institute of Technology
Pasadena, California 91109

ICEFIELD RANGES RESEARCH PROJECT
SCIENTIFIC RESULTS

Volume 3

ICEFIELD RANGES RESEARCH PROJECT
SCIENTIFIC RESULTS

Volume 3

Edited by

VIVIAN C. BUSHNELL
American Geographical Society

and

RICHARD H. RAGLE
Arctic Institute of North America

Published jointly by

AMERICAN GEOGRAPHICAL SOCIETY, NEW YORK

and

ARCTIC INSTITUTE OF NORTH AMERICA, MONTREAL

1972

This series of volumes is dedicated to
the people of Yukon Territory.

CONTENTS

	Page
Editors' Preface	ix
Steele Glacier, 1935–1968 <i>by Walter A. Wood</i>	1
Kluane Lake Map Area (abstract) <i>by J. E. Muller</i>	9
Geology of the Wolf Creek Area, St. Elias Range <i>by Robert P. Sharp</i>	11
Movement Observations on the Terminus Area of the Steele Glacier <i>by S. Thomson</i>	29
Comparison of Moraines Formed by Surging and Normal Glaciers <i>by Nathaniel W. Rutter</i>	39
Some Aspects of the Geomorphology of Meltwater Streams, Steele Glacier <i>by A. J. Broscoe</i>	47
Observations on an Alpine Mudflow, Steele Creek <i>by A. J. Broscoe and S. Thomson</i>	53
Observations of the Surge of Steele Glacier <i>by A. D. Stanley</i>	61
The Ice-Dam, Powder-Flow Theory of Glacier Surges <i>by Lawrence B. Nielsen</i>	71
Summary of Rusty Glacier Mass-Balance Study, 1968 <i>by Thomas Brewer</i>	75
Some Results of the Hydrological Investigation of the Rusty Glacier Basin <i>by Theodorik Faber</i>	83
Gravity and Shallow-Ice Temperature Measurements on the Rusty Glacier <i>by David J. Crossley and Garry K. C. Clarke</i>	93
Thermal Drilling and Deep-Ice Temperature Measurements on the Rusty Glacier <i>by David F. Classen and Garry K. C. Clarke</i>	103
Abundances of Isotopic Species of Water in the St. Elias Mountains <i>by K. E. West and H. R. Krouse</i>	117
Snow Accumulation in the Icefield Ranges <i>by Melvin G. Marcus and Richard H. Ragle</i>	131
The Reflection Characteristics of Radio Waves on the Surface of a Subarctic Glacier in Summer <i>by Takeo Yoshino</i>	143
Supraglacial Streams of the Kaskawulsh Glacier <i>by Karen J. Ewing</i>	153
Infrared Radiometric Temperatures in the Alpine/Periglacial Environment as Related to Thermal Remote Sensing <i>by Ray Lougeay</i>	163

	Page
Up-Heaved Blocks: A Curious Feature of Instability in the Tundra <i>by Larry W. Price</i>	177
The Sedimentology of a Braided River <i>by Peter F. Williams and Brian R. Rust</i>	183
Vegetation, Microtopography, and Depth of Active Layer on Different Exposures in Subarctic Alpine Tundra <i>by Larry W. Price</i>	211
A Checklist of Vascular Plants from the Icefield Ranges Research Project Area at Kluane Lake <i>by James A. Neilson</i>	221
New and Important Additions to the Flora of the Southwest Yukon <i>by James A. Neilson</i>	241
Behavior Study of the Arctic Ground Squirrel <i>by Betsy Jo Lincoln</i>	245
Geomorphic Effect of the Arctic Ground Squirrel in an Alpine Environment <i>by Larry W. Price</i>	255
Pesticide Residues in Selected Yukon Mammals <i>by Donal W. Halloran and Arthur M. Pearson</i>	261

Editors' Preface

The studies reported in this volume fall into three general categories: (1) those related to surging-glacier research (pp. 1-130); (2) topics of general interest in the physical sciences (pp. 117-220); and (3) topics of general interest in the biological sciences (pp. 211-261). Included in the first category are studies of the Steele Glacier, which surged in 1965-1968, and studies of the Rusty Glacier, which is believed to be in a presurge phase. In the first category, not all of the research reported was carried out under the auspices of the Icefield Ranges Research Project, but is included here because it is directly related to the IRRP research.

Papers of general interest, in both the physical and the biological sciences, follow the pattern of those of the two previous volumes in that some are by senior researchers and some are by students. Some articles have been published previously and others have not. Articles being published for the first time have been reviewed by experienced specialists. Previously published papers are reprinted as they first appeared, except for stylistic changes.

One of the papers reprinted here (pp. 11-27) reports some of the earliest (1943) geologic work done in the area. The reader's attention is called to more recent (1967) geologic studies by the inclusion of an abstract taken from a published memoir (p. 9).

VIVIAN C. BUSHNELL
RICHARD H. RAGLE

Steele Glacier 1935–1968

Walter A. Wood*

Introduction

Steele Glacier—also referred to in the early literature as Wolf Creek Glacier—is about 35 km long and rarely more than 2.5 km wide. It is one of many ice streams which drain the northeastern slopes of the St. Elias Mountains. Water discharged by the glacier enters the Donjek River via Steele Creek and eventually reaches the Bering Sea by way of the White and Yukon Rivers. Together with Steele Creek Steele Glacier is the principal distributary of a watershed that encompasses 700 km² and within which the topography is dramatically alpine. A perennial mantle of ice and snow covers the crests of the watershed and individual summits range in elevation from 2500 m to more than 5000 m. The western boundary of the watershed is a high ridge which links Mt. Steele (5070 m) and Mt. Wood (4840 m) and forms the divide between drainage of the Yukon River system and that which reaches the Gulf of Alaska via the Chitina and Copper Rivers. Approximately thirty glaciers comprise the system within the Steele watershed. Of these some twenty-five are connected or disjuncted tributaries of the Steele Glacier. The remainder belong to an isolated system, the drainage from which is carried by Hazard Creek and flows into the valley of Steele Creek about 15 km above the terminal moraine of the last advance.

Climatologically the continental slope of the St. Elias Mountains is semi-arid. Mean annual precipitation at Kluane is of the order of 35 cm, while that of Yakutat on the Gulf of Alaska exceeds 300 cm. While some maritime moisture reaches the Steele watershed, most of the effect of Pacific airmasses is lost before they cross the high Steele–Wood–Walsh ridge, and the environment of the Steele watershed must be considered dry as compared to the Pacific littoral. The equilibrium line on Steele Glacier and on its major tributaries is between 2750 and 2900 m. Tree line in the valley of Steele Creek approximates 1400 m and more than 90% of the watershed is treeless. Tundra vegetation is continuous to about 2150 m but isolated alpine plant communities are to be found near the 2800-m contour.

Exploration of Steele Glacier, 1935–1947

Although the high summits of the Icefield Ranges (name first used by Bostock, 1948) were seen by early

travelers from vantage points many miles away on the Yukon Plateau (McConnell, 1905), and several of the more prominent peaks among them were named, exploration was restricted to the courses of the major river valleys. The valley of the Donjek River, in the same area which contains Steele Glacier, was well known to prospectors and to hunting parties from the time of the Gold Rush, and in 1913 Mt. Steele and Mt. Wood were surveyed by mapping parties of the International Boundary Commission from stations within the White River drainage area. A crude recognition of the existence of Steele Glacier appears as early as the 1920's and this probably dates from the work of McConnell (1905). It is doubtful, however, whether prior to 1935 any party penetrated Steele Creek region for more than a few miles. Inhabitants of Burwash Landing, some of them still alive, have reported that Steele Creek was a "forbidden valley," and no Indian would enter it for fear of annihilation from flood waters and crashing ice (Wood, 1967).

In 1935, Steele Glacier became the central setting for a field program in high-mountain photogrammetry. In 1930 O. M. Miller of the American Geographical Society began research in the use of high oblique aerial photographs for mapping areas of high relief (Miller, 1931). One such area selected as a target for this study was the portion of the St. Elias Mountains rising between Kluane Lake and the International Boundary. This area was chosen because of the dramatic relief presented by the terrain, the presumed accessibility by pack train from Burwash Landing on Kluane Lake, the presence of a triangulation network adjacent to it done by the International Boundary Commission Survey of 1913, and the availability in the Yukon of aircraft to serve as platforms for high oblique photography.

Under the sponsorship of the American Geographical Society the Wood Yukon Expedition went into the field in July of 1935 (Wood, 1936). With a pack train of 34 horses provided by the Jacquot Brothers of Burwash Landing, it succeeded in breaking a trail along the trim line above the true right margin of Steele Glacier until four-footed progress was stopped by the lowest connected tributary glacier of the Steele system (Fig. 1). A base camp was established at this point and became the hub of field operations for that year, and for other seasons to follow.

The primary objective of the 1935 season was to establish a network of local ground control points of such

*American Geographical Society

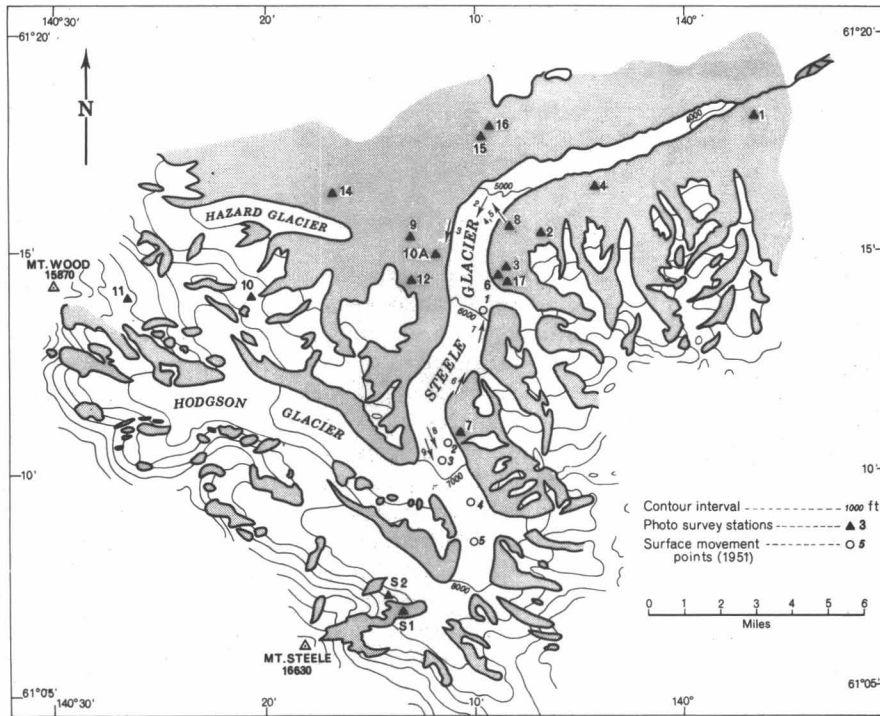


Fig. 1. Map of Steele Glacier region showing locations of survey stations and points where movement observations were made. Numbered arrows give locations and directions of exposure of aerial photographs (Figs. 2-9).

prominence and distribution as to permit identification in air photographs, and strong resections from photogrammetric measurements to be made in the laboratory. Six such stations were established between the terminus of Steele Glacier and the base of Mt. Steele in July and August (Fig. 1).

Important as were these stations to the establishment of geographical references, of far greater significance are the photographic panoramas exposed at nine sites, including the survey stations, for the purpose of developing minor control. Each of these panoramas illustrates a portion of the surface of Steele Glacier, and the 1935 field season, therefore, is the datum from which any photo interpretive analysis of the recent behavior of the glacier must begin. The first field season ended with a number of air photographic missions, from one of which we have the first aerial photographic coverage of Steele Glacier (Fig. 2). The photography, unfortunately, cannot be considered to be worthy of formal exhibition. It was the writer's first attempt at large format (13 x 18 cm) aerial work and his first exposure to high-mountain flying—the pilot's also. So menacing was the weather and so primitive was the aircraft (by present-day standards) that more concern, by pilot and photographer alike, was devoted to maintaining stability and composure than was given to *f* stops and shutter speeds. The results, however, are entirely satisfactory for interpretive purposes.

The 1935 field season was consumed in large part by reconnaissance—physical, technical, and logistical. In

1936 operations were shifted to an area some 40 km north of Steele Glacier. No work was done on the ground within the Steele watershed, but a number of aerial flights over the glacier expanded the photographic coverage of 1935, particularly in the upper reaches of the area of accumulation.

In 1937 Dr. Bradford Washburn and Dr. Robert H. Bates descended the full length of Steele Glacier following their ascents of Mts. Lucania and Steele, and several fine aerial photographs exposed by Washburn in that year give us valuable documentation at all levels of the glacier and help to bridge the gap of evidence between 1936 and 1939.

In 1939 the Third Wood Yukon Expedition again entered the Steele watershed, and it expanded familiarity with the topography by exploring the glaciers which drain into Hazard Creek (Fig. 1). These ice bodies affect Steele Glacier only through water discharged through Hazard Creek, which enters the Steele valley nine miles above the terminus.

During the summer four survey stations were added to the 1935 sites. The summer of 1939 will go down in history as one of nearly continuous foul weather. Of 61 days spent in the field the weather on 45 was so inclement as to preclude survey or photographic operations. Aerial photography, too, was thwarted in the Steele Glacier area and no meaningful coverage was obtained.

The 1941 field season was as productive as the 1939 season had been sterile. Nine survey stations were oc-



Fig. 2. Middle course of Steele Glacier in 1935. The debris-covered ice in the foreground was inactive if not stagnant at that time (August 30, 1935; 16:30; 3550 m).

cupied and photo panoramas were exposed at each. Six of the nine records were repeats of earlier years. Also in 1941 the first professional assessment of the glacial history of a large portion of the Steele watershed was under-

taken by Sharp (1951). In the light of the dramatic recent (1965-1968) behavior of Steele Glacier a number of Sharp's observations are of great interest.

At the time the Steele was first seen in 1935, it was



Fig. 3. Steele Glacier in surge, 1967. Note the lake impounded in the valley of Hazard Creek at lower right (August 9, 1967; 11:15; 3050 m).

obvious that the lower eight miles of its trunk were inactive if not stagnant (Fig. 2). From the stability of alluvial fans built onto the glacier from tributary valleys along both margins below the 1500-m contour and other evidence, Sharp concludes stagnation to have been present in 1941. This was substantiated by examination of photo panoramas exposed from Station 4 (Fig. 1) in 1935 and 1941. During the six-year interval no perceptible downvalley movement could be detected. Three kilometers farther upstream (Station 8, Fig. 1) movement of the order of 5 m was measured at points on the surface of the glacier south of the axis of flow and along the inner arc of the bend of the Steele (Fig. 4). This motion can be attributed, in part at least, to the activity of glacier A (Fig. 1) which experienced a period of rejuvenation between 1935 and 1941. As of 1941, then, it is fair to assume that Steele Glacier was barely active in the vicinity of its great bend, and stagnant below it.

Sharp has also recorded evidence of thickening and advance of a number of disjunct and connected tributaries of Steele Glacier during the period 1935-1941. Finally, because the last advance of the Steele prior to 1965 invaded a mature spruce forest, Sharp estimates from vegetational relationships that this advance culminated during the period 1850-1890.

The 1941 field season ended with a series of photographic flights over the Steele watershed from which the most complete coverage to date was obtained.

Six years intervened before Steele Glacier was revisited. In 1947 the writer, on terminal military leave, and his family spent a week in the Steele watershed during which five previously established survey stations were reoccupied. Photo panoramas were exposed at all sites. Analysis of these photographs clearly shows that activity increased in the vicinity of the great bend during the interval 1941-1947. Movement in the vicinity of Station 8 was of the order of 30 m, while the ice opposite Station 4, stationary between 1935 and 1941, had moved downvalley as much as 15 m during the six-year interval.

The 1947 data are the last to have been gathered on the ground prior to the surge of the Steele in 1965, and it can be said that 1947 brought to an end the period of reconnaissance exploration of the Steele watershed and of the trunk glacier in particular.

Steele Glacier, 1947-1965

The summer of 1951 was an important one for the St. Elias Mountains, and especially for Steele Glacier, for the time had come in the Canadian Government's program to map these ranges for eventual publication at the scale of 1:250,000. In July vertical aerial photography intended for stereo-photogrammetric plotting of topography was obtained at 10,670 m. The north-south flight lines covered the terrain between the 60th and 62nd parallels, and were bounded by the Alaska Highway on the east and the

International Boundary on the west and southwest. This photography, of excellent quality, marked the frontier in time between data of general interpretive interest and that with evidence of analytical value.

The 1951 photography was followed in subsequent years by further Canadian coverage of the St. Elias Mountains. Only that of 1954 and 1956 is pertinent to the area of Steele Glacier. It was from the 1951 photography that the Steele watershed was mapped as a part of the Kluane Lake Sheet of the 1:250,000 topographic series.

During the ten years prior to surge (1955-1965) the chronology of Steele Glacier is spotty. There appear to be no photographs of the glacier between 1956 and 1960, but in 1961 the writer secured partial high oblique coverage of the watershed, as did W. O. Field; Austin Post (personal communication) flew air photographic missions over Steele Glacier in 1960, 1961, 1963, and 1965 as part of his broad study of glacier fluctuations in northwestern North America. From an appraisal of his 1960 photography Post evaluated Steele Glacier as being in a state of imminent surge, and he predicted such an event for 1963. In late August of 1965 Post again overflew the Steele and noted activity in the ice of the upper trunk glacier. In April of 1966 the writer overflew the Steele on a reconnaissance for the projected Yukon Alpine Centennial Expedition of 1967. At that time the surge was in full flood and by July it had invaded the stagnant ice below the great bend. Post's photographs of August 1965 show no dramatic displacement of the ice in the upper reaches of Steele Glacier. They do, however, illustrate increased marginal crevassing as compared with his 1961 records, and there can be no doubt that unusual activity was taking place. The massive slump of the ice in the upper reaches of the glacier did not take place until after Post's observations of late August. In July 1966 the writer talked with a number of residents of Burwash Landing, some of them Indians long familiar with the local environment, to determine whether any unusual circumstance might have caught their attention during the fall of 1965 or the winter 1965-1966. Three Indians independently reported that "during the winter" (date unknown) they had heard a prolonged rumbling in the west accompanied by a "haze over the mountains." They had no recollection of such phenomena having occurred previously.

Once a "surge in being" was recognized, the history of Steele Glacier swelled with data on its behavior. Through the facilities of the Icefield Ranges Research Project a field party was established at Station 6 in July 1966. High oblique aerial photographs were exposed over the chaotic ice (Fig. 7), and ten survey stations established prior to 1947 were reoccupied by helicopter and photo panoramas exposed (Fig. 5). Movement of the ice in the vicinity of Station 6 was measured and a daily rate of 15 m was established. At the same time the significance of the surge and the scientific opportunity engendered by it was called to the attention of the Surveys and Mapping



Fig. 4. Looking northwest across Steele Glacier from Photo Survey Station 8 (Fig. 1) in 1939. The general surface of the inactive ice is about 100 m below the Station (July 18, 1939; 10:00; 1691 m).

Branch of the Department of Energy, Mines and Resources of Canada, with the recommendation that mapping photography be exposed over the Steele at the earliest possible moment. The response to this plea was enlightened and immediate. On August 13 and again on September 15, 1966 mapping photo coverage of the Steele was obtained. During the same period the National Geographic Society assisted the work of the Icefield Ranges Research Project by fielding a party which broadened the detailed coverage of Steele Glacier begun by the writer earlier in the season. Finally, in September 1966 L.A. Bayrock led a reconnaissance party which examined pro-

cesses at work in the terminal area of the advancing ice (Bayrock, 1967).

During the winter 1966-1967 M. E. Alford, Resident Water Resource Engineer of the Department of Energy, Mines and Resources in Whitehorse, photographically recorded the progress of the Steele Glacier surge in November 1966 and in January, March, April, and May 1967. His photo series of January 1967 contains the first evidence of the surge of the Hodgson Glacier, the largest tributary of Steele Glacier. So powerful was this surge that ice of the Hodgson was able to narrow the trunk of the still surging Steele by about one-third of its width



Fig. 5. View of Steele Glacier surge from Photo Survey Station 8 in 1966 (see Fig. 4 for a view from Station 8 in 1939). The general level of the chaotic ice is about 75 m above the Station (July 25, 1966; 10:30; 1691 m). Photo by R. C. Faylor.



Fig. 6. Right margin of Steele Glacier in 1961. Note the penetration of the tributary glacier into the main stream prior to surge (August 10, 1961; 15:30; 3110 m).

(Fig. 9). By mid-August this compound element of the Steele had advanced nearly 3 km downvalley before being pinched to the left margin by the main ice stream.

In 1967 the writer again obtained high oblique aerial coverage of the Steele in June and in August (Fig. 3). Fourteen photo survey stations were reoccupied, and surface movement in the vicinity of Station 6 was measured, the rate being 6.5 m/day. Though the rate was less than

50% of that measured at the same locality in 1966, it was of interest to note that the general level of the ice surface between Stations 6 and 4 was higher than that observed in 1966. In the vicinity of Stations 8 and 4 the thickening was of the order of 15 m.

During the summer of 1967 the terminal area of the advancing ice was intensively studied by a party representing the University of Alberta and the Research Council of



Fig. 7. Surging Steele Glacier in the area covered by the central portion of Figure 6. The power and initial velocity of the surge is evident in the clean decapitation of the tributary glacier by the surging glacier (July 24, 1966; 15:15; 2550 m).



Fig. 8. Upper Steele Glacier in 1936. The prominent debris mound may be seen just to the right of optical center (August 11, 1936; 11:30; 2900 m).

Alberta. Under the leadership of L. A. Bayrock micro-movement of the ice was observed throughout a network of points on the surface of the frontal ice, water discharge and sedimentation were measured, and geologic and geomorphic processes studied, especially as these relate to the contact between advancing the stagnant ice (Thomson, 1968). Although the terminus of the surging ice was still

advancing, downvalley movement was of the order of 2 m/day as compared with 10 m/day in September 1966.

Modern Behavior of Steele Glacier

Sharp (1951) has concluded that the last major advance of Steele Glacier terminated between 1860 and 1890.

Fig. 9. Upper Steele Glacier in surge, 1967. Surface velocities of the Steele at this time probably approximated 1 m/hr; yet the surge of the tributary Hodgson Glacier (right) is of sufficient thrust to divert the flow of the main stream through about one-third of its width (June 16, 1967; 09:00; 3100 m).



Since 1935 its average gradient has been about 35 m/km and the steepest break in slope occurs where the ice stream enters the east-west fault zone which determines the course of the lower Steele Glacier. It is within this depression that all stagnant ice of the glacier occurs. Active ice, then, occupies approximately 20 km of the 35 km length of the trunk stream. Within that span and through measurements of five surface features which appear on vertical photographs of 1951, 1956, and 1966, it has been possible to approximate the movement of Steele Glacier (Table 1) for the period 1951-1966; to project these rates, assuming them to have been constant, for the period 1956-1965; and to suggest the accelerated rate of flow for the period September 1965-August 1966, a period of time commencing with Post's recognition of increased activity and ending with the mapping photography of August 1966. All five points, distinct elements of medial moraine loops and kinks, survived the first year of the surge.

A reliable check on these approximations has been provided by examination of two high oblique photographs, one taken by Wood in 1941, the other by Post in 1961. Point 3 is well illustrated in both photographs, the optical axes of which were normal to the axis of flow. Semi-graphic computation gives a total downstream movement for Point 3 of 490 m between 1941 and 1961, or 25 m/yr.

Evidence is meager on the behavior of upper Steele Glacier prior to 1951. A single high oblique aerial photograph by Wood in 1936, however, clearly illustrates Point 3, a prominent debris mound (Fig. 8). By the roughest of estimates of its horizontal position relative to points on the margin of the glacier and relating this to the known positions in 1941, 1951, and 1956, the feature cannot have advanced less than 2100 m in 15 years (1936-1951), a rate of 140 m/yr, and some five times the rate indicated for 1951-1956, and the technically less reliable rate for 1941-1961. There is, however, other evidence of rejuvenation of the upper Steele Glacier in the years prior to 1941. The writer's party traveled over the upper Steele in 1935 and again in 1941. In the former year the glacier surface was smoothly molded and presented no technical problems. In 1941 the same surface was coarse in texture and was seamed with crevasses whose well-weathered contours bespoke exposure of several seasons.

The 1935 campsite at the base of Mt. Steele had been all but overrun by a swelling of the neighboring ice.

Sharp (1951) calls attention to rejuvenation of a number of the glaciers of the Steele watershed during the period 1935-1941, a cycle which had subsided by 1947. It seems probable, indeed certain, that the upper course of the Steele Glacier also experienced accelerated flow during this period. The measurements cited above, however, indicate that acceleration was shortlived and did not extend its visible effects below the confluence of the Hodgson Glacier and the middle course of the Steele.

By August 1968 the surge of Steele Glacier appeared to have run its course. The zone of contact between active ice of the surge and stagnant debris-covered ice of the last advance showed little change from the August 1967 stand. Motion was certainly present in the middle and upper reaches of the glacier, but the chaotic texture of the surface, so dramatic in 1966, had been replaced by softened lines and angles, and it was quite possible to land a helicopter at many places where, two years previously, it would have been out of the question to do so. 1968, then, is a logical punctuation point in the history of Steele Glacier. It must be a comma or a semicolon, however, and not a period, for documentation of the post-surge history of the glacier is important.

References

- Bayrock, L. A. (1967) Catastrophic advance of the Steele Glacier, Yukon, *Occas. Publ. No. 3*, Boreal Inst., Univ. Alberta, 35 pp.
- Bostock, H. S. (1948) Physiography of the Canadian Cordillera with special reference to the area north of the 55th parallel, *Mem. 247*, Geol. Surv. Can., 106 pp.
- McConnell, R. G. (1906) The Kluane mining district, *Ann. Rept., 1904*, Geol. Surv. Can., Vol. 16, pp. 1-18.
- Miller, O. M. (1931) Planetabling from the air, *Geogr. Rev.*, 21, 201-212.
- Sharp, R. P. (1951) The glacial history of Wolf Creek, St. Elias Range, Canada, *J. Geol.*, 59, 97-117.
- *Thomson, S. (1972) Movement observations on the terminus area of the Steele Glacier, Yukon, July 1967.
- Wood, W. A. (1936) Wood Yukon Expedition 1935, *Geogr. Rev.*, 26, 228-246.
- Wood, W. A. (1947) Chaos in nature, *Explorers J.*, 45.

*This article appears in the present volume.

ADDENDUM

ICEFIELD RANGES RESEARCH PROJECT SCIENTIFIC RESULTS: VOLUME 3, p.8

TABLE 1. Movement of the Steele Glacier during 1951--1966

Point no.*	Approx. elevation (m)	Total observed movement 1951--56 (m)	Average annual movement 1951--56 (m)	Total movement projected for 1956--65 (m)	Total movement projected for 1951--65 (m)	Observed movement for 11 months in 1965--66 (m)	Estimated movement for 12 months in 1965--66 (m)
1	1800	116	23	207	320	4495	4908
2	2100	134	27	243	375	4830	5268
3	2200	140	28	252	392	4816	5244
4	2300	123	25	225	348	5095	5556
5	2350	150	30	270	420	5348	5832

* See map on p. 2

Kluane Lake Map-Area *

J. E. Muller †

Kluane Lake map-area embraces some 6900 square miles of St. Elias Mountains and Yukon Plateau, separated by Shakwak Trench. Yukon Complex metamorphic rocks, with granodiorite of Ruby Range batholith and some smaller bodies, mainly underlie Yukon Plateau. The probably Precambrian and early Paleozoic schists were metamorphosed and granitized in Mesozoic and perhaps early Tertiary time. Minor Mesozoic volcanic rocks, some granite, and abundant rhyolite also occur in Nisling Range.

Eugeosynclinal deposits of St. Elias Mountains have yielded Middle Devonian, Lower Permian, Upper Triassic, and Jura-Cretaceous fossils. The volcanic rocks are pre-Permian, Permian, and Triassic; carbonate-clastic sequences are Devonian, Lower Permian, and Upper Triassic; and a greywacke-argillite sequence is Upper Jurassic to Lower Cretaceous.

Folding perhaps preceded Permian sedimentation, and

*This has previously appeared as the Abstract of *Memoir 340*, Geological Survey of Canada (1967), and is reprinted here with permission.

†Geological Survey of Canada, Department of Energy, Mines and Resources, Vancouver, British Columbia

orogeny with granitic intrusion terminated the geosyncline in Cretaceous time. Paleocene or Eocene plant-bearing beds of conglomerate, sandstone, shale, and coal are followed by a thick succession of basaltic lava and tuff, and are pierced by a few felsitic plugs.

Shakwak lineament is believed to be a major hinge line reflecting mainly vertical movements between the St. Elias geosyncline and Yukon geanticline. Duke River thrust is an important break, affecting all rocks including Tertiary beds. In Kluane Ranges low-angle thrusts have placed older rocks on Tertiary.

Three glaciations, showing increase in topographic expression coupled with decreasing age and extent, are tentatively mapped; the oldest may be pre-Wisconsin.

The explosion center of 1500-year-old volcanic ash covering much of Yukon and Alaska may be at the foot of Natazhat Glacier.

Mineral deposits, so far of minor importance, are placer-gold, possibly concentrated from till, nickel-copper sulphides near peridotite occurrences, native copper in Triassic lavas, a few tungsten and molybdenite showings in granitic rocks, gypsum in Devonian? and Triassic formations, and coal in Tertiary sediments.

Geology of the Wolf Creek¹ Area, St. Elias Range *

Robert P. Sharp †

ABSTRACT. The heretofore unmapped rock sequence on Wolf Creek provides a useful section for correlation of Canadian Yukon and Alaskan formations. The oldest rock, massive Devonian marble at least 1000 feet thick, is overlain by several thousand feet of Devonian-Mississippian slate, phyllite, schist, fissile marble, granulite, and greenstone. An unconformity separates 1500 feet of well-bedded Permian limestone, sandstone, and tuff from the older rocks, and the Permian is overlain discordantly by 4600 feet of well-layered Tertiary volcanics, about half acidic pyroclastics and half andesite and basalt flows.

Pennsylvanian (?) gabbro intrudes the pre-Permian rocks, and large bodies of late Mesozoic or early Tertiary granite and quartz monzonite are exposed. The youngest intrusives are mafic plugs and dikes associated with the Tertiary volcanism. The contact zones of the granitic and monzonitic bodies are pyritized, and a highly fractured silicified area in quartz monzonite contains molybdenite.

The Paleozoic metamorphics are compressed into east-northeast isoclinal folds. The Permian beds are tilted gently northward, and the Tertiary volcanics are largely horizontal. Two sets of high-angle reverse faults trending northwest and northeast near Wolf Creek mouth and an east-northeast monoclinial flexure with upthrust to the south along lower Wolf Creek are major features in the relatively simple structural pattern. The monocline and faults developed in the middle or late Cenozoic and may be the product of adjustments within the St. Elias block during its last major uplift.

INTRODUCTION

General Statement

During the Wood Yukon Expedition of 1941 (W. A. Wood, 1942a, 1942b; Bates, 1942) the geology of 130 square miles in the northern St. Elias Range was mapped in reconnaissance fashion. This area had been previously visited by a few hunters, prospectors, and two earlier Wood expeditions (W. A. Wood, 1936; F. H. Wood, 1940), but its geology, aside from brief notes by Wood (1936), was unreported. The region adjoining Wolf Creek and large areas to the west and south are also blank on the geological map of Yukon Territory (1917). Intermediate location of the Wolf Creek area makes it a valuable link between eastern Alaska and western Canada. This report describes only the bedrock geology, since treatment of the glaciation is reserved for a publication of the American Geographical Society covering activities of all Wood Yukon expeditions.

Every member of the party assisted in the geological work, but special acknowledgment is due Walter A. Wood, who most ably organized and led the expedition. The services of Dr. H. S. Bostock, of the Geological Survey of

Canada, who read the manuscript and offered suggestions based on his wide knowledge of the Yukon, are much appreciated. Dr. J. S. Williams, of the U. S. Geological Survey, kindly studied Permian fossil collections. The University of Illinois Graduate School Research Board aided with a grant defraying expenses of transportation, and the Reserve Officers' Training Corps of the University loaned a small plane table.

Location and Physical Features

Wolf Creek, on the northeast flank of the St. Elias Range, 25 miles east of the Alaskan border, at 61° 15' N and 140° 10' W (see inset of Fig. 1), is one of the larger western tributaries of the Donjek River, a major branch of the White. Whitehorse, the nearest convenient point of entry, lies 180 miles airline east-southeast. Burwash Landing at Kluane Lake, 3 to 4 days pack-train trip—45 miles airline—to the east, served as a final outfitting post.

Peaks of the St. Elias Range, one of the higher and more rugged mountain masses on the continent, culminate in Mt. Logan (19,850). No points on the map (Fig. 1) are over 11,000 feet, although on its western and southern periphery are Mt. Wood (15,880) and Mt. Steele (16,644) (Fig. 2). Relief within the area mapped is about 7,000 feet, and complete dissection has produced an extremely rugged topography (Fig. 3). Wolf Creek flows eastward in a broad U-shaped glacial trough (Fig. 2) with a remarkably straight course to the east-northeast in its lower half. The valley makes an almost right-angle bend to the south near its midpoint—herein identified as “the bend.”

¹ Wolf Creek is now officially known as Steele Creek and St. Elias Range is now St. Elias Mountains.

*This report has previously appeared in *Bulletin of the Geological Society of America*, Vol. 54, pp. 625-650 (1943), and is reprinted here with permission.

†Present address: Department of Geological Sciences, California Institute of Technology, Pasadena

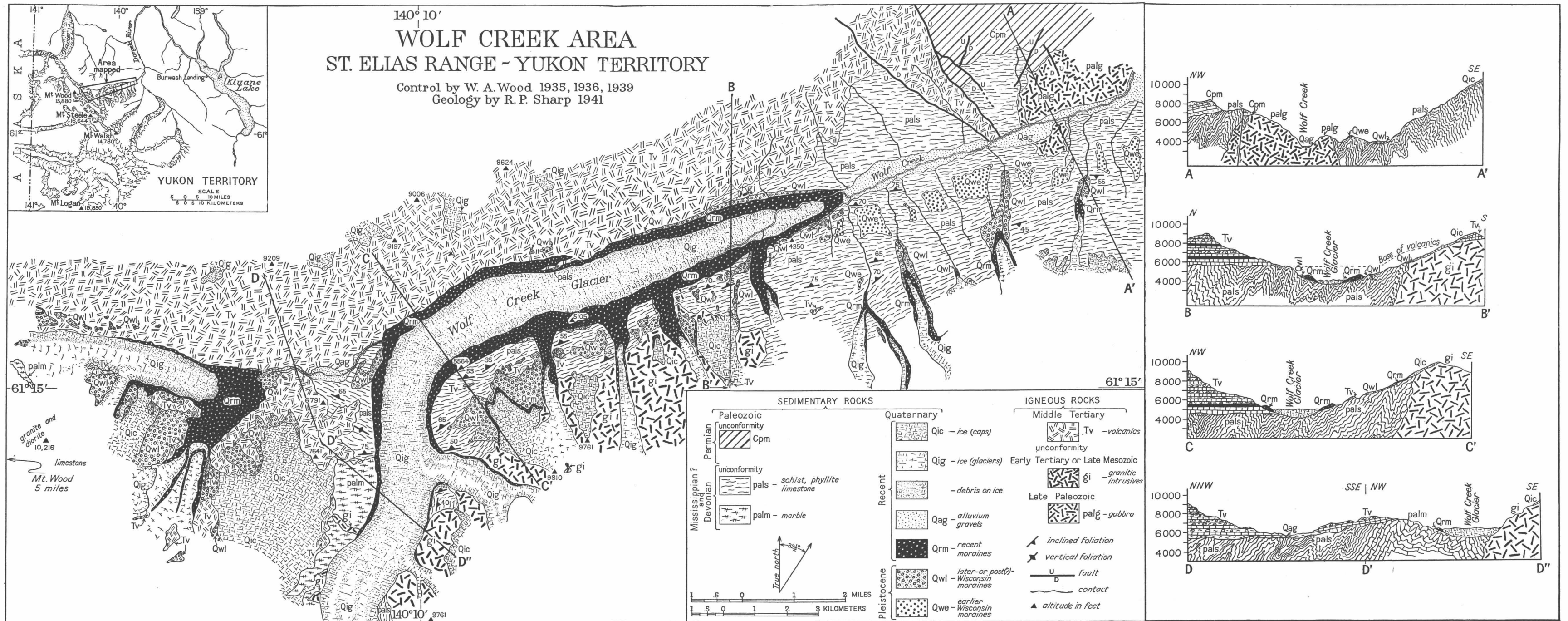


Fig. 1. Geological map and structure section of Wolf Creek area



Fig. 2. Wolf Creek valley; Mt. Steele (S), Mt. Wood (W). Donjek flood plain and Wolf Creek fan behind foreground ridge; stagnant lower Wolf Creek Glacier in center. Looking west-southwest. (Aerial photo by W. A. Wood, Sept. 9, 1941.)

Wolf Creek valley averages 4000 to 5000 feet deep with floor elevations between 3500 and 6500 feet within the boundaries of Plate 1. Timber line is close to 4500 feet, and fully 90% of the area is free of vegetation large enough to hamper geological work. Orographic snow line lies between 8000 and 9100 feet, and most of the high country is covered by ice and snow (Fig. 4). The only sources of geological information for such areas are a few isolated bare rock ledges and debris carried down by glaciers. A trunk glacier 25 miles long occupies Wolf Creek

valley to within 6 miles of its mouth. Tributary canyons indenting the high south wall contain smaller glaciers (Fig. 3), and a larger glacier occupies the major north branch near Mt. Wood (Fig. 1).

Nature of Work

Initially, supplies and equipment were obtained chiefly by parachuted loads from the air (Wood, 1942a, 1942b), but all subsequent operations were by foot and back pack.

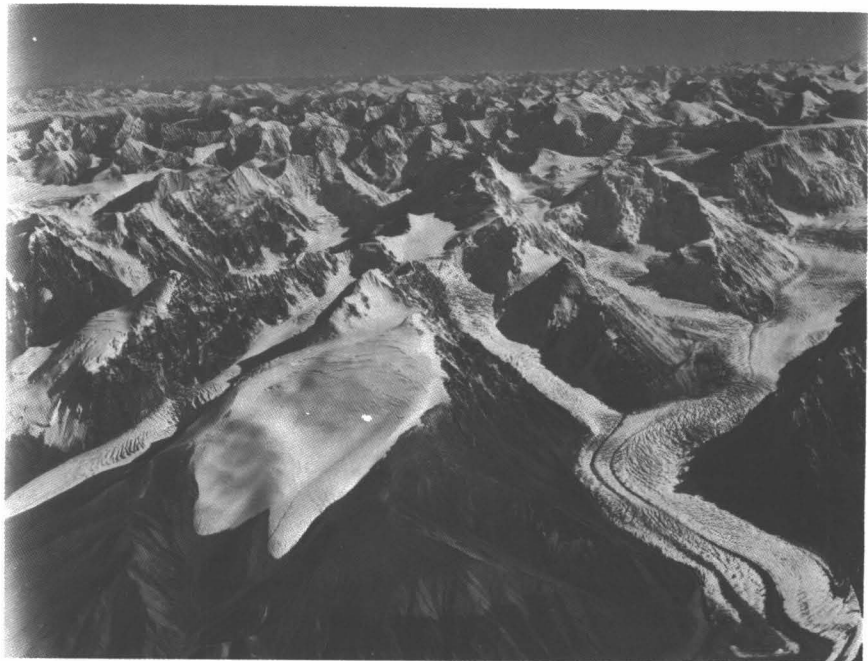


Fig. 3. East wall of Wolf Creek near bend. Rocks largely granite and quartz monzonite. Looking east-southeast. (Aerial photo by W. A. Wood, Sept. 9, 1941.)



Fig. 4. Wolf Creek Glacier above bend. Continues southward from Figure 3. Chiefly quartz monzonite and some Devonian-Mississippian metamorphics to left of glacier. Peak in right center is Mt. Walsh. Looking southeast. (Aerial photo by W. A. Wood, Sept. 9, 1941.)

Seventy-three days were spent on Wolf Creek between June 26 and September 6, 1941. Unfavorable weather handicapped the work only slightly, for the summer of 1941 was one of the driest and clearest reported in Yukon history. Geological mapping was on a 1:50,000 scale controlled by an excellent triangulation system established through theodolitic observations in previous years by Walter Wood. A small U. S. Army plane table and a Brunton compass established locations by resection. Aerial photographs furnished by Wood proved extremely helpful.

METAMORPHIC AND SEDIMENTARY ROCKS

Introduction

Table 1 summarizes the data on formations mapped along Wolf Creek, and the columnar section (Fig. 5) shows their structural relations.

Marble (Devonian)

General statement. This formation consists of uniform massive gray marble, locally argillaceous and cherty, which is best exposed on the west wall of Wolf Creek above the bend (Fig. 6). The area of exposure is small, but marble may underlie much of the high ice- and snow-covered area to the west. Poorly preserved corals indicate a Devonian age, which is consistent with the stratigraphic succession.

Total thickness may be at least 1000 feet and possibly more.

Description. The marble is uniformly massive, light to dark gray, and of medium grain. It weathers gray, brown, or reddish and contains a few thin argillaceous layers and irregular chert nodules. White, coarsely crystalline calcite fills veinlets and replaces bryozoans and corals. Stratification is obscured by fracturing, metamorphism, and weathering. The topographic habit of the marble is characterized by steep, rough surfaces with numerous spires and sharp ridges.

Age. A species of *Cladopora* and one other distorted coral with Devonian characteristics are among the poorly preserved fossils in the marble. Dr. W. H. Easton of the Illinois Geological Survey identifies these corals as definitely pre-Carboniferous and probably not older than Devonian.

The massive marble is overlain conformably by a considerable thickness of schist, phyllite, and thin marble beds unless the entire section on Wolf Creek is inverted, which seems unlikely. The schist and associated rocks unconformably underlie Permian beds and are considered Mississippian or Devonian, or both. The probable Devonian age of the fossils is thus consistent with the stratigraphic succession. Massive Middle Devonian limestone in various parts of Alaska (Brooks and Kindle, 1908; Smith, 1939; Capps, 1940) may be in part equivalent to the marble of Wolf Creek.

TABLE 1. Summary of Formations

Quaternary	Recent gravels (Qag)	Few hundred feet thick at most, largely bouldery outwash gravels of modern glaciers
	Recent moraines (Qrm)	100 to 200 feet, fresh, bouldery till of present glaciers and modern advance 100 to 200 years ago
	Later or post-Wisconsin moraines (Qwl)	100 feet, bouldery till, slightly weathered, covered with vegetation, exact age unknown
	Earlier Wisconsin moraines (Qwe)	100 feet, bouldery till, noticeably weathered, subdued topography, 500 to 1500 feet above present streams, older than preceding later or post-Wisconsin moraines, but still probably late Wisconsin
Tertiary	Volcanics (Tv)	4600 feet, well-layered basalt, andesite, trachyte, quartz latite, obsidian, ash, tuff, agglomerate, breccia, all of local origin, volume of flows and pyroclastics about equal, mafic dikes, sills, plugs associated
Early Tertiary or Late Mesozoic	Granitic intrusives (gi)	Large batholithic body of porphyritic biotite granite and hornblende-biotite quartz monzonite, locally mineralized and containing molybdenite
Permian	Sedimentary rocks (Cpm)	1500 feet, well-stratified limestone, limy sandstone, sandstone, grit, chert, sandy tuff, and water-laid tuff, containing Permian fossils
Pennsylvanian (?)	Gabbro (palg)	Stocklike body of medium- to coarse-grained augite-hornblende gabbro, intruding pre-Permian rocks
Mississippian, Devonian, or both	Undifferentiated metamorphic rocks (pals)	Several thousand feet of slate, phyllite, schist, fissile marble, quartzite, greenstone, and granulite, originally sedimentary and volcanic, closely and complexly folded
Devonian	Marble (palm)	1000 feet or more, massive, uniform, gray marble, slightly cherty and argillaceous, sparse corals

Undifferentiated Metamorphic Rocks (Mississippian, Devonian, or Both)

General statement. This formation consists of slate, phyllite, schist, marble, quartzite, greenstone,² and granulite³ produced by a low-grade regional and somewhat more intense contact metamorphism of sedimentary and volcanic beds. It outcrops over a large part of the area mapped (Fig. 1) and composes much of the south wall of Wolf Creek below the bend (Fig. 7). Most of the rocks

²Greenstone is used here for a relatively massive rock, containing enough chlorite and epidote to give it a greenish color, which was produced by low-grade metamorphism of fine-grained mafic igneous material.

³Granulite is used in the sense defined by Holmes (1929, p. 111): "A granulose metamorphic rock composed of even-grained interlocking granular minerals."

are schistose and so complexly folded that measurement of thickness is impossible. On the basis of stratigraphic relations this unit is Devonian or Mississippian, or possibly both.

Description. Marble and phyllite dominate. The marble is gray to nearly black, finely crystalline, fissile, schistose, and crenulated. It weathers gray to brown. Impure calcareous beds contain dolomite, sand, clay, and carbonaceous material. Veinlets of coarse-grained white calcite are numerous in fractured strata, and small pods of hydrothermal quartz are locally abundant. Black, paper-thin phyllite forms partings between layers of marble, and phyllite beds in groups 200 to 300 feet thick alternate with similar groups of marble strata. Most phyllite is shiny gray to nearly black, brownish weathering, and thin-bedded. Paper-thin beds are rich in clay, and platy strata contain some sand and calcite. Small-scale sharply asymmetrical crenulations, less than 0.5 mm high, give

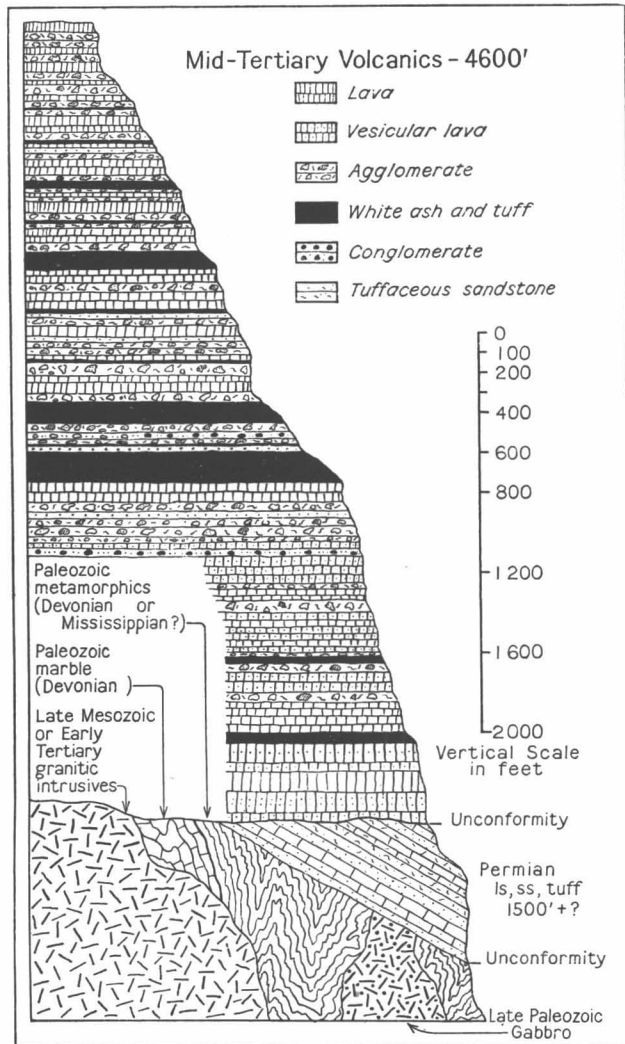


Fig. 5. Columnar section.

many phyllites a prominent linear marking on schistosity planes, and cross crenulations locally produce a reticulated pattern. Slates are not abundant, although much of the phyllite is slightly recrystallized and resembles slate. Scattered beds of gray, brown-weathering, fine, argillaceous quartzite were noted.

Near intrusives phyllite and marble gradually give way to schist and granulite. Quartz-biotite, quartz-sericite, and sericite-chlorite schists of medium grain are common. The various granulites consist of interlocking granules of calcite, quartz, diopside, hornblende, biotite, chlorite, zoisite, sericite, plagioclase, and traces of pyrite. In some beds a distinct compositional interlayering of biotite and quartz with pyroxene and calcite is apparent.

Greenish calcareous sericite-chlorite schists and greenstones crop out on lower Wolf Creek. The greenstones consist of chlorite, epidote, hornblende, plagioclase (near

albite), sericite, calcite, sphene, and traces of pyrite in interlocking granules without well-developed foliation. Veinlets and pods of coarse-grained hydrothermal quartz and ankerite (?) are abundant in these rocks.

The rocks composing this formation were developed by low-grade regional metamorphism of shale, calcareous sandy shale, limestone, impure sandy and dolomitic limestone, and argillaceous sandstone. In lower Wolf Creek, mafic volcanics, presumably flows or tuff, and possibly tuffaceous limestone were included. Granitic intrusions locally produced more intense metamorphism. These rocks are so tightly and complexly folded that the thickness cannot be determined accurately. One to several thousand feet appears a not improbable figure.

Age and relation to other sections. The only direct field evidence on the age of this unit is its conformable position above marble containing Devonian fossils and its unconformable attitude beneath Permian beds.

Metamorphic rocks of the pre-Mesozoic complex east and north of Wolf Creek are usually assigned to the Yukon group of pre-Cambrian or Paleozoic age (Lees, 1936; Bostock, 1936). The Mount Stevens group (Cairnes, 1912; Cockfield and Bell, 1926) in the Wheaton and Whitehorse districts and previously established formations of undetermined age, such as the Kluane schist (McConnell, 1905; Cairnes, 1915b), are probably Yukon equivalents. The metamorphics of Wolf Creek are somewhat similar to the Yukon group, but H. S. Bostock (personal communication) thinks the descriptions above indicate less marked regional metamorphism than shown by that group along Yukon River. This need not be a fatal objection to correlation, but there is yet no proof that the Wolf Creek rocks should be included in the Yukon group.

In Alaska deposits of every Paleozoic period are known (Smith, 1939), and many of the systems contain rocks similar to the Wolf Creek metamorphics. However, pre-Devonian rocks may be tentatively eliminated, for the Wolf Creek metamorphics overlie Devonian marble, and comparable pre-Devonian rocks are scarce in the vicinity of Wolf Creek. In contrast, Middle Devonian rocks are widespread in southeastern Alaska (Moffit, 1938b), and the Mississippian is well represented throughout the Territory (Mertie, 1930b; Smith, 1939). Both systems contain rocks similar to the Wolf Creek metamorphics. They also include metavolcanics (Capps, 1916; Mertie, 1935; Moffit, 1938a) like those on Wolf Creek and are cut by similar gabbroic intrusives (Mertie, 1937; Moffit, 1941). Since there is little reason for excluding either the Devonian or Mississippian of Alaska as possible correlatives, it is best to assume that the Wolf Creek rocks may be either Mississippian or Devonian or possibly in part both. This is consistent with the Devonian age of the underlying marble, the lack of definite break between Devonian and Lower Carboniferous beds (Brooks and Kindle, 1908), and the unconformable position of the overlying Permian.



Fig. 6. Rocks of upper Wolf Creek. Foreground ridge composed of dark horizontal Tertiary volcanics on Devonian marble. Peaks beyond Wolf Creek Glacier largely granitic. Looking east. (Aerial photo by W. A. Wood, Sept. 9, 1941.)

Similar rocks along the Donjek River just to the east contain Carboniferous fossils (McConnell, 1906). This relation and the abundance of Mississippian rocks on upper Chitina River 35 miles west (Moffit, 1938a) might suggest that the Wolf Creek metamorphics are largely Mississippian. Lack of definite correlation between the fossiliferous Donjek beds and the Wolf Creek rocks and the possibility

that McConnell's fossils may have come from strata now known to be Permian lend uncertainty to this dating. The Wolf Creek rocks are probably not younger than Mississippian, for they are unconformable beneath Permian strata, and the Pennsylvanian is poorly represented in Alaska. The only beds definitely known to be Pennsylvanian are terrestrial (J. S. Williams, 1941).



Fig. 7. Region south of Wolf Creek. Foreground rocks possibly Devonian-Mississippian metamorphics. Mt. Wood at upper left. Looking north. (Aerial photo by W. A. Wood.)

Permian Rocks

General statement. Permian strata are exposed on the north wall of lowermost Wolf Creek (Fig. 1). The following data were obtained from distant observations and study of float, for access to the Permian outcrops was prevented by Wolf Creek, which in summer is unfordable by foot. Abundant float and excellent exposures permit reasonably reliable descriptions.

About 1500 feet of well-stratified limestone, limy sandstone, grit, chert, sandy tuff, and water-laid tuff are exposed (Fig. 8). Limestone, sandstone, and tuff are about equally abundant, and Permian fossils are plentiful.

Description. The 1500 feet (estimated) of Permian beds appear from a distance to be as follows:

<i>Permian strata</i> (descending order)	Feet
7. Massive black beds	50
6. Uniform, well-bedded, gray-weathering strata . .	500
5. Interlayered yellowish-brown, white, gray, and black beds, constituting the most distinctive group within the Permian sequence.	100
4. Dark, massive beds	50
3. Dark-weathering, massive beds with some light-colored strata	250
2. Dark-weathering, well-bedded strata with two prominent white layers, 20 to 40 feet thick .	250
1. Brown-weathering, well-bedded strata	300
Total.	1500

The calcareous strata are light-gray, fine-grained, soft, argillaceous limestone; black, dense, brittle limestone with irregular fracture; and various shades of gray, medium- to fine-grained arenaceous and tuffaceous limestone. Most of these beds weather light brown or gray. The large fragments of chert suggest that it occurs as beds rather than solely as nodules. Gray, green, white, and brown dense chert layers are interbanded on a 1/2- to 1-inch scale. Arenaceous strata consist of light-gray to brownish-gray, fine- to medium- and even-grained quartz sandstone some of which is tuffaceous and some calcareous. Nearly all the sandstone is distinguished by a vivid warm-brown weathering color. Tuff beds are gray, fine-grained, weather brown, and contain considerable quartz and feldspar. The tuff is well cemented and lacks the lamination noted in calcareous strata, although it appears to be well bedded in outcrop and is presumably water laid. The grits are brownish to greenish gray and consist of subangular to subrounded fragments of quartz, tuff, limestone, chert, and unidentified materials up to 3/8 inch in diameter. The matrix is variously sandy, calcareous, or tuffaceous. The fossiliferous beds are dark-gray, arenaceous limestone and light- to brownish-gray, limy sandstone.

The northern St. Elias Range contains a greater thickness of Permian strata than the 1500 feet exposed on Wolf Creek, for these beds extend northward in a homoclinal section, and much greater thicknesses have been reported in Alaska (Capps, 1916; Ross, 1933; Moffit, 1938b).

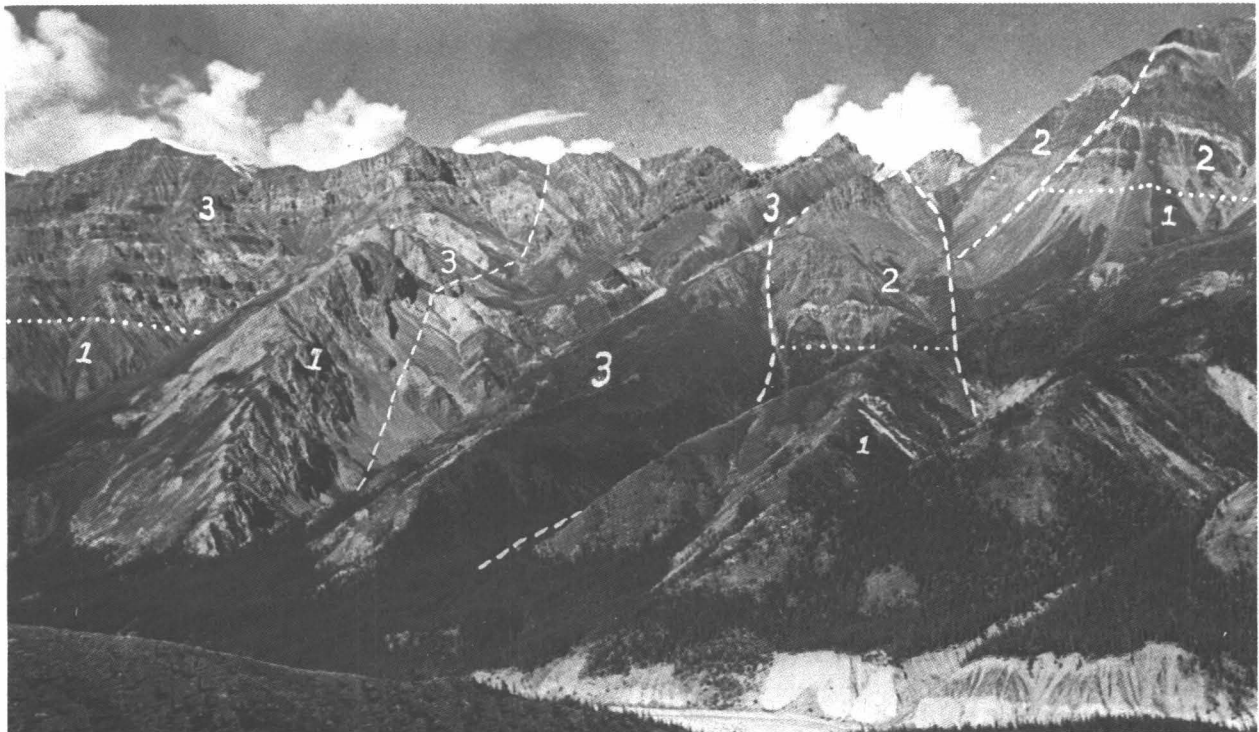


Fig. 8. Faults in north wall of lower Wolf Creek. (1) Devonian-Mississippian metamorphics; (2) Permian strata; (3) Tertiary volcanics. Dashed lines are faults, dotted lines are unconformities.

The Permian beds of Wolf Creek have a gentle northward tilt and are cut by a number of high-angle oblique faults. They are unconformable on Paleozoic gabbro and metamorphics at the mouth of the canyon and discordantly overlain by Tertiary volcanics. The pre-Permian erosion surface is smooth throughout the short distance exposed. Unconformities between Permian and Mississippian or Devonian rocks are reported in Alaska (Moffit, 1938a; Ross, 1933).

Age and relation to other sections. Fossils collected in float have been studied by Dr. J. S. Williams, who kindly furnishes the following statement.

"The collection consists of species of the brachiopod genera: *Chonetes*, *Productus*, *Marginifera*, *Spirifer* (*Neospirifer*), *Punctospirifer*, and *Rhynchopora*. Two species of bryozoans are also present. The brachiopod species are, for the most part, as yet unpublished, but they are well known in Alaskan collections of late Paleozoic age. The faunule is typical of the Alaskan faunules at present generally referred to the Permian period."

Permian strata are reported in many Alaskan districts within a 300-mile radius of Wolf Creek other than those already referred to (Capps, 1940; Moffit and Knopf, 1910; Moffit, 1933, 1941; Mertie, 1930b, 1937), and beds of possible Permian age are known in the Canadian Yukon (Cairnes, 1915a; Bostock and Lees, 1938). Brooks's (1900) Nutzotin series and Carboniferous strata near Whitehorse (Cockfield and Bell, 1926) may also contain deposits of this period. Strong lithologic similarities between the Wolf Creek rocks and Permian strata in Alaska suggest at least partial equivalence. The middle division of the Alaskan Permian, consisting of intermixed sedimentary and volcanic beds, seems to be represented here rather than either the upper or lower divisions which are predominantly volcanic (Moffit, 1930; Ross, 1933). This may indicate a Permian overlap to the east or southeast.

Quaternary Deposits

Thorough treatment of Quaternary materials requires a discussion of glacial history beyond the scope of this article. Deposits of two Wisconsin substages are mapped and designated for convenience as earlier and later Wisconsin. The older moraines resemble those of the Iowan-Wisconsin advance in the mountains of western United States (Sharp, 1941), but other considerations suggest that they may not be older than late Wisconsin.⁴ The younger substage is latest or possibly post-Wisconsin and includes moraines of two separate but closely related phases. Recent deposits of bouldery till and outwash gravels are related to existing glaciers and to a marked ad-

vance culminating 100 to 200 years ago. This dating is based in part on ecological data and parallels the established history of coastal Alaskan glaciers, many of which drain from the same snow fields.

The Recent white volcanic ash reported throughout the Yukon (Dawson, 1888; Hayes, 1892; Cairnes, 1912) is absent from Wolf Creek. According to Capps (1915) the source was about 40 miles northwest, and his isopach map indicates a possible 2 to 3 feet of ash in this vicinity. H. S. Bostock (personal communication) suggests from his observations that wind direction during eruption may not have favored deposition on Wolf Creek. Rugged local terrain, exceptionally active erosion, and the possibility that the ash fell on snow which subsequently melted and washed it away are supplementary or alternate factors. This 1400-year-old ash (Capps, 1916) is one of the best chronological markers in the region.

IGNEOUS ROCKS

General Statement

Igneous rocks on Wolf Creek are classified into four age groups, the oldest being the metamorphosed Devonian-Mississippian mafic flows or tuffs already described. A Pennsylvanian (?) gabbroic stock intrudes the Paleozoic metamorphics, and considerable late Mesozoic or early Tertiary granite and quartz monzonite are exposed. Tertiary lavas and pyroclastics cover a large area north of Wolf Creek and with associated dikes, sills, and plugs constitute the youngest igneous group.

Intrusive Bodies

Pennsylvanian(?) gabbro. A stocklike body of gabbro composes the north wall of Wolf Creek at its mouth (Fig. 1). The rock is a dark-green altered augite-hornblende gabbro of xenomorphic granular texture and medium grain size, containing finer diabasic phases and extremely coarse pegmatitic segregations. Secondary serpentine, chlorite, epidote, and calcite are abundant, and some talc is seen in hand specimen and thin section.

Exact dimensions of the gabbro body cannot be determined, but it is discordant and seemingly small, so it may provisionally be classed as a stock. The gabbro intrudes the Devonian-Mississippian metamorphics and is unconformably overlain by Permian beds. It is certainly late Paleozoic and probably Pennsylvanian, for absence of marine Pennsylvanian beds in Alaska (J. S. Williams, 1941) suggests widespread diastrophism and probably igneous intrusion during that period. Similar basic and ultrabasic Paleozoic bodies are known in Alaska (Mertie, 1937; Smith, 1939) although not all are contemporaneous.

Late Mesozoic or early Tertiary granitic bodies. The south wall of Wolf Creek westward from its midpoint is composed largely of granite and monzonite (Fig. 1).

⁴Subsequent studies tend to confirm the late Wisconsin age of the older moraines.

Aerial photographs suggest a considerable southward extension of the granitic rocks (Figs. 3,6), and debris on the glaciers shows that many of the high snow- and ice-covered peaks to the southwest are composed of similar material. A body of batholithic proportions is indicated.

The chief rocks are a pink porphyritic biotite granite between middle Wolf Creek and the bend, and varieties of white to gray hornblende-biotite-quartz monzonite farther south. These rocks are of medium grain and hypauto-morphic texture. Myrmekite, perthite, and zoned plagioclase are common. The porphyritic granite has pink orthoclase phenocrysts $1\frac{1}{2}$ inches long, and a melanocratic phase of the quartz monzonite contains considerable sphene. Gneissic structure and inclusions are prominent in the granitic rocks only near intrusive contacts. Small aplite and pegmatite dikes, some with black acicular tourmaline, were noted, and three plugs of dark biotite-hornblende tonalite containing considerable sodic oligoclase intrude the Devonian marble on the west wall of upper Wolf Creek. One plug is truncated by the erosion surface below the Tertiary volcanics, and since the tonalite is peripheral to the granitic rocks it is assigned to the same group. Time did not permit separate mapping of the various lithologies within this group, so they are not differentiated on Figure 1.

The porphyritic biotite granite is highly silicified, pyritized, and contains a few flakes of molybdenite and chalcopyrite in a 200- to 300-foot border zone north and east of peak 9761 (Fig. 1). A large medial moraine on Wolf Creek Glacier consists of highly silicified quartz monzonite containing chalcopyrite, pyrite, specular hematite, and considerable molybdenite in small veinlets and flakes. The abundance of mineralized debris in the moraine indicates a large exposure farther up the valley outside the map area (Fig. 1). Molybdenum is reported in 41 localities in Alaska, some not far west of Wolf Creek (Smith, 1942).

The granitic rocks intrude the Devonian-Mississippian metamorphics, but their relationship to the Permian beds is not known. They are unconformably overlain by Tertiary volcanics, and intrusion probably occurred before deposition of the lignite-bearing late Eocene beds (Cairnes, 1915b) a short distance east of Donjek River as indicated by the lack of metamorphism and marked deformation in the latter. On a stratigraphic basis the Wolf Creek granitic rocks may be tentatively dated as post-Devonian or Mississippian and pre-late Eocene. The lack of Paleozoic intrusives of this type in the Alaskan Yukon (Smith, 1939) and other relations indicate that they are probably post-Paleozoic.

In the Alaskan Yukon, post-Paleozoic intrusives are broadly grouped as Mesozoic and Cenozoic (Smith, 1939) but Mertie (1930a) and Moffit (1938a) show that a three-fold subdivision is feasible. On this latter basis the following classification is formulated: (1) Coast Range bath-

olith rocks, late Mid-Jurassic to early Lower Cretaceous; (2) Laramide rocks, late Upper Cretaceous to early Eocene; and (3) mid-Tertiary intrusives.

The Coast Range rocks form large batholiths and satellite bodies predominantly of granodiorite or quartz diorite, although granite, monzonite, syenite, and acidic and basic differentiates are known. Smith (1939) states that quartz monzonite is rare in the Coast Range bodies of the Alaskan Yukon, but this generalization may not hold elsewhere (Cairnes, 1912; Bostock, 1936). The Laramide bodies are also of batholithic proportions and largely granite and monzonite, with a variety of other rocks reported locally. The Laramide and Coast Range bodies are alike in size but differ in average composition. Somewhat similar relations are recognized in western United States (Lindgren, 1915).

The age of the Alaskan bodies herein termed Laramide has not been accurately determined, and failure in the past to distinguish them either from Coast Range or mid-Tertiary intrusives leads to confusion. Capps (1933) reports intrusion of granite during the Eocene in the Mount McKinley region, and Mertie (1938) favors an early Tertiary age for seemingly correlative intrusives farther west. The bodies of granite, monzonite, and diorite near Broad Pass (Moffit and Pogue, 1915) previously dated as post-Eocene because they intrude the Cantwell formation need be only late or post-Cretaceous, as the Cantwell is now known to be Upper Cretaceous and not Eocene as formerly supposed (Smith, 1939; Capps, 1940). Large intrusives of late Cretaceous or early Tertiary age have also been reported in Suslota Pass (Moffit, 1933), possibly in the upper Chitina River (Moffit, 1938a), and in the Yukon Plateau to the east of Wolf Creek (Bostock and Lees, 1938). The existence of a number of large intrusives approximately of Laramide age (late Upper Cretaceous to early Eocene) appears to be established.

Mid-Tertiary stocks, laccoliths, dikes, and sills of granite, quartz monzonite, and monzonite are exposed in the Ruby-Kuskokwim (Mertie, 1924), Yukon-Tanana (Mertie, 1937), and possibly the Nushagak (Mertie, 1938) districts. Many are related to cinnabar mineralization, and some still possess peripheral hot springs.

The size, composition, lack of cinnabar mineralization or hot springs, and inferred antecedence to the coal-bearing Eocene beds east of the Donjek indicate that the Wolf Creek intrusives are not mid-Tertiary. Furthermore, the granitic intrusives of east-central Alaska and most molybdenite-bearing bodies of that region are now considered Mesozoic (Smith, 1942). The predominance of granite and quartz monzonite in the Wolf Creek bodies favors correlation with the Laramide group, but Laramide rocks are scarce in near-by areas in contrast to the abundance of Coast Range rocks. It seems prudent for the present to recognize that the Wolf Creek bodies may be either Laramide or Coast Range (late Middle Jurassic to early

Eocene) with intrusion during the Mesozoic considered most likely.

Tertiary plugs, dikes, and sills. Coarse-grained extensively altered sodic monzodiorite containing anorthoclase and distinctive titanium-rich augite composes small pluglike bodies at the base of the Tertiary volcanic rocks in upper Wolf Creek. Sills of diabase within the volcanics near the same locality and a diabase plug intruding schists near point 5564 (Fig. 1) south of middle Wolf Creek contain the same titanium-rich augite. This suggests a common source for the monzodiorite and diabase. A number of mafic dikes 2 to 20 feet wide cut the volcanics and adjacent Paleozoic rocks. Those examined in thin section are augite andesite or diabase of fine to coarse diabasic texture. These intrusives are of essentially the same composition as the Tertiary flows and presumably of the same age.

A rhyolite porphyry dike in Paleozoic schist near peak 6791 may possibly be related to similar rocks of Cenozoic age in other areas (Cairnes, 1915a; Cockfield, 1921; Mertie, 1937).

Tertiary Volcanics

General statement. Well-layered nearly horizontal volcanic rocks at least 4600 feet thick compose much of Wolf Creek's north wall (Fig. 9). Small outliers are preserved south of the canyon, and volcanics cover a

large area west of Wolf Creek bend (Fig. 1). Pyroclastics, largely tuff and agglomerate, compose at least half this sequence, the remainder being basalt and andesite flows. Quartz latite, trachyte, and obsidian are minor constituents. The volcanics are Tertiary, of local origin, and widely distributed in this part of the St. Elias Range (Fig. 10) (Brooks, 1900; McConnell, 1905).

Lithology. Most of the flows are augite andesite and olivine-augite basalt with andesite slightly predominant. A thick flow of sodic quartz latite and a group of trachyte or possibly sodic latite flows resemble soda-rich rocks reported in corresponding volcanics of the Nabesna-White River District, Alaska (Moffit and Knopf). Except for obsidian, all the lavas are holocrystalline with fine hypautomorphic granular, pilotaxitic, or trachytic textures most abundant. Porphyritic types are slightly more abundant than nonporphyries. Common phenocrysts in andesite are augite, zoned labradorite, and less abundantly biotite. In addition, olivine and more rarely basaltic hornblende are present in the basalt flows. The quartz latite contains large crystals of quartz, anorthoclase, andesine, and aegirine-augite. A coarse-grained amygdaloidal basalt near the base of the section is distinguished by its tabular crystals of amber glassy labradorite $\frac{3}{4}$ inch long. Similar phenocrysts are reported from lavas in neighboring parts of Alaska (Moffit and Knopf, 1910; Moffit, 1938a). Pyrrhotite is the major ore accessory in the lavas, and cristobalite fills small cavities in the quartz latite and one andesite flow.



Fig. 9. Tertiary volcanics, north wall of Wolf Creek. Normal section described in text is exposed on flank of central snow-capped peak. About 4600 ft of volcanics shown.



Fig. 10. Tertiary volcanics north of Wolf Creek. Aerial photo looking north from over Wolf Creek (by W. A. Wood).

Some flows are moderately vesicular, and others are scoriaceous with horizontally flattened vesicles. Roughly spherical amygdules, up to 1½ inches in diameter, are filled with quartz, chalcedony, calcite, and aragonite. However, most flows are neither vesicular nor amygdaloidal. Columnar jointing is locally well developed in a few flows near the base of the sequence.

Obsidian showing flow lines and crude layering outcrops in cliffs 200 feet high on the flanks of peak 6791 west of Wolf Creek bend and along the river banks to the north (Fig. 1). This rock is chiefly a black vitreous to pitchy glass containing scattered crystals of potash feldspar and an irregular intermixture of 5% reddish-brown glass. Under the microscope the red material appears to be small braided layers, stringers, and spicules of hematite which represent the oxidized black particles of similar size and arrangement in the black glass. The indices of the red (1.495) and the black (1.498) glass show that they are both obsidian, with about 73% silica (George, 1924). Long splinters of gray obsidian associated with tuff near the middle of the volcanic section farther east contain crystals of potash feldspar and have slightly higher index (1.507).

The pyroclastics range from fine ash and tuff to coarse agglomerate and breccia. The fine deposits are white, gray, or brick red and usually well bedded, although some are massive. Ash beds are soft and friable, but the tuff layers are indurated, and some near the base of the sequence in the west are hard, platy, and silicified. The latter contain irregular siliceous nodules presumably formed by circulating hot waters and vapors associated

with hot-spring and solfataric action. Under the microscope the fine beds are seen to consist of glass, crystal fragments, chiefly feldspar, quartz, biotite, and augite, and much fine unidentified material. These minerals and the associated fragments of gray obsidian indicate a composition more acidic than that of the flows. Some crystal tuffs are andesitic, however, and locally so firmly welded as to be indistinguishable from altered lava. Well-bedded pyroclastics are clearly water laid, but massive layers may have been deposited directly from the air. Scattered beds of conglomerate and tuffaceous sandstone, 2 to 6 feet thick, are associated with the water-laid ash and tuff. The conglomerate contains well-rounded stones of lava, 2 to 12 inches in diameter, in a sparse sandy matrix.

Distinctive white, gray, and red lapilli tuff in groups of beds up to 200 feet thick are more abundant than the finer layers. The white beds consist largely of pumiceous fragments an inch or less in diameter set in a tuffaceous matrix of glass and crystal shards. The red and gray layers contain varicolored scoriaceous to pumiceous fragments with a few pieces of dark dense lava and obsidian, usually less than an inch in diameter, all embedded in red or gray cinders.

Crudely stratified agglomerate and breccia are abundant in beds 50 to 75 feet thick. They consist of angular to subangular pieces of vesicular basalt and andesite up to 5 feet in diameter, embedded in a scanty tuffaceous matrix.

Andesite flows well up in the section contain angular fragments of granite and schist a few inches in diameter which have been carried up several thousand feet from

the older basement rocks. The schist appears to be essentially unmodified, but the granite shows evidences of leaching and perhaps differential fusion, for it is notably cellular, frayed at the edges, and digested in appearance.

Thickness, arrangement, and structure. The thickness of these volcanics was originally greater than the 4600 feet now exposed, for the uppermost layers have been eroded. McConnell (1906) estimates their minimum thickness in this vicinity at 5000 feet, and 6000 to 8000 feet of similar rocks is reported in the Copper River region (Mendenhall, 1905).

The succession of flows and pyroclastics shown in Figure 1 represents the normal Wolf Creek sequence exposed in the lower central part of the canyon (Fig. 9). It consists of the following major units:

Tertiary volcanics (descending order)

- 11. Interbedded lava and agglomerate with minor white tuff; layers at top are cliff forming 1000(?)
- 10. Breccia, agglomerate, lava, tuff, and ash in various arrangements, white and red lapilli tuff layers abundant and separated by lava flows 20 to 40 feet thick, a few thin conglomerate beds included 1500
- 9. White lapilli tuff layers constituting the most prominent unit in the sequence 200
- 8. Massive andesite flows 100
- 7. Agglomerate, lava, tuff, ash, and a few conglomerate and sandstone beds, fragmental material predominant over flows 600 to 800
- 6. Group of 15 to 20 thin flows each characterized by a thin vesicular zone at the base, a central layer of non-vesicular but commonly porphyritic lava, and an upper zone of highly vesicular brecciated reddish lava representing the broken and oxidized top of the flow; no evidence of extended weathering between flows except in one or two instances where it might be due to modern processes accelerated by ground-water seepage. From a distance this group of flows looks like well-bedded sedimentary rocks 200
- 5. White tuff bed. 30
- 4. Cliff-forming, vesicular to dense basalt and andesite flows including layers of agglomerate and the distinctive amygdaloidal porphyritic basalt flow containing large amber phenocrysts of labradorite; many flows only 5 to 10 feet thick and notably vesicular 300 to 400

- 3. White porous ash 50
- 2. Uniform massive sodic quartz latite flows of dense and porphyritic texture 200 to 300
- 1. Massive flows forming vertical cliffs 200 to 300
- Approximate total 4600

The amounts of pyroclastics and lava in this section are about equal. Flows predominate near the base where basalt is most plentiful. The middle third has more pyroclastics than average with white ash and lapilli tuff particularly abundant. The upper third consists about half and half of agglomerate and flows. Extrusive episodes were interrupted frequently by explosive outbursts and by short periods of quiescence during which conglomerate, sandstone, and other water-laid beds containing materials of local origin were deposited.

Origin. These rocks are considered to be of local origin because: (1) The obsidian can hardly have come from a distant source, (2) large angular fragments in agglomerate and breccia beds indicate a vent of moderate proximity, (3) the flows could have been supplied from local dikes and plugs of proper composition, (4) the area between peaks 9209 and 9197 is thought to be a filled volcanic crater, and (5) the thin flows on Wolf Creek could hardly have come from a point so distant as the vents of the Wrangell Range, 130 miles west-northwest, which supplied the Wrangell lavas so widely distributed in Alaska (Mendenhall, 1905; Moffit, 1941). Furthermore, similar volcanics in neighboring areas may also be of local origin (Cairnes, 1915a; Capps, 1916).

Deviations from the normal succession are found near the bend in Wolf Creek, where the lowermost beds are obsidian and white platy ash. Near point 5564 south of the canyon the basal materials are well-bedded tuffaceous silt, sandstone, and conglomerate. Agglomerate and breccia increase in abundance and coarseness westward. The well-bedded normal sequence gives way to a jumbled mass of breccia, agglomerate, welded crystal tuff, lava, and dikes in an area bounded on the east by peak 9197 and on the west by peak 9209. This area is considered to be a filled volcanic crater because: (1) The well-developed layering seen farther east disappears here, (2) coarse agglomerate beds dip 25° inward, (3) abundant coarse pyroclastics indicate excessive explosive action, (4) more noticeable alteration of the rocks suggests circulation of hot vapors and solutions, (5) lava flows thicken up to the edge of this jumbled area and end abruptly, (6) such flows also dip slightly outward as though they had formed on the lower slopes of a broad cone.

The volcanics are largely undeformed except along sharp linear flexures and faults. This is also generally characteristic in Alaska (Moffit and Knopf, 1910; Moffit, 1930).

The Wolf Creek flows came in part from vents and possibly also from fissures. Many of the coarse agglomerate beds may have been deposited as mudflows (H. Williams, 1941). No progressive change in chemical composition of materials erupted is recognized. In the eastern part of Wolf Creek mafic flows are abundant toward the base, but in the west the lowermost layers are obsidian and acidic tuff. This suggests eruptions from different vents or fissures supplied at about the same time with magmatic materials of different composition. Fully half the volcanism of Wolf Creek was explosive, and some of the most violent explosions were from vents supplied with acidic materials.

Pre-volcanic surface. These volcanics rest on a relatively smooth erosion surface (Fig. 8) with a maximum observed relief of less than 200 feet. This does not compare with the 3000-foot relief, reported by Mendenhall (1905), on the surface beneath the Wrangell lavas. The Wolf Creek surface is more like that in the Talkeetna Mountains (Brooks, 1911) and the Chisana-White River area (Capps, 1916). Possibly these surfaces are not the same, for Mendenhall's appears to be Eocene, but that on Wolf Creek and elsewhere may be younger.

The pre-volcanic erosion surface on Wolf Creek is mantled by several feet of structureless extensively weathered detritus, and the rocks below are oxidized and kaolinized to depths of 30 feet. This weathered mantle consists of small angular fragments of the underlying rocks with a preponderance of quartz and less abundant schist and phyllite. The sandy and micaceous matrix contains kaolin and is cemented by brown hydrous iron oxides. This material is interpreted as a regolith developed on the erosion surface by subaerial weathering and subsequently buried by the volcanic materials. True soil is lacking except possibly in one place where several feet of reddish structureless clay overlies the coarser regolith.

Age. The volcanics of Wolf Creek rest unconformably on older rocks including the late Mesozoic or early Tertiary intrusives. The thickness, grain size, and proximity of the late Eocene lignite-bearing beds east of Donjek River (McConnell, 1906; Cairnes, 1915b) strongly suggest that they formerly extended into the Wolf Creek area. Lava and tuff interbedded in these strata may represent a preliminary phase of the volcanism, but absence of late Eocene deposits from Wolf Creek suggests erosion prior to eruption of the Wolf Creek volcanics. Thus, the base of these volcanics need be no older than Oligocene. Local deformation and dissection to a depth of 5000 feet or more prior to the later Wisconsin glaciation suggests that the uppermost layers are not younger than middle or late Quaternary.

The Wrangell lavas of Alaska (Mendenhall, 1905) were extruded during a period extending from Eocene to Recent time. The Eocene age of the basal Wrangell

lavas is confirmed by Moffit's (1930, 1938a) evidence, and Recent activity of the Wrangell vents is a matter of historical record. Capps (1916) believes that local phases of the volcanism began in Eocene time, but the major activity was post-Eocene, a conclusion favored by Schrader and Spencer (1901). Capps (1916) has further established the Pleistocene age of most of the lavas north of White River by finding them interbedded with and overlying pre-Wisconsin Pleistocene tillite. Canadian Yukon rocks similar to those of Wolf Creek are the Carmacks volcanics (Bostock, 1936) and the Newer volcanics (Cairnes, 1916; Cockfield, 1921), which are Eocene to Miocene.

Presumably the Wolf Creek volcanics are at least partly equivalent to these formations and represents a fraction of the total span of Wrangell activity, but none of these names is adopted because the Wolf Creek rocks are of local origin. The Wolf Creek volcanism probably centered around the mid-Tertiary, although it could have been initiated as early as Oligocene and may have continued into the Quaternary.

STRUCTURE

Structures along Wolf Creek are relatively simple except in the closely folded Paleozoic metamorphics and in a faulted area at Wolf Creek mouth. Recognizable folds in the metamorphics are small, the largest being 100 to 200 feet from limb to limb, but these may be superimposed on larger structures. Many folds are isoclinal, and the almost universal parallelism between bedding and foliation suggests that this is the predominant habit. Most fold axes trend east-northeast, but the direction and degree of plunge is not consistent. The foliation dips 50° to 75° northwest except near Wolf Creek mouth (Fig. 1). Deformation of the metamorphics was well advanced or completed prior to intrusion of the gabbro and may be tentatively dated as Pennsylvanian.

High-angle faults with apparent reverse displacements (Fig. 8) cut the Permian beds and the unconformably overlying volcanics in lower Wolf Creek (Fig. 1). They are divided into a minor set trending northeast and a major set trending northwest. The fault planes dip 80° to 90° , and displacements are relatively small (500 to 800 feet) on all except the two easternmost faults which have throws of at least 2000 feet. Direct examination of fault planes was not possible, so the exact direction of relative movements cannot be given. An oblique, dip-slip or strike-slip movement could have produced the observed stratigraphic displacements. If these faults are essentially contemporaneous and related to the same stress, their high angle and orientation suggest an essentially horizontal

shear couple acting in a northwest and southeast direction with the northeast side moving southeast. The superior development of the faults trending northwest could be attributed to their approximate parallelism with the shear couple (Fig. 11).

Since these faults cut the Tertiary volcanics, they are probably middle or late Cenozoic. It has been suggested (Russell, 1891, 1892; Spencer, 1903) that the St. Elias Range is a horst bounded on the northeast and southwest by faults showing considerable late Cenozoic displacement. Differential uplift along such fractures would set up stresses within the St. Elias block which may well have caused the Wolf Creek faults.

The Tertiary volcanics are deformed by a sharp monocline trending east-northeast from north of Mt. Wood to lower Wolf Creek where it is lost in the fault complex. The straight course of Wolf Creek from the bend eastward (Fig. 2) and of its north fork westward has been determined by this structure. The monocline has an upward shift on the south of several thousand feet, which accounts for the almost complete lack of volcanic rocks south of Wolf Creek. Dips up to 60° N have been measured along this flexure. Parallelism between the monocline and foliation in the metamorphics (Fig. 1) indicates some degree of control by the latter. However, the foliation shows no evidence of warping or tilting within the monoclinical zone. This suggests a fault in the metamorphics over which the volcanics were draped in monoclinical fashion. Such a fault would be difficult to locate because it would parallel the bedding and schistosity. Location of the monocline along the margin of the massive granite batholith is probably not accidental. Since the volcanics are displaced by this structure, it is middle or late Cenozoic and may be related to the same stresses which caused the faults at Wolf Creek mouth, particularly if it is due

to compression (Baker, 1935; Blackstone, 1940). Figure 11 is a generalized analysis of the possible stress relations which might have produced both the faults and the monocline.

SUMMARY OF GEOLOGICAL HISTORY

The earliest event recorded is deposition of at least 1000 feet of relatively pure limy sediment in a Devonian sea shallow enough to be inhabited by corals. Subsequent changes introduced much mud and some sand without interrupting deposition of calcareous material. The resulting sediments were impure limy and dolomitic beds interlayered with thin mud strata. Contemporaneous igneous activity supplied interbeds of basic volcanic debris. Deposition of several thousand feet of these mixed sediments continued through part of the Devonian or Mississippian, or both.

Diastrophism tightly compressed the Devonian-Mississippian (?) sediments into folds trending roughly east-northeast, imparted a low-grade metamorphism to the rocks, and uplifted the land. Following culmination of the deformation, but possibly contemporaneous with its closing phases, a stock of gabbro was intruded near the mouth of Wolf Creek. By some time in the Permian erosion had exposed the gabbro and developed a land surface of low relief across the older rocks. These relations suggest that the Pennsylvanian was largely a period of diastrophism, intrusion, and erosion, and this seems to have been true over much of Yukon and Alaska.

A Permian sea eventually submerged the land, and on its slowly subsiding floor many thousand feet of sand, lime, and volcanic materials were deposited. Brachiopods and bryozoans flourished in parts of the Permian sea. These strata were deformed by moderate tilting prior to intrusion of granite and quartz monzonite in upper Wolf Creek. These large intrusives are related either to the Jurassic-Cretaceous Coast Range batholith or to Cretaceous-Eocene Laramide bodies. They metamorphosed the Paleozoic rocks and produced considerable silicification and sulphide mineralization, including introduction of molybdenite.

Diastrophism associated with or subsequent to the intrusion uplifted the land and initiated erosion which exposed the granitic batholith, and developed a surface of low relief across all the older formations. A regolith was formed by weathering on this surface prior to eruption of the Tertiary volcanics which buried the area to a depth of nearly 5000 feet in basaltic and andesitic flows and more acid pyroclastics. In other regions the period between granitic intrusion and volcanism involves deposition of Cretaceous or Eocene formations and several episodes of deformation and erosion. Evidence of these events is lacking along Wolf Creek, although Eocene coal-bearing beds crop out just to the east. During the volcanic

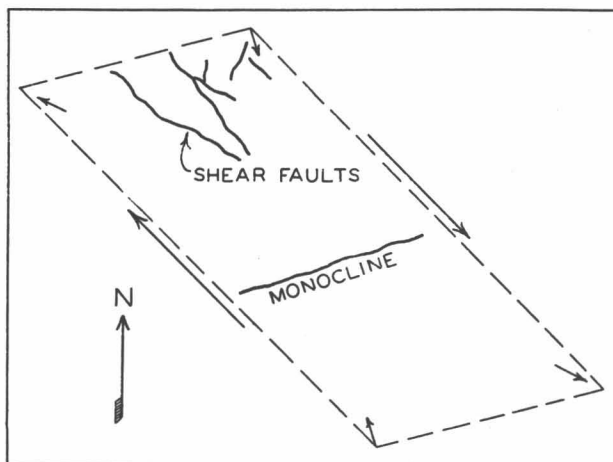


Fig. 11. Analysis of middle or late Cenozoic stress-strain relations on Wolf Creek (southeast-northwest shear couple is postulated).

activity extrusions of lava and explosive outbursts were about equally abundant with flows dominant in the early stages and explosions more abundant in the middle. Volcanism did not continue into the latest Pleistocene here as in other Alaskan and Yukon areas.

The volcanics were deformed by high-angle reverse faults and a monoclinical flexure in middle or late Cenozoic time, perhaps contemporaneously with phases in the last major uplift of the St. Elias block. The erosion initiated by uplift cut canyons many thousand feet deep which served as passageways for the great Pleistocene valley glaciers. The complex history of erosion, deposition, advance, and retreat of the glaciers occupying the Wolf Creek drainage is reserved for treatment in other publications. It involves several Wisconsin or partly post-Wisconsin episodes and a modern advance 100 to 200 years ago followed by retreat and stagnation interrupted by minor advances, one of which is currently in progress.

References

- Baker, A. A. (1935) Geologic structure of southeastern Utah, *Am. Assoc. Petrol. Geol.*, 19, 1472-1507.
- Bates, R. H. (1942) Above the whirlwind, *Am. Alpine J.*, 4, 348-354.
- Blackstone, D. L. (1940) Structure of the Pryor Mountains, Montana, *J. Geol.*, 48, 590-618.
- Bostock, H. S. (1936) Carmacks district, Yukon, *Mem. 189*, Geol. Surv. Can., 67 pp.
- Bostock, H. S., and Lees, E. J. (1938) Laberge map-area, Yukon, *Mem. 217*, Geol. Surv. Can., 32 pp.
- Brooks, A. H. (1900) A reconnaissance from Pyramid Harbor to Eagle City, Alaska, *21st Ann. Rept.*, Pt. 2, U.S. Geol. Surv., pp. 331-391.
- Brooks, A. H. (1911) The Mount McKinley region, Alaska, *Prof. Paper 70*, U.S. Geol. Surv., 234 pp.
- Brooks, A. H., and Kindle, E. M. (1908) Paleozoic and associated rocks of the upper Yukon, Alaska, *Bull. Geol. Soc. Am.*, 19, 255-314.
- Cairnes, D. D. (1912) Wheaton district, Yukon Territory, *Mem. 31*, Geol. Surv. Can., 153 pp.
- Cairnes, D. D. (1915a) Upper White River district, Yukon, *Mem. 50*, Geol. Surv. Can., 191 pp.
- Cairnes, D. D. (1915b) Exploration in southwestern Yukon, *Summ. Rept. 1914*, Geol. Surv. Can., pp. 10-33.
- Cairnes, D. D. (1916) Wheaton district, southern Yukon, *Summ. Rept. 1915*, Geol. Surv. Can., pp. 36-49.
- Capps, S. R. (1915) An ancient volcanic eruption in the upper Yukon basin, *Prof. Paper 95D*, U.S. Geol. Surv., pp. 59-64.
- Capps, S. R. (1916) The Chisana-White River district, Alaska, *Bull. 630*, U.S. Geol. Surv., 130 pp.
- Capps, S. R. (1933) The eastern portion of Mount McKinley National Park, *Bull. 836D*, U.S. Geol. Surv., pp. 219-300.
- Capps, S. R. (1940) Geology of the Alaska Railroad region, *Bull. 907*, U.S. Geol. Surv., 201 pp.
- Cockfield, W. E. (1921) Sixtymile and Ladue Rivers area, Yukon, *Mem. 123*, Geol. Surv. Can., 60 pp.
- Cockfield, W. E., and Bell, A. H. (1926) Whitehorse district, Yukon, *Mem. 150*, Geol. Surv. Can., 63 pp.
- Dawson, G. M. (1888) Report on an exploration in the Yukon district, Northwest Territory, and adjacent portions of British Columbia, *Summ. Rept. 1887-1888*, Geol. Surv. Can., pp. 5B-277B.
- George, W. O. (1924) The relation of the physical properties of natural glasses to their chemical composition, *J. Geol.*, 32, 353-372.
- Hayes, C. W. (1892) An expedition through the Yukon district, *Nat. Geogr. Mag.*, 4, 117-162.
- Holmes, A. (1929) *The Nomenclature of Petrology; With Reference to Selected Literature*, Murby, London, 284 pp.
- Lees, E. J. (1936) Geology of Teslin-Quiet Lake area, Yukon, *Mem. 203*, Geol. Surv. Can., 30 pp.
- Lindgren, W. (1915) The igneous geology of the Cordilleras and its problems, in *Problems of American Geology*, edited by W. N. Rice, pp. 234-286, Yale Univ. Press, New Haven.
- McConnell, R. G. (1905) The Klauane mining district, *Ann. Rept.*, Geol. Surv. Can., Vol. 16, pp. 1A-18A.
- McConnell, R. G. (1906) Headwaters of White River, Yukon, *Summ. Rept. 1905*, Geol. Surv. Can., pp. 19-26.
- Mendenhall, W. C. (1905) Geology of the central Copper River region, Alaska, *Prof. Paper 41*, U.S. Geol. Surv., 133 pp.
- Mertie, J. B. (1924) The Ruby-Kuskokwin region, Alaska, *Bull. 754*, U.S. Geol. Surv., 129 pp.
- Mertie, J. B. (1930a) Mountain building in Alaska, *Am. J. Sci.*, 5th Ser., 20, 101-124.
- Mertie, J. B. (1930b) Geology of the Eagle-Circle district, Alaska, *Bull. 816*, U.S. Geol. Surv., 168 pp.
- Mertie, J. B. (1935) Pre-Cambrian and Paleozoic vulcanism of interior Alaska, *Trans. Am. Geophys. Union*, 16, 292-302.
- Mertie, J. B. (1937) The Yukon-Tanana region, Alaska, *Bull. 872*, U.S. Geol. Surv., 276 pp.
- Mertie, J. B. (1938) The Nushagak district, Alaska, *Bull. 903*, U.S. Geol. Surv., 96 pp.
- Moffit, F. H. (1930) Notes on the geology of upper Nizina River, Alaska, *Bull. 813D*, U.S. Geol. Surv., pp. 143-163.
- Moffit, F. H. (1933) The Suslota Pass district, upper Copper River region, Alaska, *Bull. 844C*, U.S. Geol. Surv., pp. 136-162.
- Moffit, F. H. (1938a) Geology of the Chitina Valley and adjacent area, *Bull. 894*, U.S. Geol. Surv., 137 pp.
- Moffit, F. H. (1938b) Geology of the Slana-Tok district, Alaska, *Bull. 904*, U.S. Geol. Surv., 54 pp.
- Moffit, F. H. (1941) Geology of the upper Tetling River district, Alaska, *Bull. 917B*, U.S. Geol. Surv., pp. 115-155.
- Moffit, F. H., and Knopf, A. (1910) Mineral resources of the Nabesna-White River district, Alaska, *Bull. 417*, U.S. Geol. Surv., 64 pp.
- Moffit, F. H., and Pogue, J. E. (1915) The Broad Pass region, Alaska, *Bull. 608*, U.S. Geol. Surv., 80 pp.
- Ross, C. P. (1933) Mineral deposits near the west fork of the Chulitna River, Alaska, *Bull. 849E*, U.S. Geol. Surv., pp. 289-333.
- Russell, I. C. (1891) An expedition to Mount St. Elias, Alaska, *Nat. Geogr. Mag.*, 3, 53-203.
- Russell, I. C. (1892) Mt. St. Elias and its glaciers, *Am. J. Sci.*, 3rd Ser., 43, 169-182.
- Schrader, F. C., and Spencer, A. C. (1901) The geology and mineral resources of a portion of the Copper River district, Alaska, *Spec. Publ.*, U.S. Geol. Surv., 94 pp.
- Sharp, R. P. (1941) Wolf Creek glacier system, St. Elias Range, Yukon Territory, *Bull. Geol. Soc. Am.*, 52, 1932-1933 (abstr.).
- Smith, P. S. (1939) Areal geology of Alaska, *Prof. Paper 192*, U.S. Geol. Surv., 100 pp.
- Smith, P. S. (1942) Occurrence of molybdenum minerals in Alaska, *Bull. 926C*, U.S. Geol. Surv., pp. 161-207.
- Spencer, A. C. (1903) Pacific mountain system in British Columbia and Alaska, *Bull. Geol. Soc. Am.*, 14, 117-132.
- Williams, H. (1941) Volcanology, in *Geology 1888-1938; Fiftieth Anniversary Volume*, Geol. Soc. Am., New York, pp. 367-390.

- Williams, J. S. (1941) Late Paleozoic faunas of Alaska, *Bull. Geol. Soc. Am.*, 52, 1978 (abstr.).
- Wood, F. H. (1940) An attempt on Mt. Wood, St. Elias Range, *Am. Alpine J.*, 4, 1-8.
- Wood, W. A. (1936) The Wood Yukon Expedition of 1935,

- Geogr. Rev.*, 26, 228-246.
- Wood, W. A. (1942a) The parachuting of Expedition supplies, *Geogr. Rev.*, 32, 36-55.
- Wood, W. A. (1942b) Parachutes in the St. Elias Range, *Am. Alpine J.*, 4, 341-347.

Movement Observations on the Terminus Area of the Steele Glacier

July 1967

S. Thomson *

ABSTRACT. The Department of Geology of the University of Alberta placed an expedition on the Steele Glacier from July 10 to 24, 1967 to study the effects of a surging glacier on the formation of glacial deposits and to observe the means of incorporating debris into the ice mass. A part of this study consisted of measurements of the movement of the active ice mass and the reactivation of dead ice.

Observations consisted of angles turned from each end of a known base line to stations established on the dead ice and to recognizable features on the active ice. During the first few days, rates of movement were approximately 0.4 ft/hr but by the end of the observation period the motion had slowed to less than half this value. The portion of the dead ice being reactivated had rates of movement of the same order of magnitude. The dead ice appears to be reactivated by the generation of a series of shear planes, some of which rise from the ground surface through the entire ice mass. Suggested mechanisms for incorporation of debris into the ice mass are motion on shear planes and overriding of superglacial debris on the dead ice.

Introduction

The Department of Geology of the University of Alberta supported a party which studied some aspects of the geomorphology of the terminus area of the Steele Glacier in July 1967. The major purposes of the study were to observe the effects of a surging glacier on the formation of glacial deposits and to observe means of incorporating debris into the ice mass. The party arrived in the terminus area of the glacier on July 10, 1967 and left on July 24, 1967.

A necessary part of the study was the determination of the direction and rate of movement of the active ice and the reactivation of the dead ice. This report deals exclusively with movement observations in the terminus area and an analysis of the resulting data.

The Steele Glacier is 32 air miles west of Burwash Landing; the latter locality is at the northwestern end of Kluane Lake and was the base of operations for the expedition (Plate 1).¹ A camp was established in the terminus area of the glacier.

Steele Creek is an easterly flowing tributary of the Donjek River which it joins at a point about 25 mi upstream from the Alaska Highway crossing. Steele Creek valley is 4000-5000 ft deep and about 4000 ft wide near river level. At its confluence with the Donjek River, river elevation is some 3200 ft. The elevation of the camp site

near the terminus of the glacier at the time of study was approximately 4200 ft. The Steele Glacier occupies the valley to within some 8 mi of its mouth.

The valley was glaciated during Wisconsin time; Sharp (1943) mapped two moraines resulting from late sub-stages of this glacial advance. These appear as a series of morainal ridges on the lower part of the valley walls. The recent deposits of bouldery till and outwash gravels as well as remnants of debris-covered dead ice in the valley, are related to a marked ice advance which culminated 100-200 years ago (Sharp, 1943). The downstream limit of this advance is marked by a well-developed terminal moraine.

The present glacier advance is considered to have begun in 1965; since that time the ice has advanced some 7 mi. Rates of advance in the order of 35 ft/day were reported (Bayrock, 1967). The moving or active ice is incorporating the dead ice, its superglacial debris, and adjacent material.

Observation Points

When the party arrived on site, the active ice was impinging upon a large block of dead ice located in about the center of the valley. Two lobes or tongues were advancing around the dead ice. In order to observe ice movements, it was decided to establish two base lines roughly parallel to the glacier advance, for transit surveying. Subsequently, a third short base line was set up in the vicinity of the camp. Figure 1 is a schematic diagram illustrating the location of the survey stations and the general areas in which the observed points were located.

*Department of Civil Engineering, University of Alberta, Edmonton

¹Plate 1 is a map inside the back cover of this volume.

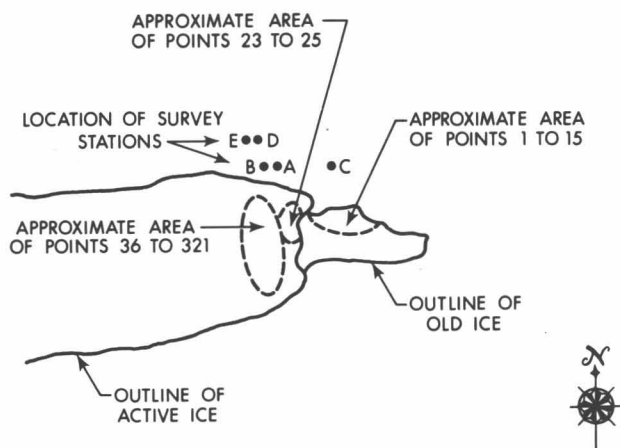


Fig. 1. Schematic diagram illustrating location of survey stations and areas of points.

Observation points established on the dead ice consisted of one-inch diameter red and white range poles or crosses painted on large rocks. Where possible, identifying numbers were painted beside the points. Access to the active ice was not only very dangerous but virtually impossible; hence, prominent features on the ice were chosen as observation points. These ice features had to be easily identifiable by shape, yet contain some small characteristic, such as a boulder or pebble, on which the hair lines of the instrument could be centered. Several observational points on the active ice were subsequently lost due to ablation or collapse of the features.

Base Lines

Three base lines were used for observation of the movements. Base Line AB, 100 ft long, was located on a moraine ridge immediately adjacent to the camp on the north wall of the valley. Station B was located to the west of Station A. The length and location of Base Line AB were dictated solely by convenience. AB was approximately parallel to the glacier and was near the terminus of the active ice. The length of this line is accurate to ± 0.05 ft.

The second base line, AC, ran from Station A eastward to Station C, located on the edge of an alluvial fan. AC is very roughly an extension of BA. It is at an angle of about 30° to the axis of the dead ice in front of the glacier and extends nearly the length of the dead ice mass. The horizontal distance between A and C was 1918.88 ft. A very difficult chaining task was fortunately eliminated by the presence in the valley of the Mapping and Charting Establishment, Canadian Forces. Members of this unit measured Base Line AC by tellurometer; its accuracy is ± 0.01 ft.

The third base line, DE, was located higher up the valley wall in such a position that the surface of the moving

ice could be observed. Base Line DE was 420 ± 0.5 ft in length. The time available did not permit the expenditure of effort that would have been necessary to establish a longer or more accurately chained base line.

Survey Instrument

The instrument used for the survey work of the expedition was a standard Winslow transit. The horizontal circle is calibrated to read angles to 20 seconds of arc. The vertical circle allows the reading of angles to one minute of arc. With reasonable care, surveying to an accuracy of one part in 5000 may be achieved (Davis and Foote, 1953). In rugged topography, the chaining of base lines is a limiting factor in the accuracy of the surveying; therefore, the transit used was considered adequate for this work.

The points could not, under the field circumstances, be observed simultaneously from both ends of the base line. Since the points were observed from one end of the base line about two hours later than from the other end, and assuming a rate of movement of 0.4 ft/hr, the point moved 0.8 ft during times of observations. In the calculations for the coordinates of the point, simultaneous readings were assumed. There is, therefore, an inherent error in the measurements of about one part in 2000.

Results of Survey Observations

The survey data consisted of the known base-line length and the angles from each end of the base line to the point under consideration. The time of the observation was taken as the average of the two actual times of observation. The calculations yielded X, Y, and Z coordinates of the observed point—assuming Station A to have coordinates 0,0,0—for Base Lines AC and AB. The X axis was arbitrarily chosen to coincide with the particular base line. The Y axis is, therefore, perpendicular to the base line and southerly distances are positive. The Z coordinate is the vertical distance below the zero station. A schematic diagram to illustrate the preceding is given in Figure 2. Since the three base lines were not tied together by surveying, they must be considered as separate entities.

A computer program was set up to sort the data in chronological order for each point, to calculate the X, Y, and Z coordinates, and to calculate the errors in the coordinates based on an error of one minute in the angles and on the chaining errors in the base-line length. In general, the errors computed were small and have been neglected. In those instances where the error is significant, however, the data were rejected.

Base Line AC

Figure 3 shows typical terrain and the location of some of the points observed. Plots of the data for this base line are presented in Figures 4, 5, 6, and 7. Figure 4 shows the

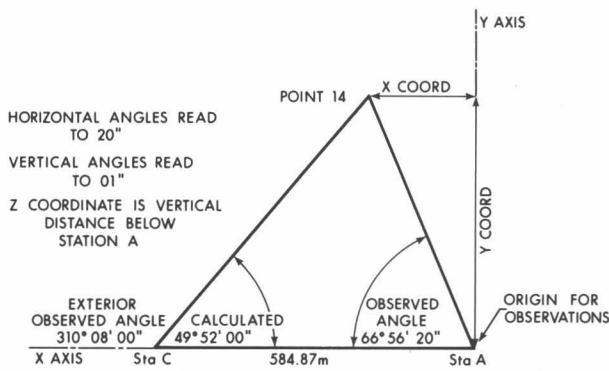


Fig. 2. Schematic diagram illustrating observations for a typical point.

relative positions of the 15 points observed. Observations showed that Points 1 to 8 were located on dead ice. Figure 5 is a plan view of the movements, all points having been brought to a common datum by taking the first reading at each point as zero. The slight movement of Point 9 suggests that it is located on top of shear planes which were just beginning to be activated. Point 10, also located above a set of shear planes, was moving; hence, it is inferred that the shear planes were active at this location. Points 11 and 12 moved farther than Point 10; hence, there may be another shear plane between these two points and Point 9. Another alternative is the presence of a rather wide shear zone with Point 10 on the lower side. Differential movement exists within this zone, the upper part moving slightly more rapidly than the lower part. In a plan view, Points 10, 11, and 12 moved along a line that is at an angle of 10° to 12° with Base Line AC.



Fig. 3. Location of some of the points observed from Base Line AC.

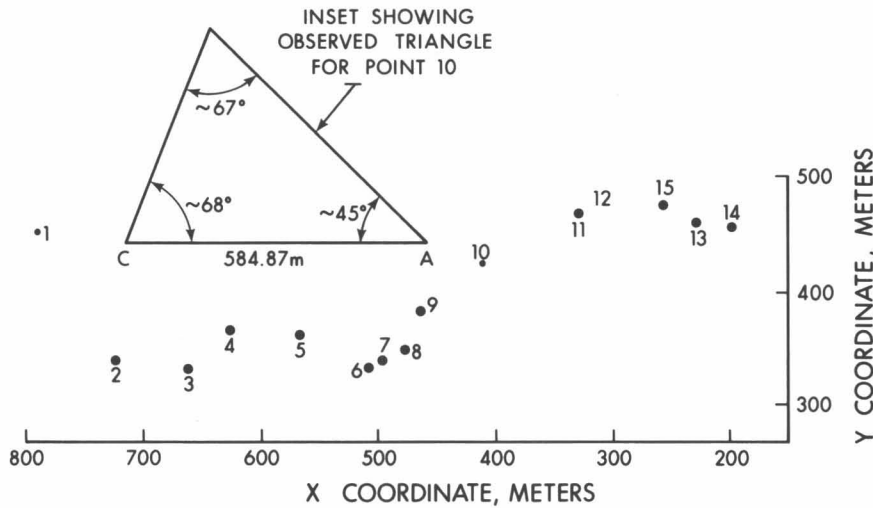


Fig. 4. Relative position of points for Base Line AC.

Points 13, 14, and 15 (Fig. 5) moved at an angle of about 25° to AC. They moved farther than the preceding points, which indicates that they were in an area that was being actively incorporated by the moving ice. This explains their greater total movement and also the greater Y component; that is, the active ice was moving toward a free face and going around the old ice which was being reactivated. The movements depicted on Figure 5 appear reasonably uniform in that they do not depart very far from a straight line or smooth curve.

Figure 6 depicts the changes in elevation of Points 10-15. Most of the points show a general tendency to rise, which is the anticipated movement. The abrupt changes in the plots for Points 11 and 15 are considered to be due to effects of ablation.

Average rates of movement are shown on Figure 7. These rates were calculated by dividing the movement between successive pairs of observations by the time between the observations. The average rate of movement

from zero time to 39.2 hours is plotted against 39.2 hours. Similarly, for the next set of observations (July 18), made at 89.9 hours from zero time, the average rate of movement over the 50.7-hour interval is shown against 89.9 hours. As is indicated by the abrupt change in slope of the lines, the glacier slowed down considerably between July 14 and 16. After July 18 the rate appears to be slowing more gradually and steadily. If the curve for the last three observations for Point 10 is extrapolated the movement would have stopped in about two weeks. This assumes the decrease in the rates of movement to be constant. It is more likely that the rates decrease with time and therefore a substantially longer time would be required for the glacier to come to a stop.

Figure 8 is an overlay from Figure 3 showing the proposed shear planes in an attempt to explain the movement of Points 10-15. The shear plane denoted I is just starting to be activated; hence, Point 9 indicates start of movement, whereas Point 8 is stationary. Shear Plane II is

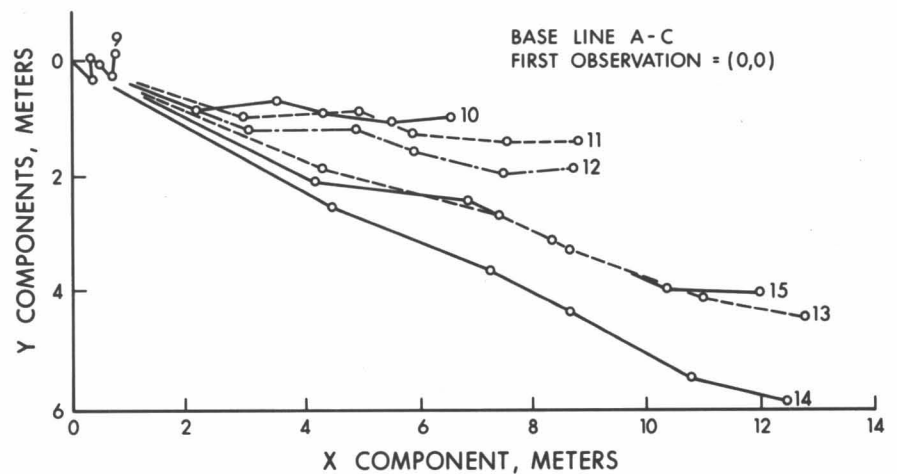


Fig. 5. Movement of Points 9-15 from a common datum.

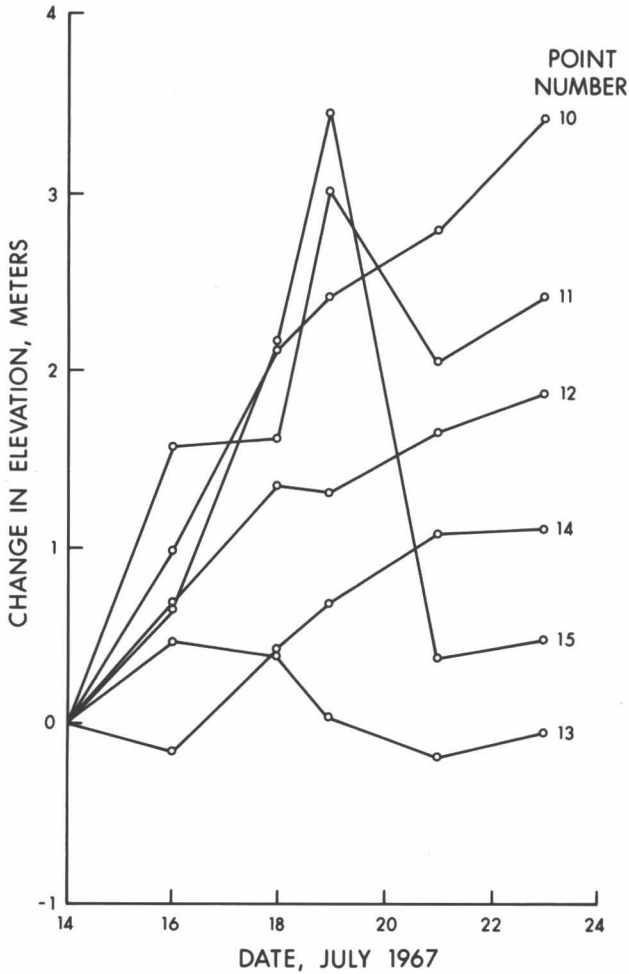


Fig. 6. Change in elevation versus time, Points 10-15, Base Line AC.

active, as is Shear Plane III. Points 11 and 12 have moved farther than Point 10 and have also increased in elevation. Points 13 and 14 have not risen very much but have moved considerably in a horizontal plane. Point 15 appears to be subjected to "bulldozing" and crumpling, hence it is rising in elevation.

In general, it would appear that the active ice creates in the dead ice shear surfaces that curve upward from the base of the dead ice. The slopes of these shear planes appear to be steep as they are first formed some distance in front of the ice. The slopes seem to decrease in steepness as the active ice advances. In this particular instance there is a large knob of old ice, on which Points 11 and 12 are located, that is being sheared. This may account for the flat attitude of the shear planes in this location.

Base Line AB

Plots of the data for the Base Line AB are given on Figures 9 and 10. In order to avoid ambiguity and error in the computer program, the points observed for this base line are preceded by a "2." This base line was immediately adjacent to the camp and only 100 ft long. The points under observation were near the front of the active ice and were in the range of 1000-1500 ft away from the base line; hence, the angle subtended at the point by the base line is in the order of 5° to 3°. Such a very small angle of intersection does not lend itself to accuracy.

Figure 9 shows the relative positions of the points with the vectors indicating direction of motion in a horizontal plane. The three points are moving in about the same direction and appear to be deflected toward the north by the dead ice. The horizontal direction of movement makes an angle of 27° with Base Line AB and about 37° with Base Line AC. The motion has a greater Y component than points on the dead ice.

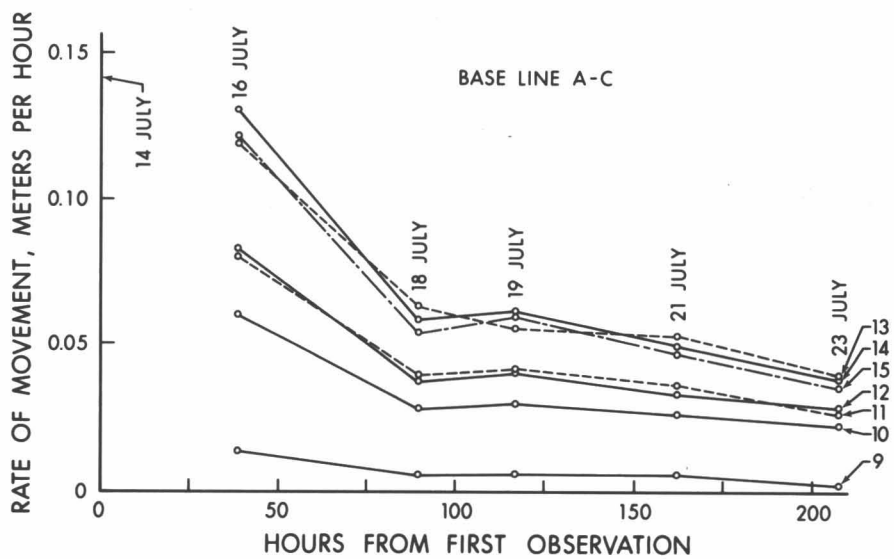


Fig. 7. Average rate of movement between observations versus time from first observation.

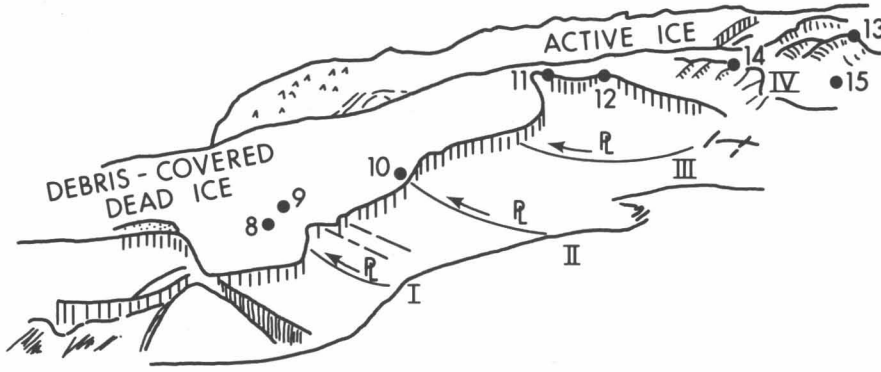


Fig. 8. Overlay from Figure 3 showing proposed shear planes.

Figure 10 shows the changes in elevation of Points 23, 24, and 25 from a common datum. Points 23 and 24 are decreasing in elevation, whereas Point 25 is rising. Figure 9 shows that the former two points are closer to the terminus than is the latter point. Point 23 is on the snout of the active ice, Point 24 is a triangularly shaped block of clear ice on a larger ice block, and Point 25 is the tip of an ice block within the moving ice mass. The decrease in elevation of Point 23 can be explained by visualizing the movement of Shear Plane III of Figure 8. As Points 11 and 12 are rising at one end of this shear plane the other end must be going down. It is postulated that the downward movement of Point 23 is due to its being near the upstream end of the shear plane. Point 24 is going down simply due to the downward movement of the individual block. The block on which Point 25 is located is rising probably as a discrete unit. The movements infer a somewhat random movement of the jumbled mass of ice blocks that appear to make up the general terminus area of the active ice. Statistically the movement is forward or downhill but an individual block may have a component of movement in virtually any direction. If one imagines a block with a rather planar face that is tilted uphill then the weight of a block moving downhill

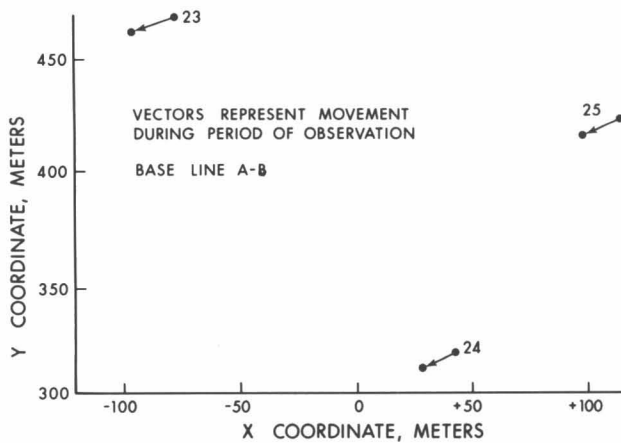


Fig. 9. Relative position of points for Base Line AB.

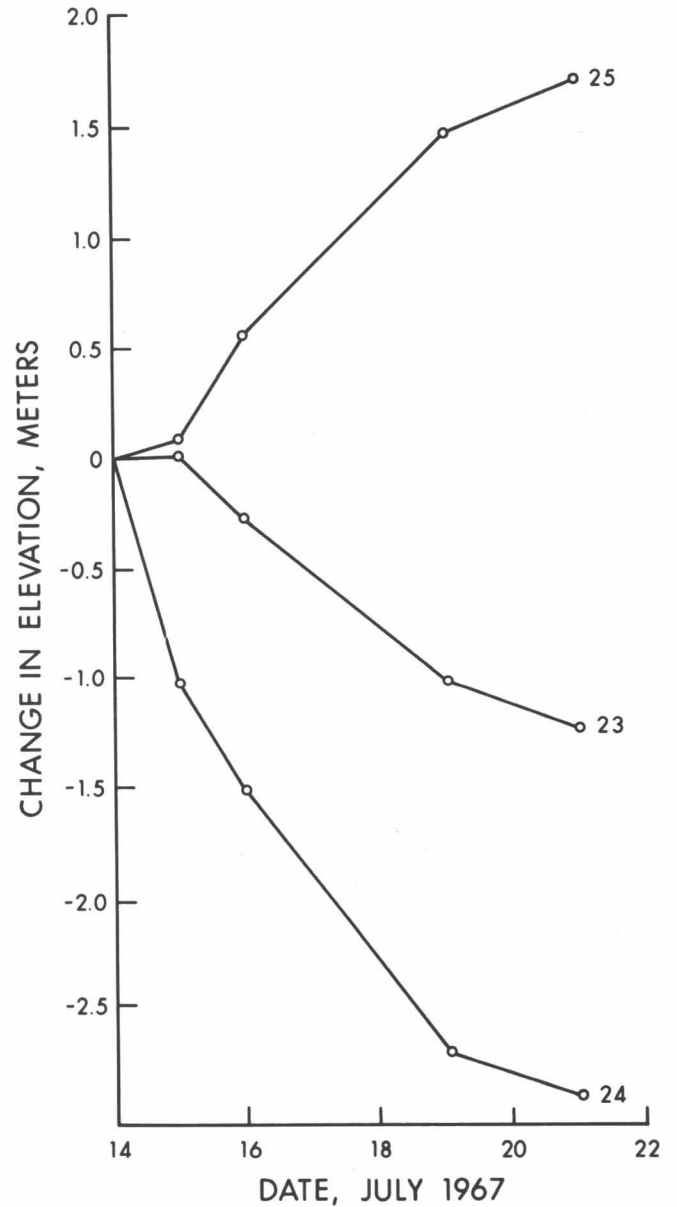


Fig. 10. Change in elevation versus time for Base Line AB.

would create a force having a downward component. If this force were sufficiently high the block would move downward, perhaps occupying void space, displacing material, or forcing an adjacent block sideways or upward. A like argument applies to a block having a downstream tilt. A force on this face would have an upward component which could lift the entire block upward. This random motion may be considered analogous to turbulent flow in a river.

In general, the rates of movement of Points 23, 24, and 25 were the same order as Points 13, 14, and 15 (Fig. 7) for the period July 14-15. Subsequently, however, the latter points were moving about 0.15 ft/hr (July 21) whereas the former points on the active ice were moving at approximately 0.25 to 0.3 ft/hr; that is, considerably faster. If one compares only the X components of motion they are relatively the same; the active ice was moving considerably faster. A brief check on the Y components shows both sets of points to be about the same order of magnitude. Since only surface velocities were measured in both cases, one is led to conjecture that the upper part of the active ice was overriding the old ice which was being re-activated but at that time had a slower rate of movement.

Base Line DE

Many difficulties were encountered in the surveying associated with Base Line DE which was located on the valley wall several hundred feet above Base Line AB. The early priority assigned to other tasks of some importance to the expedition delayed the establishment of the base line. Survey observations made were fitted into the general work schedule as time became available; hence, fewer readings were taken.

Observations of seven naturally occurring features are available for use in this report. Additional points were lost through ablation. The points associated with this base line are preceded by a "3."

Figure 11 gives the relative positions of the points; fortunately, the 7 points are spread over the surface of the glacier. The origin used in these calculations was Station D. The points on the south or far side of the active ice were moving southward and undoubtedly reflect the deflection of the glacier around the old ice mass. The components of motion are at a high angle to the general eastward motion of the ice. On the north, or near, side the ice was also being deflected by the old ice mass, but the vector representing motion does not make as great an angle with the general ice movement direction.

Figure 11 also depicts the total direction and magnitude of the observed points for Base Line CD. Points 315, 316, and 319 had a dominant southward component of motion. Point 321, located on the north edge of the ice, was moving essentially parallel to the general direction of glacier flow. Points 36 and 39, which were near the snout of the moving ice, appeared to have an initial

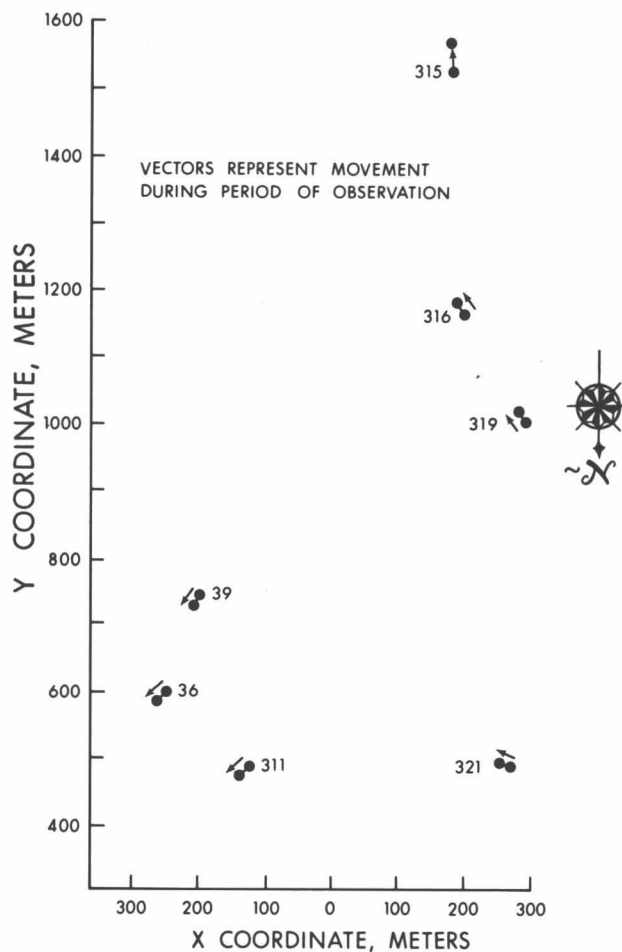


Fig. 11. Relative position of points, Base Line DE.

movement toward the north edge of the glacier then, having attained this position, moved along the valley. Another way of considering the motion of these two points is that the early northward movement reflects deflection by the old ice, a core of which extends upvalley into the moving mass, and subsequent motion reflects the ice in the lobes flowing roughly parallel to valley walls and the edge of the dead ice.

The rates of movement for the points observed from Base Line DE are listed in Table 1. Comparison of the data in this table with that in Figure 12 indicates a general agreement in the rates of movement of the points observed except for Point 315, the movement of which is much greater than any other point. It is believed that the rates for this point do not present a true picture. The direction of movement of this point was almost directly away from the observer. Due to a short base line and the great distance involved to Point 315, the lines drawn from each end of the base, which define the location of the point, intersected at a small angle. There is, therefore, the

TABLE 1. Rates of Movement of Points on Active Ice, Base Line DE

Point No.	Time Interval		Rate of Movement ft/hr
	From	To	
36	15 July	21 July	0.248
	21	23	0.162
39	18	21	0.283
	21	23	0.246
311	15	18	0.406
	18	21	0.195
	21	23	0.214
315	18	21	0.94
	21	23	1.48
316	18	21	0.250
	21	23	0.494
319	18	21	0.38
	21	23	0.312
321	18	21	0.164
	21	23	0.166

possibility of a considerable error in the Y coordinate. There is also a strong suggestion that the rate of movement slowed considerably about July 15, 1967.

Conclusions

It would appear that the dead ice becomes incorporated into and forms an integral part of the moving ice mass in stages. The stages are not distinct but merge with one another. From this brief study, the stages may be postulated as follows. Initially, the shear surface develops in front of the moving ice at which time movement is quite slow (see Point 9, Fig. 5). The inertia of the old ice is still quite high despite the fact that it is moving slowly; therefore, the active ice overrides the old ice. When sufficient shear displacement has occurred along one of the shear planes, stationary dead ice is exposed to the force exerted by the moving ice, whereupon it is set into motion. This latter stage probably initiates shear planes farther downvalley. It is only when overriding and considerable shear displacement have occurred that the old or previously dead ice has lost its identity and become an integral part of the moving mass.

A comparison of the rates of movement for the three base lines shows that the rates of movement were compatible. Highest rates of movement were recorded for the active ice and the rates decreased toward the terminus area. The edge of the old ice, which was incorporated by the moving ice, had rates of movement of the same order as the active ice. The rates decreased to zero in the vicin-

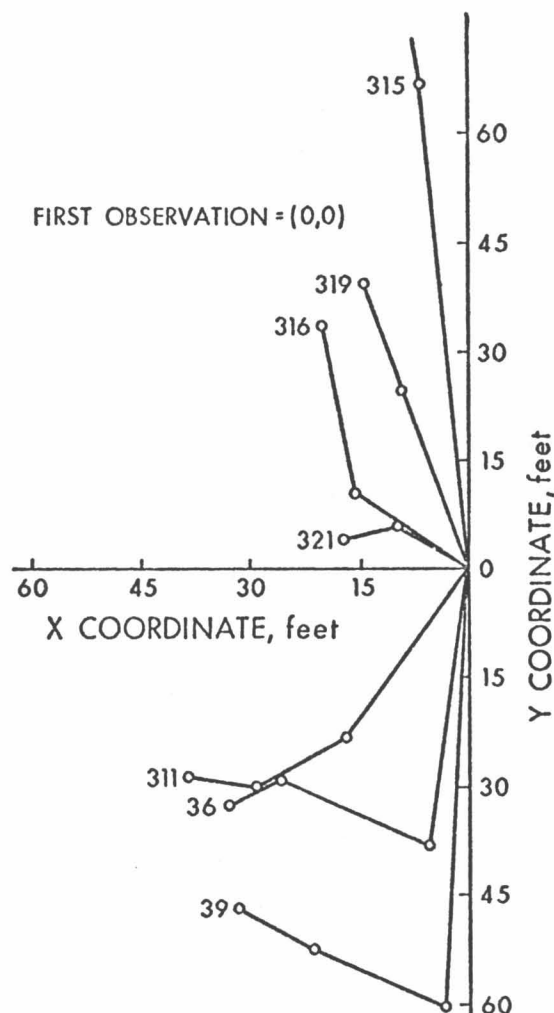


Fig. 12. Movement of points observed from Base Line DE from a common datum.

ity of Point 9, which was located about 900 ft eastward along the old ice from the active ice front.

The changes in elevation were not very great for any of the observations. The points on the old ice observed from Base Line AC all showed a general tendency to rise. Changes in elevation ranged from 2 ft to nearly 12 ft and were a response to the formation of and movement along shear planes. Points on the active ice showed a general tendency to decrease in elevation in amounts ranging up to about 8 ft. It is suggested that these decreases were a result of the spreading of the ice front and development of lobes around the dead ice.

The movements, depicted on Figure 11 for the points observed from Base Line DE, suggest that the ice mass tended to flow around the old ice, which in large part was being reactivated. It is postulated that the moving ice was piling up against the old ice and expending some energy in

reactivating it. At the same time, a gradient developed toward the valley walls giving rise to a sideways or spreading-out tendency of the moving ice mass. It appears, also, that the old ice occupied only the center portion of the valley bottom in the terminus area; hence, room was available between this ice and the valley walls for the development of two active ice lobes which moved around the old ice.

The old ice appeared to be activated by the generation of shear planes, (Fig. 8), and subsequently it became a part of the active ice mass. It is suggested that a wedge-shaped mass of old ice protruded upstream under the center of the active ice; that is, the active ice overrode the old ice before the latter became fully incorporated. This mechanism accounts for the nearly horizontal shear planes near the top of the old ice. The former resulted from the "bulldozing" effect at the upper levels and the latter were caused by forces on the wedge-shaped mass near the base of the ice.

The reactivation of the dead ice by the development of shear planes appears to be a mechanism whereby debris becomes incorporated into the ice mass. The nearly horizontal shear planes, that in one instance extended the entire thickness of the old ice mass, also appear to be a

source of englacial debris by bringing up basal material. It is possible that continued thrusting along one of these latter shear planes could cause overriding of superglacial debris resulting in its becoming englacial material.

Acknowledgments

The author is indebted to Prof. J. B. Nuttall, Department of Civil Engineering, for the development of the computer program. Mr. D. V. Currie, a graduate student in the Department of Geology, aided in the field work. Dr. A. J. Broscoe, Department of Geology, provided much helpful criticism during interpretation of the data.

References

- Bayrock, L. A. (1967) Catastrophic advance of the Steele Glacier, Yukon, *Occas. Publ. No. 3*, Boreal Inst., Univ. Alberta, Edmonton, 35 pp.
- Davis, R. E., and Foote, F. S. (1953) *Surveying Theory and Practice*, McGraw-Hill, New York, pp. 32-37 (4th ed.).
- *Sharp, R. P. (1943) Geology of the Wolf Creek area, St. Elias Range, Yukon Territory, Canada, *Bull. Geol. Soc. Am.* 54, 625-650.

*This report is reprinted in the present volume.

Comparison of Moraines Formed by Surging and Normal Glaciers *

Nathaniel W. Rutter †

ABSTRACT. A Neoglacial moraine of Bighorn Glacier, St. Elias Mountains, probably formed by a surging glacier, and a Neoglacial normal moraine of nearby Grizzly Glacier were studied. Surficial deposits and erosional features were mapped. Fabric analyses were done in till at five sites in each moraine. Samples were subjected to laboratory lithologic and texture analyses.

The Bighorn (surge) moraine is a thin, discontinuous, irregular mantle, mostly till, but including ice-contact stratified material. Lateral moraines show subdued ridges marking the upper limit of glaciation. Ground moraine of the Grizzly (normal) glacier is an irregular, continuous, thick mantle, mostly till and ice-contact stratified material. Upper ice limits are marked by prominent ridges. Rocks of similar lithologies within the till are concentrated in bands parallel to glacier flow.

Stones in till of the Grizzly moraine have strong preferred orientation roughly in the direction of glacier flow. In the Bighorn moraine, rocks in till are weakly oriented. Where orientation is apparent, it is not necessarily in the flow direction. For the size fraction finer than 2 mm, Bighorn till is coarser than Grizzly till although the bedrock terrain is similar.

These differences are useful in distinguishing moraines of normal and surging glaciers.

Introduction

Glacier investigations in recent years indicate that surging glaciers are relatively common in many parts of the world. Surging glaciers show a marked increase in flow velocity, commonly with surface displacement of over 2 mi in a year. The increased flow lasts about 1-5 years before the terminal area stagnates or nearly stagnates. Surges that are well documented include Black Rapids Glacier, Alaska (Hance, 1937; Moffit, 1942; Post, 1960); Brúarjökull Glacier, Iceland (Todtman, 1965); Medvezhii Glacier, Pamir, U.S.S.R. (Dolgushin, *et al.*, 1963); Muldrow Glacier, Alaska (Post, 1960; Harrison, 1964); a glacier on Northern Ellesmere Island, Canada (Hattersley-Smith, 1964); a glacier in Spitsbergen (Glen, 1939); a glacier in Stak Valley, Pakistan (Desio, 1954); Steele Glacier, Yukon (Bayrock, 1967); Susitna Glacier, Alaska (Post, 1960); Walsh Glacier, Yukon-Alaska (Paige, 1965; Post, 1960, 1966, 1967); and the Yakutat Bay glaciers, Alaska (Tarr, 1909; Tarr and Martin, 1914).

Assuming that surging glaciers were as common a phenomenon in the Pleistocene period as now, a glacial geologist must be able to identify and interpret deposits and features associated with this activity. Perhaps the most important reason for this is to avoid inferring regional climatic variations from deposits that represent catastrophic activity unrelated to climate, or if so, only locally.

The present study was initiated to investigate differences in recent moraines left by normal and surging alpine glaciers in order to distinguish between these types.

Moraines of the Bighorn and Grizzly Glaciers, a surging and normal variety respectively, situated in the Donjek

Range on the northeast flank of the St. Elias Mountains, Yukon (Bighorn Glacier, 61°02' N, 139°08' W; Grizzly Glacier, 61°05' N, 139°06' W), were selected for study (Figs. 1, 2, 3).

A typical normal alpine glacier in the St. Elias Mountains has a gently dipping terminus area, distinct medial and lateral moraines, and relatively few crevasses. Forward motion takes place during recession or when the glacier is in equilibrium. The annual displacement may be only a few feet. The morainal complex left following deglaciation consists of typical arcuate end moraines, ridged lateral moraines, and usually, a continuous cover of ground moraine.

Moraines of glaciers in which surging has been observed have not developed past the ice-cored stage. Hence, identification of a surge moraine is by necessity circumstantial. The Bighorn moraine is judged to be a surge moraine for the following reasons.

First, the difference in moraine morphology compared to the majority of recent moraines in the area. The latter have characteristics common to moraines deposited by normal glaciers. Data available on recently surged glaciers indicate that the morphology of the moraines, although in part ice-cored, is similar to the Bighorn (Walsh) Glacier (Post, 1966).

Secondly, where observations have been made over a period of time on glaciers that have surged in the Alaska Range and St. Elias Mountains, surging is a recurring phenomenon, for example, Muldrow Glacier, Alaska (Harrison, 1964, p. 368) and Bighorn (Walsh) Glacier, Yukon (Post, 1966, p. 377). It can be demonstrated that the Bighorn has surged recently. In 1947, Bighorn Glacier had characteristics typical of normal glaciers in the St. Elias Mountains (Government of Canada photograph A11014-68). A 1951 photograph (A13232-234) showed a dramatic change; a forward displacement of the toe of at least ½ mi. By 1956, it had reached another ½ mi (Government

*This report has previously appeared in the *Canadian Journal of Earth Sciences*, Vol. 6, pp. 991-999 (1969), and is reprinted here with permission.

†Geological Survey of Canada, Calgary, Alberta, Canada

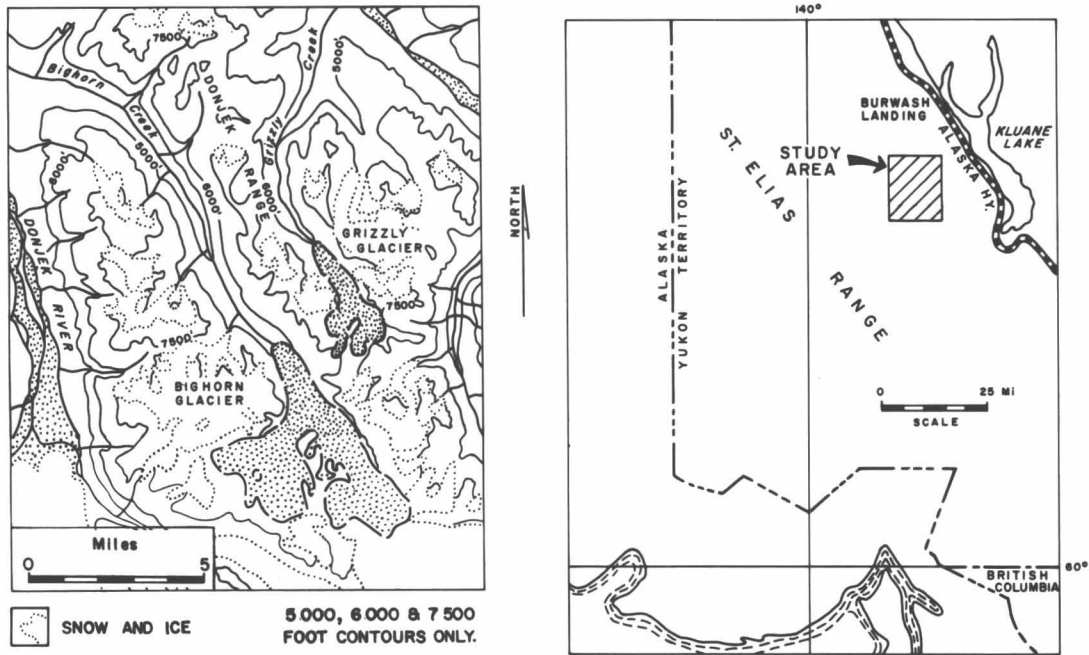


Fig. 1. Index maps of study area.

of Canada photograph A15434-113). The previously smooth surface was now highly fractured and crevassed, and the thickness of the ice near the snout had increased greatly. Since 1956, there has been no appreciable advance of the snout. The morphology and stagnated condition of the snout are typical of glaciers that have surged in the past few years.

It follows then, that if surging is often a recurring phenomenon, and since it has been demonstrated that the Bighorn has surged recently, the moraine selected for study was most likely formed by an earlier surge.

Other factors considered in the selection of the two moraines include proximity to each other, same general exposure, similar bedrock terrain, relatively small size, and accessibility. In addition, proximity to Steele Glacier was desirable in order to discuss mutual problems with personnel from the University of Alberta who were studying movement and drift deposition at the snout of the surging Steele Glacier.

Glacier and Morainal Characteristics

Bighorn Glacier. Bighorn Glacier is comprised of northeastern- and northwestern-trending tributaries 3 and 4 mi long, respectively, that join to form a main ice stream 3 mi long (Fig. 1). Below the confluence there is a prominent medial moraine and several minor ones. The firn limit on northerly exposed surfaces is at an elevation of approximately 7500 ft (1961 air photographs), whereas the toe of the glacier is at an elevation of between 5600 and 5800 ft.

The Bighorn surge moraine extends from the toe of

the glacier downvalley for 2 mi. It is roughly $\frac{1}{2}$ mi wide uninterrupted by moraines from tributary valleys except toward the north, where drift deposited from a northeastward-trending normal glacier has been incorporated into a portion of the surge moraine.

Except for minor patches, drift older than that of the Bighorn surge moraine has almost completely been eroded out of the valley. This is because of the low resistance of the bedrock to weathering (mainly basic metasediments) and to the high rate of physical weathering and mass wasting in the area.

A radiocarbon date derived from wood and plant debris found in stratified drift about 20 ft below the morainal surface yielded a date of 170 ± 140 years old (GSC-895). This would place the age of the moraine as late Neoglacial (Porter and Denton, 1967).

Grizzly Glacier. The Grizzly Glacier flows northward from the head of Grizzly Creek valley for about 3 mi. The accumulation area consists of two cirques whose glaciers unite to form the main ice stream divided by a medial moraine, not far below the firn limit which lies at an elevation of about 6000 ft (1961 air photographs).

Prominent lateral and terminal moraines are present near the snout area of the glacier, representing at least two glacier advances or a glacier advance and an equilibrium phase. Although no absolute dates are available on the age of these moraines, they are probably Neoglacial because only incipient vegetation has taken hold, the inner lateral moraines are partially ice-cored, and moraines with similar characteristics and setting are dated as Neoglacial throughout the North American Cordillera (Porter and Denton, 1967).

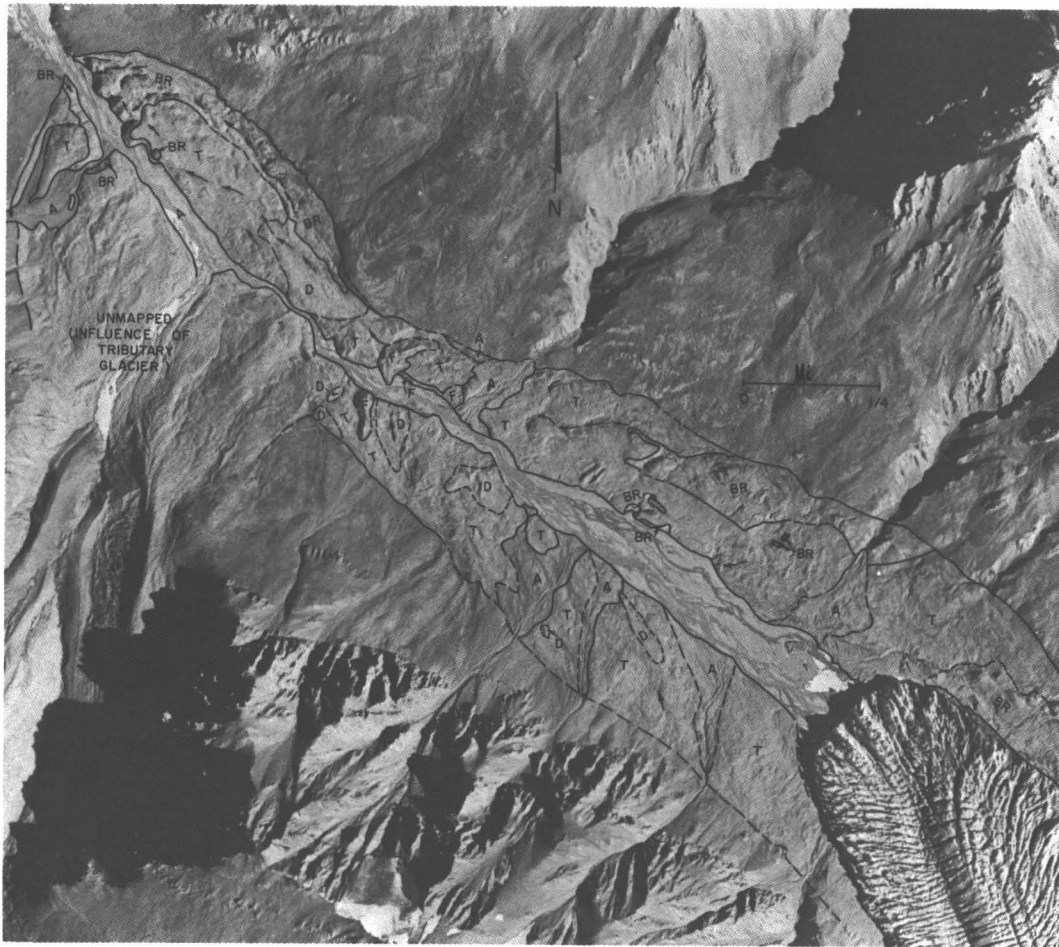


Fig. 2. 1956 air photograph of the Bighorn moraine. T = till, some reworked with minor stratified drift; F = glacio-fluvial deposits, some till; A = modern alluvium or talus; D = glacial drift, undifferentiated, mostly till and glacio-fluvial deposits; BR = bedrock; → meltwater channels; — defined boundary; - - approximate boundary (Government of Canada photograph A15434-114).

Study Methods

Glacier surges last at most only a few years, after which the terminal area becomes stagnant or nearly so. The short duration of the glacial activity suggests that the volume of "lodged" or accreted material will be relatively minor. Therefore, because of the stagnation of the terminal area, most till deposited will be ablation.

In a normal glacier, where the regional climatic change affects the economy of the glacier relatively slowly over many years, most of the terminal area, although thinning from the surface, is still active. Much of the material deposited could be lodgment till or, if not, deposited by a lodgment mechanism, a method that can similarly crush, compact, and orient stones with their long axes parallel to the direction of glacier flow.

The field methods employed were based on the above concepts. Five sites in each moraine were selected in un-

modified till, most about 3 ft above the bedrock surface near the valley bottom. Fifty stones with three unequal axes, the long axis about one and a half lengths greater than the intermediate axis, were selected for measurement at each site. The azimuth of the long axis was recorded. The purpose of this was to determine the degree of preferred orientation of pebbles and boulders in till in each moraine. Also, if preferred orientation was indicated, what relation did it bear to the direction of glacier flow?

Samples for mechanical analyses were collected at the site where the orientation studies were made. In the laboratory the percentages of sand, silt, and clay were determined for the less than 2-mm size fraction. The texture was analyzed to aid in distinguishing the two varieties of moraine.

Both moraines were mapped and compared with respect to geomorphology and deposits. This is intended to aid in differentiating surge from normal moraines when

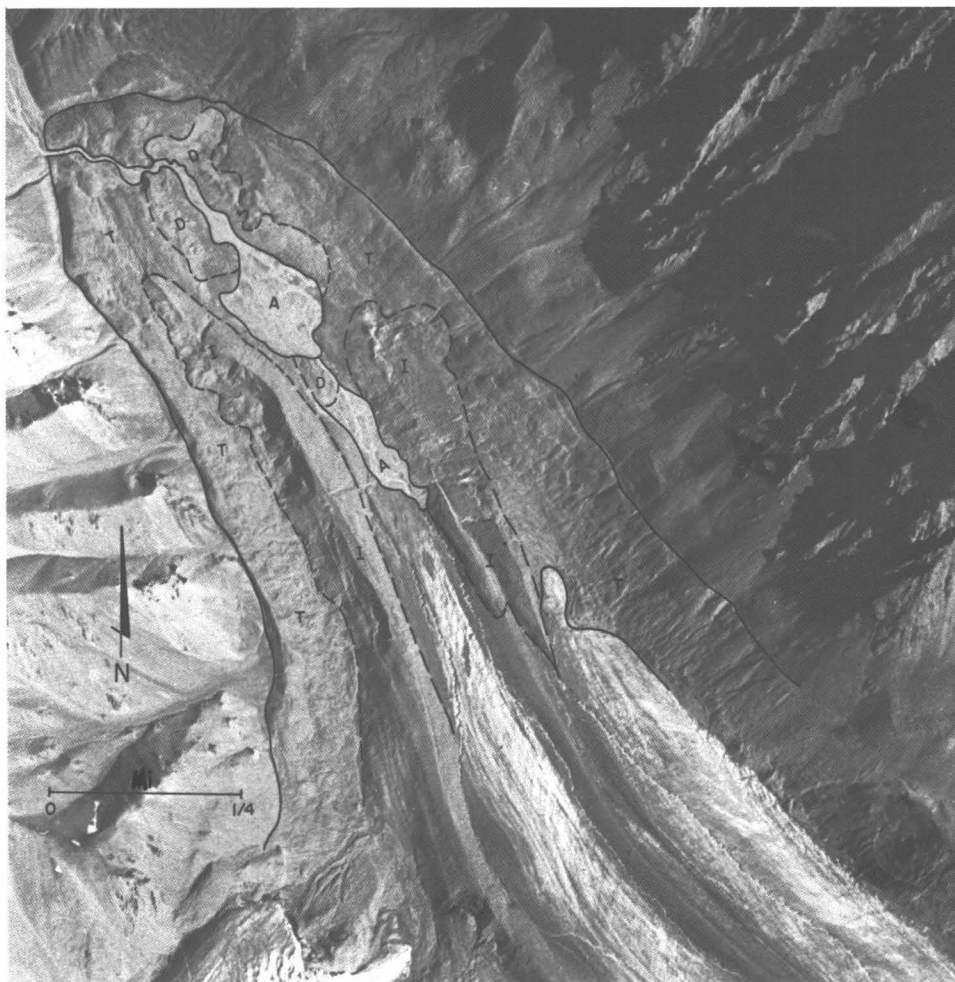


Fig. 3. 1956 air photograph of the Grizzly moraine. T = till, some reworked with minor stratified drift; I = ice-cored moraine; F = glacio-fluvial deposits, some till; A = modern alluvium or talus; D = glacial drift, undifferentiated, mostly till and glacio-fluvial deposits; BR = bedrock; — defined boundary; - - approximate boundary (Government of Canada photograph A15434-114).

moraines are freshly exposed, not having been eroded greatly or overridden by later ice. Many Neoglacial moraines are in this state of preservation.

Results

Geomorphology and sedimentation. The Bighorn and Grizzly moraines show differences principally in their geomorphology which show up strikingly on air photographs (Figs. 2, 3). In the Bighorn, a thin discontinuous hummocky mantle of coarse drift overlies the area of the moraine. The thickness of the deposits is less than 10 ft, although there are restricted deposits of stratified drift that reach 40 ft. In the Grizzly moraine, the mantle of glacial drift is continuous, averaging more than 10 ft in thickness with little variation in local relief except for

ice-cored material. In Grizzly till, pebbles and boulders of similar lithology are commonly strung out along orderly bands parallel to the direction of ice movement. In the Bighorn no such order exists; lithologic varieties form a heterogeneous composite.

Although till is the dominant deposit in each moraine, there is relatively more stratified or sub-aerially reworked material in the Bighorn moraine. The important part played by water during the formation of the Bighorn moraine is further supported by a large number of melt-water channels.

Probably the most striking differences in the two moraines are the upper margins. In the Grizzly, prominent lateral moraines with ridges of till about 12 ft high mark a former upper limit of ice (Fig. 4), whereas in the Bighorn,



Fig. 4. Prominent ridge marking the upper limit of the southwest lateral moraine left by the Grizzly Glacier. View photographed near Site G4 (see Fig. 7) toward the southeast. Figure near moraine-bedrock contact and former ice-marginal stream.

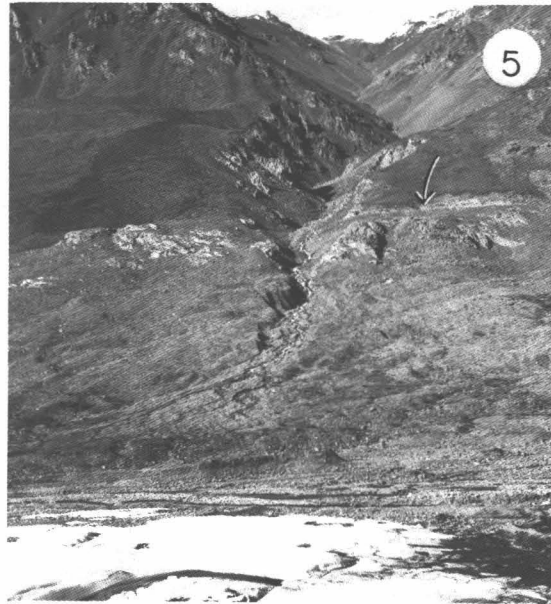


Fig. 5. Freshly scoured bedrock and thin drift marking the upper limit of ice during the surge that left the Bighorn moraine. View toward the northeast taken from a site about 1/5 mi downstream from the present-day glacier snout.

the upper limit is indicated by freshly scoured bedrock covered locally by thin till (Fig. 5) with no appreciable break in slope (Fig. 5).

The depth of erosion in valley bottom caused by the surging glacier can be observed near the downvalley limit of the moraine. Here a 7-10 ft scarp in bedrock separates the pre-surge valley surface from that formed by the surge.

Fabric analyses. The fabric studies show (1) that stones in Grizzly till, as indicated by rose diagrams and standard deviations, are more strongly oriented than those

of Bighorn till (Figs. 6, 7; Table 1), (2) that with one exception (site G4), orientation in Grizzly till is in, or nearly in, the direction of flow of the former glacier; orientations in Bighorn till show no consistent patterns.

The random orientation in Bighorn till is consistent with deposition as ablation till from wasting stagnant ice; the pattern in Grizzly Glacier (excepting site G4) suggests deposition as lodgment till, or at least in a manner that produces strong orientation in the direction of ice movement. Site G4 is on a steep slope near the upper limit of

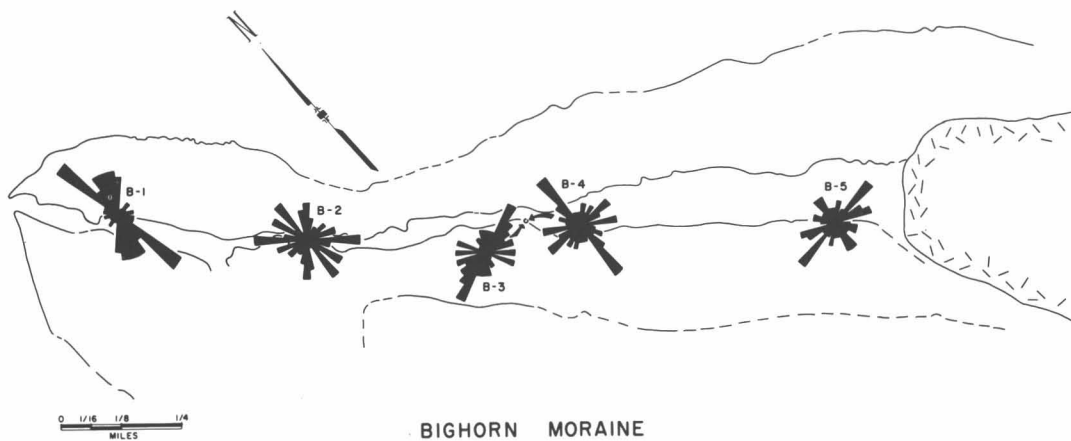


Fig. 6. Rose diagram (10° divisions) of the orientation of the long axes of 50 till stones measured at five sites on the Bighorn moraine. Site locations indicated on moraine outline. Measurements at B3 were taken at 5 ft below the till surface and B4 about 8 ft lower, near the bedrock surface.

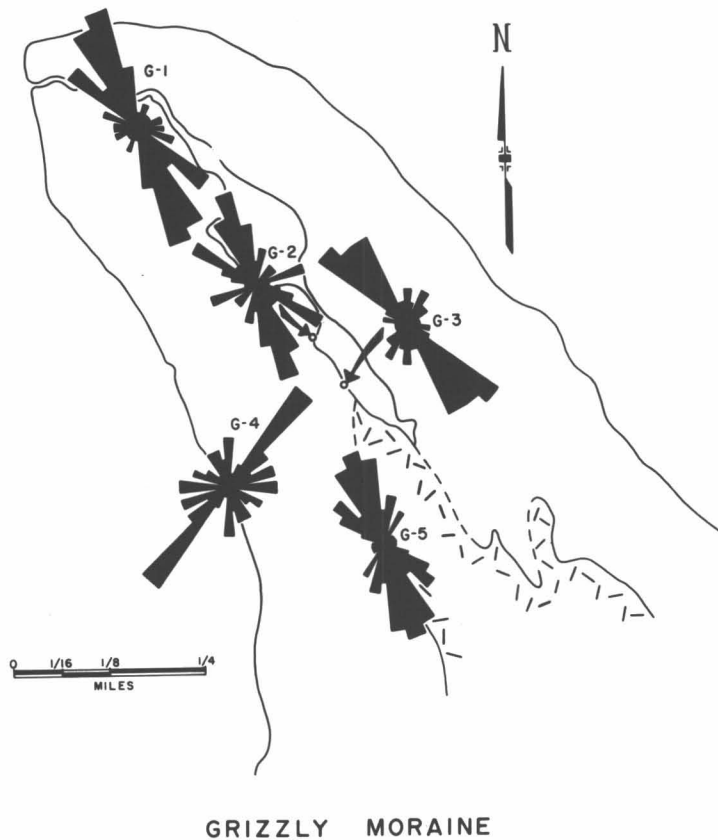


Fig. 7. Rose diagrams (10° divisions) of the orientation of the long axes of 50 till stones measured at five sites on the Grizzly moraine. Site locations indicated on moraine outline.

the lateral moraine of Grizzly Glacier, where the till may have suffered post-depositional slumping. Alternatively, the till may consist of ablation debris deposited at the ice margin.

Texture and petrographic composition. Mechanical analyses of till collected in the two moraines clearly indicate that till of the Bighorn moraine is coarser than that of the Grizzly (Table 2; Fig. 8). Pebble counts at each fabric analysis site indicate that in Bighorn till the dominant

materials are low-grade metamorphic rocks consisting of green schist, greenstone, slate, schistose sandstone, and quartzite. Granodiorite pebbles are present in four out of five samples and constitute between 7% and 51% of the total. Phyllite and quartz are minor constituents. The pebbles and boulders in Grizzly till have essentially the same lithologic varieties as that of the Bighorn except no granodiorite is present. The lower silt-clay content of the Bighorn till could result from granodiorite among source materials

TABLE 1. Arithmetic means and standard deviations (method outlined by Krumbein, 1939) of groups of 50 stones taken at selected sites on the Bighorn and Grizzly moraines

Site	Arithmetic mean (Ma)	Standard deviation (σ)
Bighorn moraine		
B1	N.8° E.	32°
B2	N.34° E.	50°
B3	N.81° E.	40°
B4	N.5° W.	50°
B5	N.73° E.	51°
Grizzly moraine		
G1	N.28° W.	40°
G2	N.19° W.	42°
G3	N.33° W.	36°
G4	N.40° W.	48°
G5	N.24° W.	33°

TABLE 2. Mechanical analyses (hydrometer method, Bouyoucos, 1951) of the less than 2-mm size fraction of till of the Bighorn and Grizzly moraines collected at the fabric analysis sites

Site	% Clay	% Silt	% Silt + Clay	% Sand
Bighorn moraine				
B1	4.76	24.75	29.51	70.49
B2	4.84	22.29	27.13	72.87
B3	3.71	15.81	19.52	80.48
B4	4.58	16.53	21.11	78.89
B5	4.53	21.78	26.31	73.69
Grizzly moraine				
G1	12.42	32.51	44.93	55.07
G2	12.34	34.17	46.51	53.49
G3	11.32	32.95	44.27	55.73
G4	10.92	24.83	35.75	64.25
G5	13.23	37.12	50.35	49.65

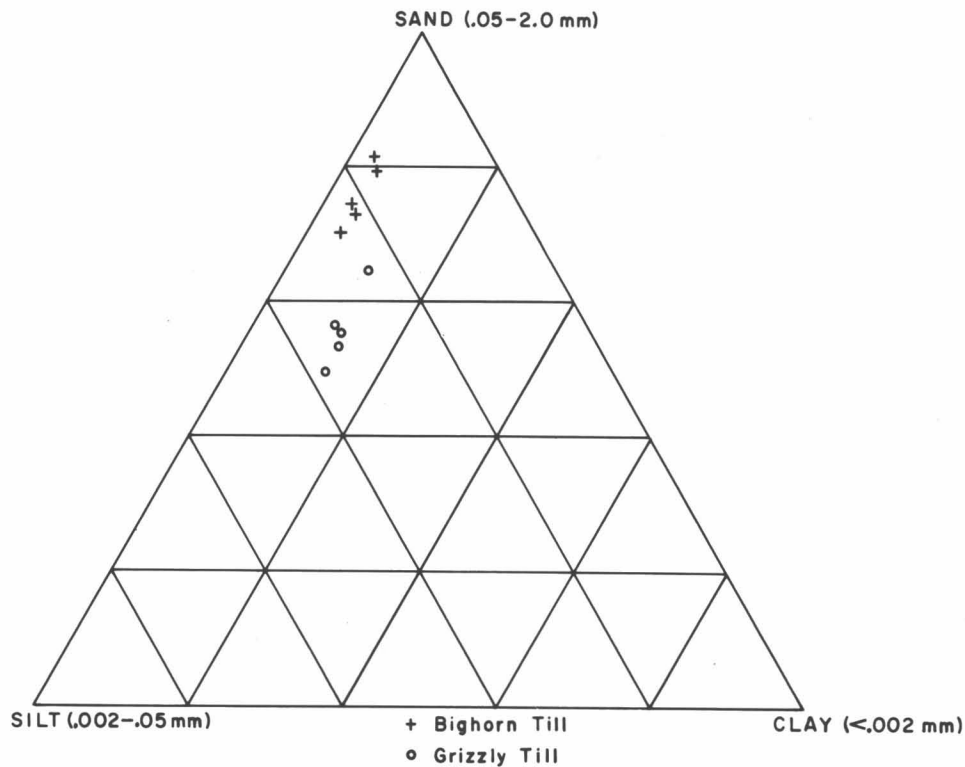


Fig. 8. Texture of the less than 2-mm size fraction of till samples.

rather than the depositional history, but this is probably not so. The proportion of granodiorite pebbles in the till has no consistent relationship to sand content (and conversely to silt-clay content), which suggests that depositional history is the governing factor. Supported by fabric analyses and geomorphological comparisons, it is more likely that the textural differences are due to a high percentage of ablation till in the Bighorn moraine and a high percentage of non-ablation till in the Grizzly moraine.

Summary

Evidence favors the conclusion that the Grizzly moraine was formed by a normal glacier. The Bighorn moraine was most likely the result of a surge. The till fabrics, mechanical analyses, and gross characteristics of each moraine indicate a large proportion of ablation till present in the Bighorn moraine, whereas the Grizzly moraine, at least near the till-bedrock interface, contains a large proportion of lodgment till or some other non-ablation variety. Although there are unsolved problems on the mechanics of till deposition, and the present study is limited in its scope, the fact remains that till in each moraine has different characteristics and therefore may be useful in solving the primary problem, namely, to differentiate between till deposited by a normal alpine glacier or a surging glacier. More studies will have to be undertaken to verify the conclusions presented.

Acknowledgments

This study was made under project 670060 of the Geological Survey of Canada. Close cooperation was maintained with the University of Alberta party studying flow characteristics and till deposition on the snout of the surging Steele Glacier. Discussions with members of this group headed by A. J. Broscoe, Department of Geology, were extremely beneficial. Special thanks are extended to my field assistant, L. A. Barrie, Queen's University, who aided the writer during field work. The present manuscript was kindly reviewed and commented on by O. L. Hughes and W. Blake, Jr. of the Geological Survey of Canada.

References

- Bayrock, L. A. (1967) Catastrophic advance of the Steele Glacier, Yukon, Canada *Publ. No. 3*, Boreal Inst., Univ. Alberta, 35 pp.
- Bouyoucos, G. J. (1951) Recalibration of the hydrometer method for making mechanical analyses of soils, *Agron. J.*, 43, 434-438.
- Desio, A. (1954) An exceptional glacier advance in the Karakoram-Ladakh region, *J. Glaciol.*, 2, 383-385.
- Dolgushin, L. D., Yevteyev, S. A., Krenke, H. N., Rototayev, K. G., and Svatkov, N. M. (1963) The recent advances of the Medvezhii Glacier, *Priroda*, 11, 85-92.
- Glen, A. R. (1939) The glaciology of North East Land, *Geogr. Ann.*, 21, 1-23.
- Hance, J. H. (1937) The recent advance of Black Rapids Glacier, Alaska, *J. Geol.*, 45, 775-783.

- Harrison, A. E. (1964) Ice surges on Muldrow Glacier, Alaska, *J. Glaciol.*, 5, 365-368.
- Hattersley-Smith, G. (1964) Rapid advance of glacier in Northern Ellesmere Island, *Nature*, 201, 176.
- Krumbein, W. C. (1939) preferred orientation of pebbles in sedimentary deposits, *J. Geol.*, 47, 673-706.
- Moffit, F. H. (1942) Geology of the Gerstle River district, Alaska, *Bull. 926-D*, U.S. Geol. Surv., pp. 146-157.
- Paige, R. A. (1965) Advance of Walsh Glacier, *J. Glaciol.*, 5, 876-878.
- Porter, S. C., and Denton, G. H. (1967) Chronology of Neoglaciation in the North American Cordillera, *Am. J. Sci.*, 265, 177-210.
- Post, A. S. (1960) The exceptional advances of the Muldrow, Black Rapids, and Susitna Glaciers, *J. Geophys. Res.*, 65, 3703-3712.
- Post, A. S. (1966) The recent surge of Walsh Glacier, Yukon and Alaska, *J. Glaciol.*, 6, 375-381.
- Post, A. S. (1967) Walsh Glacier surge, 1966 observations, *J. Glaciol.*, 6, 763-765.
- Tarr, R. S. (1909) The Yakutat Bay region, Alaska, *Prof. Paper 64*, U.S. Geol. Surv., 183 pp.
- Tarr, R. S., and Martin, L. (1914) *Alaskan Glacier Studies*, Nat. Geogr. Soc., Washington, D.C., 498 pp.
- Todtman, E. M. (1965) Über den Vorstoss des Brúarjökull, Nordrand des Vatnajökull Island, 1963/64, *Tech. Field Conf. F.*, 7th Congr., Intern Assoc. Quatern. Res., abstr.

Some Aspects of the Geomorphology of Meltwater Streams, Steele Glacier Terminus

A. J. Broscoe *

Introduction

This paper is a description of several aspects of the geomorphology of the headwaters of Steele Creek, which originates at the terminus of the Steele Glacier ($61^{\circ}18' N$, $139^{\circ}58' W$).

Steele Creek emerges from the terminus of the glacier at an elevation of about 4000 ft (1200 m), and flows about $N 70^{\circ}E$ in a deep, narrow, steep-walled valley toward the valley of Donjek River. At the junction, Steele Creek has built a fan with a radius of about two miles (3 km) and has forced the Donjek River against the east side of its broad valley. Steele Creek is joined by a number of tributary streams which rise on the valley walls. Similar streams rise on the valley walls above the Steele Glacier and disappear into tunnels in the glacier. Some of these streams were observed to be intermittent, but others, particularly on the south valley wall, are fed by meltwater from small valley glaciers. A small lake is impounded at the large bend in the glacier and discharges into a tunnel on the north side of the glacier.

The geology of the Steele Creek area was mapped by Sharp (1943). The high ridges which form the north valley wall are underlain by nearly flat-lying volcanic rocks of Tertiary age. The volcanic rocks form well-defined bench-and-slope topography and weather to a rusty brown rubble of angular fragments. The south valley wall is underlain by metamorphic rocks, mainly phyllites, of Devonian or Mississippian age. The foliation of the phyllite strikes parallel to the trend of the main valley and dips steeply toward the valley. The topography of the uplands shows little reflection of this structure. The phyllites disintegrate into small, dark-gray fragments. Because of the differences in lithology on the two sides of the valley, the colors of the streams draining the two valley walls are markedly different: rusty brown on the north and dirty gray on the south. The fan deposits on the two sides of the valley show this color distinction quite clearly.

Geomorphic observations were made on two channels: a small channel to the north and the major channel of Steele Creek to the south and east. The small channel emerged from the north side of the terminus and flowed

around erosional remnants of stagnant ice about 4500 ft (1400 m) to the junction with the main channel. Observations were made on this channel adjacent to the advancing glacier and immediately upstream from the junction. The main channel emerged from the south side of the terminus and flowed as a vigorous river to the Donjek valley. This channel was studied downstream from the junction with the northern tributary. The following properties were investigated: stream gradient (stadia survey), stream width (direct measurement or triangulation), cross-sectional profile, surface velocity, suspended sediment concentration, and composition of dissolved solids. Additional observations were made on the flow regimen of the streams. The available data, though limited, permit estimation of the rate of discharge of the streams and the rate of transport of suspended sediments. Many fundamental problems remain unsolved; some discussion of these problems is included in the final part of the paper.

Observed Data

Channel properties. Cross sections of the channel of the north fork of Steele Creek immediately adjacent to the glacier margin are shown in Figure 1. From the data presented in Table 1, it is concluded that the discharge through this section was about $80 \text{ ft}^3/\text{sec}$ ($2.3 \text{ m}^3/\text{sec}$). It should be emphasized that there is no vertical exaggeration in these sections. The channels are quite deep in proportion to their width, at least in comparison to many nonglacial channels. The Froude number in this reach is about 0.9. Measurements of sediment concentration (Table 2) from samples taken at this locality on three separate days indicate an average suspended load of about $10 \text{ lb}/\text{sec}$ ($4.5 \text{ kg}/\text{sec}$) through the reach. No quantitative observations were made of bed-load transport, but the stream was observed to move boulders up to 1 ft (0.3 m) in diameter. There was a constant rumbling sound indicating the continual movement of large fragments in the bed load. This channel was flanked by the steep front of the advancing glacier on the southwest and by an extensive gravel flat on the northeast. The surface of the gravel flat contained fragments of ice, which melted out to produce shallow depressions on the surface of the flat. Materials on the gravel flat ranged in size from angular boulders 1 ft (0.3 m) across to silty sand, the matrix in which the boulders were found.

*Department of Geology, University of Alberta, Edmonton, at time of writing; present address: Texaco Canada Limited, Calgary

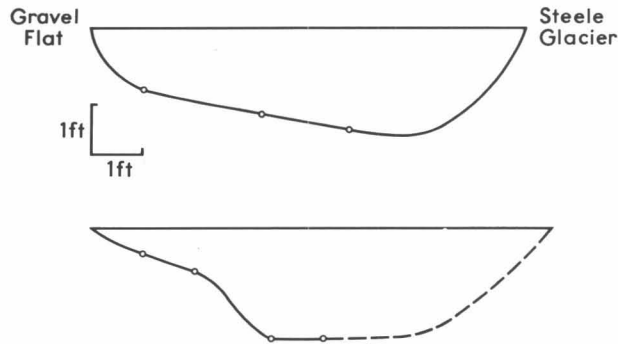


Fig. 1. Cross sections of meltwater stream north of stagnant ice. See Table 1 for related data.

TABLE 1. Data for Figure 1

	Upper Section (July 17)	Lower Section (July 20)
Cross-sectional area (ft ²)	12.9	12.5
Surface velocity (ft/sec)	7.4	7.4
Mean velocity (ft/sec)	≈6.3	≈6.3
Discharge (ft ³ /sec)	81.4	78.8
Sediment concentra- tion (%)	0.20	0.18
Suspended sediment load (lb/sec)	10.2	8.9
	(Sample 5)	(Sample 5A)

Observations on the lower part of the north channel and along the main channel (Fig. 2) consisted primarily of stadia surveys of the long profiles of selected reaches, measurements of surface velocities, and collections of water samples. The size and vigor of the streams in these reaches, particularly the main channel, precluded measurements of depths of flow, so the following discharges are based on field estimates of the depth of flow. Channel widths were measured by triangulation.

The estimated discharge through the lower part of the north channel was 172 ft³/sec (4.87 m³/sec) and suspended sediment about 20 lb/sec (9 kg/sec). The Froude number was about 0.58. There was no indication of bed load movement at the time of the observations. The gradient ranged from one to three percent along the lower reach.

In the narrows of the main channel, Steele Creek was a fairly large and very rapid stream. The discharge was estimated at about 1740 ft³/sec (49.3 m³/sec) and the suspended sediments transport at about 140 lb/sec (63 kg/sec). The Froude number was about 1.2. Supercritical flow was strongly indicated by the presence of standing waves up to 5 ft (1.5 m) high. These figures are based on an assumed average depth of about 2 ft (0.6 m). When the site was revisited on May 23, 1968, the rate of flow was much less, and parts of the channel floor were exposed. The observations made at this time indicate that the depth estimate was reasonably close. The sound of the stream during the 1967 observations was a continuous roar, indicating constant and rapid movement of large particles in the bed load. In this reach of stream, the gradient was steep, commonly more than 4%, and the channel was confined between a mass of stagnant ice on the south and by a mound of boulders up to 8 ft (2.5 m) across on the north. The presence of the ice on the south side of the channel made accurate determination of channel width

TABLE 2. Summary of Suspended Sediment Concentration at Sampling Stations

Station	Date	Time	Sediment Concentration ¹ (%)	% Sand ²	Froude Number	
1	17 July	1145	1.35	} 21 %	1.19	
1A	17 July	1350	1.30			
2	17 July	1200	1.24	} 10 %		
2A	17 July	1345	1.21			
3	17 July	1230	0.18	} 22.5%		0.58
3A	17 July	1330	0.24			
4	17 July	1235	0.26	} 36.5%		
4A	17 July	1325	0.25			
5	17 July	1715	0.20	} 31.5%	0.86	
5A	20 July	1025	0.18			
5C	22 July	1315	0.27			
6	20 July	0945	0.12	40.5%		

¹ Sediment concentration is expressed as the ratio of the weight of suspended solids to the weight of water.

² The percent sand indicates the percentage of all of the sediment collected at the given localities within the sand size.

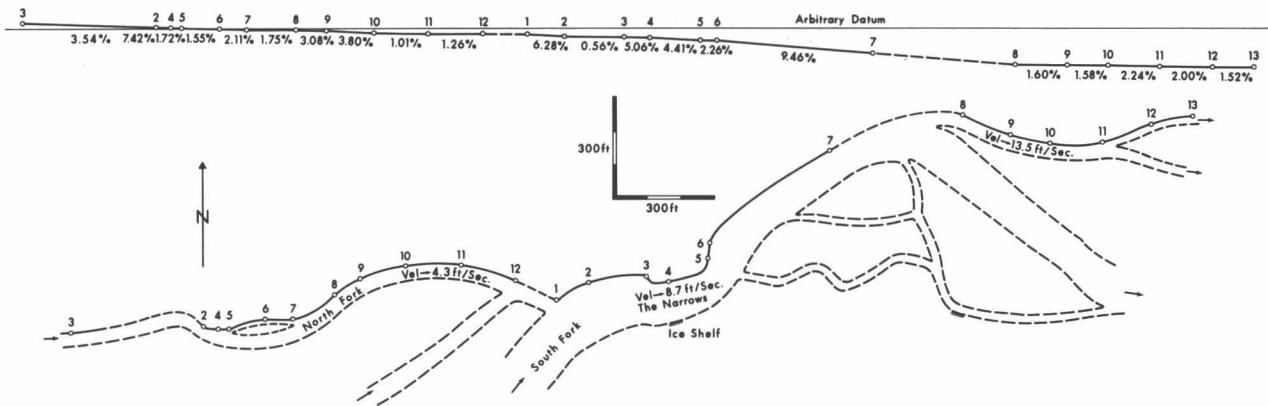


Fig. 2. Planimetric map and long profile, Steele Creek, July 1967.

very difficult; a thermo-erosional niche was present, but its width could not be measured. Farther downstream, the channel was unconfined, and a clearly defined braided pattern was present. The main channel downstream from the narrows crossed the valley floor obliquely, and a transverse bar was present on the downvalley side of the channel. Similar transverse bars are known in other gravel-bed rivers. The gradient along one minor branch of the braided channel pattern was 2%. The surface velocity in this reach was unusually high, and standing waves were present on the water surface.

Chemical composition of stream waters. Samples of water collected at the localities described in the preceding section were analyzed for the concentration of sodium, calcium, magnesium, iron, carbonate, bicarbonate, and sulphate, in addition to measurements of pH and conductivity. It was hoped that the compositions would reflect the source of the water and hence indicate something of the nature of the tunnel system under the glacier. Concentrations of total dissolved solids were estimated by multiplication of the conductivity by 0.7. The observations are summarized in Table 3. The horizontal line through the table separates entries pertaining to the main channel (above the line) from those for the north fork (below the line). Within each of the two groups, the data seem quite consistent, with very little change from station to station, and from one time of observation to another. Two definite differences exist between the data for the two channels. The water from the main channel is much higher in sulphate content than that from the north fork, whereas the water from the north fork is somewhat higher in bicarbonate. Iron and carbonate ions were lacking. Interpretation of the chemical data is difficult, in part because of the limited number of sample localities. The data indicate that the two streams are derived from different sources, but the sources are not defined. The calcium, magnesium, and bicarbonate ions can be readily explained as derived from crushed carbonate rock in morainal material. Marble crops out

on the west side of the glacier south of the large bend. The source of the high sulphate content in the main stream is not known.

The interpretation of tunnel distribution under the glacier is further complicated by the occurrence on the evening of July 14, 1967, of a very rapid increase in flow of the north fork as the result of an abrupt outburst of water from the north margin of the terminus. In this area, water flooded the north marginal depression adjacent to the glacier, an area that was formerly dry. The flood was first indicated about 20:00 by a marked increase in the noise level of the meltwater stream and lasted at least three hours. The water flooded entirely over the gravel flat normally crossed by the north fork. In the course of the flood, a deep channel was cut into the floor of the north marginal depression, in which stagnant ice was exposed, and boulder-bearing material in slopes above the depression slid into the channel. All of the particles were swept downstream. The source of the flood was not apparent, but there must have been a marked, though temporary, change in the subglacial channels. There was no definite indication of a drop in level of the impounded lake at the bend of the glacier after the flood, but no reliable observations were made of the lake levels prior to the flood.

Inferences from Observed Data

Sediment load. The sediment and discharge measurements permit conclusions to be drawn concerning the amount of sediment moved in suspension by the meltwater river, particularly the main channel. If the estimate of 140 lb/sec (63 kg/sec) is accepted, and if one assumes a duration of meltwater flow of 100 days per year, then the total volume of sediment moved in suspension through the narrows of Steele Creek would be about 400,000 yd³ (300,000 m³) per meltwater season. This would result in deposition of 0.8 ft (0.25 m) of sediment over a channel width of ¼ mile (0.4 km) within the 2-mile (3

TABLE 3. Summary of Water Properties

Sample No.	Date	Time	Location	Ca (ppm)	Mg (ppm)	Na (ppm)	HCO ₃ (ppm)	SO ₄ (ppm)	pH	Conductivity μ mhos/cm	Total dissolved solids (=0.7 x cond.)
1	17 July	1145	"Quiet" water close to shore near Sta. 4 in narrows	26	10	6.38	44	47	8.2	215	150
1A	17 July	1350	Same	28	9	6.38	39	51	8.0	215	150
2	17 July	1200	Standing wave in margin of stream in shooting flow in narrows below Sta. 4	32	6	6.76	39	51	8.0	220	154
2A	17 July	1345	Same	32	6	6.66	39	47	8.0	220	154
3	17 July	1230	Tranquil flow area in downstream reach of north fork	26	8	5.86	54	16	8.0	180	126
3A	17 July	1330	Same	29	6	5.86	51	15	8.3	170	119
4	17 July	1235	Rapids upstream from sample locality 3	22	10	5.70	51	15	8.3	180	126
4A	17 July	1325	Same	33	3	5.64	57	15	8.3	180	126
5	17 July	1715	Below push moraine on north fork of Steele Creek	31	4	5.64	51	14	8.3	165	115
5A	20 July	1025	Same	29	5	5.58	49	14	8.3	165	115
5C	22 July	1315	Same	27	7	5.30	54	16	8.2	170	119
6	20 July	0945	Small rapids on north fork of Steele Creek near push moraine	27	7	5.64	54	15	8.3	170	119

km) radius of the fan at the junction with Donjek River. To this figure must be added the still undetermined amount of material moved as bed load. Observations of the gravel flats adjacent to the narrows locality indicate that the bed load consists of particles ranging in size from sand to boulders at least a foot in diameter, and probably larger.

The order of presentation of data in Table 2 is such that the general changes in sediment concentration from upstream to downstream are indicated from the bottom of the table toward the top. There is a general increase in sediment concentration from Sample 6, the locality farthest upstream, to Sample 3, in quiet water near the junction with the main stream. The slightly high values for Samples 4 and 4A are probably a reflection of turbulent water in rapids at that point. Further, there is a general downstream decrease in the percentage of sand found within the samples in a downstream direction. It is tentatively concluded from this information that the bulk of sediment in the channel is obtained from the channel floor and banks rather than the glacier itself. The complex nature of the channel of the north fork makes these conclusions somewhat tenuous. There are

several waterfalls along the channel, several braided reaches, and there is an increase in discharge, partly from a tributary from the north valley wall, and probably from melting stagnant ice in front of the active glacier.

There is little obvious difference in the sand grains within the suspended load along the north fork. All sand samples are composed dominantly of very sharp, angular fragments; some (about 5%) calcite, some fragments of phyllite, but mostly quartz. The carbonate grains are probably derived originally from outcrops of marble along the west margin of the glacier south of the large bend.

Possibility of basal melting. The major question that arises out of all these considerations is: did the melting take place under the glacier at a rate rapid enough to provide a significant contribution to stream flow, and did some of this water exert a hydrostatic pressure on the sole of the glacier? One can only speculate.

The real problem is the means of determination of the water budget of the entire glacier-tributary stream system to the degree of accuracy needed to determine the presence of water resulting from basal melting. It is apparent that the precipitation would have to be measured carefully through the year in the vicinity of the glacier, and the rate

of ablation, both by melting and sublimation, determined with care. These measurements would be virtually impossible on such a rough and variegated surface as that of the Steele Glacier. Difficulties would also be experienced in obtaining exact measurements of discharge of the many streams that flow into tunnels under the glacier. Further, the outflow from the terminus of the glacier would have to be gauged far more precisely than the measurements described in this paper. Finally, the contributions to the valley from groundwater and the losses under the channel by groundwater flow would have to be evaluated. If all these measurements could be performed, then we might have some basis for a statement as to the effectiveness of basal melting in contributing to the flow of the meltwater stream and, perhaps, to the exertion of hydrostatic pressure on the sole of the glacier.

Conclusions

Two channels drain from the glacier. The smaller channel to the north had a discharge in July of about 80 ft³/sec (2.3 m³/sec) adjacent to the glacier, and a suspended sediment load of about 10 lb/sec (4.5 kg/sec). The bed load included boulders. At a distance of 4500 feet (1400 m) from the front of the glacier, the channel had a discharge of 172 ft³/sec (4.87 m³/sec) and a suspended sediment load of about 20 lb/sec (9 kg/sec). Bed load discharge was not active during the time of the observation. The main channel had a discharge of about 1740 ft³/sec (49.3 m³/sec) and a sediment load of about 140 lb/sec (63 kg/sec). Bed load transport was strongly effective in the main channel.

The chemical composition of the water indicates that the two forks of Steele Creek have separate sources under the glacier, but does not indicate the exact sources of the water. The high content of calcium and bicarbonate is easily explained as the result of crushed marble in

the morainal deposits. The high sulphate content of the main channel is not readily explained. A glacial flood which occurred during July of 1967 indicated a sudden change in the tunnel system under the glacier.

The measurements of sediment transport indicate the possible removal of 400,000 yd³ (300,000 m³) of material in suspension during a meltwater season. The measurements of sediment concentration along the north fork indicate that material is being eroded mainly from the channel floors rather than removed from the glacier directly. The sediment in suspension contains high percentages of sand which is very angular and consists of quartz plus small fragments of the local bedrock.

Additional measurements of substantial physical and technical difficulty must be made before any valid conclusions can be made concerning the possibility of basal melting.

Acknowledgments

The field investigation was supported by grants from the National Research Council and the Boreal Institute of the University of Alberta. Most of the chemical analyses were done by the Environmental Health Services Division of the Departments of Health, Government of Alberta. The sodium determinations were performed by the laboratory of the Department of Soil Science, University of Alberta. Dr. S. Thomson and D. V. Currie assisted in the field, and Dr. Thomson aided the writer in laboratory determinations.

Reference

- *Sharp, R. P. (1943) Geology of the Wolf Creek area, St. Elias Range, Yukon Territory, Canada, *Bull. Geol. Soc. Am.*, 54, pp. 625-650.

*This article is reprinted in the present volume.

Observations on an Alpine Mudflow, Steele Creek*

A. J. Broscoe † and S. Thomson ‡

ABSTRACT. Alpine mudflows occurred on the ridges above Steele Creek, St. Elias Mountains, on July 11, 1967, during a rainfall of 2.19 inches in 36 hours. One flow was observed in an area of flat-topped, steep-sided morainal terraces on the lower part of the north valley wall. This mudflow emerged in pulses from a notch at the upper margin of the terrace surface, and formed fronts 6 to 8 ft high. The arcuate fronts broke either to the east or west and the mud flowed across the fan, and through erosional notches to the valley floor. A detailed map and profiles show the topography and distribution of materials.

The stream deposited coarse bed load on the alluvial fan on the upper terrace, then cascaded down the notch. Undercutting of the notch caused periodic collapse of the morainal material, which formed temporary dams. Water and finer bed load were impounded and the dam was saturated but not overtopped. Saturated material emerged from the notch as viscous, rock-charged mud.

Particles in the mudflow ranged in size from colloids to boulders 13 ft across. Pebbles from a mudflow sample included 70% locally derived lava and 18% granite from the moraine. Material finer than 2 microns was predominantly montmorillonite. Rain and runoff washed fine material from mudflow deposits, leaving the lag deposit similar to alluvial gravel.

Botanical evidence indicates that mudflows occur at intervals of decades. The collapse of material from the sides of the steep-walled, high-gradient notch, cut into easily erodable till, controlled the pulsating nature of the observed mudflow.

Introduction

In the course of field work in the St. Elias Mountains in July of 1967, the writers had the opportunity to witness the occurrence of an alpine mudflow and subsequently to study the deposit laid down by it. Some inferences are made concerning the mechanism of transport of large boulders by the mudflow.

The mudflow occurred on the north flank of the valley of Steele Creek (61° 18' N, 139° 58' W) about 30 miles west of Burwash Landing. The location is shown in Figure 1. Steele Creek is an easterly flowing tributary of the Donjek River and joins the Donjek about 25 miles upstream from the Alaska Highway bridge. The mudflow occurred at an elevation of about 4200 ft, some 8 miles west of the junction of the Steele and Donjek.

Geological Setting

Metamorphic rocks, chiefly phyllite, of late Paleozoic age underlie surficial deposits on the southern valley wall and the lower part of the northern valley wall. The metamorphic rocks are unconformably overlain by Tertiary

volcanic rocks, which are essentially flat lying. The volcanic rocks form the upper part of the north valley wall and are expressed topographically as prominent steep cliffs. Along the lower part of the valley walls the bedrock is concealed by moraines of both Pleistocene and Recent age. The Recent moraines form a group of flat-topped steep-sided, discontinuous topographic terraces on both valley walls. The individual terraces are 10 to 20 ft wide and 30 to 40 ft high. On both valley walls, steep-gradient streams have eroded V-shaped notches along the faces of the moraines and deposited material in the form of alluvial fans on the flat upper surfaces of the moraines. The central part of the valley is occupied by masses of stagnant ice, which are remnants of a glacier whose advance culminated about 100 years ago (Sharp, 1943, 1951).

The till forming the moraines was observed at several places to include the usual wide range of particle sizes and to demonstrate the usual lack of any stratification. It differed from many tills, however, in that this material was loose, cohesionless, and highly permeable. In surface exposures, the angularity of the granitic cobbles and boulders that made up a large part of the till was clearly evident. A grain-size distribution curve is presented in Figure 2. The Trask sorting coefficient for the samples is 11.4 and the inclusive graphic standard deviation is 4.7 ϕ , which is at the lower end of the range of values given by Folk (1968) for till. A count of pebbles greater than 4.76 mm in diameter revealed that 48.8% were granite, 28.3% were carbonate, 5.1% were volcanic and the remainder were of metamorphic origin (Table 1). The material finer than 0.074 mm was essentially cohesionless, which indicates a lack of clay minerals (Table 2).

*This report has previously appeared in the *Canadian Journal of Earth Sciences*, Vol. 6, pp. 219-229 (1969), and is reprinted here with permission.

†Department of Geology, University of Alberta, Edmonton, at time of writing; present address: Texaco Canada, Ltd, Calgary, Alberta

‡Department of Civil Engineering, University of Alberta, Edmonton

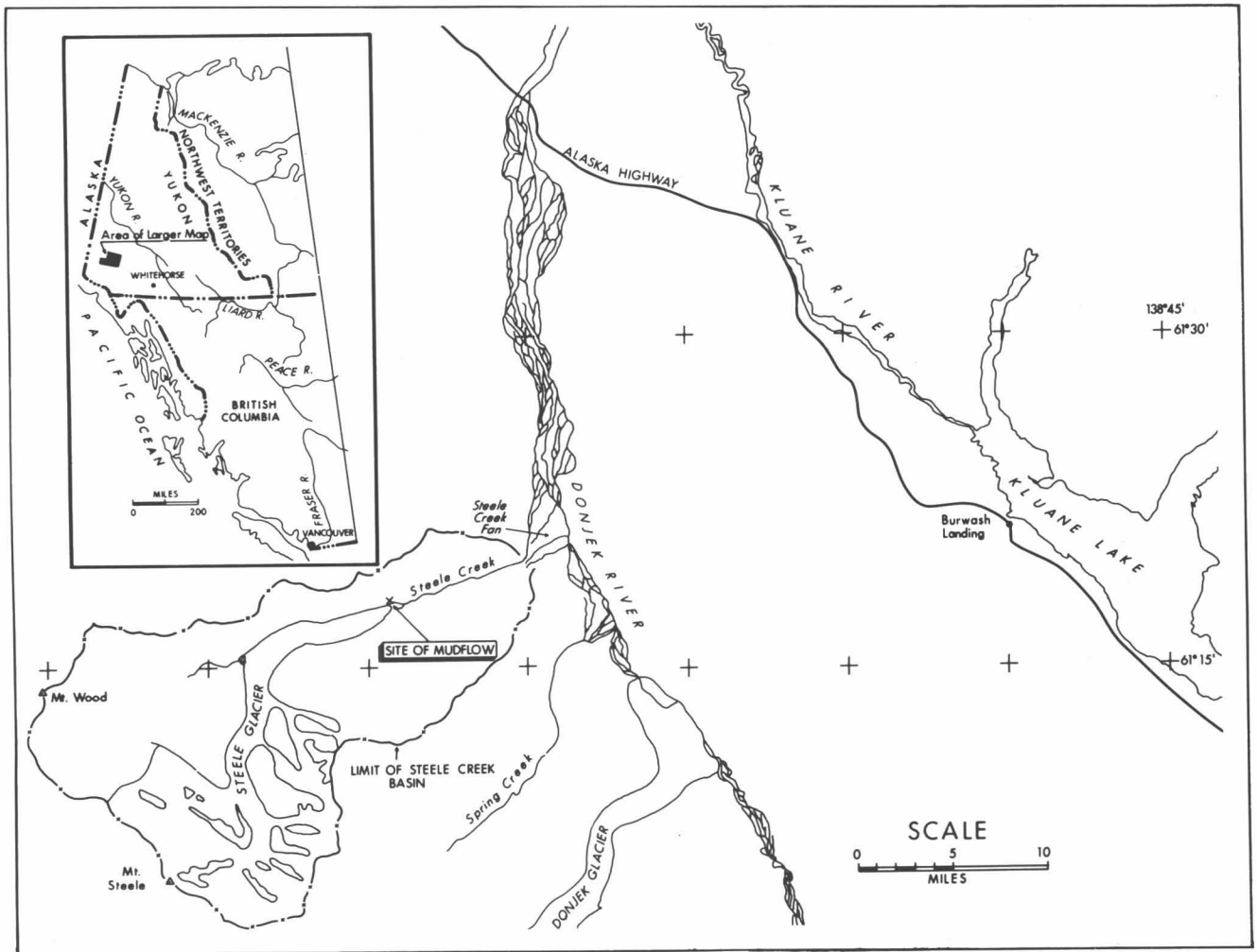


Fig. 1. Map showing the location of the Steele Creek mudflow.

TABLE 1. Results of Pebble Counts

	Composition %	
	Mudflow material	Moraine material
General rock grouping		
Granite	18.4	48.8
Volcanic (including basalt, pumice, lava)	71.7	5.1
Carbonate (limestone and dolomite)	6.9	28.3
Metamorphic (including gneiss and phyllite)	3.0	17.8

Description of Mudflow

Rain began about 10 p.m. the evening of July 10, 1967, and by 9 a.m. on July 12 the total recorded was 2.19 in. The rainfall, probably augmented by snow melt from the

TABLE 2. Plasticity Characteristics*

Material	Liquid limit (%)	Plastic limit (%)	Plasticity (%)
Mudflow	61	30	31
Till	26.5	19	7.5

*Limits were determined for material finer than 0.074 mm.

upper part of the valley wall, resulted in a flood that emerged from the notch at the upper margin of the terrace surface in a series of mudflows during the early morning of July 11, 1967. Pulsating flow has been observed in many other mudflows (Blackwelder, 1928; Sharp and Nobles, 1953; Curry, 1966). The mudflow moved onto the fan with fronts 6 to 8 ft high, which advanced as arcs of circles with increasing radii, accompanied by noises that sounded like continuous peals of thunder. In one instance,

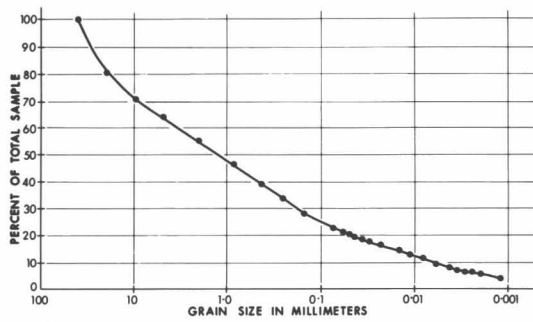


Fig. 2. Grain-size distribution of till, Steele Creek mudflow.

the arcuate front broke at the eastern side and the mud impounded behind the front flowed eastward roughly parallel to the upper face of the terrace, and then southward to the valley floor through another erosional notch. Other pulses of the mudflow built up similar fronts, some

of which broke to the west, whereupon flow was directly across the fan. The individual pulses were immediately preceded by a rapid and remarkable increase in the noise level created by the mudflow. It is estimated that the deposition on the fan ranged from a minimum of a few inches to a thickness in the order of 12 ft in a span of about 2 hours. The oblique air photograph (Fig. 3) shows the channels followed by the mudflow and the distribution, topographic features, and materials deposited by the flow. The topographic map (Fig. 4) was prepared from a stadia survey to show the slopes formed by the mudflow as well as the distribution of materials on that part of the fan east of the notch. Only a small part of the fan was west of the notch.

Figure 3 shows the presence of a fan-covered moraine surface directly above the area described in this report. The stream desposited some coarse bed load material on the upper terrace level and cascaded over the terrace scarp, into which it further eroded the steep-walled notch.



Fig. 3. Oblique air photograph showing the distribution of deposits of Steele Creek mudflow (photograph by T. E. Berg).

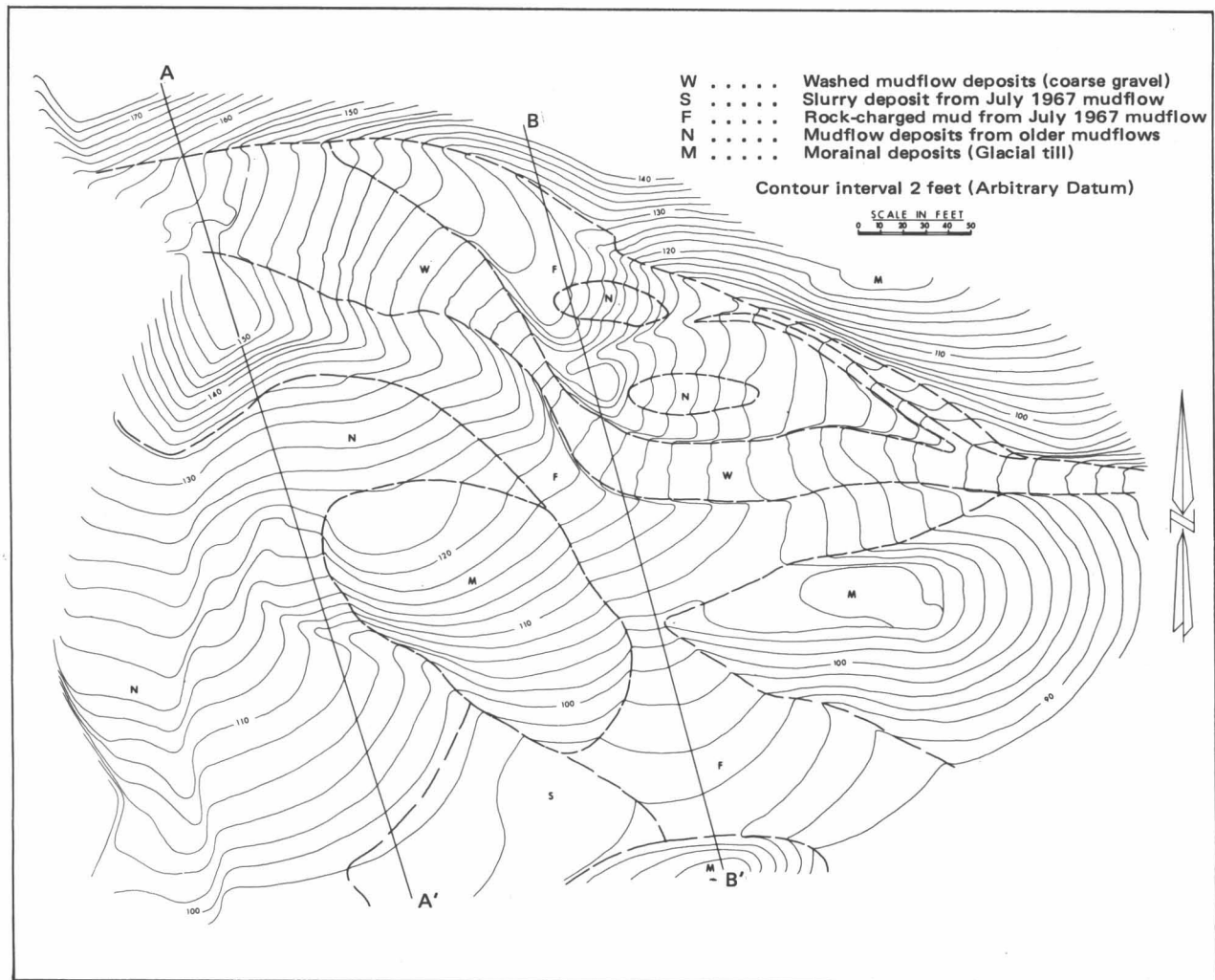


Fig. 4. Topographic and geologic map, Steele Creek mudflow, July 1967.

The extremely loose state of the material in the moraine must be stressed as contributing to the origin and the pulsating nature of the mudflow, since deformation would cause material in this state to break up completely. Erosion of the notch by local undercutting was observed to result in the periodic collapse of morainal debris into the stream in such large quantities that temporary dams were formed. As water and finer bed load backed up behind these dams, the material in them was quickly saturated but not overtopped. The saturated mass under the influence of the hydrostatic head moved down the channel and emerged from the notch as viscous, rock-charged mud. Sharp and Nobles (1953) described a similar mechanism for the explanation of pulsating flow of the Wrightwood mudflow. Fryxell and Horberg (1943) noted the collapse of materials into channels of alpine mudflows. The failure of the water to overtop the dam is important in this concept because overtopping would have led to the generation of a slurry rather than a large mud wave.

Material Deposited by Mudflow

The material deposited by the mudflow was a dark russet brown in its moist state and a light brown to buff color in its dry state. The grain sizes covered a very wide range as might be expected from the source of the material. Boulders up to 13 ft across (Fig. 5a) were observed and grain-size analyses (Fig. 6) revealed particles as small as 1 micron. The sample of material subjected to the laboratory grain-size analysis was collected from a point about 10 ft north of the morainal knob at the south edge of the map-area. Because of the location from which the sample was obtained, it is deficient in the coarser sizes that could be observed on the upper part of the fan. A representative sample of the material on the upper part of the fan could not be obtained because of transportation difficulties. In the opinion of the authors, however, the presence of this coarse material would serve to shift that part of the grain-size curve coarser than about 0.5 mm in the direction of the coarser sizes. The curve for the

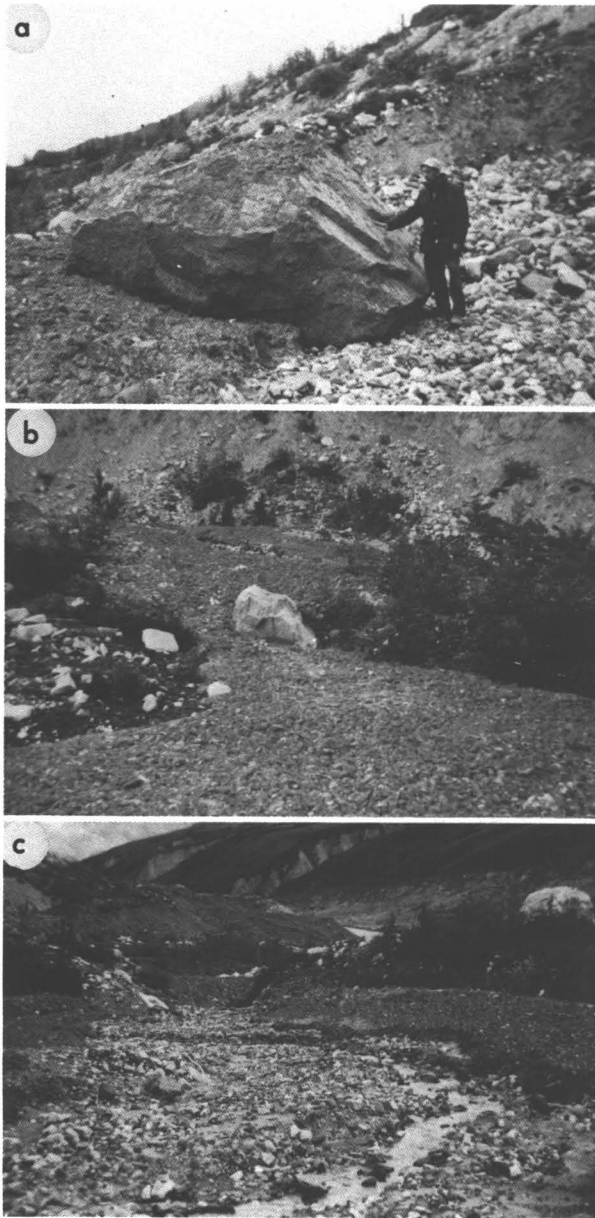


Fig. 5. Photographs of parts of the Steele Creek mudflow; (a) Large boulders moved by the mudflow. Mudflow material is to the left. The man is standing on washed mudflow deposits; (b) Surface of mudflow between two morainal knobs. The moraine face is in the background; (c) Washed mudflow deposits, flanked by unwashed material.

particles finer than 0.5 mm would not change appreciably and the entire curve would be more linear. The very wide range of grain sizes is common in mudflows (Blackwelder, 1928; Sharp and Nobles, 1953; Fryxell and Horberg, 1943). The sorting coefficient of the mudflow material (7.0) is unusually high, at least compared to values quoted by Sharp and Nobles (1953, p. 556). The mudflow material has an inclusive graphic standard deviation of 4.6ϕ .

A count was made of the pebbles larger than 4.76 mm

obtained from the sieve analysis (Table 1). Of these, 70% consisted of locally derived lava and 18% consisted of granite derived from the moraine. Limestone, dolomite, phyllite, chert, and gneiss were relatively rare. The pebbles were sharp and angular, with the exception of the limestone, of which less than half showed clear-cut evidence of water rounding. In general, the rock composition and angularity of the pebbles indicate a local source of the fan material. The lava fragments are considered to be derived from the fan on the next higher terrace or possibly from the flanks of the channel still farther upstream (Fig. 3). The remaining pebbles were derived from the moraine as the notch deepened.

The comparison of the pebble count and plasticity characteristics of the fan material with comparable data from the moraine (Tables 1 and 2) indicates that the two materials are markedly different. It is concluded that most of the mudflow was composed of volcanic material from the upper fan or possibly from the channel above that fan. This evidence indicates that the notch was cut over a period of years and the resulting debris spread over the fan mingled with lava material from above. This aids in explaining the high proportion of montmorillonite in the samples, as discussed in the next paragraph.

The plasticity characteristics of that part of the soil sample smaller than the 200 mesh sieve (74 microns) were determined by procedures in wide use in the field of soil mechanics and are reported in Table 2. The test results are commonly referred to as the Atterberg Limits, which are discussed in many textbooks dealing with soil mechanics (see, for example, Means and Parcher, 1963). In mountainous terrain, one would expect materials having a high liquid to be rather rare and rock flours to predominate. X-ray diffraction analyses on that portion of the sample finer than 2 microns revealed this portion to be almost exclusively the clay mineral montmorillonite. The presence of this mineral explains the high values of the limits obtained, and contributes in large measure to the ease with which the rock-charged mud flowed, often on slopes as flat as 6° . The source of the montmorillonite is the ash associated with the Tertiary volcanic rocks that cap the ridge.

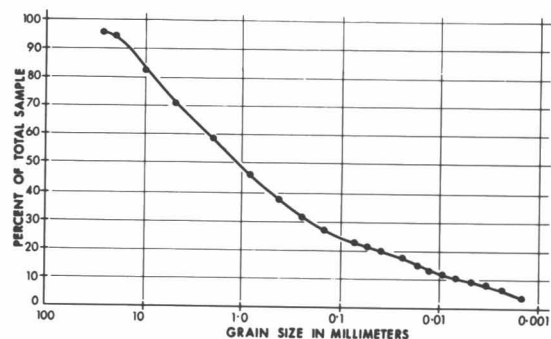


Fig. 6. Grain-size analysis of mudflow deposit, Steele Creek mudflow.

Washed Mudflow Deposits

One point of considerable significance is the very rapid removal of the fine material from the surface of the mudflow by subsequent rain and the accompanying runoff. Immediately after the mudflow, that part of the fan subjected to flooding was covered with a soft, sticky deposit, which included an abundance of sand, silt, and clay sizes (Figs. 5a, b). In the short period of a few days, the gravel sizes had been washed clean over several areas occupied by a small stream (Fig. 5c). The effect of the runoff was to change the appearance of the mudflow to the point where one would be led to believe it to be almost exclusively gravel sizes and to be misled concerning its manner of formation. The clean gravels so formed are referred to as 'washed' and their location is marked by the letter 'W' on Figure 4. Similar washed mudflow deposits have been described by Singewald (1928), and Fryxell and Horberg (1943). Curry (1966) inferred that ridges of boulders were the result of the washing of fine materials out of old mudflow deposits, which conclusion is supported by the observations in the Steele Creek mudflow.

Frequency of Occurrence

The deposits on the fan prior to the observed mudflow included both washed and undisturbed mudflow material from earlier floods. The areas of undisturbed old mudflow deposits were marked by well-defined mudflow levees and by a continuous mat of mountain avens (*Dryas drummondii*). The presence of mountain avens indicates the ready availability of groundwater, as might be expected on a fan. Such a mat requires decades to become established (Anderson, 1967; Lawrence, *et al.*, 1967; G. H. LaRoi, personal communication, 1968), indicating that the fan had not been subjected to a mudflow of this magnitude for some tens of years. One plant that was collected from the fan was dated at not less than 15 years old (G. H. LaRoi, personal communication, 1968). Similar vegetative conditions were observed on other fans on the north valley wall, and similar mudflows took place on these fans during the same storm. It is concluded that the mudflows occur infrequently, triggered by unusually intense rainfalls, but contribute substantially to the deposits making up the fan.

Drying History of Mudflow Deposits

The washed fan deposits consist of a veneer of clean gravel having a high porosity. A fresh mudflow advancing over a surface of this nature would lose a slurry of water and fine sediment into the open voids of the gravel. This would result in the development of intergranular friction and the eventual retardation of the flow. Material accumulating behind would tend to flow over and around such obstacles. This would explain the observed piling up of the mudflow close to the apex of the fan and the diversion of

the flow through gaps either to the east or west. The release of a slurry of fine sediments was observed during the flood. This slurry escaped from the front of the mud wave and flowed down a narrow channel across the old mudflow deposits into the area labeled 'S' on Figure 4. The slurry was impounded in this area by a tongue of the mudflow; the topography so formed was extremely smooth and flat.

Immediately after the mudflow, in all areas except the levee, the deposited material was still in an essentially quasi-fluid state. About one week after the flood occurred, that is, about July 18, 1967, a crust had formed so that there were local areas that could be safely walked upon and other areas in which the crust broke readily, exposing the still fluid material beneath. By July 24, 1967, the crust was approximately 6 in. thick in the area of the lower end of Profile B and was sufficiently extensive that one could walk anywhere on the flow. Under this crust, however, the material was still fluid. A similar drying history was described for mudflow deposits in Argentina (Singewald, 1928) and Wyoming (Fryxell and Horberg, 1943).

Topographic Profiles

Topographic profiles A and B (Fig. 7) were drawn from the plan on Figure 4. Profile A shows the levee at the head of the fan to be some 12 ft high at its maximum. The slope between the toe of the levee and the little gully represents a true slope of the fan, which has an angle of approximately 13° . The downhill face of the levee is at an angle of 32° , which is essentially the same as the slope on the face of the moraines. Since the morainal material is in a loose state, it is suggested that these latter angles are repose angles for the material and reflect the angle of shearing resistance for the loose state. Downhill from the gully, the profile crosses the contours obliquely.

Profile B (Fig. 7) starts on the morainal face showing an apparent slope, and then crosses a section of the mudflow levee including a small notch. The flat area represents the stream bed in which the gravel had been washed clean. The profile then descends through a notch between two unflooded morainal knobs and represents the surface of the mudflow material. The two morainal knobs constricted the flow at this point, thus producing a steep slope whose value is 14° . The topographic rise at the foot of the profile is another morainal knob. As shown in Figure 3 this knob is at the edge of the terrace. Just outside the map-area, the slope descends to the main valley floor.

A number of minor terraces form the composite major terrace on which the fan has been deposited. The individual steps are visible in Figure 3 to the west (left) of the fan. These terraces formerly extended into the area of mudflow and are now represented by morainal knobs, which rise a few feet above the level of the fan.

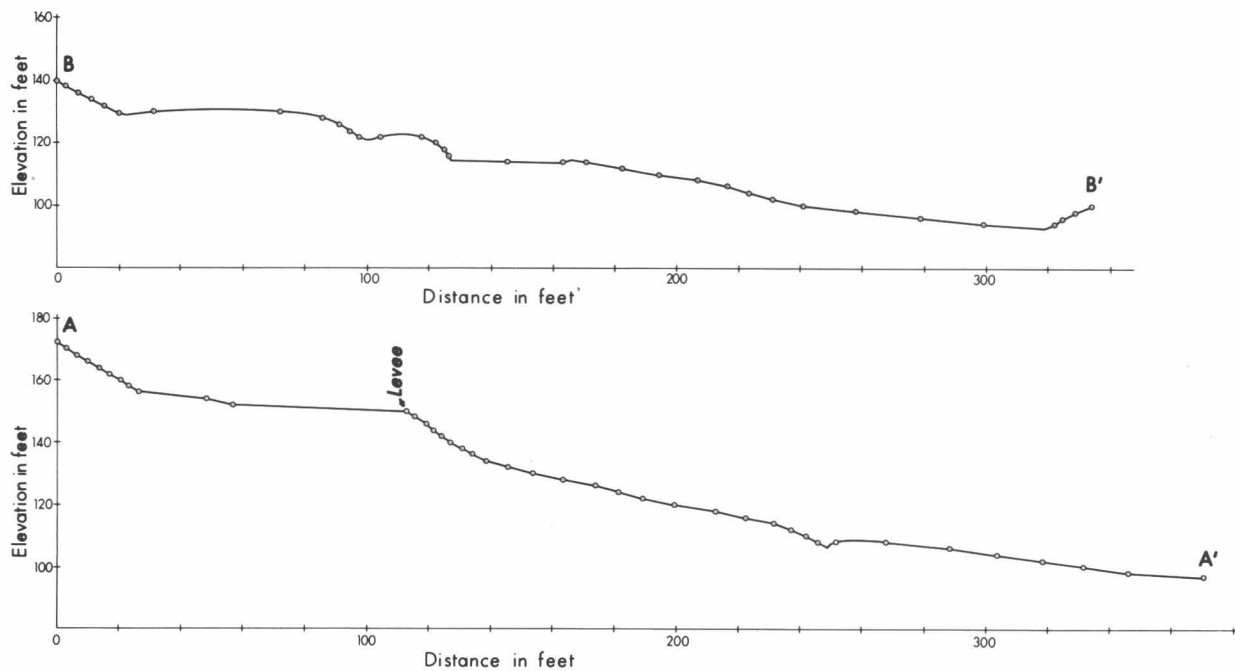


Fig. 7. Topographic profiles, Steele Creek mudflow, July, 1967.

Mechanism of Boulder Transport

The mechanism of transport of the large boulder shown in Figure 5a is of some interest. Many instances of the transport of similar boulders have been cited in the literature (Blackwelder, 1928). This boulder, which has an estimated total weight of about 80 tons, was transported at least 130 ft during the mudflow. During its transport, it was observed to be partly submerged. From theory, the fluid in which it was immersed can be shown to have a unit weight in the order of 100 lb/ft^3 (pcf). Therefore the effective or submerged weight of the boulder is about 28 tons. On a 19.5° slope (gradient of the notch) the component of this weight parallel to the slope is 9.4 tons, which is the force tending to cause movement. A further downhill force may be derived from the hydrostatic head of fluid built up behind the boulder. At 100 pcf, this head would exert a total thrust in the order of 25 tons if the head were the same as the height of the rock. The resisting force would be derived from frictional resistance between the rock and the bed. This is of the form $F_f = \sigma \tan \theta$ where F_f is the frictional resistance, σ is the normal force, and $\tan \theta$ is a coefficient of friction. The force normal to the bed is 26.5 tons, and from the lower part of Profile B the predominantly fluid material has a friction angle of some 6° . From this value of θ , a resisting force of 2.8 tons is obtained. There is little doubt that the boulder should move and, in fact, accelerate. One might argue that the 6° chosen for θ is an extreme value on the low side. The upper extreme value is the slope angle, 19.5° . Even if θ were as high as 19.5° , the head provided

by the mud need only be 5.4 ft, that is, less than half the height of the rock, to create a force equal to the downhill component. Once movement started, it would seem reasonable that the mud would get under the boulder and the frictional resistance would drop to some value intermediate between these extreme values. This implies that it is not necessary that the head of mud behind the rock be maintained. The abrupt change of slope from the notch to the fan changes the magnitude of the forces, and the downslope component on the flatter slope is only slightly greater than the frictional resistance. As the mudwave built up on the fan and fluid was lost from it, the frictional resistance increased somewhat and the boulder came to rest. It is assumed that the rock collapsed into the stream bed of the notch and formed part of one of the temporary dams described previously. These concepts do not include the direct effects of cobbles or pebbles under the rock, which may be considered to increase or decrease the resistance provided by friction. Their effect is included in the coefficient of friction expressed as the angle θ . An infinite slope analysis (Taylor, 1948) of that part of the fan derived from the more fluid part of the mudflow suggests the angle of shearing resistance to be in the order of 6° , that is the observed slope angle.

Summary of Observations

The following appear to be the major observations arising from this work:

(a) There is little doubt that this alpine mudflow was triggered by the intense rainfall. The mats of mountain

avens suggest that storms of this intensity occur at intervals of several decades.

(b) The pulsating nature of the mudflows was largely the result of the creation of temporary dams within the major notch. This type of flow has been observed in both alpine and semiarid type mudflows.

(c) Deposition took place at the rate of 8 to 12 ft in 2 hours on the upper part of the fan. The lower part of the fan was covered by the finer particles in a slurry. The major portion of the material deposited came from the fan on the terrace above with relatively little from the notch in the fan face.

(d) The subsequent history of the mudflow material is notable in two aspects. The first aspect is the length of time it remained essentially fluid. In 2 weeks a crust about 6 in. thick had formed on a deposit about 2 ft deep. The second aspect is the rapid rate at which certain areas were washed clean of fines leaving a veneer of coarse clean gravel on the surface of the fan. This is of some importance, since the presence of the clean gravel is very misleading concerning the mechanism of formation of the fan. Washed mudflow deposits have been described for both alpine and semiarid type mudflows.

(e) The observed slope on the faces of the moraines of 32° and the loose state of these deposits suggest that this angle represents the angle of shearing resistance for the loose state.

Conclusions

From this study of this particular alpine mudflow the following conclusions are offered:

Such mudflows are intermittent, appear to occur at intervals of several decades, and are triggered by intense rainfalls. Sharpe's (1938) conclusion that alpine mudflows are the result of snowmelt is not supported by these observations.

The rates of deposition can be very high for short intervals, the maximum in this instance being observed to be some 12 ft. Ponded slurred material was about 2 ft deep.

The creation of a veneer of clean gravel by stream and rain washing presents a misleading picture concerning the formation of such fans, either in a semiarid or alpine environment. There is no apparent difference between the large-scale features of this alpine mudflow and the semiarid mudflows described in the literature. The deposit formed by the flow shows a wide dispersion of particle sizes, common for this type of deposit.

It is suggested that the major requirement for pulsating mudflows such as that observed is a steep-sided, high-gradient notch cut into easily erodable material. In this instance, the notch was eroded into the upper terrace, which was composed of loose till. It is also likely that erosion of the upper fan supplied volcanic material, which increased the viscosity of the mudflow and the height of the front of the mudflow.

The abrupt change in gradient caused by the upper fan resulted in the deposition of the coarser fraction of the stream load, but the stream remained heavily charged with fine volcanic debris including montmorillonite. The stream changed its regimen from one of deposition to one of erosion as the stream entered the notch. Where the stream left the notch and emerged on to the lower face, the regimen reverted to that of deposition. The deposit consisted of the volcanic material plus any material picked up in the notch.

Acknowledgments

The party was financially supported by grants from the National Research Council of Canada, Ottawa and the Boreal Institute, University of Alberta. D. V. Currie assisted in the field survey. X-ray diffraction analyses were carried out by the Alberta Research Council. Grain-size distribution and the Atterberg Limits were determined in the Soils Laboratory of the Department of Civil Engineering, University of Alberta.

References

- Anderson, D. J. (1967) Studies of structure in plant communities, Pt. 4; Cyclical succession in *Dryas* communities in northwest Iceland, *J. Ecol.*, 55, 629-635.
- Blackwelder, E. (1928) Mudflow as a geologic agent in semiarid mountains, *Bull. Geol. Soc. Am.*, 39, 465-480.
- Curry, R. R. (1966) Observations of alpine mudflows in the Tenmile Range, Central Colorado, *Bull. Geol. Soc. Am.*, 77, 771-776.
- Folk, R. L. (1968) *Petrology of Sedimentary Rocks*, Hemphill's, Austin, Texas, 120 pp.
- Fryxell, F. M., and Horberg, L. (1943) Alpine mudflows in Grand Teton National Park, Wyoming, *Bull. Geol. Soc. Am.*, 54, 457-472.
- Lawrence, D. B., Shoenike, R. E., Quispel, A., and Bund, G. (1967) The role of *Dryas drummondii* in vegetation development following ice recession at Glacier Bay, Alaska, with special reference to its nitrogen-fixation by root nodules, *J. Ecol.*, 55, 793-813.
- Means, R. E., and Parcher, J. V. (1963) *Physical Properties of Soils*, Merrill Books, Columbus, Ohio, 464 pp.
- *Sharp, R. P. (1943) Geology of the Wolf Creek area, St. Elias Range, Yukon Territory, Canada, *Bull. Geol. Soc. Am.*, 54, 625-650.
- Sharp, R. P. (1951) Glacial history of Wolf Creek, St. Elias Range, Canada, *J. Geol.*, 59, 97-117.
- Sharp, R. P., and Nobles, L. H. (1953) Mudflow of 1941 at Wrightwood, southern California, *Bull. Geol. Soc. Am.*, 64, 547-560.
- Sharpe, C. F. S. (1938) *Landslides and Related Phenomena; A Study of Mass-Movements of Soil and Rock*, Columbia Geomorph. Stud. No. 2, Columbia Univ. Press, New York, 137 pp.
- Singewald, J. T., Jr. (1928) Discussion of mudflow as a geologic agent in semiarid mountains, *Bull. Geol. Soc. Am.*, 39, 480-483.
- Taylor, D. W. (1948) *Fundamentals of Soil Mechanics*, Wiley, New York, 700 pp.

*This article is reprinted in the present volume.

Observations of the Surge of Steele Glacier*

A. D. Stanley †

ABSTRACT. For part of 1966, Steele Glacier in the Icefield Ranges made a spectacular advance at a rate exceeding 500 m per month. The main part of the surge continued for two years, but by early 1968 the advance had slowed to less than one tenth of the maximum rate. For most of the 35-km length of the main trunk the surface was a chaotic jumble of ice blocks, spires, and pinnacles, but large structures outlined by surface moraine were preserved. Most of these structures had been displaced 8 km by August 1967, irrespective of their original location. Preliminary measurements indicate structures were displaced similar distances down the length of the glacier and suggest that most of the glacier moved forward as a block. The surge has not been correlated with any local earthquake activity, and there is no evidence for a short-term climatic change. The movement is considered to result from critical dynamic conditions within the glacier, possibly facilitated by increased amounts of water along the ice-bedrock contact.

Introduction

In the summer of 1966, ice in the lower part of Steele Glacier suddenly advanced after several years of down-wasting (Fig. 1). The advance of the ice tongue was dramatic and the popular press referred to it as the 'galloping glacier.' The date of initial movement is not known but was probably during 1965. By August 5, 1966, an ice wall more than 30 m high had traveled down the lower part of the glacier for a distance of 12 km. The front advanced a further 3 km during the following year but photographs taken in early 1968 show that movement had slowed to less than one tenth the maximum rate.

For at least 30 years before the surge, the lower part of the glacier had been relatively inactive, and there is no ready or obvious explanation for the dramatic advance. There was no obvious change in climate nor any known seismic activity that preceded the surge, and the meltwater from the glacier shows no evidence of any unusual discharge associated with the advance. Although the information presently available does not give a ready explanation for a surge, pertinent data obtained from aerial photographs may assist in evaluating proposed theories of glacier surges and contribute to the study of 'normal' glacier flow.

Glacier surges, or catastrophic advances, have been identified in several parts of the world, including that of Medvezhii Glacier, Pamir, U.S.S.R. (Dolgushin, *et al.*, 1963), a glacier in Spitsbergen (Glen, 1939), and Otto Fiord Glacier in North Ellesmere Island, Canada (Hattersley-Smith, 1964). Several surging glaciers in western North America have been described in detail, including several in Alaska, for example, glaciers in the Yakutat Bay area of Alaska (Tarr, 1909; Tarr and Martin, 1914), the Black Rapids Glacier (Moffit, 1942; Post, 1960),

Susitna Glacier (Post, 1960), Muldrow Glacier (Post, 1960; Harrison, 1964), Walsh Glacier, Yukon-Alaska (Paige, 1965; Post, 1966, 1967), and Steele Glacier, Yukon (Bayrock, 1967; Roots, 1967), within the St. Elias Mountains.

Part of the St. Elias Mountains is used as a field laboratory for scientific investigations by the Icefield Ranges Research Project that is sponsored by the Arctic Institute of North America and the American Geographical Society (Wood, 1963). During the last seven years scientists from several disciplines have undertaken a number of studies, primarily during the summer months. The projects have included meteorological observations and several sets of terrestrial photographs for a number of glaciers within the Icefield Ranges. Steele Glacier is one of the glaciers studied, and when the surge was recognized in 1966 the Surveys and Mapping Branch of the Department of Energy, Mines and Resources arranged for two sets of aerial photographs to be obtained. These were taken to compile large-scale maps to study morphological changes of the glacier and to measure displacement of surface features so that quantitative data could be obtained to evaluate theories proposed to explain glacier surges.

A study of the photographs and the maps compiled from them shows that the ice surface developed a number of distinctive features that are characteristic of a glacier surge. This paper describes some of the features and lists data derived from a preliminary examination of available material.

Location and Physical Setting

Steele Glacier (known as Wolf Creek Glacier before 1963) is one of the larger glaciers on the northeastern slopes of the Icefield Ranges that form part of the north-west-trending St. Elias Mountains along the Yukon-Alaska border.

The north-facing slopes between Mt. Harrison, Mt. Steele, and Mt. Wood are a complex of basins and small cirques which form an accumulation area for Steele Glacier and its tributaries. From these peaks the precipitous snow-mantled slopes extend down to a series of broad

*This report has previously appeared in the *Canadian Journal of Earth Sciences*, Vol. 6, pp. 819-830 (1969), and is reprinted here with permission.

†Inland Waters Branch, Environment Canada, Ottawa, Ontario, Canada

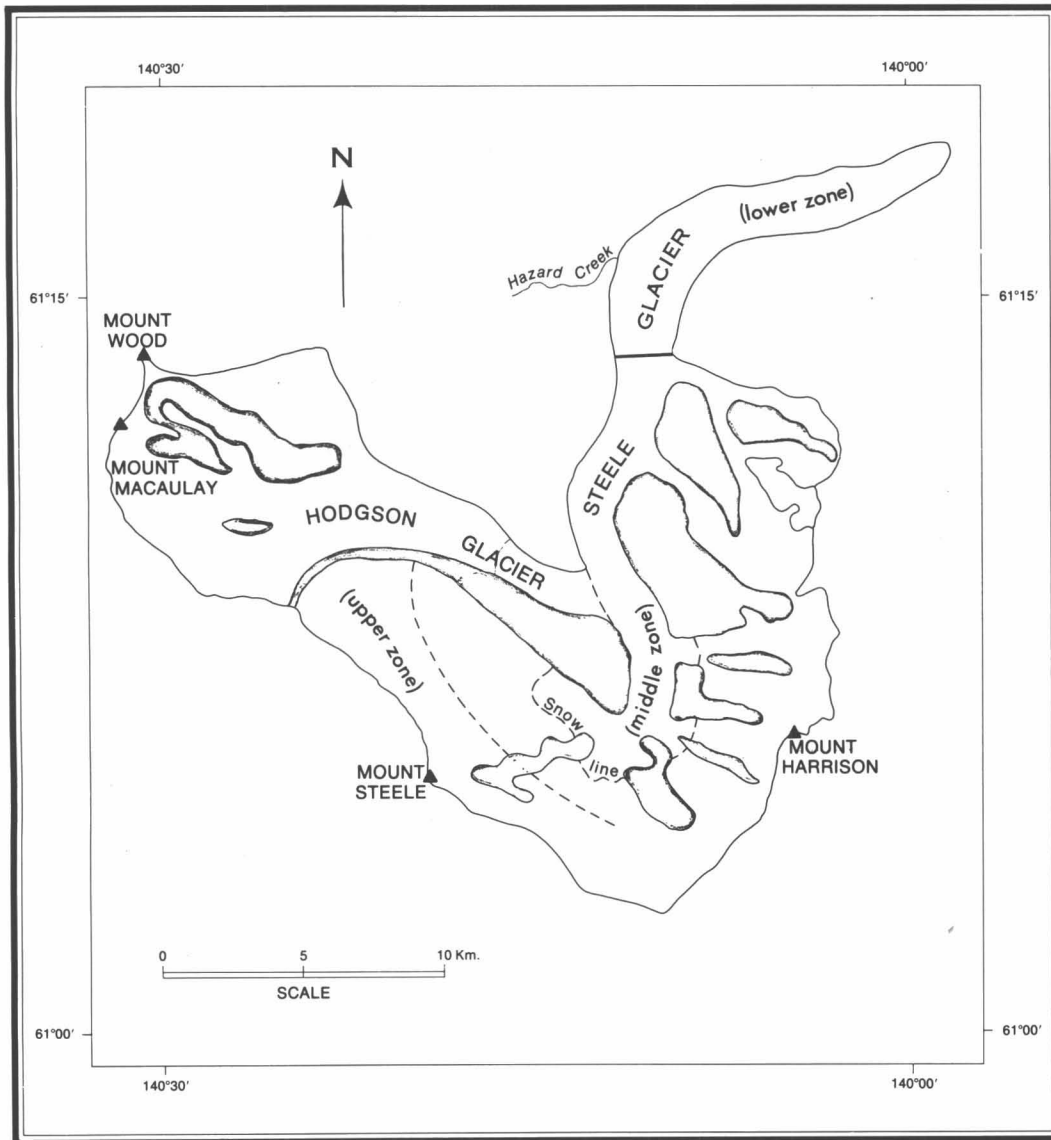


Fig. 1. Map of Steele Glacier showing location of tributaries and the accumulation basin of the Steele and Hodgson Glaciers. The generalized snow line is based mainly on the 1951 photography.

snowfields below 4000 m. Below 2500 m the snow and ice are confined to one main sinuous valley that extends northward for 20 km before turning east into a broader valley below the junction with Hazard Creek. Meltwater from the glacier flows into Steele Creek to the Donjek River, a tributary to the Yukon River, some 40 km west of Kluane Lake.

The valley section of Steele Glacier is more than 35 km long and, on the average, 2 km wide. The main trunk of 60 km² is nourished by ice and firn from an accumulation basin of approximately 240 km², including six tributary glaciers. Hodgson Glacier, a left-hand tributary covering an area of 100 km², is the most important. It joins the main glacier just below the accumulation zone, and extends westward for nearly 23 km to Mt. Wood (Fig. 1).

Sources of Information

In 1935, W. A. Wood led the first of a series of expeditions into the Icefield Ranges and has maintained records of several glaciers over the past 30 years (Wood, 1936, 1942). Detailed descriptions of the valley geology are given by Sharp (1943) and Muller (1967). The glacial history of the surrounding area is outlined by Muller (1967), and Sharp (1951) studied the glacial geology of the immediate area.

A valuable series of photographs have documented changes of the glacier since the mid-thirties. The records can broadly be divided into photographs taken for specifically photogrammetric purposes and those taken for scientific interest. The photogrammetric record listed in

Table 1 clearly reflects the extensive support the Canadian Government, through its Surveys and Mapping Branch of the Department of Energy, Mines and Resources, has given to the study of this unusual glacier.

W. A. Wood has taken numerous photographs during a series of expeditions to the area, and A. S. Post of the United States Geological Survey has taken several series of aerial photographs over the last 10 years. In fact, Post predicted the surge of the Steele Glacier, and his photographs taken in late summer 1965 show extensive crevasses that formed during the initial phase of the surge.

After the surge began it was arranged for M. E. Alford of the Whitehorse Office of the Water Survey of Canada to fly over the area and photograph the glacier, particularly the advancing ice front. Photographs were taken in 1966 November; 1967 January, February, March, April, and May; and 1968 March. In the summer of 1967, W. A. Wood took a further set of photographs of many parts of the glacier.

Large-scale maps of sections of Steele Glacier have been compiled by the Surveys and Mapping Branch from the photographs listed in Table 1, as a basis for measurements of glacier movement and changes in surface elevation. A map of the main part of the glacier at the scale of 1:50,000 was prepared from photographs taken in 1951, and 1:25,000-scale maps were compiled from aerial photographs taken in 1966. The first maps, produced for field use, were based on limited ground control and more accurate maps are to be prepared using ground control established in 1967 by the Canadian Army Map Service. The map prepared from the 1967 photography with the most recent ground control has been used as a base map to locate surface features identified on aerial photographs from previous years.

Pre-Surge Features

There is no description of the pre-surge appearance of the accumulation area, but a detailed account of the lower part of the glacier in 1941 was given by Sharp (1951). Large sections of the accumulation basins have steep rock walls but most of the slopes were covered with a thick mantle of snow. In all the available photographs of the accumulation zone, the snow cover has a smooth surface that is unbroken except for small crevasses near the glacier margins and extensive crevasses associated with changes in slope.

Below the junction with Hazard Creek the glacier was covered by a mantle of debris that obscured the ice and merged with lateral moraines in the valley. Because of this mantle it was not possible to define clearly the ice margins or terminus. Bayrock (1967) identified the 1951 terminus of the glacier as the lower limit of the exposed ice. However, ice undoubtedly extended farther down-glacier beneath the debris mantle for another 18 km to a prominent moraine which Sharp (1951) considered the terminal moraine of the last advance.

A series of well-defined medial moraines extends along most of the length of the main trunk. These moraines outline the boundaries of ice streams from tributary glaciers that join the main glacier below the accumulation zone. Many of the moraines have distinct loops, and the enclosed ice streams terminate in a bulbous lobe. These loops and irregular bulges in constituent ice streams are the result of a previous surge or irregular advances of individual tributaries.

The entire ablation zone, including that of Hodgson Glacier, had very few crevasses and many of the features of stagnant ice. The average surface slope was 50 m/km and the early expeditions were able to walk most of the distance up the glacier. In detail the topography was highly irregular with short water courses, large closed depressions, and irregular knobs and ridges that were debris covered. Nearly all supraglacial streams were deeply entrenched, and englacial arches together with numerous passages and tunnels showed the ice in an advanced state of decay.

The best evidence for lack of movement was in the section of the glacier below Hazard Creek, where alluvial cones from tributary valleys extended onto the glacier surface from the northern side. From field studies in 1941, Sharp (1951, p. 109) considered the cones were more than 25 years old but he was unable to detect any perceptible downvalley displacement for parts of the cones projecting onto the ice surface.

Below the junction with Hazard Creek the extensive mantle of debris covered the ice and obscured the terminus so it was not possible to estimate the amount of recession. Down-wasting was the main process during stagnation and moraines on the valley walls showed that the ice surface had been 100 to 150 m above the existing dirt surface. If the ablation rate is assumed to be 1.5 m each year, down-wasting must have been continued for several decades. This period of quiescence probably terminated in the fall of 1965 and by June 1966 the main part of the advance had occurred.

TABLE 1. Aerial Photography of Steele Glacier

Year	Organization	Flight lines
1951	Surveys and Mapping Branch	A-13132/33
1966 August	Surveys and Mapping Branch	A-19647
1966 September	Surveys and Mapping Branch	A-19739
1967 August	Surveys and Mapping Branch	A-20128/29

Surge Features

Aerial photographs of Steele Glacier taken during the surge show all the features described by Post (1960) for the sudden advance of Muldrow Glacier, Alaska. The surface is heavily crevassed and has become a jumble of blocks, columns, and spires that tower several meters above the general surface (Fig. 2). Despite the chaotic ice surface and extensive displacement, large-scale features are still defined clearly and occur in the same relative position with respect to each other.

On the basis of the surface features and the change in elevation determined from detailed topographic maps, the glacier can be divided into three distinct zones (Fig. 1). These zones are independent of the ablation and accumulation areas and they have a characteristic appearance. The lower zone has a convex transverse profile and the surface is much higher than before the surge, the middle zone has an ice surface lower than before, and the upper zone comprises those areas where there is no apparent change in elevation. The upper zone is entirely within the accumulation area, but the middle zone covers part of the accumulation and ablation areas.

Lower zone. The lower zone extends from the advancing ice front to a position 3 km above the junction

with Hazard Creek. Throughout the zone the surface has thickened by an average of 100 m and the transverse profile has become convex (Fig. 4, profiles v-v', w-w'). Above the junction the thickness increase is much less, and at an elevation of 1750 m above sea level there is no apparent change in the level of the ice surface.

For most of the zone the margins are well marked by steep walls of ice that tower 20 to 30 m above the lateral moraines on either side of the glacier. Moraines of tributary glaciers that once spread out over the glacier are truncated by this ice wall, and streams that once flowed onto the ice surface have been dammed and now form large ponds or flow as marginal streams along the foot of the wall. The most conspicuous ponded waters are trapped in the valley of Hazard Creek, and in 1967 formed an ice-dammed lake with an area of 1 km².

In 1951 the lower part of the glacier had a debris-covered surface broken by few crevasses. Aerial photographs taken in 1965 by A. S. Post show no unusual features. In 1966, the surface was completely different, with a complex pattern of fractures and a set of arcuate roll-like structures sub-parallel with the actively advancing ice front. By August 1967, the front had moved down-glacier 12 km and the series of rolls extended back up the glacier more than 3.5 km.



Fig. 2. Steele Glacier, May 1967. View looking south to Mt. Steele, showing chaotic surface of glacier and the preservation of surface moraines. Width of glacier is 2 km.

Studies by Bayrock (1967) in 1966 showed that the advancing front was a 30-m-high wall of dirt-covered ice. The wall was apparently formed from push moraines that were later overridden and incorporated into the active ice.

Measurements taken by Bayrock during a four-day period showed the advance was not regular but occurred along parts of the front as successive movement planes developed in the dirt-covered dead ice. These planes were nearly horizontal or dipped upglacier, and the overlying ice was pushed forward and upward to give a roll-shaped structure in front of the active front. The movement planes cropped out as arcuate fractures about 100-200 m ahead of the advancing front, and with further movement subparallel fractures were developed downglacier. As the roll continued to develop it was gradually incorporated into the active ice and became one of the series of arcuate structures that extended upglacier from the terminus.

Individual rolls are 5 to 10 m high, and most are distinct features clearly separated from adjacent structures by obvious depressions. Some rolls have a set of crevasses at right angles to their length. The crevasses, originally developed as the ridges formed before the advancing ice front, now serve to separate these structures.

Middle zone. The middle zone refers to all parts of the glacier where the surface has been lowered (Fig. 4, profiles $x-x'$, $y-y'$, and $z-z'$). It extends from above the junction with Hazard Creek at an elevation of 1750 m, to well above the snow line, a distance of almost 26 km. The surface lowering is generally 50 to 100 m but in the section immediately above Hodgson Glacier the maximum value is 130 m. The previous ice surface is identified readily by 'stranded' masses of debris-covered ice adhering to the valley walls well above the present glacier surface.

Complex crevasse systems occur in all parts of the zone, and continue well into several tributary basins. Although many glaciers have contributed to the surge, several small tributaries showed no movement and their junctions with the main glacier are marked by steep ice walls or a series of prominent crevasses.

Hodgson Glacier, the largest tributary, did not contribute to the surge in 1966, and its junction was marked by a steep 20-m-high ice wall. Although a series of crevasses had developed near the junction, the surface had not been lowered and the moraine pattern was similar to that photographed in 1951. However, as a result of the surface lowering of the Steele Glacier, the damming influence of the main trunk was effectively removed and the tributary subsequently surged. Aerial photographs taken in August 1967 show that several surface structures on Hodgson Glacier were displaced 1.5 km downstream and the wall was halfway into the main stream with the leading edge on the western margin 3.0 km downstream.

During the surge of the main trunk, tributary ice streams retained their identity, and although displaced several kilometers, in general they retained their original width and relative position. The medial moraines formed

large ridges between individual streams of clean ice that were commonly 20 m below the general ice surface. The moraines stand well above the surface and one of the most prominent formed a wall that extended several kilometers down the glacier before merging with an extensive area of debris.

At higher elevations the moraines become less prominent and gradually merge with the ice surface, and the 'stranded' ice on the valley sides becomes closer to the level of ice surface. The zone extends well into the accumulation area, and at high elevations a blanket of snow obscures all details of surface lowering except en echelon crevasses at the margins of the glacier and traverse crevasses at the upper limit of the surface lowering.

Upper zone. The upper zone includes the head walls of most tributaries and covers all areas where there has been no obvious surface lowering. Available maps do not cover this area of the glacier in sufficient detail to detect any changes in surface contours, and it is not possible to recognize surface lowering by direct inspection of aerial photographs. The photographs taken in 1966 and 1967 do not cover all the accumulation zone and it is difficult to define the boundary of the area that has not been affected by the surge. This boundary is assumed to be marked by a series of crevasses, extending across some sections of individual basins, marking the upper third of the accumulation area.

Movements

A preliminary estimate of the gross movement of the main part of Steele Glacier has been obtained by comparison of aerial photographs and large-scale base maps compiled from the 1967 photographs. No direct measurements were made in the field, and the figures given for displacement during the surge are all based on the inspection of aerial photographs and the recognition of distinctive moraine patterns on the glacier surface.

The 1951 photographs show many surface features including well-defined patches of clear ice, looped moraines, and streams of clear ice with small irregularities and bulbous terminations. Most of these distinct features are confined to the main trunk of the glacier and do not occur above 2500 m above sea level or within the accumulation zone.

More than thirty features were identified on each set of photographs and their positions were sketched on the large-scale map. Figure 3 shows their location in August 1967, and Table 2 lists some of the surface features and the displacement scaled from the map along the probable line of glacier movement. The measurements have an accuracy of ± 100 m, for locations were plotted without the aid of a mechanical plotter and some features became less distinct during the surge and were difficult to define.

Nearly all structures were displaced more than 8.0 km during the surge, and as first noted by Roots (1967) there appears to be no progressive change in the displacements down the glacier irrespective of the original location of the feature on the ice surface. In 1951 all the well-defined

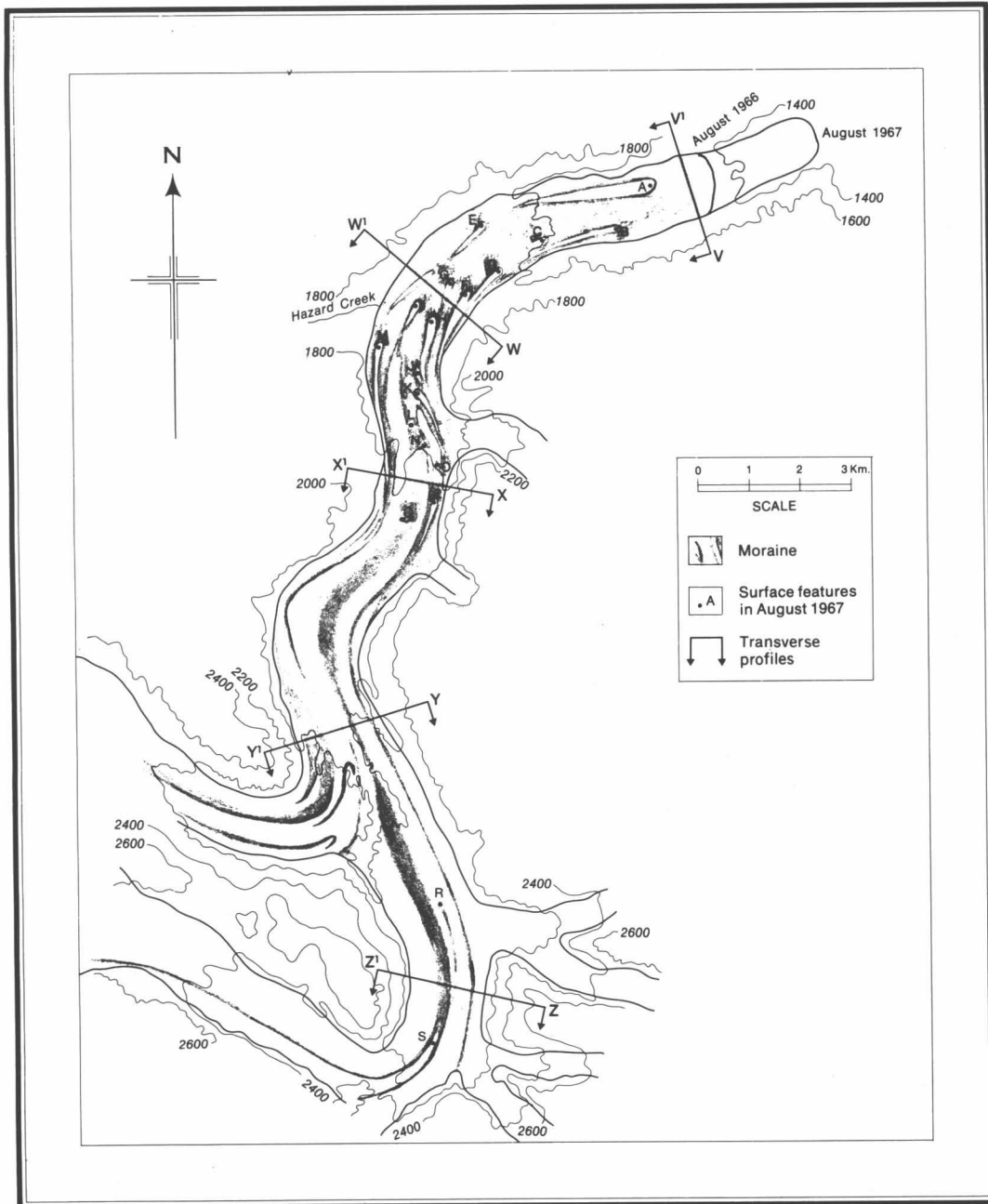


Fig. 3. Map of Steele Glacier, August 1967, showing moraine pattern and 1967 position of surface features identified in aerial photographs of 1951, 1966, and 1967, together with transverse profiles.

features were in the section above the junction with Hazard Creek, and during the surge they were displaced down the main trunk. The material transferred from near the snow line has few distinct features.

During the surge all structures occupied the same relative positions, and in straight sections of the valley it was not possible to detect any significant movement difference between features near the center line and those to within 200 m of the glacier margins. Most of the differences in displacement occurred in sections near large bends.

The most interesting movements occurred near the prominent bend above Hazard Creek. As indicated in Table 2, features A and B show total displacements of 9.5 km and 7.8 km. Above the bend at Hazard Creek, the 1951 photographs show two very clear structures, a moraine (feature A) on the west side and a clear ice patch (feature B) on the east side, 1 km upstream. In August 1966 the two structures still occupied the same relative positions 1 km apart, but the ice patch had moved 5.0 km compared with the moraine that had been displaced

TABLE 2. Table Listing Displacement of Surface Features During Surge of Steele Glacier

Features	Displacement in km between photographs							Total displacement (km)
	1951	1966 August		1966 September		1967 August		
A	x	6.4	x	0.5	x	2.5	x	9.4
B	x	5.0	x	0.5	x	2.3	x	7.8
C			x	0.5	x	2.3	x	
D	?	4.7	x	0.5	x	2.3	x	7.5
E	x	5.2	x	0.9	x	2.7	x	8.4
F	x	5.5	x	0.5	x	1.9	x	7.9
G	x	5.3	x	0.5	x	2.5	x	8.3
H	x	5.4	x	0.5	x	2.3	x	8.2
I	x	5.4	x	0.5	x	2.8	x	8.7
J	x	5.3	x	0.5	x	2.5	x	8.3
K	x	4.9	x	0.5	x	2.4	x	7.8
L	x	5.1	x	0.5	?	2.4	x	8.0
M	x	5.1	x	0.5	?	2.5	x	8.1
N	x	5.0	x					
O	x	5.0	x			3.6	x	8.6
P	x	5.1	x			3.6	x	8.7
Q	x	5.5	x			3.5	x	9.0
R	x	5.5	x?			3.0	x	8.5
S			x?			3.0	x	

Note: x, clearly identified; ?, not well identified.

6.4 km. By August 1966 both structures were in a straight portion of the valley, and during the next month both moved about 0.5 km and in the following 11 months were displaced 2.5 km.

Cause and Flow Mechanism

The available photos show no reason for the sudden advance but do assist in the evaluation of existing theories. The mass movement of ice down the main trunk indicates that for the section where most structures occur there was little differential movement in any transverse profiles. This lack of differential motion suggests that the glacier moved as a unit by sliding along the base. The preservation of large-scale surface features suggests that (in spite of extensive fragmentation near the surface) there was little vertical exchange of ice within the glacier.

Both Weertman (1969) and Lliboutry (1969) considered that surges result from an increase in water at the base of the glacier. Once the surge has started any film or water-filled channels would be maintained by the water generated by the rapid motion. The additional water would not remain at the base of the glacier but would drain downglacier and contribute to the meltwater stream. This contribution would be difficult to detect, for the surge would result in an increase of meltwater due to the transfer of ice to lower, warmer elevations, and the increased ablation that results from a greater exposed surface area as the ice surface becomes chaotic.

Although it was possible to estimate the discharge for a short time during the summer of 1966, there are no hydrologic records available for any previous period. The discharge may have been greater in 1966 but the increase was not sufficient to cause extensive changes to the stream channels, and the section of the river below the terminus showed no evidence of unusual flooding.

According to Robin (1969) surges may result from an instability within the glacier due to changes in temperature or stress. For Steele Glacier there is no information about temperatures within the ice and no information of ice depths to determine the bedrock topography. A surge may be governed by constrictions in the valley or reverse slope in the bedrock surface. If this control occurs in the Steele Glacier, the most likely position for the reverse slope would be in the area above the junction with Hazard Creek.

Summary and Conclusions

Steele Glacier has several features common to surging glaciers described by other authors. The glacier has an extensive accumulation zone at high elevations, but the main trunk of the glacier occupies a sinuous valley more than 35 km in length. Before the surge the ice tongue was virtually stagnant and had down-wasted for several decades. There was no great change in surface gradient along the main trunk and values ranged from 25 m/km to 50 m/km.

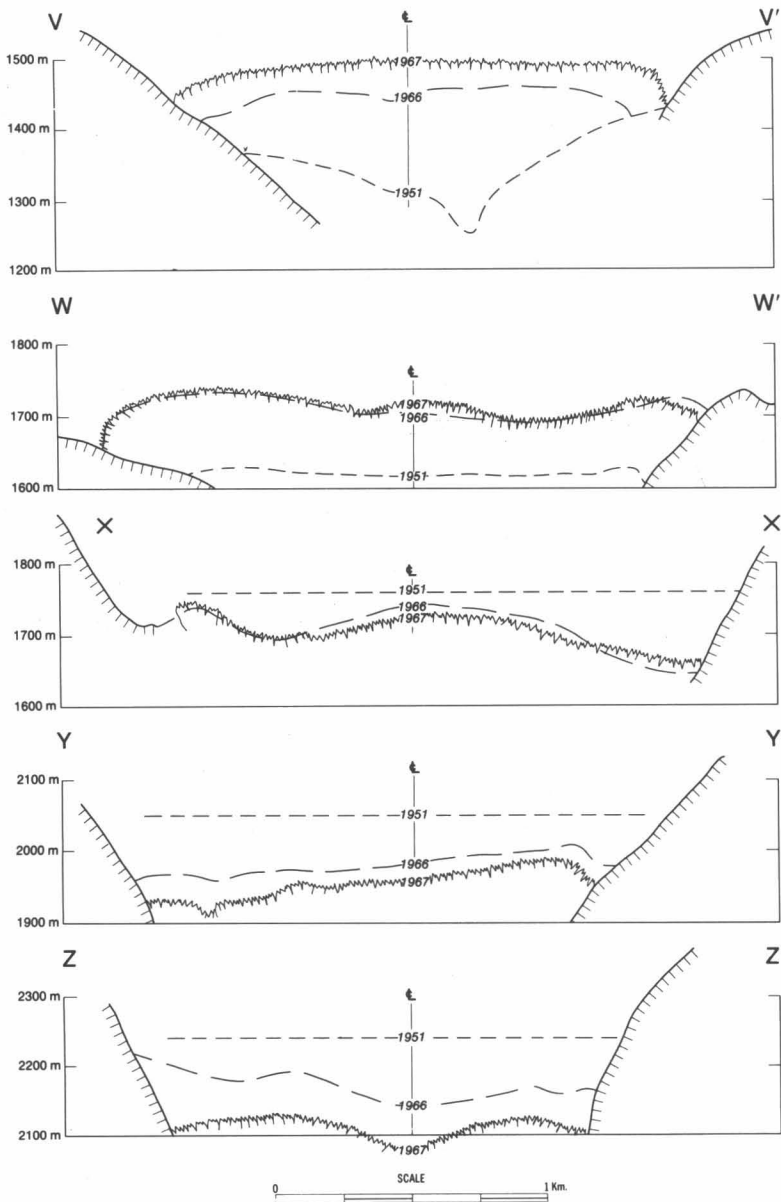


Fig. 4. Transverse profiles of the Steele Glacier showing changes in surface elevations during the surge. Positions of profiles are shown on Figure 3.

The first crevasses appeared in 1965, and by the following year the surface became chaotic but large-scale features were not obliterated. The increase in glacier thickness in the lower part of the valley was compensated for by a lowering of the ice surface over an area extending from Hazard Creek to well above the snow line. In the section below Hazard Creek, the debris-covered ice of the lower 13 km of the glacier had been pressed into a series of subparallel arcuate ridges that extended 3.5 km back from the advancing ice front.

Large structures along the length of the glacier had been displaced a total of 8 km by late 1967. Generally the features maintained the same relative position on the glacier surface but were displaced greater distances when on the outside of the main bends.

From an examination of the surface features it is not possible to identify the cause of the surge. There is no obvious relation between the present surge and possible external causes. Other glaciers in the immediate area have not surged so it is not possible to consider any general climatic change, or local seismic activity. The advance can be attributed to changes within the glacier or along the bedrock contact. Photographs taken in 1966 do not show evidence of unusual flooding or any significant changes in the stream channels for the river below the ice front.

The surge is attributed to unstable conditions in the middle zone of the glacier, particularly the main trunk above Hazard Creek. This part of the glacier may have constituted an ice reservoir, with the discharge triggered by the decrease of ice thickness in the downstream area

and facilitated by an increase in water at the ice-bedrock contact.

Acknowledgments

This initial study of the Steele Glacier surge was only possible with the assistance of many individuals. Most information was obtained from aerial photographs ordered for the completion of the National Topographic Series, and base maps compiled by the Surveys and Mapping Branch from photographs taken during the surge. Supplementary information was obtained from photographs by A. S. Post of the United States Geological Survey, M. E. Alford of the Water Survey of Canada, and W. A. Wood of the Arctic Institute of North America. Their generous cooperation is gratefully acknowledged.

References

- Bayrock, L. A. (1967) Catastrophic advance of the Steele Glacier, Yukon, Canada, *Publ. No. 3*, Boreal Inst., Univ. Alberta, 35 pp.
- Dolgushin, L. D., Yevteyev, S. A., Krenke, H. N., Rototayev, K. G., and Svatkov, N. M. (1963) The recent advance of the Medvezhii Glacier, *Priroda*, 11, 85-92.
- Glen, A. R. (1939) The glaciology of North East Land, *Geogr. Ann.*, 21, 1-23.
- Harrison, A. E. (1964) Ice surges of Muldrow Glacier, Alaska, *J. Glaciol.*, 5, 365-368.
- Hattersley-Smith, G. (1964) Rapid advance of glacier in Northern Ellesmere Island, *Nature*, 201, 176.
- Lliboutry, L. A. (1969) Contribution à la théorie des ondes glaciaires, *Can. J. Earth Sci.*, 6, 943-953.
- Moffit, F. H. (1942) Geology of the Gerstle River district, Alaska, *Bull. 926-D*, U.S. Geol. Surv., pp. 146-157.
- Muller, J. E. (1967) Kluane Lake map-area, Yukon Territory, *Mem. 340*, Geol. Surv. Can., 137 pp.
- Paige, R. A. (1965) Advance of Walsh Glacier, *J. Glaciol.*, 5, 876-878.
- Post, A. S. (1960) The exceptional advances of the Muldrow, Black Rapids, and Susitna Glaciers, *J. Geophys. Res.*, 65, 3703-3712.
- Post, A. S. (1966) The recent surge of Walsh Glacier, Yukon and Alaska, *J. Glaciol.*, 6, 375-381.
- Post, A. S. (1967) Walsh Glacier surge, 1966 observations, *J. Glaciol.*, 6, 763-765.
- Robin, G. de Q. (1969) Initiation of glacier surges, *Can. J. Earth Sci.*, 6, 919-928.
- Roots, E. F. (1967) Yukon centennial projects—A variety of survey problems, *Can. Surv.*, 21, 250-259.
- *Sharp, R. P. (1943) Geology of the Wolf Creek area, St. Elias Range, Yukon Territory, Canada, *Bull. Geol. Soc. Am.*, 54, 625-650.
- Sharp, R. P. (1951) Glacial history of Wolf Creek, St. Elias Range, Canada, *J. Geol.*, 59, 97-117.
- Tarr, R. S. (1909) The Yakutat Bay region, Alaska, *Prof. Paper. 64*, U.S. Geol. Surv., pp. 11-144.
- Tarr, R. S., and Martin, L. (1914) *Alaskan Glacier Studies*, Nat. Geogr. Soc., Washington, D. C., 498 pp.
- Weertman, J. (1969) Water lubrication mechanism of glacier surges, *Can. J. Earth Sci.*, 6, 929-942.
- Wood, W. A. (1936) The Wood Yukon expedition of 1935; An experiment in photographic mapping, *Geogr. Rev.*, 26, 228-246.
- Wood, W. A. (1942) The parachuting of expedition supplies, *Geogr. Rev.*, 32, 36-55.
- Wood, W. A. (1963) The Icefield Ranges Research Project, *Geogr. Rev.*, 53, 163-184.

*This report is reprinted in the present volume.

The Ice-Dam, Powder-Flow Theory of Glacier Surge*

Lawrence E. Nielsen †

ABSTRACT. In this theory it is assumed that a stagnant ice block or dam develops in the lower regions of a glacier. Ice gradually builds up above the dam while the dam itself becomes thinner by ablation. Eventually the upper end of the stagnant ice block crumbles from the force of the ice above it, and much of the glacier is changed from a state of compression to one of tension. The breaking of the ice dam results in the glacier rapidly becoming broken into a mass of blocks or powdered ice. The apparent viscosity of the broken-up glacier is much less than that of bulk ice, so high velocities of flow are possible, and a phenomenon similar to a mudflow results. This theory explains why some glaciers repeatedly surge yet appear stagnant between surges. The broken-up appearance of surging glaciers and the delayed surging of tributaries are explained. Additional substantiating observations on several of these phenomena are presented.

Introduction

Recently Nielsen (1968) published a new theory of surging glaciers that explained many of the observed phenomena. A number of calculations were given which indicated the reasonableness of the theory. Figure 1 illustrates the proposed steps in one cycle of a surging glacier. An over-extended glacier develops a stagnant ice dam in its lower regions. As ablation occurs in the stagnant area and excess ice builds up in the upper regions, a point is reached at which the ice fractures and breaks the dam. A state of tension then develops in much of the glacier, which causes it to break into blocks. The broken-up glacier is capable of flowing and sliding much more rapidly than a normal glacier. This theory emphasizes the brittle nature of ice rather than its plastic nature (Nye, 1951, 1952, 1958). The theory also differs in several important aspects from those of Lliboutry (1964, 1965) and Weertman (1962, 1964). Details are given in the above mentioned paper by Nielsen (1968).

Additional Observations

The surging mass of powdered ice has several characteristics not found in normal glaciers, but instead behaves much like a mudflow or a landslide. At the upper end of the broken-up glacier, the blocks can have a backwards rotation as they move forward, similar to the slumping of soil banks (unpublished observations, L. Nielsen). The movement may be quite erratic, and adjacent sections across the glacier may be moving with different velocities (Bayrock, 1966). Such behavior is characteristic of powdered materials, but not of continuous masses. As the glacier advances, its lower end greatly increases in thickness while its upper end becomes much thinner—sometimes as much as a hundred meters. Again, this behavior is characteristic of the flow of concentrated suspensions such as mudflows rather than the flow or sliding of a

single continuous mass as proposed by other theories. Figures 2 and 3, showing the Backe¹ Glacier after it surged, look very much like a giant landslide. The dam for the Backe was the large lateral moraine and the ice of the Rusty¹ Glacier visible in front of the Backe in Fig. 2.

After the main stream of a glacier has surged, it is generally observed that its upper tributaries surge also. For instance, after the Steele Glacier surged in 1966, the Hodgson Glacier (a tributary) and several other smaller tributaries surged in 1967. Figures 4 and 5 show the surging of the Hodgson Glacier into the Steele Glacier in 1967 after the surging Steele had sliced off the Hodgson in 1966. An explanation is as follows: the surging of the main stream greatly lowers its surface, and at the same time the fluidized powder blocks flow easily compared to solid ice. This is like removing a dam from the tributary, so it breaks up and starts to surge as explained above. The broken-up ice of the tributary easily pushes aside the powdered ice of the main stream and so flows far out into the main glacier, cutting across the original flow lines of the main stream. This subsequent surging of the tributaries into the main body of the glacier is the cause of the twisted moraine patterns so typical of surging glaciers (Fig. 6).

After a glacier has surged and the velocity has reduced, the ice blocks soon become converted into a solid mass again by regelation and freezing of meltwater. Normal flow mechanisms then take over, and the easy flow of fractured ice blocks can no longer take place. The stage is now set for a repetition of the whole cycle.

Acknowledgments

The author wishes to express his appreciation to the Icefield Ranges Research Project and to his field companions on this project for making it possible to observe at firsthand the surging glaciers of the Yukon Territory during the summer of 1967. It was gratifying to see how many of the characteristics of the surging Steele, Hodgson,

*This report has previously appeared in the *Canadian Journal of Earth Sciences*, Vol. 6, pp. 955-961 (1969), and is reprinted here with permission.

†Monsanto Company, St. Louis, Missouri

¹The Backe Glacier was formerly unofficially known as the Jackal; the Rusty Glacier was known as the Fox.

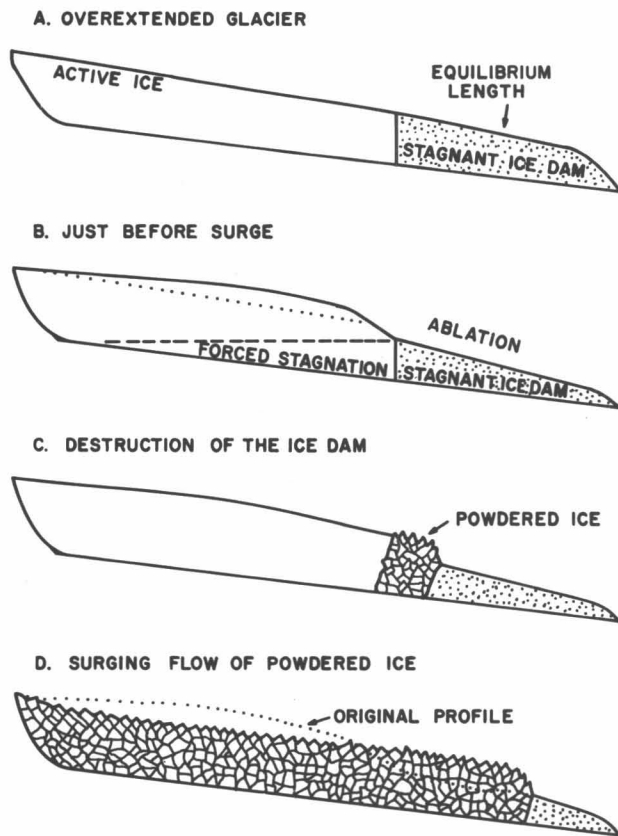


Fig. 1. Schematic diagram of the steps in the cycle of a surging glacier.



Fig. 2. Backe Glacier terminus, Yukon Territory, after it had surged out over the surface of the Rusty Glacier.



Fig. 3. The Backe Glacier after surging. Note the broken, slumped, and sunken appearance of the upper glacier and the towering bulge of the terminal region. The Backe Glacier is approximately one mile in length.



Fig. 4. The junction of the Steele Glacier (left) and Hodgson Glacier (right) in August 1966. The surging Steele has sliced off the Hodgson Glacier, which had not yet surged. (Courtesy of Department of Energy, Mines and Resources, Ottawa, Ontario, Canada.)

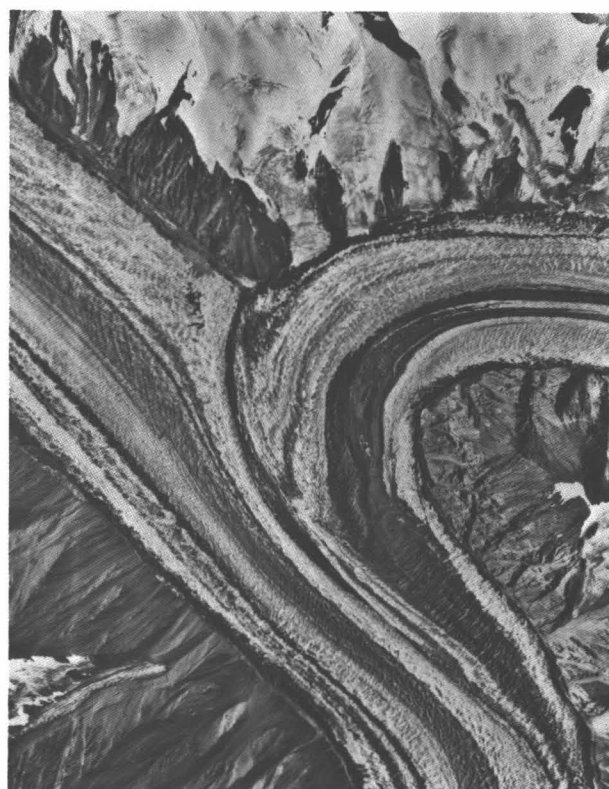


Fig. 5. The junction of the Steele Glacier (left) and Hodgson Glacier (right) in August 1967. The Hodgson is surging out into the powdered main stream of the Steele Glacier and distorting the medial moraines. (Courtesy of Department of Energy, Mines and Resources, Ottawa, Ontario, Canada.)



Fig. 6. The twisted moraine patterns of a glacier which surged, and then later its upper tributaries surged. (Photo of the Susitna Glacier, Alaska, courtesy of Austin S. Post, University of Washington.)

and Backe Glaciers could be understood in terms of the theory presented here. The Icefield Ranges Research Project is jointly sponsored by the Arctic Institute of North America and the American Geographical Society. Special thanks are due Dr. George Rigsby, Mr. Richard Ragle, and Dr. Walter A. Wood.

References

- Bayrock, L. A. (1966) Catastrophic advance of the Steele Glacier, Yukon, Canada, *Publ. No. 3*, Boreal Inst., Univ. Alberta, Edmonton, 35 pp.
- Lliboutry, L. (1964) Sub-glacial "Supercavitation" as a cause of the rapid advances of glaciers, *Nature*, **202**, 77.
- Lliboutry, L. (1965) How glaciers move, *New Sci.*, **28**, 734-736.
- Nielsen, L. E. (1968) Some hypotheses on surging glaciers, *Bull. Geol. Soc. Am.*, **79**, 1195-1201.
- Nye, J. F. (1951) The flow of glaciers and ice-sheets as a problem in plasticity, *Proc. Roy. Soc. London*, **A207**, 554-572.
- Nye, J. F. (1952) The mechanics of glacier flow, *J. Glaciol.*, **2**, 82-93.
- Nye, J. F. (1958) Surges in glaciers, *Nature*, **181**, 1450-1451.
- Weertman, J. (1962) Catastrophic glacier advances, IUGG Symposium at Obergurgl, Assoc. Sci. Hydrol., pp. 31-39.
- Weertman, J. (1964) The theory of glacier sliding, *J. Glaciol.*, **5**, 287-303.

A Two-Year Mass-Balance Study of the Rusty Glacier

1968-1969

Thomas Brewer *

ABSTRACT. The 1968 mass balance is seen to be $+6.0 \times 10^{12}$ g of water, while the 1969 balance is found to be -1.59×10^{12} g. This yields a two-year balance of -0.99×10^{12} g. Statistical examination of the data indicates that this two-year result is reliable to $\pm 44\%$. The distribution of snow in 1968 confirms the presence of a bedrock hump under the ice predicted from gravity measurements. It is speculated that the five-year mass balance (1967-1971) is negative and about 1.0×10^{12} g.

Introduction

Rusty Glacier¹ is a small valley glacier with a known history of glacial surging. It is located approximately 80 km west of Kluane Lake near Steele Glacier (Plate 1).² The center of the accumulation zone of Rusty Glacier has coordinates $61^{\circ}13'N$, $140^{\circ}20'W$. It is found on the Department of Energy, Mines and Resources 1:250,000-scale map sheet entitled *Kluane Lake*. This paper is a report of the mass-balance study carried out on Rusty Glacier during 1968 and 1969. The work is part of an extensive investigation to determine characteristics of the glacier before its next surge.

In so far as possible, the terminology used in this paper is that suggested by Meier (1968) and reprinted in the *Journal of Glaciology* (1969). The general approach is that which Meier calls the fixed-date system. Initially, a stratigraphic system was attempted (Brewer, 1969), but the data taken in the summer of 1969 showed that an elaborate meteorological estimate worked out for the 1967-1968 budget had been ambiguous. Fortunately, sufficient data had been taken during 1967 and 1968 to allow recalculation on a fixed-date basis.

Field Observations

The array of stakes used for measuring ablation and accumulation was initially established in 1967. This array, shown in Figure 1, was used with only minor changes throughout the study. The stakes are 3.17-cm diameter steel tubing implanted with wooden plugs in the bottom to prevent them from melting in (Ostrem and Stanley, 1969). Rusty Glacier is a subpolar glacier (Crossley, 1969; Classen, 1970), so that once stakes are set, they freeze solidly into place almost at once. About once a year, however, replacement of the stakes on the lower part of the

glacier was necessary. When this was done, the stakes were kept in their original location, except where a short displacement was dictated by obstructions. Careful notes were kept of the date and magnitude of all displacements, resettings, and extensions.

Three sorts of measurements were taken. These were (1) ablation or accumulation of snow; (2) snow densities; and (3) ice densities. All measurements were made during the summer field seasons only.

The ablation and accumulation measurements were made weekly; readings were to the nearest centimeter. Snow-probe measurements were made to establish the thickness of the 1967-1968 snowpack. The summer surfaces determined this way are in agreement with those indicated by stratigraphic markers (copper screens) placed at the end of 1967, and again in 1968. Using a stratigraphic surface to define the base of the annual snow accumulation is permissible here even though this is a fixed-date study since in both years the entire snow pack accumulated after the fixed date of August 15.

In pits dug down to the 1967 horizon, snow densities were determined by using the standard CRREL snow-density kit. Samples were taken horizontally rather than vertically because layers and lenses of ice made vertical sampling difficult and unreliable. Total thickness of ice apparent on the wall of the pit was recorded so that a correction for total accumulation could be made. Samples of ice were weighed on an Ohaus triple-beam balance (± 0.1 g), and volumes were calculated by measuring the displacement of the sample in a specially constructed $0^{\circ}C$ bath (Fig. 2). After immersion of the ice sample the change in level of the liquid was measured to 0.05 mm with a vernier caliper.

Since Rusty Glacier is subpolar, superimposed ice can form. In 1968, a detailed reconnaissance was conducted to look for significant areas of superimposed ice. In the flat region on the upper glacier around Stake 32, about 25 cm of ice had formed on top of the 1967 stratigraphic markers. The region where this ice formed is evident as a

*Research Associate, Department of Geology, Boston University

¹Rusty Glacier was formerly unofficially known as Fox Glacier.

²Plate 1 is a map on the inside back cover of this volume.

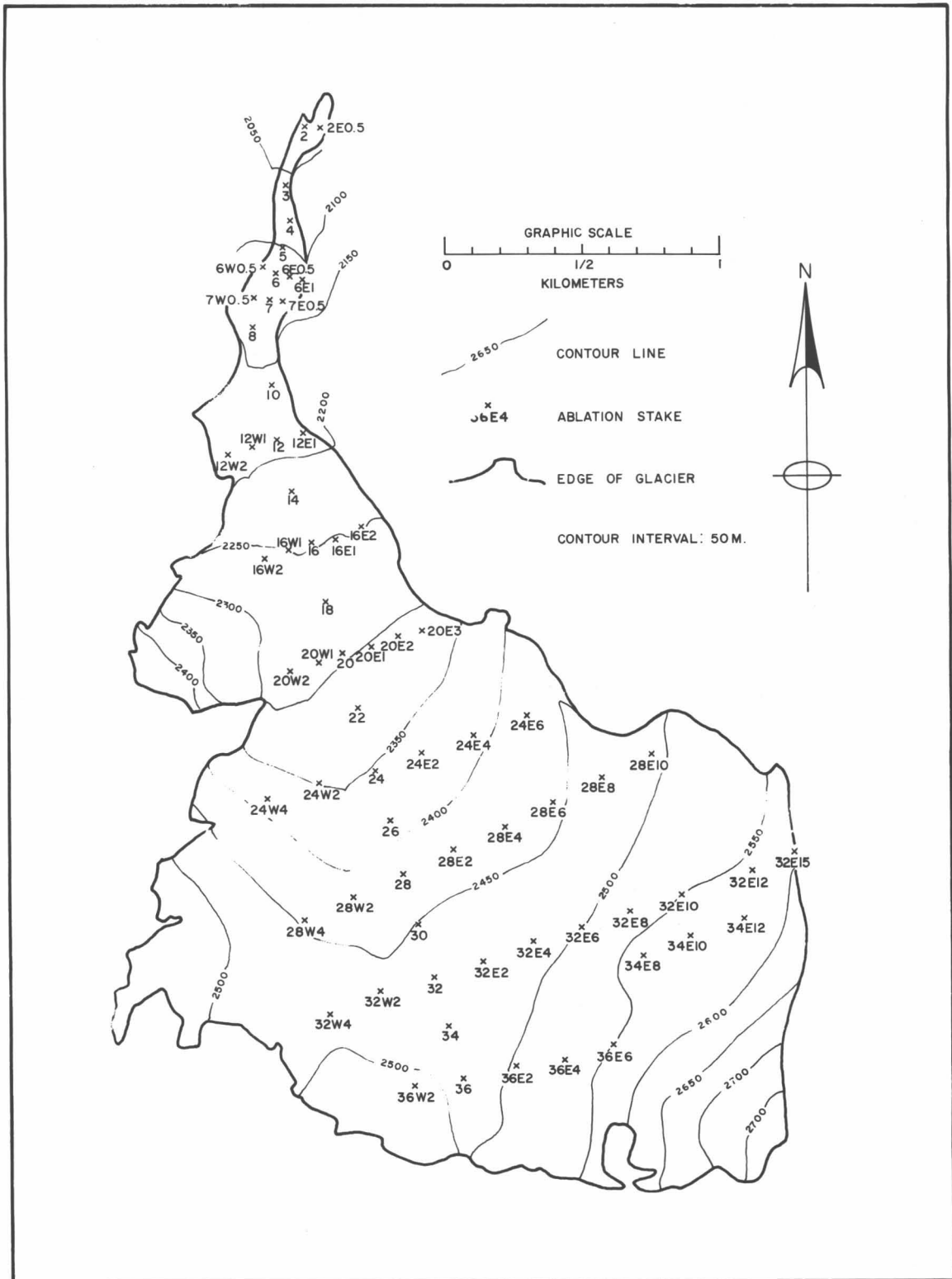


Fig. 1. Topographic map of Rusty Glacier. Locations of ablation stakes are shown.

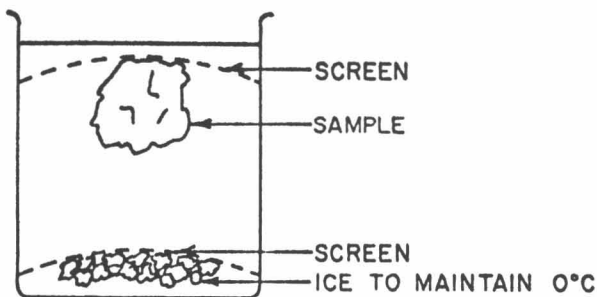


Fig. 2. Diagram of density-measuring device.

medium gray region slightly to the west of the glacier's center line on the 1967 air photo (Fig. 3). The calculated water equivalent value of this ice is 0.04×10^{12} g. This has been added to the 1968 accumulation. No superimposed ice was noted in 1969, probably because of improved drainage in the early spring.

Calculations

Since this is a fixed-date study, it is not possible to report net winter and summer ablation and accumulation (Meier, 1969). For ease in calculation, however, it is desirable to separate events taking place during the field season from those that occur in the winter. Therefore the following four categories of ablation and accumulation were determined for each of the two years:

- (1) Remnant winter accumulation: any snow and firn accumulation remaining from precipitation which occurs in the interval between the last day of measurement of one summer field season and the first day of the next.
- (2) Apparent winter ablation: material which disappears during the interval of (1), which was there at the end of the preceding field season.
- (3) Remnant summer accumulation: any accumulation on the glacier which is present on the last day

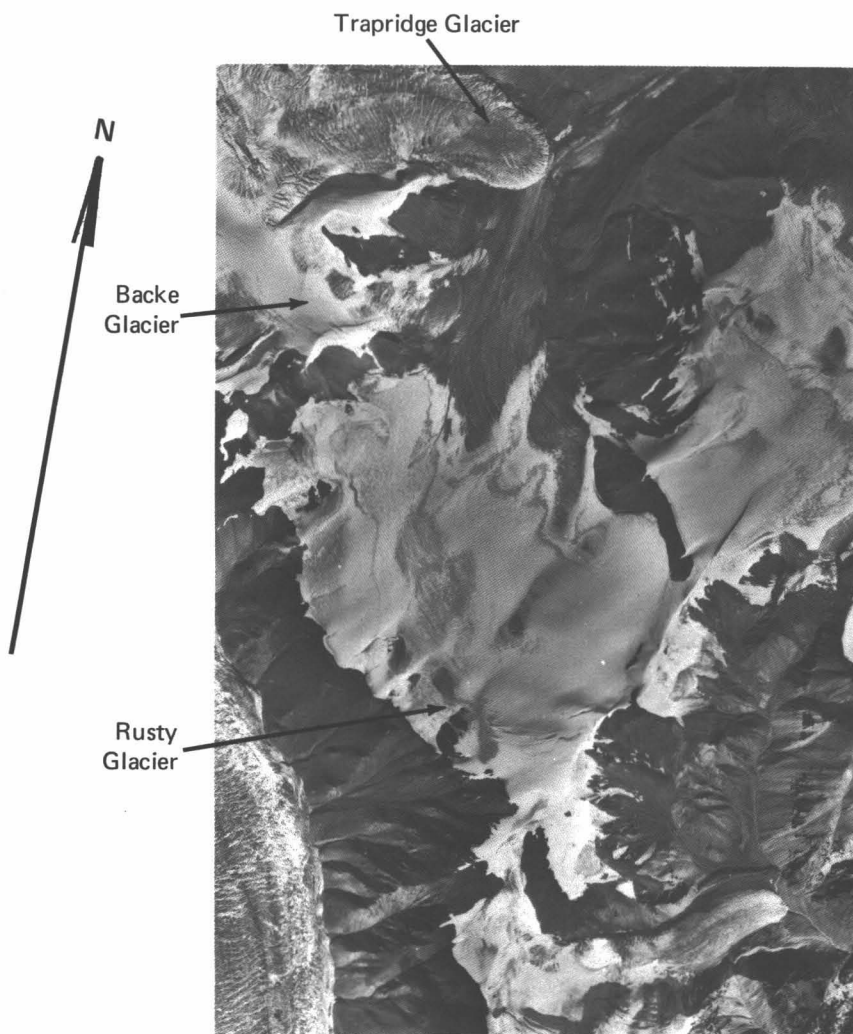


Fig. 3. Aerial photo of Rusty Glacier. Lateral moraines near the terminus are the result of a considerable amount of ablation. (Courtesy of National Air Photo Library, Surveys and Mapping Branch, Department of Energy, Mines and Resources, Ottawa. Photo No. A 20128-28.)

of the field season which was not there on the first day of measurement.

- (4) Apparent summer ablation: material which disappears during the interval of (3), which was there at the start of the interval.

The last day of measurement of the field season is the fixed date—August 15.

Remnant accumulation for the first winter (1967–1968) was determined in the following manner: (1) constructing a detailed isopach map of the 1968 snowpack (Fig. 4); (2) computing the end of summer volume represented on the isopach map. Frustrums of cones were used to approximate isopach “hills”; (3) converting this volume to water-equivalent mass; and (4) adding to this end-of-season value the amount of 1967–1968 snow which ablated during the summer to establish the amount which had been present at the beginning of summer.

The other three categories of accumulation and ablation for 1967–1968 and all four categories for 1968–1969 were determined by the following relationships:

$$\text{Accumulation (C)} = \sum_{\text{over all points}} \left(\text{Accumulation at a point (c)} \right) \times \left(\text{Area attributable to that point} \right) \times \left(\text{appropriate density} \right)$$

$$\text{Ablation (A)} = \sum_{\text{over all points}} \left(\text{Ablation at a point (a)} \right) \times \left(\text{Area attributable to that point} \right) \times \left(\text{appropriate density} \right)$$

The area attributable to each point was established by field reconnaissance and examination of aerial photographs. It was measured with a polar planimeter on a 1:10,000 topographic map of Rusty Glacier which was drawn by the Department of Energy, Mines and Resources (Canada) from 1967 air photos. The annual balance was computed on August 15 since the field party generally left the glacier at about this time. Snow ablation rates determined by measurements throughout the summer were used to extrapolate final readings in the few cases when they were taken before August 15.

In most mass-balance studies of this sort, it is necessary to add a correction for movement of the ice. On Rusty Glacier the movement has been very small, only about 3 to 4 m a year (Collins, 1972), so no correction of this sort was applied.

The 1967–1968 mass balance was computed by determining the mass of the 1968 snowpack at the end of the season (August 15, 1968) from the isopach map (Fig. 4) and deducting the 1967–1968 winter ablation and the 1968 summer ablation of pre-1968 firn and ice.

When the field party reached the glacier in June of 1969, virtually all the 1968–1969 winter accumulation

had vanished. By mid-July, only traces of it remained. Therefore, no 1968–1969 isopach accumulation map was constructed. The 1969 mass balance is found to be the sum (with due regard to sign) of a small summer accumulation and winter and summer apparent ablations for the year. The two-year balance is simply the sum of the balances for each of the two years.

Error Study

It has been the observation of this author that few, if any, mass-balance studies include an estimate of the reliability of the final value. Such an estimate is readily performed, and has been completed for this study.

Because of the natural variability of density, accumulation, and ablation, there is always uncertainty as to how close to the “true” value of these quantities a calculated value lies. As a result, there is an uncertainty in the mass-balance which is calculated from these values. By computing standard errors for values with significant uncertainty, an estimate can be made at a given confi-

dence level as to the size of the uncertainty in the mass balance (Koch and Link, 1970; Arkin and Coulton, 1939).

Preliminary analysis in this study showed that the variability and number of measurements of ablation and accumulation implied that these factors had about four times more effect on the precision of the study than anything else. Based on the accumulation and ablation variabilities, confidence intervals were constructed for the quantities leading to the two-year mass balance, and finally for the two-year balance. A confidence level of 99.4% was used. These limits are reported in Table 1, column 4, as percentage errors.

Results and Discussion

The results of this study are summarized in Table 1. Some of the water-equivalent values stated in column 3 are the sums of two or three quantities which were calculated separately. The materials measured to produce these figures are given in column 5. The snow-density values are based on snow pit data collected as indicated in Table 2.

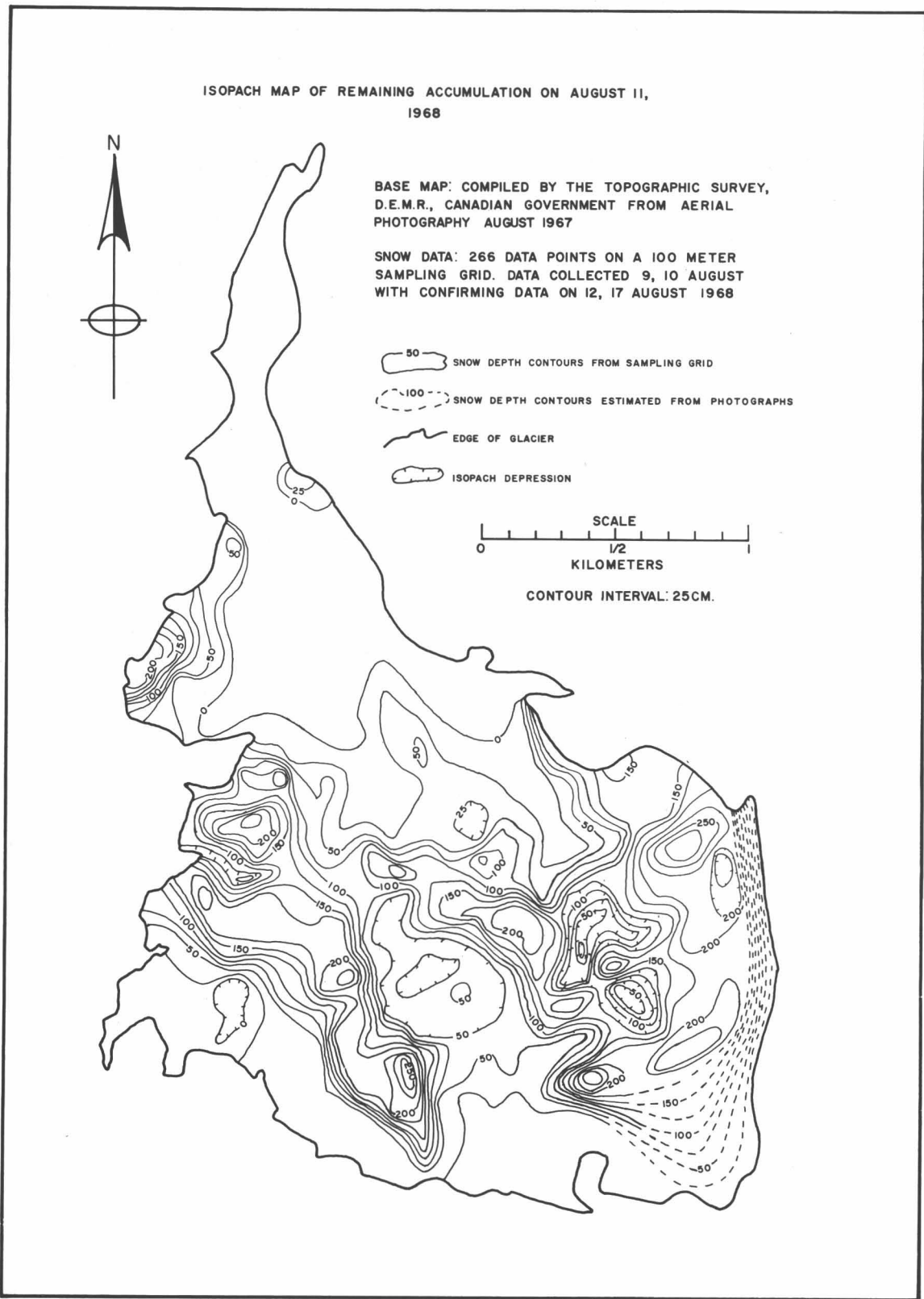


Fig. 4. Snow depths on Rusty Glacier on August 11, 1968 (1967-1968 accumulation).

TABLE 1. Results of the 1968-1970 Rusty Glacier Mass-Balance Study

Date	Calculated values			Measured accumulation or ablation								
	Name of calculated value	Value H ₂ O (g)	Error ¹	No. of stations	Type of reading	Range of readings ²				Average readings		Density
							ΔH (cm)	H ₂ O (g)	Station No.	ΔH (cm)	H ₂ O (g)	
Aug. 15, 1967	Arbitrary zero											
June 28, 1968	Remnant winter accumulation ³	2.51 × 10 ¹²	8%	32 266	Abln. rate ³ Isopach map	min max	0 300	0 120	2 36E6	58	28	0.49
	Apparent winter ablation	-0.53 × 10 ¹²	32%	45	Old ice ablation	max min	70 0	63 0	2E5 28E8	23	21	0.90
				20	1967 snow ablation	max min	101 17	47 8	28W4 36W4	36	17	0.47
Aug. 15, 1968	Remnant summer accumulation	0										
	Apparent summer ablation	-1.37 × 10 ¹²	16%	26	Old ice ablation	max min	199 0	179 0	3 22	108	97	0.89
				32	1968 snow ablation	max min	98 36	49 18	24 36	58	28	0.49
	1968 mass balance	0.60 × 10 ¹²	32% = 0.342 × 10 ¹² g									
June 23, 1969	Remnant winter accumulation	0.13 × 10 ¹²	44%	10	1969 snow accumulation	max min	30 7	14 3	36E4 28W4	21	10	0.47
	Apparent winter ablation	-0.98 × 10 ¹²	15%	34	1968 snow ablation	max min	55 13	29 7	28E10 24W4	27	14	0.51
				41	Old ice ablation	max min	120 7	108 6	2 20E3	59	53	0.90
Aug. 15, 1969	Remnant summer accumulation	0.28 × 10 ¹²	20%	35	1969 snow accumulation	max min	70 7	14 6	32E10 20E2	42	8	0.19
	Apparent summer ablation	-1.02 × 10 ¹²	15%	10	1969 snow ablation	max min	30 7	14 3	36E4 28W4	21	10	0.47
				34	1968 snow ablation	max min	48 0	25 0	24E6 34E12	17	9	0.59
				29	Old ice ablation	max min	163 0	147 0	4 24	110	99	0.90
	1969 mass balance	-1.59 × 10 ¹²	15% = 0.215 × 10 ¹² g									
	Two-year mass balance	-0.99 × 10 ¹²	41% = 0.40 × 10 ¹² g									

¹ According to the statistical methods used, there is a 99.4% probability that the values of column 3 are representative of the true values within the stated percentage limits in column 4.

² Maximum and minimum values are given for the accumulations and ablations listed in columns 5 and 6 for the time intervals listed in columns 1 and 2; the stations where extremes were found are designated. This information is included as a measure of the dispersion of the data.

³ Ablation rates at permanent ablation stakes were used to determine the remnant winter accumulation from the snow mass indicated at the end of the summer season on the isopach map. This information is only needed for comparative purposes, and contrasts strongly with the 1969 remnant winter accumulation.

ΔH is the recorded difference at stakes.

H₂O is the water equivalent.

TABLE 2. Origin of Calculated Densities

Year	Observer	No. of snow pits	No. of readings
1967	Steinke	15	62
1968	Brewer	10	108
1969	Brewer and Griggs	9	66

It is apparent that the mass of the glacier decreased considerably during the two-year period of the studies. The two-year mass balance is -0.99×10^{12} g of water $\pm 0.40 \times 10^{12}$ g.

Observations of the terminus also indicate wastage. In 1969 subglacial bedrock was visible at Stake 7 in streams incised through the ice. During the period from the time of the 1967 observations until Rusty Glacier was visited in 1971 (S. G. Collins, personal communication) the terminus receded several hundred meters and the entire lower tongue was stagnant and very thin.

A rough estimate of mass balance over a longer period of time can be made by comparing the position of the transient snow line in other years with its position in 1968 and 1969. Data taken in 1967 (Steinke, 1968) indicate that the transient snow line for 1966–1967 had receded to about Stake Row 28 at the end of the season,

about 3 rows farther up the glacier than the snow line a year later. According to S. G. Collins (personal communication, 1971) 1970 was a year of heavy accumulation in which the transient snow line had not receded past Stake Row 12 when the field party left in August. In 1971, however, virtually all the 1970–1971 snow cover melted off as it did in 1969, indicating a considerable deficit. It is therefore estimated that over the five-year period from 1966 to 1971 the glacier has a mass-balance deficit of approximately 1×10^{12} g.

Figure 5 is a longitudinal profile of the snow distribution on Rusty Glacier combined with a topographic profile along the same line. It is of some interest that the snow depth on the flat top of the well-defined hump in the upper accumulation zone is a region of minimum snow accumulation. This tends to support Crossley's and Clarke's (1970) conclusion that the hump overlies a bedrock projection. The leading edge of the hump unexpectedly seems to be a region of maximum snow accumulation. It appears in general that regions of maximum snow depths occur in topographic pockets.

An important aspect of the study is the estimation of errors in the computed mass-balance value. It appears that the possible ranges of values computed are considerably greater than most others imply when reporting mass balance to two significant figures without qualification. It should be realized, however, that the estimated errors in the present study might be reduced by a factor of two if a lower confidence level were used.

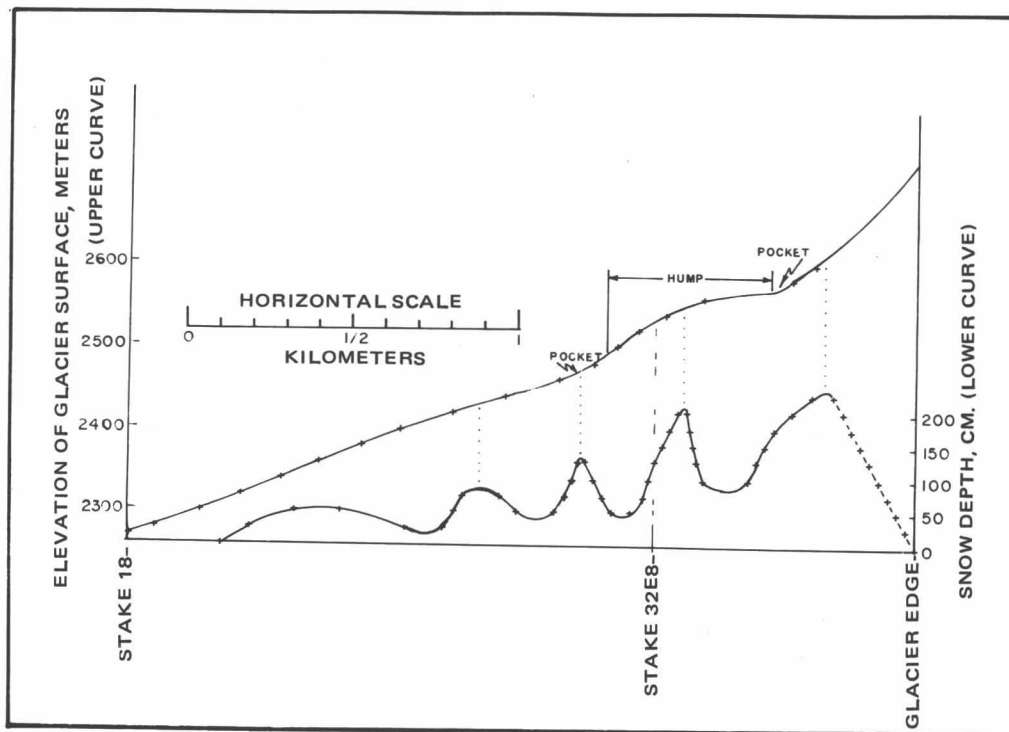


Fig. 5. Longitudinal profile of Rusty Glacier with 1967-1968 snow accumulation curve superimposed.

Acknowledgments

Several people deserve special thanks for their help in this study. Richard Ragle, Senior Scientist of the Arctic Institute of North America, was most helpful in finding financial support. Dr. Melvin Marcus offered many helpful suggestions in the summer of 1968. Vibjurn Karlen was responsible for setting out the array of ablation stakes in the summer of 1967.

A very successful (and inexpensive) ice drill for setting stakes in a subpolar glacier was designed by S. G. Collins for use during the latter half of the study. Ted Steinke's (1968) carefully recorded measurements, summarized in a report to the Arctic Institute, made the 1967-1968 winter calculations possible. Tom Griggs, my very capable field assistant in 1969, made about one-half of the ablation measurements that year. A preliminary report of the 1968 mass-balance study (Brewer, 1969) was prepared as partial fulfillment of the requirements for the A. M. degree in Geology at Boston University. Dr. D. W. Caldwell and Dr. M. A. Gheith of that institution were particularly helpful while the study was being completed.

References

- Arkin, J., and Coulton, R. (1957) *Statistical Methods*, Barnes and Noble, New York, pp. 113-124 (4th ed.).
- Brewer, T. (1969) A mass balance study of "Fox Glacier," Yukon Territory, Canada, A. M. thesis, Boston Univ., Boston, 43 pp. (unpubl.).
- Classen, D. (1970) Thermal drilling and deep-ice temperature measurements on the "Fox Glacier," Yukon, M. Sc. thesis, Univ. British Columbia, Vancouver, 66 pp. (unpubl.).
- Collins, S. G. (1972) Survey of the Rusty Glacier area, Yukon Territory, 1967 through 1970, *J. Glaciol.* (in press).
- Crossley, D. J. (1969) Gravity and temperature measurements on the "Fox Glacier," Yukon, M. Sc. thesis, Univ. British Columbia, Vancouver, 81 pp. (unpubl.).
- Crossley, D. J., and Clarke, G. K. C. (1970) Gravity measurements on "Fox Glacier," Yukon Territory, Canada, *J. Glaciol.*, 9, 363-374.
- Journal of Glaciology* (1969) Mass-balance terms, 8, 3-7.
- Koch, G. S., and Link, R. F. (1970) *Statistical Analysis of Geological Data*, Wiley, New York, 375 pp.
- Meier, M. (1968) Combined heat, ice, and water balances at selected glacier basins; A guide to measurement and data compilation, *Tech. Paper Hydrol.*, UNESCO.
- Ostrem, G., and Stanley, A. (1969) *Glacier Mass-Balance Measurements; A Guide*, Can. Dept. Energy, Mines Res., Ottawa, pp. 12-17.
- Steinke, T. (1968) "Fox Glacier" study, 1967, data report submitted to Arctic Inst. North Am., 94 pp. (unpubl.).

Hydrological Study of the Rusty Glacier

Theodorik Faber*

ABSTRACT. The Rusty Glacier—considered to be in a presurge phase—and two other glaciers, the Trapridge and the Backe, occupy a common basin in the St. Elias Mountains. Hydrological data from the basin as a whole and from each of the individual glaciers were gathered during the period July 9–August 15, 1968. During this period the total discharge from the basin was 6.9×10^6 m³. Rusty Glacier contributed 24% of this discharge; the other two glaciers together contributed 52%, and the ice-free part of the basin contributed 12%. Since the Rusty Glacier occupies 36% of the total area of the basin, the Backe and the Trapridge 52% together, and the remainder of the basin 12%, the contribution of the Rusty Glacier to the total discharge is distinctly lower than that of the other glaciers. The low discharge from the Rusty Glacier is in accordance with the expectation that this glacier will surge. Statistical formulas are given for the relationship of discharge to temperature and to precipitation. Measurements showed that the calcium content of both the water and its suspended sediment in the discharge near the exit of the basin is mainly due to the calcium content of the discharge from a Trapridge Glacier stream which flows across moraine containing limestone fragments. Evidence is presented for the presence of magnesium-bearing rock in the area of one of the streams on the Backe Glacier.

Introduction

The Rusty Glacier is situated between the Steele Glacier, 6 km to the east, and the Canada–United States border, 36 km to the west. The nearest settlement is Burwash Landing, 70 km to the east-northeast (Plate 1).¹

In the same basin as the Rusty Glacier are the Backe and Trapridge Glaciers (Fig. 1). The maximum length of the entire basin is 5.5 km, in a north-south direction; the maximum width is 5 km, in an east-west direction. Elevations within the basin range from 1800 to 3000 m. Within the basin, ice-cored moraine occurs; bedrock is exposed at only a few isolated spots. The meltwater of the three glaciers drains by a complex system to Rusty Creek,² which runs from the terminus of the Rusty Glacier to the northern end of the glacial basin where it joins Hazard Creek. The latter drains via Steele Creek to the Donjek and White Rivers and finally into the Yukon River.

Purpose of the Investigation

The Rusty Glacier is considered to be in a presurge phase. Since the mechanism for the surge of a glacier is not completely understood, it is important to gather data prior to an anticipated surge for comparison with post-surge data. Hydrological data pertinent to the problem include total discharge from the basin and discharge from each of the three glaciers in the basin. Also of

interest are the chemical characteristics of the discharge and the amount of sediment transported.

Prior Investigations

In 1967 a hydrologist accompanying a glaciological party from the Glaciology Subdivision of the Department of Energy, Mines and Resources (Canada) made a brief survey of the hydrological conditions in the basin. The total outflow from the basin was determined by using data from a water-level recorder operating on Rusty Creek from July 19 to August 19. Other measurements permitted estimates of the quantities of water discharged from each of the glaciers in the basin. The relative amounts from each area studied are given in Table 1.

Methods and Instruments Used in 1968

Since a detailed map of the area was not available, distances and areas in the basin were measured on an enlarged aerial photograph (No. A20128-829 of the Department of Energy, Mines and Resources). The scale of the enlargement was 1:10,000 near the Rusty I water-level recorder (Fig. 2). Since distances and areas used in this discussion are based on that scale, they are only approximate.

Discharge measurements. Most of the streams in the basin lacked any form of control, so water-level recorders could not be installed on them. Near the exit of Rusty Creek from the basin, however, the control (as defined by Grover and Harrington, 1966) was provided by the reach of the channel itself. It was here that the Rusty I water-level recorder was installed (Fig. 3). At this site a

*Instituut voor Aardwetenschappen, Vrije Universiteit, Amsterdam, The Netherlands

¹Plate 1 is a map inside the back cover of this volume.

²Unofficial name



Fig. 1. Rusty Glacier Basin looking south; (a) = Rusty Glacier, (b) = Backe Glacier, (c) = Trapridge Glacier. Foreground left and mid: Rusty Creek. Foreground right: Trapridge stream A.

good rating curve was obtained (Fig. 4) which permitted computation of daily discharges at Rusty I and at other points in the basin.

To establish the relative contribution of a stream somewhere in the basin to the total outflow from the basin, the following procedure was adopted:

- (1) The time of travel, T_x , of the water from the point of observation, x , to the Rusty I water-level recorder was measured by means of dye.
- (2) The amount of water, Q_{xt} , passing the point of

observation at a time, t , was measured by means of a current velocity meter.

- (3) The amount of water, $Q_F(t+T_x)$, passing the site of the Rusty I water-level recorder during the period between the time of observation at point x and the time of arrival at Rusty I water-level recorder was computed from the stage recording and the rating curve (Fig. 4).
- (4) The measured amount of water, Q_{xt} , at the observation point, x , was expressed as the percentage of the discharge, $Q_F(t+T_x)$ at Rusty I water-level recorder, so

$$\text{contribution (C)} = \frac{Q_{xt}}{Q_F(t+T_x)} \cdot 100$$

TABLE 1. Contributions to Total Discharge from the Basin—July 19 to August 19, 1967 (A. Stanley and J. Plommer, personal communication)

Meltwater stream ¹	% of total discharge
Trapridge A	20
Trapridge B	3
Trapridge C	4
Trapridge D	12
Total Trapridge	39
Backe A	22
Backe B	7
Total Backe	29
Rusty	25
Heidi	7
Rusty I water-level recorder	100%

¹ See Figure 2.

A Leopold and Stevens horizontal drum recorder with a 7-day clock was used at the Rusty I station for recording water level. The current velocity used in determining discharge in the basin was measured with a small Price current meter last calibrated on January 5, 1968. Current measurements were obtained by suspending the meter from a rod and wading into the stream (Fig. 5).

Chemical characteristics. Samples were taken from several glacial streams for chemical analysis. Hardness, Ca^{++} , and alkalinity were determined in a field laboratory according to methods described by Goedendorp (personal communication) and Hem (1970). At the sampling site, electrical conductivity and pH were measured by means of portable equipment similar to that described by Dekker and Faber (1969).

Sediment transport. The measurement of suspended

sediment transport was carried out according to the method described by Hinrich (1965). The treatment of the samples was in accordance with the findings con-

cerning the influence of temperature on CaCO_3 content described by Engelen (1968).

There was an attempt to measure the bedload transport at the site of the Rusty I water-level recorder, but the sediment proved to be too fine for the quarter-mesh basket sampler used.

Meteorological measurements. Ambient air temperatures were measured 200 m downstream from Rusty I water-level recorder by a Lambrecht thermo-hygrograph installed in a Stevenson screen 2 m above the surface; maximum and minimum thermometers were read daily.

Precipitation was measured on the Rusty Glacier by the glaciologists camped there. This was the only location in the basin where precipitation was measured since the rain gauges for the hydrologists did not arrive.

Results

Discharge of water-level recorder. A curve of discharge as a function of water depth was computed from the results of 33 discharge measurements ranging from a minimum of 790 liters/sec to a maximum of 4300 liters/sec (Fig. 4). The computation assumed a double logarithmic regression. For the Rusty I water-level recorder, the equation used was:

$$Q = 316 h^{3.667}$$

where Q = discharge in liters/sec and h = water depth in feet above zero discharge level. The correlation coefficient was found to be 0.983.

Daily discharge at Rusty I was derived from the water-level records and the computed relationship between discharge and water depth. Table 2 gives mean, minimum, and maximum daily discharge values and total discharge for the periods of operation. Difference between discharge varies by only 10% from 1967 to 1968.

To determine whether mean, minimum, and maximum daily discharges show any obvious trends, 7-day running averages were plotted (Fig. 6). All curves show a distinct peak on July 26.

Relationship between discharge, precipitation, and temperature. The sources of run-off in the basin are meltwater from the glaciers and rain at temperatures above 0°C ; very little water infiltrates the glaciers and ice-cored moraines because of their low permeability.

The area of the basin is 17 km^2 , so that 1 mm of rain amounts to $1.7 \times 10^4 \text{ m}^3$. Assuming no evaporation, 1 mm of rain per day corresponds to 197 liters/sec of discharge. Total rainfall measured on the Rusty Glacier was 75.6 mm in 38 days, or an average of 1.98 mm/day. This would amount to a discharge of 390 liters/sec due to rain, which is 18.6% of the total mean daily discharge of 2100 liters/sec.

Daily discharge due to meltwater was computed as the discharge of the day minus half the sum of the

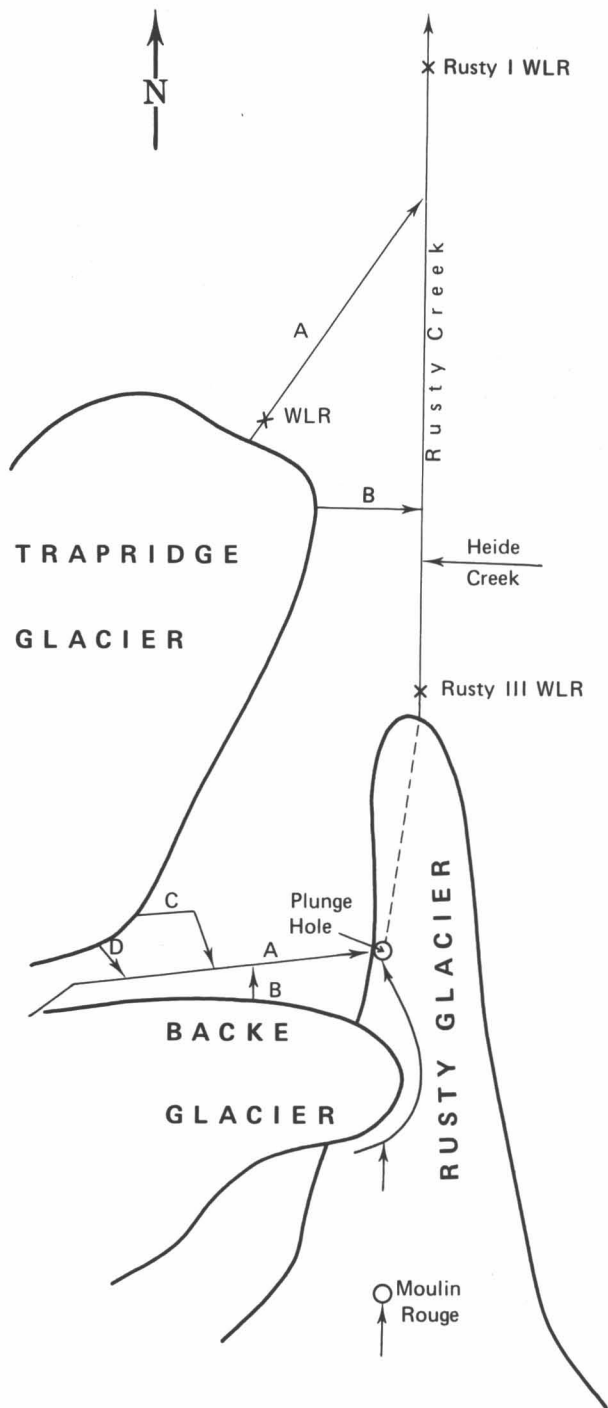


Fig. 2. Schematic diagram showing locations of streams and observation sites. WLR = water-level recorder.



Fig. 3. Rusty I water-level recorder and the reach of Rusty Creek to the north of it.

discharges due to rain on that day and the previous day. That is

$$Q_{md} = Q_d - \frac{1}{2}(Q_{Rd} + Q_{Rd-1})$$

where Q_m = discharge due to meltwater, in liters/sec
 Q_R = discharge due to rain, in liters/sec
 Q = total discharge in liters/sec
 d = the day of the discharge
 $d-n$ = the n^{th} day previous to the discharge day.

Over the period of July 10-August 15, 1968, the daily mean discharges due to meltwater were summed per day

$$\sum_{d=d}^{d=n} Q_{md} = Q_{md} + Q_{md-1} + \dots + Q_{md-n}$$

Over the same period the mean daily temperatures (T in $^{\circ}\text{C}$) were summed in the same manner. The relation between

$$\sum_{d=d}^{d=n} Q_{md} \text{ and } \sum_{d=d}^{d=n} T_d$$

was computed as the linear regression of values Q_m on values of T . This relation is

$$\sum_{d=d}^{d=n} Q_{md} = 331 \left(\sum_{d=d}^{d=n} T_d \right) + 435 \quad (1)$$

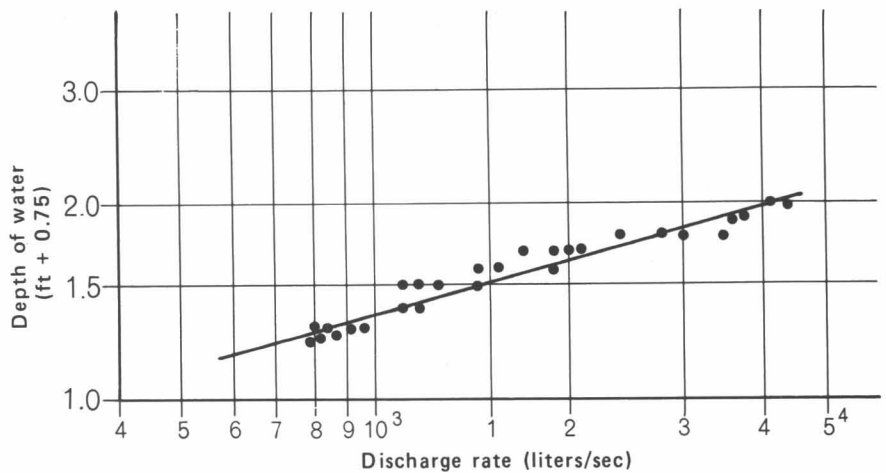


Fig. 4. Relationship of discharge rate to water depth at Rusty I water-level recorder.



Fig. 5. Current measurement at the site of Rusty I water-level recorder.

In the same way the relations between the total discharge, the precipitation, and the temperature were computed. These relations are

for total discharge and rain (R) in millimeters

$$\sum_{d=d}^{d=n} Q_d = 833 \left(\sum_{d=d}^{d=n} R_d \right) - 4101 \quad (2)$$

and for total discharge and temperature (T) in °C

$$\sum_{d=d}^{d=n} Q_d = 400 \left(\sum_{d=d}^{d=n} T_d \right) + 688 \quad (3)$$

With the above-mentioned relations it is possible to compute the discharge at the site of Rusty I water-level recorder from precipitation measured on the Rusty Glacier and from ambient air temperatures measured at 2 m above the ground near the site of Rusty I water-level recorder. For all computations, $n = 37$. Correlation coefficients were: 0.993 for equation 1, 0.967 for equation 2, and 0.994 for equation 3.

Discharge contributed by each of the elements of the basin. The contributions of each of the glaciers in the

TABLE 2. Mean and Extreme Values of Daily Discharge

	1967 July 19–August 19 (m ³)	1968 July 9–August 15 (m ³)
mean	2.0 × 10 ⁵	1.8 × 10 ⁵
minimum	1.1 × 10 ⁵	0.78 × 10 ⁵
maximum	3.1 × 10 ⁵	2.6 × 10 ⁵
Total for period	60 × 10 ⁵ (30 days) 76 × 10 ⁵ (extrapolated to 38 days)	69 × 10 ⁵ (38 days)

basin and of the snow-free regions were computed according to the method outlined earlier. The results are given in Table 3. More detailed data for 1968 are given in Table 4. The 4% variation between the total for 1967 and that for 1968 is well within the limits of accuracy of the methods used. In 1967 no estimate was made for discharge from the ice-cored moraines.

Chemical analysis. The results of the chemical analyses of water taken from the streams in the basin are given in Table 5. The values in this table are the mean values of all samples from a given location. Table 6 gives the total dissolved solids measured; sampling locations on each glacier are listed according to increasing distance the water has traveled over ice or moraine. It is apparent that the total amount of dissolved solids increases with distance. The increase is greater when the water flows through morainal material than when it flows over ice.

The Ca⁺⁺ and Mg⁺⁺ contents and the Ca/Mg ratios for the water samples from various localities are given in Table 6. Four groups can be distinguished according to the value of Ca + Mg:

- (1) Stagnant meltwater: (Ca + Mg) < 2.0
- (2) Water on the ice or near the border of the ice: 2.0 < (Ca + Mg) < 9.1
- (3) Water in contact with morainal material with: 9.1 < (Ca + Mg) < 15
- (4) Water in contact with morainal material with: (Ca + Mg) > 15

When we look at the ratio (Ca/Mg) we can distinguish three groups:

- (1) A group with (Ca/Mg) > 2.50
- (2) A group with 1.00 < (Ca/Mg) < 2.50
- (3) One sample with Ca/Mg = 0.72

Group 1 consists of two components. The first is water on or near the ice with a chemical composition that still resembles that of precipitation; that is, Ca/Mg high through lack of Mg, and Ca + Mg low (< 9.1). (In precipitation Ca⁺⁺ = 1.4 ppm and Mg⁺⁺ = < 0.1 ppm so Ca/Mg > 14.) The second component of Group 1 is water from Trapridge location A which is rich in both Ca⁺⁺ and Mg⁺⁺. The ratio

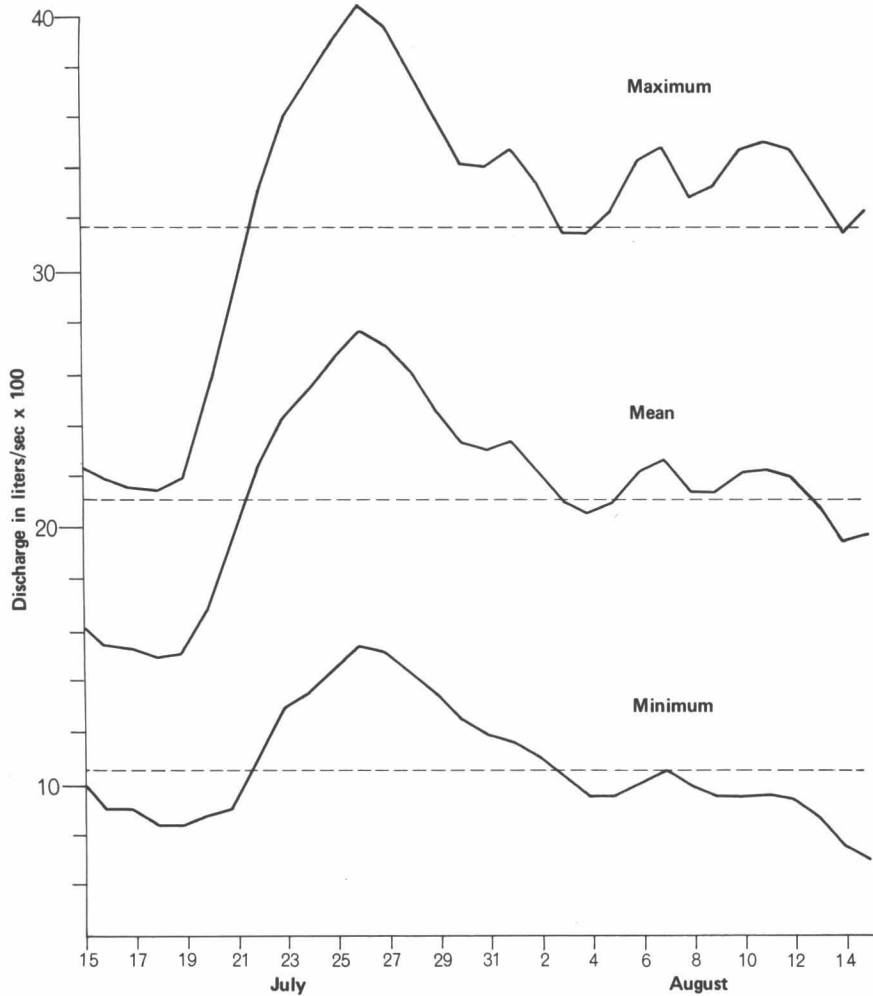


Fig. 6. Seven-day running averages of maximum, mean, and minimum discharge (Q) values.

of Ca/Mg may represent the ratio of Ca/Mg in the rock fragments from which the Ca^{++} and Mg^{++} are derived.

Group 2 represents water in contact with the "normal" morainal material in the basin. From this material, which consists of a mixture of tuff, igneous rock, and limestone particles, the water dissolves both Ca^{++} and Mg^{++} . The

lower Ca/Mg ratio shows that Mg^{++} is relatively preferred over Ca^{++} . "Group" 3, a single sample from Backe stream A (Fig. 2), shows that dolomitic limestone or an amount of ferro-manganese minerals is exposed to contact with the water. The presence and/or the nature of the supplier of the magnesium have not been ascertained in the field. According to Muller (1967), however, magnesium-bearing rocks do occur in the area.

Summarizing the results of the divisions in groups according to Ca + Mg content and to Ca/Mg ratio, we can discern four groups of water:

(1) Water on or near the ice. This water resembles in its high Ca/Mg ratio (5.27) and its low content of Ca + Mg (6.9 ppm) the character of the precipitation it is derived from.

(2) Water in contact with the "normal" moraine material. This water has a ratio of Ca/Mg of 1.45 and a content of Ca + Mg of 12.5 ppm.

(3) Water in contact with moraine material containing considerable amounts of calcareous rock or in contact

TABLE 3. Amounts of Discharge

Source	1967 ¹ (% of total)	1968 (% of total)
Backe	29	29
Trapridge	39	48
Rusty	25	24
Ice-cored moraines	---	2
Heidi Creek	7	1
Total	100%	104%

¹ From Table 1.

TABLE 4. Contributions to Total Discharge from the Basin July 9–August 15, 1968

Meltwater stream ¹	% of total discharge
Trapridge A	35
Trapridge B	7
Trapridge C	3
Trapridge D	3
Total Trapridge	48
Backe A	10
Backe B	4
Backe front	12
Backe S. side	3
Total Backe	29
Rusty	24
Total discharge from glaciers	101
Heidi Creek	1
Ice-cored moraines	2
Total discharge at basin outlet	104

¹ See Figure 2.

with calcareous rock *in situ*. This water has a content of Ca + Mg of 22.6 ppm and a ratio of Ca/Mg of 1.97. The presence of limestone *in situ* in the Heidi Creek area was observed in the field; Trapridge C and A both run through areas where moraine material mainly consisting of limestone fragments is exposed.

(4) Water in contact with magnesium minerals. This water is characterized by a Ca/Mg ratio of 0.72 and a Ca + Mg content of 13.4 ppm.

The Ca/Mg ratio and the Ca + Mg content in the foregoing are the mean values for these quantities. A summary of the chemical character of each group is given in Table 7.

Suspended sediments. On July 15 suspended sediments were measured at the site of Rusty I water-level recorder. The results are given in Table 8. The maximum load of suspended sediments was recorded at 13:50. The minimum load recorded was the first load measured and so it may not be the actual minimum. The discharge at the time it was measured, however, is approximately equal to the minimum discharge for the entire period of observation, so it seems probable that the suspended sediment load (106 g/m³) recorded at 09:10 is close to the absolute minimum to be carried at the site of Rusty I water-level recorder.

The CaCO₃ content of the suspended sediment on July 15 was rather high (mean value = 36.6%). The peak value of 44.3% at 11:00 may possibly be attributed to suspended sediment from Trapridge A, which would be contributing a major proportion of water to the recorded discharge early in the day because of the relative proximity of Trapridge stream A to the Rusty I water-level recorder.

The amount of suspended sediment measured on July 15 at Rusty I is small when compared with the 1721 g/m³ measured on July 26 at Rusty III (Fig. 2) with a discharge of 2100 liters/sec.

On July 12 suspended sediment was measured in

TABLE 5. Results of the Chemical Analyses of Water Samples (Mean Values)

Sample location ¹	No. of samples	EC (μ mho)	pH	Hardness (ppm)	Ca ⁺⁺ (ppm)	Alkalinity (ppm)	Mg ⁺⁺ (ppm)	TDS ² (ppm)
Moulin Rouge	4	22	7.3	24	5.6	27	2.2	58.8
Plunge hole	2	25	7.6	26	4.4	35	3.6	69.0
Backe A	4	48	8.2	46	5.6	55	7.8	114.4
Trapridge D	2	30	8.4	24	8.9	43	0.4	76.3
Trapridge C	2	60	7.9	57	12.0	60	6.6	135.6
Backe B	2	30	8.4	25	7.5	36	1.5	70.0
Mung Creek	4	39	8.6	43	8.5	51	5.3	107.8
Rusty III	12	44	8.0	43	9.0	54	5.7	111.7
Heidi Creek	4	104	7.7	87	17.0	90	11.0	205.0
Trapridge B	4	64	8.5	46	8.8	62	5.9	122.7
Trapridge A	10	46	8.3	62	17.0	77	5.1	161.1
Rusty I	16	102	8.0	72	16.0	83	8.0	179.0
Meltwater*	2	12.5	6.4	5.2	1.4	7.5	0.4	14.5
Rainwater	2	11.5	4.9	2.4	1.4	6.3	---	10.1

All samples were analyzed in duplicate.

Mean values differ less than 10% from individual analyses.

¹ See Figure 2.

² TDS = total dissolved solids.

*From crevasse in Backe Glacier.

TABLE 6. Total Quantity of Dissolved Solids and Calcium Content at Measuring Sites Arranged (for Each Glacier) According to Increasing Distance from Source

Measuring site	Dissolved solids (ppm)	Ca + Mg (ppm)	Ca/Mg
Source: Rusty Glacier			
Moulin Rouge ¹	58.8	7.8	2.65
Plunge hole ¹	69.0	8.0	1.22
Rusty III ²	111.7	14.7	1.58
Rusty I ²	179.0	24.0	2.00
Source: Backe Glacier			
Crevasse on glacier ¹	14.5	1.8	3.50
Backe B ²	70.0	9.0	5.00
Backe A ³	114.0	13.4	0.72
Source: Trapridge Glacier			
Trapridge D ¹	76.3	9.3	20.2
Trapridge B ²	122.7	14.7	1.49
Trapridge C ⁴	135.6	18.6	1.82
Trapridge D ⁴	161.1	22.1	3.33
Source: Heidi Creek	- -	28.0	1.54
Rainwater	10.1	1.4	>14

¹ Water on or near ice.

² Water in contact with "normal" moraine material.

³ Water in contact with magnesium materials.

⁴ Water in contact with moraine material containing considerable amounts of calcareous rock.

Trapridge stream A. The results are given in Table 9. It is apparent that the suspended sediment load of Trapridge stream A is much greater than that at the site of Rusty I water-level recorder for comparable discharge

TABLE 7. Mean Values of Ca⁺⁺, Mg⁺⁺, Ca + Mg, Ca/Mg, and Total Measured Ions

Group	Ca ⁺⁺ (ppm)	Mg ⁺⁺ (ppm)	Ca + Mg (ppm)	Ca/Mg	Total ions (ppm)
1	1.58	1.1	6.9	5.27	54.9
2	7.4	5.1	12.5	1.45	101.1
3	15.0	7.6	22.6	1.97	167.2
4	5.6	7.8	13.4	0.72	114.4

rates. The CaCO₃ content of the suspended sediment is also very high (mean value, 63.1%); this high CaCO₃ content can be accounted for by the presence of limestone fragments in the morainal material. The decrease of CaCO₃ content with increasing discharge is probably due to dilution with meltwater that has not been in contact with the calcareous moraine. It is concluded that Trapridge A is the main source of CaCO₃ in the discharge at the site of Rusty I water-level recorder.

Precipitation and temperature. Precipitation was measured at the glaciologists' camp on the Rusty Glacier; air temperatures at 2 m above the ground were measured in a Stevenson screen located 200 m downstream from Rusty I water-level recorder. Results are given in Tables 10 and 11.

Summary

The mean discharge rate at Rusty I water-level recorder for the period of observation was 2100 liters/sec or 124 liters/sec/km², with a total discharge of 6.9×10^6 m³. The contributions of each of the three glaciers, and their areas, are given in Table 12. It is clear that the discharge from Rusty Glacier is much less than that from

TABLE 8. Suspended Sediment in Water near Rusty I Water-Level Recorder on July 15, 1968

Time	Discharge rate (liters/sec)	Water temperature (°C)	Suspended sediment (g/m ³)	CaCO ₃ (% of suspended sediment)
09:10	450	1.1	105.7	37.7
10:15	520	1.6	108.0	34.2
11:00	700	2.8	245.7	44.3
11:35	800	2.8	350.3	38.6
12:09	910	2.8	453.1	36.3
13:00	1050	3.0	580.6	38.2
13:50	1200	2.8	766.5	35.7
15:00	1300	2.8	692.3	32.0
16:00	1350	2.8	519.1	32.1
				mean 36.6

TABLE 9. Suspended Sediment in Trapridge A, July 12, 1968

Time	Discharge rate (liters/sec)	Water temperature (°C)	Suspended sediment (g/m ³)	CaCO ₃ (% of suspended sediment)
10:45	470	0.9	668	67.5
11:50	560	1.2	1210	63.9
12:45	850	1.5	1139	63.2
13:30	960	1.6	1998	57.9
				mean 63.1

TABLE 10. Precipitation at Glaciological Camp on Rusty Glacier, July 9–August 15, 1968

Maximum daily	17.3 mm (13.5 rain + 3.8 snow) (July 13)
Mean daily	2.5 mm (2.0 rain + 0.5 snow)
Total snow	18.2 mm (density 0.1)
Total rain	75.6 mm (1.28 × 10 ⁶ m ³ water = 18.6% of total discharge from basin)
Total snow and rain	93.8 mm

TABLE 11. Temperatures (°C) near the Rusty I Water-Level Recorder

Mean daily temperature	5.5
Mean daily minimum temperature	0.4
Mean daily maximum temperature	10.7
Mean temperature, coldest day	- 1.5 (July 13)
Mean temperature, warmest day	11.5 (July 23)
Minimum recorded temperature	- 4.5 (July 13, 14; August 8)
Maximum recorded temperature	18.5

the Trapridge and Backe. This difference supports the expectation that the Rusty Glacier may surge before long. A certain amount of accumulation might be expected before a surge; that is, the melt regime before a surge could be described as below normal while the regime during a surge would be above normal, with normal melt regime being that of a nonsurging glacier, such as the Trapridge. The Backe Glacier did surge some time ago, but its rate of melting has since diminished and is now more or less equivalent to that of the Trapridge.

The contribution of Rusty Glacier to the total discharge measured at Rusty I water-level recorder was computed from data on discharge from the various streams draining the Rusty Glacier. T. Brewer (personal communication) also computed the discharge from Rusty Glacier using accumulation, ablation, and precipitation data. The results are given in Table 13; they support the conclusion that discharge from the Rusty Glacier is less than that from the Trapridge or the Backe.

Acknowledgments

The hydrological studies reported here were carried out by a team from the Glaciology Subdivision, Inland Waters Branch, Department of Energy, Mines and Resources, Canada. The team consisted of assistants J. R.

TABLE 12. Discharge in Relation to Area of Glacier

Glacier	Area (km ²)	% of total area ¹	Contribution (% of total)	Discharge rate (liters/sec)	Specific discharge (q) (liters/sec/km ²)	$\frac{q}{q(\text{Rusty I WLR})^2}$
Rusty	6.15	36.2	24	500	81	0.66
Trapridge	5.30	31.2	48	1000	189	1.53
Backe	3.53	20.8	29	600	170	1.38

¹ Area unaccounted for is occupied by ice-cored moraines.

² q(Rusty I WLR) = 124 liters/sec/km².

TABLE 13. Total Discharge during the Period of Observation (July 9–August 15, 1968)

Area considered	Discharge (m ³)
Entire area (measured at Rusty I water-level recorder)	6.9 × 10 ⁶
Rusty Glacier only	1.66 × 10 ⁶ (Faber) 1.45 × 10 ⁶ (Brewer) (1.56 ± 10) × 10 ⁶ (average of two values)
Balance attributed jointly to Trapridge and Backe	5.34 × 10 ⁶

Plommer (June 21–July 23) and H. Reisenleiter (July 23–August 23), with the author as party chief. This team received logistic support in the field from the Icefield Ranges Research Project. Most of the field equipment

was furnished by the Glaciology Subdivision. The Institute for Earth Sciences of the Free University, Amsterdam, made the author's stay in Canada possible by granting him leave.

References

- Dekker, H. G., and Faber, Th. (1969) New portable, battery powered instruments for hydro(geo)logical fieldwork, *Geol. Mijnbouw*, 48, 240-246.
- Engelen, G. B. (1968) Schwebstoffmessungen in einem Gebirgsbach in Südtirol bei Hochwasser, *Deutsche Gewässerkundl. Mitt.*, 12, 66-71.
- Grover, N. C., and Harrington, A. W. (1966) *Stream Flow; Measurements, Records and Their Uses*, Dover, New York, 363 pp.
- Hem, J. D. (1970) Study and interpretation of the chemical characteristics of water, *Water Suppl. Paper 1473*, U.S. Geol. Surv., 363 pp. (2nd ed.).
- Hinrich, H. (1965) Beitrag zur Schwebstoffmessung in Wasserläufen mit Beschreibung eines einfachen Filterverfahrens, *Deutsche Gewässerkundl. Mitt.*, 9, 49-60.
- Muller, J. E. (1967) Kluane Lake map-area, Yukon Territory (115G, 115F E½), *Mem. 340*, Geol. Surv. Can., 137 pp.

Gravity and Shallow-Ice Temperature Measurements on the Rusty Glacier

David J. Crossley* and Garry K. C. Clarke*

ABSTRACT. The Rusty Glacier has a history of surging but is at present quiescent. In 1968 a gravity survey indicated the glacier has a maximum depth of 88 m. Near-surface temperature measurements identify the Rusty as a subpolar glacier.

INTRODUCTION

The Rusty¹ Glacier is a small valley glacier in the Yukon; it is located between the Steele and Hodgson Glaciers and shares a common drainage basin with the Backe¹ and Trapridge¹ Glaciers (Fig. 1). All five of these glaciers have surged and only the Rusty and Trapridge are at present inactive. The fragmented condition of an actively surging glacier makes surface measurements impractical. In anticipation of a future surge of the Rusty Glacier an extensive study of the glacier, coordinated by the Icefield Ranges Research Project, was begun in 1967. In 1968 a gravity survey was carried out to find the ice thickness; near-surface temperature measurements were also made.

The earliest work in the Rusty Glacier area was by the Wood Yukon Expedition in 1935, which conducted a program of reconnaissance aerial survey during the ascent of Mt. Steele (Wood, 1936). Sharp (1943) reported a geological study of the Steele Glacier valley which included some of the terrain to the northeast of the Rusty.

THE GRAVITY SURVEY

The Measurements and their Reduction

A Sharpe Gravity Meter was used in the survey. Readings at 66 stakes, erected in 1967, constitute the gravity network (Fig. 2) on the glacier. In addition, 9 elevated stations on outcrops around the glacier and 14 cairns on bedrock at the ends of glacier traverses were occupied. The UTM (Universal Transverse Mercator) coordinates and elevation above sea level of the glacier stations were determined from a theodolite survey in 1968 to an absolute accuracy of ± 1 m for the UTM coordinates and about ± 0.02 m for the elevations. The coordinates and elevations of the edge stations were obtained from a less precise independent survey, within ± 1 m and an estimated ± 0.15 m respectively. Combined errors in the station ele-

vations, allowing for stake-height measurements, amounted to ± 0.05 m for the glacier stations and ± 0.18 m for the edge stations.

Loop misclosures were adjusted by the weighted least-squares method of Gibson (1941). The rms deviation of calculated-minus-measured differences between junctions was 0.07 mgal. No sampling of rock was attempted for density and the value of 2.67 g/cm^3 was used. The average surface density of ice was measured as 0.89 g/cm^3 but allowing for compaction at depth a value of 0.90 g/cm^3 was used. The resulting density contrast of 1.77 g/cm^3 is probably accurate to $\pm 0.20 \text{ g/cm}^3$. Conventional corrections for station latitude and elevation were applied; details can be found in Crossley (1969).

Lack of symmetry in the form of topographic features precluded two-dimensional integration; therefore hand computations using the zone system of Hammer (1939) were considered suitable. The attractions of the zones were computed for both rock and ice densities to allow for compartments which included both materials. Within 90% confidence limits the error in the topographic correction was ± 0.37 mgal for a station. Corrections for distant zones were incorporated into the regional gradient which was obtained by least-squares fitting of a polynomial to edge stations. Figure 2 shows the Bouguer anomalies with the topographic corrections applied and Figure 3 shows the residual anomalies.

Interpretation

Estimated errors in the least-squares fitting of the initial data, standard reduction errors, and topographic corrections total 0.39 mgal and 0.40 mgal for the glacier and edge stations respectively (90% confidence limits). Errors arising from the regional gradient rms deviation of 0.51 mgal reflect random errors and the simplicity of the least-squares function. Assuming these two causes contribute equally, 0.25 mgal might reasonably be combined with the random errors. Assuming further a Gaussian error distribution, 95% confidence limits on the residual anomalies are ± 0.67 mgal. Due to errors in the data, the problem of finding a satisfactory depth interpretation becomes one of adjusting some model to the residuals to within the accuracy desired. For a three-dimensional body of arbitrary shape, the integrated mass attraction requires dividing the body

*Department of Geophysics, University of British Columbia, Vancouver, Canada

¹The names Fox, Jackal, and Hyena were formerly unofficially used for these glaciers; Rusty, Backe, and Trapridge are names that have recently been approved.

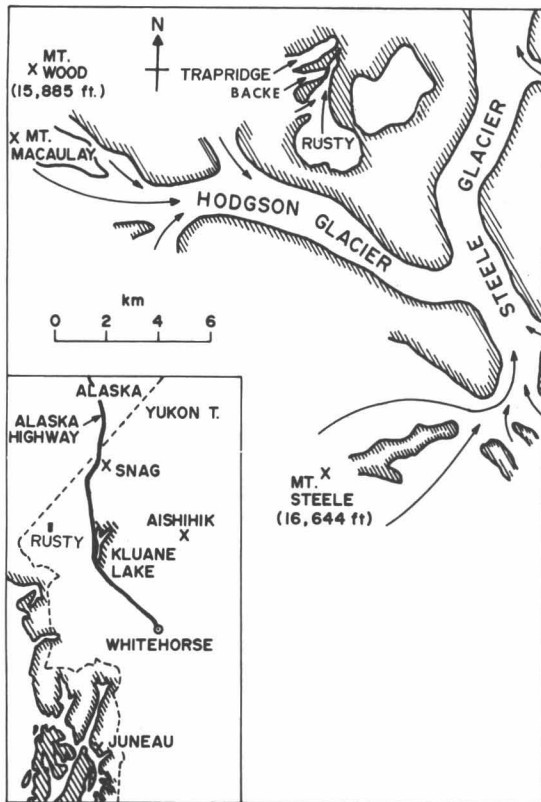


Fig. 1. Location of the Rusty Glacier.

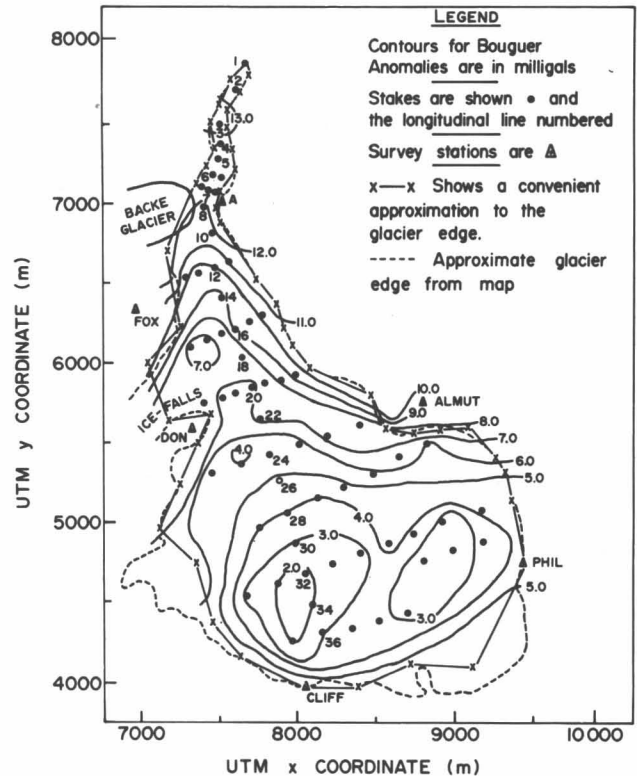


Fig. 2. Glacier sketch showing Bouguer anomalies. Terrain correction applied.

into simpler shapes which can be handled analytically. The computerized sum of horizontal laminae formulated by Talwani and Ewing (1960) has been widely used. This method has the disadvantage that each time an approximation is made to the outline of body the coordinates of the laminae have to be redetermined.

An alternative method of integration of a depth distribution was attempted, based on the attraction of triangular vertical prisms. The vertices of each prism at the surface of the glacier are the known coordinates of the gravity stations and remain fixed. The *z* coordinate of a vertex at the glacier bed is obtained from an initial model, with the depth of a prism taken as the average of three vertices. Figure 4 shows that any number of edge stations can be accommodated without adding unknown depths.

The calculation of the attraction of a single prism is outlined in Appendix I. Integration of the glacier in this way required an initial depth profile and this was obtained by an infinite slab assumption. Figure 5 shows the resulting depth distribution; cross sections at the glacier traverses (Fig. 6) and a longitudinal profile (Fig. 7) are also shown. The mean deviation of observed-minus-calculated anomalies is 0.44 mgal which is within the desired confidence intervals. Adjustments to the depths were obtained by the least-squares procedure used by Corbató (1965a, b); but the results obtained were unacceptable. Further discussion of the integration procedure and the interpretation is given in Crossley and Clarke (1970) and Crossley (1969).

Discussion

Thermal drilling results from D. F. Classen (personal communication, 1969) are given in Table 1 with the predicted gravity depths at three stations. Errors in the gravity depths resulted from a combination of uncertainty in density contrast and 95% confidence limits on the residual anomalies.

Comparison of the gravity and drilling depths shows good agreement, well within the accuracy of the gravity data. The gravity depths in the snout of the glacier are unreliable because of the thinness of the ice and large terrain corrections. There is also some doubt about the depths in the region below the ice falls (Fig. 2) because the depth of the small tributary glacier which joins the Rusty there is unknown. Although the mean deviation between observed and calculated anomalies is 0.44 mgal, for some stations a difference of one or two mgal remains; it is expected that the depth model requires adjustment in these areas. Examination of Figures 5 and 6 reveals no unusual

TABLE 1. Drilling Results

Station (Stake No.)	Depth (m)		Difference
	Gravity	Drilling	
12	29.0 ± 12.3	31.4	-2.4
16	30.6 ± 12.5	27.0	+3.6
20	50.6 ± 14.7	47.9	+2.7

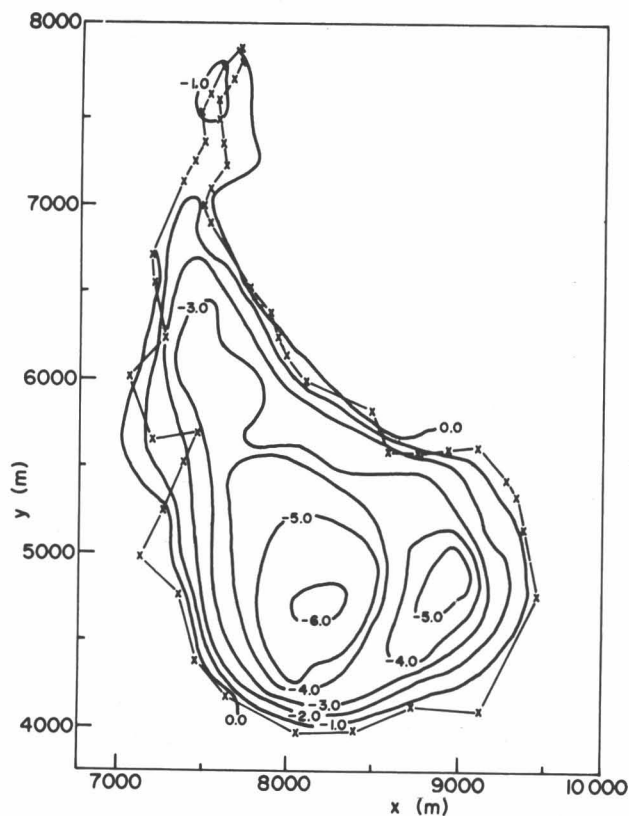


Fig. 3. Residual anomalies, regional gradient removed. Contour interval 1.0 mgal.

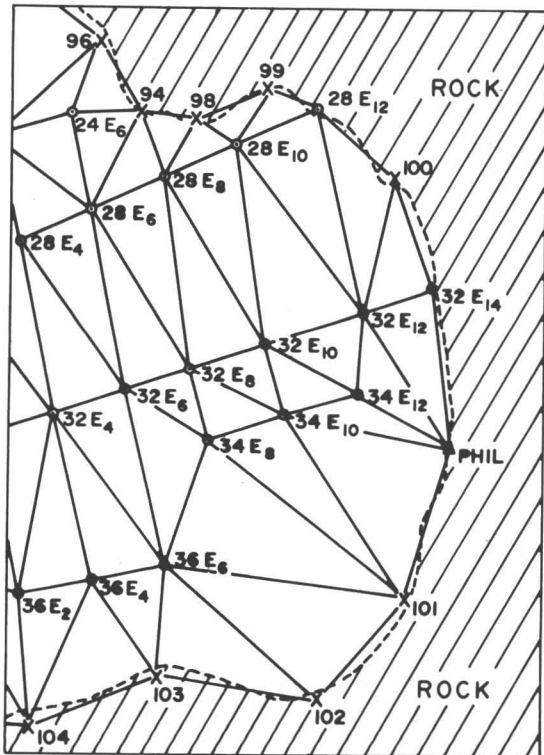


Fig. 4. Portion of integration scheme. Stations created for network are shown with a cross.

features in the bedrock profile. The inherent smoothing of relief associated with gravity interpretation may, however, account for this. A prominent bulge in the ice surface in the area of stake 34E₁₀ may be associated with a slight bedrock rise immediately downglacier (Figs. 6c, 6d).

TEMPERATURE MEASUREMENTS

The Results

During the summer of 1968 near-surface temperature profiles were obtained at Stakes 2, 7, 16, and 34 (Fig. 2). Two mechanical drills were used, a three-inch SIPRE coring auger and a one-inch ice drill. When the drill froze, hot water was used for recovery; this thermal disturbance was unimportant. Thermocouple temperatures were taken within sealed, water-free, one-inch polyethylene tubing. Hourly measurements over a period of 18 hrs for the hole at Stake 7 indicated that the temperatures had stabilized within twelve hours after drilling. The results, to an estimated accuracy of $\pm 0.2^\circ\text{C}$, are shown in Figure 8.

Factors Influencing Glacier Temperatures

Climate. Meteorological stations in the Yukon are sparsely situated and none of them are in the St. Elias Mountains. Although a weather record for the Rusty was kept for July and August, there is no direct information concerning the climate for the rest of the year.

The meteorological data accumulated at the nearest two all-year stations, Aishihik and Snag, were reported in Kendrew and Kerr (1955). Marcus (1964) presented a year's data for the Juneau Icefield region in southern Alaska and found that the temperature gradient between the icefield and sea level was seasonally dependent. Using data from these two sources, the annual variation at the Rusty Glacier was estimated to be a sinusoid of mean $-15 \pm 5^\circ\text{C}$, and amplitude $20 \pm 5^\circ\text{C}$. From the mass balance results of T. Brewer (personal communication, 1969) the snowfall averaged over one year was deduced to be about one meter.

Thermal history. The past surges of the Rusty involved appreciable thickness changes, hence the temperature profiles obtained are time dependent. Considering the Greenland and Antarctic ice sheets, Wexler (1959) has shown that large ice masses are in a quasi-equilibrium state. All temperature calculations should ideally consider the duration of the assumed boundary conditions. Unfortunately lack of data concerning the past surges of the Rusty Glacier precludes such treatment.

Penetration of the winter cold wave. The effect of harmonic temperature fluctuations at the surface of a semi-infinite solid was treated by Carslaw and Jaeger (1959). The treatment of a composite solid (snow on ice) requires further application of the diffusion equation (Appendix II). Calculation of the effect of one meter of

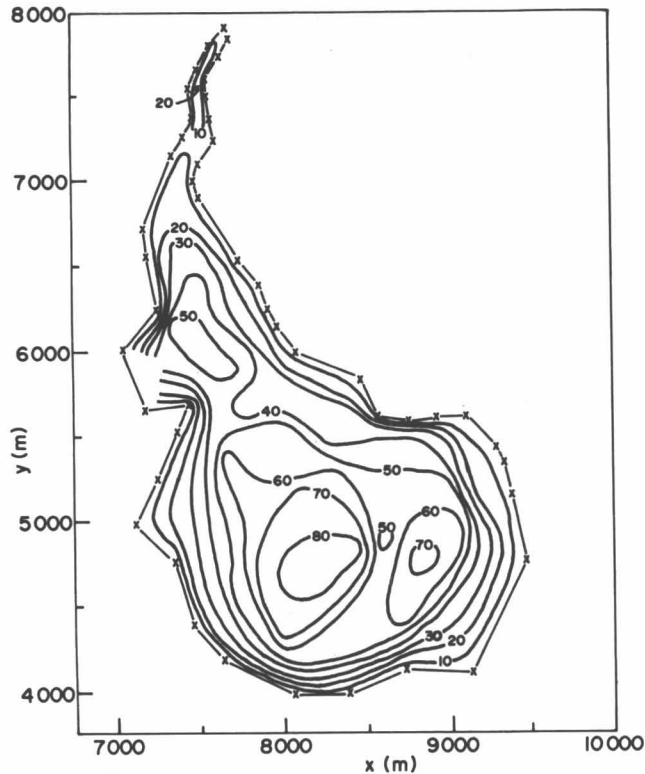


Fig. 5. Glacier depths, contour interval 10 m.

snow on a glacier indicates that the 8-m temperature of -5°C (Fig. 8) is not due to the cold wave. Modifications of the effect of the cold wave due to dynamic accumulation (Benfield, 1952) fail to account for the low ice temperature on the Rusty Glacier.

Effect of ice movement on temperature profiles. Robin (1955) discussed the effect of downward ice movement on temperature profiles. Application of the expression

$$T_H - T_h = \frac{q}{K} \sqrt{\frac{2H\kappa}{A}} \left[\text{erf} \left(h \sqrt{\frac{A}{2H\kappa}} \right) \right]^{-H}$$

to glaciers 50 m and 100 m thick results in Figure 9 (H = ice thickness, q = geothermal heat flow taken as $1.2 \mu\text{cal cm}^{-2} \text{sec}^{-1}$, A = accumulation rate, K = thermal conductivity and κ is thermal diffusivity). For ice accumulation of less than $50\text{--}100 \text{ cm yr}^{-1}$ there is negligible perturbation of the geothermal gradient.

Strain heating. Survey results for 1968 and 1969 were compared by S. Collins (personal communication) to assess surface velocity of the Rusty Glacier. The flow rates obtained were approximately one meter a year, about the accuracy of the UTM coordinates; thus it appears the glacier is virtually stagnant and strain heating can be discounted.

Discussion

With reference to Figure 8 the following points are noteworthy:

- (1) At Stake 34 there was a firn cover of one meter; the temperature profile indicates that the thermal gradient is smooth from the surface and through the firn-ice interface. Comparison with the profiles at holes with no firn cover confirms that the snow insulates the ice beneath from surface temperatures. This effect is seen more clearly in the penetration of the cold wave (Appendix II, Figs. 2, 3).
- (2) Comparison of the July 10 and August 16 profiles for Stake 7 shows that the top few meters of ice had warmed by about a degree.
- (3) The 8-m hole at Stake 7 shows that the glacier temperature remains fairly constant at about -4.7°C below a depth of 4 m. Hence the minimum glacier temperature may well be in the region of -5°C ; warming towards the glacier bottom is to be expected due to geothermal heating.

Near-surface temperatures were determined on the Backe and Trapridge glaciers; although measurements are sparse, the temperatures obtained were below zero.

The penetration of the annual temperature fluctuations at the glacier surface has been considered for conduction and solid convection only, but the effects of summer ablation and the heat carried down into the glacier by percolating meltwater and subsurface streams is unknown. The role of fluctuating temperature profiles in providing trigger mechanisms for glacier surges has often been discussed (for example, Robin, 1969), especially in conjunction with the mechanism of glacier sliding as proposed by Weertman (1969). As Nielsen (1969) has pointed out, some glacier surges suggest that mechanical instabilities are present; for example, tributary glaciers often advance after the parent glacier has surged. It is possible that the diversity in size and normal flow rates of surging glaciers may indicate involvement of more than one trigger mechanism.

SUMMARY

The gravity survey results show the Rusty Glacier to have a maximum depth of 88 m in the accumulation region. Agreement with thermal drilling results is good but in two areas of the glacier the depths obtained are uncertain. Depth profiles across the glacier show no unusual bedrock features, but this may be a result of the low resolving power of gravity surveys. Consideration of the temperature measurements and the factors affecting the glacier thermal regime indicates that the Rusty and near-by glaciers are subpolar.

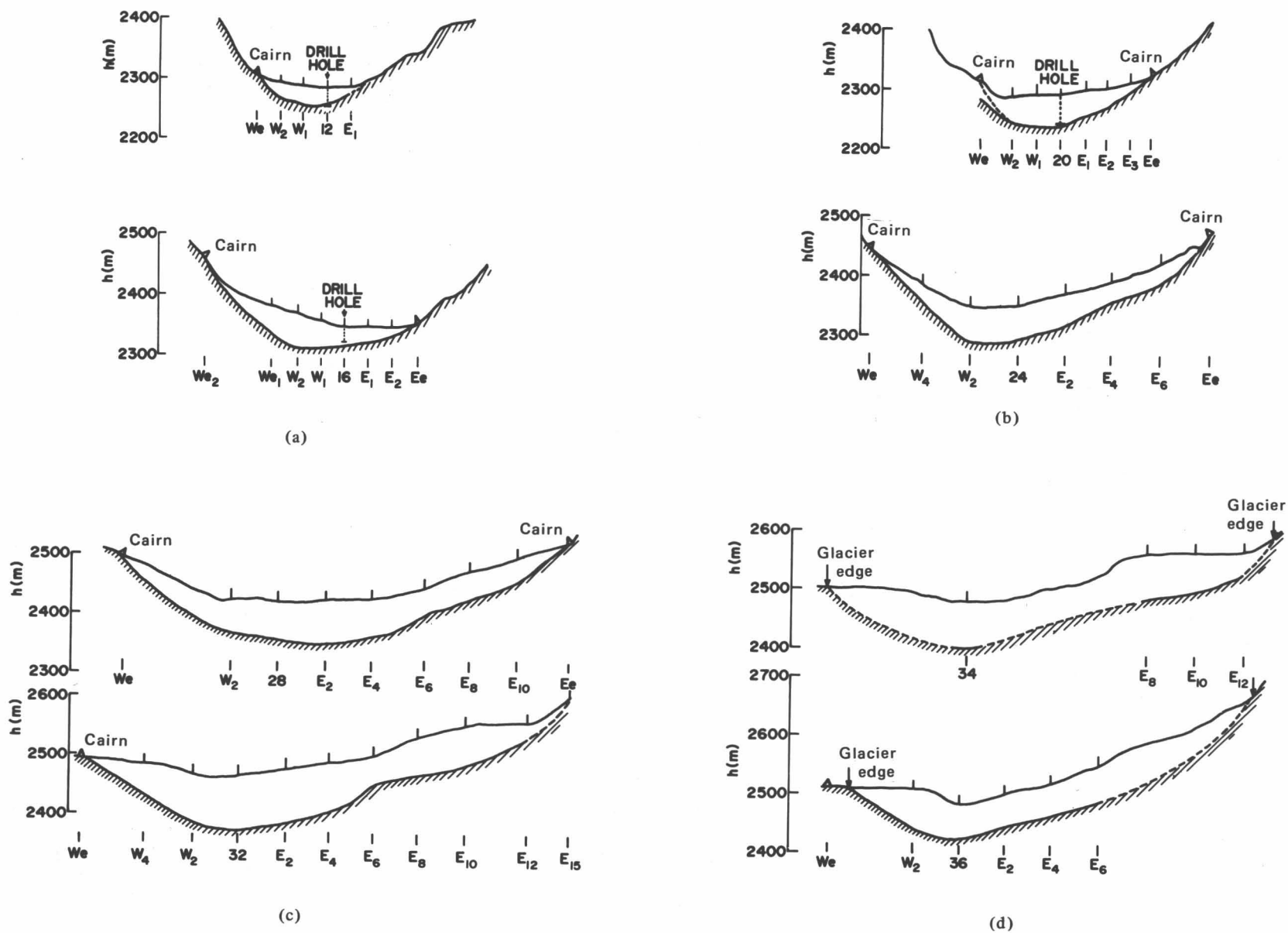


Fig. 6. Transverse depth profiles. Dashed portions of profiles are uncertain. Elevation, h , is above mean sea level. Profiles are for stake rows 12, 16, 20, 24, 28, 32, 34, and 36.

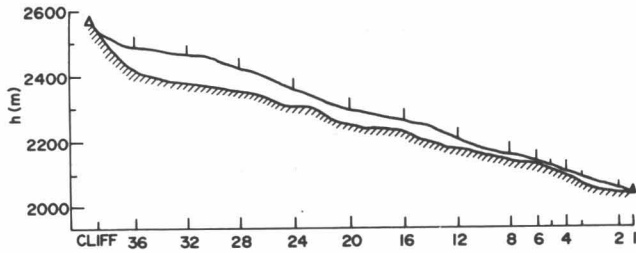


Fig. 7. Longitudinal depth profile. Vertical exaggeration 2.54.

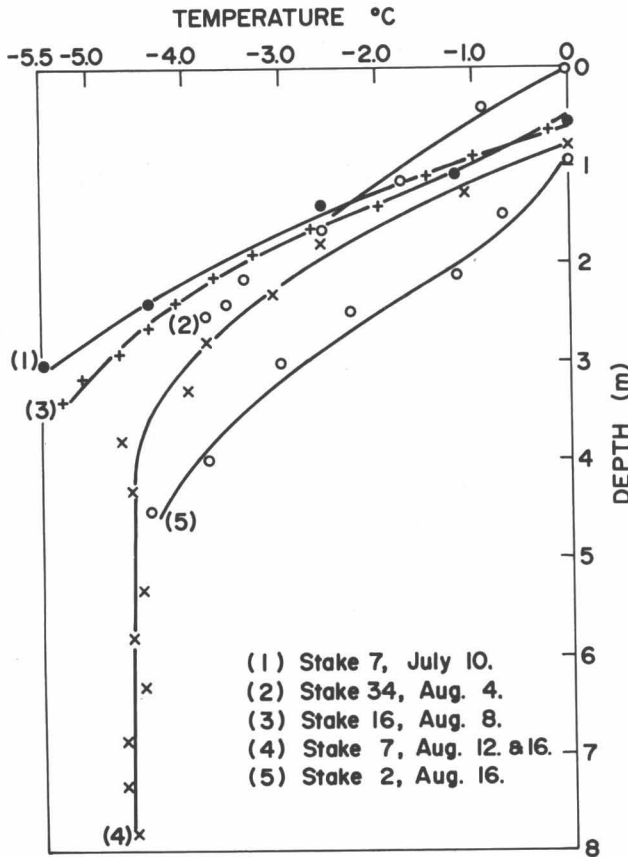


Fig. 8. Temperature results.

Acknowledgments

We wish to thank the following people and organizations for their assistance. The seismic apparatus was provided by Dr. W. A. Weeks and the U.S. Army Terrestrial Sciences Center (formerly C.R.R.E.L.), Hanover, New Hampshire; Dr. J. Tanner and the Gravity Division, Dominion Observatory, Ottawa, generously loaned a gravimeter at short notice. The Icefield Ranges Research Project gave invaluable logistic support; special thanks go to Dr. M. Marcus, the base camp director, and Phil Upton, the pilot. Sam Collins was an excellent leader at Fox

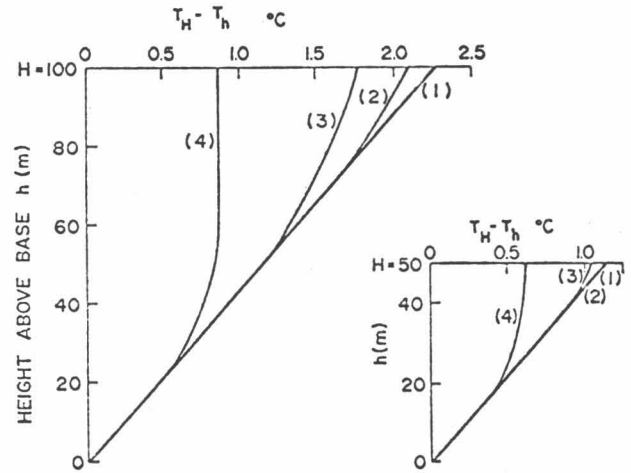


Fig. 9. Effect of accumulation rate on temperature gradient. $A = 0, 50, 100, 500 \text{ cm yr}^{-1}$ for (1), (2), (3), and (4) respectively.

Camp; David Harrison and Patrick Powell were commendable field assistants. The help given both by Dr. A. Stanley, Inland Waters Branch, Department of Energy, Mines and Resources, Ottawa, and Dick Ragle was greatly appreciated. Financial support was obtained from the Arctic Institute of North America and the National Research Council of Canada.

References

Benfield, A. E. (1952) The effect of accumulation on temperatures within a snowfield, *J. Glaciol.*, 2, 250.
 Carslaw, H. S., and Jaeger, J. C. (1959) *Conduction of Heat in Solids*, Clarendon Press, Oxford, 510 pp. (second ed.).
 Corbató, C. E. (1965a) A least-squares procedure for gravity interpretation, *Geophysics*, 30, 228-233.
 Corbató, C. E. (1965b) Thickness and basal configuration of lower Blue Glacier, Washington, determined by gravimetry, *J. Glaciol.*, 5, 637-650.
 Crossley, D. J. (1969) Gravity and temperature measurements on the Fox Glacier, Yukon, M. Sc. thesis, Univ. British Columbia, Vancouver, 81 pp. (unpubl.).
 Crossley, D. J., and Clarke, G. K. C. (1970) Gravity measurements on the Fox Glacier, *J. Glaciol.*, 9, 363-374.
 Gibson, M. O. (1941) Network adjustment by least-squares-alternative formulation and solution by iteration, *Geophysics*, 6, 168-179.
 Hammer, S. (1939) Terrain corrections for gravimeter stations, *Geophysics*, 4, 184-194.
 Kendrew, W. G., and Kerr, D. (1955) *The Climate of British Columbia and the Yukon Territory*, Edmond Cloutier, Ottawa, Chap. 10, pp. 167-178.
 Marcus, M. G. (1964) *Climate-Glacier Studies in the Juneau Icefield Region, Alaska*, Univ. Chicago Press, Chicago, Chap. 4, pp. 52-61.
 *Nielsen, L. E. (1969) The ice-dam, powder-flow theory of glacier surges, *Can. J. Earth Sci.*, 6, 955-961.
 Robin, G. de Q. (1955) Ice movement and temperature distribution in glaciers and ice sheets, *J. Glaciol.*, 2, 523-532.
 Robin, G. de Q. (1969) Initiation of glacier surges, *Can. J. Earth Sci.*, 6, 919-928.

*Sharp, R. (1943) Geology of the Wolf Creek area, St. Elias Range, Yukon Territory, Canada, *Bull. Geol. Soc. Am.*, 54, 625-650.
 Talwani, M., and Ewing, M. (1960) Rapid computation of gravitational attraction of three-dimensional bodies of arbitrary shape, *Geophysics*, 25, 203-225.
 Weertman, J. (1969) Water lubrication mechanism of glacier surges, *Can. J. Earth Sci.*, 6, 929-942.

Wexler, J. (1959) Geothermal heat and glacier growth, *J. Glaciol.*, 3, 420-425.
 Wood, W. A. (1936) The ascent of Mt. Steele, *Am. Alpine J.*, 2, 438-448.

*These articles are reprinted in the present volume.

APPENDIXES

I

PRISM INTEGRATION FOR GRAVITATIONAL ATTRACTION

According to the formulation of Talwani and Ewing (1960), the vertical component of the gravitational attraction per unit thickness of a thin horizontal triangular lamina, evaluated at a point *P* is

$$V(z) = G\rho_i \sum_{i=1}^3 \left\{ W \cos^{-1} \left[\left(\frac{X_i}{\Gamma_i} \right) \left(\frac{X_{i+1}}{\Gamma_{i+1}} \right) + \left(\frac{Y_i}{\Gamma_i} \right) \left(\frac{Y_{i+1}}{\Gamma_{i+1}} \right) \right] - \sin^{-1} \left(\frac{z q_i S}{(p_i^2 + Z^2)^{1/2}} \right) + \sin^{-1} \left(\frac{z f_i S}{(p_i^2 + Z^2)^{1/2}} \right) \right\} \quad (1)$$

where *z* is the depth of the lamina below *P*. The symbols have the same meaning as in the paper by Talwani and Ewing. The contribution of the first term is zero if *P* is over one of the vertices of the lamina. The total attraction of a prism extending from *z* = 0 to *z* = *H* is obtained by evaluation of the integral

$$g = \int_0^H V(z) dz,$$

using numerical methods.

For simplicity Simpson's rule was used in the form

$$g = \frac{H}{6} (V_1 + 4V_2 + V_3)$$

where *V*₁, *V*₂, and *V*₃ are the values of *V*(*z*) obtained from (1) at the depths 0, *H*/2, and *H* (Fig. 1a). Increasing

the number of *V*'s was not found to change *g* by a significant amount because in all cases the depth of the prism was less than, or comparable to, the distance from the prism to *P*.

For stations *P* sufficiently far from a prism, the evaluation of *g* was carried out using a center of mass approximation to adequate accuracy. The vertical attraction of a prism treated in this way is given by

$$g = \frac{G A \rho z}{r^2} \cdot \frac{d}{r}$$

where *A* is the area of the triangular face and *d* = (*z*₁ + *z*₂ + *z*₃)/6 = *z*/2 (Fig. 1b). The results obtained by comparing the whole-glacier anomaly at two representative stations is given in Table 1 for values of *D*, the distance at which the approximation formula was used. A distance of 0.7 km for *D* appears to be a good compromise between accuracy and speed of integration.

TABLE 1.

Radius <i>D</i> (km)	Anomalies (mgal)		Approximate Computer Time Per Station (sec)
	Station A	Station B	
0.0	0.217	0.473	0.7
0.1	0.217	0.473	0.7
0.5	1.940	2.778	1.3
0.7	1.941	2.782	2.0
1.0	1.942	2.783	3.0
10.0	1.942	2.783	8.0

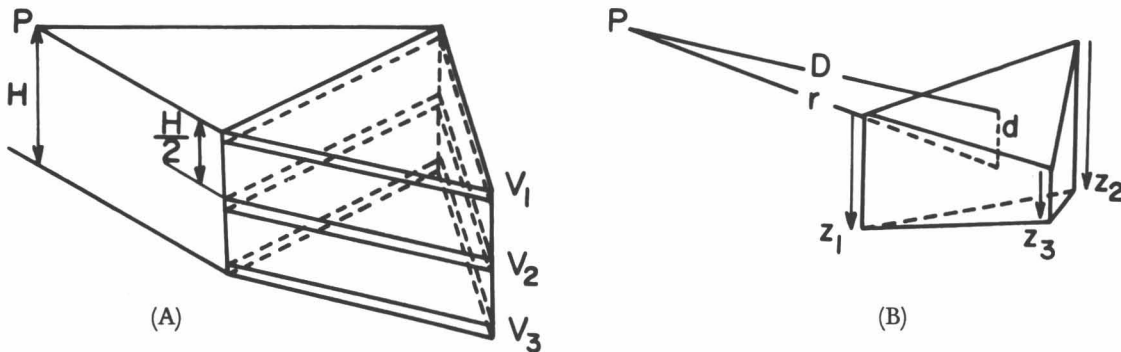


Fig. 1. Prism integration for gravitational attraction. For symbols see text.

II

THE DIFFUSION OF A THERMAL WAVE INTO A GLACIER

The problem has been simplified to the extent that the wave is applied at the surface $z = 0$ of a semi-infinite medium. The input is assumed a harmonic function of time and can be expressed as

$$T(o, t) = A \cos(\omega t - \epsilon)$$

By Fourier Analysis any desired input can be treated by the superposition of such waves, if periodicity can be assumed. Two cases are considered, called Models I and II, and the treatment is restricted to the steady state solution in which the surface fluctuations have been applied since $t = -\infty$ and the medium was initially at zero temperature.

The following symbols are used and the values have been taken from Carslaw and Jaeger (1959):

- K_1 = thermal conductivity of snow, $0.00025 \text{ cal sec}^{-1} \text{ }^\circ\text{C}^{-1} \text{ cm}^{-1}$
- K_2 = thermal conductivity of ice, $0.0053 \text{ cal sec}^{-1} \text{ }^\circ\text{C}^{-1} \text{ cm}^{-1}$
- κ_1 = thermal diffusivity of snow, $0.0050 \text{ cm}^2 \text{ sec}^{-1}$
- κ_2 = thermal diffusivity of ice, $0.0115 \text{ cm}^2 \text{ sec}^{-1}$
- ω = angular frequency of input wave, 1 cycle yr^{-1} ($1.992 \times 10^{-7} \text{ sec}^{-1}$)

The thermal diffusivity of average rock is $0.0118 \text{ cm}^2 \text{ sec}^{-1}$.

The object of the treatment is to determine the effect of a snow cover on the diffusion of the annual winter cold wave into a glacier, to decide whether the temperatures measured on the Rusty Glacier were due to the cold wave.

Model I—The glacier as an infinite half-space. The boundary condition is

$$T(o, t) = A \cos(\omega t - \epsilon)$$

$$\lim_{z \rightarrow \infty} T(z, t) = 0$$

and the method is described fully in Carslaw and Jaeger. The solution is a wave diminishing in amplitude as $Ae^{-0.294z}$ and with a phase lag of 17.1z days, with z in meters.

Model II—The glacier as a layered half space. Model I would serve as a good approximation for a glacier provided the thermal properties of ice were constant with depth and not too different from the underlying bedrock. Most glaciers, however, have a firn cover which may be many meters thick: Model II considers the effect of a layer of snow of uniform thickness over a glacier. The boundary between ice and snow is assumed perfect thermally, and is located at a depth d below the surface.

The boundary conditions for this problem are

$$T_1(o, t) = A \cos(\omega t - \epsilon)$$

$$T_1(d, t) = T_2(d, t)$$

$$K_1 \frac{\partial T_1}{\partial z} \Big|_d = K_2 \frac{\partial T_2}{\partial z} \Big|_d$$

$$\lim_{z \rightarrow \infty} T_2(z, t) = 0$$

and they express the continuity of heat and temperature across the firn-ice interface.

Writing T_1 and T_2 in the forms

$$T_1(z, t) = u(z) e^{i(\omega t - \epsilon)}$$

$$T_2(z, t) = v(z) e^{i(\omega t - \epsilon)}$$

and solving the diffusion equations

$$\frac{\partial^2 T_1}{\partial z^2} = \frac{1}{\kappa_1} \frac{\partial T_1}{\partial t}$$

$$\frac{\partial^2 T_2}{\partial z^2} = \frac{1}{\kappa_2} \frac{\partial T_2}{\partial t}$$

in the appropriate regions leads directly to the solutions

$$T_1(z, t) = P_1 \left(\frac{X^2 + Y^2}{U^2 + W^2 \sin^2 R} \right)^{1/2} \cos \left\{ \omega t - \epsilon + \arctan \left(\frac{UX - XW \sin R}{UX + YW \sin R} \right) \right\} \quad (1)$$

$$T_2(z, t) = P_2 (U^2 + W^2 \sin^2 R)^{-1/2} \cos \left\{ \omega t - \epsilon + \arctan \left(\frac{U \tan Q_2 - W \sin R}{U + W \tan Q_2 \sin R} \right) \right\} \quad (2)$$

where

$$P_1 = A e^{S_1}$$

$$S_1 = z k_1$$

$$R = 2 k_1 d$$

$$W = S e^R$$

$$U = 1 + W \cos R$$

$$Q_1 = -2 k_1 (z - d)$$

$$V = S e^{Q_1}$$

$$k_1 = \sqrt{\omega / 2 \kappa_1}$$

and

$$P_2 = A(1+S)e^{Qz}$$

$$Q_2 = d(k_1 + k_2) - zk_2$$

$$S = \frac{K_1 k_1 + K_2 k_2}{K_1 k_1 - K_2 k_2}$$

$$X = \cos S_1 + V \cos(S_1 + Q_1)$$

$$Y = \sin S_1 + V \sin(S_1 + Q_1)$$

$$k_2 = \sqrt{w/2\kappa_2}$$

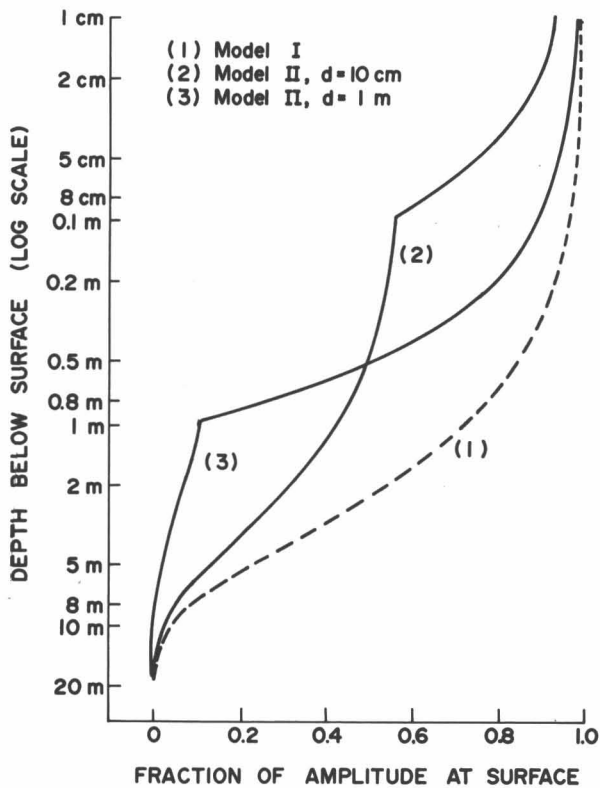


Fig. 2. Effect of snow cover on amplitude penetration of annual cold wave.

Details of the intermediate steps can be found in Crossley (1969).

Figures 2 and 3 show the amplitude and phase of the thermal wave obtained from (1) and (2). A comparison is given by plotting the values obtained from Model I.

It is sufficient to note that the amplitude of the diffused wave is strongly affected by a shallow snow cover to a distance of $5-10d$ below the surface. This phase lag is not greatly affected, and 10 m is the approximate depth of the coldest temperature to be expected, half a year after the passing of the winter cold wave.

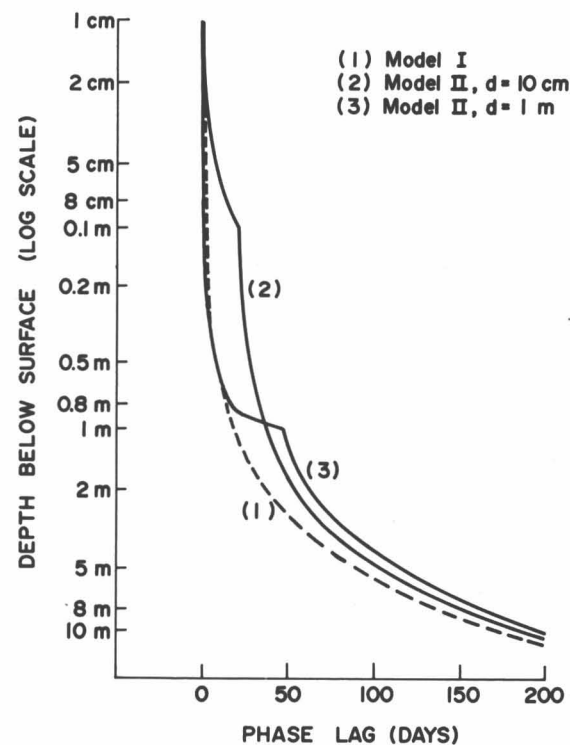


Fig. 3. Effect of snow cover on phase penetration of annual cold wave.

Thermal Drilling and Ice-Temperature Measurements In the Rusty Glacier

David F. Classen* and Garry K. C. Clarke*

ABSTRACT. During the summer of 1969 a thermal drilling and deep-ice temperature measurement program was carried out on the Rusty Glacier.¹ The thermal drilling produced seven instrumented holes at six locations on the glacier, three reaching bedrock. Temperature measurements indicated that the glacier was below the pressure-melting point throughout, and that evidence of a disturbed thermal regime existed.

Estimates of geothermal heat flow were determined, and an anomalous value of $4.73 \mu\text{cal}/\text{cm}^2 \text{ sec}$ was obtained. Bottom temperature models were developed which indicate the possibility of basal melting.

INTRODUCTION

It is the purpose of this paper to present the results of thermal drilling and deep ice-temperature measurements made during the summer of 1969 on the Rusty Glacier.

Surging Glaciers

A surging glacier, as defined by Post (1969), is one which periodically (15-100+ years) discharges an ice reservoir by means of a sudden, brief, large-scale ice displacement, which moves many times faster than the glacier's normal flow rate between surges. During its active phase a surging glacier can be recognized by intense crevassing, sheared margins, and large ice displacements. When inactive it retains distinctive surface features from past variations of flow rate.

Through the use of aerial reconnaissance, Meier and Post (1969) and Post (1969) have identified 204 surging glaciers in western North America. These glaciers occur in the Alaska Range, the Chigmit, eastern Wrangell, eastern Chugach, and St. Elias Mountains.

This limited distribution of surging glaciers suggests the presence of certain common features which induce periodic instabilities. Indicated factors are unusual bedrock roughness or permeability in certain areas, anomalously high ground-water temperatures, and abnormal geothermal heat flow.

The phenomenon of glacial surging is not well understood. Initiation mechanisms have been proposed and discussed by a number of authors and reviewed by Robin (1969). Stress instabilities have frequently been suggested as a mechanism for triggering surges. Temperature instabilities (instabilities which result from deformation of basal ice due to an increased basal temperature) were suggested by Robin (1955). Theories that require an increase in basal temperature commonly propose basal sliding, surface accumulation, or fluctuating geothermal heat flow as the cause. Water-film instabilities at the ice-rock boundary surface have been suggested by Weertman (1962). Nielsen (1968)

has indicated the probable presence of mechanical instabilities associated with surging tributary glaciers. It is quite possible that more than one mechanism may be involved in initiating a glacier surge.

Glacier-flow velocities are extremely sensitive to the ice temperatures near the channel boundary and in other regions of high shear stress. The relationship of temperature to glacier flow has been given by Glen (1955); the possibility of sliding due to regelation of ice at its pressure melting point (Weertman, 1957, 1964, 1967; Lliboutry, 1968) is also a factor to be considered.

Purpose of the Program

For a quantitative theory of surge mechanisms and glacier flow, information concerning the channel shape and temperature regime of a surging glacier is essential. This information, however, has not yet been obtained because of the tremendous difficulty of making *in situ* measurements during and immediately after a surge. Therefore, it is likely that measurements on a presurge glacier may provide the most useful information for understanding surge mechanisms. For this reason, a program was initiated in 1967 on the Rusty Glacier. The intent is to produce a detailed description of the physical state of a glacier before a surge.

Rusty Glacier

The Rusty Glacier, a small valley glacier, is located on the continental side of the Icefield Ranges, and lies within the Steele Glacier drainage basin west of the Steele Glacier and north of the Hodgson Glacier (Fig. 1). The glacier is at an approximate elevation of 2250 m with the accumulation area at its southern end. It is 6-7 km long, its surface is relatively steep and it shares a common run-off system with its neighbors, the Backe² and Trapridge² Glaciers, to the west. The surrounding region is mountainous with Mt. Wood (4842 m) to the west and Mt. Steele (5073 m) to the south.

*Department of Geophysics, University of British Columbia, Vancouver

¹ Formerly unofficially known as the Fox Glacier

² Formerly unofficially known as the Jackal and Hyena Glaciers

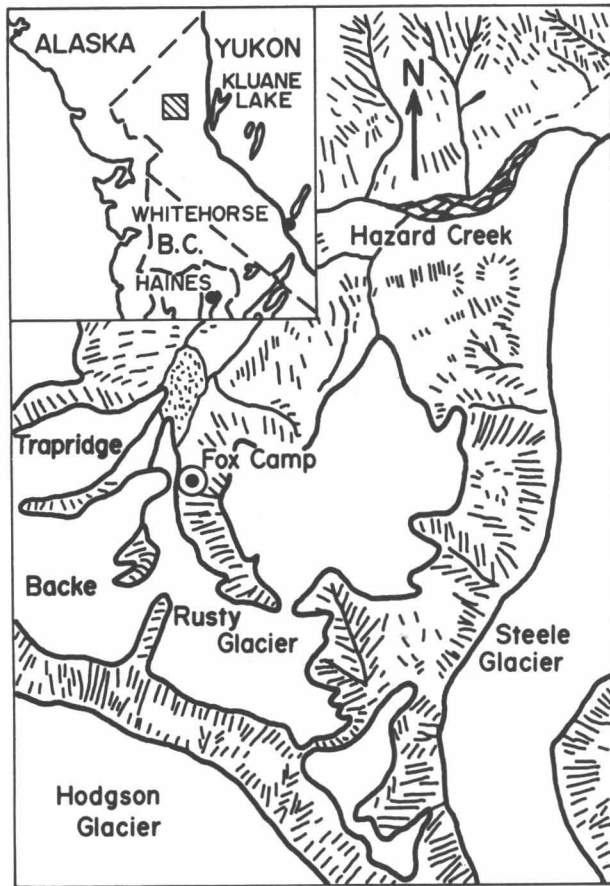


Fig. 1. Rusty Glacier location map.

The Steele Creek basin is reported to have sixteen surging glaciers. The Steele and Hodgson Glaciers, and certain tributaries, have surged as recently as 1966. Examination of morainal patterns (Sharp, 1943) suggests a general advance in the area, with a simultaneous advance of the Rusty, Backe, and Trapridge Glaciers about 100-200 years ago. Further evidence indicates that the Rusty, Backe, and Trapridge Glaciers have surged independently since that time.

EXPERIMENTAL RESULTS

Drilling Results

Thermal drilling produced a total of seven instrumented holes at six locations on the glacier; three holes apparently reached the base of the glacier. Figure 2 indicates the position of these sites in relation to the network of survey markers on the glacier. Five of the locations were along the longitudinal axis of the glacier; the sixth was near a headwall at the southern end of the accumulation region. The holes are numbered 1 through 6 in the order of their completion; two holes were drilled at Site 2. Survey-marker numbers are also included in the diagram.

Figure 3 is a gravity depth map of the Rusty Glacier showing the drilling locations.

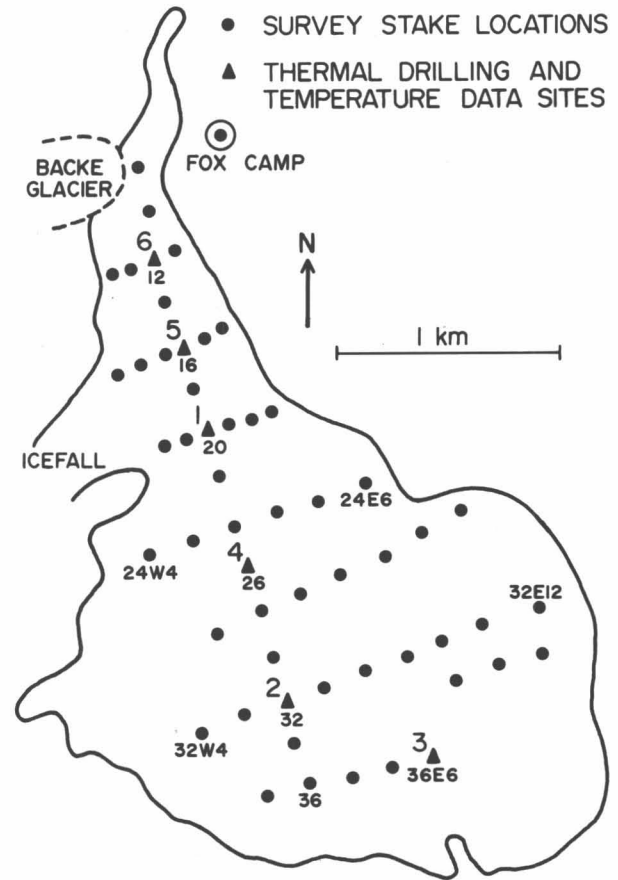


Fig. 2. Location map of Rusty Glacier thermal drilling sites.

Table 1 gives a condensed summary of the drilling results and compares drilled depths with gravity depths. The conclusion that a probe reached the bottom of the glacier was based on rapid reduction in drilling rate, or cessation of drilling, without evidence of probe burn-out or hole closure; and the compatibility of the depth reached with that determined by gravity. For these holes the depths as determined by gravity are within 5%-10% of the drilled depths. Probe and generator failures accounted for failure to drill to the bottom of the glacier in the other holes.

TABLE 1. Depths to Bottom of Glacier

Hole No.	Stake No.	Depth (m)		Bottom of glacier reached
		Drilling	Gravity	
1	20	48.8	50.6	x
2A	32	20.4	87.6	
2B	32	30.5	87.6	
3	36E6	30.2	64.6	
4	26	14.6	57.7	
5	16	27.7	30.6	x
6	12	32.0	29.0	x

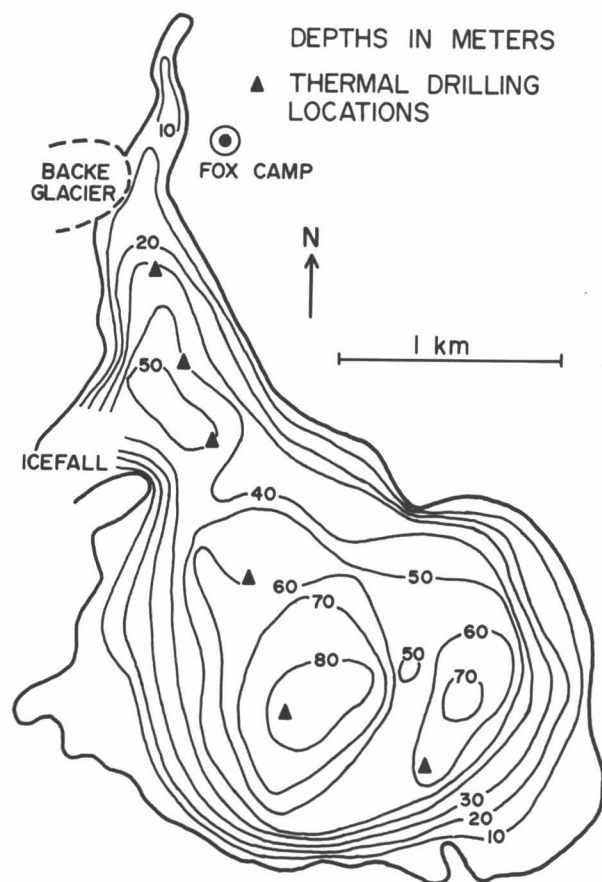


Fig. 3. Contour map of bedrock depths calculated from gravity observations for Rusty Glacier, after Crossley (1969). Thermal drilling locations are superimposed.

Temperature Results

Thermistor distribution. Thirty-six thermistors were placed in the Rusty Glacier during the course of the project. Of these, six were placed with a small glycol-circulating hand drill for a temperature comparison experiment which will be described later in this paper. The remainder of the thermistors were set with the thermal drilling apparatus. One additional thermistor was placed in the tongue of the Trapridge Glacier to determine its geophysical classification by monitoring temperature with depth (Ahlmann, 1948, 1953).

Figure 4 is a cross section of the glacier showing the thermistor distribution along the longitudinal axis. Holes 1 and 5 give the most complete temperature coverage.

Cooling curve. The use of hot-point drilling procedures results in a large thermal contamination of the surrounding ice. Cooling curves were plotted in order to determine the time required for the disturbed ice to reach an equilibrium temperature.

Thermistor measurements were made at Hole 4 over short time intervals after power to the probe was shut off. Data were obtained for depths of 5.5 m and 14.6 m. These data are plotted in Figure 5. The temperature drift for both depths is approximately 0.20°C between the fourth

and eighth day and 0.10°C between the eighth and twelfth day. There is no indication that equilibrium has been reached. Weather conditions which forced an evacuation of the field camp prevented continuation of the measurements.

An additional cooling curve was constructed for a fifty-day period from the primary field data. The thermistors at each drilled location were measured three times over the course of the field season and the dates noted. This information was sufficient to establish the curve in Figure 6. In this Figure, temperature offset is plotted against elapsed time and indications are that equilibrium is reached after thirty-six days. Temperatures measured at the twenty-fifth day are at equilibrium within the accuracy of measurement and reduction. Measurements prior to the twenty-fifth day can be adjusted to equilibrium values by using the curve.

The possibility of additional drift over a longer period of time, such as 0.10°C over fifty more days, cannot be excluded. It is felt, however, that all final temperatures are well within $\pm 0.10^{\circ}\text{C}$ of equilibrium value.

Rusty Glacier temperature data. Resistance measurements were made on each thermistor three times during the two-month field season. A standard Wheatstone bridge arrangement (L+N 4760) was employed and errors due to self-heating were avoided by maintaining the input voltage at 0.2 v. Lead resistance was determined by measuring the resistance of the two common conductors connected in series.

The "final" temperature was in most cases the last measured temperature for a particular thermistor. In every case, except that of Hole 4, the final temperature was taken twenty-five or more days after placement and can be considered at equilibrium within the accuracy of measurement, $\pm 0.05^{\circ}\text{C}$, and definitely within a $\pm 0.10^{\circ}\text{C}$ accuracy. The error involved in calibration and reduction of calibration data, never greater than $\pm 0.01^{\circ}\text{C}$, is included in the measurement accuracy value.

Temperature values were averaged for thermistors which were at equilibrium for two or three of the measurements. Thermistors above the 10-m level showed, without exception, an increase in temperature with time at a rate which decreased with depth. This effect is attributed to the penetration of the warming segment of the annual temperature wave and does not influence the profiles at greater depths.

Temperatures for Hole 4 were corrected to equilibrium values by adding -0.20°C , the correction obtained from Figure 6.

Figures 7-12 show the temperature profiles for Holes 1-6; bedrock depths deduced from gravity values are indicated.

The temperature data for Hole 3 must be discounted in an analysis of the glacier's thermal regime because the meltwater drained from the hole through a subsurface crack and prevented the thermistors from being frozen into the surrounding ice. As a result the temperatures measured were probably of the air or snow.

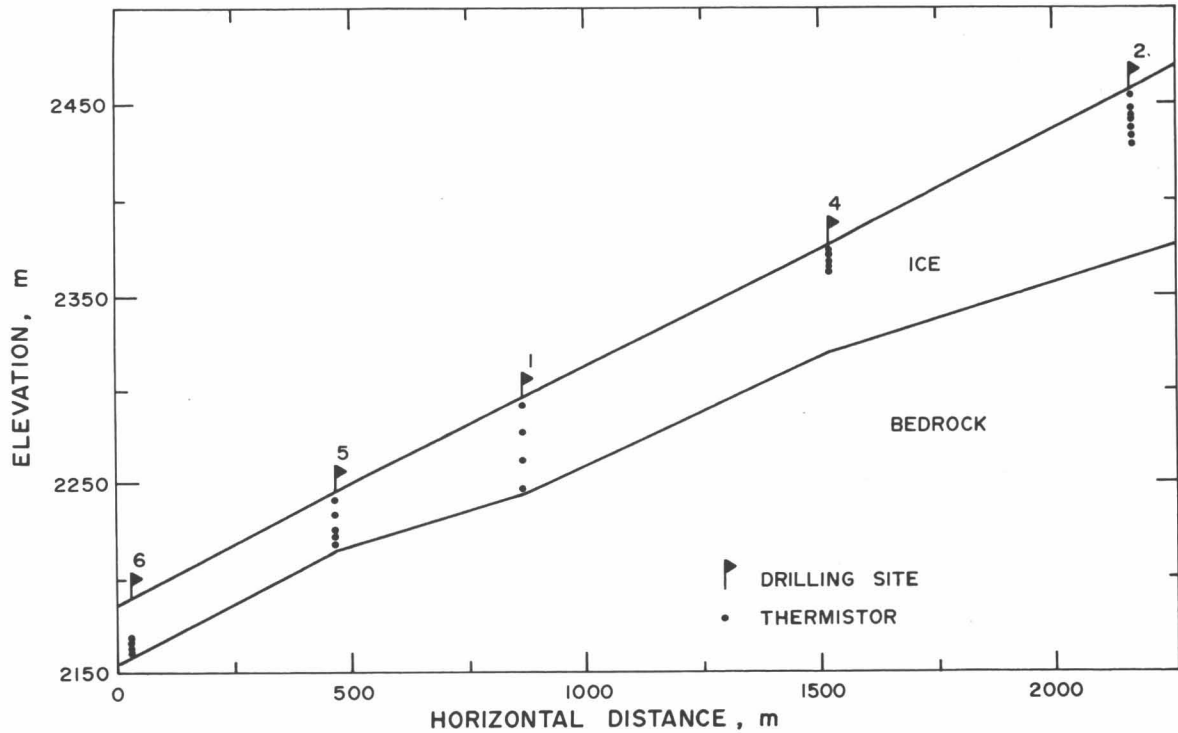


Fig. 4. Thermistor distribution along the longitudinal axis of the glacier (vertical exaggeration 4 x).

Additional results. A 6.4-m hole was drilled in the tongue region of the Trapridge Glacier with a small brine-circulating hand drill designed by S. Collins. A salt solution was used for the drilling operation and flushed out of the hole with fresh water before the thermistor was placed. A measurement taken after nine days and corrected to an equilibrium value indicated that the temperature was -6.75°C .

The same drill was used for a hole at Site 4 and an ethelene glycol solution circulated through the hole. This solution was left in the hole and thermistors were

placed at depths equal to those placed by thermal drilling and within 10 m of that location. Table 2 compares the equilibrium temperatures for the two methods.

Except for the 5.5-m depth, the glycol temperatures are slightly warmer. The differences, however, are not systematic, which may indicate the influence of local features. Since these results are not conclusive, and the effect of glycol on ice-temperature measurements is a matter of controversy, a rigidly controlled experiment would be valuable.

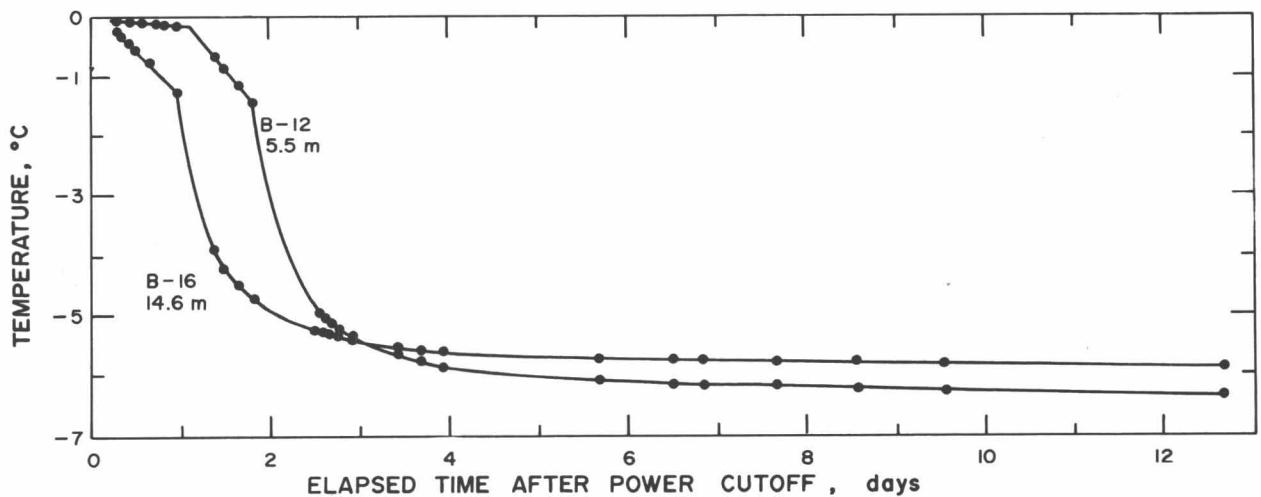


Fig. 5. Cooling curve from data taken at Hole 4.

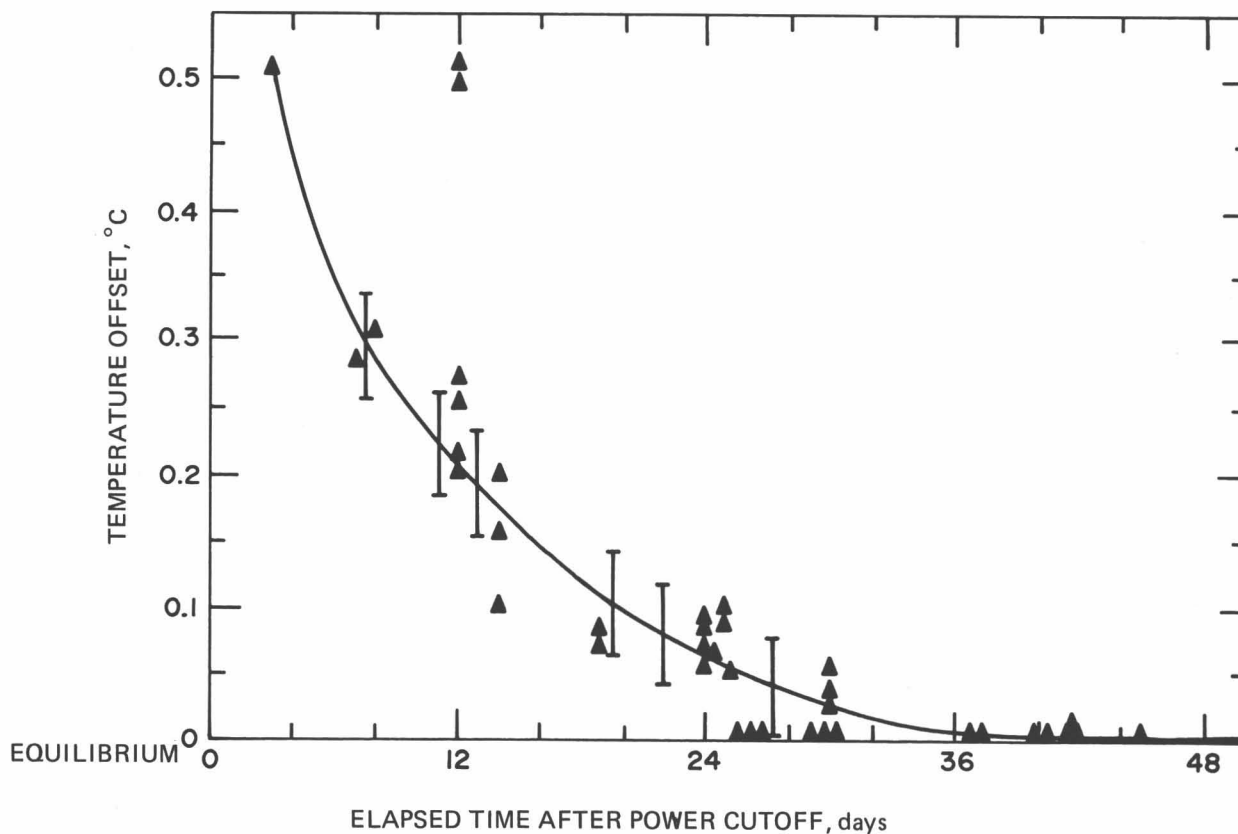


Fig. 6. Fifty-day cooling curve.

DISCUSSION

Geothermal Heat Flow

Estimates of geothermal heat flow were determined for the three drilling locations at which glacier bottom was reached. These values, corrected for the effects of topographic distortion, indicate an anomalous heat flow.

The heat flux Q was calculated using the relationship for uniform heat flow through a slab, $Q = (k/d) (t_1 - t_2)$ where k = the thermal conductivity; d = distance between the bottom two thermistors; t_1 = bottom temperature; t_2 = temperature at distance d from the bottom.

The thermal conductivity of ice varies with temperature and density. For the geothermal estimates based on the Rusty Glacier data, values of k were determined from

Pounder's (1965) formula $k = 5.35 \times 10^{-3} (1 - 4.8 \times 10^{-3} \theta)$ where θ is the ice temperature in $^{\circ}\text{C}$ between t_1 and t_2 . It was not necessary to adjust the conductivity for density variations since such variations were slight.

An examination of the gradients of Figures 7, 11, and 12 indicate a nonlinearity of the profiles with the gradient values decreasing with depth. An increase in density with depth is not sufficient to totally explain this curvature. It is likely that the curvature reflects the effects of a previous surge and thinning of the glacier, or a general climatic change in which case the heat-flow estimates are completely unreliable. In order to obtain these estimates it was assumed that the bottom gradients were near equilibrium and this would certainly not be the case if thermal instability surge theories have any validity.

The pattern of heat flow from the earth's interior is distorted near the surface by topographic relief. The flux is intensified by valleys and attenuated by ridges. To obtain regionally significant heat-flow values in areas of appreciable relief, these effects must be corrected.

A rapid estimation method (Lachenbruch, 1968), based on superficial gradient measurements at a horizontal surface between two plane slopes, was applied to the previously determined values. Plane valley models were constructed using topographic profiles, the anomalies calculated, and the corrections applied. The results are given in Table 3.

TABLE 2. Comparative Temperatures at Site 4

Depth (m)	Temperature ($^{\circ}\text{C}$)	
	Thermal hole	Glycol hole
3.1	-5.12	-4.68
5.5	-6.55	-6.62
8.5	-6.74	-6.68
14.6	-6.12	-5.82

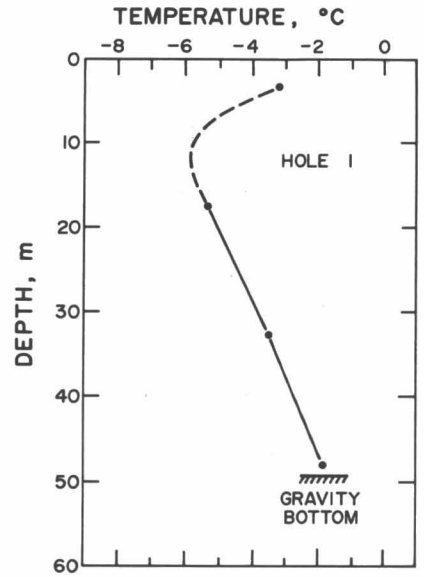


Fig. 7. Temperature profile, Hole 1.

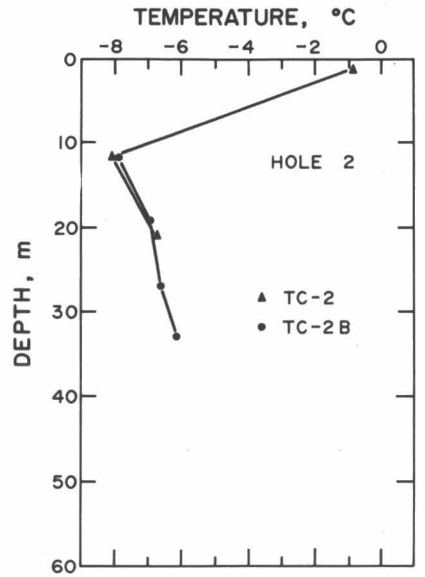


Fig. 8. Temperature profile, Hole 2.

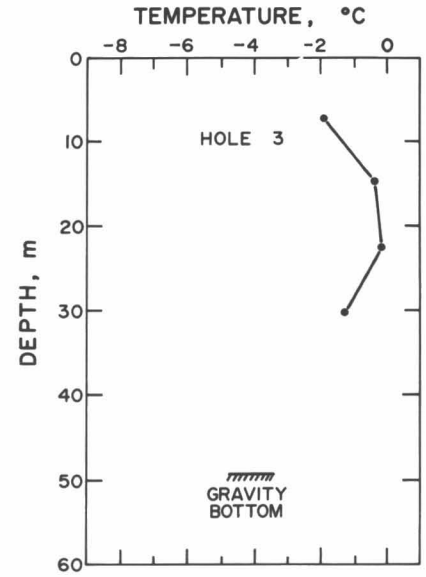


Fig. 9. Temperature profile, Hole 3.

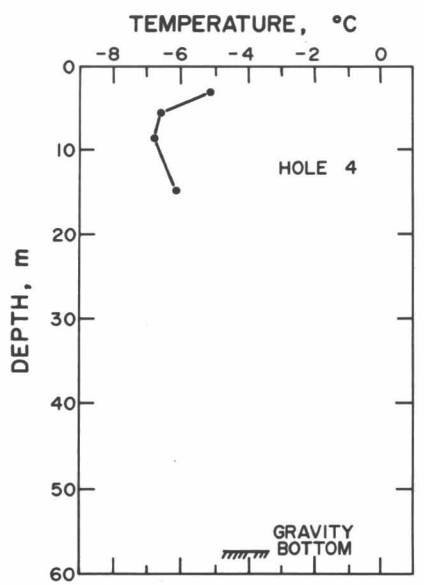


Fig. 10. Temperature profile, Hole 4.

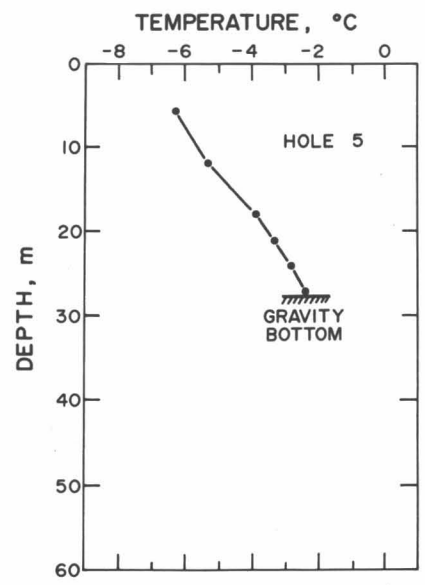


Fig. 11. Temperature profile, Hole 5.

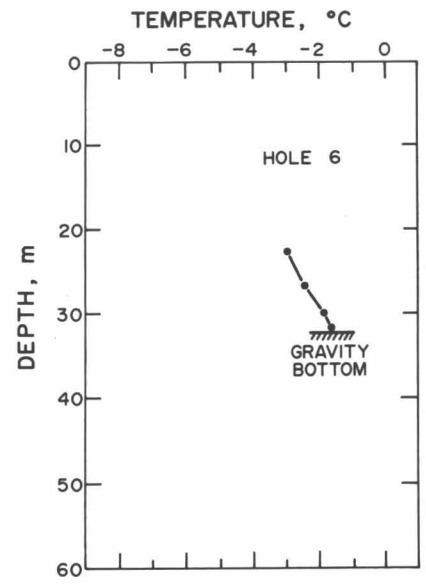


Fig. 12. Temperature profile, Hole 6.

TABLE 3. Heat Flux (Q) at Three Sites

Hole No.	Q ($\mu\text{cal}/\text{cm}^2 \text{ sec}$)	
	Calculated	Corrected
1	5.45	4.36
5	7.59	5.62
6	5.39	4.21

A method for calculating climatic corrections to heat-flow measurements was presented by Crain (1969). It was shown that small details of the climatic variations have little ultimate effect on the heat-flow correction. The critical factors are the transition times between glacial and interglacial periods and the difference in mean annual temperature between these periods. The most recent deglaciation alone accounts for 70% of the corrections.

Calculations based on the near-surface approximation for depths less than 150 m give corrections of $+0.52 \mu\text{cal}/\text{cm}^2 \text{ sec}$ for the most recent deglaciation (about 10,000 years ago) and $-0.21 \mu\text{cal}/\text{cm}^2 \text{ sec}$ for the previous glaciation (about 60,000 years ago), assuming a temperature increment of 10.0°C . The total correction is $+0.32 \mu\text{cal}/\text{cm}^2 \text{ sec}$. This indicates that the apparently high heat flow is not due to an uncorrected Pleistocene effect.

The averaged corrected Q is $4.73 \mu\text{cal}/\text{cm}^2 \text{ sec}$. Reasonable changes in the various parameters would not significantly change the heat-flow estimates. Since the commonly cited world average heat flow is $1.20 \mu\text{cal}/\text{cm}^2 \text{ sec}$, it is evident that the value obtained from the Rusty Glacier data is anomalous. Heat-flow values in the range $3.00\text{--}4.00 \mu\text{cal}/\text{cm}^2 \text{ sec}$ and higher are not uncommon, however (Lee and Uyeda, 1965), and have been known to occur near the crests of oceanic ridges, geothermal areas, and Cenozoic volcanic areas. The latter are often associated with some of the highest heat-flow values recorded. Since geological investigations by Sharp (1943) in the Steele Creek vicinity indicate that the Icefield Ranges is an area of Cenozoic volcanic activity, the high estimates of heat flow obtained from the Rusty Glacier data appear reasonable.

Our heat-flow estimates support Post's (1969) suggestion that a contributing factor to the extensive regional occurrence of surging glaciers in the St. Elias Mountains, and especially those in the Icefield Ranges, is a broad region of anomalous heat flow.

Lapse Rate

In the troposphere, mean air temperature decreases with altitude. In the dry snow and upper percolation facies of glaciers and ice sheets, the snow temperature measured at 10-m depth gives a reliable estimate of the mean annual air temperature at the surface (Benson, 1962). It is possible, then, to determine atmospheric lapse rate from 10-m temperatures.

TABLE 4. Data Used in Computing Lapse Rate

Elevation (m)	Temperature ($^\circ\text{C}$)	Hole No.
2182	-4.8	6
2242	-5.7	5
2291	-6.2	1
2378	-6.4	4
2459	-8.1	2

A lapse rate was calculated using 10-m temperatures from five bore holes on the Rusty Glacier. The data (Table 4) were plotted and a least-squares fit to the points determined.

The resulting gradient was $-10.6^\circ\text{C}/\text{km}$. This is compared in Figure 13 with the value $-16.0^\circ\text{C}/\text{km}$ found in the St. Elias Mountains by Grew and Mellor (1966), and $-14.0^\circ\text{C}/\text{km}$ for the same latitude (61°N) in Greenland determined by Mock and Weeks (1965). As a matter of interest, the dry adiabatic lapse rate, $-10.0^\circ\text{C}/\text{km}$, and the U.S. Standard rate (U.S. Standard Atmosphere, 1962), $-6.5^\circ\text{C}/\text{km}$, are plotted with the Rusty Glacier gradient in Figure 14.

Mock and Weeks (1965) found that gradients for northern Greenland were close to the dry adiabatic lapse rate and surmised that adiabatic warming of katabatic winds was the controlling mechanism. In southern Greenland gradients were markedly greater than those in the north.

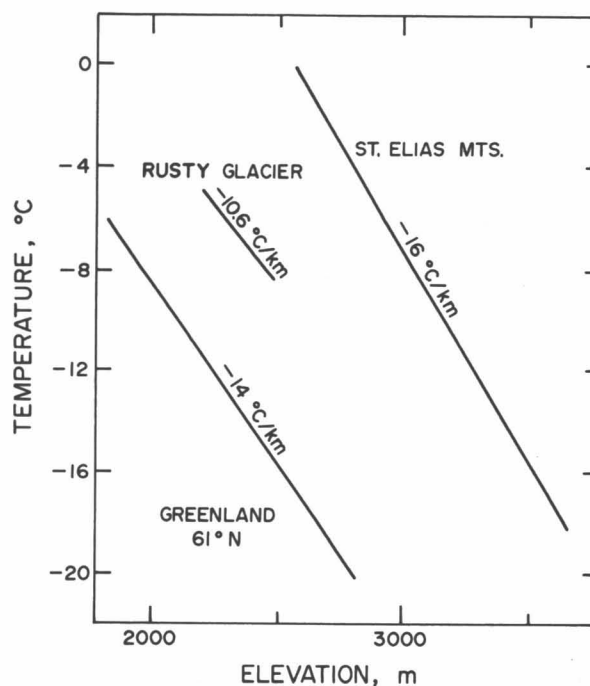


Fig. 13. Variation of temperature with surface elevation. Lapse rate from Rusty Glacier data is compared with other lapse rates at the same latitude.

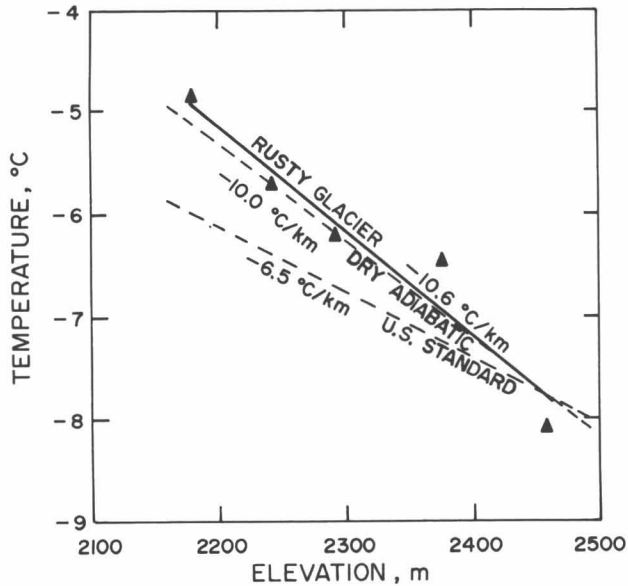


Fig. 14. Rusty Glacier, dry adiabatic, and U.S. Standard lapse rates.

This is thought to indicate the downward transfer of latent heat in the snow due to percolating meltwater.

Since the Rusty Glacier is a small, north-facing valley glacier surrounded by a complex topographic system, katabatic winds are not likely to be the primary controlling factor in determining the lapse rate.

Since percolating meltwater increases the lapse-rate value determined from snow temperatures, it is interesting to note the effect of eliminating such data. If the data from Hole 2, the only location influenced by this factor, are discarded from the Rusty lapse-rate calculation, a value of $-8.0^{\circ}\text{C}/\text{km}$ is obtained. This value is remarkably similar to summer environmental lapse rates determined by Marcus (1965) for the Kluane area using radiosonde data from a Whitehorse station. His values range from $-6.5^{\circ}\text{C}/\text{km}$ to $-8.4^{\circ}\text{C}/\text{km}$ for the continental slope. This suggests that the local climatology is the most directly controlling factor.

Bottom Temperature Models

Hypothetical glacier bottom temperature models were developed based on lapse rate, ice thickness, and englacial temperature gradients.

Using the previously determined lapse rate of $-10.6^{\circ}\text{C}/\text{km}$ for the Rusty Glacier, 10-m temperatures were calculated for each survey stake position. Each temperature was then extrapolated, based on ice depth and a selected temperature gradient, to obtain a basal value.

Two bottom temperature maps were created (Figs. 15, 16). For the first, Model A, a single reasonable temperature gradient was selected as representing the entire glacier and applied to determine the basal temperatures. The gradient, $0.11^{\circ}\text{C}/\text{m}$, was obtained from Hole 1 and

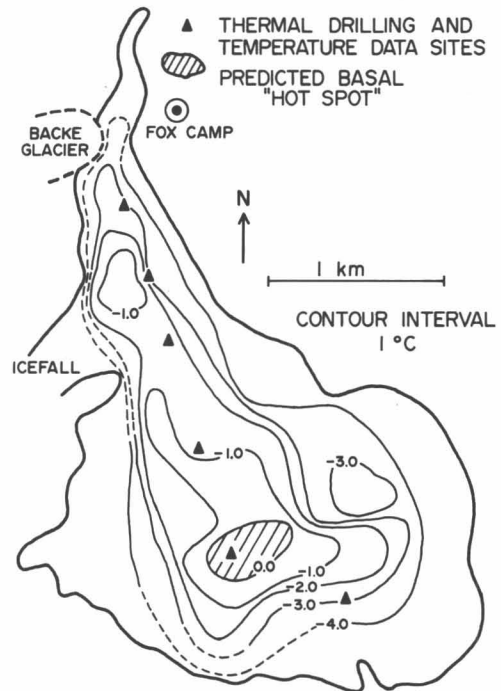


Fig. 15. Rusty Glacier bottom temperature map, Model A. Temperatures in degrees Celsius.

is a linear fit to the data. A variable gradient was used for Model B. Each drilling site was given a gradient value (Table 5), derived from the temperature profile for that location. This value was applied to the neighboring points so that the glacier was divided into five regions characterized by these gradients.

Both models indicate the presence of a hot spot, an area in which the predicted basal temperature is at the pressure melting point.

In Model A the hot spot is located in the accumulation region near Stake 32. Since the gravity interpretation was based on an infinite slab model, depths are likely to be underestimated. It is therefore possible that the actual depths in the upper regions of the glacier are greater, in which case the hot-spot area would be more extensive than indicated. Results of the 1969 survey (S. Collins,

TABLE 5. Temperature Gradients Derived from Profiles

Stake No.	Hole No.	Gradient ($^{\circ}\text{C}/\text{m}$)
12	6	0.14
16	5	0.16
20	1	0.11
26	4	0.10
32	2	0.08

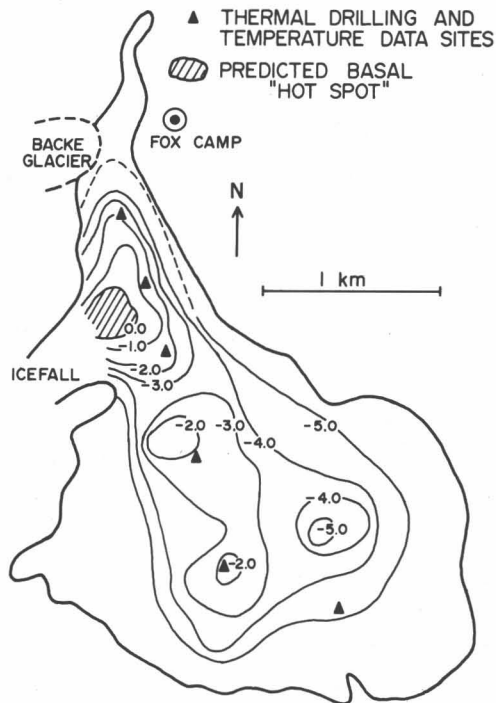


Fig. 16. Rusty Glacier bottom temperature map, Model B. Temperatures in degrees Celsius.

personal communication) reveal this to be the area of maximum glacier movement. This flow-rate maximum may, however, be a consequence of the ice thickness rather than an indication of melting at the bed.

Model B shows no basal melting zone in the upper regions of the glacier. The gradient information for this area, however, is not conclusive since the only available data were from holes very shallow relative to the glacier depth at that location. Since slight changes in the gradient value cause reasonably large variations in basal temperature at these depths, the possibility of basal hot spots cannot be disregarded for this model.

Conclusions

Thermal drilling on the Rusty Glacier resulted in three holes to the bottom of the glacier. Temperature measurements indicated that the glacier was below the pressure-melting point throughout. Temperature profiles suggest a disturbed thermal regime due to a previous surge.

Estimates of geothermal heat flow were determined and corrected for the effects of topographic distortion. These values indicate a heat flow which is anomalous but not unreasonable for the area.

Lapse rates determined from 10-m ice temperatures at a range of elevations give values in agreement with other lapse-rate information for the area.

Two glacier bottom-temperature models were developed and both indicate the possibility of areas in which the basal temperature is at the pressure melting point. One of the models suggests a hot spot in the accumulation region, the other a hot spot in the ablation region.

Confirmation of the basal temperature in the upper regions of the glacier by future drilling would be valuable in relating surge mechanism theories and the development of surge conditions for the Rusty Glacier.

Acknowledgments

We wish to express our sincere appreciation to the following people and organizations for their assistance: To H. W. C. Aamot, for design of the thermal probe system; to A. Stanley for his continued interest; to D. Crossley, T. Brewer, and S. Collins for helpful discussions; to B. Chandra for advice on thermistor calibration and for providing a computer program for the calibration reductions; to P. Michalow and D. Schreiber for technical advice and construction of equipment; and to D. Gray for his help in the field.

Special thanks also go to W. A. Wood, R. H. Ragle, and the Arctic Institute of North America for valuable support; to the Chemical Engineering Department of the University of British Columbia for use of calibration equipment; and to the U.S. Army Cold Regions Research and Engineering Laboratory for loan of seismic equipment.

This project was supported by grants from the National Advisory Committee on Water Resources Research, from the National Research Council, and from the U.B.C. Committee on Arctic and Alpine Research. Their assistance is gratefully acknowledged.

References

- Aamot, H. W. C. (1967a) Pendulum steering for thermal probes in glaciers, *Spec. Rept. 116*, U.S. Army Cold Reg. Res. Engin. Lab., 8 pp.
- Aamot, H. W. C. (1967b) Heat transfer and performance analysis of a thermal probe for glaciers, *Tech. Rept. 194*, U.S. Army Cold Reg. Res. Engin. Lab., 15 pp.
- Aamot, H. W. C. (1968) A buoyancy stabilized hot point drill for glacier studies, *Tech. Rept. 215*, U.S. Army Cold Reg. Res. Engin. Lab., 5 pp.
- Ahlmann, H. W:Son (1948) *Glaciological Research on the North Atlantic Coasts*, Roy. Geogr. Soc., London, 83 pp.
- Ahlmann, H. W:Son (1953) *Glacier Variation and Climatic Fluctuations*, Bowman Mem. Lects., Ser. 3, Am. Geogr. Soc., New York, p. 23.
- Benson, C. S. (1962) Stratigraphic studies in the snow and firn of the Greenland ice sheet, *Res. Rept. 70*, U.S. Army Cold Reg. Res. Engin. Lab., 93 pp.
- Crain, J. K. (1969) A simple method of calculating climatic corrections to heat flow measurements, *Can. J. Earth Sci.*, 6, 499-502.
- Crossley, D. J. (1969) Gravity and temperature measurements on the Fox Glacier, Yukon, M. Sc. thesis, University of British Columbia, Vancouver, 81 pp. (unpubl.).
- Glen, J. W. (1955) The creep of polycrystalline ice, *Proc. Roy. Soc. London*, Ser. A, Vol. 228, pp. 519-538.
- *Grew, E., and Mellor, M. (1966) High snowfields of the St. Elias Mountains, *Tech. Rept. 177*, U.S. Army Cold Reg. Res. Engin. Lab., 18 pp.
- Guest, P. G. (1950) Orthogonal polynomials in the least-squares fitting of observations, *Phil. Mag.*, 41, 124-137.

- LaChapelle, E. (1963) A simple thermal ice drill, *J. Glaciol.*, 4, 35.
- Lachenbruch, A. H. (1968) Rapid estimation of the topographic disturbance to superficial thermal gradients, *Rev. Geophys.* 6, 365-400.
- Lee, W. H. K., and Uyeda, S. (1965) Review of heat flow data, in *Terrestrial Heat Flow*, pp. 87-190, *Geophys. Monogr. No. 8*, Am. Geophys. Union, Washington.
- Lliboutry, L. (1968) General theory of subglacial cavitation and sliding of temperate glaciers, *J. Glaciol.*, 7, 21-58.
- *Marcus, M. G. (1965) Summer temperature relationships along a transect in the St. Elias Mountains, Alaska and Yukon Territory, *Man and the Earth, Ser. Earth Sci. No. 3*, Univ. Colorado, Boulder, pp. 15-30.
- Meier, M. F., and Post, A. S. (1969) What are glacier surges? *Can. J. Earth Sci.*, 6, 807-817.
- Mock, S. J., and Weeks, W. F. (1965) Distribution of 10-m snow temperatures on the Greenland ice sheet, *Res. Rept. 170*, U.S. Army Cold Reg. Res. Engin. Lab., 21 pp.
- Nielsen, L. E. (1968) Some hypotheses on surging glaciers, *Bull. Geol. Soc. Am.*, 79, 1195-1202.
- Philberth, K. (1966) Sur la stabilisation de la course d'une sonde thermique, *Compt. Rend.*, 262, 456-459.
- Post, A. S. (1969) Distribution of surging glaciers in western North America, *J. Glaciol.*, 8, 229-240.
- Pounder, E. R. (1965) *Physics of Ice*, Pergamon Press, Toronto, 151 pp.
- Raspet, R., Swartz, J. H., Lillard, H. E., and Robertson, E. C. (1966) Preparation of thermistor cables used in geothermal investigations, *Bull. 1203-C, C1-C11*, U.S. Geol. Surv., 11 pp.
- Robin, G. de Q. (1955) Ice movement and temperature distribution in glaciers and ice sheets, *J. Glaciol.*, 2, 523.
- Robin, G. de Q. (1969) Initiation of glacier surges, *Can. J. Earth Sci.*, 6, 919-928.
- †Sharp, R. (1943) Geology of the Wolf Creek area, St. Elias Ranges, Yukon Territory, Canada, *Bull. Geol. Soc. Am.*, 54, 623-649.
- Stacey, J. S. (1960) A prototype hotpoint for thermal boring on the Athabaska Glacier, *J. Glaciol.*, 3, 783-786.
- U.S. Standard Atmosphere (1962) United States Committee on Extension to the Standard Atmosphere, 278 pp.
- Weertman, J. (1957) On the sliding of glaciers, *J. Glaciol.*, 3, 33-38.
- Weertman, J. (1962) Catastrophic glacier advances, *Res. Rept. 102*, U.S. Army Cold Reg. Res. Engin. Lab., 8 pp.
- Weertman, J. (1964) Theory of glacier sliding, *J. Glaciol.*, 5, 287-303.
- Weertman, J. (1967) Sliding of non-temperate glaciers, *J. Geophys. Res.*, 72, 521-523.

*These reports were reprinted in an earlier volume of Icefield Ranges Research Project, Scientific Results.

†This report is reprinted in the present volume.

APPENDIX: INSTRUMENTATION

I

THERMAL PROBES

Probe Constructed at the University of British Columbia

The placement of temperature-sensing devices in the Rusty Glacier required a small practical drill capable of producing vertical holes to depths of 100 m or more in subpolar ice. The development of an electrically powered, cable-suspended drill to penetrate mountain glaciers is reported by LaChapelle (1963). Philberth (1966) and Aamot (1967a) discuss means of attitude stabilization. Aamot (1968) describes a buoyancy-stabilized hot-point drill for use on temperate glaciers and suggests adaptations for drilling in subpolar ice.

Drilling in cold ice, such as that of the Rusty Glacier, presents a special problem since the hole is likely to re-freeze, anchoring the power cable in the ice, before any great depth can be reached. Hole closure must be prevented or reduced to a rate compatible with drilling speed and estimated ice thickness. H. W. C. Aamot (personal communication, 1969) designed a thermal probe suitable for use on the Rusty Glacier. The design was based on an earlier model used for temperate ice (Aamot, 1968) with an added provision for line heating to reduce the hole closure rate.

Design description. The hot point suggested for use on the Rusty Glacier project is shown in Figure 1. The solid copper point is long, to achieve a large contact pressure with the ice. The electric heating element contained in the lower two-thirds of the cartridge is soldered into the copper. The buoyancy section consists of a tube of

laminated plastic, and it is bonded to the hot point and cap with an epoxy resin adhesive. Fusite feedthrough terminals in the cap connect to the power cable.

The probe dimensions and power specifications were selected to permit completion of 160-m holes in -6.0°C ice (Aamot, 1967b). A probe diameter of 7.6 cm was chosen with 2500 watts of power to be dissipated in the tip and 15.75 watts/m to be dissipated along the 160-m power cable. This arrangement provided a drilling speed of 4.0 m/hr and 40 hours of drilling time before the hole closed to 2.2 cm, a diameter slightly larger than the cable package.

Several modifications of Aamot's design were introduced. The original system, which called for high voltage and low current (1150 v, 4.3 amp) was replaced with a high-current, low-voltage arrangement (240 v, 20.6 amp). This eliminated the need of an isolation transformer, a high-voltage auto-transformer, and expensive high-resistance nichrome wire.

Tests prior to field use indicated that the wall thickness of the buoyancy chamber was not sufficient to withstand the anticipated pressures. Insufficient time prevented replacing the chamber, therefore the chambers of six probes were completely filled with an epoxy resin; in two others the buoyancy chambers were perforated to allow them to be filled with water, thus equalizing the pressure. The end cap was redesigned to permit attachment of a steering rod—about 2 m long—to replace the buoyancy guidance mechanism. The steering rod was not needed, however, since depths actually encountered were very shallow (50-80 m) and cavities in the ice were not evident.

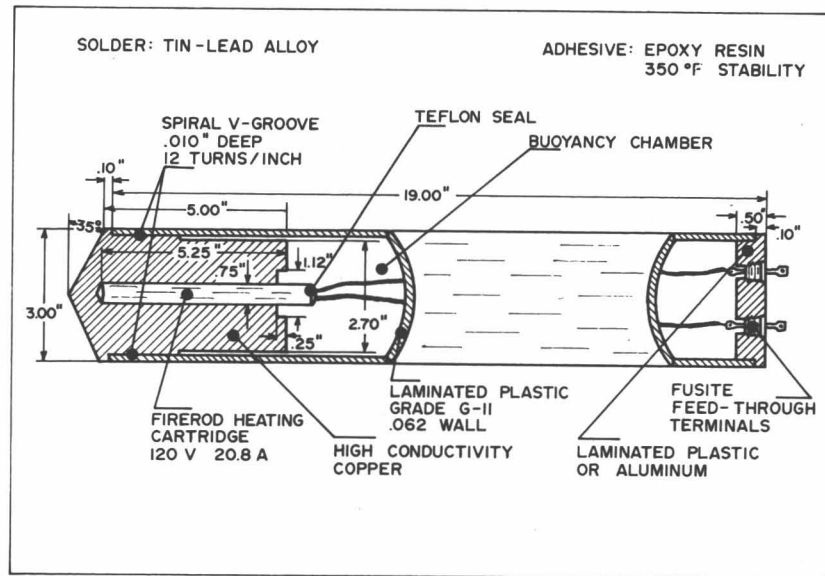


Fig. 1. Thermal probe design.

Field operations. A 5-kva Kohler generator (Model 5RMS65) supplied electrical power to the hot point. The generator, rated at 120/240 v, 20.8 amps, was equipped with a voltage regulator to allow a continuous current to be drawn, plus a fuel pump and line, and a control panel with voltmeter and ammeter. Voltage was varied by adjusting the engine speed, eliminating the necessity of a variable transformer. Fuel was taken from a fifty-gallon drum so that no drilling time was lost filling a small mounted tank.

The power supply cable, Belden 8471, was selected to dissipate approximately 15.75 watts/m. Since 17-gauge wire was unavailable, 16-gauge was used which provided a resistance of about 5 ohms per 300 m at 82°C with 14.10 watts/m power dissipation in the line.

Provisions were made for total as well as partial line heating with the addition of a 22-gauge, Belden 8740, copper cable. By connecting this cable in series with one of the conductors, the total 5 kva power could be dissipated in the line, doubling the heat delivered to the melt-water. If the hole closure proved to be less than estimated, the line heating could be reduced to one-half by parallel connection of the cables. Figure 2 shows line heating arrangements and power dissipation values.

The power cable package was laid out on the ice to prevent the overheating and resulting insulation deterioration which could occur with the cable on a spool. A thermistor cable was attached to the package at 5-m intervals as the probe descended.

Stacey-Type Probes

An additional eight hot-point probes were purchased from J. C. Savage of the University of Toronto. These were designed for drilling in temperate glaciers and the general construction was based on the prototype model developed by Stacey (1960). The main differences were

the shape in which the Calrod heaters were wound, the termination of the heater (no longer a copper block), and

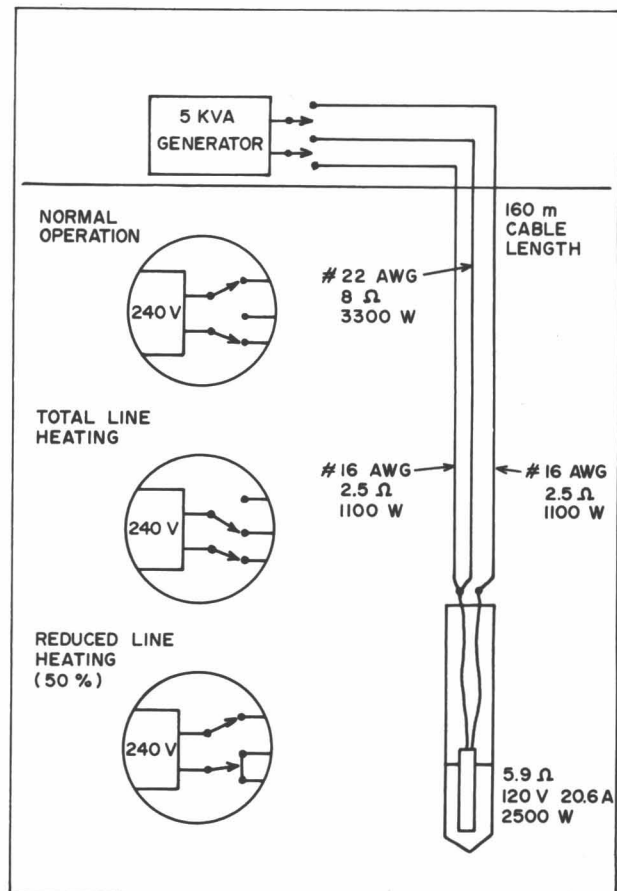


Fig. 2. Line heating—240-v operation.

the threaded seal with annealed copper gasket which replaced the Kovar seal.

The probes, heated by Calrod elements with nominal resistance of 17 ohms, drew approximately 10 amps. As a result only one-quarter of the power was dissipated in the line and the probes had a 35-m depth limit in the -6.0°C ice.

Probe Performance

Performance of the U.B.C.-constructed probes was below expectations. In only one instance did the actual drilling rate match the anticipated rate of 4.0 m/hr. In the remaining cases, the rates ranged from 1.0-1.5m/hr with substantial sidewall melting. There were a number of factors which apparently explain this. Dissection of a faulty probe revealed that the Silastic-140 seal in the moat around the upper section of the element had failed. Since the element had not been soldered into the copper tip (a thermal compound was used), water seeped into

the small cavity at the base of the heating element. This reduced conduction to the tip of the probe causing greater sidewall heating and a slower drilling rate.

In addition, it was later noted that the Firerod heating element resistances were as much as one ohm less than specified by the manufacturer. This resulted in a 17% power loss at the point. It is also possible that the elements were not inserted far enough into the copper tip. All of these factors presumably contributed to the overall probe performance.

Only one element burn-out was experienced during drilling and this was due to accidental overloading. Persistent generator difficulties, however, prevented completion of three holes.

The Stacey-type probes performed well, but due to their lower power and smaller diameter were limited to shallow holes. Only 10 amps were drawn by these probes which reduced the line heating to 25% of the desired value. The resulting 35-m depth limit restricted their use to the thinner sections of the glacier.

II

THERMISTORS

For the englacial temperature measurements Fenwal GB31P2 thermistors were selected. These glass bead thermistors were probe mounted for ease of handling, the probe being 14 mm long with 51 mm leads. The units had a nominal resistance of 1000 ohms at 25°C , β of 3500, and a dissipation constant of 1 mwatt/ $^{\circ}\text{C}$.

Results accurate to 0.10°C over the range -10.00°C to 0.00°C were sought. This unit with the appropriate bridge would allow an accuracy of $\pm 0.03^{\circ}\text{C}$ for the field measurements.

Calibration

Calibration of 56 thermistors was performed using the following equipment: Haake TP-41 constant temperature bath with a PolyScience Corporation model KR-30, quarter-horse compressor cooling unit; a Dymec model 2801-A digital readout quartz thermometer as a standard; a General Radio Company 1432M decade resistor with a Leeds and Northrup 2437 null detector in a bridge circuit with 25,000-ohm legs; and a voltage divider monitored by a KEW66 multimeter.

A selector switch allowed batch calibration of 23 thermistors. The thermistors were prepared by connecting one lead of each to a conductor of a 24-conductor cable and the other lead to a common conductor. The leads were covered with plastic tubing and the joints insulated to prevent current leakage and shorting.

The constant temperature bath fluid was a mixture of 80% water and 20% methyl alcohol which allowed temperatures below 0.00°C . The thermistors were calibrated in $3.00 \pm 0.01^{\circ}\text{C}$ intervals over the range -12.00°C to 0.00°C , the anticipated range of glacier temperatures. Figure 3 shows the thermistor calibration circuit.

The calibration data were reduced to tables of temperature versus resistance. Values of resistance were given for each individual thermistor over the range of calibration temperatures in increments of 0.01°C . The difference between calibrated resistance and computed resistance at the calibration points was also recorded to provide an estimate of the fit accuracy.

The data reduction was based on a method developed for least-squares curve-fitting of non-equidistant data in terms of orthogonal polynomials and power moments (Guest, 1950). The technique was applied to the thermistor calibration data for the function $R = \text{EXP}(A + B/T + C/T^2)$ using a computer program written by B. Chandra of the Department of Geophysics, University of British Columbia.

Self-Heating Considerations

The Fenwal GB31P2 thermistor has a dissipation constant of 1 mwatt (dc)/ $^{\circ}\text{C}$. This in turn changes the resistance by 5%.

To reduce the self-heating and the resulting errors in measurement, it is necessary to limit the current through the thermistor to a level compatible with the desired accuracy. This is accomplished by placing a voltage divider across the bridge power supply so that the voltage may be reduced to the required level.

The bridge input voltage, E_{in} , is determined from the relationship $E_{in} = 2E$, where $E = (PR)^{1/2}$. R is the resistance of the thermistor at midpoint of the temperature range and P is the dissipation constant of the thermistor which will give the desired accuracy. For 0.01°C allowable offset, $P = 0.01$ mwatts. In this case R is 4000 ohms which gives an E of 0.2 v. The maximum input is thus 0.4v.

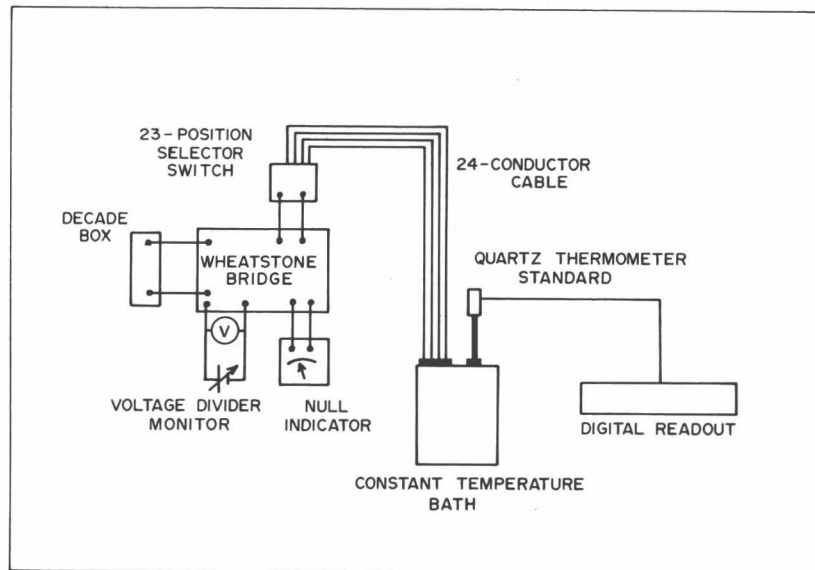


Fig. 3. Thermistor calibration unit.

A bridge voltage of $E_{in} = 0.2\text{v}$ was used for the field measurements which reduced the error due to self-heating far below the error involved in the measurement apparatus itself.

Preparation of Thermistor Cables

The installation of thermistors in a multiconductor cable required careful attention, since each thermistor had to be cushioned, waterproofed, and properly identified. The construction of the thermistor cables was based on procedures developed by the U. S. Geological Survey (Raspert, *et al.*, 1966).

Belden 8488, eight-conductor, 22-gauge, antenna-rotor cable was selected for use as the thermistor cable. Each conductor was vinyl insulated and the entire package encased in a chrome vinyl jacket.

The cable was cut to the proper length as determined from gravity depths (Crossley, 1969) and thermistor positions indicated. Markers were also placed at 10-m intervals for determining hole depth.

Approximately 10 cm of the outer jacket was cut away at the proper position to accept the thermistor. The conductor, located by color code, was cut, stripped, and covered with insulating tubing. The thermistor leads were soldered to the conductor with a low-powered iron and the tubing placed over the joints to prevent shorting. The thermistor was then placed against the cable, cemented with Ambroid, and sealed with Alpha FIT-300 heat-shrink tubing. A final wrapping with self-vulcanizing tape completed the pod.

Only six thermistors were installed on a cable; the two remaining conductors were used to measure the lead resistance. The lead resistance is subtracted from the total circuit resistance to give the thermistor resistance.

Since the cables were to be used only once, no special connectors were installed on the upper end; the leads were

simply taped into a plastic bag until it was time to take the measurements.

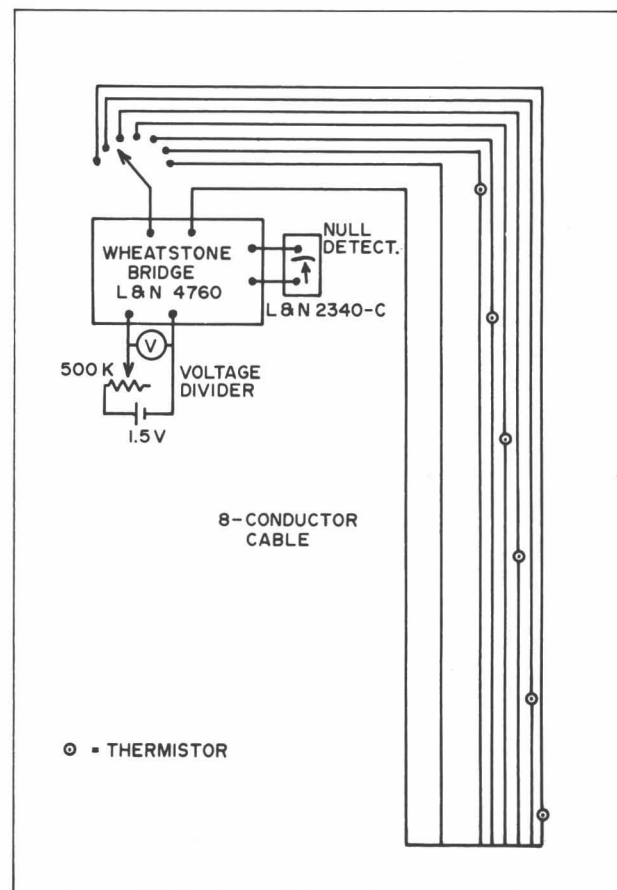


Fig. 4. Field measurement circuit.

Field Measurements

Field measurements were made with a Leeds and Northrup 4760 D-C Wheatstone Bridge and a 2340-C pointer type galvanometer. Power was supplied by a 1.5-v dry-cell battery. A voltage divider monitored by a KEW66 multimeter permitted the use of low voltages

(0.2 v) thus eliminating errors due to self-heating of the thermistor. Figure 4 shows the field measurement circuit.

This arrangement allowed resistance measurements of moderate precision. The limit of error was $\pm 0.15\%$ of the dial reading, or ± 0.02 to $\pm 0.03^\circ\text{C}$ over the range of resistances encountered.

Abundances of Isotopic Species of Water

in the St. Elias Mountains

K. E. West and H. R. Krouse**

ABSTRACT. Snow and ice samples were collected from the St. Elias Mountains during the summers of 1968 and 1969. The collection sites included Mt. Logan (elevations up to 5800 m), Divide (the accumulation area of the Hubbard and Kaskawulsh Glaciers), and Rusty Glacier (a glacier with possible surging properties). The $\delta\text{H}_2\text{O}^{18}$ values varied from -45.1‰ (SMOW) on Mt. Logan, elevation 5680 m, to -14.8‰ (SMOW) at the Rusty Glacier, rainfall at 2460 m elevation. The $\text{H}_2\text{O}^{18}/\text{H}_2\text{O}^{16}$ data elucidated complex weather patterns caused by the St. Elias Mountains acting as an obstacle to easterly flow, as well as giving insight into the flow pattern of the Rusty Glacier.

INTRODUCTION

In the summer of 1968 and 1969, ice and snow samples were collected in the St. Elias Mountains of the Yukon. The collection sites included Mt. Logan, Divide, and the Rusty Glacier (Plate 1).¹ The data reported will be given in det units where:

$$\delta\text{H}_2\text{O}^{18} \text{ or } \delta\text{O}^{18} = \left[\frac{(\text{H}_2\text{O}^{18}/\text{H}_2\text{O}^{16}) \text{ SAMPLE}}{(\text{H}_2\text{O}^{18}/\text{H}_2\text{O}^{16}) \text{ SMOW}} - 1 \right] \times 1000$$

SMOW = STANDARD MEAN OCEAN WATER
($\delta_{\text{SMOW}} = 0.00\text{‰}$).

In the discussion we have assumed that the precipitation in this area is the result of a Rayleigh condensation process (Dansgaard, 1964) from a limited vapor reservoir. The data therefore will be interpreted in terms of latitude, altitude, and seasonal effects.

Continental temperatures generally decrease with increasing latitude. Greater temperature gradients between the source and the location of precipitation result in greater isotopic selectivity, as witnessed by greater depletion of H_2O^{18} with increasing latitude. Altitude effects are due to preferential loss of the heavier isotopic species at lower altitudes, and the fact that higher elevations usually have lower temperatures (that is, air masses cool as they rise, causing Rayleigh condensation, which means lower δ values as the vapor reservoir becomes depleted at higher elevations). Seasonal variations in the isotopic composition of precipitation arise mainly from the varying temperature gradients between the source and the

precipitation area. Minimum δ values are encountered in the winter and maximum values in the summer or early fall.

The isotopic composition of snow that falls in the accumulation area of a glacier is affected by all the fore-mentioned mechanisms. Latitude normally affects only the average δ value while altitude has a more complex effect. Since the majority of snow basins of glaciers have a fairly steep gradient, the δ values of the snow decrease as one gets farther above the firn line. Upon disappearing below the surface, the snow transforms into ice to reappear later below the firn line. It should then be possible to elucidate the origin of the ice and hence the mechanics of the glacier's flow since the altitude effect, in principle, places an isotopic label on the origin of the ice.

DIVIDE STATION

In mid-July of 1968, a 5.4-m deep snow pit was dug at the Divide camp (elev. 2640 m) which is located in the accumulation area of the Hubbard and Kaskawulsh Glaciers. This area was the first to be sampled since a helicopter could not be reserved to reach the Rusty Glacier until late July.

Results

Temperature. Temperature readings were taken every 10 cm from a freshly cut wall. The average temperature was -0.3°C down to a depth of 370 cm (Fig. 1). From 370 cm to 490 cm there was a steep temperature gradient which showed signs of stabilizing at -2.8°C between 490 and 540 cm.

In accordance with density and δO^{18} determinations, the previous summer level, 1967, was placed at 360 cm.

*University of Alberta, Edmonton, at time of writing; present address, Department of Physics, University of Calgary, Alberta
¹Plate 1 is a map inside the back cover of this volume.

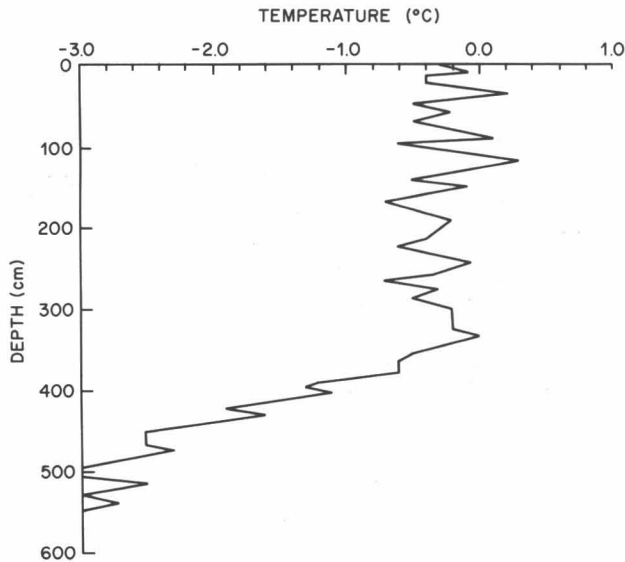


Fig. 1. Temperature profile of Divide Pit (elev. 2640 m; July 1968).

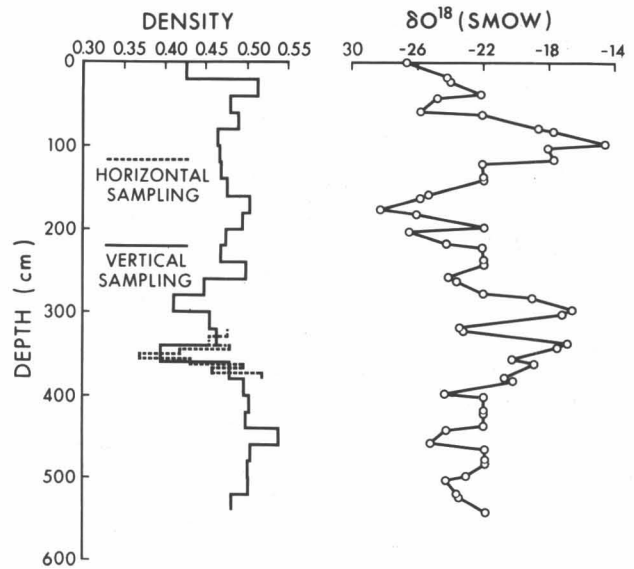


Fig. 2. Density and isotopic profiles of Divide Pit (elev. 2640 m; July 1968).

This means that the warming by mid-June had removed all indications of temperatures identified with the previous winter's accumulation. Supposedly, this warming effect would have penetrated deeper as the melt season progressed. The reasons for this warming effect are:

- (1) latent heat released by refreezing of meltwater;
- (2) penetration of heat from the warmer summer radiation.

The temperature profile of Figure 1 would indicate that this pit was in an area of percolation facies. Observations by other workers (Wagner, 1969; Grew and Mellor, 1969) agree with this conclusion.

Density. The density measurements were taken with CRREL-designed equipment. The average density was found to be 0.478 gm/cm^3 . This is greater than expected for percolation facies (0.43 to 0.39 gm/cm^3) but it is similar to the densities found by Wagner (1969). The density at the surface of the pit was low, and increased sharply to a local maximum at 20–40 cm (Fig. 2). Density usually remains low at the surface, where low body stress limits mechanical compaction, and grain growth reduces capillary retention of meltwater, thus allowing it to drain to lower layers.

Ice lenses were found at 60, 160, and 245 cm. It seems unlikely that direct solar radiation alone would have caused melting at a sufficient rate to form these lenses, since the daytime heating would have been offset by nightly cooling. It seems more likely that these lenses were formed by sustained convective heating during warm spells of several days' duration or perhaps from rainwater.

The two low-density anomalies at 280 and 356 cm were in depth hoar. This was presumably formed in the autumn when vapor, due to the latent heat released by

refreezing summer meltwater, contacted the cooler autumn snows and froze, forming a layer of large, loosely packed snow crystals. The two anomalies indicate a sort of Indian Summer at 280–300 cm with the cold spell from 300 to 340 cm and the end of the summer near 356 cm. The high density at 440–460 cm was probably due to small, closely packed firn crystals from the winter of 1966–1967. Wind packing could also be a cause.

The small variation in the density shows that considerable homogenization has been achieved by the action of percolating meltwaters. Little mechanical compaction, however, seemed to have occurred in the snow pit.

Oxygen isotopes. The oxygen isotope profile of the snow pit was quite complex. The classical profile of minimum δ values corresponding to winter precipitation and more positive ones for the summer precipitation can be seen in Figure 2 if the upper 60 cm are ignored. A positive peak at 350 cm corresponds closely to the end of the melt season as suggested by the corresponding low-density anomaly. Another positive peak at 300 cm corresponds to the density anomaly at 290–300 cm, attributed to an Indian Summer. Below 360 cm, there is evidence of another negative peak, representing the winter of 1966–1967. The spread of the δ values is much less than for the 1967–1968 samples as a consequence of homogenization.

If the upper 60 cm are again disregarded the results are comparable to those of MacPherson and Krouse (1967) from a pit dug on June 30, 1963 near Divide camp (Fig. 3). The MacPherson pit had a smaller range of δ values and a slightly more negative average δ value. This indicates that while the 1962–1963 average temperature was colder than 1967–1968, the winter minimum and summer maximum

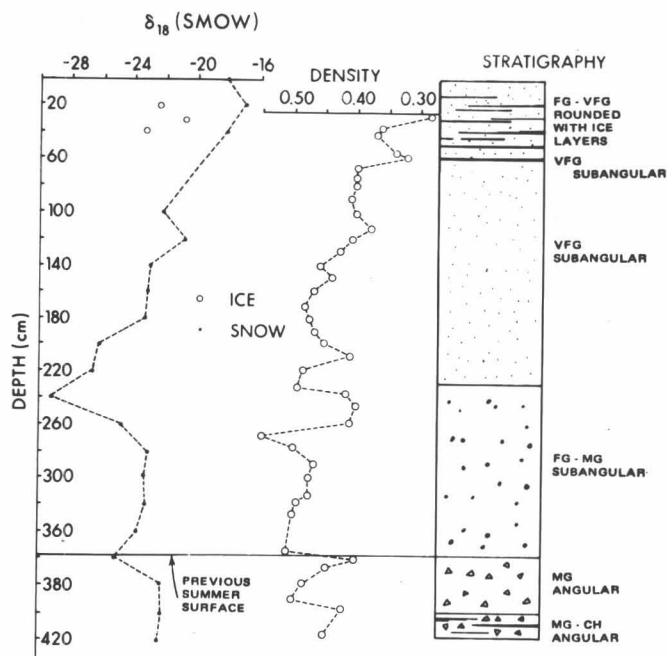


Fig. 3. Pit I of MacPherson and Krouse (1967) (elev. 2640 m; June 30, 1963).

temperatures were greater in 1967-1968. The relative positions of the minimum δ values suggest that 1962-1963 had more snow in the spring than fall or early winter while equal amounts of snow fell after and before the δ minimum in 1967-1968. The latter was probably due to snowfall during the warming spell indicated at 270 - 300 cm. The density profile of the MacPherson pit was less uniform, probably because it was sampled earlier in the melt season. There may also have been less uniformity of the δ values if this pit had been sampled in more detail. MacPherson's data points between 20 and 40 cm, attributed to ice layers, are similar in their δ values to the snow of the present study between 0 and 60 cm. Unfortunately, samples of ice layers were not collected in the present study.

The relatively negative δ values from 0 to 60 cm, (more positive δ values would be expected from spring and summer snowfall) allow some interesting conjectures which cannot be alluded to in the density, temperature, or stratigraphic observations. Divide camp is in an area of complex weather patterns; it is located near or in a zone of a climatological divide between continental and marine weather. Taylor-Barge (1969) has suggested that the oscillation of this climatological divide could place Divide camp in either weather pattern, or in the zone of change. Also Divide camp lies in the rain shadow of Mt. Logan.

Friedman and Smith (1970) analyzed the deuterium content of snow cores of several transverse of the Sierra Nevada divide. The altitude relationship was particularly

well defined west of the divide, but was not well defined east of it. Samples from east of the divide tended to be 10‰ to 15‰ less than samples collected at the same elevation west of the crest. Therefore, if the climatological divide moved to the west of the Divide camp pit in the spring and early summer, one would expect more negative δ values as found by Friedman and Smith.

Another explanation of these data could be the fact that during this period most of the precipitation could have been brought by westerlies which first had to pass over Mt. Logan. This again would place the meteorological divide west of Divide camp and the pit would be in the rain shadow of Mt. Logan. The expected decrease in precipitation because of the rain shadow, however, is not seen for this period.

The phenomenon of an easterly flow, although uncommon, is a third possible explanation. This might give Divide a simulated continental source, which would be expected to give more negative δ values. Although cloud build-up was seen in the east in mid-June, no weather observations were taken in the spring to confirm or refute this explanation.

Therefore, although the $\delta\text{H}_2\text{O}^{18}$ data point out meteorological complexities in the spring and early summer not revealed by density, temperature, or stratigraphic observations, more information is needed to discern the mechanism which caused these complexities. Depletion of $\delta\text{H}_2\text{O}^{18}$ by meltwater percolation, although a factor, was not considered a controlling factor.

MT. LOGAN

Introduction

Accumulation on Mt. Logan is controlled by several factors including topography, wind, elevation, and temperature. In a dry-snow region such as Mt. Logan, the total accumulation is equal to the sum of the precipitation, the snow blown in, and the hoar formation, minus the snow blown away and evaporation (Mellor, 1961). It is often impossible to determine the relative contribution of each factor.

Previous work by Alford (1967), Alford and Keeler (1968) and Keeler (1969) has given insights into accumulation on the lower slopes of the mountain and the summit plateau. Keeler (1969) found that above 2500 m, elevation appeared to exert little control over precipitation amounts. He stated that the reason for this may be that precipitation on Mt. Logan is associated primarily with frontal, as opposed to purely orographic, processes and that site-to-site differences in accumulation reflect local processes, such as redistribution by wind rather than elevational control. From these studies there is also no evidence that precipitation increases with elevation to a maximum before declining because of a depletion in the

moisture reservoir. This effect has been seen in Antarctica and Northern Greenland where topography plays a minor role in determining accumulation.

Results

In the summer of 1968, two snow pits were sampled, and in 1969 a 15-m snow core was taken. Unfortunately neither pit was sampled in great detail; nevertheless valuable information may be deduced from the results.

Pit I. Pit I was located in a narrow pass called the Northwest Col at an elevation of 5400 m. Stratigraphy and density relationships in this pit seemed to indicate an annual layer (J. C. La Belle, personal communication).

A low-density anomaly, associated with fall depth hoar, was found at 130 cm. The layer was also recognized by its friable appearance. This indicated a total annual thickness for 1967-1968 of 1.3 m of snow, with a mean water equivalent of accumulation of 0.41 m. This is considerably less than the accumulation that has been found on the summit plateau (up to 0.84 m water equivalent, Keeler, 1969). High winds which stream through the narrow pass were assumed to be responsible for the low accumulation.

The temperature and density data establish this region as one of dry-snow facies. The temperature profile did not seem to stabilize or show yearly fluctuations; this indicates that summer temperatures penetrate deeper than the previous annual layer.

The oxygen isotope data showed no seasonal trend. In fact, the profile was almost the inverse of what would normally be expected, with the positive peak in midwinter instead of summer (Fig. 4). This was probably due to

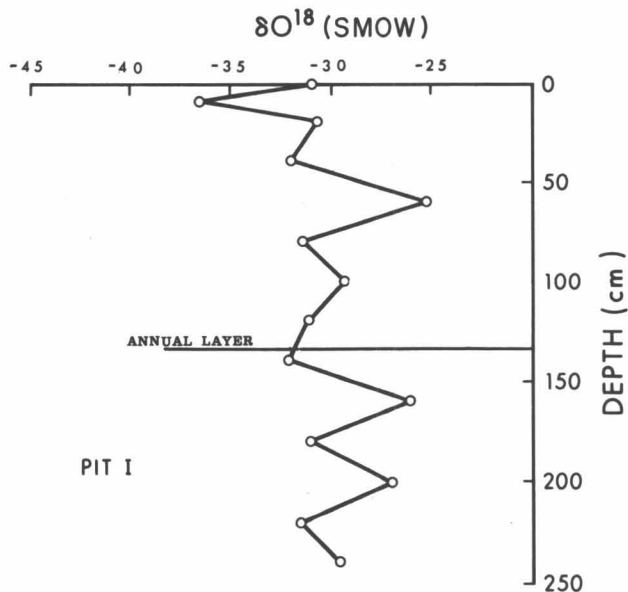


Fig. 4. Isotope profile of Pit I (Mt. Logan, Northwest Col; elev. 5400 m).

mixing, depletion, and replenishment from other areas by high winds. It is interesting to note that a negative peak, similar to the one in the Divide camp pit, appeared just below the surface. The pit had not been sampled in enough detail to make any assumptions from this coincidence, however. The average δ value of the pit was -31.7‰ .

Pit II. Pit II was in the snow dome, elevation of 5680 m, on the AINA Peak.² There were many layers of varying composition in the pit, but between the depths of 140 and 163 cm there was a layer of low density snow. Below this, layers of considerably greater hardness were found. If the low-density anomaly indicates the previous summer horizon, the accumulation of 1967-1968 would be 1.5 m of snow or 0.6 m water equivalent. This figure seems high for a summit, but this summit has no windward rocks to control or cause wind-scour (J. C. La Belle, personal communication).

The isotopic data showed a definite negative trend with depth (Fig. 5). Unfortunately, the pit was only sampled to a depth of 120 cm, so there is no way of knowing if the δ values would have become more positive between 120 and 160 cm, giving the normal annual isotopic profile. The most striking thing about both Pit I and Pit II is their minimum δ values, -38.6‰ and -45.1‰ . These values are normally associated with the extremely cold and arid regions of Antarctica and Northern Greenland. The average δ value of Pit II is -33.9‰ , which is more negative than the average of Pit I (-31.7‰), but this would be expected because of the change in elevation.

The temperature profile showed that this is a region of dry-snow facies and that summer heating has penetrated beyond the previous annual layer. Little or no information is given by these or other data, however, as to why snow accumulates on this particular peak. When compared to other peaks on Mt. Logan, it can only be described as

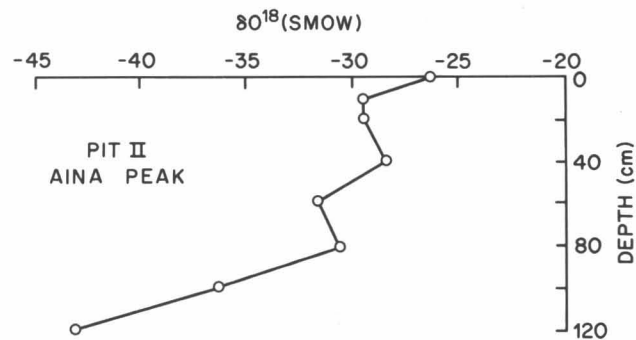


Fig. 5. Isotope profile of Pit II (Mt. Logan, AINA Peak²; elev. 5680 m).

²Unofficial name

an accumulation anomaly caused by peculiar topographic or orographic conditions which will require more detailed studies to be understood. It is of interest, however, that the presence of the isotopic trend with depth implies negligible wind mixing, which is a necessary condition to retain snow on this peak.

The snow core. A snow core was taken from the summit plateau (elevation 5400 m) near the AINA camp. Figure 6 shows the oxygen isotope profile, with the depth converted to water equivalent (W.E.). Two low-density anomalies, one at 1.0 m and the other at 2.5 m, were found. The one at 2.5 m (0.96 m W.E.) indicates the summer of 1968. This was positively identified by C. M. Keeler (personal communication) by using the 1968 spring surface as a reference horizon.

If we assume that a normal seasonal isotopic trend dominates, then the profile can be interpreted as in Table 1. The 82 cm accumulation for 1967-1968 agrees well with the accumulation measured by Keeler (1969) in 1968 on the summit plateau. His measurements ranged from 60 to 84 cm with an average of 70 cm for the year 1967-1968. The summer of 1967 was a high accumulation period and therefore 125 cm may not be unreasonable for 1966-1967. The accumulation at Divide in the snow budget year 1965-1966 was low. Therefore 139 cm would seem to be much too high, since both Divide and Mt. Logan experience the same major meteorological patterns. It is more reasonable to consider this depth as the sum of 1965-1966 and 1964-1965 precipitations since 1964-1965 was also a low accumulation year for Divide. This would mean that the summer isotopic maximum had either been

TABLE 1. Interpretation of Isotopic Profile

Year	Depth (W.E.) (cm)	Accumulation (W.E.) (cm)
1968-69	0-96	96
1967-68	96-178	82
1966-67	178-303	125
1965-66	303-442	139
1964-65	442-524	71
1963-64	524-593	69
1962-63	593-665	72
1961-62	665-742	77
1960-61	742-	---

erased by wind or missed because of sparse sampling. The latter seems the most likely and points out the need for detailed sampling to obtain a complete isotopic profile. 1962-1963 was a year of high accumulation at Divide, but this does not seem to coincide with the core data from Mt. Logan even if both interpretations of the 1964 to 1966 time span are considered. The expected winter minima of 1961-1962 and 1966-1967 are missing. This should not be surprising when one considers the dynamic mixing and wind-scour arguments invoked to explain the results of Pit I. It may also have been that small snowfalls occurred in these winters because of extreme cold. Isotopically this would result in thin layers with relatively negative δ values, which could be easily missed during sampling.

The average δ value of the core, -29.8‰ , is more positive than the average for Pit II (-33.9‰). This is expected on the basis of the elevation differences between Pit II and the core location. On the other hand when we compare the average δ^{18} values for two locations at the same elevation (the core and Pit I) for the same year (1967-1968), the agreement is remarkable (-31.6‰ and -31.7‰ respectively). Therefore, although elevation does not seem to affect the amount of precipitation on Mt. Logan (Keeler, 1969), it does alter the δ values significantly.

Discussion

If one plots the Mt. Logan results on a δ^{18} versus latitude graph, one readily ascertains the importance of altitude in determining the isotopic composition of precipitation (Fig. 7). The bars in the graph show the range of δ values of each of the cited locations. The Divide δ values are in the same range as those of the Rusty Glacier (see discussion below) and thus fit the general trend. Therefore, although accumulation studies show no depletion of the precipitation reservoir in the area of Mt. Logan, isotopic values do. In order to find the δ^{18} depletion with altitude, it would be necessary to do a traverse from the Gulf of Alaska to the summit plateau of

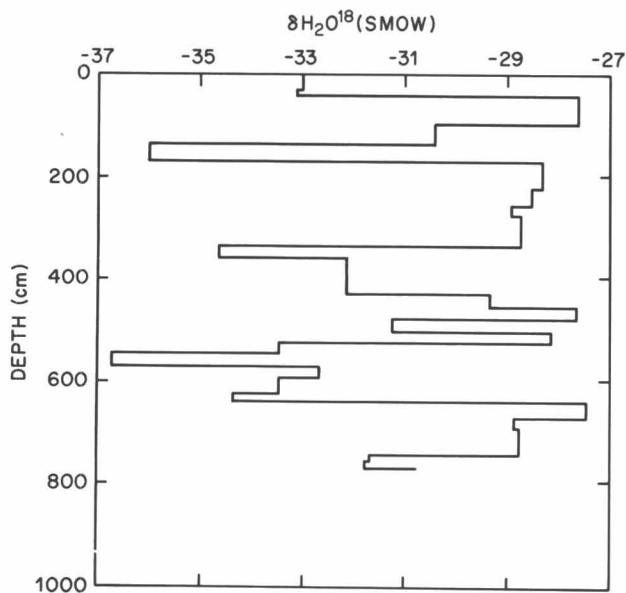


Fig. 6. Snow core from plateau on Mt. Logan (elev. 5400 m; summer 1969).

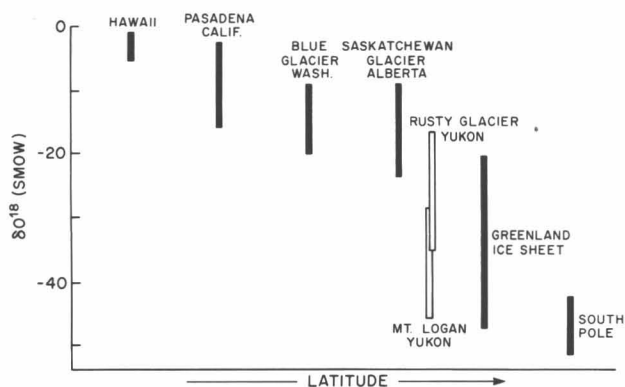


Fig. 7. $\text{H}_2\text{O}^{18}/\text{H}_2\text{O}^{16}$ composition of the precipitation at Rusty Glacier and Mt. Logan compared with the composition of precipitation at other latitudes (after Sharp, 1960).

Mt. Logan, along the path of the predominant precipitation storms. Using just the theoretical Rayleigh distillation model (Dansgaard, 1964) it would seem that the cloud systems have lost over 95% of their initial vapor. Dansgaard (1964) calculated the amount of vapor left if isobaric cooling from 20° to -20°C had occurred. His calculations gave 5.2% of the vapor left with the condensation (snow) having a δ value of -28.2‰ . Since the mean yearly temperature, recorded in a bore hole, of the summit plateau is -25.4°C (Keeler, 1969) and the average δ value of the Mt. Logan core was -29.8‰ , this precipitation model of straight isobaric cooling from 20°C , according to the Rayleigh condensation formula, seems to fit the Mt. Logan results. A completely analyzed traverse would be necessary to confirm this, however.

To check for kinetic effects due to orographic or other processes, samples from Mt. Logan, Divide Camp, and Rusty Glacier were sent to the Environmental Research Branch, Atomic Energy of Canada Ltd., Chalk River, Ontario for deuterium analysis. The results are plotted in Figure 8 against their respective δO^{18} values.

The resulting relationship

$$\delta D = 8.2 \delta\text{O}^{18} + 6.5\text{‰} \quad (1)$$

is very close to the northern hemisphere results of the International Atomic Energy Agency and the World Meteorological Organization world survey of isotopic concentration in precipitation:

$$\delta D = (8.1 \pm 0.1) \delta\text{O}^{18} + (11 \pm 1)\text{‰} \quad (2)$$

This means that the snow found in the St. Elias Mountains was formed during later stages of an equilibrium condensation from ocean vapor, which has been evaporated in a non-equilibrium process fast enough to give a deuterium surplus, $d = +6.5\text{‰}$ as compared to the world survey surplus of 11‰ (Dansgaard, 1964). This surplus in

deuterium can be described qualitatively by the difference in evaporation rates, R , of the isotopic species;

$$R_{\text{H}_2\text{O}^{16}} > R_{\text{HDO}} > R_{\text{H}_2\text{O}^{18}}$$

The lower kinetic isotope effect contribution to the vapor source would seem consistent with the quasi-stationary lows that built up in the Gulf of Alaska. (The vapor would have more opportunity to equilibrate isotopically with the ocean.)

The slope of 8.2 in Figure 8 indicates that the snow at these altitudes has been condensed under near-equilibrium conditions. Although previous visual observations had established that precipitation occurred at these altitudes, workers had generally placed more emphasis on the mechanism of the precipitation forming at lower altitudes and then being blown upward. The δO^{18} values, their interrelationship, and the latitude anomaly of the Mt. Logan samples, all present strong evidence that snow actually forms at these high altitudes. Although snows from lower altitudes may be blown into the area, this does not seem to represent a major contribution. There is no doubt that snow deposition at this altitude can be greatly influenced by wind conditions, however, as witnessed by the data from the Northwest Col.

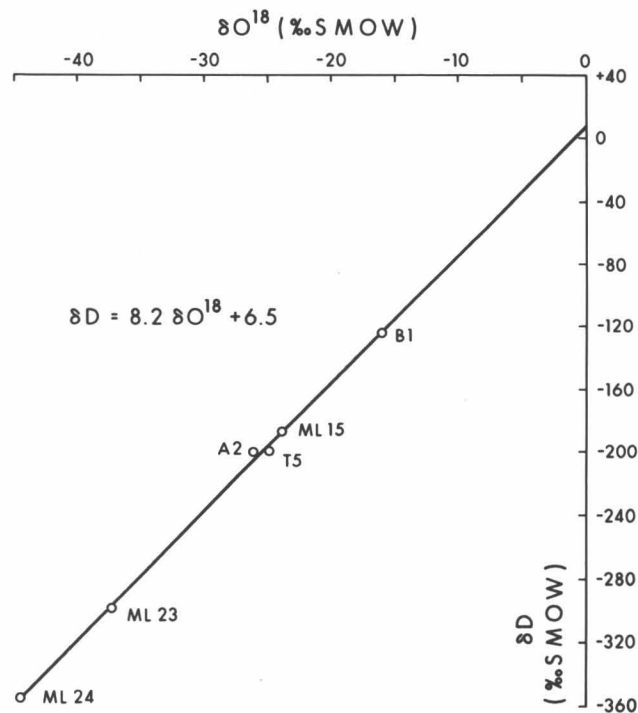


Fig. 8. Plot of δD vs. δO^{18} . ML = Mt. Logan snow, A = Divide snow, T = Rusty snow, and B = Rusty rainfall.

RUSTY GLACIER

Introduction

The Rusty Glacier is a small valley glacier that shares a common drainage basin with the Backe and Trapridge Glaciers. All three of these glaciers are believed to have surged in the past, with the Backe being in active surge during 1967 and 1968. The Steele and Hodgson Glaciers are also surging glaciers, with the Hodgson in active surge during 1968, while the Steele had just reached the end of its latest surge.

Early in 1967, glaciologists from Canada and the U.S.A. selected the Rusty Glacier for study in an effort to explain the mechanisms of a surging glacier. The moraines and glacial surface features were found to have much in common with the Steele Glacier before its surge. The choice of the Rusty Glacier was good also because ablation had smoothed the surface, permitting easier travel.

The mean daily temperature recorded at Fox Camp between July 6 and August 18, 1968 was 44.4°F, with a low of 39.5°F on July 13 and a high of 48.7°F on July 22. Winds were mainly from the south or southeast. The wind directions were determined on the glacier, however, and may be representative of the katabatic surface winds rather than the prevailing winds of the region, since a number of storms were seen to come from the north.

The Rusty (length, approx. 4 km) is believed to be a Type III surging glacier (Meier and Post, 1969). The lower portion of the Rusty seems to have been virtually motionless for a considerable period of time. The movement is only a few meters per year in the active portions of the upper glacier.

The classic flow patterns of normal glaciers were first proposed by Reid (1896). He suggested that snow from the top of the accumulation area submerges and eventually appears downglacier, at the surface near the terminus, while snow deposited just above the firn limit appears just below the equilibrium line as shown in Figure 9a. In the ideal case, this should give rise to a longitudinal isotopic profile below the equilibrium line which is the reverse to that above (Fig. 9c).

Figure 9b is a top view of an ideal glacier. The flow vectors show that if a traverse is taken, the center ice normally would have a more negative value, again due to the altitude effect. The center flow vectors are faster, because movement near the edges of the glacier is retarded by the valley walls. In the longitudinal profile, the bottom motion is also retarded by the drag of the bedrock.

Results

Upper glacier. Seven snow pits in the accumulation area of the Rusty Glacier were analyzed. The pits were located near Stakes, 24W2, 28W4, 28E4, 32, 32E8, 36, 36E8 (Fig. 10). The elevation change from Stake 20 (the

lower limit on the firn line) and the highest point of the accumulation area was 400 m. The thick dark line passing through Stake 24 was the firn limit from aerial photography in 1965. It was lower in 1968 but the melt season had not ended before the camp was abandoned.

Snow pits. Snow Pit 36E8 was at the highest elevation (2550 m) and was the last (August 15) snow pit dug on the Rusty. The densities ranged from 0.4 to 0.6 gm/cc with a low anomaly at 100 cm (Fig. 11). Dirt bands appeared at 40 cm, 115-145 cm, and 185 cm while the only ice lens appeared at 60 cm.

Oxygen isotopes give a seasonal profile which would locate the horizon for summer 1967 at a depth of 140 cm. The discrepancy between this value and that determined by density, 100 cm, can probably be explained by an unusually warm midsummer period while the low-density anomaly is caused by depth hoar, which is usually formed in the fall. The isotope data from 160 to 240 cm seem to be fairly homogeneous while the density is markedly lower than that of 1967-1968 (110 cm depth). This indicates that meltwater percolation has homogenized the 1966-1967 δ values and at the same time has warmed

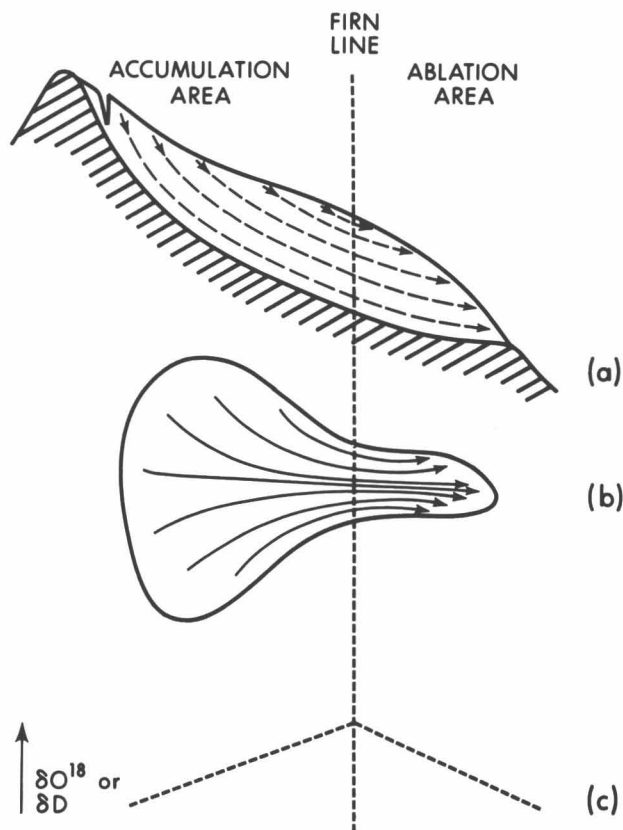


Fig. 9. (a) Longitudinal profile of glacier flow (after Reid, 1896); (b) top view of glacier flow (after Reid, 1896); (c) isotopic variation of a longitudinal profile.

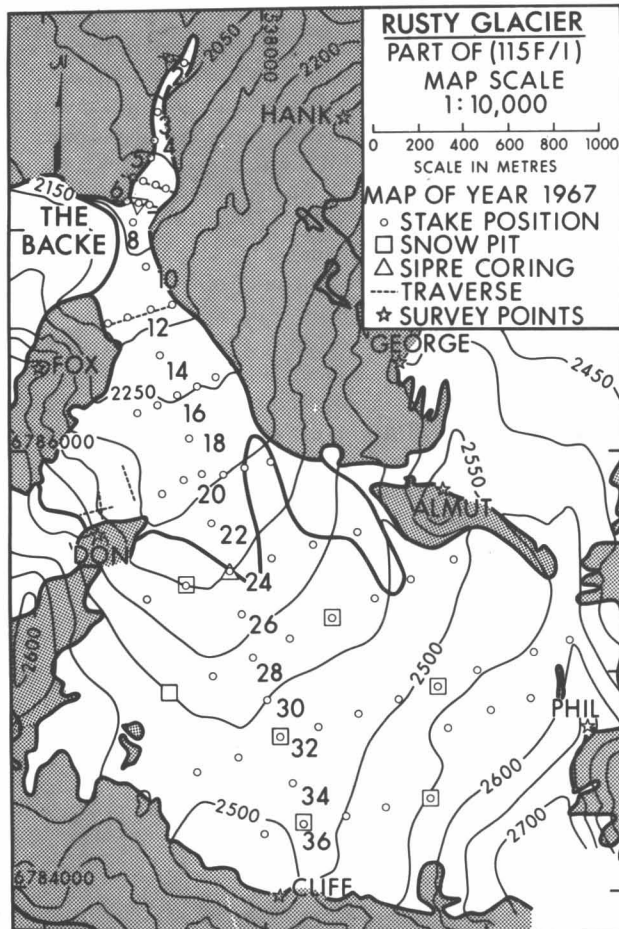


Fig. 10. The Rusty Glacier showing sampling scheme for H_2O^{18}/H_2O^{16} determination. (For additional stake numbers see Fig. 1 of Brewer on p. 76 of this volume.)

up the snow when it refroze to the point that vapor was formed. This vapor then formed large crystals of loosely compacted firn similar to depth hoar. This explanation is supported by the fact that large amounts of dense snow and ice below 240 cm prohibited further sampling.

The dirt bands occurred in either midsummer or mid-winter. They probably are from small dust tornadoes or just high southerly winds coming off the ridge near survey point "Cliff" (Fig. 10). Small "dust devils" were often observed near point "Cliff" on a bright sunny day. Therefore, these dirt layers may be indicators of periods of minimum cloud cover in this area.

The density values indicate that this pit is in a zone of soaked facies. One would expect, however, because of the proximity to the end of the melt season, that the isotopic values would be much more homogenized (MacPherson and Krouse, 1967). It may be that the snow, because of loss of albedo due to the dirt cover, has been heated enough to allow faster compaction, thus giving the high density values. This would allow the pit to be in a percola-

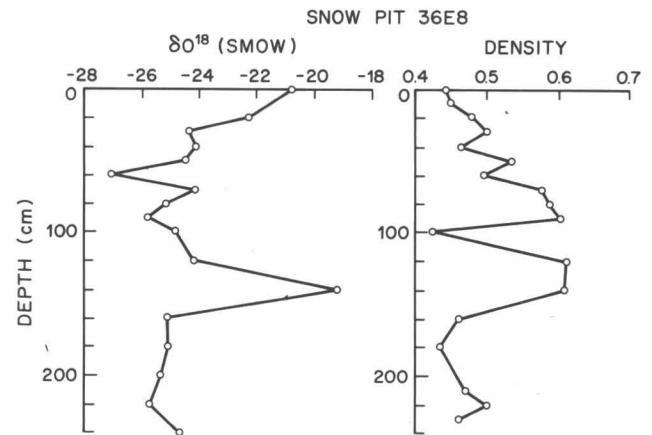


Fig. 11. Snow Pit 36E8 (Rusty Glacier; elev. 2550 m; August 15, 1968).

tion zone, yet explain the lack of homogenization of isotopic values and ice lenses.

Snow Pit 32E8 was located at an elevation of 2525 m. The density data were very homogeneous, ranging from 0.4 to 0.5. Two low densities were located to either side of the isotopic winter minimum. Since they were not very prominent and were close to the isotopic midwinter, neither seems to be a fall season density (Fig. 12). Similarly, low densities were seen in Pit 36E8 at 40 cm and 60 cm. The isotopic profile of 32E8 was strikingly similar to that of 36E8, although the large positive value for the summer of 1966 was not found. This is probably due to faster transformation into extremely hard firn or ice, which was encountered after the 1967-1968 budget year (110 cm depth). Again, because of the preservation of the isotopic data, the density values and the general stratigraphic conditions, Pit 32E8 was assumed to be in an area of percolation facies.

The snow pit near 28E4 (elevation 2425 m) was sampled on the same day, August 1, 1968, as Pit 32E8. Homogenization had started, however, and may have penetrated to the horizon of the previous year by the end of

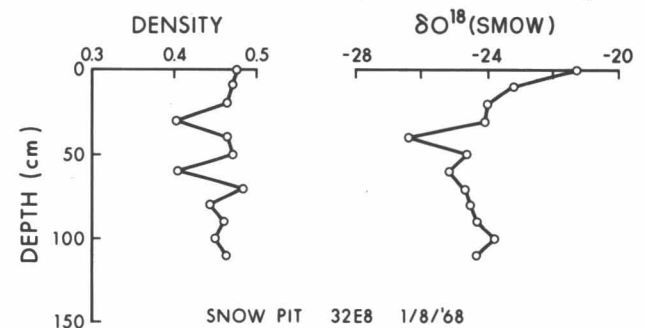


Fig. 12. Snow Pit 32E8 (Rusty Glacier; elev. 2525 m).

the melt season (Fig. 13). The low density anomaly corresponding to the fall season was at 90 cm and the isotopic summer was at 100 cm. Relatively high density at 80 cm and low δ values at 80 and 90 cm may correspond to cool periods in the early summer of 1967. Ice was encountered at 110 cm. This pit was believed to be in a transition zone from percolation facies to wetted facies. The reason for the two facies in such a small area with very little elevation change is the angle which the northward-facing slope of the Rusty makes with the sun. Pits 32E8 and 36E8 were both located on steep, northward-facing slopes and therefore had a high albedo. The rest of the snow pits were located in much flatter areas. This is consistent with Brewer's (1972) observation that maximum snow depth occurs in 'pockets' at the bottoms of topographic hills.

The snow pit near Stake 36 (Fig. 14) was sampled on August 1, 1968. Although the recent snow fall gave the isotopic profile a positive peak, the rest of the pit was well homogenized. At a depth of 40 cm, ice was encountered. Pit 32 was similar, except that slush had formed at 30 cm. This was as expected, since both pits were located near a slush pond at the top of the accumulation area.

Snow Pit 24W2 also seems to be fairly well homogenized, even though surface snow gave the isotopic data a definite summer peak (Fig. 15). No isotopic summer peak was obvious for 1967, but the ice at 80 cm was assumed to mark the end of the 1967 melt season.

Snow Pit 28W4 had dirt layers at 65 and 100 cm. Below 100 cm, ice was encountered. The isotopic data show that the 1967 summer horizon was at 90 cm (Fig. 16). Homogenization seemed to be well in progress, since the δ value range was from -21.5 to -26 ‰. Tentative temperature and density measurements suggest that this was in a zone of wetted facies. The dirt, as in pit 36E8, is probably from the ridge behind survey point "Cliff."

The accumulation area of the Rusty Glacier seemed to be divided into two glacial zones with pits 36E8, 32E8 and perhaps 28E4 in the percolation zone, while pits 36, 32, 28W4 and 24W2 were in the wetted zone.

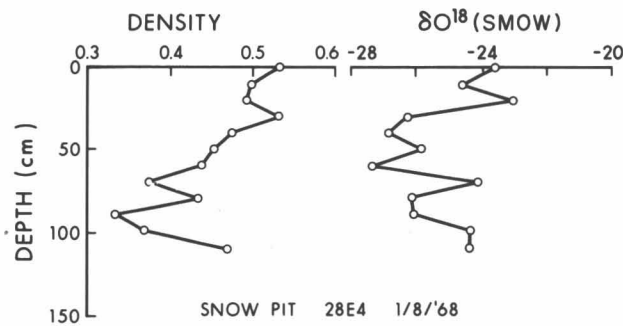


Fig. 13. Snow Pit 28E4 (Rusty Glacier; elev. 2425 m).

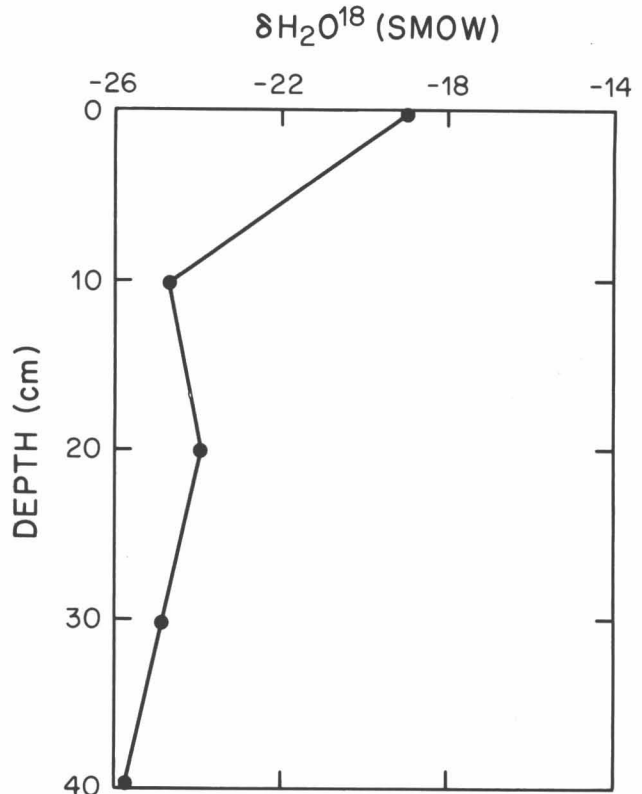


Fig. 14. Snow Pit 36 (Rusty Glacier; elev. 2490 m; August 1, 1968).

The water equivalent accumulation at Pit 36E8 was 55.6 cm at 100 cm and 73.0 cm at 140-cm depth. The water equivalents at 32E8 and 28E4 were 45.4 cm and 46.1 cm. Using scanty density data at 28W4 the water equivalent was 46.3 cm. Therefore the average accumulation in the wetted zone seemed to be near 46 cm of water while in the percolation zone it may

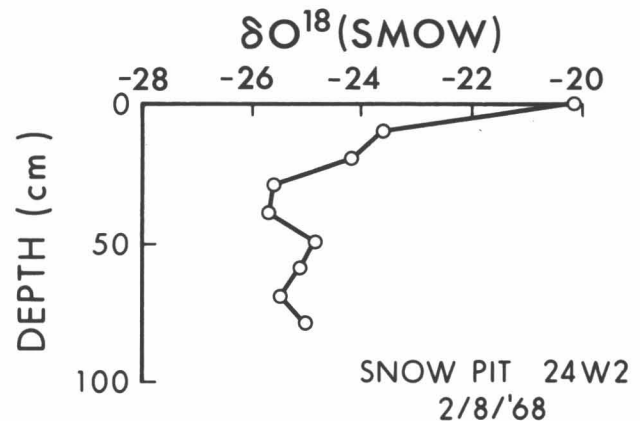


Fig. 15. Snow Pit 24W2 (Rusty Glacier; elev. 2350 m).

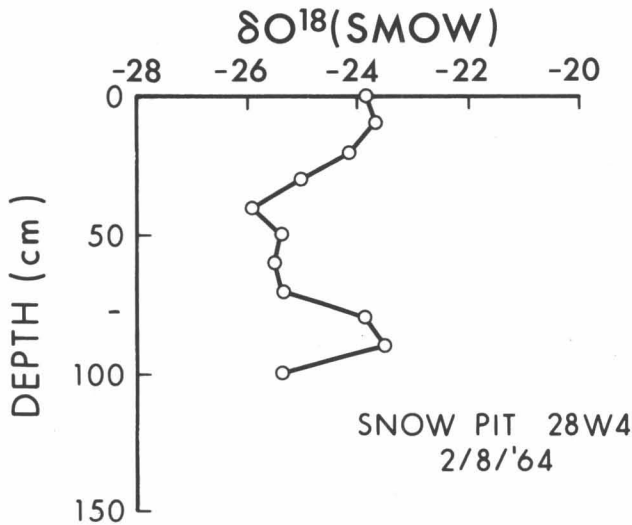


Fig. 16. Snow Pit 28W4 (Rusty Glacier; elev. 2450 m).

have been slightly higher. The 73.0 cm (W.E.) at 140 cm in Pit 36E8 strengthens the idea that the positive isotopic peak was a midsummer peak and did not indicate the end of the melt season. Accumulation around Stakes 32 to 36 was depleted, probably by drainage into the melt pond southwest of Stake 32.

The isotopic average and elevations for all the snow pits except 32 and 36 are given in Table 2. The elevation change on the west side of the glacier gave an isotopic change of 0.4 ‰/100 m. Sharp, *et al.* (1960) found 0.5 ‰/100 m on the Blue Glacier, Washington. The east side does not show this, however, which could be due to the transition from the wetted to the percolation zone.

Lower glacier. Lower glacier sampling was done to elucidate the glacial flow patterns. The flow of the Rusty Glacier is controlled by four factors:

- (1) It is a glacier with a presumed history of surging.
- (2) It apparently has not moved significantly since its last surge, at least in the lower third.
- (3) A tributary on the west side goes over the ice falls before joining the main stream.

TABLE 2. Average Isotope Values

Pit No.	δ Average (SMOW)	Elevation (m)
36E8	-24.4	2553
32E8	-24.1	2528
28E4	-25.0	2426
28W4	-24.7	2450
24W2	-24.3	2350

- (4) The Backe has surged over part of the Rusty (Stakes 7 to 11, Fig. 10).

Surface sampling included four transverse and a longitudinal profile. Cores were sampled at Stakes 2 and 7 as well as snow and rainfall at the camp just west of Stake 8.

Traverses. A peak in positive $\delta^{18}\text{O}$ values (see * in Fig. 17) in all traverses is assumed to mark the boundary of the Rusty and its west arm. This is consistent with the flow lines which are evident in the aerial photograph of the Rusty taken by the Canadian Defence Force in 1965.

The oxygen isotope data on the western portions of the traverses must be considered in conjunction with: (1) the ice falls, and (2) distortion and contamination by the Backe. The moraine-covered samples at Stake 6 are possibly superimposed ice. The rest of the δ values west of the asterisk in Figure 17 show no trends. This is expected since the flow had been perturbed by the ice falls. The traverse at Stake 7 was terminated at 7W0.6 because of the presence of the melt stream and the Backe Glacier.

The east sides of the traverses show that the edges of the main stream have more positive δ values than the centers, which is consistent with the center ice moving faster than the side ice (Fig. 9). The inconsistent variations in δ values below the snow at Stake 12 is probably due to varying degrees of meltwater contamination, while the δ value at 2E0.9 is attributed to superimposed ice from the lateral moraine.

Longitudinal profile. A longitudinal profile was made by sampling at the center survey stakes from 1 to 12. The $\delta^{18}\text{O}$ results are given in Figure 18. From surface observations on the Rusty Glacier, this longitudinal profile appeared to be in the center of the main arm of the glacier. From the results of the traverses, however, one

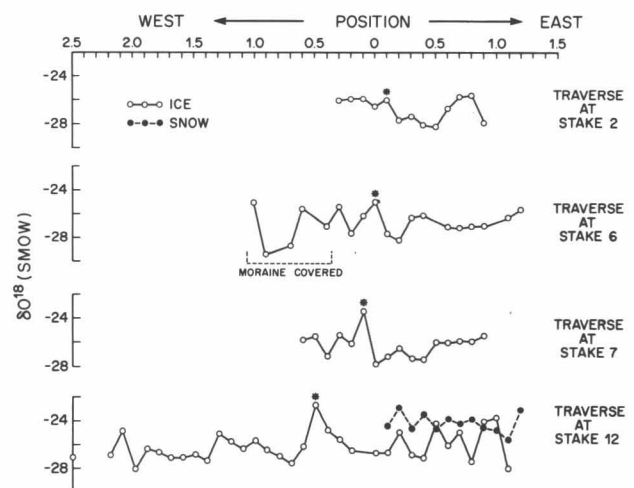


Fig. 17. Transverse profiles of $\text{H}_2\text{O}^{18}/\text{H}_2\text{O}^{16}$ composition on the Rusty Glacier.

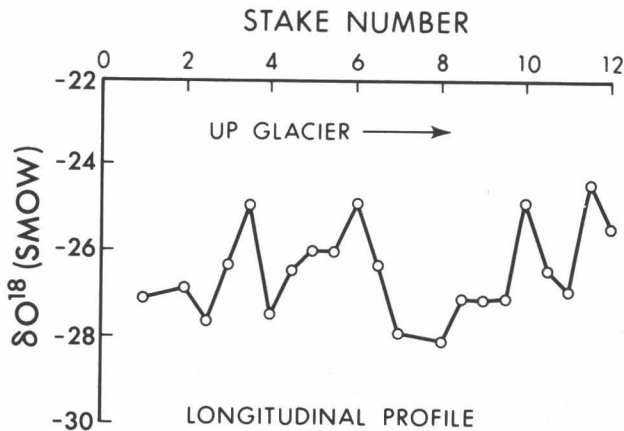


Fig. 18. Uncorrected longitudinal profile of the Rusty Glacier.

can see that this profile went from the main arm at Stake 12 into the west arm by Stake 2 (Fig. 17). It was therefore necessary to apply a position correction so the longitudinal profile would not cross several flow lines. The criterion chosen was an average of the minimum values of δO^{18} found to the east of the asterisk in Figure 17. That is the center of the main arm for Stakes 7, 6, and 2. Unfortunately, no sampling was done east of Stakes 3, 4, and 5. The values near Stake 8 were possibly contaminated by the terminus of the Backe. The rest of the δ values, because of their position, were considered to be representative of the center of the main arm. The corrected longitudinal profile gives a positive slope (Fig. 19). This indicates that this particular surging glacier's flow is similar to the general mechanism proposed by Reid (1896). Although this general observation cannot distinguish between the theories of Robin (1969), Weertman (1969), or Lliboutry (1969), it does cast doubt on the ice-dam, powder-flow theory of Nielsen (1969) for this particular glacier.

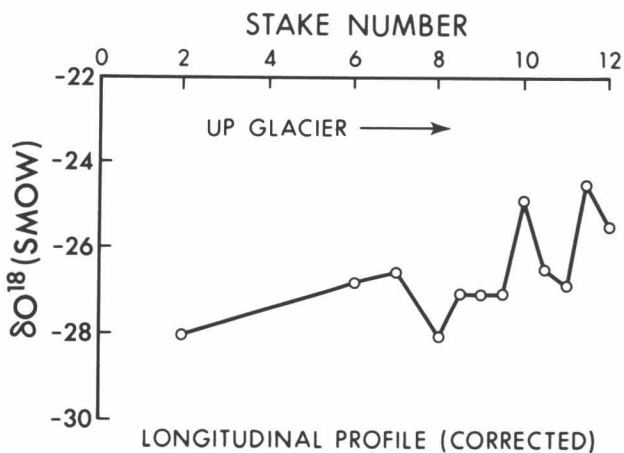


Fig. 19. Positionally corrected profile of the Rusty Glacier.

Ice cores. The core at Stake 7 was drilled until it became physically impossible to retrieve the core, while coring at Stake 2 was stopped because of meltwater entering the hole at 5 m. Unfortunately, these cores, according to Figure 17, are located on opposite sides of the boundary between the west and main arms.

The variation found in the core at Stake 7 (Fig. 20) is almost as great as the variation found in the longitudinal profiles (Fig. 18, 19). (A discussion as to whether the trend observed in Figure 19 is significant is given near the end of this report.) It is difficult to assess whether these variations are remnants of seasonal variations or general climatic changes. Because of the size and surging properties of the glacier, however, it is concluded that this ice is probably not more than 300 years old. Further interpretations are rendered impossible by the unknown parameters of this glacier's flow history, that is, the period of surge, etc.

The core at Stake 2 was more homogeneous. The only large deviation from the average δ value (-25.8 ‰) was at 50 cm (Fig. 21). Whether this corresponds to the

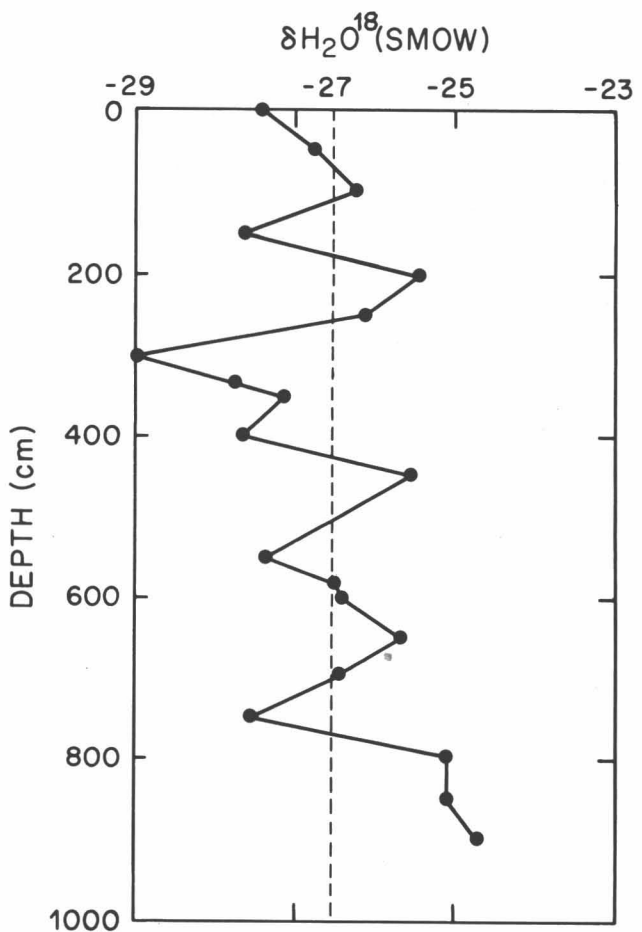


Fig. 20. Ice core at Stake 7, Rusty Glacier.

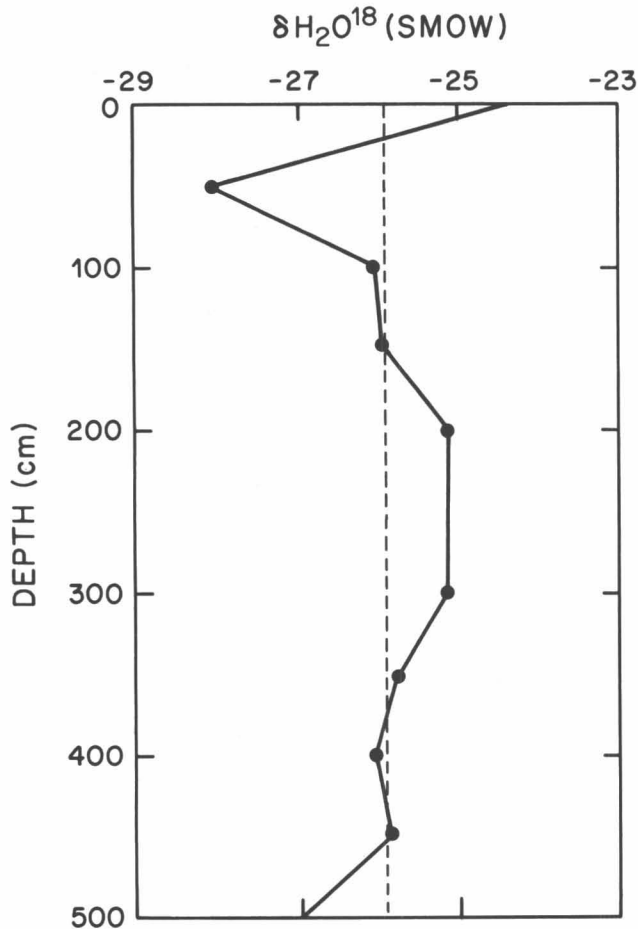


Fig. 21. Ice core at Stake 2, Rusty Glacier.

negative peak at 300 cm of the core at Stake 7 is impossible to say. Correspondence between the cores is not expected, however, since the cores probably experienced different histories by being located in different arms of the Rusty.

Snow and rainfall. The snow and rainfall at Fox Camp were very sparse during the period of July 6 to August 8, 1968. A total of 9.3 cm (W.E.) of precipitation occurred in the form of rain or snow. Relatively large amounts of precipitation occurred on July 25 and 27. On both days, snow samples were collected on a traverse from the Rusty Camp (near Stake 7) to survey point "George" (an elevation difference of 350 cm). No altitude trend was found however. Rain and snowfall samples were also collected at Rusty Camp. The average δO^{18} and temperatures at the time of deposition are given in Table 3. All of the $d\delta O^{18}/dt$ values range from $-0.9\text{‰ per }^{\circ}\text{C}$ to $+2.43\text{‰ per }^{\circ}\text{C}$ with the average being $1.27\text{‰ per }^{\circ}\text{C}$. These values are not very consistent with the values found by Dansgaard (1964) and Picciotto, *et al.* (1960) of $0.69\text{‰ per }^{\circ}\text{C}$ and $0.95\text{‰ per }^{\circ}\text{C}$. This incon-

TABLE 3. Average Values of δO^{18} and Temperature

Date	Temperature ($^{\circ}\text{C}$)	δO^{18} (SMOW)	Description
July 25	2.5	-14.8	rain
	3.2	-16.5	snow (traverse)
July 27	1.3	-20.9	snow (traverse)
	0.3	-20.0	snow (from south)
	1.6	-18.0	rain (from north)

sistency is believed to be caused by the glacier's moderating effect on the air temperatures, since all temperature measurements were taken directly above the glacier surface (Marcus, 1965).

Two storms on July 27 were sampled hourly. The results are given in Table 4. Both storms' δ values became more negative as the storms progressed. In order to determine whether this effect is due to reservoir depletion, temperature changes, or a combination of both, a detailed temperature regime would have to be known. If one applies isobaric cooling from an initial temperature of 20°C to the Rayleigh condensation formula, the above δ variations correspond to a depletion from 18% (of the original vapor reservoir) to 10% of the original vapor reservoir. Since small amounts of precipitation were observed, and this area is directly east of Mt. Wood, and perhaps in its rain shadow, these depletions do not seem unreasonable.

DISCUSSION

Dansgaard (1964) plotted the mean air temperatures of six Greenland weather stations against the δ values for the same periods and obtained the following relationship:

$$\delta O^{18} = 0.69 t - 13.6 \text{‰} \quad (3)$$

where t - temperature ($^{\circ}\text{C}$)

TABLE 4. δO^{18} Values Observed during Storms

	Time	δO^{18} (SMOW)
First Storm	4 P.M.	-17.0
	5 P.M.	-17.2
	6 P.M.	-21.9
Second Storm	8 P.M.	-17.8
	9 P.M.	-18.8
	10 P.M.	-20.7
	11 P.M.	-21.2
	12 P.M.	-21.6

Applying equation 3 to the average δ value of the snow pits of the Rusty Glacier (-24.5‰) gives an average yearly temperature of -15.8°C . Applying the lapse rate of $.65^{\circ}\text{C}/100\text{ m}$ (Grew and Mellor, 1966) to the yearly average temperature of Bethel, Alaska, a maritime station, and Whitehorse, Yukon, a continental station, and averaging the results, one gets a temperature of -15.2°C for an elevation of 2460 (the average snow pit elevation). This agreement suggests that the isotopic composition of precipitation on the Rusty Glacier is due to a mean yearly temperature near -15.8°C and a combination of marine and continental weather patterns, such as found at Divide.

The rapid transformation of snow to ice (one year in wetted facies, 2 to 3 years in percolation facies) seems to be an effect of both the surging and temperature properties of the Rusty Glacier. The last surge has lowered the slope of the accumulation area, allowing heavy melting from direct radiation, while the subfreezing temperatures of the Rusty refroze much of this percolating meltwater into ice when it made contact with the previous annual layer. Dirt layers from the surrounding ridges also seem to play an important role in this transformation by lowering the albedo of the surface snow.

The lower glacier results are very similar to the results of Sharp, *et al.* (1960) on the Blue Glacier, Washington. Their longitudinal profile also showed a small "inversion" of the δ values below the firn line. In this case a core taken below the firn line was extremely homogeneous; since the Blue Glacier is about the same size as the Rusty, one might expect to see similar paleoclimatic variations in both glaciers. Accepting the Blue Glacier's homogeneous results as proof of little or no paleoclimatic trends in glaciers of this size, two explanations of the δO^{18} variations in the lower glacier cores of the Rusty are possible:

- (1) These variations may be preserved seasonal variations. This seems unlikely however, because of the homogenization of the δO^{18} observed on the Rusty, in the wetted facies and on Divide in percolation facies (MacPherson and Krouse, 1967) by the end of the melt season.
- (2) These variations may be due to firn and snow recently incorporated into the crevasses caused by the surging of the Rusty Glacier.

If the latter explanation is correct, then the longitudinal profile of Figure 19 may be significant, since most of these samples should represent old glacial ice.

A peak in δO^{18} corresponding to a boundary between 2 arms (marked by a medial moraine) was also found on the Blue Glacier. MacPherson and Krouse (1967) and Epstein and Sharp (1959) found no such peak, but both of these studies based their traverses on very few samples. It would seem that if a traverse is sampled in enough detail, boundaries between arms of glacier may be identified. The identification of boundaries may have important applications in the interpretation of glacier dynamics.

In the case of the Rusty, this information elucidates the basal hot spot reported by Classen and Clarke (1971) at Stake 16W2. The isotope data would identify this feature with the west arm. Since the basal hot spot is just below the icefall, it may be a consequence of the icefall rather than the surging properties of the glacier as suggested by Classen and Clarke (1971). This interpretation does not exclude the temperature regime from being a contributing factor to the surging properties of the Rusty; rather, it allows for another mechanism to create the temperature regime.

Acknowledgments

Financial support for this project was derived from the National Research Council of Canada and the Boreal Institute of the University of Alberta. Field assistance was provided by the Icefield Ranges Research Project of the Arctic Institute of North America. We would also like to thank the field crews for their assistance and especially J. C. LaBelle, J. Underwood and C. M. Keeler for making the Mt. Logan samples available.

References

- *Alford, D. (1967) Density variations in alpine snow, *J. Glaciol.*, 4, 495-503.
- *Alford, D., and Keeler, C. (1968) Stratigraphic studies of the winter snow layer, Mt. Logan, St. Elias Range, *Arctic*, 21, 245-254.
- †Brewer, T. (1972) Summary of "Rusty" Glacier Mass Balance Study, 1968, unpublished.
- Classen, D., and Clarke, G. K. C. (1971) Basal hot spot on a surge type glacier, *Nature*, 229, 481-483 (see also pp. x to xx of this volume).
- Dansgaard, W. (1964) Stable isotopes in precipitation, *Tellus*, 16, 436-468.
- Epstein, S., and Sharp, R. P. (1959) Oxygen isotope variation in the Malaspina and Saskatchewan Glaciers, *J. Geol.*, 67, 88-102.
- Friedman, I., and Smith, G. I. (1970) Deuterium content of snow cores from Sierra Nevada area, *Science*, 169, 467-470.
- *Grew, E., and Mellor, M. (1966) High snowfields of the St. Elias Mountains, *Tech. Rept. 177*, U.S. Army Cold Reg. Res. Engin. Lab., 18 pp.
- *Keeler, C. M. (1969) Snow accumulation on Mt. Logan, Yukon Territory, Canada, *Water Resources Res.*, 5, 719-723.
- Lliboutry, L. A. (1969) Contribution à la théorie des ondes glaciaires, *Can. J. Earth Sci.*, 6, 943-953.
- *MacPherson, D., and Krouse, H. R. (1967) $\text{O}^{18}/\text{O}^{16}$ ratios in snow and ice of the Hubbard and Kaskawulsh Glaciers, in *Isotope Techniques in the Hydrological Cycle*, edited by G. E. Stout, pp. 180-194, *Monogr. No. 11*, Am. Geophys. Union, Washington, D. C.
- *Marcus, M. (1965) Summer temperature relationships along a transect in the St. Elias Mountains, Alaska and Yukon Territory, in *Man and the Earth, Ser. Earth Sci. No. 3*, Univ. Colorado, Boulder, pp. 15-30.

*These articles were reprinted in previous volumes of Icefield Ranges Research Project, Scientific Results.

†Incorporated in article on pp. 75 to 82 of the present volume.

- Meier, F., and Post, A. (1969) What are glacier surges? *Can. J. Earth Sci.*, 6, 807-816.
- ‡Nielsen, L. E. (1969) The ice-dam, powder-flow theory of glacier surges, *Can. J. Earth Sci.*, 6, 955-961.
- Picciotto, E. E., Demaere, X., and Friedman, I. (1960) Isotopic composition and temperature of formation of Antarctic snows, *Nature*, 187, 857-859.
- Reid, H. F. (1896) The mechanics of glaciers, *J. Geol.*, 4, 912-928.
- Robin, G. de Q. (1969) Initiation of glacier surges, *Can. J. Earth Sci.*, 6, 919-926.
- Sharp, R. P. (1960) *Glaciers, Condon Lects., 1960*, Oregon State Syst. Higher Educ., Eugene, 78 pp.
- Sharp, R. P., Epstein, S., and Vidziunas, I. (1960) Oxygen-isotope ratios in the Blue Glacier, Olympic Mountains, Washington, U.S.A., *J. Geophys. Res.*, 65, 4043-4059.
- Taylor-Barge, B. (1969) The summer climate of the St. Elias Mountains region, in *Icefield Ranges Research Project, Scientific Results*, edited by V. C. Bushnell and R. H. Ragle, Vol. 1, pp. 33-49, Am. Geogr. Soc., Arctic Inst. North Am., New York.
- Wagner, W. P. (1969) Snow facies and stratigraphy on the Kaskawulsh Glacier, in *Icefield Ranges Research Project, Scientific Results*, edited by V. C. Bushnell and R. H. Ragle, Vol. 1, pp. 55-62, Am. Geogr. Soc., Arctic Inst. North Am., New York.
- Weertman, J. (1969) Water lubrication mechanism of glacial surges, *Can. J. Earth Sci.*, 6, 929-942.

‡This article is reprinted in the present volume.

Snow Accumulation in the Icefield Ranges, St. Elias Mountains*

Melvin G. Marcus † and Richard H. Ragle ‡

ABSTRACT. Snowpack characteristics in the St. Elias Mountains were examined as part of the Icefield Ranges Project for 1961 to 1965, emphasizing particularly the 1964-1965 glacier balance year, together with reconstructions for 1953 to 1961. Analysis was carried out along a hydrological traverse on the Kaskawulsh, Hubbard, and Seward-Malaspina Glaciers, and at a single location through a period of time. The data obtained are summarized in graphs and tables. The relationships between precipitation, elevation, and topography, and effects of continentality and exposure are considered. In neither case are the relationships clearly defined, but it is evident that elevation is a critical factor in the maintenance of continental slope glaciers and spring runoff. Fluctuations in net accumulation are determined and evaluated; a stable period is indicated for the late 1950's, followed by an increase of 200 to 300 mm in the early 1960's and a minimum in 1964-1965 and 1965-1966 of winter nourishment and mass balance. Climatic implications are drawn from the snow accumulation data.

Introduction

The temporal and distributional variations of gross and net snow accumulation which occur over glacierized alpine terrain provided important clues to the nature of high mountain environments. A knowledge of snowpack characteristics is essential to calculations of glacier mass balance, inventory and prediction of water storage and runoff, and interpretation of annual climatic cycles. Unfortunately, snow data are relatively sparse for most mountain regions, especially those which are isolated from human settlement and traffic. The Icefield Ranges of the St. Elias Mountains are a particular case in point (Fig. 1). Covered by the most extensive permanent snow mantle in continental North America and dissected by the longest valley glaciers outside of Greenland and Antarctica, the environment of the St. Elias Mountains has, until recently, received relatively little scientific attention.

Since 1961, interrelated environmental studies have been carried out in this area by the Icefield Ranges Research Project. Project activities in climatology, glaciology, geomorphology, ecology, and human physiology have been summarized for the period 1961 to 1968 by Wood (1963, 1969), Ragle (1965, 1967), and Marcus (1969a, 1969b). Included in the investigations have been annual determinations of snow accumulation in the region and reconstructions of net accumulation for the period 1953 to 1961. This paper summarizes and interprets this snowpack record for a 13-year period, placing particular emphasis on the 1964-1965 glacier-balance year.

The objectives of these field studies were twofold: (1) to seek knowledge of the effects of topography, elevation, and distance from the ocean on snow accumulation in the St. Elias Mountains; and (2) to determine and evaluate fluctuations of net accumulation through time.

Meaningful sampling of environmental elements and processes in mountain regions is, however, extremely difficult; "representative" stations are weak surrogates for continuous spatial coverage. Thus, while the data presented are considerable for a little-explored area, they represent only a small sample for a mountain system of such great magnitude. This is because rapid variations of environmental elements and processes occur at all scales across an alpine system and are reflected in steep climatic gradients near the surface.

If the parameters of climate—energy, moisture, and momentum—change significantly over small horizontal distances, local variations in snow cover and glacier mass-balance will occur. Thus, local budgets may be calculated with considerable accuracy for point-sampled sites; serious errors may result where spatial extrapolations are attempted. The hydrological data presented herein should therefore be viewed primarily as point-sample information. Even where traverse data are included, no attempt is intended to suggest integrated mass-balance relationships over entire glacier units.

Study Area

The St. Elias Mountains form a major element of the Pacific Mountain Ranges of North America (Wahrhaftig, 1965). Physiographically, they comprise roughly parallel ranges, trending in a shallow arc through 500 km (Fig. 1). The topography is that of a high alpine region, and the major valleys are largely submerged beneath glacier ice. The St. Elias Mountains form the core of the Icefield Ranges (Bostock, 1948), 16 peaks of which exceed 4500 m in elevation, including Mounts Logan, St. Elias, and Vancouver at 6040, 5488, and 4785 m, respectively, within 100 km of the Pacific shore. Glaciers descend from all the summits, feeding the major snow-accumulation zone between 1500 and 3000 m. Equilibrium line elevations average approximately 2100 m on the continental slope and 1100 m on the marine slope.

These mountains form an impressive topographic barrier between the Gulf of Alaska and the continental

*This report has previously appeared in *Arctic and Alpine Research*, Vol. 2, pp. 277-292 (1970), and is reprinted here with permission.

†Department of Geography, University of Michigan, Ann Arbor
‡Arctic Institute of North America, Washington, D.C.

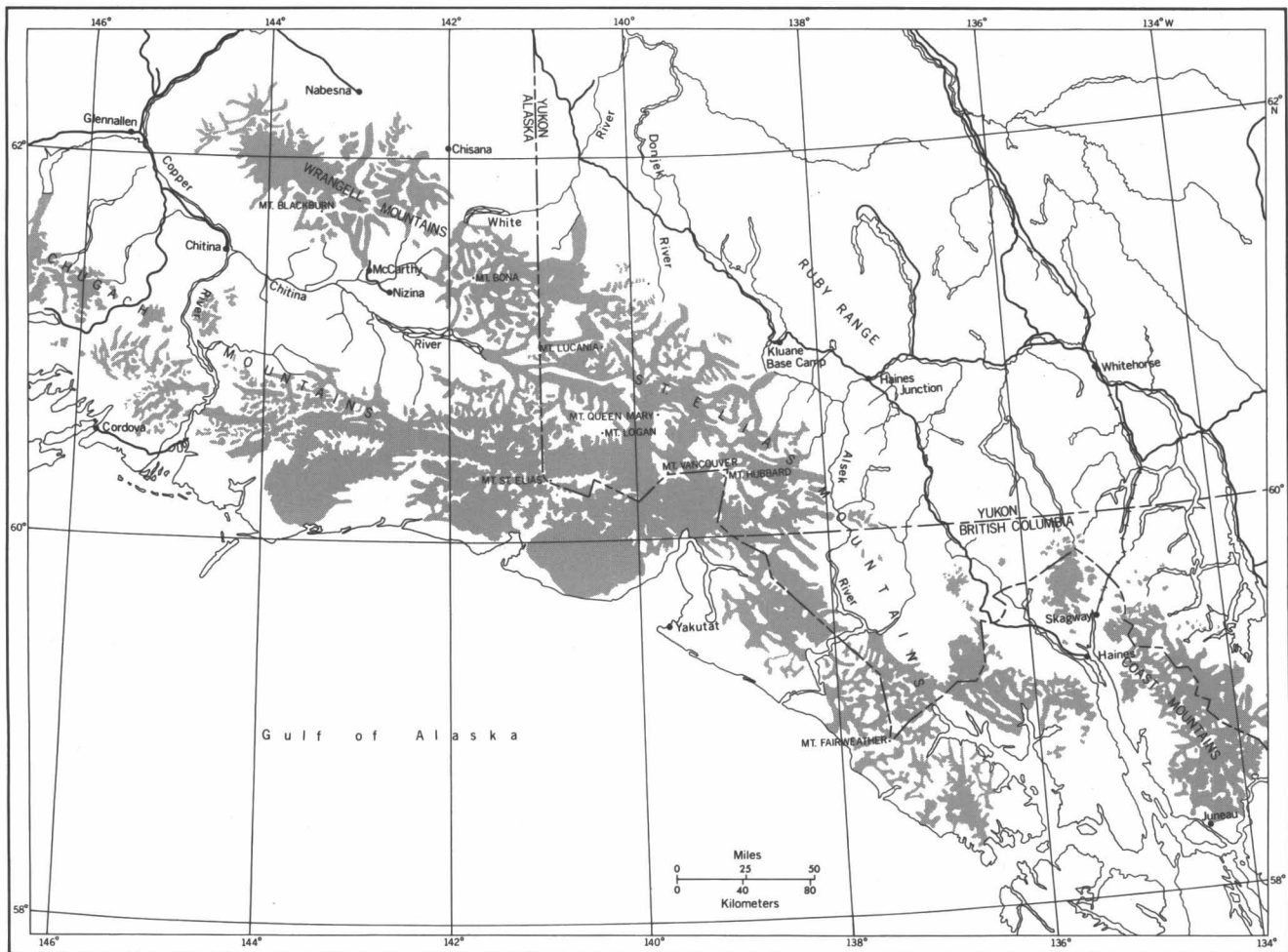


Fig. 1. The St. Elias Mountains and environs.

interior. The climate of the Pacific Littoral is a classical cool Marine West Coast type, while the interior—some 250 km from tidewater—is characterized by Subarctic regimes. The importance of these highlands in separating these climatic regions cannot be overemphasized. Frequent and intensive moisture-bearing storms are an outstanding facet of marine slope climate. The St. Elias Mountains are a massive obstacle, standing normal to these vectors of moisture transport and zonal flow.

Important glaciers draining the Icefield Ranges include (1) the Kaskawulsh, some 72 km long, which flows to the continental interior; (2) the Hubbard, approximately 120 km in length; (3) the Seward-Malaspina network, in area the world's second largest valley-piedmont system (Fig. 2). The snow studies described herein were carried out over these three glaciers, with the bulk of the data collected at or near the Divide Research Station (Fig. 2).

Before 1948 the interior of the St. Elias Mountains had been little studied or explored, although a few early

investigators (Gilbert, 1910; Tarr, 1907; Tarr and Butler, 1909; Tarr and Martin, 1914) focused their attention on peripheral glacier zones. Early penetrations of the Icefield Ranges were accomplished by Russell (1891, 1892, 1893) and the International Boundary Commission (Wood, 1967). During the 1930's and early 1940's, expeditions led by Wood (1936, 1942) and by Washburn (1935, 1936) provided the first comprehensive mapping and photographic coverage of the interior mountains. From 1948 to 1951, under the auspices of the Arctic Institute of North America's Project Snow Cornice, glaciological studies were accomplished in the heart of the Icefield Ranges. Notable among the published results, and providing a temporal link to this study, were a series of papers by Sharp (1951a, 1951b, 1951c, 1951d, 1953, 1958a, 1958b).

Field Methods

Over extensive glacier systems, field analysis of snow accumulation and stratigraphy is usually accomplished

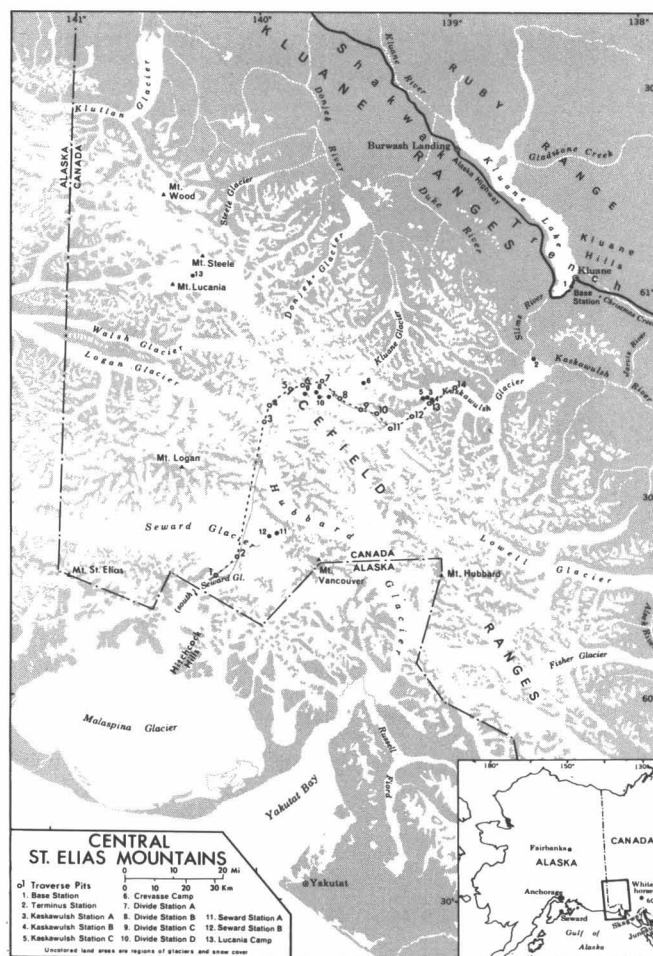


Fig. 2. Snow measurement sites, Icefield Ranges. The dotted line connects pits along the 1965 hydrological traverse.

by one of two methods: (1) analysis of the snowpack at selected pit sites along a traverse line, or (2) interpretation of the snowpack at a single pit site over a period of time (Alford, 1967). Each system has obvious temporal and spatial advantages and disadvantages. Both methods were used in the Icefield Ranges, but most data gathering was necessarily conducted at established field stations in association with other research activities. Divide Station (Fig. 2) and environs provides the longest record, although pits were also established near Seward Station in 1964 and 1965. In order to obtain better altitudinal and distributional relationships, however, a reconnaissance hydrological traverse was conducted in May and June 1965. The principal objective was to obtain accumulation and winter precipitation data for a transmountain profile of the Icefield Ranges.

The traverse was established across the Icefield Ranges from the lower Seward Glacier—across the glacier divide of the Hubbard and Kaskawulsh Glaciers—to the lower Kaskawulsh Glacier (Fig. 2). Pits were excavated at 14 sites (Fig. 2; Table 1). Six were located along the lower Seward, upper Seward, and Hubbard glaciers, all glaciers

which flow toward the Pacific Ocean; the lowest of which was at 1370 m elevation. Unfortunately, weather and travel difficulty made it impossible to establish pits at lower elevations on the Seward-Malaspina system. At the divide between the Hubbard and Kaskawulsh Glaciers (2640 m), a pit was excavated on May 31, and four additional pits and/or core holes were established at nearby Divide Station in June, July, and August. On the continental slope (Kaskawulsh Glacier), seven pits were placed between Divide Station and the transient snow line. The lowest of these was at 1615 m, some 150 m above the snow line at the time of excavation.

Location and density data are given for each traverse pit in Table 1. Pit sites are numbered from the lowest Pacific slope position across the divide to the lowest continental slope location. Dates of excavation do not show chronological agreement with the pit-numbering sequence; this is because it was intended that the complete set of pits should be occupied before snow and air temperatures rose to 0°C and before free water appeared in the snowpack. Sites of lowest elevation on either side of the Icefield Ranges were, therefore, occupied as early as possible

TABLE 1. Preliminary Data: Pit Locations and Densities, Icefield Ranges (May to June, 1965)

Pit	Glacier	Eleva- tion (m)	Interval (m)	Lat. N.	Long. W.	Date of excavation	1964-65 Accum- ulation (mm snow)	Mean density of snow (Mg m ⁻³)	Water equiva- lent (mm)
1	Lower Seward	1,370	395	60°18'	140°13'	May 21-22	4,600	0.378	1,739
2	Upper Seward	1,765	215	60°23'	140°15'	May 21-22	5,800	0.366	2,120
3	Hubbard	1,980	155	60°37'	139°57'	June 9	3,100	0.419	1,300
4	Hubbard	2,135	150	60°40'	139°54'	June 9	2,120	0.437	927
5	Hubbard	2,285	215	60°45'	139°51'	May 30	2,600	0.392	1,019
6	Hubbard	2,500	120	60°46'	139°47'	May 29	2,100	0.388	815
7	Divide	2,620	20	60°46'	139°41'	May 31	3,200	0.407	1,302
8	Kaskawulsh	2,640	220	60°44'	139°35'	May 28	3,700	0.409	1,513
9	Kaskawulsh	2,380	155	60°42'	139°31'	May 27	2,600	0.394	1,024
10	Kaskawulsh	2,225	155	60°42'	139°24'	May 26	2,700	0.364	983
11	Kaskawulsh	2,070	155	60°39'	139°20'	May 24	2,400	0.388	931
12	Kaskawulsh	1,915	150	60°42'	139°13'	May 19	1,780	0.385	685
13	Kaskawulsh	1,765	150	60°44'	139°08'	May 17	1,650	0.390	643
14	Kaskawulsh	1,615		60°45'	139°01'	May 17	910	0.342	311

in anticipation of ablation and the ascending 0°C surface. Only at the last pits excavated, Hubbard Glacier Pits 4 and 5, were free water and 0°C temperatures encountered. In both cases, only the upper few centimeters of the snow were affected. Since free water and ice banding were not otherwise discovered, it is believed that measurement errors due to early ablation are negligible in determinations of the winter accumulation layer. Figure 3 shows temperature profiles in the snowpack during each pit excavation; for Divide Station the migration of the snowpack temperature gradient is followed through the field season.

At each pit, continuous density measurements were taken through the 1964-1965 pack. Density values were determined with the standard SIPRE snow-density kit. Mean densities were obtained by integrating individual readings over the depth of the pit. Similar methods were used at Divide and Seward Stations for pits excavated in other years. When coring was employed, it is noted in figures, tables, and text. A standard, Teflon-coated SIPRE corer was used.

No problems were encountered in identification of the base of the annual snow layers. Pits along the lower Kaskawulsh Glacier terminated at the ice surface. In other cases, the 300- to 500-mm zone immediately above the annual boundary was characterized by lower densities

than levels above and below it. On the average, densities dropped from the 0.43 to 0.48 Mg m⁻³ range to the 0.35 to 0.40 Mg m⁻³ range. Examples from two pits are given in Figure 4. Pit 4 is representative of those dug before disappearance of the cold wave; Pit 3 contains ice bands formed in the early ablation season. The basal layer of low density is typified by loose, coarse-grained crystals. Similar layers have been reported for the Devon Island Ice Cap (Koerner, 1966) the Greenland Ice Cap (Benson, 1962), and the 1963 summer boundary in the St. Elias Mountains (Grew and Mellor, 1966). This depth hoar is generally attributed to late summer and early autumn snowfall when sharp thermal gradients are established between new snow, firn, and the atmosphere. Additional verification of the previous summer's surface was obtained by the identification of sharp density increases at that boundary, as well as excellent agreement between density and hardness for sites where ram soundings were taken (Pit 3 in Fig. 4).

It is significant that, in almost every pit, visual identification of the previous summer's firn surface was impossible; dust or dirt were not present in sufficient quantity. Dirty layers were sometimes encountered, however, within the annual snowpack, in each case within 500 mm of the upper surface. The eventual disposition and transport of this debris is unknown, but its mode of

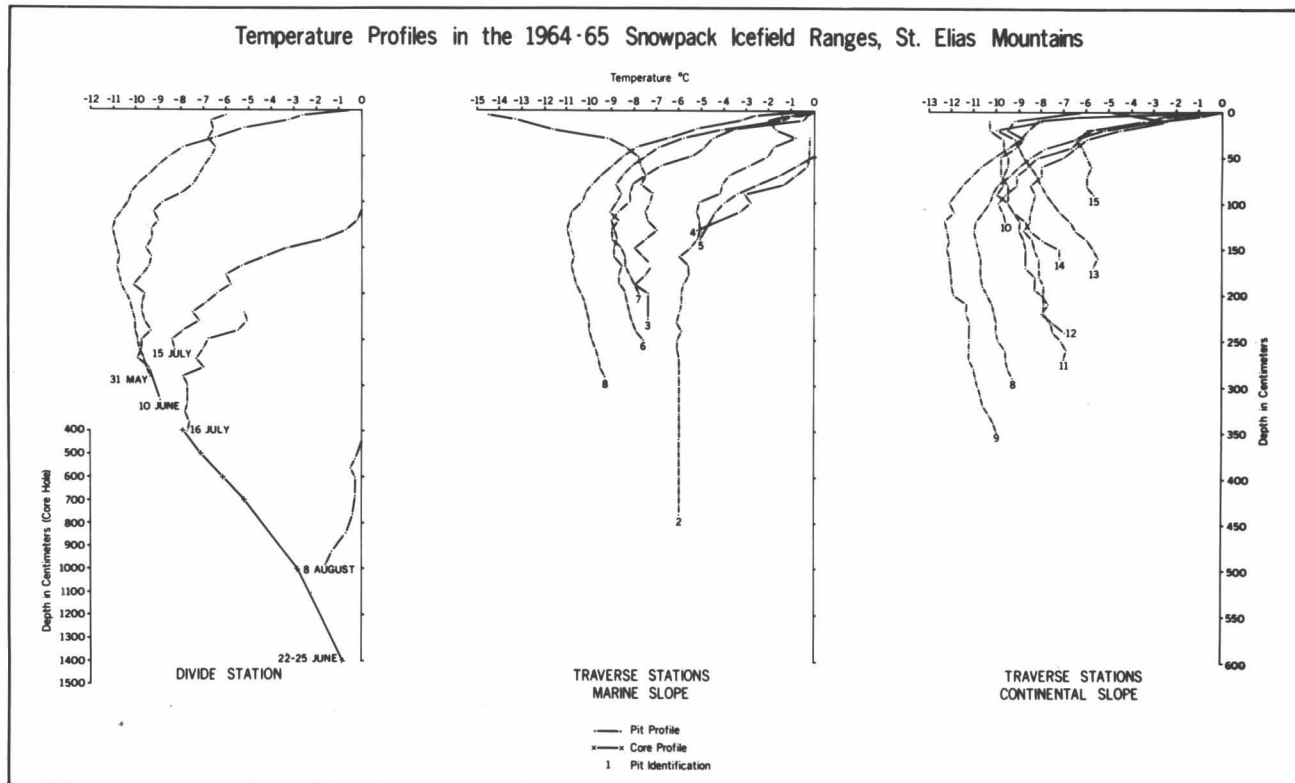


Fig. 3. Temperature profiles in the 1964-1965 snowpack, Icefield Ranges, St. Elias Mountains.

occurrence does suggest that investigators may be misled if dirt layers are used to define the basal boundary.

Transmountain Accumulation: 1964-1965

Winter accumulation data for the transmountain profile are summarized in Table 1. Figure 5 expresses precipitation, slope, and exposure along the transect. The diagram is schematic in that the hydrological traverse follows lowest valley elevations across the mountains. Adjacent peaks of the Icefield Ranges significantly disrupt the dome-like appearance of the profile and distort boundary layer air flow from both marine and continental sources. This has been demonstrated by Benjey (1969) who determined the lower limits of geostrophic flow at approximately 1700 and 2600 m, respectively, over the Kaskawulsh and Seward Glacier surfaces, and by Taylor-Barge (1969) who identified major changes in the alignment and movement of summer storm tracks as they encountered the St. Elias Mountains. Precipitation shadows also occur along the hydrological transect; they are especially affected along the East Arm of the upper Hubbard Glacier (Pits 5 and 6).

Relationships between precipitation, elevation, and topography. It is generally assumed that precipitation increases with elevation to some maximum value, but that it eventually declines due to a reduction in moisture supply. There is a definite increase of moisture with elevation along the lower continental slopes of the Icefield Ranges (Figs. 5, 6). Between 1615 (Pit 14) and 2640 m

(Pit 8) there was a precipitation gradient of 1170 mm km^{-1} of elevation in 1964-1965. Most of this precipitation was orographic and continental in origin (Taylor-Barge, 1969, p. 135). Extending the continental transect toward Kluane Lake, Keeler (1969, p. 722) has calculated a vertical gradient of 650 mm km^{-1} of elevation between 1000 and 2500 m. Thus, when it is also considered that September to May precipitation is usually less than 250 mm at Kluane Lake and Whitehorse, it is apparent that elevation is a critical factor in the maintenance of continental slope glaciers and the production of spring runoff.

Relationships between moisture and elevation are not clearly defined on the Pacific slope of the Icefield Ranges, although it is for just such marine-oriented windward slopes that the precipitation-altitude model is most frequently cited. An increase of precipitation with elevation has been shown, for example, in the Juneau, Alaska area, where Murphy and Schamach (1966) measured three times as much precipitation on Mt. Juneau (1136 m) as at the Juneau City weather station (22 m). For the same region, Marcus (1964) calculated a ratio of 2:2 between precipitation at Juneau Airport (6 m) and the Lemon Creek Glacier research station (1275 m). Between 1370 m (Pit 1) and 2640 (Pit 8) of the St. Elias transect, however, winter precipitation rises, falls, and again rises. This may be partially because of precipitation shadows which affect locations between the upper Seward Glacier and Divide. Keeler (1969, p. 722) has suggested alternatively

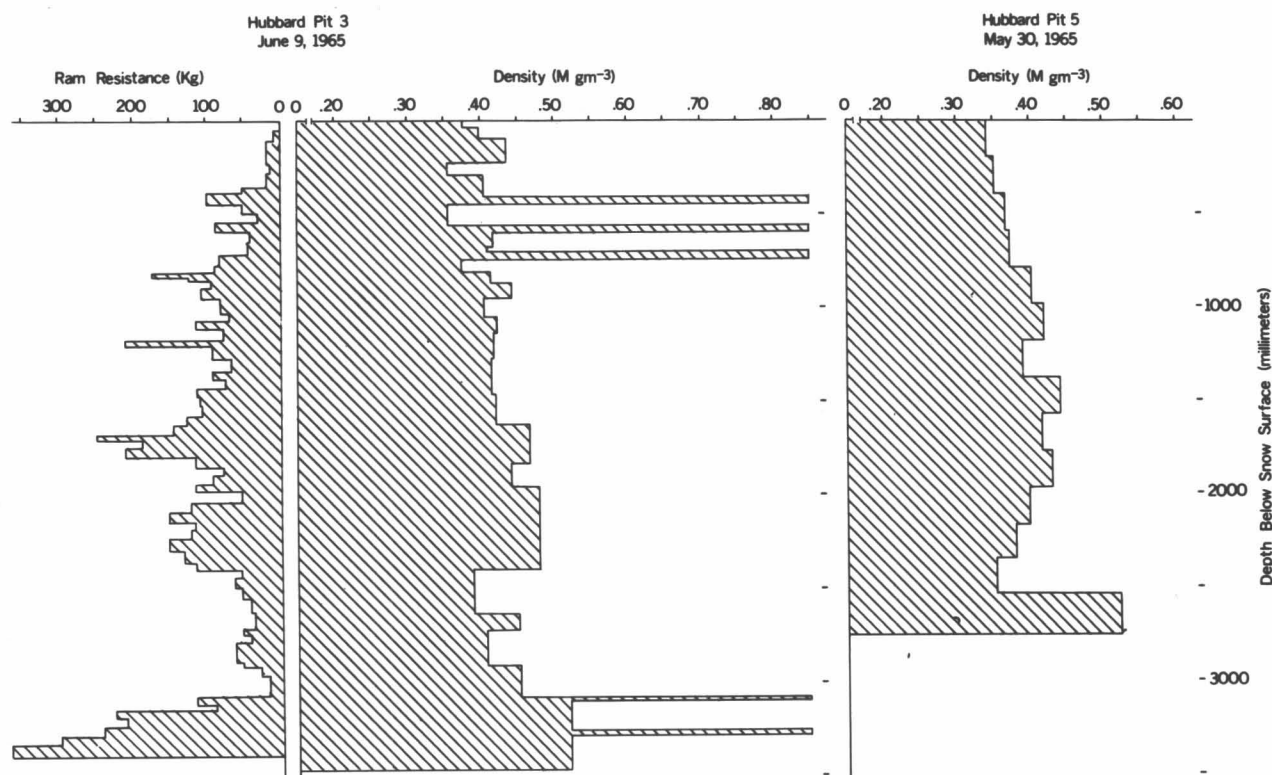


Fig. 4. 1964-1965 accumulation data for Hubbard Glacier Pits 3 and 5. Density decreases inversely with depth in the layer above the 1963-1964 surface. The ram hardness profile for Pit 3 also shows excellent agreement with density as a measure of the 1963-1964 surface. Ice bands near the surface in Pit 3 indicate it as one of two pits in which the deep freeze had disappeared by the date of excavation.

that there may be a negative precipitation gradient between Yakutat and Divide (lower dashed line in Fig. 6). For the portion of the slope sampled on the hydrological traverse, the erratic scatter probably results from a combination of topography and negative gradient. Unfortunately, because of terrain and logistical difficulties, it was impossible to obtain data between sea level and 1370 m. This is the zone in which maximum precipitation might be expected; A. Post (1969; personal communication, 1969) suggests that the area of the Samovar and Hitchcock Hills should receive between 4000 and 5000 mm. The upper dashed line in Figure 6 schematically represents the most probable trend.

Stratigraphic studies of the Mt. Logan snowpack between 2280 and 4500 m were accomplished by Alford and Keeler (1969) concurrently with the hydrological traverse. They found generally low snow accumulations, although an increase in accumulation occurred at higher elevations (Fig. 6). Keeler (1969, p. 722) again surveyed the Mt. Logan transect in 1968, extending the profile to 5400 m. He concluded, on the basis of his pit data (Fig. 6), that "... above 2500 m, elevation appears to exert little control on precipitation amounts. The reason for this may be that precipitation here is associated primarily with frontal as opposed to purely orographic processes.

Site to site differences in precipitation on Mt. Logan itself reflect local processes such as redistribution by the wind rather than elevational control."

Effects of continentality and exposure. Distance from the Pacific shore undoubtedly affects the availability of precipitable moisture across the Icefield Ranges. It is difficult, however, to isolate changes in the moisture regime caused by continentality from those caused by topography and leeward slope position. In any case, the differential influences of marine and continental environments are apparent in a comparison of stations at equivalent elevations on opposite slopes (Table 1). Between Pits 2 and 14 (both at 1765 m) there is a marine-to-continental differential of better than 3 to 1. Below this elevation the difference is accentuated. On the lower Seward Glacier, however, 1740 mm of water was still present at 1370 m, and the transient snowline was observed well below 700 m in late May. The pattern is not as clearly defined above 2000 m because of local topographic conditions and proximity to the climatic divide, which is defined as a zone between Divide and Kaskawulsh Weather Stations (Taylor-Barge, 1969, p. 182). Analysis of upper-air temperatures (Marcus, 1965) indicates that the effectiveness of this divide appears to die out above 3000 m mean sea level in the free atmosphere.

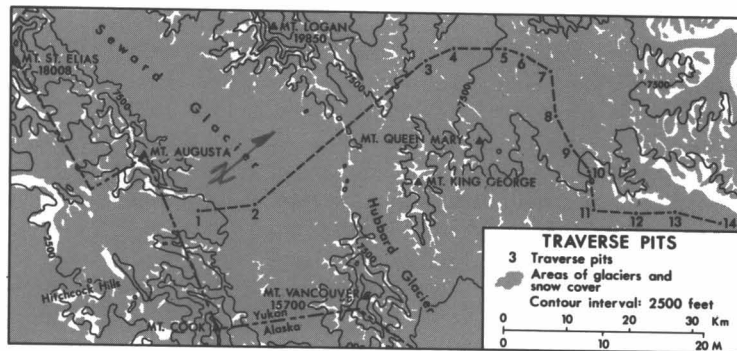
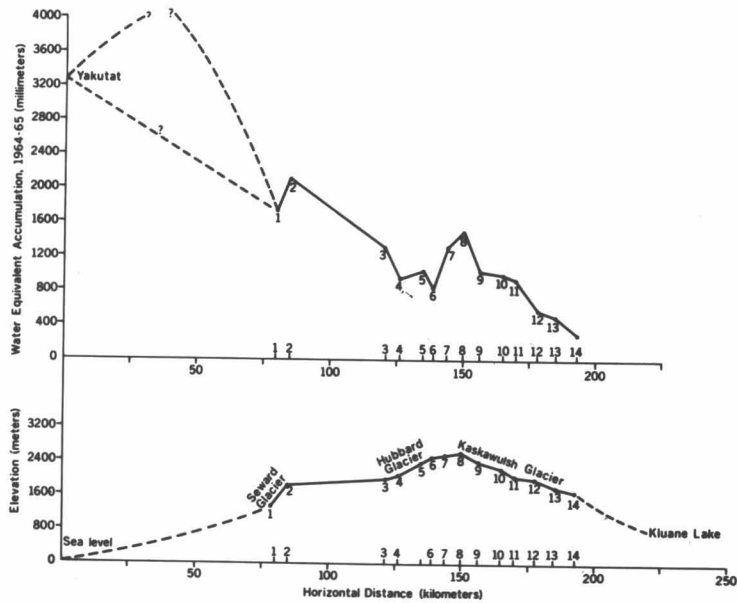


Fig. 5. Profiles of 1964-1965 water accumulation along the corresponding transmountain profile. Pit locations for the 1965 hydrological traverse are numbered (see Table 1).

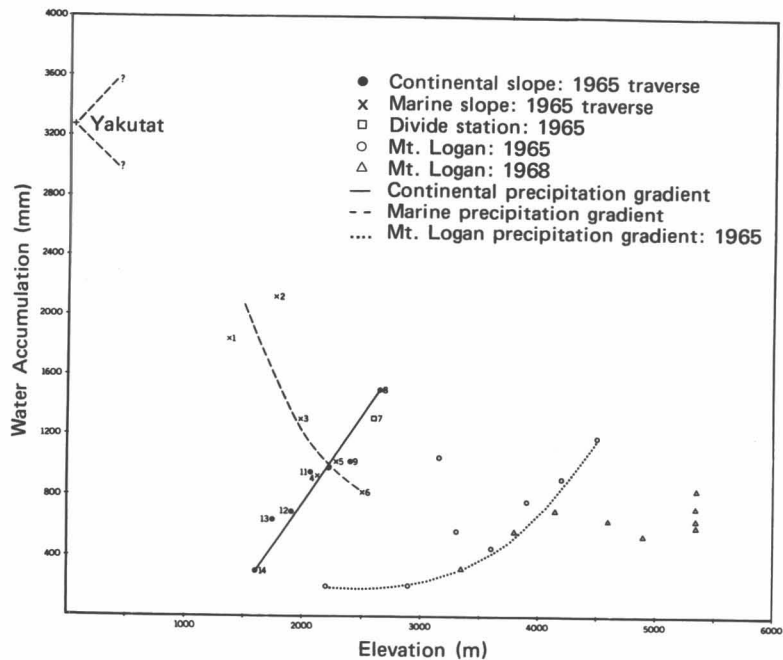


Fig. 6. Relationships between elevation and water accumulation in the Icefield Ranges, St. Elias Mountains. All observations are for the 1964-1965 winter season on the glacier with the exception of 1968 Mt. Logan data. Mt. Logan data are after Alford and Keeler (1968) and Keeler (1969).

Temporal Variations of Snow Accumulation

Utilizing pit and coring data, annual accumulations of water have been calculated for the period 1953 to 1966. Additional but less reliable accumulation values were measured at movement stakes on the east arm of the Hubbard Glacier. The locations, dates, and methods of measurement for each site are given in Appendix 1. Observations taken from firn cores or crevasse profiles represent net budget year accumulations. Depth, mean density, and water equivalent of snow or firn are given for each measurement site in Appendix 2. Temporal trends are also graphed (Fig. 7).

The combined curves for Divide Stake No. 10 and Divide Station (Fig. 7) provide a continuous picture of net water input on the Divide area accumulation plateau. This is an area in which negligible net ablation occurs; therefore, snow and firn accumulation essentially represents total annual precipitation. Precipitation was generally stable between 1954-1955 and 1959-1960, but an additional 200 to 300 mm of water was deposited each budget year during 1960 through 1963. The mass-balance period 1964-1965 through 1965-1966 was characterized by a dramatic drop in precipitation. In 1965-1966, only 1240 mm accumulated, some 1360 mm lower than the maximum net budget of 2600 mm attained in 1961-1962. Short-term values measured in local rain shadows along the Hubbard Glacier and at Glacier Central¹ reflect the lower absolute accumulations that are expected. On the upper Seward Glacier, where ablation is more effective, the accumulation values for 1963-1964 and 1964-1965

¹ Editor's note: Glacier Central, also known as Divide Station A, is location 7 of Plate 1 on the inside back cover of this volume.

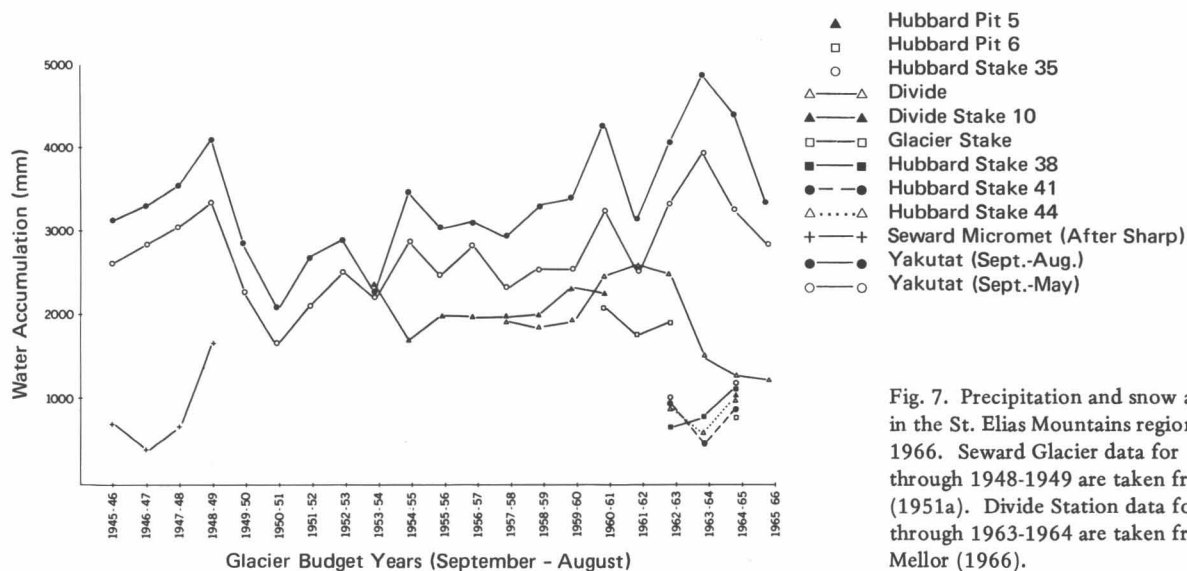


Fig. 7. Precipitation and snow accumulation in the St. Elias Mountains region, 1945 to 1966. Seward Glacier data for 1945-1946 through 1948-1949 are taken from Sharp (1951a). Divide Station data for 1961-1962 through 1963-1964 are taken from Grew and Mellor (1966).

show good agreement with the range of Sharp's calculations for the late 1940's.

If only winter nourishment of glaciers in the Icefield Ranges is considered, the budget years 1964-1965 and 1965-1966 still represent the minimum values for recent years. A gross water accumulation of 1302 mm was measured at Divide (Pit 8 of the hydrological traverse) on May 31, 1965. In previous years Divide pits were established 4 to 5 weeks later in the season, yet yielded much higher figures: 2430, 2600, 2500, and 1550 mm for 1960-1961 through 1963-1964, respectively. Substantiating these figures is the fact that the number and sizes of crevasse exposures in 1965 and 1966 was much greater than those observed during previous field seasons. This was true of all glaciers and did not appear to relate to the flow dynamics of one particular glacier.

Climatic Implications

The snow survey sites graphed in Figure 7 are located in areas which receive most of their moisture from maritime sources. A positive correlation exists between on-shore, orographic flow, and the amounts of cloud cover and precipitation along the Pacific slopes. The effect is strengthened when intense Aleutian Low pressure cells hold position for several days or more in the Gulf of Alaska. Yakutat, across the bay from the terminus of the Malaspina Glacier (Fig. 2), is the first-order weather station closest to the Icefield Ranges; presumably it is also the most representative station. It should be expected, therefore, that precipitation trends of Yakutat should show close agreement with those on the windward mountain slopes.

This is not necessarily the case. Yakutat precipitation, shown for September to August glacier years in Table 2

TABLE 2. Precipitation at Yakutat, Alaska¹
(September to August budget years)
1945-1946 to 1965-1966

Budget year	Precipitation (mm)	Departure from 1945-46/1965-66 mean (mm)
1945-46	3,147	- 202
1946-47	3,309	- 40
1947-48	3,550	- 201
1948-49	4,107	+ 758
1949-50	2,826	- 523
1950-51	2,079	-1,269
1951-52	2,661	- 688
1952-53	2,910	- 439
1953-54	2,235	-1,114
1954-55	3,452	+ 103
1955-56	3,029	- 319
1956-57	3,119	- 230
1957-58	2,951	- 398
1958-59	3,320	- 29
1959-60	3,406	+ 57
1960-61	4,296	+ 947
1961-62	3,180	- 168
1962-63	4,089	+ 741
1963-64	4,868	+1,519
1964-65	4,411	+1,063
1965-66	3,378	+ 29

¹Data from U.S. Weather Bureau (1945-1966).

and Figure 7, only partially follows accumulation trends on the upper slopes. Increased sea-level precipitation is often accompanied by decreased glacier nourishment and vice versa; that is, coastal precipitation is not necessarily accompanied by precipitation in the interior of the Icefield Ranges. Such conditions are especially apparent in 1954-1955, 1961-1962, 1962-1963, and 1963-1964. Only in the late 1950's do values at the two levels remain relatively stable in relation to each other. Similar results are obtained if approximate accumulation-season precipitation (September to May) is compared for the two elevations (Fig. 7). This evidence may be valid only for the St. Elias Mountains, but it does suggest that the common practice of extrapolating upper-slope precipitation on the basis of low-level observations may sometimes be erroneous; a 1-year transect record may be inadequate to set a curve for other years.

The causes of these variations in year-to-year precipitation relationships are not clear and require further research. It is not likely that complex mountain topography alone accounts for them, since topography remains constant. It is tentatively suggested that variations in air-mass characteristics and the extent of their penetration

of mountains are significant factors. Three synoptic situations, for example, would yield dramatically different elevation-precipitation relationships.

(1) In this region upper-air troughs and fronts usually have their greatest impact at the 800- and 700-mb levels, that is, in the glacierized zones. Thus, if associated sea-level and orographic gradients are weak, more precipitation may occur at the higher levels.

(2) When high-pressure cells or weak dry-weather systems prevail, cloud cover and precipitation is minimized throughout the region. Weak onshore or orographic movements sometimes develop locally and counter to the larger system, producing clouds and precipitation in the zone below 1500 m.

(3) Intense low-pressure cells and their associated fronts may extend sufficiently in depth to bring large quantities of precipitation to all levels of the marine slope.

The above synoptic patterns have many possible permutations and there are many variations between individual weather systems as well as from one glacier year to the next.

Climatic change also plays an important role in the year-to-year evolution of the Icefield Ranges snowpack. Variations in the frequency and intensity of air masses and storm tracks probably have greater impact on upper-slope accumulation than do short-term temperature fluctuations. Certainly the relationship between temperature change and glacier mass balance is not as clearly defined for the St. Elias Mountains as it is for the lower coastal mountains of southeast Alaska and British Columbia. In the latter areas, most of the glaciers have their total surface below 2500 m, with a majority below 2000 m. Their mass balances, therefore, are significantly affected by small vertical migrations of the summer 0°C surface, causing readjustments of equilibrium line heights and accumulation/ablation zone ratios (Marcus, 1964; Meier and Post, 1964). A number of investigators have suggested that these glaciers (south of the St. Elias Mountains) have enjoyed healthier regimes due to cooling temperature trends identified since the early 1940's (Hubley, 1956; LaChapelle, 1960; Heusser and Marcus, 1964; Meier and Post, 1964; Hamilton, 1965).

Water accumulation did not increase during the late 1950's on the upper slopes of the Kaskawulsh and Hubbard glaciers. Precipitation was in fact lower than usual at Yakutat and in the mountains during this period (Fig. 7). Colder temperatures and greater snow retention may have compensated for this lower precipitation in zones of the glaciers near the equilibrium line. Since there has been greater terminal activity on most of the Icefield Ranges glaciers during the 1960's and since a 5- to 10-year lag effect would not be unusual for glaciers of their size, it appears that these glaciers also enjoyed improved health during the period of lower precipitation in the 1950's. It follows that the 1960-1961 to 1962-1963

increase in Divide accumulation (accompanied by a maintenance of low equilibrium lines) may be reflected by further short-term improvements of the glaciers' economy. Similarly the effects of recent decreases in accumulation, which have been accompanied by a regional rise in the elevation of equilibrium lines, may be felt in the next decade.

Acknowledgments

The field research discussed herein was accomplished as part of the Icefield Ranges Research Project under joint sponsorship of the American Geographical Society and the Arctic Institute of North America. Hydrological traverse elements of the research were supported by a National Geographical Society Research Grant. Members of the traverse party included John Griffin, the University of Michigan; Lawrence Nielsen, Monsanto Chemical Company; and the authors. Philip Upton piloted the project aircraft in support of the traverse. Overall project operations during the research period were under the supervision of Walter A. Wood, Project Director. Austin Post, United States Geological Survey, who critically reviewed the text, made many helpful suggestions. We wish to express our gratitude to the above individuals and organizations for their efforts and valued counsel. Our appreciation is also extended to the many Project personnel who took time from their own research to assist us in the collection of snow data over the years.

References

- *Alford, D. (1967) Density variations in alpine snow, *J. Glaciol.*, 6, 495-496.
- *Alford, D., and Keeler, C. (1969) Stratigraphic studies of the winter snow layer, Mt. Logan, St. Elias Range, *Arctic*, 21, 245-254.
- †Benjey, W. (1969) Climatological investigations in the Icefield Ranges, summer 1965; Pt. 1, Upper-air wind patterns, *Res. Paper No. 54*, Arctic Inst. North Am., pp. 1-50.
- Benson, C. S. (1962) Stratigraphic studies in the snow and firn of the Greenland Ice Sheet, *Res. Rept. 70*, U.S. Army Snow, Ice, Permafrost Res. Establish., 93 pp.
- Bostock, H. S. (1948) Physiography of the Canadian Cordillera, with special reference to the area north of the fifty-fifth parallel, *Mem. 247*, Geol. Surv. Can., 106 pp.
- Gilbert, G. K. (1910) *Glaciers and Glaciation, Harriman Alaska Series*, Smithsonian Inst., Washington, Vol. 3, 231 pp.
- *Grew, E., and Mellor, M. (1966) High snowfields of the St. Elias Mountains, Yukon Territory, Canada, *Tech. Rept. 177*, U.S. Army Cold Reg. Res. Engin. Lab., 18 pp.
- Hamilton, T. D. (1965) Alaskan temperature fluctuations and trends: Analysis of recorded data, *Arctic*, 18, 104-117.
- Heusser, C. J., and Marcus, M. G. (1964) Historical variations of Lemon Creek Glacier, Alaska, and their relationships to the climatic record, *J. Glaciol.*, 5, 77-86.
- Hubley, R.C. (1956) Glaciers of the Washington Cascade and Olympic Mountains: their present activity and relation to local climatic trends, *J. Glaciol.*, 2, 669-674.
- *Keeler, C. M. (1969) Snow accumulation on Mount Logan, Yukon Territory, Canada, *Water Resources Res.*, 5, 719-723.
- Koerner, R. M. (1966) Accumulation of the Devon Island ice cap, Northwest Territories, Canada, *J. Glaciol.*, 6, 383-392.
- LaChapelle, E. R. (1960) Recent glacier variations from western Washington, *J. Geophys. Res.*, 65, 2505.
- Marcus, M. G. (1964) Climate-glacier studies in the Juneau Ice Field region, Alaska, *Res. Paper 88*, Dept. Geogr., Univ. Chicago, 128 pp.
- *Marcus, M. G. (1965) Summer temperature relationships along a transect in the St. Elias Mountains, Alaska and Yukon Territory, *Univ. Colorado Stud., Ser. Earth Sci., No. 3*, pp. 15-30.
- Marcus, M. G. (1969a) High Mountain Environment Project, 1968 field season, *Arctic*, 22, 162-163.
- Marcus, M. G. (1969b) Icefield Ranges Research Project, 1968, *Arctic*, 22, 161-162.
- Meier, M. F., and Post, A. S. (1964) Recent variations in mass net budgets of glaciers in western North America, *Publ. 58*, Comm. Snow Ice, Intern. Assoc. Sci. Hydrol., pp. 63-77.
- Murphy, T. D., and Schamach, S. (1966) Mountain versus sea level rainfall measurements during storms at Juneau, Alaska, *J. Hydrol.*, 4, 16-19.
- Post, A. (1969) Distribution of surging glaciers in western North America, *J. Glaciol.*, 8., 229-240.
- Ragle, R. H. (1965) Icefield Ranges Project, *Arctic*, 18, 269-270.
- Ragle, R. H. (1967) Icefield Ranges Project, 1966, *Arctic*, 20, 49-53.
- Russell, I. D. (1891) An expedition to Mt. St. Elias, Alaska, *Nat. Geogr. Mag.*, 3, 53-204.
- Russell, I. D. (1892) Mt. St. Elias and its glaciers, *Am. J. Sci.*, 43, 169-182.
- Russell, I.D. (1893) Malaspina Glacier, *J. Geol.*, 1, 219-245.
- Sharp, R. P. (1951a) Accumulation and ablation on the Seward-Malaspina Glacier system, Canada-Alaska, *Bull. Geol. Soc. Am.*, 62, 725-744.
- Sharp, R. P. (1951b) Features of the firn on upper Seward Glacier, St. Elias Mountains, Canada, *J. Geol.*, 59, 599-621.
- Sharp, R. P. (1951c) Meltwater behavior in firn on upper Seward Glacier, St. Elias Mountains, Canada, *Proc. Intern Assoc. Sci. Hydrol.*, 1, 476-487.
- Sharp, R. P. (1951d) Thermal regimen of firn on upper Seward Glacier, Yukon Territory, Canada, *J. Glaciol.*, 1, 476-487.
- Sharp, R. P. (1953) Deformation of bore hole in Malaspina Glacier, Alaska, *Bull. Geol. Soc. Am.*, 64, 97-100.
- Sharp, R. P. (1958a) Malaspina Glacier, Alaska, *Bull. Geol. Soc. Am.*, 69, 617-646.
- Sharp, R. P. (1958b) The latest major advance of the Malaspina Glacier, Alaska, *Geogr. Rev.*, 48, 16-26.
- Tarr, R. S. (1907) The Malaspina Glacier, *Bull. Am. Geogr. Soc.*, 39, 273-285.
- Tarr, R. S., and Butler, B. S. (1909) The Yakutat Bay region, *Prof. Paper 64*, U. S. Geol. Surv., 183 pp.
- Tarr, R. S., and Martin, L. (1914) *Alaska Glacier Studies*, Nat. Geogr. Soc., Washington, 498 pp.
- Taylor-Barge, B. (1969) The summer climate of the St. Elias Mountains region, *Res. Paper No. 53*, Arctic Inst. North Am., 265 pp.
- U. S. Weather Bureau (1945-1966) Local climatological data: Yakutat, Alaska, January 1945 to December 1966.
- Wahrhaftig, C. (1965) Physiographic divisions of Alaska, *Prof. Paper 482*, U. S. Geol. Surv., 52 pp.
- Washburn, B. (1935) Morainic banding of Malaspina and other glaciers, *Bull. Geol. Soc. Am.*, 46, 1879-1890.
- Washburn, B. (1936) Exploring Yukon's glacial stronghold, *Nat. Geogr. Mag.*, 69, 715-747.
- Wood, W. A. (1936) The Wood Yukon Expedition of 1935, *Geogr. Mag.*, 26, 228-246.
- Wood, W. A. (1942) The parachuting of expedition supplies; an experiment by the Wood Yukon Expedition, 1941, *Geogr. Rev.*, 32, 36-55.

- Wood, W. A. (1963) The Icefield Ranges Research Project, *Geogr. Rev.*, 53, 163-184.
- Wood, W. A. (1967) *A History of Mountaineering in the St. Elias Mountains*, Yukon Alpine Centennial Exped., Scarborough, Ontario, 45 pp.
- Wood, W. A. (1969) Icefield Ranges Research Project, in *Icefield Ranges Research Project, Scientific Results*, edited by V. C.

Bushnell, and R. H. Ragle, Vol. 1, pp. 3-13, Am. Geogr. Soc., and Arctic Inst. North Am., New York.

*These articles were reprinted in previous volumes of Icefield Ranges Research Project, Scientific Results.

†A modified version of this report appeared in a previous volume of Icefield Ranges Research Project, Scientific Results.

APPENDIXES

I

SITE DESCRIPTIONS FOR SNOW ACCUMULATION MEASUREMENTS, ICEFIELD RANGES, YUKON

Location	Budget year	Date measured	Type of measurement
DIVIDE			
Stake 10	1953-54	Aug. 22, 1962	Corehole
Stake 10	1954-55	Aug. 22, 1962	Corehole
Stake 10	1955-56	Aug. 22, 1962	Corehole
Stake 10	1956-57	Aug. 22, 1962	Corehole
Stake 10	1957-58	Aug. 22, 1962	Corehole
Stake 10	1958-59	Aug. 22, 1962	Corehole
Stake 10	1959-60	Aug. 22, 1962	Corehole
Stake 10	1960-61	Aug. 22, 1962	Corehole
Divide	1957-58	July 31, 1961	Corehole
Divide	1958-59	July 31, 1961	Corehole
Divide	1959-60	July 31, 1961	Corehole
Divide	1960-61	July 30, 1960	Pit
Divide	1961-62 ^a	July 23, 1964	Corehole
Divide	1962-63 ^a	July 23, 1964	Pit/Core
Divide	1963-64 ^a	July 22, 1964	Pit
Divide	1964-65	May 31, 1965	Pit
Divide	1965-66	Aug. 10, 1966	Pit
Glacier Station	1960-61	July 2, 1961	Pit
Glacier Station	1961-62	June 29, 1962	Pit
Glacier Station	1962-63	June 29, 1963	Pit
HUBBARD ARM			
Stake 44	1962-63	July 15, 1963	Movement Stake
Stake 41	1962-63	July 15, 1963	Movement Stake
Stake 44	1963-64	Aug. 6, 1964	Movement Stake
Stake 41	1963-64	Aug. 6, 1964	Movement Stake
Stake 44	1964-65	May 30, 1965	Movement Stake
Stake 41	1964-65	May 30, 1965	Movement Stake
Pit 5	1964-65	May 30, 1965	Pit
Stake 35	1962-63	July 15, 1963	Movement Stake
Stake 38	1962-63	July 15, 1963	Movement Stake
Stake 38	1963-64	Aug. 6, 1964	Movement Stake
Stake 38	1964-65	May 30, 1965	Movement Stake
Stake 35	1964-65	May 30, 1965	Movement Stake
Pit 6	1964-65	May 30, 1965	Pit
SEWARD			
Crevasse	1945-46 ^b	Aug. 28-29, 1949	Crevasse
Airstrip	1946-47 ^b	Aug. 28-29, 1949	Pit
Airstrip	1947-48 ^b	Aug. 28-29, 1949	Pit
Airstrip	1948-49 ^b	Aug. 28-29, 1949	Pit
Micromet	1963-64	Aug. 3, 1964	Pit
Micromet	1964-65	July 14, 1965	Pit
Micromet	1964-65	July 25, 1965	Pit
Pit 2	1964-65	May 21, 1965	Pit

^aData from Grew and Mellor (1966).

^bData from Sharp (1951a).

The Effects of a Subarctic Glacier on Radio-Wave Propagation in Summer

Takeo Yoshino *

ABSTRACT. This paper describes the investigation of the attenuation of radio waves reflected on a glacier surface, and propagation loss through ice. Reflection coefficients are determined over a range of air temperatures. In summer, the air temperature a short distance above the snow and ice surface of a Subarctic glacier rises above 0°C during a warm day. We found that the reflection coefficient during such a warm day exceeds 0.4, and drops below 0.1 during a cold night; the average value of the coefficient is 0.35. These reflection coefficients at MF and HF ranges are less than those of any other ground surface except the Antarctic and Greenland ice sheets. This paper also gives measured values of the dielectric constant of glacier ice for air temperatures from -15°C to 0°C, and presents a simple method of calculating dielectric constants for a known temperature using parameter U which we determined from our data.

Introduction

The North American continent has several glacier areas. The surface temperature of the glaciers in these areas sometimes falls to below -45°C in winter, but in summer it is usually 0°C or warmer. When the air temperature rises above 0°C, the moisture of the air contained in the spacing between ice crystals increases; the motion of the ice molecules also increases, and the dielectric constant becomes greater.

The studies were carried out on the divide of the Kaskawulsh and Hubbard Glaciers in the St. Elias Mountains, an area located on the great circle between North America and the Far East. Radio waves which take this propagation route are influenced by the reflection coefficients of the glacier surface, which are determined by surface air temperatures. No study had previously been done of the reflection or scattering of MF and HF radio waves by a glacier in summer when air temperatures are between -15°C and 0°C or slightly higher.

The author measured dielectric constants and loss tangents from core samples which were taken from the glacier. Reflection coefficients at the glacier surface and propagation loss in the glacier ice were calculated from the measurements.

Structure of a Subarctic Glacier

A Subarctic glacier consists of new snow, wet snow, compacted snow, granular snow, and glacier ice, from surface to bottom. At altitudes below the snow line, glacier ice is exposed. A crystal of new snow has dendritic structure; when the surface air temperature remains below 0°C, with lapse of time the snow crystal is deformed into small particles; the resulting material is called compacted snow. When the surface air temperature rises above 0°C, new snow changes to wet snow due to the moisture of melting. With a drop in temperature, the wet snow freezes into larger grains forming granular snow. Granular snow eventually changes to polycrystal-

line glacier ice by metamorphosis. Densities in a Subarctic glacier are given in Table 1.

TABLE 1. Glacier Densities

Material	Density
New snow	0.1–0.25 g/cm ³
Compacted snow	0.25–0.4
Wet snow	0.25–0.4
Granular snow	0.4–0.7
Glacier ice	0.7–0.9

In the gap between ice and bedrock at the bottom of a glacier, the humidity is usually very high, and often we find water at this boundary. Typical crevasses, especially transverse crevasses, are about 28 m deep (Holdsworth, 1965). In summer there is usually about two meters of water standing at the bottom of a crevasse. Typical sections across crevasses are shown in Figure 1.

At depths greater than 20 m in a glacier the temperature remains at 0°C as shown in Figure 2, since only the top 20 m are influenced by air temperature.

Instruments and Methods of Measurement

For sampling, a steel pipe core sampler 5 cm in diameter was screwed into the snow by hand auger. Core samples of snow and ice have a fragile structure, so care was taken to protect them from compression, mechanical shock, and variations in temperature.

The density of each sample was computed from the measured values of its mass and volume; then sections about 1 cm in thickness were cut for the measurement of dielectric properties. Each section was inserted between the plates of a condenser which was connected to a Boonton-type Q meter to form a resonance tank circuit as illustrated in Figure 3. The dielectric constant, ϵ , was calculated by the shift in the capacity of the standard variable condenser required for resonance when the core sample was inserted in the "sample condenser."

*University of Electro-Communications, Chofu, Tokyo, Japan

That is

$$\epsilon = \frac{C_a}{C_x} + 1 \quad (1)$$

where

- C_a = decrease in the capacity of the standard variable condenser when the sample is inserted into sample condenser
- C_x = capacity of sample condenser without sample

The loss tangent ($\tan \delta$) is measured by a Q meter in the circuit. The $\tan \delta$ is given by

$$\tan \delta = \frac{C}{C_x} \left(\frac{1}{Q} - \frac{1}{Q_0} \right) \quad (2)$$

where

- Q = value of Q when the sample is inserted in sample condenser
- Q_0 = value of Q when the sample is not inserted in sample condenser
- C = total capacity of circuit

In the study area, the researchers and the instruments were transported by small aircraft, which have a problem with landing and taking off on the rough surface of a glacier, particularly with a heavy load. Therefore it was impossible to take in a gasoline engine generator and a large Q meter such as were used on Antarctic expeditions. For this investigation the author devised a homemade all-transistorized instrument, small and light, and designed for simplicity of performance and high accuracy; Figure 4 is a schematic diagram of this equipment. The oscillator stage is in a plug-in module; frequencies are stabilized by 1 MHz, 10 MHz and 100 MHz quartz crystals. The transistor circuit of this equipment uses a "posister" self-bias resistance inserted in the emitter circuit for temperature compensation; the drifting frequency of the oscillator was less than 10^{-5} , and the output power deviation was less than 0.05 dB. The standard variable condenser consisted of an indium plate and steatite insulator.

Dielectric Constant Measured

At temperatures below -15°C . The author used an experimental formula for computing the dielectric constant of snow and ice, at -15°C , based on studies in Antarctica (Yoshino, 1967).

That is

$$\ln \epsilon^* = 1.1 \rho \ln \epsilon_2 \quad (3)$$

where ϵ^* is the dielectric constant at the density ρ of the sample, and ϵ_2 is the dielectric constant of pure ice at the frequency measured.

The RF dielectric constant is the complex quantity

$$\epsilon = \epsilon' (1 - j \tan \delta) \quad (4)$$

where $\epsilon' \doteq \epsilon^*$, the dielectric constant of snow and ice, and the loss tangent of snow and ice is

$$\tan \delta = \frac{\sigma}{\omega \epsilon_0 \epsilon^* (\omega)} \quad (5)$$

where σ is conductivity of snow and ice, ω is angular frequency, and ϵ_0 is the dielectric constant of free space, in MKS units.

At temperatures above -15°C . As temperatures in ice increase from -15°C to 0°C , the thermal motion of ice molecules increases rapidly; the dielectric constant increases in proportion to the increased thermal motion and the relaxation time of ice molecules.

At or near the melting point the dielectric constant of snow and ice is variable; its value depends on water content. In the frequency range considered, the dielectric constant of pure ice is about 3.2, while that of pure water is about 78.5. Therefore, when the air temperature rises above 0°C , the dielectric constant becomes greater, because of increasing water content (Evans, 1965).

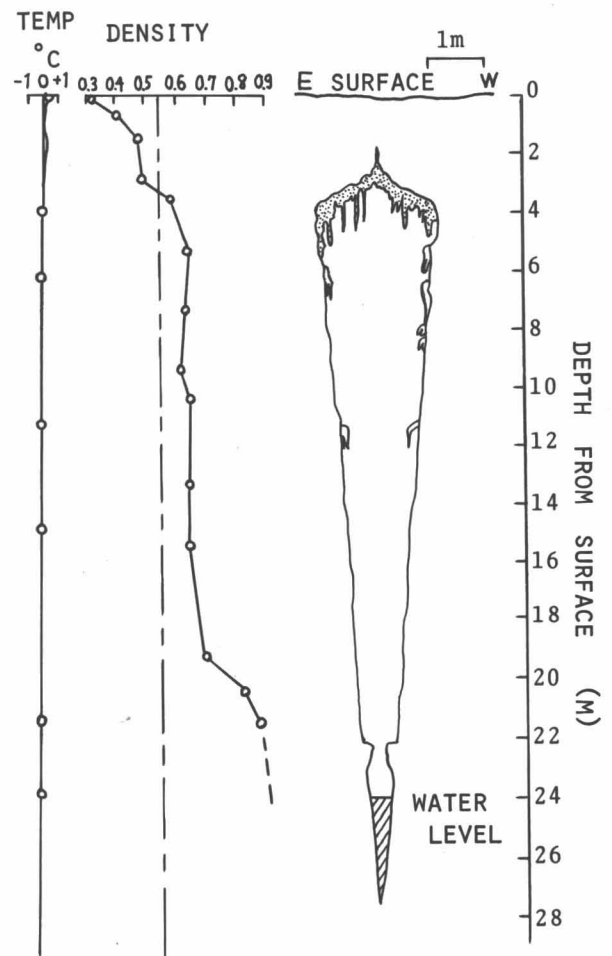


Fig. 1. Profile of a typical crevasse in a Subarctic glacier (after Holdsworth, 1965).

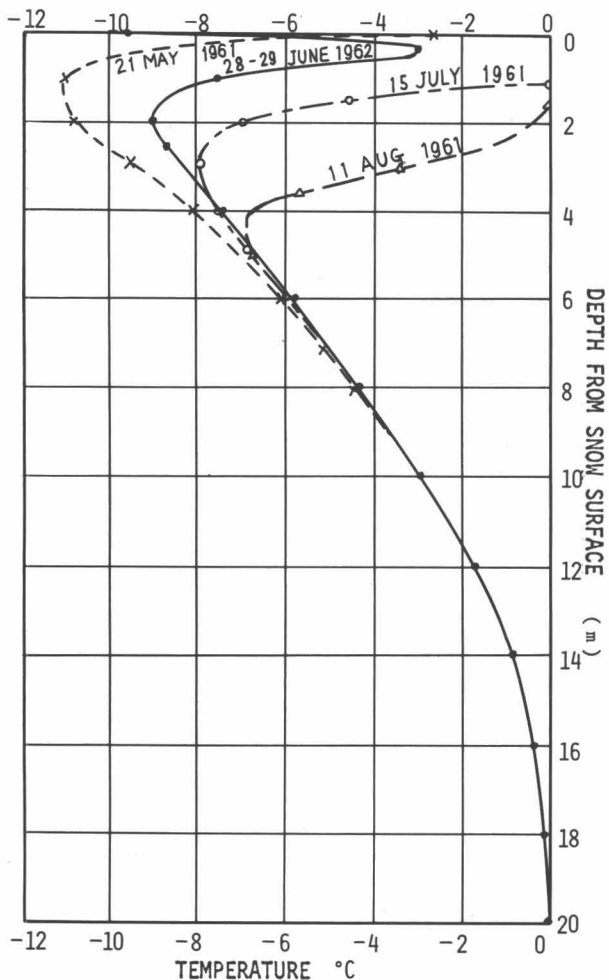


Fig. 2. Temperature profiles in a Subarctic glacier.

Figure 5 gives measured values of dielectric constants at 1 MHz from -15°C to around 0°C from 1965 Icefield Ranges' data. The temperatures used are air temperatures a small distance above the snow and ice surface. Figure 6 gives the dielectric constants at 10 MHz, and Figure 7

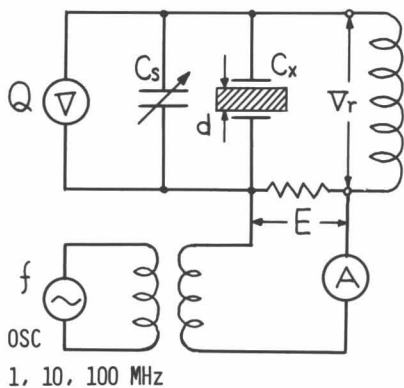


Fig. 3. Circuit diagram of setup used to measure dielectric constants and dielectric losses by means of a Q meter.

at 100 MHz. All three Figures show the same relationships to variations in air temperature. They also show that the dielectric constant of wet snow and compacted snow differ somewhat even though their densities are the same.

The lower curves in these Figures show the value computed by equation 3 for the Antarctic ice sheet, for temperatures of -15°C or lower. The upper curves are for dielectric constants at 0°C . For the computation of these, the author also used a formula of Wiener (1910), relating the variation of the dielectric constant of snow and ice with density for temperatures from -15°C to 0°C .

That is

$$\frac{\epsilon^* - 1}{\epsilon^* + U} = \frac{\rho}{\rho_i} \frac{\epsilon_2 - 1}{\epsilon_2 + U} \quad (6)$$

where

- ϵ^* = dielectric constant of snow and ice
- ϵ_2 = dielectric constant of pure ice
- ρ = density of snow and ice
- ρ_i = density of pure ice
- U = parameter for formula (the form factor).

Equation 6 is important in determining the relationship between air temperature and parameter U in the high-frequency band. In Figures 5, 6, and 7 the upper curves show the values calculated by equation 6 when $U = 10.0$; these curves are in good agreement with measured values at 0°C . Moreover, the author found the very interesting result that the value of U has a simple relationship to air temperature as shown in Figure 8.

Figure 9 gives measured values of dielectric constants at temperatures from -15°C to 0°C . Values of dielectric constants at temperatures above 0°C increase irregularly depending on the volume of contained water. In addition, the density increased rapidly when the sample was kept above 0°C , as shown by the lower set of curves.

The relationship of the dielectric constant of snow to water content is known from data (Evans, 1965). The dielectric constant of dry snow is assumed to be 2.0, corresponding to a specific gravity of approximately 0.5.

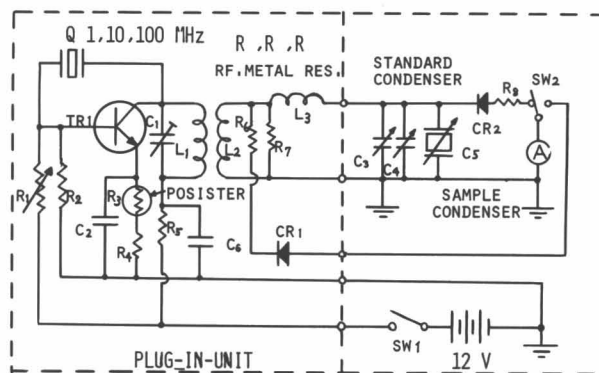


Fig. 4. Schematic diagram of transistorized equipment for measuring the dielectric properties of ice.

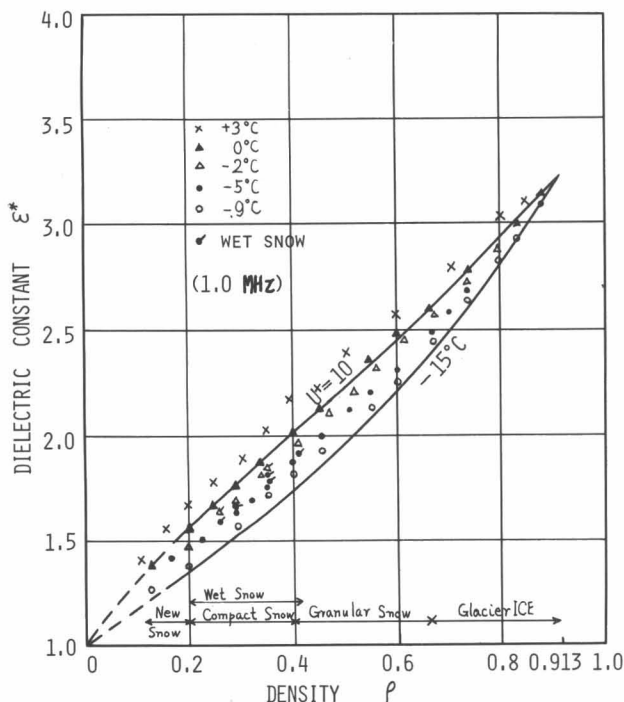


Fig. 5. Dielectric constant versus density in a Subarctic glacier for a radio frequency of 1 MHz.

Figure 10 shows the distribution of measured values of dielectric constants at the divide of the Kaskawulsh and Hubbard Glaciers in 1965. Figure 11 shows the distribution of the measured values of dielectric constants on the vertical wall of the west side of the pit at Divide camp.

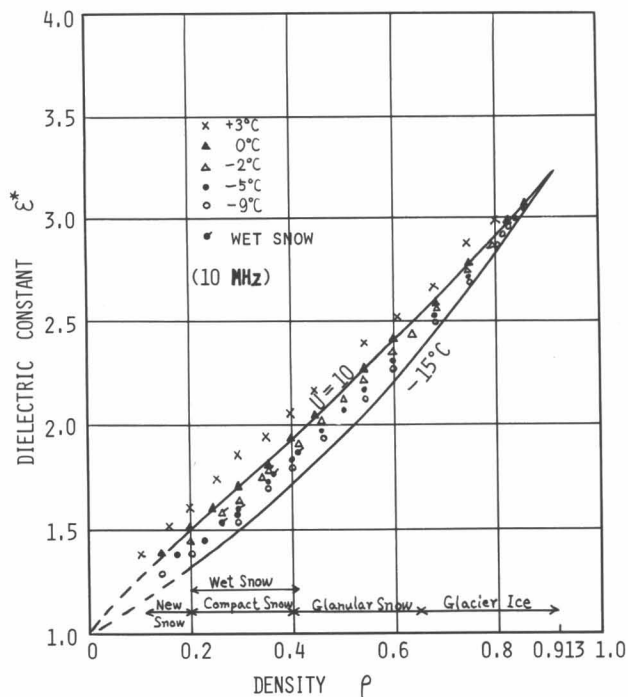


Fig. 6. Dielectric constant versus density in a Subarctic glacier for a radio frequency of 10 MHz.

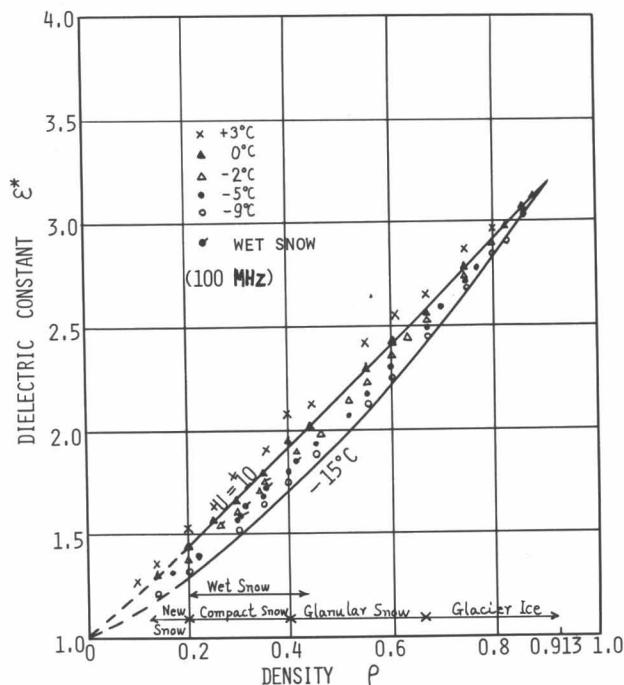


Fig. 7. Dielectric constant versus density in a Subarctic glacier for a radio frequency of 100 MHz.

Loss tangent and conductivity. Figure 12 illustrates the relationship of loss tangent ($\tan\delta$) to propagation frequency. The solid curves show the values calculated by using equation 5.

At high radio frequencies the loss tangent for air temperatures greater than 0°C increases rapidly as the percentage of contained water increases.

The variation of the conductivity (σ) with frequency was computed from the measured values of Figures 6, 7, 8, 9 by using equations 5 and 6. Conductivities of Subarctic glacier ice at temperatures of 0°C and -15°C

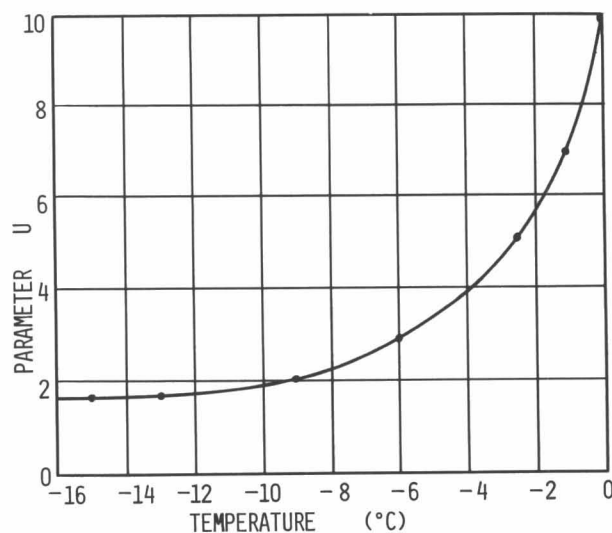


Fig. 8. Relationship of temperature to parameter U of Wiener's formula (see text).

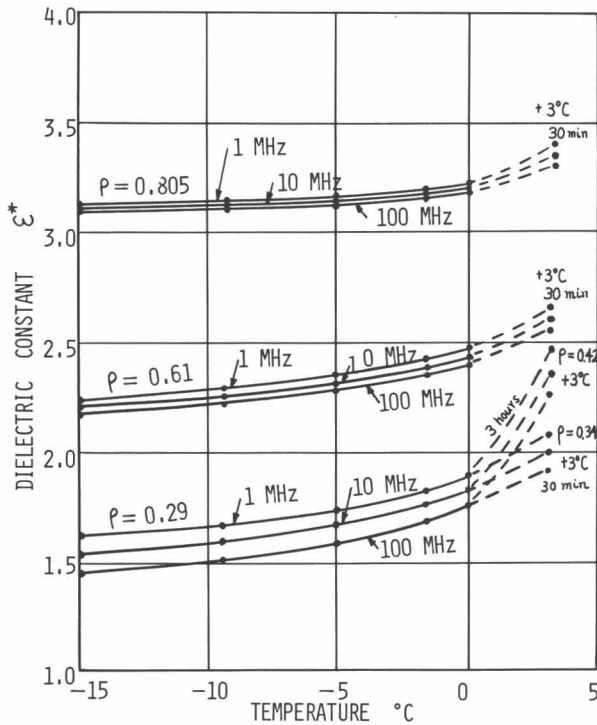


Fig. 9. Temperature dependence of the dielectric constant of snow.

are in the order of 10^{-7} to 10^{-9} mho/m; for fresh snow of density 0.2 at 0°C the conductivities are in the order of 10^{-8} to 10^{-10} mho/m. For wet snow at temperatures above 0°C , conductivity is calculated by multiplying the value for fresh snow by a factor of from 10 to 100. The values from the measured dielectric constant do not change greatly with frequency.

Reflection of Radio Waves on a Subarctic Glacier Surface

Reflection coefficient. The reflection coefficient of plane waves on a snow surface has a very important relation to the radio-wave propagation loss across a glacier. A glacier surface of fresh snow, wet snow, compacted snow, or ice has densities ranging between 0.2 and 0.9 gm/cm^3 . In the analysis of the reflection of radio waves in the frequency range covered in this paper, the glacier surface may be considered flat.

The reflection coefficient for a plane wave is given by Snell's law. For horizontal polarization this is:

$$|R_c|_h = \frac{\cos\theta - \sqrt{n^2 - \sin^2\theta}}{\cos\theta + \sqrt{n^2 - \sin^2\theta}} \quad (7)$$

For vertical polarization the relationship is:

$$|R_c|_v = \frac{n^2 \cos\theta - \sqrt{n^2 - \sin^2\theta}}{n^2 \cos\theta + \sqrt{n^2 - \sin^2\theta}} \quad (8)$$

where

- θ = the incident angle of radio wave from normal to snow surface
- n = relative index of refraction.

The following formula may be used to calculate n :

$$n^2 = \frac{\epsilon_2 - j \frac{\sigma_2}{\omega \epsilon_0 \epsilon_2}}{\epsilon_1 - j \frac{\sigma_1}{\omega \epsilon_0 \epsilon_1}} \quad (9)$$

In this paper $\epsilon_1 = 1$, and $\sigma_1 = 0$; the conductivity of the surface snow is $\sigma_2 = 10^{-6}$ mho/m over the entire frequency range.

Figure 13 shows the relationship of reflection coefficient to frequency for radio waves at vertical incidence. The curves for -15°C are for the Antarctic ice sheet. Reflection coefficients as a function of angle of incidence for frequencies of 1 MHz and 100 MHz are given in Figure 14. The dashed curves show the values at 0°C , and the solid curves show the values at -15°C .

Reflection loss and transmission loss at the snow and ice surface. The reflection loss, S_R (in decibels), is calculated as follows:

$$S_R = -10 \log_{10} |R_c|^2 \quad (10)$$

where the reflection coefficient R_c is the value calculated by equations 7 and 8.

The transmission loss, S_T (in decibels), —the loss of the incident wave penetrating the snow surface—is expressed by

$$S_T = -10 \log_{10} (1 - |R_c|^2) \quad (11)$$

Figures 15 and 16 show the relation of S_R and S_T to incident angle. The dashed curves are for values at 0°C , and the solid curves for values at -15°C . In Figure 15 it is seen that the vertically polarized wave penetrates completely when the incidence angle is 50° (the Brewster angle).

Daily variation of reflection coefficient. The typical temperature variation in a 24-hour period at the surface of a glacier in summer is given in Figure 17. For radio waves of frequencies above the VHF range, the reflection coefficient varies with surface temperature. Calculated values of the reflection coefficient throughout a day at the surface of a glacier in summer are shown in Figure 18. These values are calculated by equations 10 and 11 using data from Figure 17. The variation of reflection coefficients is very important in the determination of the field intensity at receiving sites on communication routes crossing a glacier area. Figure 18 shows that the surface of the glacier is a good reflector in the clear daytime, but it changes to a poor reflector when the temperature drops to below -5°C at night or on cloudy and blizzard days.

Figure 19 shows the tendency of the dielectric constant of snow to increase with the lapse of time after snowfall. Figure 20 shows the average variation of the coefficient during one snowfall interval.

Energy Loss in Radio Waves Propagated Through a Subarctic Glacier

Signal attenuation. The thickness of snow cover on the glacier surface is about 20 m at the divide of the Kaskawulsh and Hubbard Glaciers; but in the region below the snow line plane waves are incident directly upon ice, and can be considered to propagate into a homogeneous dielectric medium.

The propagation loss, S_{RF} (in dB/m), of high-frequency plane waves in a uniform dielectric is calculated by the following equation:

$$S_{RF} = 8.686 \frac{2\pi}{\lambda} \left[\frac{\epsilon^*}{2} (\sqrt{1 + \tan^2 \delta} - 1) \right]^{1/2} \quad (12)$$

where λ is the wavelength in free space.

Figure 21 shows the calculated relationship of signal attenuation (S_{RF}) as a function of frequency for a plane wave propagating in a unit volume of glacier ice. The

measured values from Figures 6, 7, 8, and 12 were used in the calculations. According to the values in Figure 21, the propagation loss is about 0.05 dB/m for frequencies of 10 to 100 MHz at 0°C. The loss for a wave propagated through 500 m of glacier ice would be 50 dB, resulting in the absorption of the greater part of the energy.

Scattering loss. The analysis of the scattering phenomenon for radio waves propagating through glaciers is very difficult, because the size of deeply located ice crystals cannot be easily determined. Where the size of ice crystals is known, it is possible to calculate the scattering loss of a radio wave by a formula given by Waite and Schmidt (1961). According to them, the scattering loss, S_s , for one meter is:

$$S_s = 10^{-1/2} \log_{10} \left[1 + \left(\frac{2\pi}{3} \right)^3 V^{4/3} \left(\frac{\epsilon^* - 1}{\epsilon^* + 2} \right)^2 f^4 \right] \quad (13)$$

where V is the volume of a single ice crystal. Values calculated for the Antarctic ice sheet are given in Figure 22.

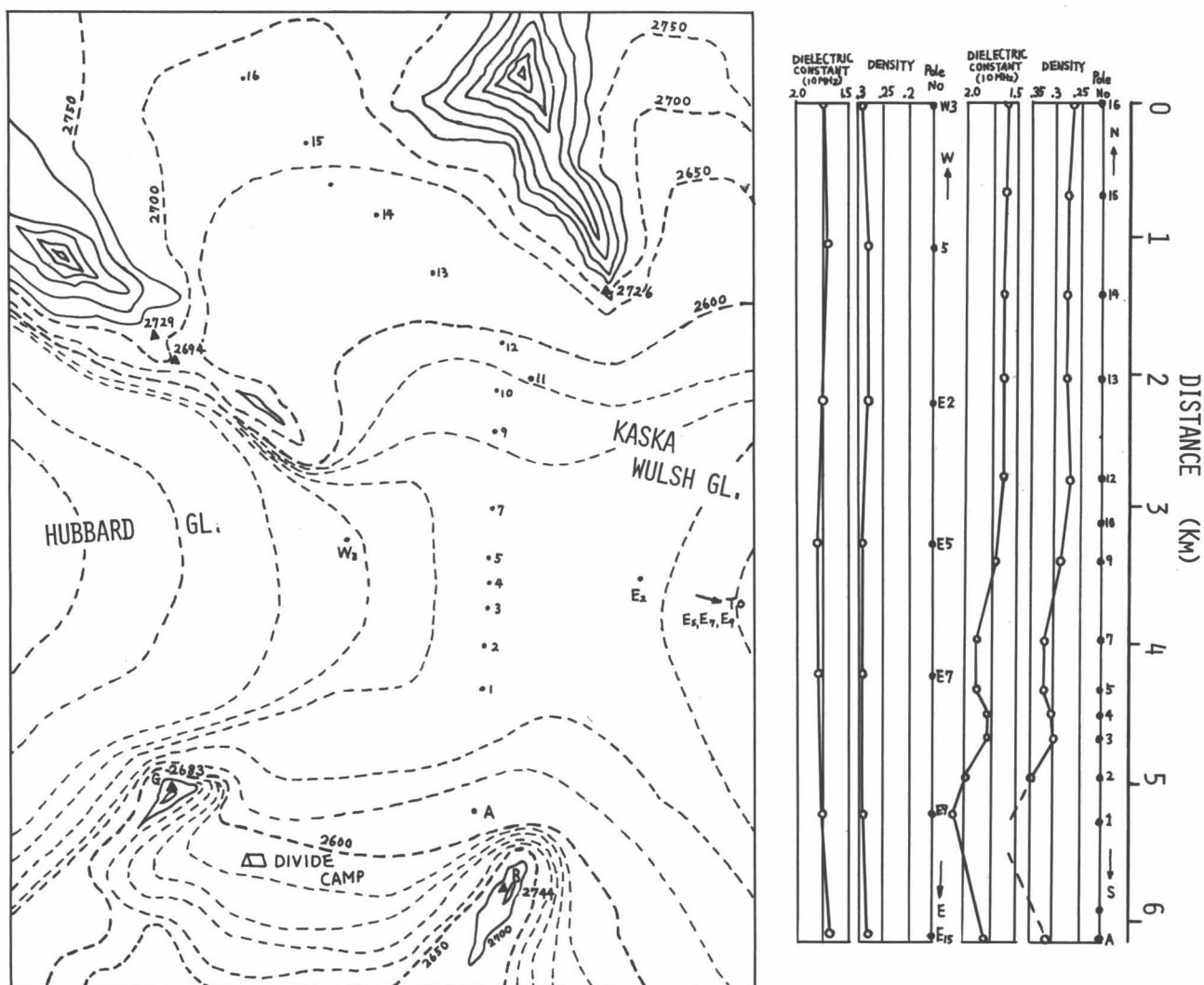


Fig. 10. Distribution of measured values of dielectric constants at the divide of the Kaskawulsh and Hubbard Glaciers in 1965. Locations of coring sites are given on the map.

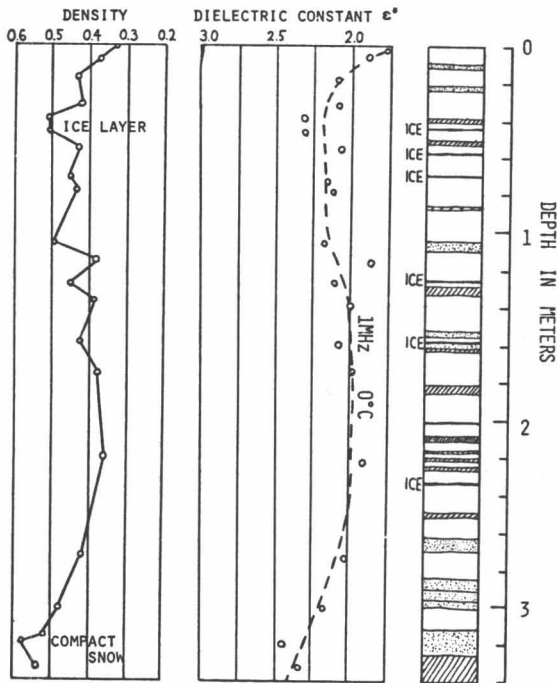


Fig. 11. Measured values of density and dielectric constant the vertical surface of the west wall of the pit at Divide camp.

In addition, the value of V used in Figure 22 is larger than that for the Icefield Ranges. The fact that scattering loss increases as the fourth power of the frequency results in its being the dominant factor in UHF band, while it

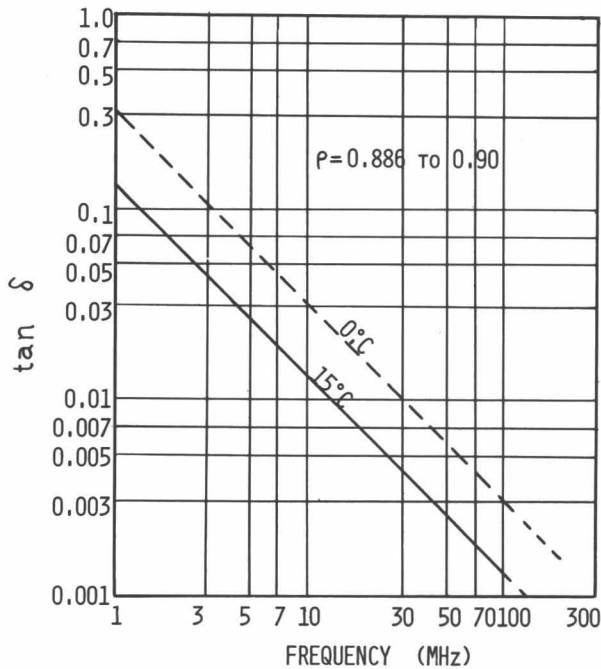


Fig. 12. Relationship of loss tangent to propagation frequency.

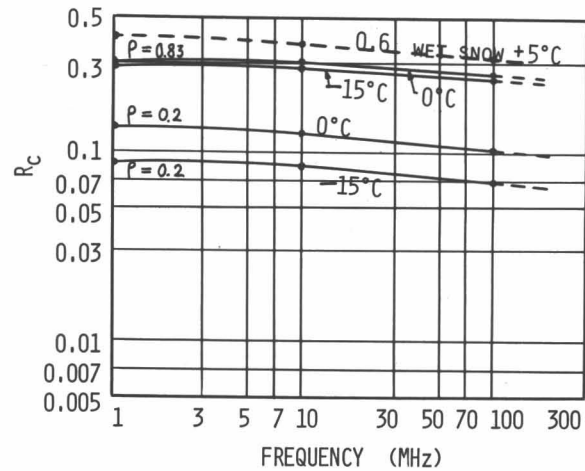


Fig. 13. Frequency dependence of reflection coefficient for radio waves with vertical incidence at the surface of a Subarctic glacier.

is negligible in the HF and VHF bands at Icefield Ranges.

Reflection loss at the ice bottom. Two types of conditions exist at the bottoms of glaciers. In the first, either standing or flowing water is found at the ice-rock boundary. The second category has no water at the ice-rock boundary.

When there is water at the ice-rock boundary, the reflection loss, S_B , is given by equation 10, using the dielectric constant of water, 78.5. Figure 23 illustrates the frequency dependence of reflection loss for vertical incidence of radio waves when water is present at the bottom of the glacier.

The dielectric properties of the terminal moraine of Kaskawulsh Glacier were measured; the dielectric constant was found to be about 6 to 7, and the conductivity was 10^{-3} mho/m. These values were used to compute the frequency dependence of the reflection loss for vertical incidence at the ice-rock boundary when no water is present. Results are given in Figure 24.

Reflection and refraction by crevasses. Almost all glaciers in the study area have many transverse crevasses. The profile of a typical transverse hidden crevasse is given in Figure 1. When the transmitted wave in the glacier propagates across the crevasse, the transmission loss is calculated by equation 11, for the two ice-air boundaries. The calculated value is approximately 21 dB for frequencies from 1 MHz to 100 MHz. In the case of radio-wave propagation through standing water in a crevasse, most of the energy is lost.

Conclusions

This study shows that the reflection loss of radio waves on a Subarctic glacier is not as great as on the Antarctic and Greenland ice sheets, but is greater than that of any other ground surface on the earth except the polar ice sheets.

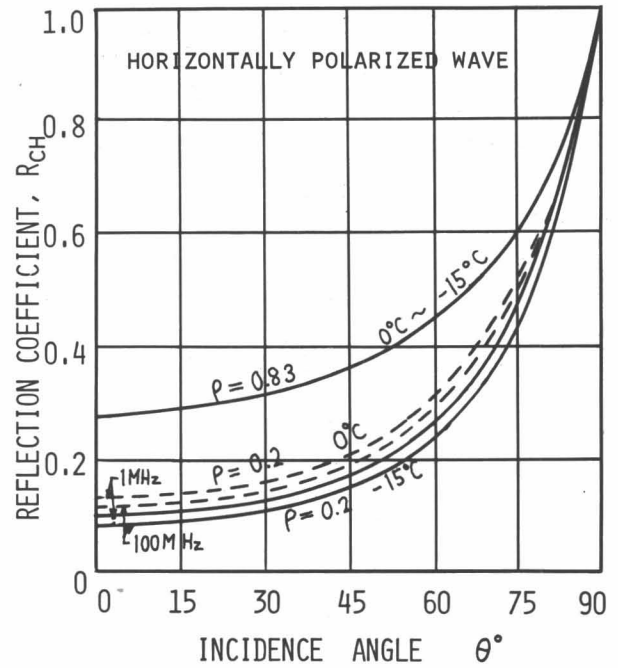
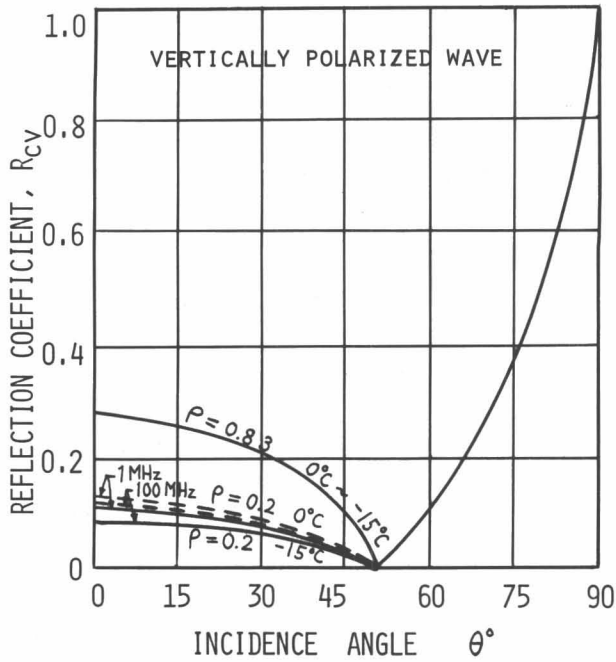


Fig. 14. Relationship between incidence angle and reflection coefficient at the surface of a Subarctic glacier.

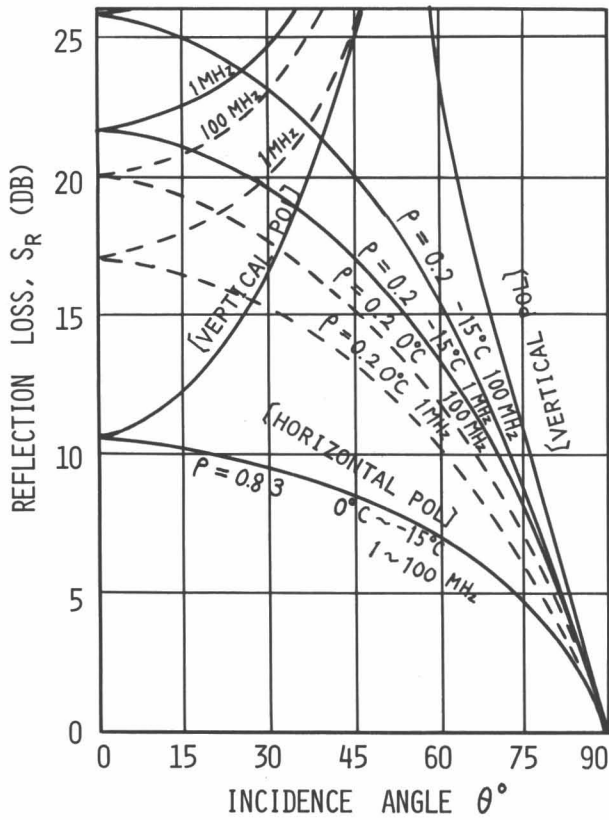


Fig. 15. Relationship between reflection loss and incidence angle at surface of a Subarctic glacier.

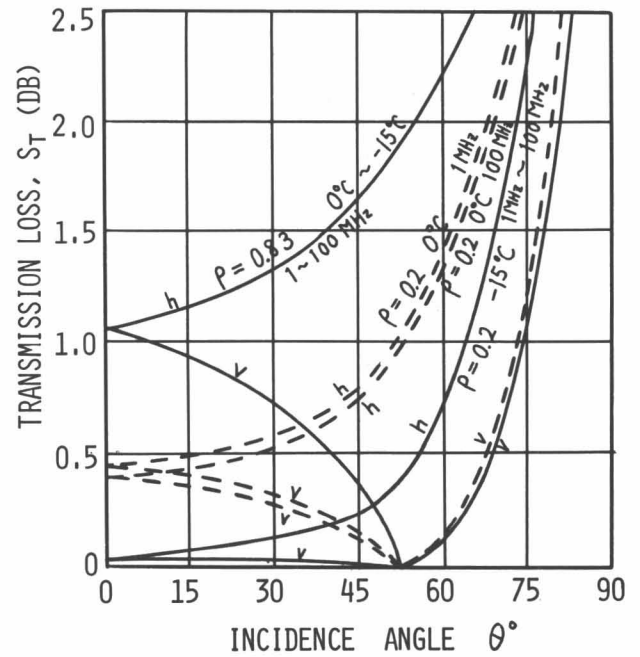


Fig. 16. Relationship between transmission loss and incidence angle at the surface of a Subarctic glacier.

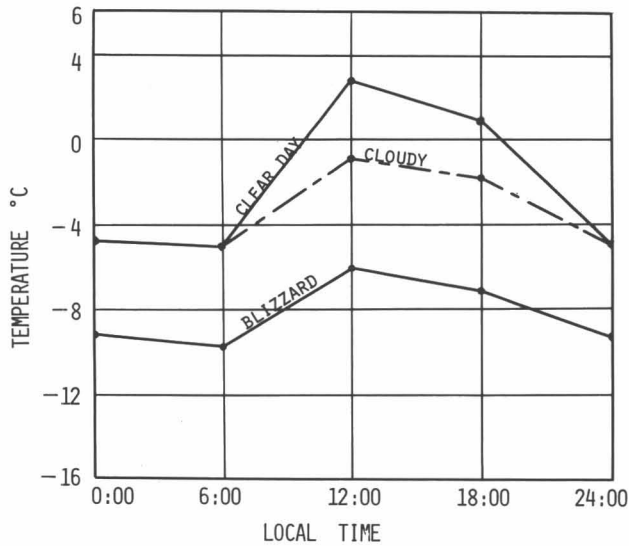


Fig. 17. Typical daily variation of surface temperature at Divide camp in the summer (after Marcus, Rens, and Taylor, 1966)

Waves refracted downward into the glacier were found to have large attenuation. Very useful relations were found between temperature and dielectric constant of a Subarctic glacier for temperatures between -15°C and 0°C . We found it possible to determine the value of reflection properties by calculations using measured values of density and temperature which are easier to obtain than direct measurements of reflection coefficients.

The results of this investigation have significance for research on radio communication in Subarctic glacier areas in the summer.

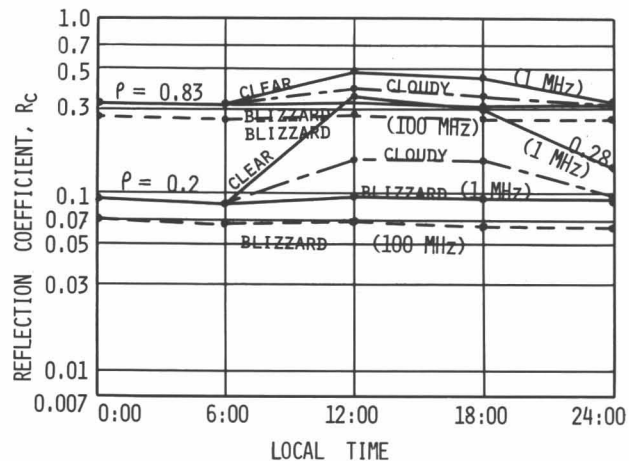


Fig. 18. Daily variation of the reflection coefficient at the surface of the glacier in summer.

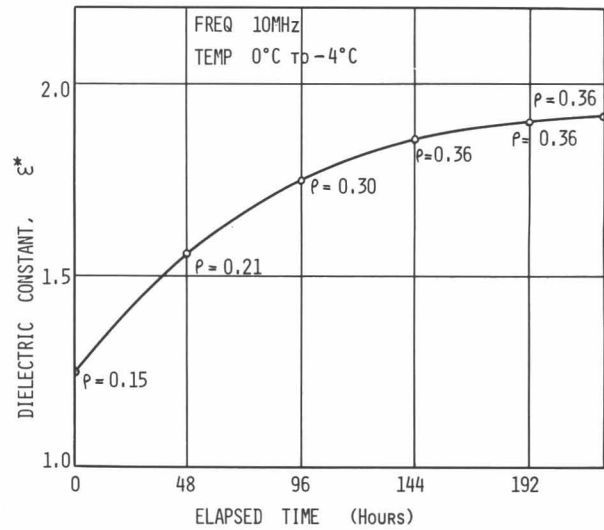


Fig. 19. Variation of dielectric constant of snow during period immediately after snowfall.

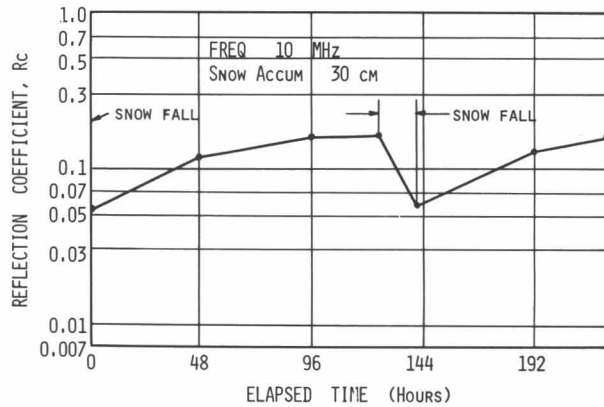


Fig. 20. Average variation of reflection coefficient during an interval between snowfalls.

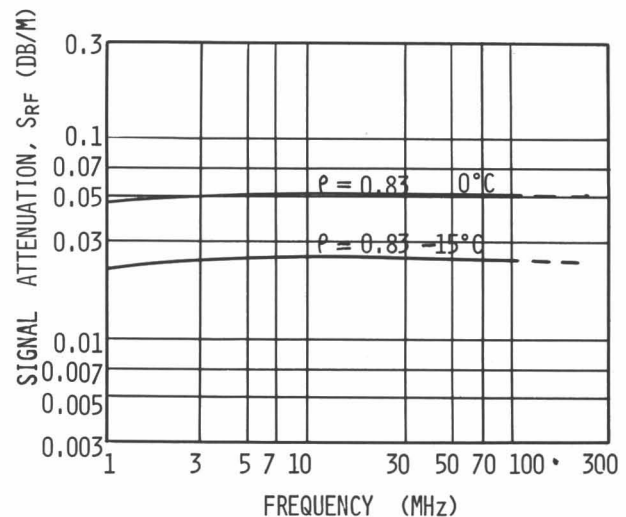


Fig. 21. Relationship of signal propagation loss to frequency of propagation.

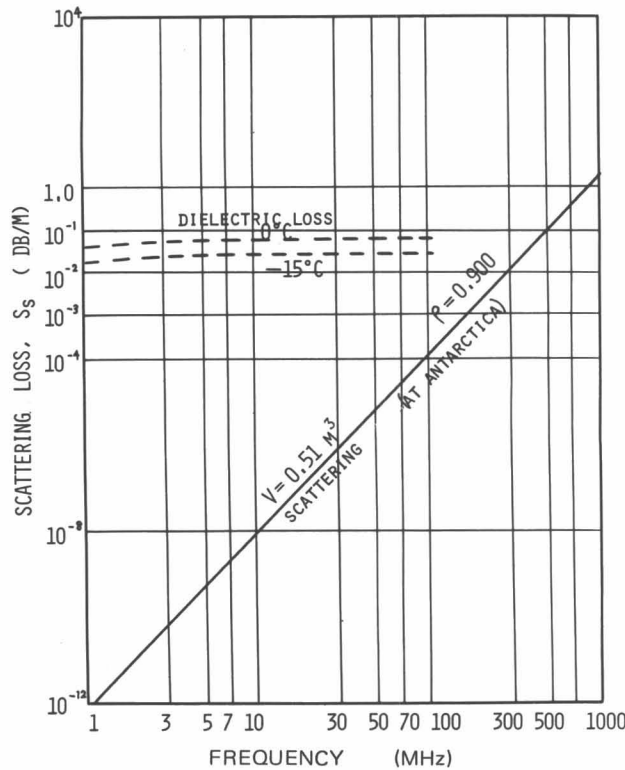


Fig. 22. Relationship of scattering loss to frequency of propagation.

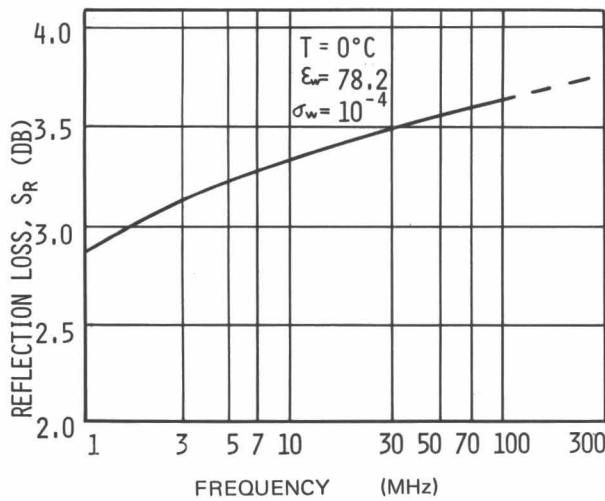


Fig. 23. Relationship of reflection loss to frequency of propagation for vertical waves reflected at an ice-water interface at the bottom of a glacier.

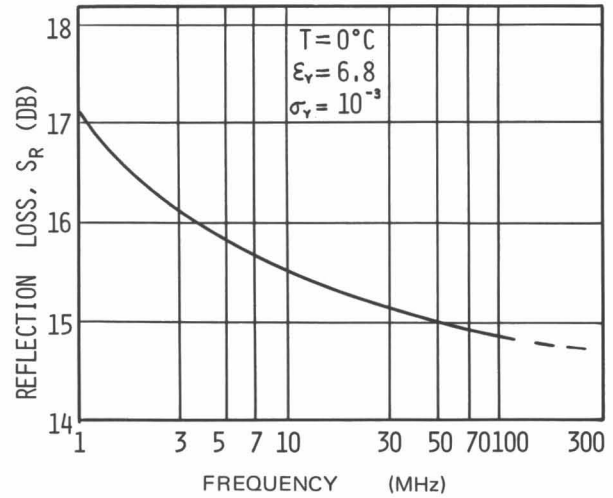


Fig. 24. Relationship of reflection loss to frequency of propagation for vertical waves reflected at an ice-rock interface at the bottom of a glacier.

Acknowledgments

The author is indebted to Richard Ragle, Melvin Marcus, and other members of the Arctic Institute of North America for many helpful suggestions and support, and to K. Yoshino for assistance in measurement.

References

Evans, S. (1965) Dielectric properties of ice and snow—A review, *J. Glaciol.*, 5, 773-792.
 *Holdsworth, G. (1965) An examination and analysis of the formation of transverse crevasses, Kaskawulsh Glacier, Yukon Territory, Canada, *Rept. No. 16*, Inst. Polar Studies, The Ohio State Univ., 91 pp.
 Marcus, M. G., Rens, F., and Taylor, B. E. (1966) Icefield Ranges climatology program, 1965 data presentation and programming analysis, *Res. Paper No. 33*, Arctic Inst. North Am., 111 pp.
 Waite, A. H. and Schmidt, S. J. (1962) Gross errors in height indication from pulsed radar altimeters operating over thick ice or snow. *Proc. IRE*, Vol. 50, 1515-1520.
 Wiener, O. 1910. Zur Theorie der Refraktion Konstanten. *Verhandl. der König. Sächsischen Ges. der Wiss.* 30 Leipzig, Mathematisch-Physikalische Klasse, Bd. 62, 256-268.
 Yoshino, T. 1967. The Reflection Properties of Radio Waves on the Ice Cap. *IEEE Transaction on Antenna and Propagation* AP-15, 542-551.

*A modified version of this report appeared in a previous volume of Icefield Ranges Research Project, Scientific Results.

Supraglacial Streams of the Kaskawulsh Glacier *

Karen J. Ewing †

ABSTRACT. Two general categories of supraglacial streams were identified during the summers of 1965 and 1966 on the Kaskawulsh Glacier: (1) annual streams having shallow channels, and (2) perennial streams having deeper channels which are reused from year to year. Perennial channels were found to have depths of one meter or more; they were generally parallel to the glacier flow, and were often regularly spaced across the glacier. The dynamic factors, climate and glacier movement, are particularly important to the formation of supraglacial streams, in addition to the static factors of relief, structure, and gradient. Daily maximums and minimums in stream discharge were found to lag behind daily maximum and minimum temperatures, as would be expected. This lag increased downstream. Glacier movement was found to bring about changes in stream gradient, the realigning of stream patterns, and the elongation of stream patterns. It was found that the static factors, ice type, presence of crevasses, type of relief, and the presence of surface debris all contributed to the nature and volume of the streams. It was learned that certain patterns are typical of annual streams while others are found more often in perennial streams.

STUDY AREA

During the summers of 1965 and 1966, the author studied supraglacial streams on the Kaskawulsh Glacier. A valley glacier, approximately 60 km long, located on the eastern side of the St. Elias Mountains, the Kaskawulsh has three major arms: the north, central, and South (Fig. 1). Studies were conducted from a research camp (elevation 1770 m) located on the large moraine formed by the confluence of the central and north arms of the glacier (Fig. 1). A preliminary two-week reconnaissance of streams over the entire glacier was accomplished in the summer of 1965. The main field study, lasting about two months, was carried out during 1966 on the central arm, adjacent to the research station.

One of the reasons this area was chosen was because it was known to develop surficial streams during the summer months. Surficial streams develop more fully on bare ice than over a snow or snow-ice base. In the vicinity of the study area, bare ice is exposed from about mid-July through mid-September each year. Although areas of the glacier at lower elevations and near the terminus are free of snow for a longer period, the confluence study area has the advantage of being within the zone where, during the summer field research season, the transition from spring snow to névé to bare ice can be observed, and

the streams can be studied through the several changes which take place from first appearance to final freeze-up.

A second reason for selecting the central arm of the Kaskawulsh Glacier for this study was because other attributes of the environment were the subject of associated studies. During the 1965–1966 field seasons a complete meteorological station was operated on the moraine and an eight-day hygrothermograph was maintained on a nearby knoll at 1828 m (Fig. 1). Temperature, humidity, wind, precipitation, and cloud cover were recorded and have been reported by Marcus, *et al.* (1966); Marcus (1965), and Taylor-Barge (1969). Ablation studies were made over both moraine and glacier ice. Oblique and vertical aerial photographs were taken in 1965 and 1966 respectively for mapping purposes, and were supplemented by theodolite and plane table surveys.

The Kaskawulsh Glacier is located in a Subarctic, continental-slope climatic zone (Taylor-Barge, 1969). At the Kaskawulsh camp, the average daily temperature for the field summer of 1966 was 41°F, with an average diurnal range of 13°F. Relative humidity averaged 76% during the field season. These figures correspond closely with the averages computed by Taylor-Barge (1969) for the summers of 1964 and 1965: average temperature, 38.2°F; diurnal temperature variation, 11.5°F; relative humidity, high 70's. The most notable feature of the Kaskawulsh summer weather is a surface katabatic wind which blows downglacier most of the time, and often complicates field work. The average speed of this wind is approximately 10 kn; winds reaching greater than 15 kn often occurred during mid-afternoon (Benjey, 1969).

The study area is relatively flat except for a local depression at the confluence of the north and central arms

*This report is a modified version of a report on pp. 121-167 of *Research Paper No. 57*, Arctic Institute of North America, 1970.

†Department of Geography, University of Michigan, Ann Arbor, at time of writing; present address, Department of Geography, University of British Columbia, Vancouver

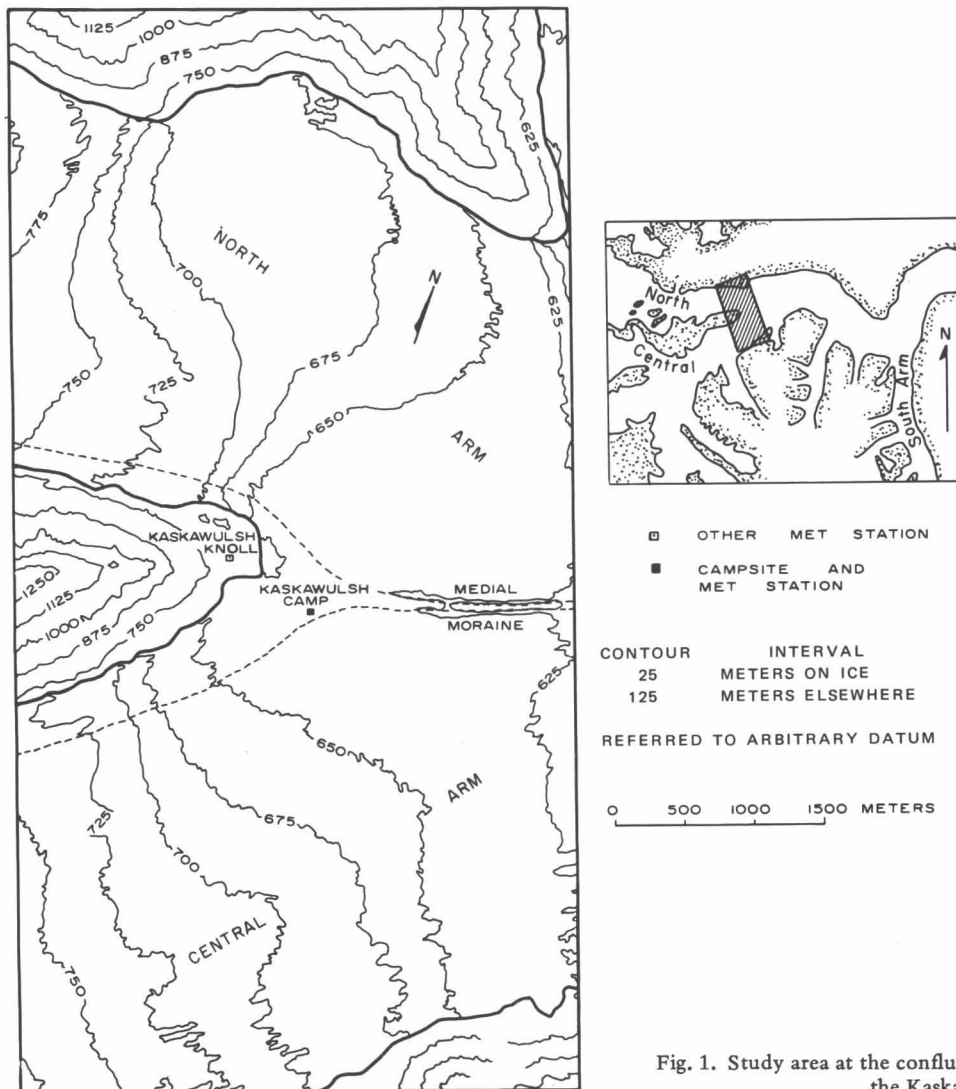


Fig. 1. Study area at the confluence of the north and central arms of the Kaskawulsh Glacier.

along the medial moraine. Ablation measurements for 1966—taken from 30 stakes placed laterally out from the moraine for 300 m—indicate that average ablation of 5.9 cm day^{-1} is generally uniform at all positions. Flow rate is greatest in the summer and a maximum of 152 m/yr has been observed (Anderton, 1967).

FACTORS WHICH INFLUENCE STREAM FORMATION

Introduction

A dense drainage net of supraglacial streams covers the Kaskawulsh Glacier. There are two major types of surficial meltwater channels on the glacier: (1) annual, which develop new channels each ablation season, and (2) peren-

nial, which occupy channels from previous years. Many supraglacial streams begin to develop before the snow has melted off the ice and as soon as enough free water has accumulated to begin flowing downslope. At first the water merely percolates through the snow, contributing to occasional slushflows as the snow base becomes saturated. As the snow melts, the streams become more clearly defined (Fig. 2). Because of the high ablation rate in the area, annual stream channels rarely attain a depth greater than 0.5 m, and, because they are so shallow, flooding often occurs during the summer and contributes to the relative instability of channel location. Remnant stream channels which have survived the winter are often clogged with snow and frozen slush; this may prevent renewal of flow in these channels in the spring. Consequently, annual streams are quite dependent upon local ice topography.

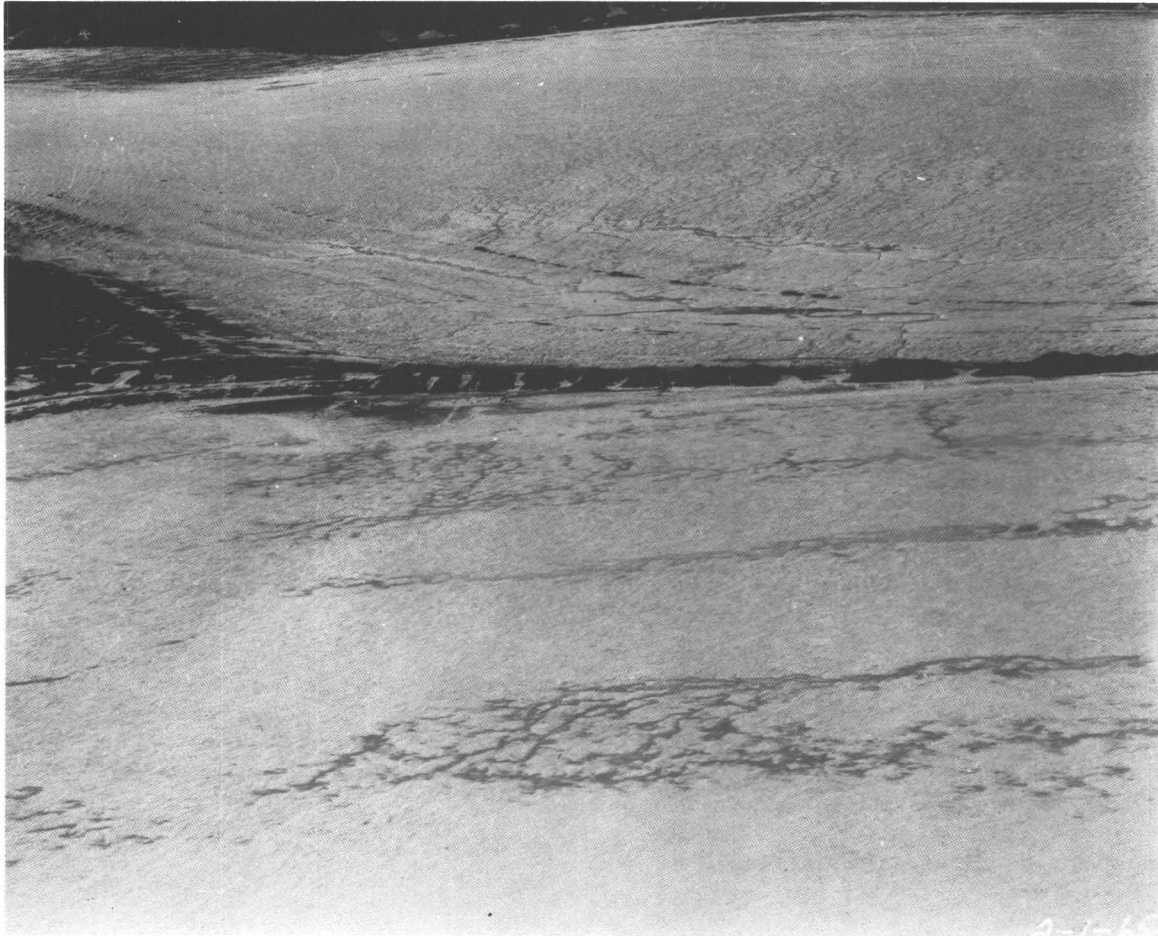


Fig. 2. Streams beginning to form in a snow base. The central arm of Kaskawulsh Glacier is in the lower half of the picture. Drainage is from left to right.

Perennial streams use the same channel from year to year. Due to larger discharge, these channels usually reach depths of one meter or more; this helps to preserve them throughout the year. Significant characteristics of these streams are that (1) a majority parallel the flow of the glacier ice, (2) they are often regularly spaced across the glacier, and (3) they often have elongated patterns. Since most of the early spring ablation is eventually discharged into perennial channels, these streams are the first to appear in the melt season. This creates an unusual stream pattern since there may be no definite tributaries. Some of these singular stream channels extend for several kilometers.

Supraglacial streams have much in common with streams flowing over land. Static factors that influence the development of both land and supraglacial streams are relief, structure, gradient, and biota. In addition, the dynamic factors, climate and glacier movement, are of particular importance to supraglacial streams.

Static Factors

Ice type. Blue and white ice foliation, common to most glaciers, consists of alternating layers of bubbly and bubble-free ice. Bubble-free ice usually appears bluish in color and the bands are often thinner than the corresponding white, bubbly ice. On the central arm of the Kaskawulsh Glacier, blue-white ice bands parallel the general direction of flow (Anderton, 1967, Fig. 21), although folding and truncation often occur. Other alignments of blue ice found in the study area are believed to be water-filled crevasses which have subsequently frozen (Anderton, 1967). The bands of blue ice vary in width from a few centimeters to almost a meter.

When exposed to air, white ice may break down into large, irregularly shaped crystals which cover the surface in depths up to several centimeters. Blue ice usually remains solid, ablating at the surface only. Even with these different weathering characteristics, however, the ice

surface usually maintains a smooth appearance. This situation changes where blue and white ice are subjected to water erosion; white ice has a much higher resistance to water erosion. Therefore, the channels of streams that flow at angles to the blue and white ice foliation usually develop ridges of white ice at the bottom.

Crevasses and moulins. Crevasses influence stream flow patterns; those which are shallow enough to become water-filled are often a cause of stream diversion. Where crevasses are numerous, pre-existing drainage patterns may be completely redeveloped. Patterns then are determined by crevasse type. Occasionally water-filled crevasses lead to subterranean passages, and moulins. Crevasses of this sort commonly appear within specific areas of the glacier and tend to extend across the entire width of the glacier. Sometimes the meltwater streams all terminate at approximately the same distance downglacier. Although such surface fractures may eventually close as the glacier moves downslope, new fractures frequently appear at the same location. Subterranean passages often remain open after crevasse reclosure due to moulin formation (Ewing, *et al.*, 1967). Renaud (1936) has observed that moulins also move downglacier even after their former streams have been diverted. This is true on the Kaskawulsh Glacier, but it is not known how long the inactive moulins last.

Relief and gradient. As can be seen from Figure 1, the longitudinal gradient of the north and central areas is slight. Gradient in the study area is generally less than 2° . Slope increases upglacier on both arms, but especially on the north arm. Relief in the study area is relatively small. The total surface relief does not exceed 3–4 m. This figure includes perennial stream channels, but does not include crevasses, since they are quite narrow in this area and depth is not easily determined. Sometimes flooding of annual streams occurs during high sun periods, causing excess water to overflow downslope and erode new channels. Perennial streams with higher banks than annual streams were never observed to flood.

Surface sediments. Silt and larger debris are scattered across the Kaskawulsh Glacier in varying amounts and thicknesses. Sediment larger than silt is found mostly within 10 m of moraines. The major portion of this larger debris is deposited by water action and/or slumping. Beyond 10 m from a moraine most deposits appear to be wind-blown. Seldom is any spot completely free of debris. Ice which may appear clean from a few meters distance is usually found to be permeated with small pinholes each containing minute amounts of silt or clay.

Very little sediment is found in the meltwater streams because of their high velocity. Some debris is captured in channels having white ice ridges, but more is concentrated in zones near moraines and in surface lake and deltaic areas on the glacier ice. When sediments accumulate sufficiently, ablation is markedly retarded. Creation of small cones, 10 cm or so in height, is typical as the surrounding ice surfaces ablate. As the sides of the mounds become steeper, slump occurs and the debris is washed into nearby

depressions. Eventually these depressions become filled with enough sediment to inhibit ablation and the cycle begins again.

The amount of debris covering the ice surface is influential in development of large-order stream channels. Although they were not measured, it was observed that most streams which were entrenched in the ice remain stable because stream erosion rates nearly equal ice-surface ablation rates.

Not all debris remains on the ice surface. Many areas are honeycombed with small cylindrical holes roughly 0.5–4 cm in diameter and between 5 and 15 cm in depth. Almost all are filled with water and while a few may have only a single pebble lying at the bottom, the majority contain a thick sludge up to several centimeters thick. These holes may remain as single cells or be interlocked with others through ablation processes. Small order streams developing in such regions have poorly defined channels; often the excess water merely flows along the surface from one hole to another. Even when partitions between holes have been melted away, flow is usually random.

Biota. It is not known whether the cylindrical holes on the Kaskawulsh Glacier contain biota as do the cryocoonite holes of the Thule area (Gerdel and Drouet, 1958). A reddish-brown organic stain observed near the moraine in the study area suggests that micro-flora exist there.

Dynamic Factors

The two dynamic factors influencing supraglacial stream development are glacier movement and climate. Climate is the more important because of its effects on annual and daily changes in the surface of the glacier. Stream development caused by glacier movement—although slower than variations caused by climate—are nonetheless significant.

Climate. Climatic processes work more rapidly on snow and ice than on land surfaces. Although not enough data were gathered to correlate climate and stream discharge, there is certainly some correlation between daily mean temperature and daily ablation (Fig. 3). Because little meltwater is stored as ground water (except in the snow above the firn line), a higher percentage is discharged from a glacier directly into streams than would be discharged from land. Therefore, a relationship can be inferred between temperature and stream discharge.

There is a time lag between the daily maximum and minimum temperatures and the daily maximum and minimum stream flow. The main flow usually comes around 14:00, a little after the maximum temperature of the day. There is a greater lag downstream with increasing stream complexity. During this time of day there is a thin veneer of water over the entire surface of the glacier. The headwater regions are usually characterized by pools of slush. Such regions may be the headwaters for several drainage

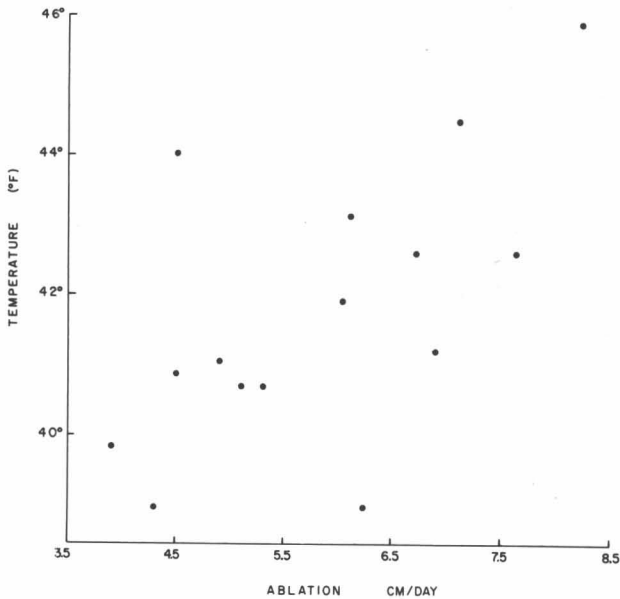


Fig. 3. Correlation of mean temperature and daily ablation on the central arm of the Kaskawulsh Glacier.

basins having streams flowing out in two or more directions. It is during the afternoon in these areas that a stream system may acquire additional branches. This happens when the melting becomes so intense that a set of small rills and rivulets is added. These minute systems do not have the clearly defined stream channels that higher orders have, and are easily diverted by the smallest protuberances. They show no remnant characteristics from day to day and become semipermanent only if ablation becomes heavy enough to allow for entrenchment. They may be classified as a type of intermittent stream.

Streams which are greatly reduced in volume cannot maintain their channel depth and eventually have their banks ablated. Occasionally a channel will carry no water except that ablated from its own banks. This usually happens when streams have been pirated or diverted. The lower reaches of the stream are then ablated to the point that the channel is maintained by its own volume of meltwater.

Movement. The three major observed effects of glacier movement on stream morphology are: (1) changes in stream gradient, (2) realignment of stream patterns by surficial cracks, and (3) elongation of stream patterns.

Undulations of the ice surface are usually due to an uneven valley floor, compression flow, or passage of kinematic waves. Glacier movement may cause changes in gradient either longitudinally or latitudinally. When change does occur, stream channels may be diverted downslope. Also, stream flow reversals are not uncommon. When reversal occurs, tributaries may enter at an upstream

angle until water erosion and ablation allow for more normal entry.

Fracture patterns develop in zones. Small, superficial crevasses are sometimes carried downglacier. If such crevasses are numerous, realignment of stream patterns often takes place. Although crevasses may reseal, others continue to form in some localities. Crevasses which open and close within a drainage basin can have several effects: one set of events is diagrammed in Figure 4. In the figure, A, B, and C are tributaries of the main stream D. When a crevasse divides the basin, A, B, and C form individual basins terminating in the crevasse. The lower reaches of A and B which were left downstream of the crevasse become the headwaters for D. After the crevasse reseals, A terminates in a moulin, C is rechanneled along the crevasse to B, and B is reunited with D.

At first consideration, it seems impossible that ice flow could cause elongated stream patterns. Brittle surface ice cannot be 'stretched' without severe fracturing. Because of the different rates of ice flow across the glacier, however, stream lengths can be distorted. As shown schematically in Figure 5, the headwaters of A and C are in a slower moving zone than is stream B. Gradually, the main branches A and C elongate to compensate for the faster moving zone of stream B. Stream B remains the same length. If this process does in fact occur, it would have a greater effect on annual than perennial streams. Annual streams develop on a snow base and form a dendritic pattern; this allows opportunities for a drainage basin to extend through zones of different flow rates. Since annual streams reform each year, the effects of distortion would not be pronounced.

Another possible explanation for the apparent elongation of stream patterns is illustrated in Figure 6. Figure 6 shows that an elongated stream pattern can develop if headwater areas remain stationary or retreat while lower reaches move downglacier. This is, of course, only a relative situation: all the ice is moving, but the headwater areas remain in snow or firn and usually migrate upglacier with the transient snow line. Perennial streams in the confluence area of the Kaskawulsh Glacier have their headwaters in the upper zones of the firn line. The melting

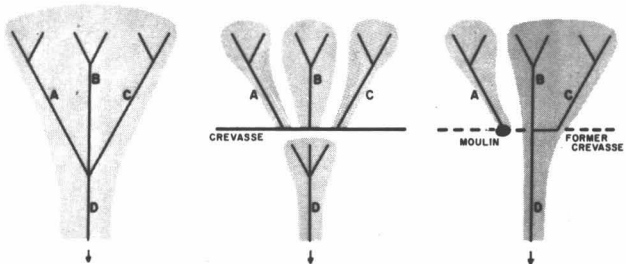


Fig. 4. Hypothetical model of a drainage basin pirated by a crevasse.

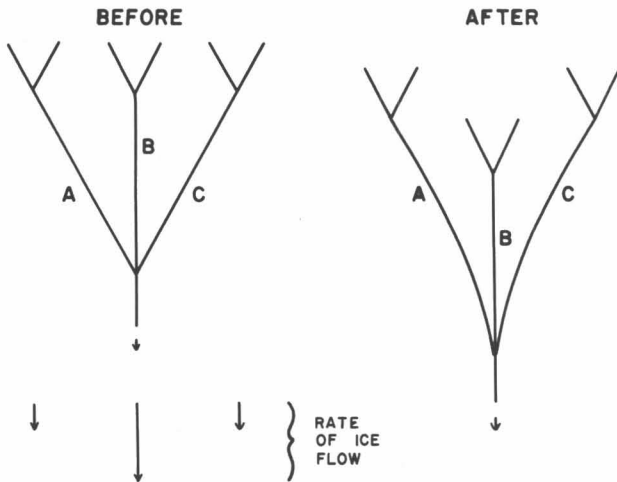


Fig. 5. First hypothetical model of stream elongation.

snows release large amounts of water in an almost continuous wash across the glacier. This water soon separates into distinct stream branches, some of which entrench deep enough to create perennial channels; enough water is released so that the perennial channels are extended downglacier with no lessening of their depth. Eventually, crevasses divide the streams into several smaller drainage areas. In most instances, however, enough annual streams become tributaries of the perennial channels to allow yearly continuation of the latter.

STREAM MORPHOLOGY

Planimetric Patterns

Supraglacial stream patterns on the Kaskawulsh Glacier are hard to analyze by conventional methods used for streams on land. The ablation of the entire surface creates a denser drainage net than is usually found. One count

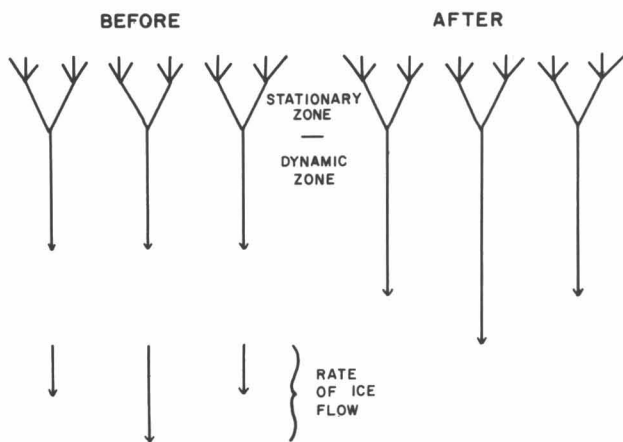


Fig. 6. Second hypothetical model of stream elongation.

showed that a perennial stream was of the tenth order. The low gradient often creates a deltaic or swamp effect in many places, with drainage basins poorly defined. The banding of blue-white ice and linear surface cracks tend to deflect water from one drainage basin to another. Both braiding and distributaries are common. Nevertheless, classical planimetric stream patterns can be identified and related to specific environmental elements.

Almost every type of stream pattern can be found on the Kaskawulsh Glacier. While other glaciers may have a predominance of one or two types (for example, the Jan Meighen with its radial pattern), the Kaskawulsh has a wide variety. This is probably due in part to its large size. Two rules were found to apply to most streams: (1) most annual streams empty into perennial streams, and (2) most perennial streams eventually terminate in moulins. Following is a brief summary of stream patterns and the conditions under which they exist.

Dendritic patterns are common in areas which are largely free from cracks and coarse blue-white ice foliation. Annual streams predominate in this pattern, especially when developing on a snow base early in summer.

A rectangular pattern is normally formed by annual streams in areas where fractures or coarse foliation are present. The blue ice, being more susceptible to water erosion, is usually a factor in alignment. Small fractures not reaching into subterranean depths are also a major cause for alignment. This pattern is common late in summer, after snows have melted (Fig. 7). A subform of this pattern is the angulate, found where streams flow across crevasses or foliation at acute angles.

A barbed pattern is present when either annual or perennial streams have had a reversal of flow due to a change in gradient. It may also be formed when an entering tributary is rerouted by blue-ice foliation.

A parallel pattern is usually found in perennial streams, especially at the start of the ablation season. In these instances, structure is not a primary factor. Small annual streams, however, sometimes develop along blue-ice foliation, creating a parallel pattern.

Many parallel perennial streams develop into trellis patterns late in the ablation season as annual streams become tributaries (Fig. 8).

A deranged effect occurs most frequently in icefalls, although an area of intense crevassing may yield the same results. Icefalls may also produce a "rice paddy" effect of small pools.

Braided streams occur in low-gradient areas of the glacier, frequently near moraines. The streams have high width-to-depth ratio and meandering channels; they do not carry large sediment loads, however, which is a common factor in the formation of braided streams on land (Leopold, *et al.*, 1964). Both perennial and annual streams may form braided patterns, but when perennial streams form such a pattern, they become more shallow.



Fig. 7. Rectangular stream pattern on the north arm of the Kaskawulsh Glacier near confluence with the South Arm. Area shown in photo is approximately 1.5 km wide and is clear of snow.

Distributaries are quite common over the entire glacier surface. They appear to be due mainly to structural factors (that is, ice foliation and stress phenomena), although low gradient is probably another factor. Both annual and perennial streams show distributary patterns, but annual streams apparently show them more often. (Fig. 9).

Disappearing streams occur mainly in perennial channels and present a rough analogue to certain karst features. The creation of moulins (sinkholes) will often create an underfit channel downstream. Upstream a blind valley may develop. Hanging valleys may occur when annual streams enter a perennial channel.

Almost all stream systems on the Kaskawulsh Glacier are complex. Since most annual streams drain into perennial ones, a complex dendritic-parallel, trellis-parallel, or rectangular-parallel pattern may develop. One predominant type, common to the entire glacier, consists of low-order annual streams which occupy areas between major tributaries—areas which, in nonglacial terrain, would absorb water through ground seepage. In these instances, distributaries and braids develop, which resemble a de-ranged effect.

Cross-Sectional Observations

Cross-sectional observations were made on several annual stream channels. Observations were taken on August 4, 5, and 6, 1965, at approximately 07:30, 14:30, and 19:30 local time. Figure 10 shows the cross sections of the largest stream studied. The slight undulations in the channel profile are caused by differential weathering of blue and white ice.

Water depths at 14:30 and 19:30 (Fig. 10) illustrate how discharge varies throughout the day; 14:30 represents the time of maximum flow and 07:30 the time of minimum flow. As expected, very little free water is found in the channels late at night and in the early morning. Figure 10 also reveals that channel shape and water depth for a given hour did not fluctuate widely over the three-day period.

The variations in stage resulted in an easily distinguishable high-water mark, especially on annual streams. As the meltwater rose higher in the afternoon it scoured the upper levels clean of any debris, leaving a pure white ice rim along the outer and uppermost levels of the streams. This white ice had a higher albedo than the surrounding



Fig. 8. Trellis pattern forming in snow early in the ablation season. Area shown is approximately 1.5 km wide.

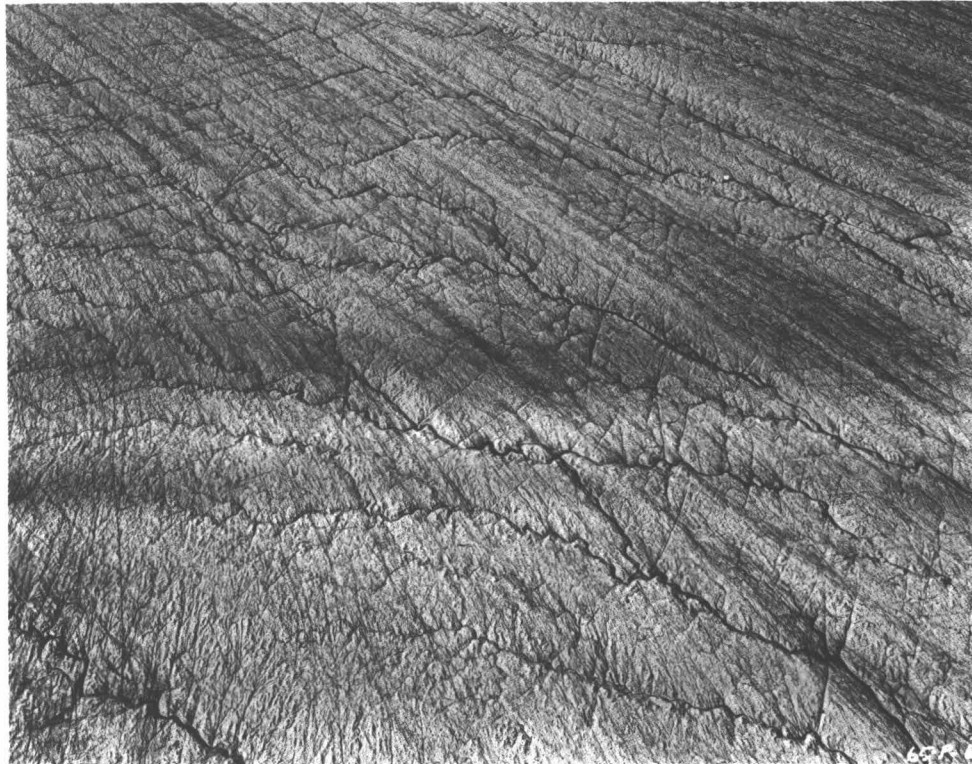


Fig. 9. Perennial and annual streams in a highly fractured area of the north arm of the Kaskawulsh. Major streams are between 0.5 and 1 m wide.

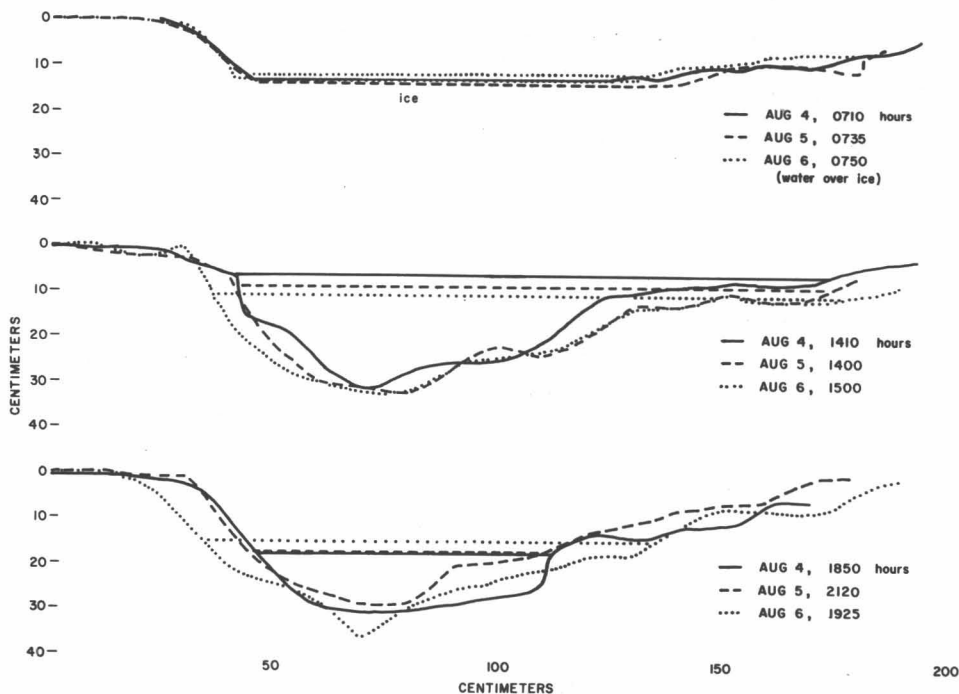


Fig. 10. Profiles of an annual stream over a 3-day period.

areas and consequently was ablated less. As the stream levels lowered, the entire basin was outlined by this white ice rim.

Each night a flat layer of ice formed across the stream channel, above the water level of the following morning. It was first assumed that this ice had formed sometime during the night, before the minimum flow had been reached. It was later observed, however, that the ice layer was also above the water level at 19:30 hours. The ice layer consisted of large interlocking crystals usually indicative of calm water. It is believed that this phenomenon was caused by ice damming farther downstream, allowing the ponded water to freeze over in the manner described. This flooding was never observed, but a dam consisting of ice crystals was found each morning some distance below the profile.

Of interest is the fact that as the amount of water in the stream increased during the morning, it often flowed in two layers: one in the channel and the other over the ice layer. This left a large layer of air between the two streams of water. Eventually, both the ice dam and the ice layer melted and the stream resumed normal flow.

CONCLUSIONS

There are two kinds of streams on the Kaskawulsh Glacier: annual and perennial. Annual streams form each year on a snow base and achieve a shallow entrenchment into the glacier ice by the end of the ablation season.

They have patterns similar to streams developing on land surfaces and, like them, are influenced by local topography. Perennial streams, with deeply entrenched channels, are more dependent upon glacier movement for their pattern characteristics than upon topographical factors. Most drainage networks are complex, consisting of both annual and perennial streams and frequently terminate in moulins. All supraglacial streams reflect the influence of temperature changes, even on a diurnal basis.

Although supraglacial streams are described in this paper in classical terminology, they are rather special cases. Further detailed studies of channel development, microclimatic influences, and energy exchange between ice and water are needed to prove just how distinctive they are.

Acknowledgments

This study was done through the support of the Arctic Institute of North America. Special thanks are due Philip Upton and Richard Ragle of the Icefield Ranges Research Project for their help with logistics. Dr. Walter Wood's contribution of photographic equipment and helicopter support was indispensable and is greatly appreciated. The field assistance of Ray Lougeay and Stuart Loomis helped make the study possible. My advisor, Melvin Marcus, is especially deserving of my thanks. Dr. Thomas Detwyler made many helpful comments on the final report.

References

- Anderton, P. W. (1967) Structural glaciology of a glacier confluence, Kaskawulsh Glacier, Yukon Territory, Canada, Ph.D. dissertation, Ohio State Univ., Columbus, 192 pp. (unpubl.).
- *Benjey, W. (1969) Climatological investigations in the Icefield Ranges, summer, 1965; Pt. 1, upper air wind patterns, *Res. Paper No. 54*, Arctic Inst. North Am., 50 pp.
- †Ewing, K., Loomis, S., and Lougeay, R. (1967) Waterspout on Kaskawulsh Glacier, Yukon Territory, *J. Glaciol.*, 6, 956–959.
- Gerdel, R. W., and Drouet, F. (1958) The cryoconite of the Thule area, *Res. Rept. 50*, U.S. Army Snow Ice Permafrost Res. Establ., 14 pp.
- Leopold, L., Wolman, G., and Miller, J. (1964) *Fluvial Processes in Geomorphology*, Freeman, London, 522 pp.
- Marcus, M. G. (1965) Icefield Ranges Climatology Program, St. Elias Mountains, 1964; Pt. 1, data presentation, *Res. Paper No. 31A*, Arctic Inst. North Am., 109 pp.
- Marcus, M. G., Rens, F., and Taylor, B. E. (1966) Icefield Ranges Climatology Program; 1965 data presentation and programing analysis, *Res. Paper No. 33*, Arctic Inst. North Am., 160 pp.
- Renaud, A. (1936) Les entonnoirs du Glacier de Gorner, *Mém. Soc. Helvét. Sci. Nat.*, Vol. 71, 27 pp.
- Taylor-Barge, B. (1969) The summer climate of the St. Elias Mountains region, *Res. Paper No. 53*, Arctic Inst. North Am., 265 pp.

*A modified version of this report appeared in a previous volume of Icefield Ranges Research Project, Scientific Results.

†This article was reprinted in a previous volume of Icefield Ranges Research Project, Scientific Results.

Patterns of Surface Temperature in the Alpine/Periglacial Environment as Determined by Radiometric Measurements

Ray Lougeay *

ABSTRACT. Observations were conducted in the St. Elias Mountains to determine some aspects of the applicability of thermal remote sensing in the alpine/periglacial environment. Techniques of obtaining ground observations were tested by which a researcher might determine the usefulness of infrared scanning to his study without the financial investment of airborne remote sensing on a trial and error basis. An attempt was also made to determine the effects of changing meteorologic conditions on both actual and radiometric temperatures of several terrain surfaces. These surfaces include various types of ice-cored moraine, glacial ice, and morainic outwash at the terminal margins of a large valley glacier. Also included were rubble and turf surfaces of a rock glacier, and talus and bedrock at the rock glacier margins.

It was found that temperatures obtained radiometrically were directly linked to insolation, which is in turn a function of cloud cover and atmospheric transmissivity. When comparing radiometric temperatures with the various components of the energy balance over an environmental surface, it was found that trends in radiometric temperature closely mirrored trends of net radiation at the surface, as expected. Relatively large variations in the trends of other energy budget components (latent-, soil-, and sensible-heat fluxes) seemed to affect radiometric temperature only slightly, however.

The techniques developed in this study appear useful in predicting the best time for thermal remote sensing overflight, and in indicating the intensity of ground observations needed at that time.

Introduction

Researchers in alpine and periglacial environments have often encountered the problem of relating observations from an intensively studied, small area to the more generalized, broad-scale picture. Many ground-based observations are necessarily limited to small areas, with great effort expended in the collection of relatively small amounts of data. This study was conducted to test the feasibility of using airborne, thermal infrared remote sensing as a guide in extrapolating large-scale thermal patterns from data collected at intensively studied small areas.

The major objective of this study was to observe the changing patterns of radiometric temperature under varying environmental conditions. A secondary objective was to devise and test a simple technique by which one might observe patterns of thermal infrared emissions from ground stations in order to predict the applicability of remote sensing before actually employing an airborne infrared radiometer over the area; and also to determine the best time of day, season, or set of meteorologic conditions for remote sensing. Previously, most remote sensing of the alpine/periglacial environment has been linked only tenuously with ground-based observations, and the full potential of remote sensing has not been realized.

Relationship between Surface Temperature and Infrared Radiation

The heart of a thermal infrared scanning system is the detector, any of several forms of transducer capable of giving off an electrical signal in response to incident radia-

tion of shorter wavelength. All substances with a temperature above absolute zero (-273°C) emit electromagnetic energy. The amount of energy emitted from a substance is dependent upon its surface temperature. Assuming the material is a perfect (that is, blackbody) radiator the amount of radiation emitted will vary directly with the surface temperature of the substance according to the Stefan-Boltzmann law: $M = \sigma T^4$, where M is the emitted radiation in ly min^{-1} ; σ is a constant $= 8.26 \times 10^{-11}$; and T is the surface temperature in degrees Kelvin. Terrain features are not perfect radiators and the amount of radiation emitted is always less than that calculated in this way. The ratio of the energy given off by a real object and the energy that would be given off by a blackbody at the same temperature is called the emissivity (ϵ) of the object; and the Stefan-Boltzmann law may be rewritten as $M = \epsilon \sigma T^4$. Thus, as surface temperature increases, the amount of radiant energy emitted from the substance increases.

The wavelength at which the maximum amount of energy will be emitted also varies as a function of the surface temperature of a substance. This relationship is expressed by Wien's displacement law: $\lambda_{\text{max}} = 2890 T^{-1}$, where λ_{max} is the wavelength of maximum intensity of emission, and T is the surface temperature in degrees Kelvin. Most substances at the earth's surface have temperature varying only a few tens of degrees from 300°K . The wavelength of maximum radiation is approximately $9.5 \mu\text{m}$, well within the infrared portion of the spectrum.

In this study, temperature data were collected with both surface thermometers and an infrared radiometer (Barnes PRT-10L) and used to monitor changing thermal patterns to determine the potential usefulness of thermal infrared remote sensing in the alpine/periglacial environment. Throughout the study the infrared radiometer was

*Department of Geography, State University College, Geneseo, New York

filtered for a spectral window of 6.9 to 20.0 μm so that only emitted infrared radiation would be monitored. The atmosphere is relatively transparent to infrared radiation from 8.0 to 14 μm , the center portion of this spectral window. Reflected sunlight was excluded, however, for almost all solar radiation incident on the earth falls between 0.3 and 3.5 μm in wavelength.

An infrared remote sensing device responds to varying amounts of electromagnetic energy in the infrared portion of the spectrum incident upon the detector and slight changes in surface temperature will cause different amounts of radiation to be emitted from various substances at the earth's surface. By understanding the factors controlling the variation in surface temperature one can understand the thermal patterns recorded by an infrared scanning system.

Infrared Remote Sensing in an Alpine/Periglacial Environment

Extreme temperature variations are characteristic of the alpine/periglacial environment and ice-cored features, such as permafrost, ice-cored moraines, and rock glaciers, are numerous. It was hypothesized that varying thermal emission patterns (both temporal and spatial) would be associated with specific features, many of which are only otherwise observable by intensive ground observations.

To date, infrared remote sensing has been used primarily for such things as detection of sea ice or vegetation types without a general overall environmental perspective, rather than as an interpretive tool of the total environment. Of the many remote sensing projects which have been conducted in Arctic and alpine environments, two are cited here as examples of the unexplored potentials of infrared scanning in the environment. Meier, *et al.* (1966), investigating the potentials of remote sensing of the glacial environment conclude that, since thermal-emission patterns detected by infrared imagery are directly related to the heat budget of the surface, "the thermal infrared scanner may be potentially the most useful tool for remote sensing of glaciers." Their statement is reinforced by Poulin and Harwood (1966), who cite a number of features of the Arctic environment which are observable only through infrared remote sensing: coastlines, hydrologic features, and subtle topography, all masked by snow cover.

Previously, little work had been done on the ground to gain an understanding of the factors which control surface temperature, which would in turn affect the resultant infrared radiation patterns. This study sought an understanding of these factors and also sought to develop ground techniques for determining (1) if infrared remote sensing might be useful for a given study; (2) the best time of day or season for the remote sensing; and (3) how intensive the ground observations must be at the time of a thermal infrared overflight.

Study Areas

For this study two major study areas were chosen within the St. Elias Mountains, the first at the terminal margins of the Donjek Glacier, and the second, a rock glacier on Sheep Mountain (see Plate 1¹ and Table 1). Observations made at these locations were supplemented by observations at the Steele Glacier as well as observations over a muskeg surface at the IRRP base camp at Kluane Lake, where facilities and instruments were available to conduct a microclimatic study to isolate the components of the energy balance. Observations were also made at the Athabasca Glacier, in the Canadian Rockies, in a setting quite similar to that of the Donjek area.

Terminal moraine of the Donjek Glacier. Studies were made from June 8-20, 1970, along a transect across four types of surfaces at the terminal margin of the Donjek Glacier (Figs. 1, 2, 3). The first surface consisted of poorly sorted morainic material which had been washed from the Donjek Glacier terminal moraine and deposited in an alluvial fan. This surface was comprised mostly of gravels, with a few low willow bushes and sparse *Dryas* mats. The second surface along the transect of the Donjek study area was that of a stable ice-cored moraine. The topography of this moraine was relatively rugged, with most slopes at or near the angle of repose. Relief of the distal side of the moraine was approximately 70 m. Detrital material formed an almost continuous mantle, 1-3 m thick, over a relatively clean ice core. Only a few ice faces were exposed where slumping had recently taken place. Numerous small ponds occupied depressions within the stable ice-cored moraine and a few streams cut across it. The morainic mantle consisted of a heterogeneous mixture of coarse to fine rocks with almost no vegetation growing upon it. The third surface was that of a veneer ablation moraine. Here a thin veneer of rock material, averaging less than 10 cm thick, covered the surface of active glacier ice. The topography was rugged with many clean ice faces exposed. The detrital material here was somewhat angular, having very few fines and thus minimal cohesion. There was no vegetation growing on the veneer moraine. The fourth type of surface along the Donjek transect was relatively clean glacier ice. This was well weathered—rough and granular—with rugged topography. Except for a small amount of silt and fine pebbles, the surface of the ice was fairly clean, differing only in exposure. On level surfaces there were often cryoconite holes. There were numerous ponds and rivulets upon the ice.

Sheep Mountain rock glacier. The second study area, occupied from June 26 to August 4, 1970, was a small glacier on the southern flanks of Sheep Mountain near Mile 1061 of the Alaska Highway (Figs. 4, 5). Five major types of surfaces were identified either upon or adjacent to the rock glacier (Fig. 6). Glacial rubble and glacial

¹Plate 1 is a map inside the back cover of this volume.

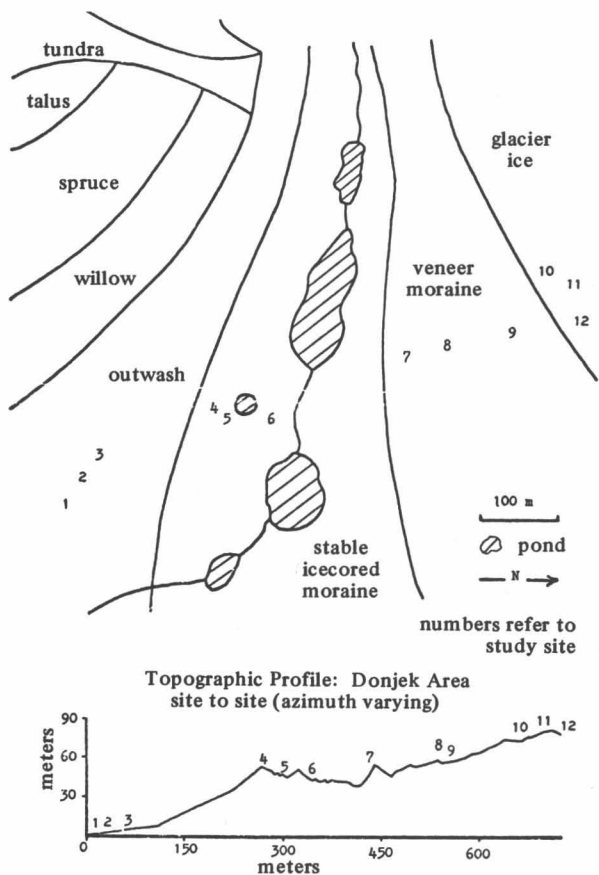


Fig. 1. Sketch map of the Donjek Glacier study area showing predominant surface types and locations of study sites. A topographic profile is also given.

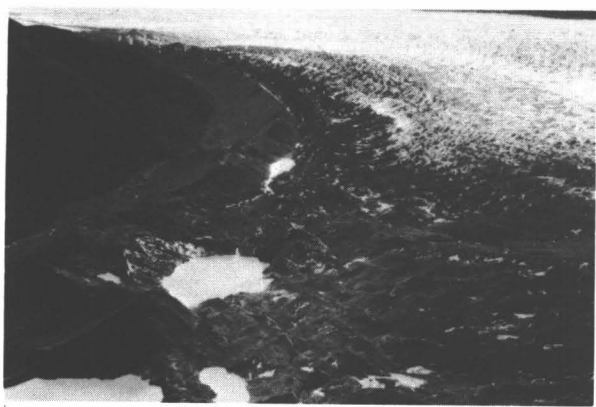


Fig. 2. Oblique aerial view of the Donjek Glacier study area showing morainic outwash (far left), stable icecored moraine, veneer moraine, and bare glacier ice surfaces.



Fig. 3. Contact between stable icecored moraine (left) and veneer moraine (right); west of the study transect in the Donjek Glacier study area.

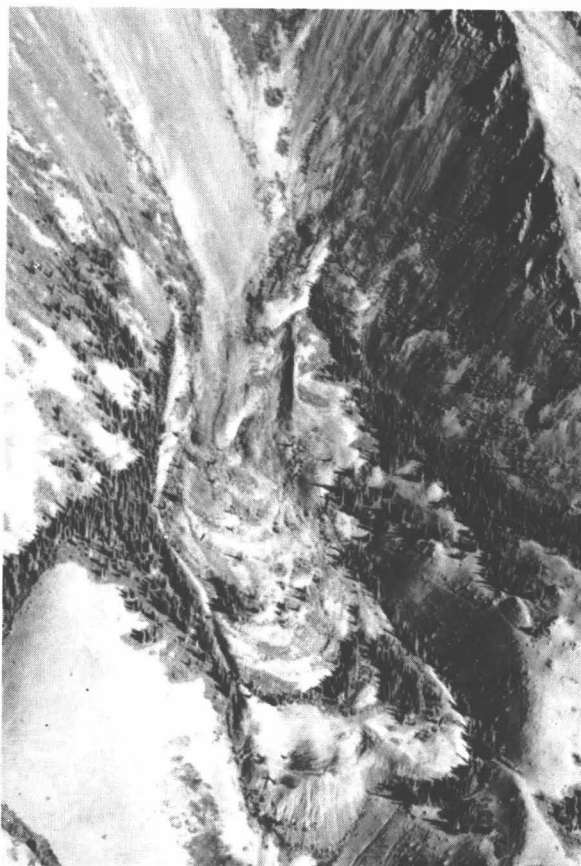


Fig. 4. Oblique aerial view of the Sheep Mountain rock glacier.

TABLE 1. Study Area Locations

Study area	Latitude (N)	Longitude (W)	Base elevation	
			ft	m
Donjek Glacier	61°09'	139°21'	3650	1110
Sheep Mountain rock glacier	61°01'	138°32'	3300	1010
Steele Glacier	61°15'	140°09'	5700	1740
Kluane muskeg	61°02'	138°24'	2620	1160
Athabasca Glacier	52°10'	117°10'	6800	2040

turf were most prevalent on the rock glacier with some talus at the terminal margins. Glacial rubble, predominant on the risers of the lobes of the rock glacier (presumably the most active portion of the glacier) was free of vegetation and contained very few fines. Glacial turf was prevalent on the more level, presumably less active, portions of the rock glacier where there was a relatively continuous mat of vegetation, especially lichens. Patches of brush and small stands of spruce were also found on the

glacier. Talus, the third kind of surface identified here, occupied slopes above the rock glacier. These talus slopes were generally at the angle of repose, providing the detrital input to the rock glacier. In addition, nonglacial turf and bedrock were identified as two additional surfaces adjacent to the rock glacier. Nonglacial turf comprised much of the lower slopes of Sheep Mountain.

Steele Glacier. Observations of the ice and the lateral moraines of the Steele Glacier were made on July 30, 1970. These observations were valuable in determining some degree of predictability in relating observations from



Fig. 5. Ground view, looking upglacier from Site 7 on Sheep Mountain rock glacier. Glacier turf is in the immediate foreground with bare rubble exposed just beyond the pyrheliograph (lower right). Upper portions of the rock glacier and talus slopes are visible in the background.

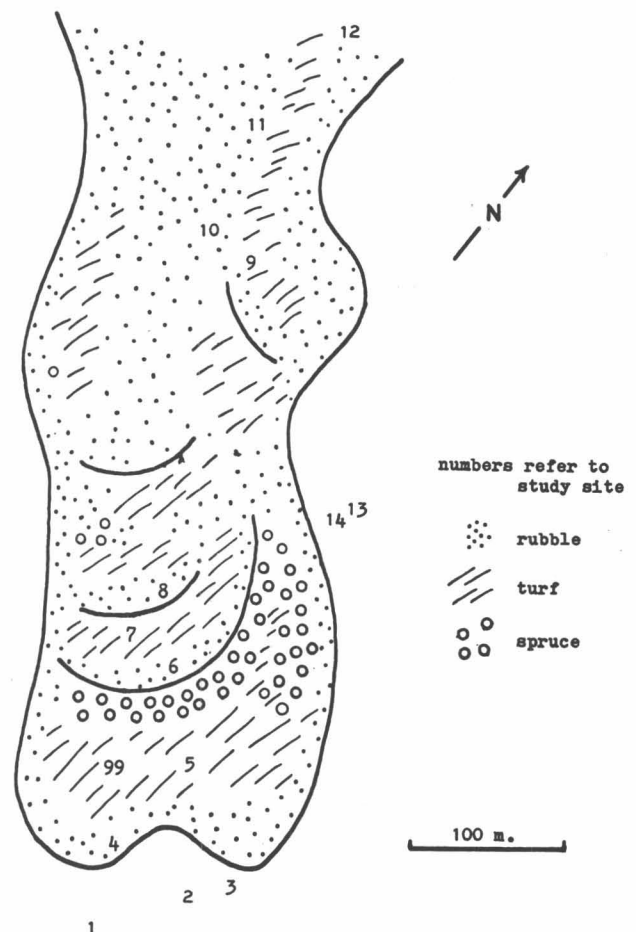


Fig. 6. Sketch map of the Sheep Mountain rock glacier and talus surface types and locations of study sites.

one area to another. Features of the Foster Glacier, a tributary of the Steele, were also observed at this time.

Kluane Lake muskeg. Proper instrumentation was available at the Kluane Lake base camp to monitor the energy budget and microclimate over a muskeg surface. It was possible to determine the total energy balance and to isolate its various components. Concurrent radiometric temperature measurements over various surfaces in the area (gravel, dirt, muskeg, water) proved quite valuable in understanding the relationship between radiometric temperature and surface-energy balance. These observations were conducted for a five-day period beginning August 5, 1970.

Athabasca Glacier. The Athabasca Glacier, in the Canadian Rockies, was visited on August 21 and 22, 1970, and observations were conducted during two cloudless nights. These observations were valuable, since the study sites in the Yukon during the Arctic summer offered no true nighttime conditions. The observations on this glacier provided data on trends of radiometric temperature and on thermal contrasts under conditions of extreme surface irradiation.

Methodology

In the two major study areas, periodic observations of radiometric temperature and related environmental parameters were made at all sites. These study sites formed a transect across all environmental surfaces within the study area. In addition, soil, rock, and vegetation samples were collected, where relevant, and elementary mapping was done to determine site location, local topography, and slope aspect. Sun elevations and azimuths were recorded throughout the high sun period on a few sample days in order to relate incident solar energy to slope aspect at each site. Albedo of each study site was determined by a home-made shortwave radiometer, consisting of a cadmium sulfide cell attached to a portable volt-ohm meter.

At each study site the sensor of a dial thermometer was placed at the ground surface, and another 15 cm below the surface. Since it was impossible to place a thermometer directly at the surface without having it exposed to direct solar radiation, the sensor was usually covered with about one millimeter of soil. At sites with coarse rubble the sensor was placed under a small stone. Originally, it was feared that there would be large discrepancies between the temperatures recorded in this manner and the actual temperatures of the ground surface. This fear later proved largely unfounded when thermometer temperatures were compared with readings made with a contact pyrometer. Also, the agreement between surface temperatures registered by dial thermometers and radiometric temperature measurements was fairly good. Where it was not possible to place a thermometer close to the surface the recorded temperatures were somewhat inaccurate and did affect the final data analysis.

Air temperatures were also observed, using dial thermometers. These thermometers were shielded from solar radiation by an aluminum foil cone attached to the thermometer's stem, and were mounted on a pole one meter

above the surface. Both a hygrothermograph and a pyrliograph were in operation continuously at each major study area. At the time of each observation, wind velocity was recorded with small Dwyer hand anemometers at 0.1 and 1.0 m above the surface. With each observation, records were made of cloud cover, precipitation, surface-moisture characteristics, and effects of topographic shadow upon the study site.

In addition to radiometric temperatures observed along the transect of each study area, observations were made to determine radiometric temperature from afar. These distant observations were accomplished by climbing above the study area and radiometrically observing the study site in such a way as to get a broad-scale view of each type of surface, and to determine thermal contrast in a manner much like that of the airborne scanning system. At the time of these distant observations, simultaneous data were collected at control locations in the study area. This provided a measure of the effectiveness of the Barnes PRT-10L radiometer for observation through a relatively long (0.5-1.0 km) air path.

Instrumentation

One of the objectives of the study was to develop a method of evaluating the applicability of infrared remote sensing by using simple and inexpensive instrumentation. With the exception of the pyrliograph and the infrared thermometer, all instruments and field equipment used are generally available to most field workers in the alpine/periglacial environment. The infrared thermometer and pyrliograph were used in this study to provide a base datum in gauging the reliability of data collected with simpler equipment.

The Barnes PRT-10L infrared thermometer, used to record radiometric temperatures, proved to be ideally suited to the purpose. It is actually a radiometer calibrated in degrees Celsius (accuracy: approximately $\pm 1^\circ\text{C}$). While it has the advantages of being relatively inexpensive, light in weight, compact, and easily transported and operated, it does not have the accuracy of more sophisticated and more expensive large infrared radiometers, nor does it have the capability of filtering to narrower spectral windows.

A contact pyrometer was used at times to determine surface temperature, but for the most part reliance was placed on the metallic dial thermometers. These thermometers had a range of -50° to 100°C and an accuracy of $\pm 1^\circ\text{C}$. They were chosen because they are durable, portable, and self-contained. The loss of one unit does not result in the loss of all data, as can be the case when depending on thermistors or thermocouples with an electronic bridge or potentiometer. It would have been possible to use even simple hardware-store mercury thermometers, but these break more easily than the Weston ones.

The majority of mapping done in conjunction with this study was done with a Brunton pocket transit and a 30-m tape, with supplementary data provided by a pocket altimeter. The accuracy obtained with these instruments was quite adequate for the purpose, as most infrared imagery contains considerable geometric distortion.

The pyrheliograph (provided by the Arctic Institute of North America) was clock driven, recording incoming solar energy in langley's per minute, within a spectral band of 0.36 to 2.0 μ m. The hygrothermograph (supplied by the University of Michigan) was mounted just above the ground surface, and the sensing elements were shielded from direct solar radiation by aluminum foil.

Over the total study period under fairly rigorous conditions of both shipment and field use, no instrumentation problems were experienced, except for a grazing moose mistaking one dial thermometer for a succulent flower.

Analysis

In order to determine the usefulness of thermal remote sensing to a given problem it is necessary to distinguish temporal and spatial patterns of thermal contrast within a study area. Because various ground surface materials tend to heat and cool at different rates, thermal contrasts between environmental surfaces may vary with the time of day and changing meteorologic conditions. These changing patterns of thermal contrast are quite important in planning airborne thermal remote sensing to insure detection of those features of interest to the study at hand. This knowledge can only be obtained by an analysis of ground-truth data observations.

Diurnal Trends of Infrared Emission

General discussion. All data for the study period were aggregated according to hour of observation. Graphed curves of the diurnal trend of infrared radiometric temperature (Fig. 7) tend to be rather rough since the data for any single hour may happen to coincide with meteorologic phenomena of predominantly one type. Even without filtering this noise out of the data, however, it is possible to determine relative diurnal trends of infrared temperature.

A theoretical simulation model which predicts surface temperature, when specific environmental parameters are given, has been developed by Samuel Outcalt of the University of Michigan. Diurnal trends of surface temperature on a cloudless day for dry gravels and ice-cored gravels, as predicted by this model, are presented in Figure 8. The two major discrepancies between the real and simulated results presented in Figure 7 and 8 are: (1) the magnitude of thermal contrast is quite different throughout the day; and (2) patterns of thermal contrast in high and low sun periods are reversed, with greater contrast occurring at night in the theoretical model. One could hypothesize, and it was empirically observed, that the maximum thermal contrast occurred during the high sun period. These discrepancies point out the problems of dealing solely with theoretical data and static meteorological conditions. Holter, *et al.* (1970, p. 409) have pointed out the need for the development of such predictive models in the field of

remote sensing. At present, however, the inaccuracy of assumptions which must be made and the difficulties in measuring some environmental conditions limit the applications of such theoretical models to field studies. Such models are highly useful, however, when linked with field observations.

Transect study site data. At the Donjek study area the general pattern of infrared temperatures held constant

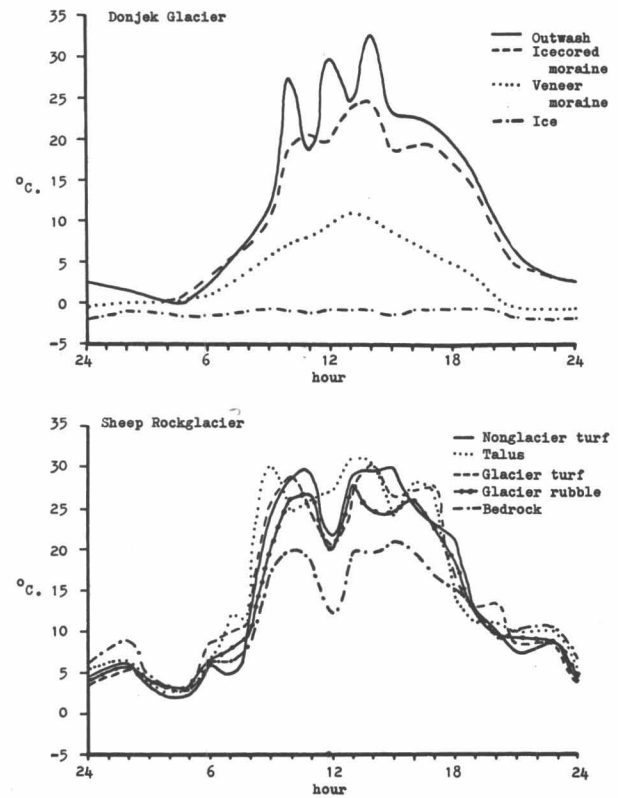


Fig. 7. Diurnal radiometric temperature trends at Donjek Glacier and Sheep Mountain rock glacier from ground observations (mean values of all observations).

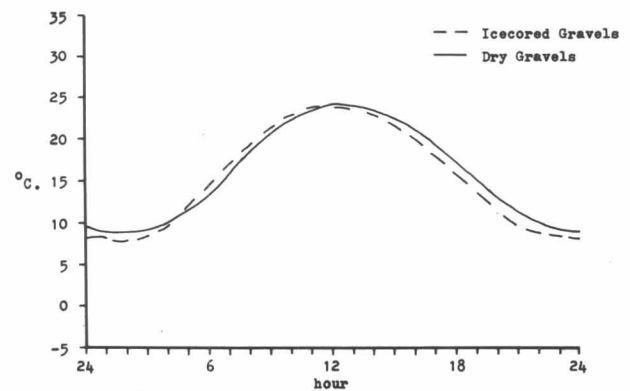


Fig. 8. Theoretical simulation of diurnal surface temperature trends on dry and ice-cored morainic material.

surface throughout the day (Fig. 7). Generally, outwash and icecored moraine appeared to have about the same temperature, with the moraine being only a degree or two cooler than the outwash. The veneer moraine remained considerably cooler than either the outwash or the ice-cored moraine, but was always warmer than the glacial ice. Glacial ice appeared to be at 0°C or a degree or two below.

The pattern of infrared radiometric temperatures for the Sheep Mountain rock glacier (Fig. 7) is not as easy to determine as that of the Donjek Glacier terminal moraine. The various environmental surfaces of the rock glacier heat and cool quite similarly. Thus, the relatively small radiometric temperature differences between environmental surfaces are masked by other environmental factors such as exposure, soil moisture, sun aspect, etc.

Figure 3 indicates that thermal infrared remote sensing might be quite useful in distinguishing two very different types of moraine and glacier ice, although there may be some difficulty in determining the boundary between ice-cored moraine and morainic outwash.

Distant infrared radiometer measurements. The diurnal trend of infrared radiometric temperature characteristics of both the Donjek Glacier and Sheep Mountain study sites was also observed from distant observation points (Figs. 9, 10). The advantage of distant radiometer readings is that one senses infrared emission from a large area, analogous to an airborne imaging system. It was observed that an increase in wind velocity could increase the observed radiometric temperature by 4°-8°C, and that clear air turbulence created a warming effect upon the radiometric temperatures. This method does, however, allow us to get relative radiometric temperature contrasts between the various environmental surfaces. These relative thermal contrasts would determine the spatial patterns depicted in thermal infrared imagery.

In the case of the Sheep Mountain rock glacier, the diurnal trend of infrared radiometric temperatures, as observed from a distant observation point, does exhibit a rank ordering of thermal contrast for the various environmental surfaces. The pattern is quite confused, however, and it would be difficult to predict any given pattern of infrared radiometric temperatures for a specific time of the day. Except in the case of bedrock, the diurnal thermal radiometric temperature graphs tend to cross too many times to give a rank ordering for any specific period of the day.

Data collected for the Donjek Glacier study area indicate, again, that infrared imagery would be useful in this location. There is significant thermal contrast between various environmental surfaces and the pattern of these radiometric temperatures tends to hold throughout the day.

The environmental surfaces observed at the Athabasca Glacier are quite analogous to those of the Donjek, and here we have diurnal radiometric temperature trends which continue throughout the day and night. Although the magnitude of radiometric temperature contrast is

most extreme at midday and minimal in the low sun period, the general pattern of thermal emissions from the various environmental surfaces remains the same throughout the 24-hour period.

It should be noted that the distant observations at both the Athabasca and Donjek study area were taken over continuous 24-hour periods. The distant observations of the Sheep Mountain rock glacier were obtained over a 6-week period. The diurnal graph for the Sheep Mountain site represents aggregate data from the entire period.

Statistical Manipulation of Data

Correlation and regression analysis. The total data field was filtered so that observations with missing data were disregarded, but no attempt was made to adjust the data for temporal lag. The high correlations of surface temperatures with infrared radiometric temperatures in Table 2 indicate the following: (1) infrared radiometric temperature is directly related to the surface temperature, as would be expected from the laws of radiation; and (2) surface temperature is indicative of the relative magnitude of infrared radiation emitted from a given surface. These correlation coefficients would have been even higher except for the limitations imposed by the use of dial thermometers; since it was difficult to put the sensor close to the surface without exposing it to direct solar radiation, surface temperatures were not recorded for bedrock, talus, and ice. Temperatures recorded with a contact pyrometer on these environmental surfaces, however, agree well with simultaneous infrared radiometric temperatures. The correlations of radiometric temperatures with incoming solar radiation (Table 2) are good considering the fact that no account was taken of lag effect in heating the ground surface by solar energy. Although incoming solar radiation is the primary source of heat energy to the ground surface, net radiation would be a better measure of energy available. Also, because it takes some time for the ground to heat or cool, one might expect a better correlation if an integration of the trend of solar radiation (or net radiation) over the previous hour were used instead of instantaneous readings. Nevertheless, the correlation indicates a rather strong dependency of infrared radiometric temperature upon insolation.

Incoming shortwave radiation is used here as a measure of atmospheric transmissivity (that is, cloud cover and density), but there is no intent to imply a direct cause and effect relationship between insolation and radiometric temperature. For this reason only simple correlation analysis has been used. The low correlation between incoming solar radiation and temperatures of glacier ice is due to the fact that ice cannot warm above 0°C no matter how much heat energy is incident at the surface.

The direct relationship between emitted infrared radiation and surface temperature, expressed by the Stefan-Boltzmann law, makes it possible to use regression analysis of infrared radiant temperature upon surface temperature

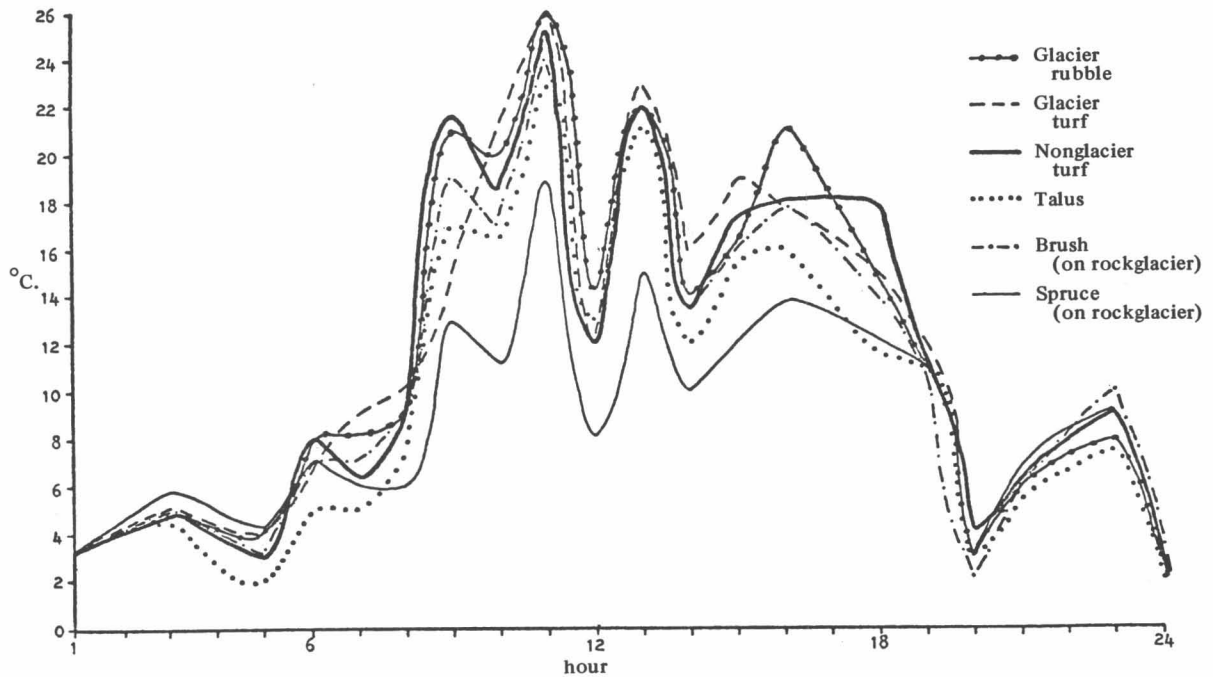


Fig. 9. Diurnal radiometric temperature trends at Sheep Mountain rock glacier from distant observations.

to determine the accuracy of the field measurements used here, in remotely determining radiometric temperature of various surfaces (Table 3). Since these results are statistically significant, one is able to discern confidence limits in the accuracy of the infrared thermometer by observing the standard error of estimate. In the case of veneer moraine, for instance, a knowledge of the surface temperature permits one to predict the radiometric temperature with an accuracy of 2.75°C. While this seems to

indicate a rather inaccurate method of field measurement, it must be noted that the major portion of these inaccuracies is not a fault of the radiometric temperature observations. The problem is one of accurately measuring the true surface temperature. The rather large difference

TABLE 2. Correlation of Infrared Radiometric Temperatures with Surface Temperature and Solar Radiation

Surface Type	Correlation Coefficients	
	Surface temperature	Instantaneous incoming solar radiation
Outwash	0.86	0.76
Ice-cored moraine	0.92	0.87
Veneer moraine	0.91	0.62
Glacial ice	(1)	0.44
Rock glacier turf	0.89	0.76
Rock glacier rubble	0.95	0.88
Nonglacial turf	0.91	0.81
Bedrock	(1)	0.73
Talus	(1)	0.83
All observations	0.65	0.66

(1) Thermometers could not be installed on these surfaces.

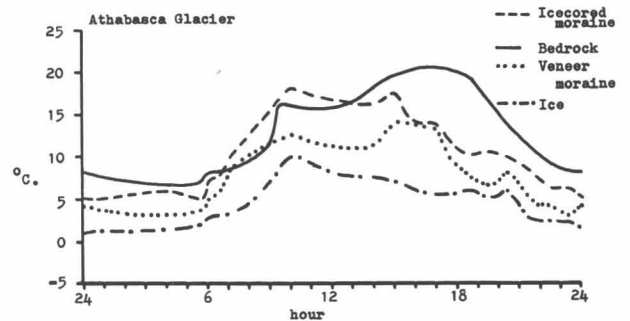
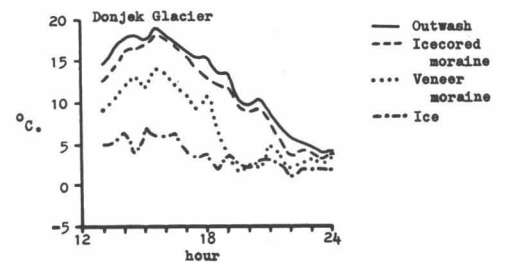


Fig. 10. Diurnal radiometric temperature trends at Donjek Glacier and Athabasca Glacier from distant observations.

TABLE 3. Regression Analysis of Infrared Radiometric Temperature and Surface Temperature

Surface type	Multiple correlation coefficient	Significance	Regression equation ($y = mx + c$)	Standard error of estimate °C
Outwash	0.86	0.94 (10^{-13})	$y = 1.38x + (-5.65)$	5.03
Ice-cored moraine	0.92	0.47 (10^{-17})	$y = 1.04x + 0.27$	3.37
Veneer moraine	0.91	0.25 (10^{-16})	$y = 1.27x + 0.35$	2.75
Glacial ice	—	—	—	—
Rock glacier turf	0.90	0.18 (10^{-27})	$y = 1.15x + (-1.16)$	4.84
Rock glacier rubble	0.95	0.60 (10^{-41})	$y = 1.22x + (-1.03)$	3.06
Nonglacial turf	0.91	0.41 (10^{-41})	$y = 1.18x + (-2.26)$	5.20
Bedrock	—	—	—	—
Talus	—	—	—	—
All observations	0.92	0.00	$y = 1.14x + (-1.00)$	4.43

between radiometric and surface temperatures in the moraine outwash area was due to the fact that it was almost impossible to accurately sample temperature of vegetation and soil simultaneously with the thermometers used. Better accuracy was obtained on the veneer moraine where it was possible to place the thermometer sensor quite close to a relatively homogeneous surface. Errors in monitoring surface temperature have resulted in rather large standard error of estimate in the regression analysis. It should be emphasized that since this study was primarily concerned with the thermal contrast between various environmental surfaces and not the absolute surface temperature, the methods used were adequate.

Relationships between surface readings and radiometrically determined temperatures in this study seem to hold constant with changing temperature magnitude. Radiometric temperature is more highly correlated with the temperature of the ground surface, and with incoming solar radiation, than with any of the other environmental parameters measured. Thus, the best indicator of infrared radiation emitted from the surface is surface temperature, whereas the radiant energy balance of the surface has the strongest effect upon changing the rate of infrared emission from the surface.

Emissivity. The use of an infrared thermometer, such as the Barnes PRT-10L, to remotely obtain surface temperatures assumes that the material of the surface in question radiates as a blackbody (that is, emissivity approaches unity). If the surface material does not radiate as a blackbody and the emissivity of this substance does not approach unity, the radiometric temperature will be

somewhat less than the absolute temperature of the surface. Emissivity is not important to the question of radiometric thermal contrast, even though it is important in obtaining the absolute temperature of these surfaces (Bliamptis, 1970).

An attempt was made to determine the relative emissivity of various environmental surfaces by looking at the difference between observed radiometric temperatures and the temperatures indicated by surface thermometers. It was hypothesized that a chi-square test would indicate if there were a significant level of consistent difference between radiometric and actual surface temperature. If there were such a consistent difference, it would indicate that the emissivity of those surfaces is not near unity. All environmental surfaces observed in this study had approximately equal emissivity values, approaching that of a blackbody radiator.

Although the Donjek Glacier ice had a melting surface and was known to be at 0°C , radiometric temperatures observed here were often cooler (-1.0°C) (Fig. 7). This lower apparent temperature can be explained by a glacial-ice emissivity value of 0.98, which is close to the value of emissivity often quoted in texts such as Geiger (1966) and Sellers (1965).

Campbell (1968) observed the cooling effect of a "cold skin evaporation layer" upon radiometric temperatures over a glacial fed lake. This phenomenon could perhaps be in operation here over a melting glacier surface. The cooling of radiometric temperatures over glacier ice, however, can be more easily explained in terms of emissivity. If one were to adjust the radiometric temperatures

observed over other environmental surfaces by their respective emissivity values it would be possible to adjust the regressions of radiometric temperature upon surface temperature (Table 4) closer to a one-to-one relationship. The c term in the regression equation $y = mx + c$ strongly reflects the effects of varying surface emissivities, where x is the surface temperature and y is the infrared radiometric temperature.

Slope and exposure. A major controlling factor in determining the amount of solar energy incident on a given site is the slope and exposure relative to the angle of direct-beam incoming solar radiation. The amount of energy incident upon a surface is a cosine function relative to the angle of slope, angle of incident radiation, and azimuth of exposure.

A theoretical simulation model developed by Outcalt (1971) provides for the separation of direct and diffuse solar radiation, the calculation of the various components of the energy balance, and yields a theoretical surface temperature. Table 5 gives surface temperatures for various slopes and exposures on the Donjek Glacier ice-cored moraine, as predicted by this simulation model. It can be seen from this table that the radiometric temperatures from different sites within one environmental surface type may be quite different due to variations of slope and exposure.

On the Donjek Glacier moraine, study sites were chosen with a variety of slope and exposure characteristics; there was still a sufficient degree of thermal contrast between environmental surface types (for example, ice-cored moraine and veneer moraine) so that variations within a particular surface type did not mask the thermal contrast between different surface types. This was not the case at the Sheep Mountain rock glacier study area, however, where the thermal contrast due to slope exposure within a given environmental surface was greater than the thermal contrast between surface types. It was found that the various surface materials studied at Sheep Mountain rock glacier tended to heat and cool at quite similar rates.

Effect of Meteorologic Conditions upon Infrared Emission

An attempt was made to understand the effect of meteorologic conditions upon infrared radiometric temperatures observed over various environmental surfaces. Daytime data (10:00-16:00) were divided according to four different weather conditions: clear, partly cloudy, light overcast, and dense overcast where precipitation had occurred within the past three hours. The data given in Table 6 indicate an obvious relationship between cloud cover and apparent radiometric temperature.

Precipitation also affects the temperature of the surface. In the data presented here, precipitation always had a cooling effect. It is significant to note, however, that although meteorologic conditions do change the general magnitude of infrared radiometric temperatures, the relative thermal contrast between surface types remains the same in most cases.

During periods of strong wind the windward side of a promontory may appear to be somewhat cooler, and wind influences radiometric temperatures recorded from a distance. Wind velocities were recorded at 0.1 and 1 m heights above the surface. The data have proven inconclusive when seeking a correlation between radiometric temperatures and wind velocity, however. Air temperature has little effect upon infrared radiometric temperatures, except as those processes of the overall energy budget of the environmental surface which control the emitted infrared radiation also control the heating of the atmosphere above the surface.

Relationship of infrared emission to surface energy balance. Radiometric temperatures were observed over four sites (Fig. 11) near the Kluane Lake micrometeorologic station in an attempt to determine the general trends of infrared thermal radiation as related to the various components of the energy balance (Sellers, 1965; Lougeay, 1969). Although four environmental surfaces were observed (muskeg, dirt, water, and gravel), the total energy balance was computed only for the muskeg site. Figure 12 indicates the general trends of the components of the energy balance as associated with the diurnal trends of infrared radiometric temperatures.

Meteorologic conditions during the time of these microclimatic observations were generally partly cloudy to overcast. A light rain fell during a 5-hour period between 03:00 and 08:00 on August 8. The trend of the various energy balance components, depicted in Figure 12, shows a sharp drop in the sensible heat flux and a concurrent rise in the latent heat flux just after this period of rainfall. At this time much of the available energy was used to evaporate water from the moist ground surface. Subsequently, about 16:00 on August 8, under relatively clear skies, there was a sharp increase in the amount of energy used in the heating of air by the sensible heat flux as the surface became drier.

Condensation occurred during each of the three nights of these observations, as evidenced by the early morning negative values of latent heat flux. The early morning of August 9 shows the most extreme example of condensation and negative latent heat flux values (Fig. 12). At this time there was greater surface cooling than on the previous two nights. This is due to reduced atmospheric back-radiation (that is, greenhouse effect) associated with a high cirrus overcast on August 9 and relatively dense stratus and altostratus overcast on August 6 and 8.

It can be seen that infrared radiometric temperatures most closely follow the diurnal trend of net radiation, while sensible and latent heat fluxes can change drastically without affecting the radiometric temperature. The soil heat flux, which is most closely related to surface temperature, is only a small percentage of the total energy balance. Therefore, the soil heat flux does not seem to follow any specific trends. In cases where condensation has caused soil heating and changes in the soil heat flux curve, there was little effect in the trend of infrared radiometric temperature.

TABLE 4. Effect of Emissivity upon Radiometric Temperature (Calculated Example)

Blackbody infrared radiance of a surface at 0°C. (emissivity = 1.0)

$$\sigma 273^\circ \text{K}^4 = 0.459 \text{ ly min}^{-1}$$

$$\text{where } \sigma = 8.26 \times 10^{-11}$$

Blackbody infrared radiance of a surface at -1°C. (emissivity = 1.0)

$$\sigma 272^\circ \text{K}^4 = 0.452 \text{ ly min}^{-1}$$

Infrared radiation from surface at -1°C is 98.5% of that at 0°C

$$0.452 \div 0.459 \times 100 = 98.5\%$$

Infrared radiance of a surface at 0°C with an emissivity value of 0.985

$$0.985 \times \sigma 273^\circ \text{K}^4 = 0.452 \text{ ly min}^{-1}$$

Use of Ground Observations in Conjunction with Thermal Remote Sensing

Ground-truth observations, such as those obtained in this study, are useful to the researcher in determining the usefulness of thermal remote sensing to his study. If thermal remote sensing does prove potentially applicable, ground observations are especially useful in flight planning and in image interpretation. Since remote sensing overflights are quite expensive compared to ground observations, it is important to determine the best time of day and/or season to fly in order to obtain imagery suitable for the specific problem at hand. Also, for a given problem imagery may have to be obtained under certain meteorologic conditions which produce proper thermal contrasts. In some cases direct sunlight and clear skies may be needed to produce high thermal contrast, while for

other purposes one may wish to reduce the effects of slope exposure and extreme thermal contrast by flying under an overcast.

Image contrast. Image contrasts on thermal infrared imagery are recorded only when the amount of infrared radiation emitted from the subject differs from that of its background. This thermal contrast may result from differences in surface temperatures or differing emissivities of target surfaces. One purpose of obtaining infrared ground-truth measurements is to monitor emittance patterns so that there is some assurance that the subject will be detected on airborne imagery. Ground-truth data collected in this study show strong thermal contrast between different types of glacial moraines, but insignificant contrast between surface materials on the rock glacier.

Although it was not possible to obtain airborne imagery of the various surfaces observed in this study, distant radiometric observations, which are quite analogous to instantaneous data obtainable from the air, provided considerable insight into the problems of obtaining and interpreting infrared imagery.

Glacial moraines. The glacial moraines of the Donjek and Athabasca Glaciers exhibit good radiometric thermal

TABLE 5. Simulated Diurnal Trends of Surface Temperature for Ice-cored Moraine Sites, as a Function of Exposure (June 21, Slope 16°)

Time	Exposure				
	level C°	N C°	E C°	S C°	W C°
2400	5.2	5.1	5.0	5.2	5.3
200	4.8	4.7	4.7	4.9	4.9
400	6.0	6.5	6.6	5.7	5.7
600	9.8	10.2	12.2	8.9	6.9
800	14.5	13.6	17.3	14.7	10.9
1000	18.4	16.0	20.1	19.8	15.6
1200	20.3	17.2	20.3	22.2	19.2
1400	19.8	17.0	17.9	21.5	20.6
1600	17.1	15.5	13.9	17.9	19.4
1800	12.9	12.7	9.6	12.5	15.5
2000	8.7	9.1	7.4	8.2	10.0
2200	6.1	5.9	5.7	6.1	6.3
2400	5.2	5.1	5.0	5.2	5.3

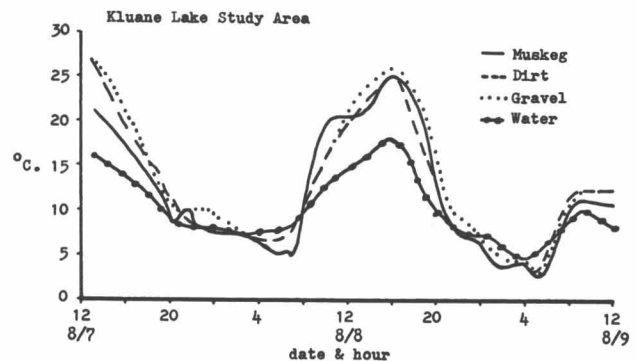


Fig. 11. Radiometric temperature trends of four surfaces at Kluane Lake study area.

TABLE 6. Radiometric Temperatures and Meteorologic Conditions; Values in °C Averaged from Daytime (10:00-16:00) Observations

Environmental Surface	Clear 0-4/10 cloud cover	Partly cloudy 5/10-8/10 cloud cover	Light overcast 9/10-10/10 cloud cover	Dense overcast 10/10 cloud cover with rain or snow in past 3 hours.
Donjek Glacier				
Outwash	25.0	21.0	27.5	11.7
Ice-cored moraine	21.0	23.0	19.0	12.6
Veneer moraine	8.7	10.0	—	5.0
White ice	-1.2	-1.2	—	-1.0
Sheep Mountain Rock Glacier				
Nonglacial turf	33.3	31.0	23.0	17.5
Glacial turf	31.0	28.0	23.5	18.5
Glacial rubble	29.0	28.0	22.0	17.0
Scree	29.0	32.0	26.0	17.0
Bedrock	23.0	22.0	18.5	13.5

contrast during midday, but they are spectrally indistinguishable on either color or black and white aerial photographs. Thus, infrared imagery from the air would be a relatively simple means of distinguishing between the various types of glacial moraines. Areas of currently active glaciation, with thinner detrital mantle and more extreme topographic textures (Loomis, 1970), could also be identified.

A specific example of how ground-truth data can help in the planning of airborne thermal remote sensing can be seen by comparing the data of the Donjek and Athabasca Glaciers depicted in Figure 10. The thermal contrasts between environmental surfaces of the Donjek Glacier behave much as would be expected, with the maximum contrast occurring at midday. Ground-truth data at the

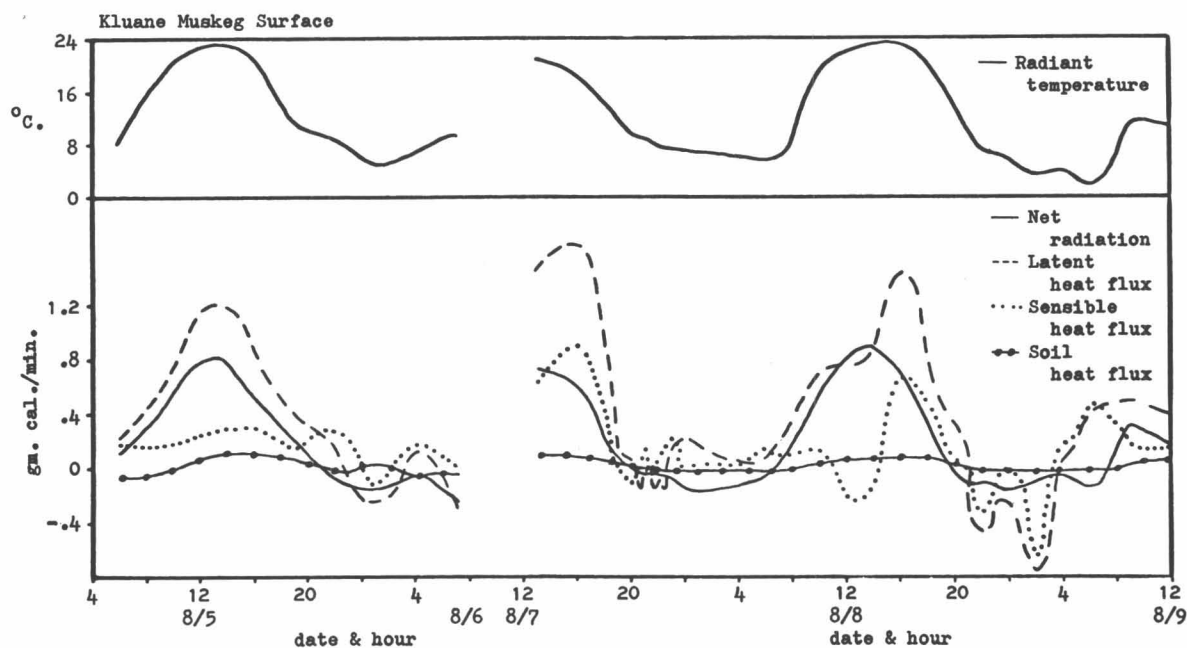


Fig. 12. Radiometric temperature of muskeg at Kluane Lake study area graphed with components of the energy balance.

Athabasca Glacier show that thermal patterns are not as predictable and useful imagery cannot be obtained as easily at this location. The various slopes and exposures of the surfaces at Athabasca show differing rates of heating and cooling throughout the day. Material such as bedrock, which is relatively cool in mid-morning, becomes the warmest surface in the afternoon and evening. Without ground truth one might assume that noon would be a good time to obtain thermal imagery. In this study area, however, the veneer moraine and bedrock surfaces have approximately equal radiometric temperatures at noon and therefore would be indistinguishable on airborne imagery obtained at this time. Ground-truth data collected at the Athabasca Glacier show that the best time to obtain airborne infrared imagery here would be in the late afternoon when the relatively erratic patterns of thermal contrast tend to stabilize.

Rock glaciers. On the Sheep Mountain rock glacier, all environmental surfaces, whether turf, rubble, or talus, tended to heat and cool at much the same rate and therefore did not exhibit strong thermal contrast patterns (Fig. 9). It is not likely that positive results could be obtained from infrared imagery of the Sheep Mountain rock glacier. It is not implied, however, that thermal remote sensing would not be useful in the identification and study of rock glacier phenomena. The Sheep Mountain rock glacier was characterized by relatively fine detrital material, the largest not usually exceeding 25 cm in diameter. The detrital material of many rock glaciers, however, is several meters in diameter. These large boulders would produce a surface topography of much greater relief than that of the Sheep Mountain rock glacier. The view of an airborne infrared system flown at midday under clear skies would encompass both the heated sunny side and the cool shaded side of the boulders. It is thus possible that rock glaciers might appear on thermal imagery as a somewhat cooler lobe on the side of a mountain where bedrock and talus surfaces would be uniformly warm.

Requirements for ground observations. The nature of the ground data needed for a given study is dependent upon the objectives of the study and the surfaces to be studied. In general, the lesser the thermal contrast between target surfaces the greater the need for more extensive ground observations. If one has a knowledge of the emissivities of the surface materials he is working with, or the thermal contrasts are sufficient to mask the effects of emissivity differences, he can then rely on ground-truth measurements of surface temperature to indicate thermal contrast which would be depicted on infrared imagery. In this case surface temperature probes, a contact pyrometer, or simple thermometers could yield valuable ground-truth data at a minimum of expense. Surface temperature data plotted on a diurnal curve would help to determine the time of day when thermal contrasts would be such that airborne imagery could detect the surface phenomena of interest.

The question of emissivity and the problems of accurately measuring thermal contrast can be eliminated by

the use of an infrared radiometer such as the Barnes PRT-10L. The radiometer responds to infrared radiation emitted from the ground surface in the same way as the airborne infrared detector. The radiometer integrates all surface temperatures within its field of view. This is important when one deals with a varied surface such as vegetation over exposed soil, or coarse gravel where there are both sunlit and shady patches. On surfaces such as these, temperatures will vary markedly and it is difficult to aggregate contact temperature measurements. The radiometer, however, does this automatically.

Summary

The field methods employed in this study have proven to be effective in determining thermal contrasts between various environmental surfaces. No instrumentation problems were encountered and accurate measurements of infrared radiant emission patterns in the alpine/periglacial environment were obtained by simple methods. It is safe to say that a researcher can easily obtain thermal contrasts over broad-scale areas by using a relatively inexpensive infrared thermometer such as the Barnes PRT-10L. This would allow accurate prediction of the applicability of thermal infrared remote sensing to the problem at hand. Also, with this method one can accurately determine the best time of day or season for identification of those features of concern.

It is also shown that, if surface emissivity differences are small, thermal contrasts between various environmental surfaces may be assessed by using simple contact thermometers without an infrared radiometer. By placing a few thermometers on each of various environmental surfaces and observing the relative values of surface temperature, one may predict whether the thermal contrast between environmental surfaces will produce significant image contrast on infrared imagery. In this manner it is possible to determine whether the variations in radiant temperature upon a single surface are of sufficient magnitude to mask the thermal contrast between that environmental surface and others adjacent to it.

Acknowledgments

Field work for this study was completed during the summer of 1970 with support from the Army Research Office—Durham and the Arctic Institute of North America.

I wish to acknowledge Dr. Melvin G. Marcus, Dr. Thomas R. Detwyler, Dr. George Kish, and Dr. Charles E. Olson, all of the University of Michigan, for their help in the preparation of this manuscript in its original and unbridged form. Also instrumental in the completion of this study were Tim Brockdorf, and Cheryl Lougeay, who worked as field assistants.

Observations of features on the Steele and Foster Glaciers were made logistically possible by Dr. Walter Wood of the Icefield Ranges Research Project. William Benjey of the University of Michigan loaned his instrumentation for microclimatic observations at the Kluane Lake base camp.

References

- Bliamptis, E. E. (1970) Nomogram relating true and apparent radiometric temperatures of graybodies in the presence of an atmosphere, *Remote Sens. Envir.*, 1, 93-94.
- Campbell, W. J. (1968) Synoptic temperature measurements of a glacier lake and its environment, *Publ. No. 79*, Intern. Comm. Snow Ice, Intern. Assoc. Sci. Hydrol., Bern, pp. 450-458.
- Geiger, R. (1966) *The Climate Near the Ground*, Harvard Univ. Press, Cambridge, Mass., 611 pp.
- Holter, M. R., Courtney, H. W., and Limperis, T. (1970) Research needs: The influence of discrimination, data processing, and system design, in *Remote Sensing with Special Reference to Agriculture and Forestry*, Committee on Remote Sensing for Agricultural Purposes, Nat. Res. Council—Nat. Acad. Sci., Washington, D. C., pp. 354-421.
- Loomis, S. (1970) Morphology and structure of an ice-cored medial moraine, Kaskawulsh Glacier, Yukon, *Res. Paper No. 57*, Arctic Inst. North Am., pp. 1-65.
- Lougeay, R. (1969) Microclimatological studies over the Seward Glacier snowpack, *Res. Paper No. 54*, Arctic Inst. North Am., pp. 51-102.
- Meier, M., Alexander, R., and Campbell, W. (1966) Multispectral sensing tests at South Cascade Glacier, in *Proceedings of the Fourth Symposium on Remote Sensing of Environment*, Ann Arbor, April 1966, Inst. Sci. Technol., Univ. Mich., Ann Arbor, pp. 145-160.
- Outcalt, S. I. (1971) A numerical surface climate simulator, *Geogr. Anal.*, 3, 379-393.
- Poulin, A. O., and Harwood, T. W. (1966) Infrared imagery in the Arctic under daylight conditions, in *Proceedings of the Fourth Symposium on Remote Sensing of Environment*, Ann Arbor, April 1966, Inst. Sci. Technol., Univ. Mich., Ann Arbor, pp. 231-234.
- Sellers, W. D. (1965) *Physical Climatology*, Univ. Chicago Press, Chicago, 272 pp.

Up-Heaved Blocks: A Curious Feature of Instability in the Tundra *

Larry W. Price †

ABSTRACT. Up-heaved blocks occurring in unconsolidated material on well-vegetated slopes in the Ruby Range were investigated. These are very similar in appearance to the already documented frost-thrust blocks which normally occur on level, poorly vegetated, bedrock areas. The up-heaved blocks in the study area are one to three feet high and show evidence of recent activity. Freshly overturned turf around the bases of some of the blocks suggest that they may have been thrust above the surface at one time by considerable force. Measurements, however, reveal an annual movement of only one to two inches.

Origin of these features is suggested as being a result of several processes. Diurnal freeze and thaw is important for two or three weeks in the spring when a narrowly thawed zone surrounding the block allows the development of frost pressure within a semi-closed system. The annual freeze in the fall contributes about one-fourth inch to the upheaval of the blocks, and solifluction is important during the summer. The size and shape of blocks, as well as local site conditions, govern the occurrence of these features which are striking evidence of the instability that characterizes the tundra.

Up-heaved blocks are probably a fairly common phenomenon in Arctic and alpine areas, although they have been infrequently documented. Colloquially, they are known as "tombstone rocks" and "cement posts" and have been mentioned incidentally by several authors (Cairnes, 1912, p. 347; Eakin, 1916, p. 81; Elton, 1927, pp. 172-173; Hogbom, 1914, p. 275). There are apparently two distinct kinds of up-heaved blocks, although the distinction has not been made previously. One is restricted to bedrock and is commonly known as a frost-thrust block (Yardley, 1951, p. 69). Washburn (1969, p. 52) has recently criticized this term, however, suggesting the term *frost-heaved* block since *heave* denotes primarily vertical, while *thrust* denotes primarily horizontal movement (Eakin, 1916, p. 76). The second type of up-heaved block is not restricted to bedrock and has not been formally recognized in the literature, although the process of up-freezing of rocks in the origin of patterned ground has been well documented (Washburn, 1956, pp. 838-839). In addition, Washburn (1969, pp. 51-58) provides an excellent discussion of these features, but considers them a result of the normal up-freezing of stones. They differ from normal up-frozen rocks, however, in that they may reach a height of several feet above the surface due to a particular set of circumstances. Bird (1967) gives an excellent review of what is known about the first mentioned type—frost-thrust (or frost-heaved) blocks. These occur in different kinds of bedrock but are best developed in schistose metasediments. The general theory of origin is that water enters the bedrock along joint planes, and upon freezing, expands and wedges the rock upward. When thaw occurs the block does not settle completely back to its original position because detritus falls into the

depression or because the block settles back at a different orientation. In subsequent years, more water accumulates along the joint planes, as well as below the block, and additional frost expansion and movement occur.

Features very similar to these in form, but not occurring on bedrock, were found in the Ruby Range of southwest Yukon, about 140 miles northwest of Whitehorse, at 61°23'N, 138°13'W. These will be called up-heaved blocks. They differ from those previously documented in that they occur on slopes rather than level areas; they occur in unconsolidated detritus as opposed to bedrock; and the associated vegetation is well-developed compared to the sparse fell-field vegetation which occurs in bedrock areas. The area has been glaciated to an elevation of about 6500 ft (Muller, 1967, pp. 9-16) and slopes are mantled with five feet or more of drift. The up-heaved blocks occur above tree line on slopes of several exposures with gradients ranging from 10° to 20°, but are particularly well-developed on a 6200-ft southeast-facing slope with a gradient of 14°. The following remarks will deal mainly with these.

The blocks average about two feet in diameter at the base, and are usually rectangular, tapering wedge-like to the top (Fig. 1). They project up to three feet above the surface and are usually devoid of lichens, especially if there is evidence of instability. On June 25, 1967, when first observed, many of the up-heaved blocks had freshly broken roots, loose mud and overturned turf around their bases, suggesting that the movement had taken place that spring. By the end of August, the overturned vegetation and turf was sodden and dull compared to the very fresh appearance it had had early in the season. Much of the mud and gravel had been washed away. On the other hand, a few of the blocks appeared quite stable with vegetation growing up closely against their bases and no evidence of recent movement. These blocks were usually heavily covered with black lichens.

Of the very fresh features, some gave the distinct impression of having been formed in one major thrust

*This article is adapted from one which appeared in the *Proceedings* of the Association of American Geographers, Vol. 2, pp. 106-110, and is used here with permission.

†Department of Geography, Portland State University, Portland, Oregon

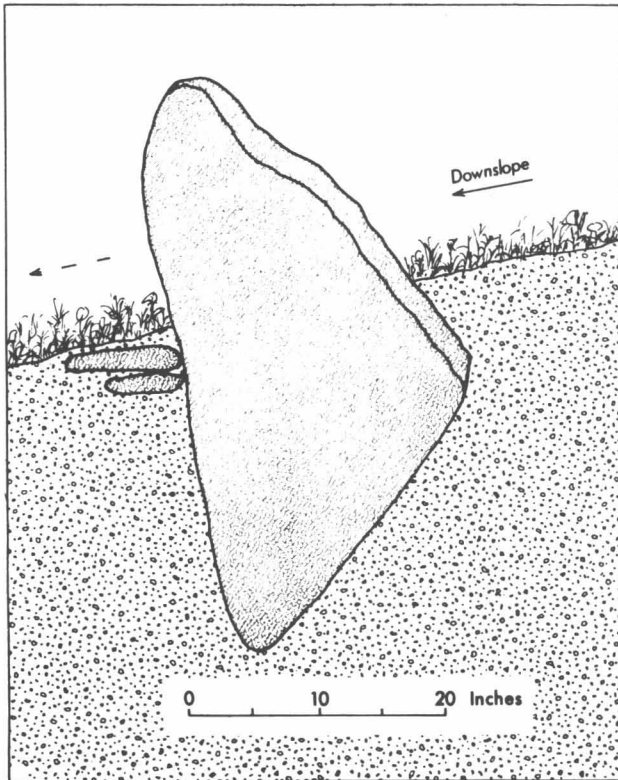


Fig. 1. Sketch of excavated up-heaved block.

above the surface. In order to investigate this possibility, several of the more active-appearing blocks were painted, photographed, and rephotographed the following year (Fig. 2). Although this is a crude method of measurement, it at least provides information as to the order of movement.

Upon return to the field on June 18, 1968, permafrost was still within four to six inches of the surface. The up-heaved blocks had been affected in different ways, but the average amount of upheaval since the previous August was one-fourth inch. By July 1, however, four of the blocks had been forced one to two inches above their original position (Fig. 2A, B, C, D, F). No appreciable movement occurred after this date and by August 5, several of the blocks had settled and tipped forward, so that the painted area was again about even with the ground. From these observations it is concluded that movement probably does not occur in one single year but in increments over a number of years. In addition, movement varies both in space and time. Some of the painted up-heaved blocks revealed very little movement, and rates of movement would presumably vary from year to year, depending upon environmental conditions.

The vegetation of this southwest-facing slope forms well-defined communities with distinct horizontal banding in relation to microhabitats provided by the risers of solifluction lobes. The community on the lobe treads consists of mossy tussocks (hummocks) one to two feet high interspersed with poorly drained basins. The distri-

bution of the up-heaved blocks is largely restricted to this community. The mossy tussocks provide excellent insulation, so the maximum depth of thaw under this community is about 36 inches. As a result, the surface remains in a saturated condition through much of the summer and measurements show that it is this section of the lobe that undergoes the greatest movement due to solifluction (author's data).

Near the end of the second field season (August 10), one of the more active up-heaved blocks was excavated (Fig. 2E). The site was very wet but permafrost was not encountered. Below the six inches of the surface organic layer the material had a grayish-blue color with a distinct hydrogen sulfide odor, a feature characteristic of poorly drained tundra soils (Tedrow, 1962, p. 345). The cross section looked very similar to frost boil areas I had excavated on the slope, with a high concentration of fine material. There were a few small rocks, two to three inches in diameter, spread about the block. On the down-slope side, tightly against the up-heaved block, were two larger rocks, ten inches and seven inches in diameter (Fig. 1).

The origin of these up-heaved blocks probably involves several distinct, but allied processes. Blocks which are incorporated in unconsolidated material may be slowly forced to the surface due to upfreezing. A mixture of fines and stones will attract moisture differentially because of capillarity, so when freezing takes place, greater expansion occurs in the area of fines. During thawing and contraction the fines have a greater affinity for each other and are drawn back together in a nucleus, while the larger sized particles do not return to their original position. This process continues at an increasing rate as the nucleus of fines increases in size. In this way, stones are slowly ejected upward through the finer material to the surface (Washburn, 1956, pp. 838-839).

When the blocks approach the surface they are susceptible to both diurnal and seasonal freeze and thaw. In the fall, movement due to diurnal freezing is not as important as the annual freeze. The bottoms of rocks may be cooled to freezing temperature more quickly than the surrounding soil because of their greater conductivity, and the growth of ice crystals beneath, as well as alongside the rock, would cause lifting toward the cooling surface. This would especially be so with a wedge-shaped rock, oriented as the one excavated (Fig. 2E). Upon thawing the intervening spaces are partially filled by detritus so that the rock cannot return to its original location. The final freeze in the winter results in a major amount of frost heave due to freezing of the interstitial water, which only occurs when temperatures are very low (Taber, 1943, pp. 1446-1456). As mentioned, however, an average of only one-fourth inch of movement was due to fall freeze.

The greatest amount of movement (one to two inches) occurred in a two-week period from June 18 to July 1. There are several possible explanations for this. The simplest, and by no means least acceptable, explanation is that when thawing takes place in the spring, the base of the rock is still encased in frozen ground. The surface

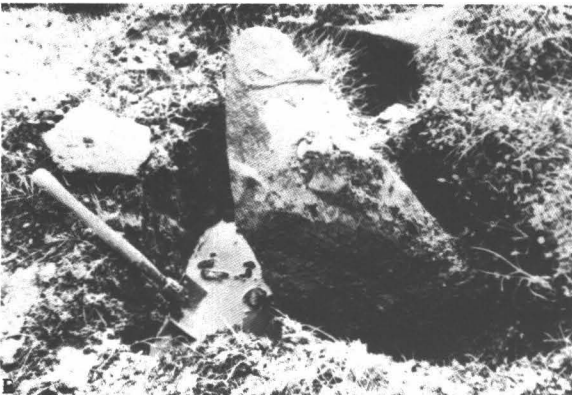


Fig. 2. Movement that occurred in one year on several up-heaved blocks on the southeast-facing slope. Photos A, C, and E are all of the same feature. Photo A was taken on July 1, 1968. The light area at the bottom of rock reveals about $\frac{1}{4}$ inches of up-heaval (hunting knife is 8 inches long and handle is one inch wide). Note disturbed turf on the upslope side of rock. Photo C of feature A was taken one month later from opposite direction. The block has settled forward so that previous amount of upheaval was not apparent. Photo E shows the feature being excavated (left is downslope). The block is wedge-shaped and is resting on one corner. Soon after the photo was taken the rock toppled forward. The rock ten inches in diameter at left of photo was one of two nestled tightly against the downslope side of up-heaved block.

In Photo B, downslope is to the upper right. It is difficult to see in photo, but this block has pulled away from the upslope turf about one inch. In this case the disturbed area is immediately downslope. Photo D is of a feature located in a poorly drained basin surrounded by tussocks. It has been forced up about $\frac{3}{4}$ inch. The right of photo is downslope. The feature in Photo F is located in drier vegetation. Downslope is to left of photo and hunting knife gives scale. Photo was taken on July 1, 1968. Considerable fresh disturbance has taken place here on upslope side of block.

is saturated and solifluction occurs within the surface material surrounding the block. This gives the impression of the block having been up-heaved when in reality the turf has settled relative to it (Hamberg, 1915, in Washburn, 1956, pp. 838-839). This process would explain the overturning and disruption of the surface layer immediately upslope from the boulder as was found in several cases (Fig. 2A, C, F).

A somewhat more involved process may also be important. The period from June 18 to July 1 is the period of highest sun and some of the clearest days of the summer occurred at this time. Permafrost was still very near the surface, but beginning to retreat at a more rapid rate. Maximum ambient temperatures range from 45° to 50° F and minimum temperatures from 29° to 30° F. Maximum temperatures of rocks at the surface on the southeast-facing slope would, however, be considerably higher than the ambient temperatures due to the higher conductivity of rock, hence, melting may occur for an inch or two around the rocks. Thawing may actually occur on sunny slopes when temperatures are slightly below freezing due to the greater absorptivity of rock compared to the surrounding frozen ground (Taber, 1943, p. 1448). The encasing soil surrounding the rock would be saturated due to the released moisture, and a semi-closed system would exist. Nocturnal freezing of the narrow thawed zone would cause expansion in the direction of the cooling surface, that is, upward at right angles to the slope. The critical factor is that thawing occurs along the underside of the rock, so when refreezing takes place enough force is provided to overcome the binding effect of permafrost on the lower part of the rock. Here the shape of the block becomes of importance: wedge-shaped blocks with one corner at depth, as the one excavated, would be greatly favored for this process.

The process just described is effective for only a short time in the spring. After permafrost has retreated below the bottom of the rock, it would cease to be important since the semi-closed system no longer exists. Upon refreezing in the fall, the semi-closed system is absent and the sun is not high enough to provide the necessary spread of temperature from day to night for this kind of movement to be significant. During the fall, a major amount of frost heave occurs, but is more of an annual event, while the process described above operates in the spring, largely on a diurnal basis.

During summer, solifluction is the most important mechanism of movement, since freeze-and-thaw does not occur very often at this site. Solifluction adds a dimension which is not present on bedrock and provides a possible alternate explanation for these features in conjunction with frost heave. It has been shown by several workers, including Lundqvist (1949, pp. 335-347) and Rudberg (1958, pp. 114-125) that in solifluction there is a high correlation between the orientation of the long axes of rocks and direction of flow. Distinctly elongated blocks would be particularly susceptible to and indica-

tive of this tendency. If a block were buried under a thick cover of detritus and oriented parallel to the surface rather than perpendicular to it, as the preceding discussion has assumed, then it would be much more susceptible to movement due to solifluction. The largest part of the block would become oriented upslope while the smallest part would be downslope (Glen, *et al.*, 1957, pp. 194-205). There is less resistance to movement at the leading smaller end of the block, and during movement *en masse* downslope it would have a tendency to rise above the surface. A slower moving area or another rock downslope may act as an obstacle and the smaller part of the block would ride over the obstacle and be forced to a higher angle. This method is favored by a larger base at depth while the frost-heave method is favored by a tapering base. Blocks with the shape of the excavated feature could be moved by either method, however.

It is doubtful that the two rocks, 7 and 10 inches in diameter, located at the surface immediately downslope from the up-heaved block, could have had enough retarding effect to bring about the present height of the excavated feature by the process suggested above. More likely, solifluction has accentuated the height of the block, forced upward primarily by differential freezing and thawing. Evidence suggests that solifluction is important in the later stages of their development, however. The fact that these features are largely restricted to the tussock community on the lobe treads, where solifluction is most active, is a reflection of this. Moreover, all of the up-heaved blocks observed on the slope were oriented with their long axes in direction of slope. Generally, the greatest disturbance was observed on the upslope side of the blocks but at one painted site the block had merely pulled away 1¼ inches from the vegetation upslope, while furrowing the material aside immediately downslope from the rock.

As indicated earlier, no major amount of upheaval was observed to occur after the early part of July. Permafrost had retreated below the bottom of the blocks by this time, apparently by allowing them to settle downslope due to gravity or to solifluction. The excavated block had settled and tipped slightly forward between July 1 and August 5. The observation that it had been up-heaved 1¼ inch was not at all obvious on August 5 since the vegetation and soil from upslope had closed in and was touching the rock again.

The method by which blocks are up-heaved in unconsolidated material appears to depend largely upon the shape of the rock and local site conditions. The exact combinations necessary are not yet known. Pointed out here are merely some of the more salient characteristics of these features as they occur within a certain set of environmental conditions. In the study area the general process of up-freezing is everywhere apparent. Many of the tussocks owe part of their height to the presence of a rock in their center. The few blocks that protrude higher above the surface are simply a more striking evidence of the instability that characterizes the tundra.

Acknowledgments

I am grateful to the Arctic Institute of North America for financial support and the Icefield Ranges Research Project for excellent logistical support. While writing this paper, I benefited from the critical comments of Dr. C.S. Alexander, Department of Geography, University of Illinois, and Dr. A.L. Washburn, Quaternary Research Center, University of Washington.

References

- Bird, J. B. (1967) *The Physiography of Arctic Canada; With Special Reference to the Area South of Parry Channel*, Johns Hopkins Press, Baltimore, 336 pp.
- Cairnes, D. D. (1912) Differential erosion and equiplanation in portions of Yukon and Alaska, *Bull. Geol. Soc. Am.*, 23, 333-348.
- Eakin, H. M. (1916) The Yukon-Koyukuk region, Alaska, *U. S. Geol. Surv. Bull.* 631, 88 pp.
- Elton, C. S. (1927) The nature and origin of soil polygons in Spitsbergen, *Quart. J. Geol. Soc. London*, 83, 163-194.
- Glen, J. R., Donner, J. J., and West, R. G. (1957) On the mechanisms by which stones in till become oriented, *Am. J. Sci.* 225, 194-205.
- Hamborg, A. (1915) Zur Kenntnis der Vorgänge im Erdboden beim Gefrieren und Auftauen sowie Bemerkungen über die erste Kristallisation des Eises im Wasser, *Geol. Foren. Forhandl.* 37, 583-619.
- Hogbom, B. (1914) Über die geologische Bedeutung des Frostes, *Bull. Geol. Inst. Uppsala*, 12, 257-390.
- Lundqvist, G. (1949) The orientation of the block material in certain species of flow earth, *Geogr. Ann.*, 31, 335-347.
- Muller, J. E. (1967) Kluane Lake map-area, Yukon Territory, (115G, 115F, E½), *Geol. Surv. Can., Mem.* 340, 135 pp.
- Rudberg, S. (1958) Some observations concerning mass movement on slopes in Sweden, *Geol. Foren. Forhandl.*, 80, 114-125.
- Taber, S. (1943) Perennially frozen ground in Alaska, *Bull. Geol. Soc. Am.*, 54, 1433-1548.
- Tedrow, J. C. F. (1962) Morphological evidence of frost action in Arctic soils, *Biul. Peryglacjal. No. 11*, pp. 343-352.
- Washburn, A. L. (1956) Classification of patterned ground and review of suggested origins, *Bull. Geol. Soc. Am.*, 67, 823-866.
- Washburn, A. L. (1969) Weathering, frost action, and patterned ground in the Mesters Vig district, Northeast Greenland, *Medd. Grøn.*, 176, 51-58.
- Yardley, D. H. (1951) Frost-thrusting in the Northwest Territories, *J. Geol.*, 59, 65-69.

The Sedimentology of a Braided River*

Peter F. Williams[†] and Brian R. Rust[‡]

ABSTRACT. A straight, four-mile tract of the Donjek River is braided throughout, discharging about 50,000 ft³/sec in flood.

The active part of the tract shows upper-regime flow in the main channels, and lacks vegetation. Higher, older levels are former river courses, partly or completely vegetated, with continuous flow (principally lower regime) only in the main channels. Comparing channel (width:depth) and topographic indices, the younger surfaces are more strongly dissected because of active channel cutting, whereas channels on older levels are subject to infilling.

The sediments vary from clays to coarse gravels; most are poorly sorted. CM plots permit division into three main groups: silt and mud of low energy environments such as abandoned channels, gravel of high energy channel-bar complexes, and a variable intermediate group which fills channels under medium-energy conditions. Seven facies are distinguished on textural, floral, and sedimentary structural characteristics. Facies relations are mostly gradational within channels, commonly fining upward. They are more complex between channels, and invariably erosional.

The origin and directional significance of hierarchical orders of sedimentary structures were studied. Six hundred and sixty measurements of small-scale structures (mostly ripples) show moderate within-bar and between-bar variation, and give a grand vector mean 22° from the river trend. Bisectors of channel directional arcs (maximum and average ranges) approximate the river trend within 5°.

INTRODUCTION

The Donjek is a braided river situated in the southwest corner of the Yukon (Fig. 1). It rises on the northeastern slopes of the St. Elias Mountains, flows northward approximately along longitude 140°W, and joins the Yukon River system some 40 miles east of the Alaska border (Fig. 1). The Donjek is fed by many small creeks, and in its upper reaches by meltwater from valley glaciers, notably the Steele, Donjek, and Kluane Glaciers.

The discharge of the Donjek River is controlled by seasonal climatic changes and by short-term variation in summer rainfall. The river is largely frozen in winter, but maintains a low discharge throughout the coldest periods. It usually begins to thaw in late April or early May, and discharge increases as the melt progresses to higher altitudes and begins to affect the glaciers. It reaches a peak in July, declines in August and September, and the river usually returns to its winter condition in October or November. Secondary peaks in the discharge may be observed over periods of three to five days after intervals of prolonged heavy rainfall during the summer.

Limited observations on the hydrology of the Donjek River were made from the highway bridge at Mile 1133, Alaska Highway (Fig. 1). A maximum surface velocity of 11.8 ft/sec was observed during flood stage, when most of the bars separating braided channels at this locality were submerged. A drop in water level of a few feet

caused separation of flow into eight channels and a decrease in maximum surface velocity to 8.5 ft/sec. It was not possible to measure discharge with the equipment available, but an estimate of flood discharge at the Mile 1133 bridge made for the Department of Public Works amounted to 50,000 ft³/sec (personal communication, 1968).

The area through which the Donjek flows was extensively glaciated in Pleistocene and Recent times, although at present the glaciers appear to be in a state of fluctuating retreat (Bostock, 1952; Krinsley, 1965; Muller, 1967). From tree-ring analysis Denton and Stuiver (1967, p. 504) estimate that the Donjek Glacier began to retreat from its Neoglacial maximum before A.D. 1874. Retreat has been irregular, and subrecent advances of the Kluane and Donjek Glaciers are indicated by scoured troughs and end moraines (Muller, 1967, p. 16). Muller estimates that the last advance of the Donjek Glacier occurred around 1930. A spectacular advance of the Steele Glacier in 1966 has been described by Wood (1967).

The present paper is based on a study of a four-mile tract of the Donjek River south of the bridge at Mile 1133 on the Alaska Highway (Fig. 1). Within this tract the river has a broad, straight valley averaging a mile in width. The valley has steep sides, which are cut into a Neoglacial succession of tills, outwash sands and gravels, and loess (Denton and Stuiver, 1967). The valley floor is covered by a complex network of channels, bars, and islands, largely formed by reworking of these glacial sediments. Four topographic levels are present on the valley floor, and will be discussed later.

The aim of this investigation is to obtain information about the sedimentary features of a river with braided channels in order to recognize and interpret similar ancient deposits in the geological record. This approach requires

*This report has previously appeared in the *Journal of Sedimentary Petrology*, Vol. 39, pp. 649-679 (1969), and is reprinted here with permission.

[†]Geology Department, University of Ottawa, at time of writing; present address, Chevron Standard Ltd., Calgary, Alberta, Canada

[‡]Geology Department, University of Ottawa, Ottawa, Ontario, Canada

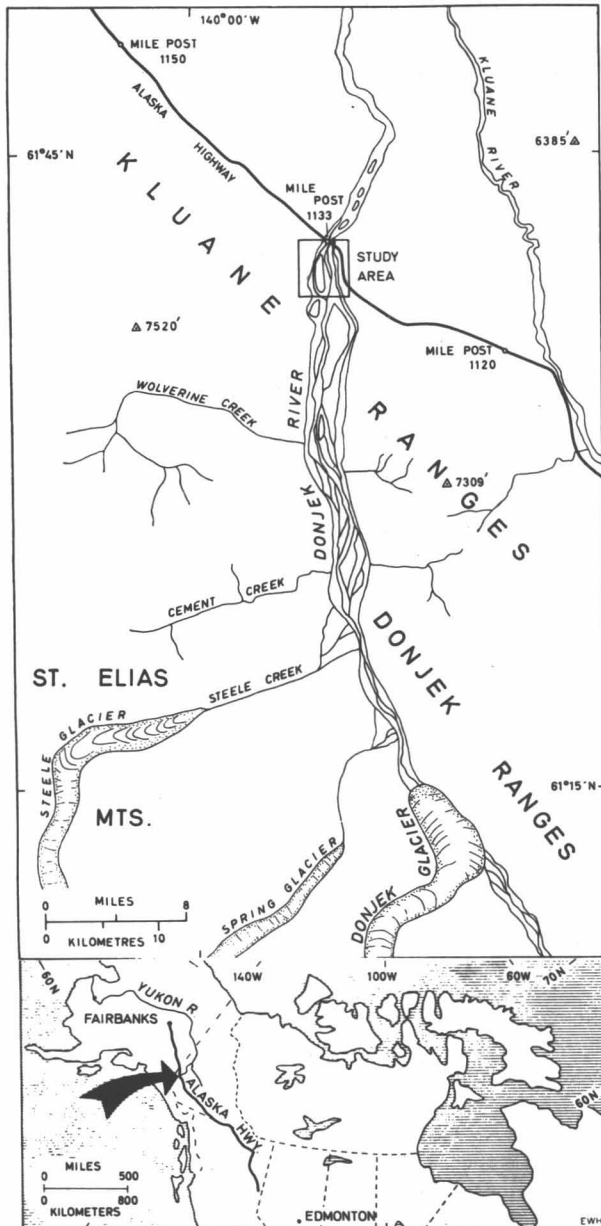


Fig. 1. Locality map of the Donjek River and study area.

a detailed multivariate study involving sedimentary textures, directional and nondirectional structures (on all scales), and facies. The various data collected were considered in association in order to produce a model of the river based on field observations.

SURFACE TOPOGRAPHY

Topographic Levels

Four topographic levels can be recognized in the tract of the Donjek River studied (Fig. 2a). They are distinguished on the grounds of elevation, the amount of vege-

tation, and the type and intensity of fluvial activity in progress. The vertical intervals between the four levels are shown diagrammatically in Figure 2a; Level 1 being the lowest and youngest, and Level 4 the highest and oldest. The areal extent of the higher and older levels is largely a function of preservation during the formation of younger levels.

Level 1. Level 1 is essentially devoid of vegetation and shows the greatest fluvial activity; the highest discharge, the highest flow regimes, and the greatest number of active channels. It may be considered as the presently active part of the river.

At low and high discharge (but especially under the latter condition) the water-air surface shows standing waves, antidunes, and chutes and pools in the principal channels (Simons, Richardson, and Albertson, 1961; Simons, Richardson, and Nordin, 1965). Sedimentary processes on Level 1 are directly related to discharge. At low discharge, with a low rate of sediment transport, there is no cutting of main channels, (first-order channels, see below), and little bar migration. However, exposure and dissection of formerly submerged bars takes place, and partial filling of abandoned channels is common. At high discharge, sediment transport is great (although not directly observable), and there is continuous migration of channels and bars.

Level 2. Level 2 is higher than Level 1 and is subject to widespread fluvial activity only during flood stage. At other times a few channels remain active, and the discharge is much less than on Level 1 but greater than on Levels 3 or 4. Large-scale changes in bed morphology caused by variation in discharge are less noticeable than on Level 1 because of the more permanent nature of the main bars and channels. The channel-bar relationships seen at low river stage are retained during flood.

A sparse vegetation colonizing the higher and more permanent bars is mostly of the vetch-willow association (see facies section). Tree-ring analysis of the willows indicates that the older bars are at least twelve years old. The area occupied by Level 2 may be considered part of a stream channel that existed at that time, which has probably been somewhat reduced in extent by lateral erosion during the formation of Level 1.

Level 3. When Level 1 (the present stream channel) has a low discharge very few channels on Level 3 have continuous water flow. The flow is almost invariably in the lower regime (Simons, *et al.*, 1961; 1965). Sediment transport is exclusive to the principal channels and is characterized by downstream migration and accretion of rippled sand bars.

At maximum or near-maximum discharge there is overbank flooding from the principal channels, carrying suspended mud into abandoned channels and other slack-water areas. The velocity of the overbank flooding varies from an almost imperceptible advance to a fast current where flow is constricted. Sedimentation from overbank floodwater is the principal mechanism of infilling channels with fine detritus.

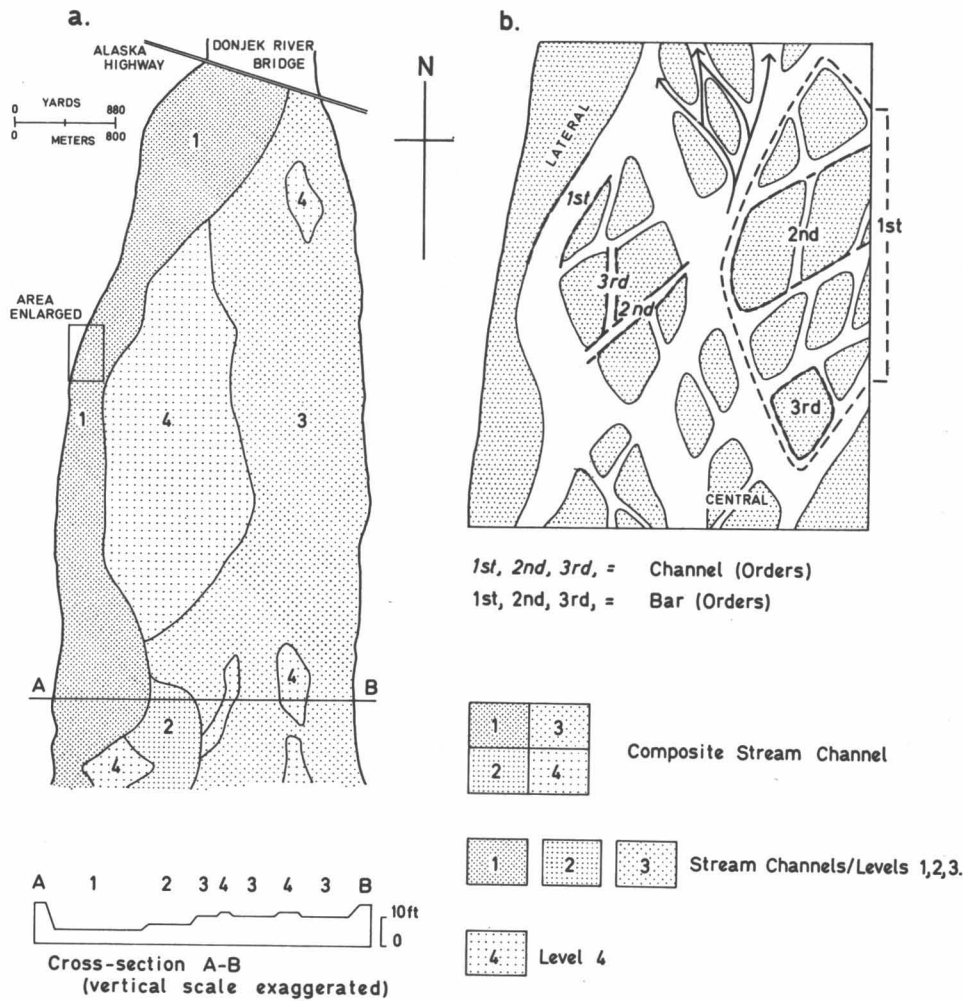


Fig. 2. (a) Areal distribution and diagrammatic profile section of stream channels and levels. Vertical scale on section is approximate. (b) Small area enlarged to show hierarchical organization of channels and bars.

Level 3 differs markedly from Levels 1 and 2 in having a good vegetative cover. The plants vary in population density and type in the different micro-environments; the more important associations being vetch-willow and sedge-horsetail. Tree-ring analysis of the willows gives a minimum age of 27 years for some of the bars.

Level 4. Level 4 is the highest and oldest surface on the valley floor, and is largely preserved as island remnants left during the formation of younger levels. All channels are abandoned, and apart from rain water and melting ground ice, the level is dry. It has a dense cover of vegetation, dominated by several species of spruce. The age of the largest spruce found was estimated to be 212 years, which indicates an age of about 250 years for the topographic surface, since the spruce is the climax vegetation in this region. The tree cover makes it difficult to recognize features such as channels, but they are indistinctly visible on the aerial photographs, and Level 4 appears to be similar to the younger surfaces in this respect.

Channels and Bars

Channels and bars are important topographic features found on all levels. Their scalar variation is considerable, and introduces a problem of classification which has, to some extent, been overcome by erecting hierarchical orders. Thus channels may be considered in terms of five orders: composite stream channel, stream channel, first-order, second-order, and third-order channels (Fig. 2). The composite stream channel is synonymous with the whole of the river tract, including active and inactive areas, that is Levels 1, 2, 3, and 4. The term stream channel refers to the contiguous parts of the river tract that are within the same level, for instance the presently active stream channel that comprises Level 1 (Fig. 2). Within each stream channel the braided character is expressed as a system of anastomosing channels and intervening bars. The channels which delineate large bars are called first-order channels, while the smaller channels that dissect the bars are called second-order channels. Anabranches

to the latter channels are termed third-order channels (Fig. 2b).

Three types of bar are present: longitudinal (lateral and central), transverse, and point bars. Longitudinal bars are by far the most abundant type. The bars have been classified into first-, second-, and third-order categories, in relation to channels of corresponding order (Fig. 2b).

Surface Topography Index

The three stream channels in the river tract have the same topographic features (principally channels and bars), but visual comparison suggests that the younger stream channels are more deeply dissected. In order to confirm this, traverses normal to the mean channel trend were accurately leveled and a series of profiles were constructed. A topographic index (T) was calculated for each section of the profile between leveling stations, such that

$$T = \frac{a_1}{a_2}$$

where a_1 is the area on the profile between the ground surface and a horizontal line through the highest point, and a_2 is the total area between horizontal lines through the highest and lowest points on the profile. The distance between leveling stations averaged 465 ft, and was dependent on conditions of visibility.

The results for stream channels 1, 2, and 3 are shown below, with significance levels calculated by "student's t " test.

Stream channel	n	\bar{x}_T	σ_T	Significance level
1	5	0.541	0.080	N.S. 5% 0.1%
2	5	0.486	0.100	
3	11	0.391	0.056	

The results show that there is no significant difference between the surface roughness of stream channels 1 and 2, but that the difference between stream channels 2 and 3 is probably significant (5 percent level). There is a highly significant difference (0.1 percent level) between stream channels 1 and 3. Essentially this test shows that stream channel 2 is more highly dissected than stream channel 3, and stream channel 1 is more highly dissected than stream channel 2. Such a relationship is to be expected, because the processes of small-scale channel formation are most active in stream channel 1, whereas channels are tending to fill in stream channel 3; stream channel 2 is intermediate in this respect.

SEDIMENTARY TEXTURES

The sediment on the tract of the Donjek River studied varies from clay-size to boulders with a maximum diameter in excess of 9 in. Lateral and vertical changes in grain

size are both common and abrupt, and an accurate estimate of relative size abundance is not possible. However, some rationalization is achieved by grouping size classes into general lithotypes: gravel, sand, silt, and clay. Gravel (mean grain size greater than -1.0ϕ) is the most abundant lithotype, followed by sand and silt, which commonly occur together.

Sediment samples were taken from a wide range of lithotypes in a variety of microenvironments. However, the size distributions of the coarsest gravels ($> -3.0 \phi$) were investigated in the field, with the results shown in Figure 3. Grain-size distributions for the remaining lithotypes were determined by dry sieving of the coarser material and pipette analysis of the silt- and clay-sized fractions. The size frequency curves of the 30 samples analysed show that 66% of the distributions are unimodal, 24% are bimodal, and 10% are poly-modal (Fig. 4). Where possible, the following parameters were calculated for each sample: median grain size (M), coarsest percentile (C), graphic standard deviation (σ_G) (Folk, 1968, p. 45), simple sorting measure (SO_s), simple skewness (α_s) (Friedman, 1967, p. 329) and graphic kurtosis (K_G) (Folk, 1968, p. 48), see Appendix 1.

The graphic standard deviations and sorting values show that the samples are moderately to poorly sorted (Folk, 1968, p. 105). The rare well-sorted samples come from migratory rippled sand bars, and the occasional very poorly sorted sediment is from channel floors liable to the deposition of both coarse bed load and fine suspended sediment. It should be noted that samples taken from such heterogeneous lithotypes were treated as admixtures. The majority of samples (75%) are positively skewed (Appendix 1), indicating an excess of fine material and general lack of current winnowing. With more than 70% of the kurtosis values between 0.90 and 1.50, the samples are predominantly mesokurtic to leptokurtic (Folk, 1968, p. 49). This indicates a tendency toward better sorting for the central part of the grain size distribution.

The coarsest percentile has been plotted against standard deviation (Fig. 5), and simple skewness against the simple sorting measure (Fig. 6) after the manner of Friedman (1967). These plots illustrate the validity of Friedman's beach: river sediment dividing lines (Friedman, 1967, pp. 329-342), and show the distribution of textural parameters in the Donjek sediments.

Values of coarsest percentile (C) have been plotted against median grain size (M), following the method of Passega (1957). The resulting distribution (Fig. 7) has been subdivided into three principal groups (1, 2, and 3), group 2 being subdivided into 2a and 2b, Group 1 combines the finer-grained sediment—silty clay and laminated mud—which accumulated in low-energy environments such as abandoned channels and other topographic lows. Group 3 includes the coarse-grained sediment—pebble beds and pebbly sands—which were deposited under high-energy conditions in channel-bar complexes. Group 2, the largest group, may be regarded as intermediate between groups 1 and 3 in terms of both grain size and

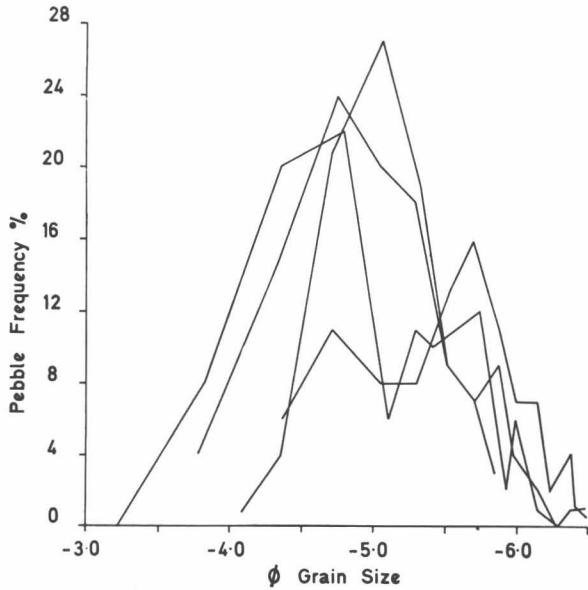


Fig. 3. Pebble-size frequency curves.

energy of environment. Group 2a is representative of rippled sand-silt bars which are always formed under conditions of lower flow regime. Conversely, group 2b is typically a heterogeneous assemblage of size grades from pebbles to silty clay, deposited in channels subject to periods of transitional and upper-flow regime currents, and periods of stagnant water following abandonment. The range of sediment sizes present in the river tract may be sometimes observed in a single channel (Fig. 8). The superposition of sediment types in this and similar examples illustrates the succession resulting from a continuous process of channel filling. Figure 8 shows the following trends:

- (1) Consistent upward decrease in median grain size and coarsest percentile
- (2) Consistent upward decrease in positive skewness (reduction in excess fines)
- (3) Minor variations in sorting, which is moderate to poor throughout
- (4) Insignificant variation in kurtosis apart from an apparently high value below the 2-ft level

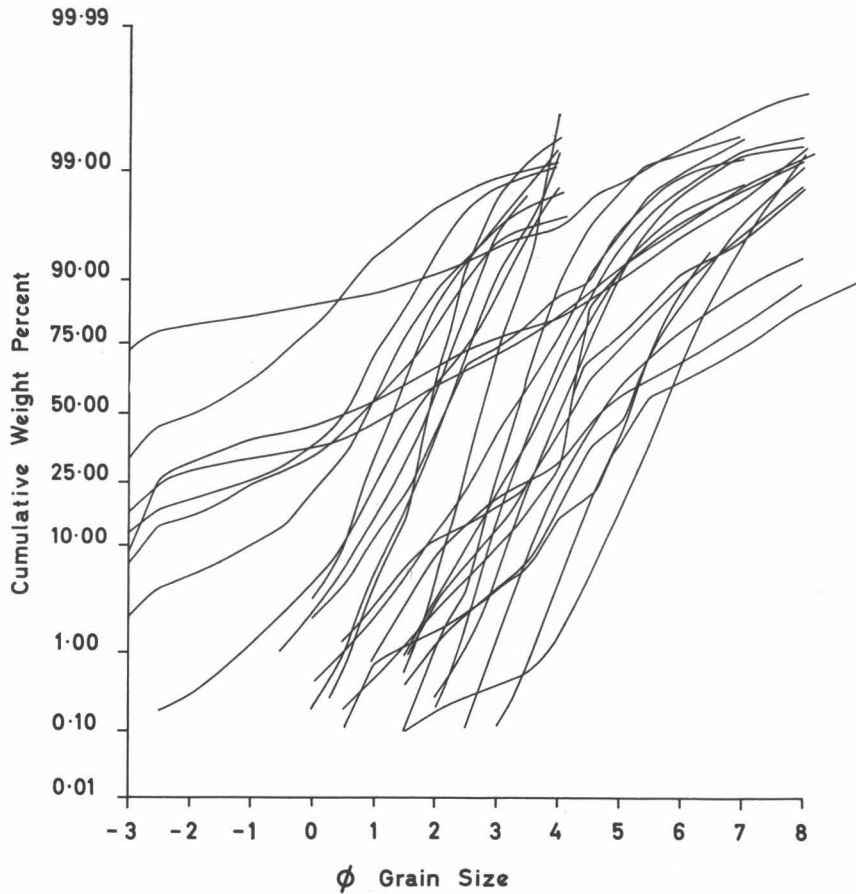


Fig. 4. Cumulative size frequency curves of the sediment samples.

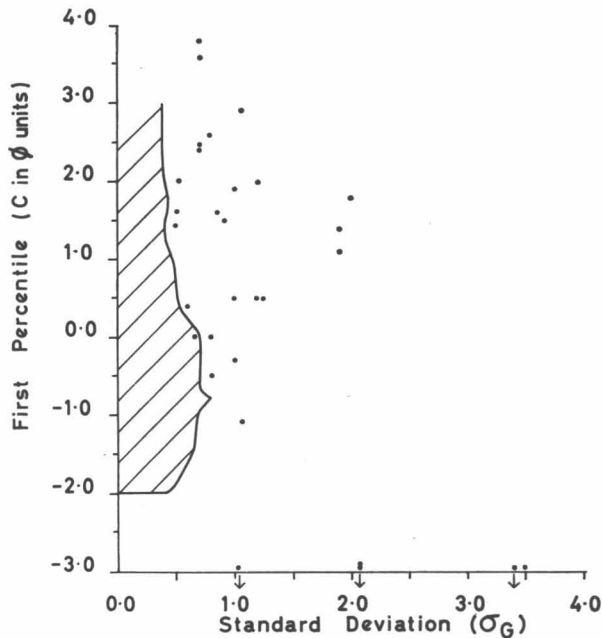


Fig. 5. Plot of first percentile and standard deviation. Shaded area and solid line represent the textural field of beach sediments and the beach-river sediment dividing line (Friedman, 1967).

SEDIMENTARY STRUCTURES

The principal types of sedimentary structure together with relative abundances are shown in Table 1. Only some of the more common and interesting structures are described in the text. Many of the structures found in the Donjek have been recognized in other braided rivers (Doeglas, 1962).

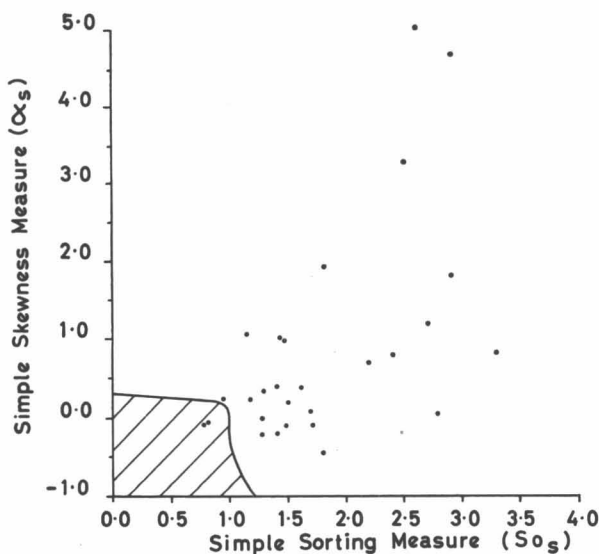


Fig. 6. Plot of simple skewness measure and simple sorting measure. Shaded area and solid line represent the textural field of beach sediments and the beach-river sediment dividing line (Friedman, 1967).

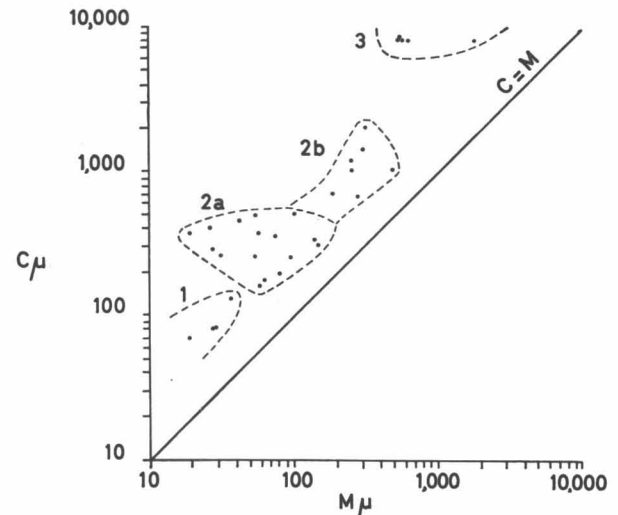


Fig. 7. CM patterns for alluvial sediment in the Donjek River.

Small-Scale Structures

Small-scale ripples. Small-scale ripples (amplitude less than 5 cm, Allen 1963b) occur in great abundance on stream channels 1, 2, and 3. The ripples are preserved in sand and silt, and frequently, in abandoned channels, are draped by a thin layer of silt or clay. Detailed variations in scale and morphology about the basic ripple types, namely straight, sinuous, linguoid, lunate (Allen, 1936a) give a multiplicity of forms. Minor variations include longitudinal ridges in the interrubble hollows and stoss-sides of lunate ripples; terraces on the ripple profile with subsidiary micro-ripples continuous with longitudinal ridges; and superimposed microripples on stoss-sides parallel in orientation to the host ripple (probably ripple-drift).

Symmetrical ripple marks have very low amplitude (few mm) with straight to gently sinuous crests which sometimes bifurcate and trifurcate. The symmetrical ripples are preserved in mud and silt, and are found on the depositional banks of channel margins (Fig. 9). The ripple crests are generally oblique to the direction of main current flow. They are formed by the regular pulsation of small lateral waves which are generated at the stream margins by the passage of channel flow around small bars and emergent ripples.

Large-scale ripples. Large-scale ripples (amplitude greater than 5 cm, Allen, 1963b) are rather uncommon, and are most abundant in stream channel 3. However, large-scale ripples could well be present on the channel floors of stream channel 1. The depth of the channels (frequently in excess of 6 ft) and consistent upper lower flow regime to upper flow regime currents are conducive to their development.

Unfortunately, water turbulence and consequent lack of clarity prevent observation of the sediment-water interface.

The large-scale ripples tend to occur in interfering grouped sets. Frequently, there is a gradual transition from large-scale to small-scale ripples. This relationship appears to be, in part, controlled by two factors, (1) original water

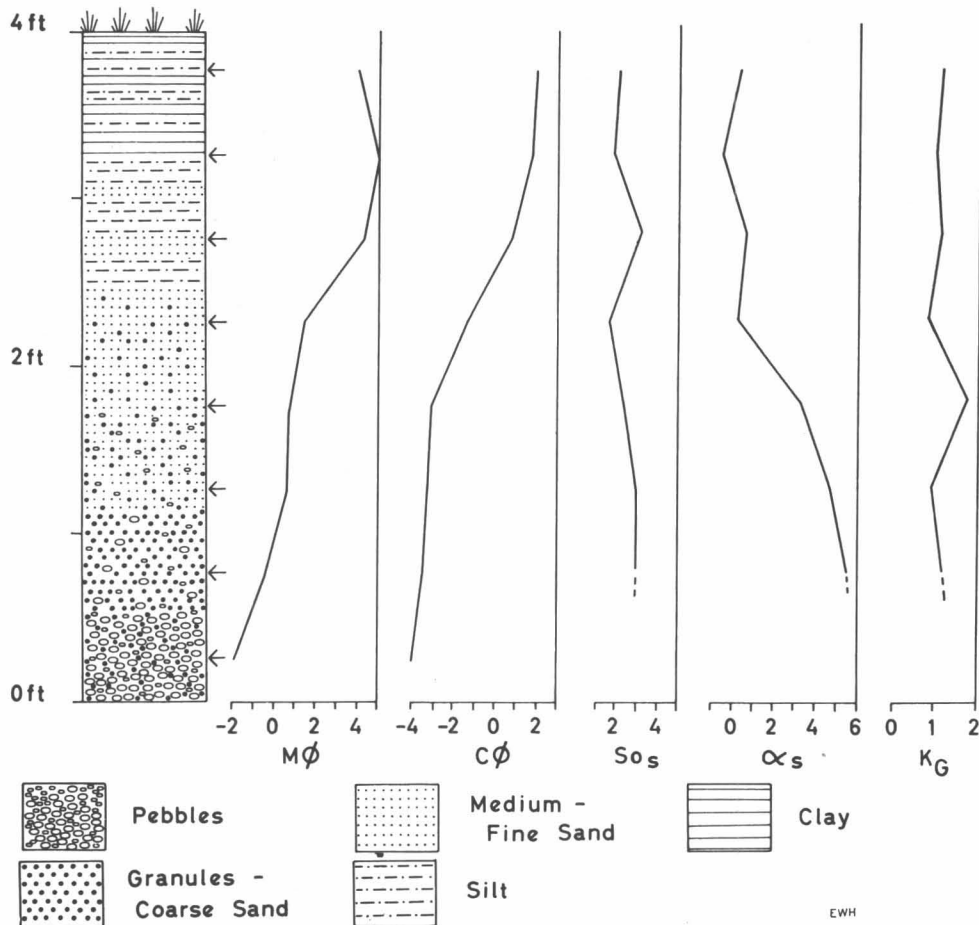


Fig. 8. Vertical variation of sedimentary textural parameters in a channel fill.

of a crescentic hollow plus contained pebble(s); the hollow becoming convergent and deeper upstream. Associated with the current crescents are longitudinal ridges of sand or silt. These develop near the crescent area and diminish and disappear downstream. Groups of current crescents are commonly transitional into small-scale ripples, especially where a bed containing pebbles changes laterally into a sand or sand-silt bed.

Silt volcanoes. Sedimentary volcanoes are common in stream channels 1 and 2, and are confined to thixotropic silt and muddy silt (Fig. 12). They are active on sediment-stagnant water and sediment-air interfaces (especially the former). The surface cones range in diameter from half an inch to 6 in., with a maximum height of half an inch.

The volcanoes are commonly found near water level on slopes between bars and channels. A typical association is a bar of gravel overlain by water-saturated silt and sand beside a channel that is partially filled with muddy silt and stagnant water. Water on the bar percolates downward from the thixotropic silt and sand to the gravel aggregate, and flows laterally, emerging in the lower part of the partially filled channel. This water, trapped in the muddy silt, is then expelled as a silt-water mixture to form eruptive cones on the sediment surface. In some instances, the lateral flow emerges on the channel at a

point *above* the water level in the channel. Here, the volcanoes occur in a layer of muddy silt which conforms to the shape of the channel. Elsewhere, the lateral flow emerges at a point *below* the water level in the channel. In this situation the volcanoes occur on top of a prograding sand/silt body.

Large-Scale Structures

Bars. Longitudinal bars are by far the most abundant type, and are discernible in all stream channels (Fig. 13). They vary in size from several hundreds of feet in length and tens of feet in width, to a few tens of feet in length and feet in width. Longitudinal bars are most commonly composed of gravel and sand admixtures, but show varying proportions of constituent lithotypes.

Longitudinal bars are commonly dissected by low-order channels. Dissection also produces small-scale terraces parallel or sub-parallel to the channel margin. The vertical interval between the individual terraces is small, generally less than 12 in. The terraces are sometimes discordant and erosional to each other, and may disappear upstream or downstream, or coalesce to form second- or third-order channels.

Transverse bars are rare, and are confined to stream



Fig. 9. Symmetrical ripples oriented upper right to lower left, under keys. Note also the low-amplitude current ripples (oriented upper left to lower right), rain pits, bird prints and gastropod tracks. Key case is 7 cm long.

channels 1 and 3. The bars are modified longitudinal bars and only appear at low discharge.

Point bars are uncommon and are best examined in stream channel 3. Their formation is favored by lower sediment load and discharge (as compared to stream channels 1 and 2), overall lower flow regime with migration of rippled silts and sands, and stable, vegetated channel banks. The bars are small, less than 1000 ft² in area, and composed of the finer size grades. Temporary point bars are present during periods of low discharge in stream channels 1 and 2.

Channels. The following discussion is concerned with first-, second-, and third-order channels (Fig. 2).

The cross-sectional profile of the channels is almost invariably asymmetrical, with no apparent preferred direction for the asymmetry. The channel floor (excluding fill) may be smooth or undulatory, the micro-relief appearing in part to be a function of channel size—greater relief with increase in channel width.

Fortunately many cross-sectional exposures both perpendicular and oblique to the dispersal trend could be

studied in erosional banks and trenches. These reveal the channel interrelationships to be a high frequency association of curved erosional surfaces with channel-fill deposits of variable thickness. Individual erosional surfaces always affect two or more adjacent channels. The mutual relationships are similar to the hypothetical model of Allen (1965, p. 164).

The lithotypes which constitute the channel fill show variation in sedimentary texture and vertical arrangement. These are considered in detail in the section on facies relationships.

A total of 167 measurements of channel index (width-depth) were made for stream channels 1, 2, and 3 (Table 2). Within-channel index variation was determined by serial measurements made in two channels on stream channel 3, and was found to be minor (Table 2). Both channels are abandoned, but one is subject to intervals of flood flow.

The channel indices for stream channels 1, 2, and 3 are summarized and compared in Figure 15. The three curves are decidedly unimodal. Further, with increasing

TABLE 2. Variation in Channel Parameters

Channel Index = Width/Depth; Sinuosity Index = Channel length/Length of meander belt axis (Brice 1964, p. 25); Transient-braiding Index = $2x$ sum of lengths of bars in reach/Length of reach midway between banks (Brice 1964, p. 27); x low = Lowest individual reading, x high = Highest individual reading of various parameters; \bar{x} = Mean; σ = Standard deviation; n = Number of observations; L = 95 percent confidence limits on \bar{x} (Folk 1968, p. 56).

Parameter	Stream Channel	x Low	x High	\bar{x}	σ	n	L at 95%
Channel Index variation within small-scale channels	3 (1)	35.0	95.0	68.0	17.9	20	± 8.36
	3 (2)	21.2	71.3	43.0	10.3	20	± 4.81
Channel Index	1	4.7	51.4	21.8	11.5	43	± 3.44
	2	6.0	49.0	22.6	11.5	38	± 3.66
	3	6.5	129.0	40.8	22.8	48	± 6.63
Sinuosity Index	1	1.02	1.17	1.07	0.055	6	± 0.059
	2	1.17	1.34	1.28	0.092	3	± 0.22
	3	1.06	1.16	1.09	0.043	6	± 0.046
Transient-braiding Index	1			2.2			

age there is a corresponding increase in the modal value of channel indices. This relationship may be accounted for by one or both of the following factors. Firstly, many of the channels in stream channel 3 are in the process of being infilled with fines, the accumulated sediment tending to reduce channel depth. Secondly, there is a very slight compositional difference between the stream channels. Stream channel 3 has a large area of abandoned channels in gravel beds, which are noticeably

deficient in the easily erodible sand-silt accumulations prevalent in stream channels 1 and 2.

The sinuosity and transient-braiding index values (Brice, 1964, pp. 25-29) are shown in Table 2. The sinuosity indices are comparable with the values suggested for braided rivers (Leopold, *et al.*, 1964, p. 281). There is only minor within- and between-stream channel variation. However, meandering reaches are also present locally, this feature being not uncommon in other braided tracts (Fahnestock, 1963).

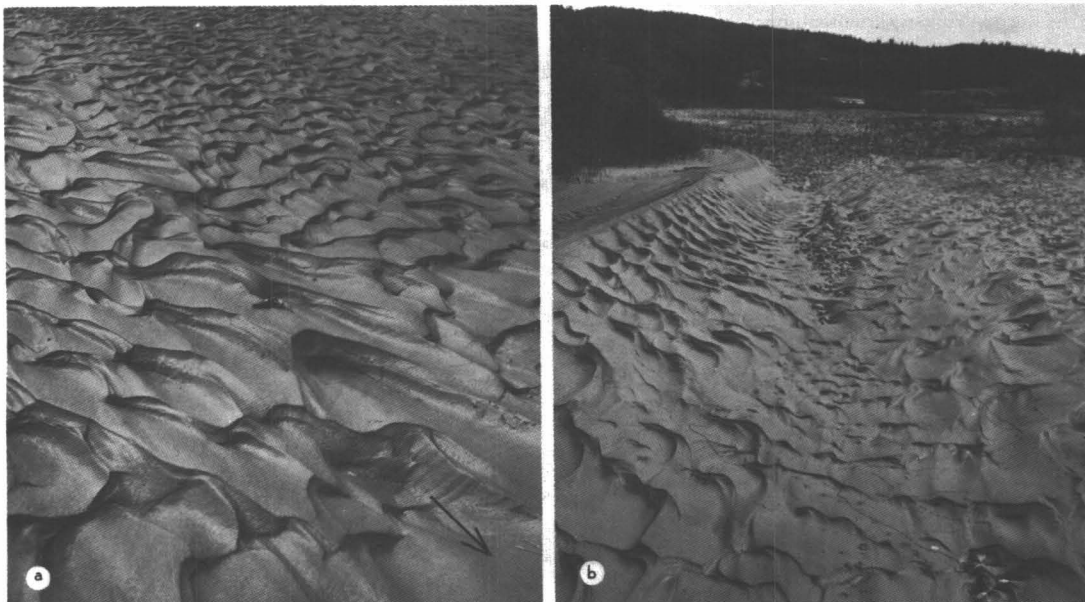


Fig. 10. (a) Passage from small-scale ripples to large-scale ripples with increase in channel depth (arrow indicates channel axis; keys give scale). (b) Lateral change from small-scale ripples on the channel floor to large-scale ripples on the channel side, corresponding to lateral increase in thickness of sand cover.



Fig. 11. Ellipsoidal scours preserved in a longitudinal sand bar.

Scour hollows. Scour hollows may be considered structures intermediate to the ellipsoidal scours and small-scale channels. The scour hollows are of short lateral extent (order of feet) and elliptical in outline with elongation parallel to the local current flow. Unlike the ellipsoidal scours they are rather deep (generally greater than 12 in.) and are erosional into more than one lithotype. Indeed, the scour hollow generally exposes a succession of lithotypes.

Migratory bar-avalanche face. This is a topography rather than a simple structure, with a horizontal to sub-horizontal bar, avalanche face, and downstream depression (Fig. 16). All three features migrate in unison.

The bar surface is covered by abundant small-scale ripples of varying type. Avalanche faces vary in vertical height (few inches to 2.5 ft), inclination (10° to 30°), and orientation with respect to channel sides (perpendicular or oblique). The downstream scour is floored by curved ripple sets, and surrounded by flatter areas of higher elevation with abundant sinuous ripples.

FACIES

Seven facies types and one facies variant have been recognized within the study area on the basis of grain size, sedimentary structures, and flora. The main characteristics of each facies type are shown in Table 3.

Facies Characteristics

Facies A. This facies is made up of laminated silty clay, almost invariably with faint color banding of alternating gray and reddish-brown layers. Thin, impersistent carbonaceous streaks are common. Sediments of facies A are found in low-lying areas which are commonly waterlogged. The flora is hydrophytic, with an abundance of *Equisetum* sp., *Eriophorum medium*, *Triglochin palustris*, and other unidentified sedges. The facies is exclusive to stream channels 3 and 4, and is preserved in abandoned channels subject to occasional flooding (Fig. 17a).

TABLE 3. Sedimentary Facies and their Sedimentary Characteristics

Facies	Grain Size						Sedimentary Structures																	Flora							
	Pebbles	Coarse Sand	Sand	Silt	Silty Clay	Clay	Lithological Banding	Parallel Lamination	Lenticular Lamination	Small-Scale X-L	Large-Scale X-L	Graded Bedding	Imbrication	Small-Scale Ripples	Large-Scale Ripples	Avalanche Faces	Ellipsoidal Scours	Current Crescents	Grain Lineation	Plant Lineation	Desiccation Cracks	Silt Volcanoes	Scour Hollows	Channels	Tracks, Trails	Bioturbation	Color Banding	Bedded Organics	Population Density	Plants present with relative abundances	
A				O	A	C	C	O													O					A	C	C	iv	13, 15, 16, (A) 16, (C) 1, 2, (R)	
B		R	C	A	A	R	A	C	C	R		R													C	C	C	O	iii	1, 16, (A) 11, 13, 15, (C) 9, 11, 14, 15, (R)	
C1		R	A	A	O		A		R	A-C		R		A-C	R		C	R	C						O	O		R	ii	1, 7, 11, 12, (A) 2, 3, 8, (C) 5, 7, 8, 9, 10, 14, (R)	
C2			C	A	A	R								C-O								A									
D		O	A	A					A-C	A-C				A-C	R	O															
E		O	A	C					O	C				C		O														i	
F	C	C	C	C	C		A-C	O	C	O	C	R	O	C		O		A	R	R	O			C	C	O	O	R	R	ii-i	As facies C1. 13, 15 (O)
G	A	A	C	C	O		C	R	O		O	R	O										R	O					i	As facies C1	

A = Abundant, C = Common, O = Occasional, R = Rare. Population density; iv = high, iii = moderate, ii = low, and i = sparse. Numbers in the column under flora refer to the following plants: 1. *Salix* spp., 2. *Deschampsia* sp., 3. *Epilobium latifolium*, 4. *Crepis elegans*, 5. *Populus balsamifera*, 6. *Oxytropis gracilis*, 7. *Potentilla fruticosa*, 8. *Aster yukonensis*, 9. *Primula* sp., 10. *Elaeagnus commutata*, 11. *Hedysarum mackenzii*, 12. *Astragalus yukonis*, 13. *Triglochin palustris*, 14. *Parnassia palustris*, 15. *Eriophorum medium*, 16. *Equisetum* sp.

TABLE 4. Small-Scale Current Directional Data at Various Hierarchical Orders

Hierarchical Order	Station Vector Means	Vector Mean of Particular Order	\bar{x} Average Variation About Order V.M.
Within-Bar	Bar 1 045, 015, 015, 119, 050	043 ($<10^{-10}$)	28°
	Bar 2 052, 015, 108, 015, 065	060 ($<10^{-10}$)	29°
Within-Stream Channel	Stream Channel 1 066, 111, 017, 021, 041, 019, 350, 338, 320, 333, 330	009 ($<10^{-20}$)	36°
	Stream Channel 2 302, 300, 346, 306, 323, 322, 292, 358, 028, 022, 358, 308, 347, 333, 358, 294, 351, 351, 350, 297, 358, 014, 276, 232, 351	330 ($<10^{-20}$)	30°
	Stream Channel 3 332, 356, 012, 318, 337, 294, 330, 309, 320, 345, 002, 031, 343, 326, 336, 281, 260, 340, 340, 308, 355, 343, 034, 343, 348, 249, 321, 023, 331, 330	333 ($<10^{-20}$)	24°
Between-Stream Channel (Composite Stream Channel)	009, 330, 333	338 ($<10^{-20}$)	15°

TABLE 5. Current Directional Data of First and Second to Third-Order Channels

Stream Channel and Location	Range of Channel Orientations (Maximum Values, degrees)		Maximum Variation from Trend of Composite Stream Channel (degrees)		Average Width of Stream Channel Section (Feet)
	1st Order	2nd-3rd Order	1st Order	2nd-3rd Order	
1A	92	88	90E	65E	2100
1B	40	105	52E	58W	1887
1C	52	60	23W	42W	1312
1D	34	20	44E	20E	975
1E	90	140	45E/W	70E/W	1910
1F	64	122	37E	75E	2060
Max. range 1A-1F	134	146	90E	70E/W	
Av. range S.C. 1	60	89			
2F	168	84	95W	56W	2585
3B	82	77	91W	63W	3000
3C	117	103	78W	63W	5250
3D	82	87	80W	60W	4280
3E	130	105	70E	60W	6390
3F	108	121	56W	65E	6125
Max. range 3B-3F	161	128	91W	65E	
Av. range S.C. 3	104	98			

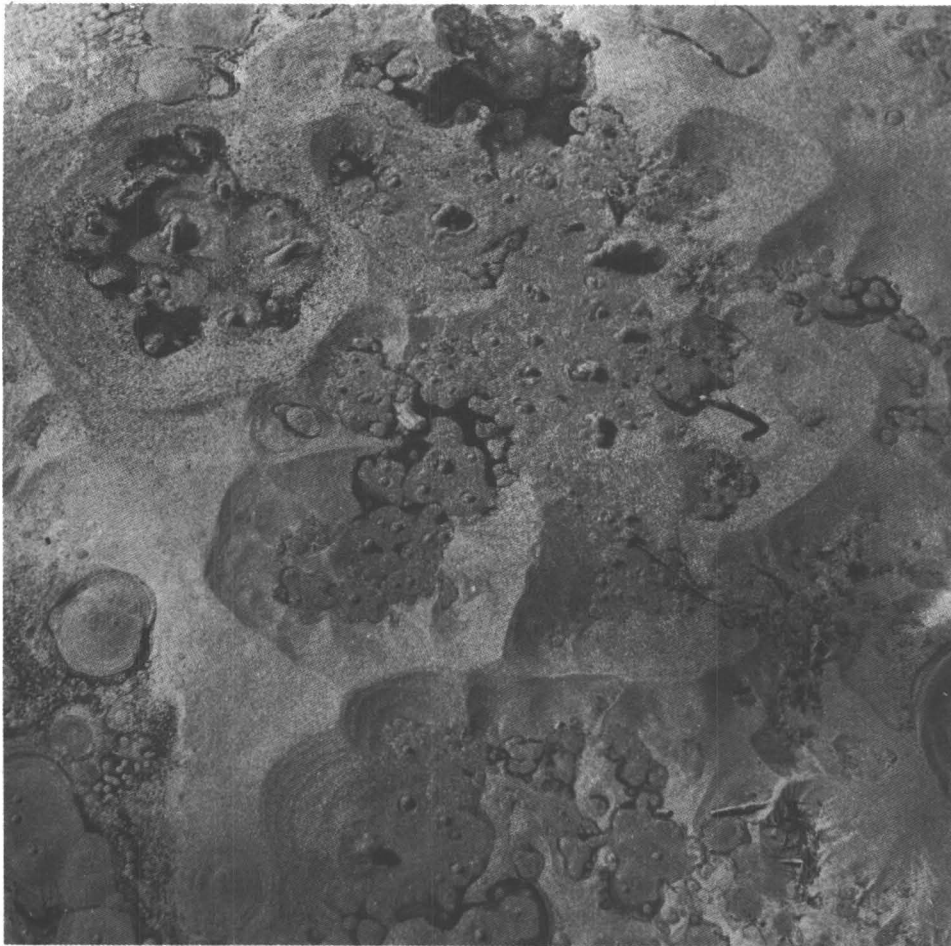


Fig. 12. Active subaqueous silt volcanoes. The area shown in the photograph is about 2 ft².

Facies B. The sediments of facies B (Fig. 17b) are banded sands, silts, and silty clays with many features in common with facies A, such as color banding and carbonaceous streaks. Banding is evident in the core shown in Figure 17b. The main differences are the overall increase in grain size, lithological banding as distinct from lamination, and a reduced plant population, of which *Equisetum* sp and *Salix* spp are abundant. Facies B is found only in stream channels 2 and 3, on the upper surface of lateral longitudinal bars and point bars.

Facies C1. This facies (Fig. 17c) is essentially made up of banded sands and silts. In many instances the contact between the lithotypes is sharp and mildly erosional. In cross section the sands appear to be massive, whereas the silts are ripple-laminated. Grain-size segregation of silt on the lee-slopes of ripples is not uncommon. The upper surface of facies C1 is generally covered with abundant small-scale ripples. Shallow ellipsoidal scours backed by migratory micro-bars and low avalanche faces (Harms and Fahnestock, 1965, Pl. 2, Fig. 2, p.111) are also common (Fig. 11). Where it has time to develop, the vegetation is commonly thick, with *Salix* spp, *Deschampsia* sp, and the vetches *Hedysarum mackenzii* and *Astragalus*

yukonis abundant. Facies C1 forms bars on stream channels 1, 2, and 3, but on the former two vegetation is sparse or absent. Some recently abandoned channels on stream channel 3 are floored by facies C1.

Facies C2. Facies C2 is a predominantly silty variant of C1 having a "quick" or thixotropic property, which is the diagnostic feature (Fig. 17d). The silt is commonly covered by a thin layer of plastic mud, which is sometimes disturbed by innumerable silt volcanoes (Fig. 12). The facies lacks a plant cover, but it is not clear whether the high water content and thixotropic nature of the sediment inhibits plant growth, or whether plants stabilize and dehydrate the sediment. The facies is confined to stream channels 1 and 2.

Facies D. Facies D is almost exclusively composed of sand, with abundant small-scale and large-scale cross-stratification (Fig. 18a). The upper surface bears abundant small-scale ripples and a few large-scale ripples. More common than the latter are avalanche faces orientated perpendicular or oblique to the channel trend. The avalanche faces are commonly present in groups, imparting a terraced morphology to the upper surface. The vegetation on abandoned bars is similar to that growing on facies C1.



Fig. 13. Apex of longitudinal bar with cross-cutting channels forming terraces.

Facies D is synonymous with the migratory sand bar, and is common in stream channels 1, 2, and 3.

Facies E. The sediment of facies E is unique in that it is produced by wind transportation. It is predominantly unvegetated sand, and forms a very small proportion of the sediment within the river tract studied. The facies is present on the more elevated areas of stream channel 3, where abandoned sandy bars and channels are exposed to the prevailing downvalley wind from the St. Elias Mountains.

Facies F. Facies F is a complex association of lithotypes ranging from gravel to silty clay (Fig. 18b). Vertical and lateral textural changes are apparent over intervals of inches or feet. The various lithotypes commonly occur in thin impersistent units, and the association is best regarded as one facies, rather than a complex mixture of several. Cross sections reveal very shallow channels in which the fill lithologies include cross-stratified pebbly sand, lenticular pebble-sand bodies, "massive" or rippled sand, and laminated silt and clay. Figure 19 is a three-dimensional model of the spatial lithological relationships observed in this facies. The surface of facies F reflects the

variability of the cross section, with an irregular topography of low channels and bars covered by poorly defined areas of pebbles, sand, and silty clay. The plant cover is similar to that of facies C1, namely the vetch-willow association (including *Salix* spp, *Hedysarum mackenzii* and *Astragalus yukonis*), except that it is less abundant, probably because of the gravel content of the sediment and its consequent rapid drainage.

Facies G. This facies is composed of gravel with occasional thin and impersistent layers of sand and silty clay (Fig. 20). The matrix of the gravel is commonly coarse- to medium-grained sand. The presence or absence of internal structure appears to be related to the pebble: sand ratio. When the ratio is high the facies lacks banding or stratification, whereas when the ratio is low (transitional to facies F) lithological banding, cross-stratification, and small-scale channels are apparent. The vegetation is similar to that of facies F, but it is again less abundant, especially on the tops of the bars which are the characteristic topography of this facies. A noticeable feature is the preferential growth of willows along the break in slope between the tops and sides of the bars (Fig. 17a).



Fig. 14. Terraces on the surface of a longitudinal bar.

Facies G is abundant in stream channels 1, 2, and 3.

Facies Relationships

The facies relationships are summarized by Figure 21 in which line diagrams (see de Raaf, *et al.*, 1965, p. 41, Fig. 22) outline the simple and complex vertical relationships, and gradational lateral relationships.

The simple vertical relationships represent the fill lithologies of individual channels, and are characterized by an upward decrease in grain size. The contacts between different facies within such a succession are commonly gradational and depositional.

More complex vertical relationships are found in cross sections which include more than one contiguous channel (Fig. 21). The contact relationships may be summarized as follows: facies G is always erosional; facies F is predom-

inantly erosional but in some cases depositional; facies D, C, B, and A are always depositional. As the cross-sectional area is increased, the relationships displayed approximate those of the composite stream channel. The gradational facies relationships (Fig. 21) give some indication of the within-channel variability of facies units in a horizontal trace. The gradation may occur over a distance varying from feet to tens of feet; in the former case the transition is commonly one of interfingering facies types, and in the latter there is overlap of one facies on another.

Figure 22 illustrates vertical and lateral facies relationships in the decadent channel. The channel is approximately 180 ft wide, and is partly occupied by a small, slowly flowing stream. On the surface of the lateral bar there is a gradational facies change toward the stream, involving an increase in grain size and a reduction in the abundance of plants. Four facies may be distinguished

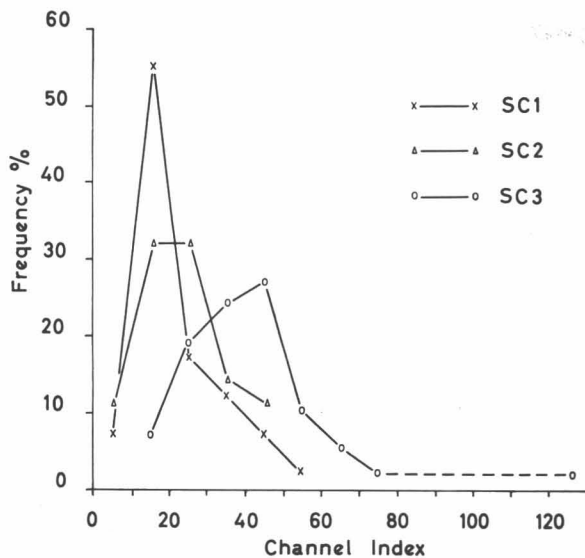


Fig. 15. Frequency plots of channel index in stream channels (SC) 1, 2, and 3.

in cross section and on the bar surface. Individual facies tend to overlap with boundaries noticeably discordant to the channel floor (as defined by the upper limit of facies G).

In Figure 22, the water level at flood stage reaches the contact between facies G and facies A, B. Flow remains within the lower regime, and ripples migrate on facies C1 and to a lesser extent on the lower level of facies B. There is little or no bed movement in facies A. As water level falls, a layer of clay and fine silt is deposited over the channel surface. However, this fine layer is removed during the following flood stage in parts of the channel immediately adjacent to the present stream. The net result is a gradual accretion of clay, silt, and sand over the greater part of the channel floor. As the regimen of the stream becomes less active there appears to be a corresponding migration of facies inward from the margins of the channel.

DIRECTIONAL CURRENT DATA

A detailed study of current directions and channel orientations was undertaken to determine:

- (1) The type of vector distributions present in a braided river
- (2) The variation of current directional data at various hierarchical orders
- (3) The relationship between the orientation of the composite stream channel (Donjek River) and the overall range of current directional data
- (4) The relationship between the maximum range of orientation of small-scale channels and stream channel width
- (5) A comparison of the directional patterns obtained from small-scale and large-scale current structures

The structures used in the study are small-scale ripples and current crescents (order 4, Allen, 1966, p. 185), and first-, second-, and third-order channels (order 1, Allen, 1966, p. 185). Measurements were taken along the "a" reference axis parallel to current flow. In some instances, particularly straight and sinuous ripples, the current direction was verified by a close study of the cross-sectional area. A minimum of ten readings was taken at each measuring station; the statistics are summarized in Appendix 2. The directional data were rationalized following Curray (1956, pp. 117-131) with a computation of vector mean, vector magnitude in terms of percent, and probability value, the latter obtained by using the Rayleigh test of significance (Curray, 1956, Fig. 4).

Small-Scale Structures

Method of analysis. The methods employed at various hierarchical orders in the directional analysis are outlined below.

(1) Within-bar order. Initially, two first order sand bars were selected in the field. On each bar five stations were selected and individual "a" axis measurements were made.

(2) Within-stream channel order. Traverses across stream channels 1, 2, and 3 were used as reference lines. Any population of directional structures numbering at least ten which happened to fall on the traverse lines was designated a station. The vector distribution for each stream channel is the combination of measurements obtained from stations within that channel.

(3) Between-stream channel order. This is a comparison of the vector distributions obtained for each stream channel.

(4) Composite stream channel order. A single value (grand vector mean) derived from the plotting of the small-scale directional current data obtained from the Donjek River (660 readings).

Results. The results of the directional analysis are presented in Appendix 2, Table 4, and Figure 23. This information is summarized below.

The "a" axis orientation of individual structures at each measuring station shows little variation from the vector mean. The significance values are consistently 10^{-3} and 10^{-4} (one exception at 10^{-2}), Appendix 2. The surface area covered by each measuring station is generally less than 150 ft².

The within-bar variation of directional data can be considered small (Table 4). The order vector means of both bars have high significance values (10^{-10}). Further, the range of station vector means encompasses an arc of only 100°.

The within-stream channel variation of vector means is greater than that of the within-bar order (Table 4). However, the means have a range of less than 180°. Again, the significance of the order vector means is very high (10^{-20}).



Fig. 16. Horizontal bar-avalanche face-erosional hollow topography.

At between-stream channel order the range of vector means is small, and is contained within an arc of 39° (Table 4). The small-scale directional current data for each stream channel are plotted as current rose diagrams in Figure 23. The rose diagrams are unidirectional, with 70% of the readings occurring within a 90° quadrant. The three vector means closely approximate the orientation of their respective stream channels.

The grand vector mean for the composite stream channel is 338, a deviation of 12° from the north-south trend of the principal channel.

Large-Scale Structures

Method of analysis. The orientation analysis of the channels was performed in the laboratory. An enlarged (4.8 in.: 1 mile) aerial photograph of the river tract shows very clearly the individual channel outlines in stream channels 1, 2, and 3. Unfortunately, the determination of channel orientations on level 4 (Fig. 2) was prevented by the dense vegetational cover.

The aerial photograph was subdivided into six rectangles labeled A-F. Areas of stream channels 1, 2, and

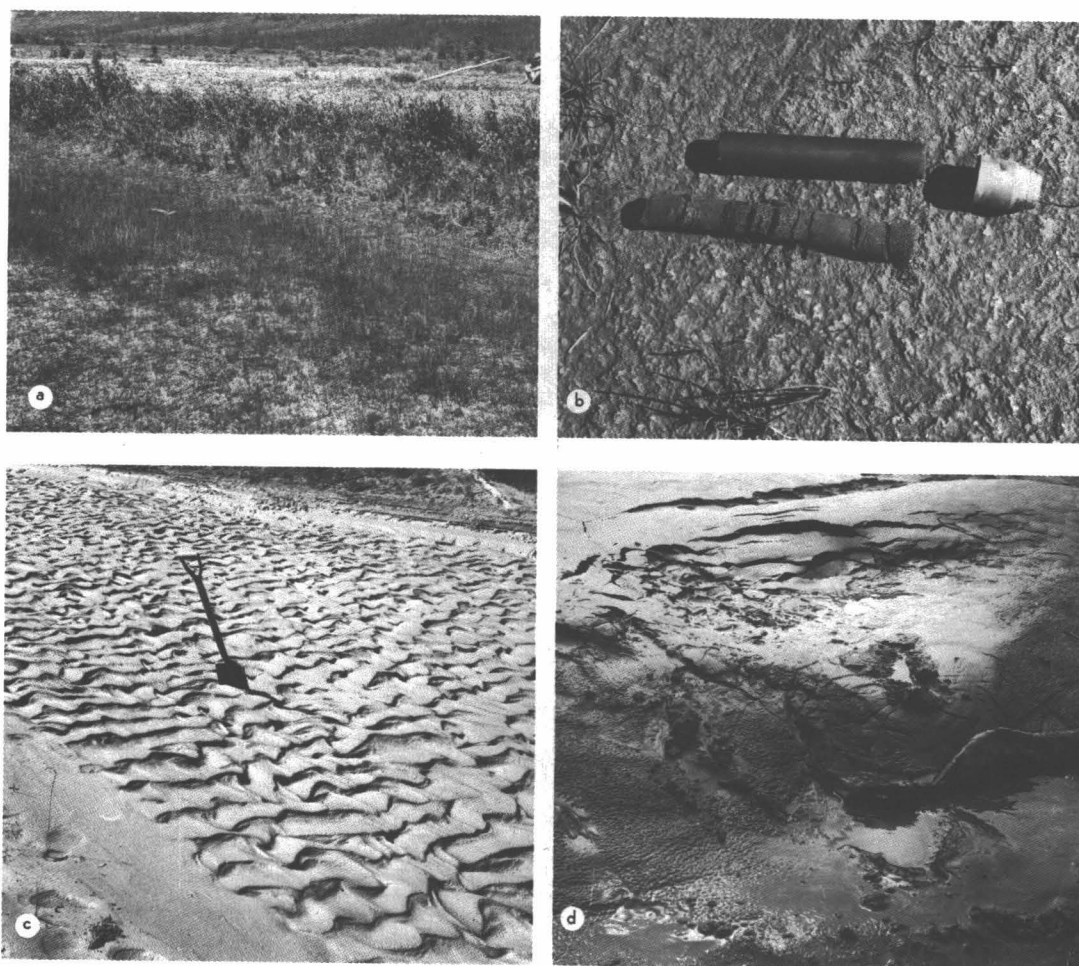


Fig. 17. Surface appearance of facies: (a) Facies A. (b) Facies B; core shows banding. (c) Facies C1. (d) Facies C2). Disturbance was caused by walking on the sediment surface; footprints can still be seen.

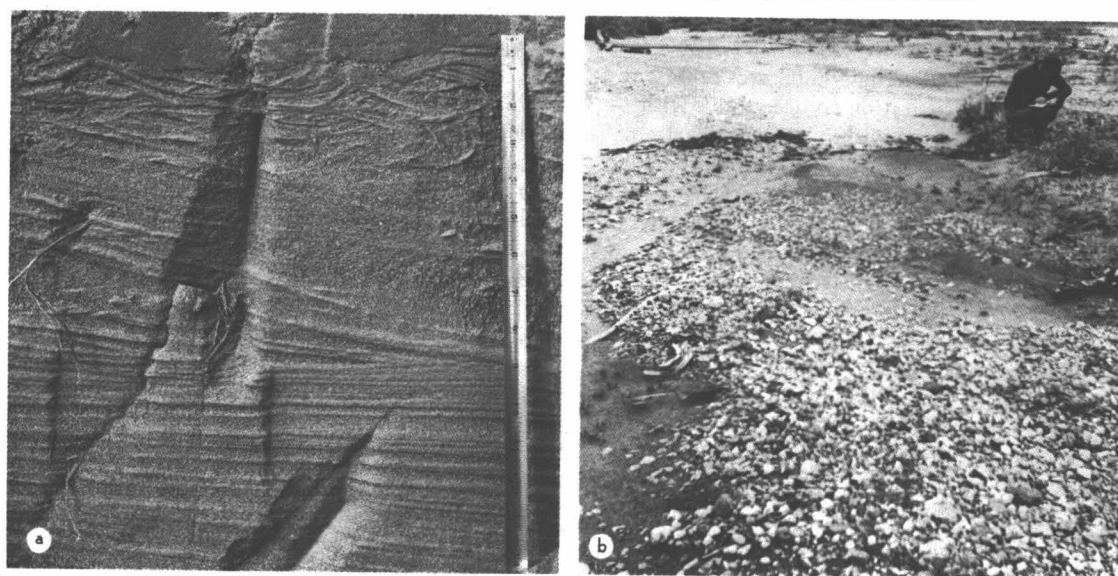


Fig. 18. (a) Cross-sectional view of facies D. (b) Surface appearance of facies F.

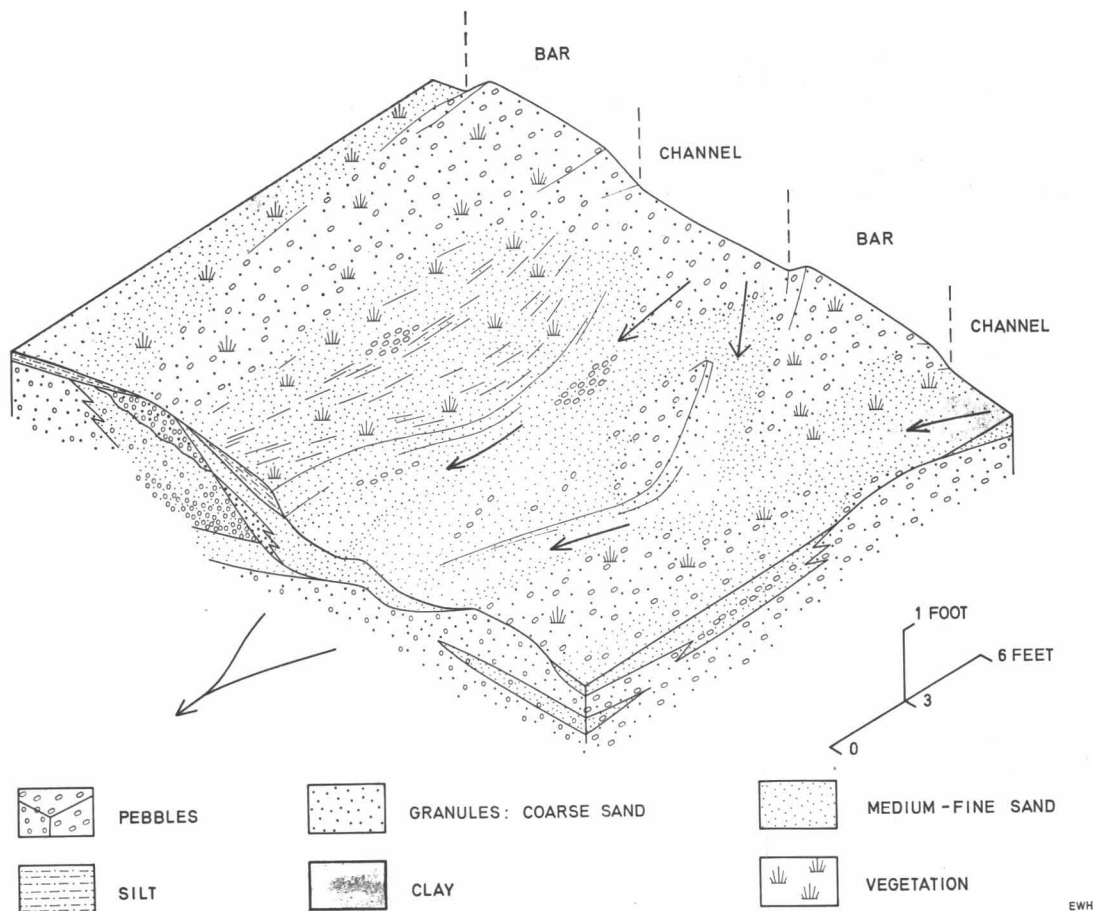


Fig. 19. Three-dimensional model illustrating the vertical and lateral variation of lithotypes in facies F. Arrows indicate direction of current flow. The different shapes of the pebble ornament are not intended to indicate preferred pebble orientation.

3 occurring within each rectangle, say F, are designated 1F, 2F, 3F; thus denoting stream channels present and position in the river tract (Fig. 24).

The channel orientations were obtained by direct tracing from the photograph. The individual arcs represent the maximum range of orientation (synonymous with maximum sinuosity) observed within a rectangle, stream channel, and composite stream channel. Measurements were made on first-order channels and second- and third-order channels (undifferentiated). The first-order channels average 210 ft in width with maximum and minimum values of 300 ft and 135 ft respectively, while the second- and third-order channels vary in width between 90 ft and 45 ft.

Results. The data obtained in the directional analysis of the channels are shown in Table 5 and Figure 24.

The within-stream channel ranges of orientation are moderate (Table 5). The average angular range varies between 60° and 104° , being higher in stream channel 3 than stream channel 1. The total angular range nowhere exceeds 180° . The larger first-order and smaller

second- to third-order channels do not show any consistent differences in the amount of angular range (sinuosity). This is apparent at within- and between-stream channel orders (Table 5).

The maximum variation of first- and second- to third-order channel orientation at different positions in the river tract and various hierarchical orders is shown in Table 5 and Figure 24. Particular emphasis is attached to the relationship of the local channel orientation and the north-south trend of the composite stream channel. Several important points may be established from Figure 24.

First, the maximum values and bisectors of the orientation arcs of the first- and second- to third-order channels have variable azimuthal angles to the trend of the composite stream. On this evidence it appears that within this hierarchical order the trend of the composite stream channel can be estimated from included channels of small as well as of large scale. Second, although more than 60% of the channels are contained within the 300-060 arc, the remaining percentage introduces a cautionary note in the number of field measurements required to

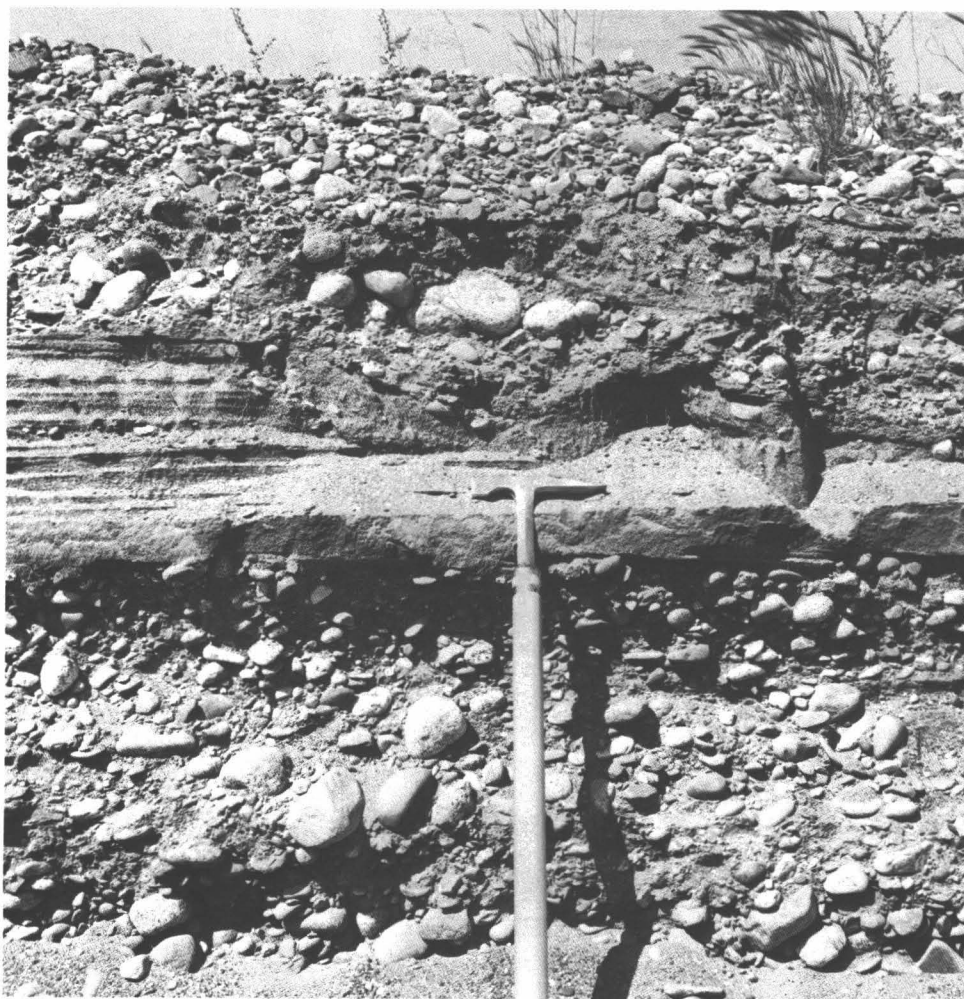


Fig. 20. Cross-sectional view of facies G. Facies G is erosional to an interbedded layer of facies D in this example. Hammerhead is 6.5 in. long.

accurately determine the trend of the principal channel. Third, in the smaller sized channels there is an increase in the range of channel orientations with successively higher hierarchical order. Fourth, the trend of stream channels 1 and 3 varies less than 30° from the trend of the composite stream.

Figure 24 suggests that there is a relationship between the angular range of orientation and stream channel width, and in Figure 25 both sets of data are plotted against each other. The curves for first-order and second- to third-order channels are remarkably similar in shape, suggesting that stream channel width as a parameter affects all types of smaller scale channel in the same fashion. The noticeable peak occurring at widths of 2000 ft and 2500 ft could well indicate an optimum relationship between the maximum range of channel orientation and stream channel width. Excluding the peak on the left-hand side of the graph the overall relationship appears to be a linear increase.

In summary, it is convenient to group and compare the directional current data for small-scale and large-scale structures (Fig. 26). The grand vector mean of small-scale structures is 338 and the bisectors of the two channel arcs are 355 and 001 respectively. The bisectors of the channel distributions are nearest to the north-south trend of the composite stream channel. Nevertheless, in this case, both large-scale and small-scale current directional data give a very good approximation of the orientation of the composite stream channel.

BRAIDED RIVER MODEL

Two types of model are considered; a three-dimensional model of the principal physical features, and a two-dimensional model of the directional current data.

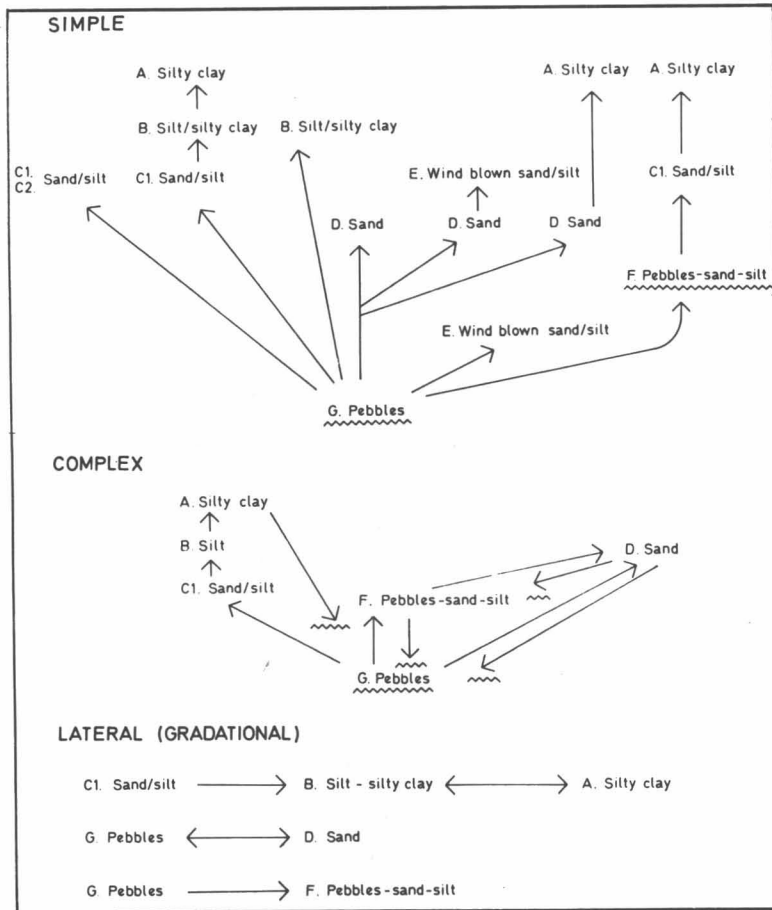


Fig. 21. Vertical (simple and complex) and lateral (gradational) facies relationships. Undulating lines indicate erosional contacts.

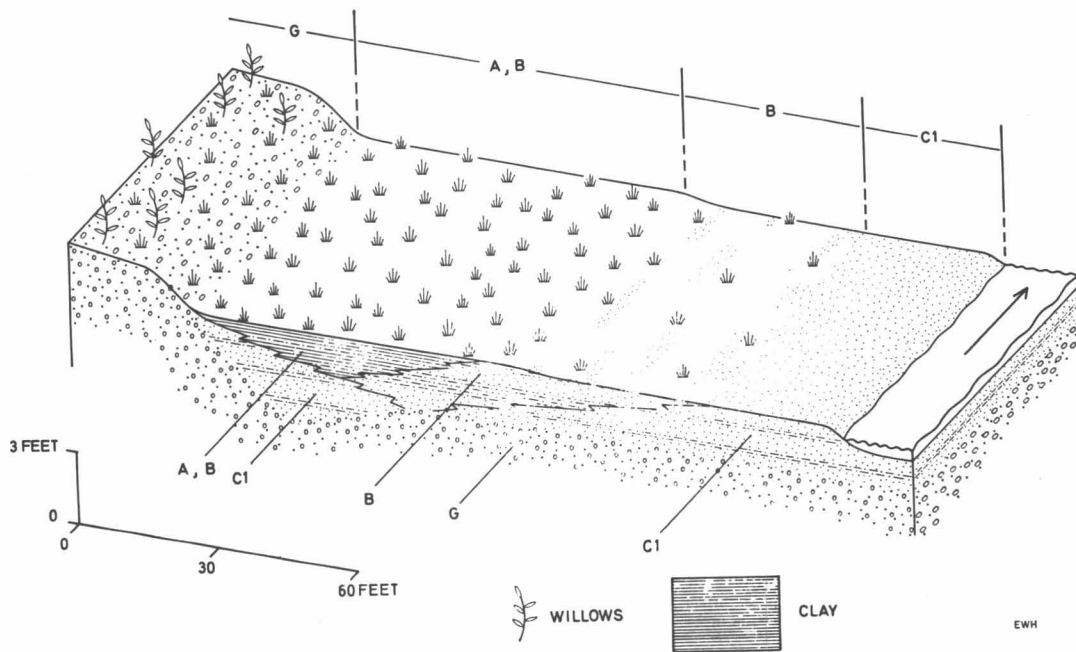


Fig. 22. Three-dimensional model of facies relationships in a decadent channel. Arrow indicates direction of current flow; ornament as for Figure 19, and as indicated here.

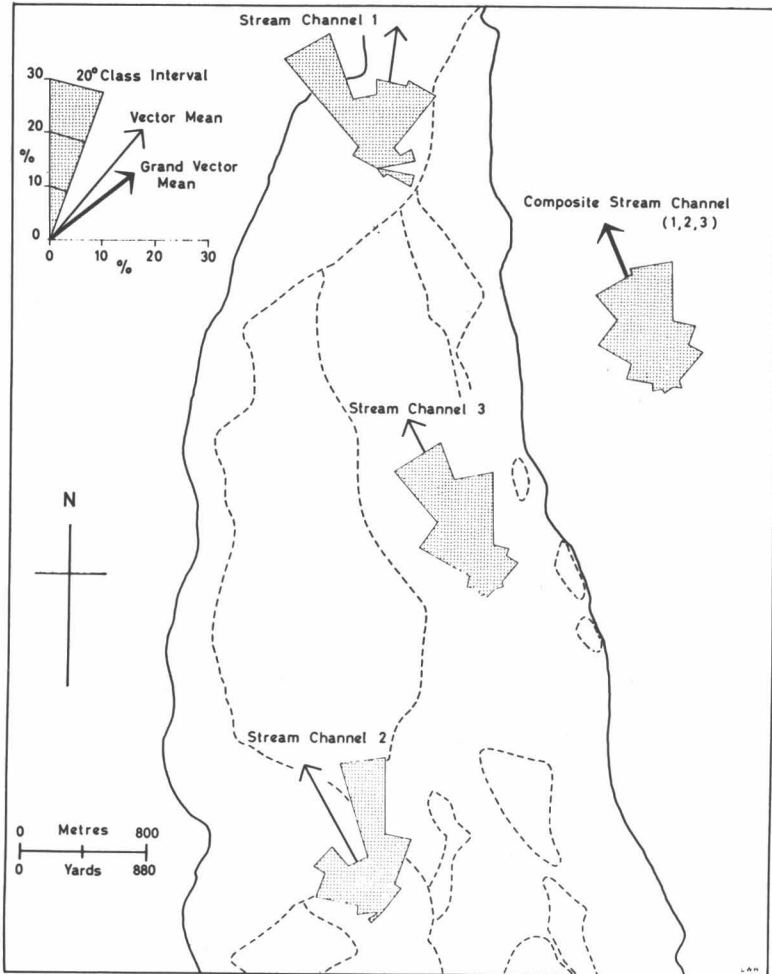


Fig. 23. Rose diagrams of small-scale directional current data for stream channel and composite stream channel orders.

Physiographic Model

The principal geomorphological features are channels (and levels), bars, and islands (Fig. 27).

Channels vary considerably in size, and five hierarchical orders are present: composite stream channel (Donjek River), stream channel, first-, second-, and third-order channels.

The composite stream channel is straight with an average width of one mile. The depth to the base of the channel has not been determined and consequently the total thickness of alluvial fill is not known.

The stream channels are synonymous with Levels 1, 2, and 3. The stream channels and Level 4 are distinguishable on the basis of elevation on the valley floor, total volume of water and maximum discharge, relative age, density and type of plant cover, and surface topography index.

The floor of the stream channels is characterized by a braided network of first-, second-, and third-order channels. These smaller channels—width dimensions in feet, tens of feet, and occasionally hundreds of feet—are generally of low sinuosity, the sinuosity index rang-

ing from 1.02 to 1.34. A few examples of highly sinuous or meandering courses are seen at low discharge in stream channels 1 and 2, and in small, slowly flowing streams with semi-permanent channels in stream channel 3 (see Fahnestock, 1963). In profile the channels are almost invariably asymmetrical with a channel floor of variable microrelief. The lithotypes which constitute the channel fill show considerable variation in type and arrangement. Nevertheless, the basic fill succession is fining-upward. The channel index averages 29.0 and ranges from 4.7 to 129.0, with minor intra-channel variation, but major interstream channel variation. This latter feature is in part the result of the progressive infilling of abandoned and decadent channels in stream channel 3. In cross section the channels are mutually erosional, occurring in a very high frequency association.

Three types of bar are present; namely longitudinal, transverse, and point bar. Longitudinal bars are easily the most abundant (greater than 95%) and occur as lateral bars along channel sides and bars in mid-channel areas. The longitudinal bars are subdivided into three hierarchical orders based on the anastomosing pattern of small-scale channels on the floor of the stream channel and on the surface of emergent bars.

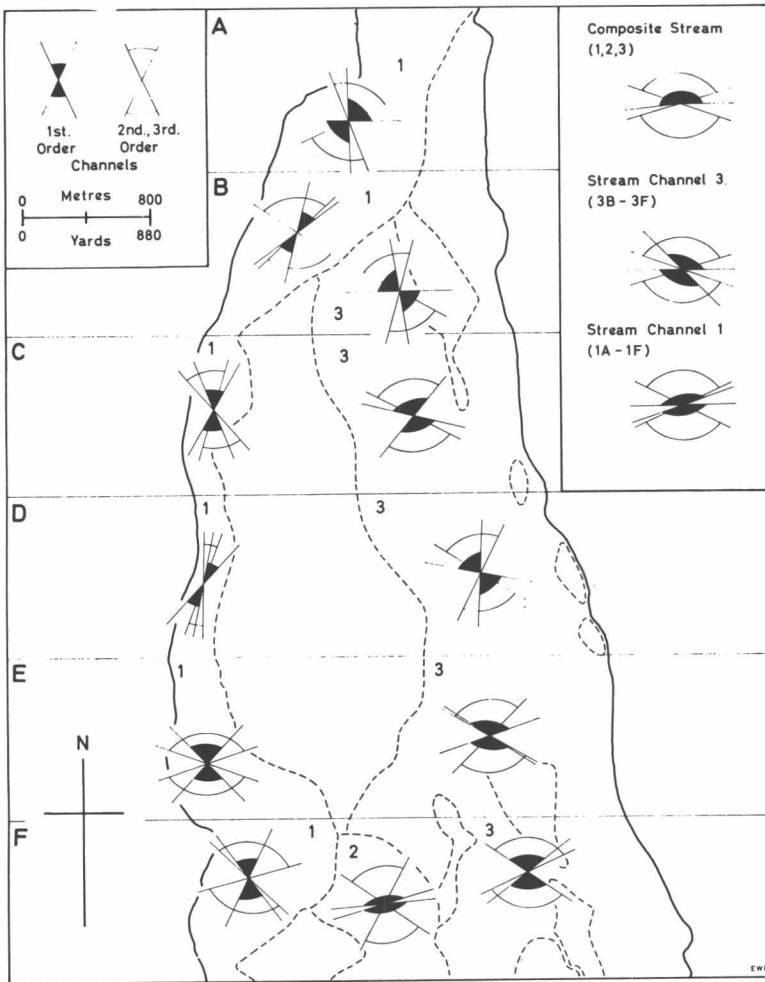


Fig. 24. Maximum ranges of first, and second- to third-order channel orientations at within-stream channel, stream channel, and composite stream channel orders.

The longitudinal bars are invariably elongate downstream but vary in shape about a basic rhombic or elliptical outline. Surface area is a variable parameter with maximum length and width dimensions varying from feet to hundreds of feet. The surface of the bar

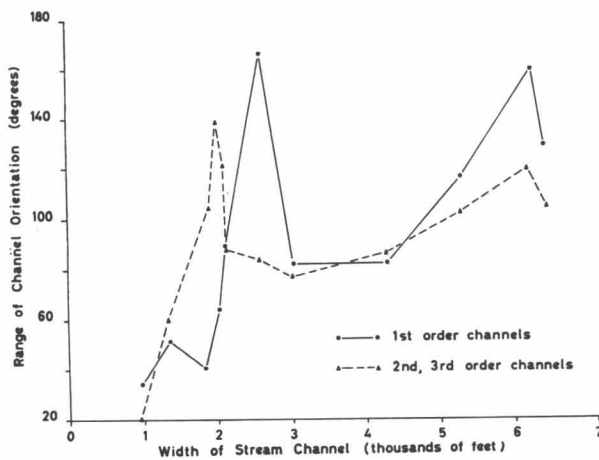


Fig. 25. Maximum range of first- and second- to third-order channel orientations plotted against stream channel width.

is never smooth, the bed roughness including a very wide range of large-scale and small-scale structures. The longitudinal bars are most commonly composed of gravel, sand, and silt-mud admixtures, with varying proportions of constituent lithotypes.

Islands are the most permanent features on the valley floor. They are also the areas of highest elevation, the upper surface corresponding to Level 4. The islands are characterized by a dense vegetational cover, which masks the original topographic roughness. The islands are elongate downstream, this feature being accentuated by subsequent erosional activity (including present day). In the few cross sections observed the islands reveal channel relationships similar to those on lower levels.

Considered as a whole, the three-dimensional model shows a valley fill eroded by three vertically distinct stream channels, each stream channel containing a braided network of smaller scale channels. In cross section the channels are mutually erosional at whatever hierarchical order is taken.

With respect to the chronology of the alluvial succession the oldest deposits occur at the highest elevation (Level 4), with progressively younger deposits at successively lower elevations.

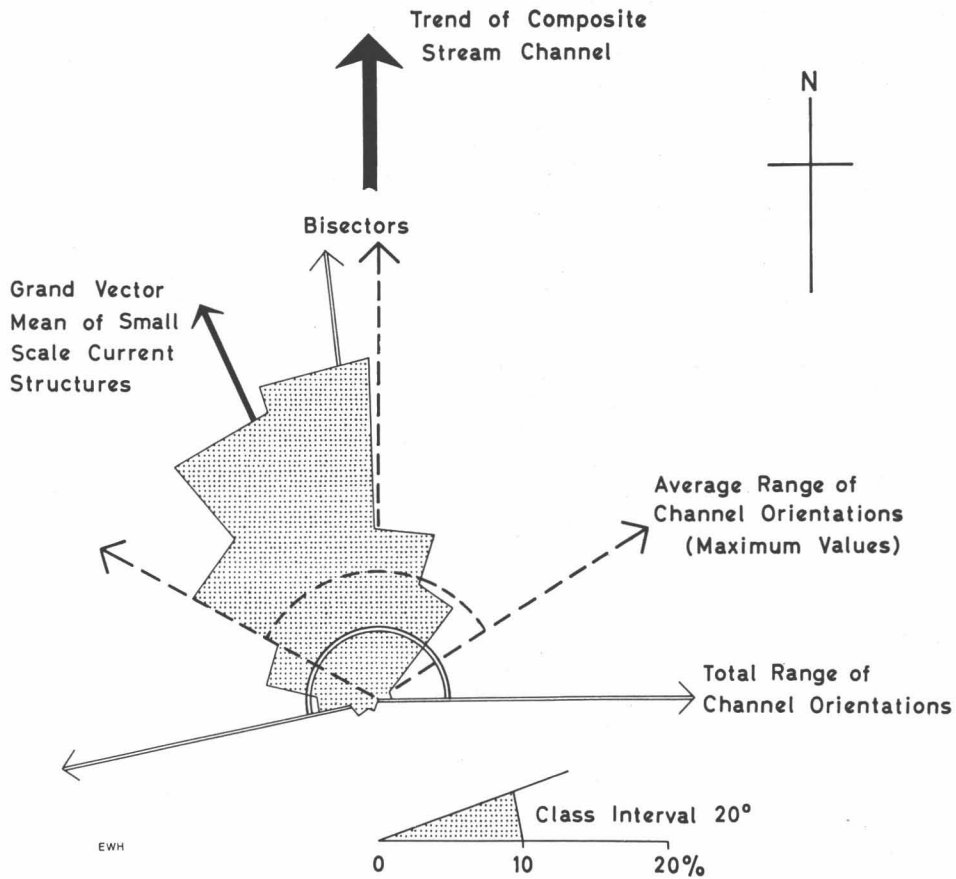


Fig. 26. Orientation diagram including the directional current data of small-scale and large-scale structures, and the trend of the composite stream channel.

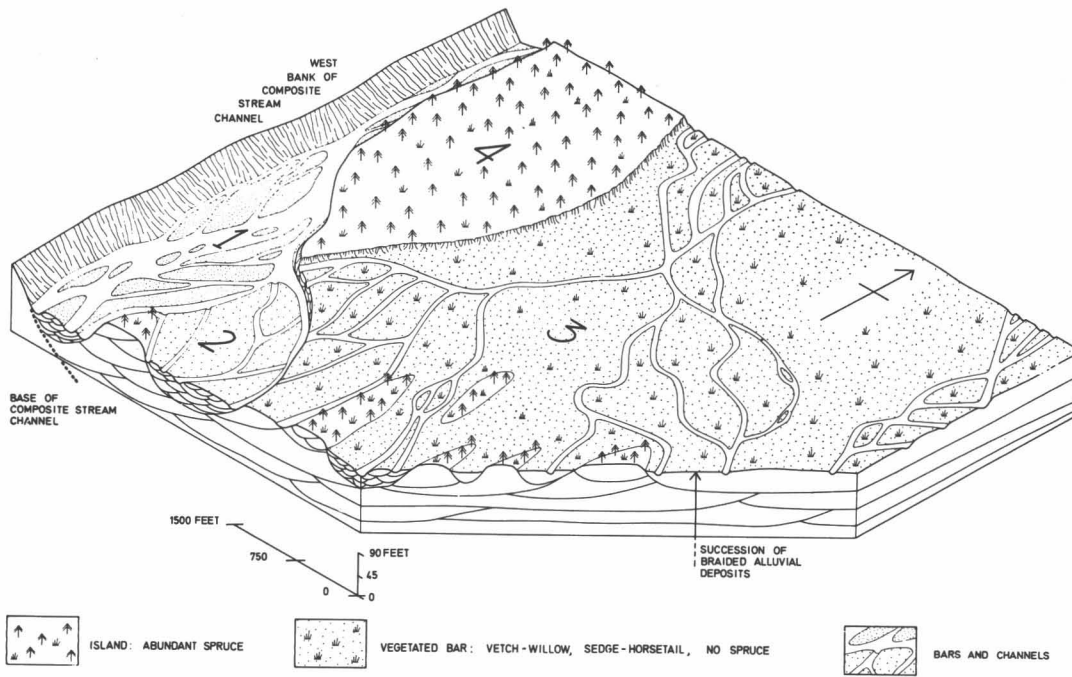


Fig. 27. Three-dimensional model of the principal features in the Donjek study area. Numbers 1, 2, 3, and 4 refer to the respective stream channels and/or levels. Vertical scale is exaggerated. Indistinct channels on level 4 are omitted.


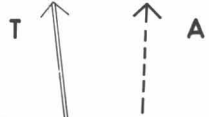
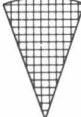
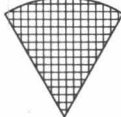
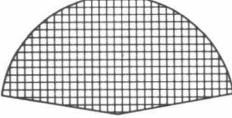
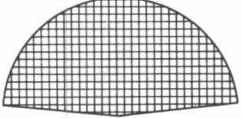
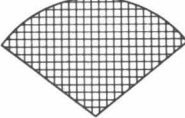
HIERARCHICAL ORDER	STRUCTURES	
	SMALL SCALE STRUCTURES	LARGE SCALE STRUCTURES
COMPOSITE STREAM CHANNEL		
BETWEEN-STREAM CHANNEL		
WITHIN-STREAM CHANNEL		
WITHIN-BAR		

Fig. 28. Two-dimensional model of directional current data from small-scale and large-scale structures. G.V.M. = grand vector mean, T = bisector of total angular range of channel orientation, A = bisector of average range of channel orientation (see Fig. 26). Trend of composite stream channel is north-south, parallel to page margin.

At the present time the river appears primarily to be in a period of degradation. Aggradation is localized, and all but confined to stream channel 3. The possible causes of degradation are well documented by Leopold, *et al.* (1964, pp.442-458), and the one most applicable to the Donjek is a change in hydrologic regimen. This could be brought about by a rise in total discharge subsequent to an increase in the amount of meltwater from prolonged glacial wastage, a process which is active in the area (Bostock, 1957, p. 121).

Directional Current Flow Model

The ranges of directional current data for the hierarchical orders of small-scale and large-scale structures are shown in Figure 28.

In the small-scale structures the variation at within-bar, within-stream channel, and between-stream channel orders can be considered small. The within-stream channel order shows the greatest range with an arc of 160° . Individual current vector distributions at all hierarchical orders are noticeably unidirectional and have very high significance values (Fig. 23; Appendix 2). The grand vector mean of the total small-scale current directional data closely approximates the trend of the composite stream channel (Fig. 28).

The range of channel orientation decreases with increase of hierarchical order (Fig. 28). The range of first- and second- to third-order channel orientations at the

within-stream channel level is 168° . The range of stream-channel orientation is very small (60°) and is symmetrical about the trend of the composite stream channel. The bisectors of the average and total angular range of first- and second- to third-order channels are less than 5° from the trend of the composite stream channel (Fig. 28).

In the braided stream the grand vector means of small-scale current structures and bisectors of average and total channel range (maximum values) are very accurate indicators of the orientation of the principal channel.

Acknowledgments

The authors gratefully acknowledge financial assistance from the National Research Council of Canada, and the Department of Geology, University of Ottawa. Particular thanks are due to members of the Icefield Ranges Research Project of the Arctic Institute of North America, for their help and hospitality during the field program. We also wish to thank Dr. J. Neilson for plant identification, Mr. E. W. Hearn for drafting, and Mr. A. Carrara for size analyses.

References

- Allen, J. R. L. (1963a) Asymmetrical ripple marks and the origin of water-laid cosets of cross-strata, *Liverpool Manchester Geol. J.*, 3, 187-236.
- Allen J. R. L. (1963b) The classification of cross-stratified units, with notes on their origin, *Sedimentol.*, 2, 93-114.

Allen, J. R. L. (1965) A review of the original characteristics of recent alluvial sediments, *Sedimentol.* 5, 89-191.

Allen, J. R. L. (1966) On bed forms and palaeocurrents, *Sedimentol.*, 6, 153-190.

Bostock, H. S. (1952) Geology of northwest Shakwak Valley, Yukon Territory, *Mem.* 267, Geol. Surv. Can., 54 pp.

Bostock, H. S. (1957) Yukon Territory, selected field reports of the Geological Survey of Canada 1898 to 1933, *Mem.* 284, Geol. Surv. Can., 650 pp.

Brice, J. C. (1964) Channel patterns and terraces of the Loup Rivers in Nebraska, *Prof. Paper* 422-D, U. S. Geol. Surv., 41 pp.

Curry, J. R. (1956) The analysis of two-dimensional orientation data, *J. Geol.*, 64, 117-131.

*Denton, G. H., and Stuiver, M. (1967) Late Pleistocene glacial stratigraphy and chronology, northeastern St. Elias Mountains, Yukon Territory, Canada, *Bull. Geol. Soc. Am.*, 78, 485-510.

de Raaf, J. F. M., Reading, H. G., and Walker, R. G. (1965) Cyclic sedimentation in the Lower Westphalian of North Devon, England, *Sedimentol.*, 4, 1-52.

Doeglas, D. J. (1962) The structure of sedimentary deposits of braided rivers, *Sedimentol.*, 1, 167-190.

Fahnestock, R. K. (1963) Morphology and hydrology of a glacial stream—White River, Mount Rainier, Washington, *Prof. Paper* 422-A, U.S. Geol. Surv., 70 pp.

Folk, R. L. (1968) *Petrology of Sedimentary Rocks*, Hemphill, Austin, Texas, 170 pp.

Friedman, G.M. (1967) Dynamic processes and statistical parameters compared for size frequency distribution of beach and river sands, *J. Sediment. Petrol.*, 37, 327-354.

Harms, J. C., and Fahnestock, R. K. (1965) Stratification, bed forms, and flow phenomena (with an example from the Rio Grande), in *Primary Sedimentary Structures and their Hydrodynamic Interpretation*, edited by G. V. Middleton, pp. 84-115, *Spec. Publ.* 12, Soc. Econ. Paleontol. Mineral.

Krinsley, D. B. (1965) Pleistocene geology of the south-west Yukon Territory, Canada, *J. Glaciol.*, 5, 385-397.

Leopold, L. B., Wolman, M. G., and Miller, J. P. (1964) *Fluvial Processes in Geomorphology*, Freeman, San Francisco, 522 pp.

Muller, J. E. (1967) Kluane Lake map-area, Yukon Territory (115G, 115F, E½), *Mem.* 340., Geol. Surv. Can., 137 pp.

Pasaga, R. (1957) Texture as characteristic of clastic deposition, *Bull. Am. Assoc. Petrol. Geol.*, 41, 1952-1984.

Simons, D. B., Richardson, E. V., and Albertson, M. L. (1961) Flume studies using medium sand (0.45 mm), *Water Supply Paper* 1498-A, U.S. Geol. Surv., 76 pp.

Simons, D. B., Richardson, E. V., and Nordin, C. F., Jr. (1965) Sedimentary structures generated by flow in alluvia channels, in *Primary Sedimentary Structures and their Hydrodynamic Interpretation*, edited by G. V. Middleton, pp. 34-52, *Spec. Publ.* 12, Soc. Econ. Paleontol. Mineral.

Wood, W. A. (1967) Steele Glacier surge, *Am. Alpine J.*, 15, 279-281.

*This article was reprinted in a previous volume of Icefield Ranges Research Project, Scientific Results.

APPENDIXES

I

TEXTURAL PARAMETERS OF SEDIMENT SAMPLES FROM THE DONJEK RIVER. SAMPLE NUMBERS REFER TO THE AUTHORS' COLLECTION IN THE DEPARTMENT OF GEOLOGY, UNIVERSITY OF OTTAWA.

Sample No.	M	C	σ	So _s	α_s	K _G	Sample No.	M	C	σ	So _s	α_s	K _G
F1-1	2.70	1.60	0.87	1.80	1.95	1.15	SA1	-1.90					
F1-2	1.90	0.60	0.40	0.80	-0.05	1.50	SA2	-0.27	> -3.00	2.05	2.60	5.05	1.17
F1-3	1.30	>0.0	0.65	1.30	0.35	1.16	SA3	0.80	> -3.00	2.05	2.90	4.70	0.95
F1-4	3.65	2.40	0.70	1.15	0.50	1.09	SA4	0.85	-3.00	1.00	2.50	3.30	1.85
F1-5	2.00	-0.30	1.00	2.40	0.80	1.25	SA5	1.65	-1.10	1.05	1.70	0.10	0.90
F1-6	4.10	2.60	0.80	1.40	0.40	1.27	SA6	4.55	1.10	1.90	3.30	0.85	1.22
F1-7	4.00	2.45	0.70	1.17	0.25	1.07	SA7	5.00	1.90	1.00	1.80	-0.45	1.13
F1-8	3.20	0.50	1.00	1.72	-0.10	1.10	SA8	4.20	2.00	1.20	2.20	0.70	1.20
F2-2	5.70	1.40	1.90	2.90	1.80	1.10	SB1	3.70	1.50	0.90	1.60	0.20	1.09
F3-1	4.15	0.50	1.25	2.80	0.05	1.80	SB2	> -3.00					
F4-1	0.68	-3.00	3.40	4.40	1.16	0.69	SB4	2.40	0.50	1.20	1.45	1.00	1.10
F4-2	0.80	-3.00	3.50	4.40	0.60	0.63	SB5	4.10	1.40	0.50	1.50	-0.10	2.50
F7-1	4.80	2.90	1.05	1.62	0.40	0.87	SB6	2.00	>0.00	0.80	1.40	-0.20	0.59
F7-2	5.20	3.60	0.70	1.45	0.95	1.30	SB7	5.20	1.80	2.00	2.70	1.20	0.92
Q1	2.80	1.60	0.50	0.82	-0.05	1.02	SB9	5.70	3.80	0.72	1.30	0.00	1.14
Q2	1.75	-0.50	0.80	1.30	-0.20	1.12							
Q3	3.35	2.00	0.51	0.92	0.25	1.08							

II

SUMMARY OF DIRECTIONAL CURRENT DATA FROM THE DONJEK RIVER. EACH STATION HAS TEN DIRECTIONAL MEASUREMENTS.

Vector Mean (Degrees)	Vector Magnitude (Percent)	Significance by Rayleigh Test	Vector Mean (Degrees)	Vector Magnitude (Percent)	Significance by Rayleigh Test
Stream Channel 1			Stream Channel 2—(Continued)		
066	98.5	<10 ⁻⁴	276	99.1	<10 ⁻⁴
111	98.0	<10 ⁻⁴	232	96.9	<10 ⁻⁴
017	99.0	<10 ⁻⁴	351	98.0	<10 ⁻⁴
021	98.0	<10 ⁻⁴			
041	98.1	<10 ⁻⁴	Stream Channel 3		
019	99.4	<10 ⁻⁴	332	98.7	<10 ⁻⁴
350	99.5	<10 ⁻⁴	356	99.1	<10 ⁻⁴
338	99.2	<10 ⁻⁴	012	96.3	<10 ⁻³
320	98.2	<10 ⁻⁴	318	99.5	<10 ⁻⁴
333	99.4	<10 ⁻⁴	337	98.9	<10 ⁻⁴
330	98.1	<10 ⁻⁴	294	97.7	<10 ⁻⁴
Stream Channel 2			330	99.3	<10 ⁻⁴
302	98.5	<10 ⁻⁴	309	99.5	<10 ⁻⁴
300	99.5	<10 ⁻⁴	320	99.3	<10 ⁻⁴
346	78.0	<.01	345	97.9	<10 ⁻⁴
306	99.1	<10 ⁻⁴	002	99.5	<10 ⁻⁴
323	98.7	<10 ⁻⁴	031	85.4	<10 ⁻³
322	99.1	<10 ⁻⁴	343	93.5	<10 ⁻³
292	98.6	<10 ⁻⁴	326	99.5	<10 ⁻⁴
358	98.8	<10 ⁻⁴	336	98.2	<10 ⁻⁴
028	99.2	<10 ⁻⁴	281	98.1	<10 ⁻⁴
022	97.5	<10 ⁻⁴	260	88.6	<10 ⁻³
358	99.2	<10 ⁻⁴	340	99.2	<10 ⁻⁴
308	99.2	<10 ⁻⁴	340	99.5	<10 ⁻⁴
347	99.7	<10 ⁻⁴	308	99.2	<10 ⁻⁴
333	98.1	<10 ⁻⁴	355	98.0	<10 ⁻⁴
358	99.2	<10 ⁻⁴	343	97.5	<10 ⁻⁴
294	92.4	<10 ⁻³	034	99.6	<10 ⁻⁴
351	94.5	<10 ⁻³	343	99.5	<10 ⁻⁴
351	98.0	<10 ⁻⁴	348	97.1	<10 ⁻⁴
250	99.5	<10 ⁻⁴	249	97.5	<10 ⁻⁴
297	97.3	<10 ⁻⁴	321	95.0	<10 ⁻³
358	99.2	<10 ⁻⁴	023	99.2	<10 ⁻⁴
014	99.5	<10 ⁻⁴	311	98.6	<10 ⁻⁴
			330	98.4	<10 ⁻⁴

Vegetation, Microtopography, and Depth of Active Layer on Different Exposures in Subarctic Alpine Tundra *

Larry W. Price †

ABSTRACT. Four slopes with different exposures (southeast-, southwest-, east-, and north-facing), but with similar gradients, elevations, and rock type, were studied in the Ruby Range. Vegetation was best developed on the southeast-facing slope, was successively less on east- and southwest-facing slopes, and least on the north-facing slope. Solifluction lobes were present in varying degrees, and their development largely followed that of vegetation in that they were best developed on the southeast-facing slope and least well developed on the north- and southwest-facing slopes. The vegetation occurred in sharply delineated communities across the lobes on the southeast-facing slope, and the communities repeated themselves in predictable patterns. The same communities were present on the east-facing slope, but were not as distinct. Plant cover was relatively impoverished on southwest- and north-facing slopes, where there were fewer microhabitats and where soil, moisture, and temperature conditions were not found in favorable combinations. Depth of the active layer largely corresponded to the presence of vegetation and microtopography. The active layer was shallowest and most variable on the southeast-facing slope. Plant cover, in general, was more important than exposure in determining the depth of thaw.

INTRODUCTION

It has been well established that in areas underlain by permafrost a close relationship exists between surface phenomena and depth of the active layer (Hanson, 1950; Hopkins and Sigafos, 1951; Lindsey, 1953; Hopkins, *et al.*, 1955; Bliss, 1956; Drury, 1962). Very few investigations, however, provide measurements of these relationships through space and time (Bliss, 1956; Drew, *et al.*, 1958). The present work was part of a larger study on the occurrence and development of solifluction lobes (Price, 1970) in which vegetation and depth to permafrost were analyzed to provide a general idea about environmental conditions on the different slopes.

The study area is located in the Ruby Range at $61^{\circ} 23' N$ and $138^{\circ} 13' W$, about 225 km northwest of Whitehorse (Fig. 1). Because of its latitude, continental location, and elevation of 1676-2134 m, the area has a subarctic alpine tundra environment. Local tree line occurs at approximately 1158 m. The specific study site consists of four slopes formed by the confluence of two ridges (Fig. 2). These four slopes face southeast, southwest, east, and north and have the same rock type and similar gradients and elevations. Gross environmental differences are, therefore, largely due to exposure to solar radiation and meltwater from late snow lie.

*This report has previously appeared in *Ecology*, Vol. 52, pp. 638-647 (1971), and is reprinted here with permission.

†Department of Geography, Portland State University, Portland, Oregon

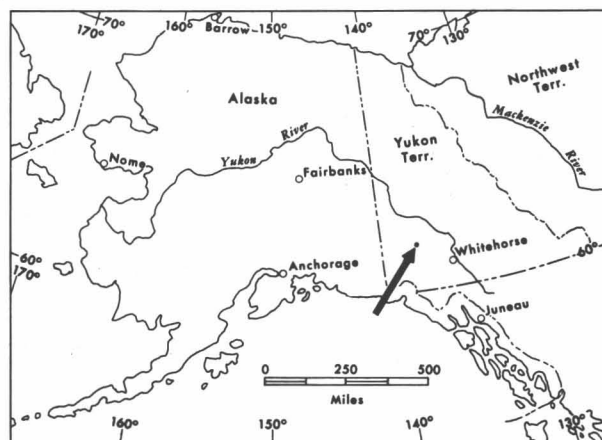


Fig. 1. Location of study area (arrow) in the Ruby Range.

METHODS

The field investigation was carried out during the summers of 1967 and 1968. Weather stations were established at an elevation of 1890 m on the southeast- and north-facing slopes (Fig. 2). Soil moisture and temperature were measured with Coleman soil-moisture and temperature cells (Coleman, 1964) at 15.2-cm intervals to a depth of 0.9 m at sites midway up each of the four slopes and monitored daily (Fig. 2). In addition, rates of mass wasting under different environmental conditions were ascertained by installing soil-movement tubes and using a strain gauge probe to measure amount of movement (Williams, 1957).

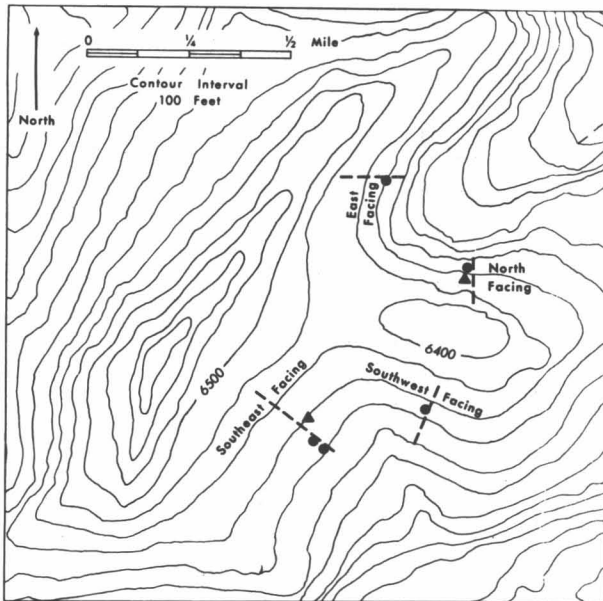


Fig. 2. Study slopes with location of weather sites (dots), and vegetation transects (dashed lines).

Most of these data will be published elsewhere and will be referred to here only to substantiate critical aspects of the study.

After plants were identified,¹ phytosociological data were gathered via a transect up each slope. Each transect was run through the soil-moisture and temperature sites (Fig. 2). Quadrats 0.1 m² (20 by 50 cm) were placed with the long axis upslope at 1.5-m intervals, although in some areas 3.0-m intervals were used.

Species were sampled for abundance, frequency, and percentage of cover, and classes were established for each measure. Abundance was described according to the following categories:

Class	Number of individuals
I—Very rare	1
II—Rare	2
III—Infrequent	3–5
IV—Abundant	6–9
V—Very abundant	10 or more

The following classes were used to describe percentage cover:

Class	Ground covered
I	Less than 5%
II	5%–25%
III	25%–50%
IV	50%–75%
V	75%–100%

¹Plants were identified by Dr. James A. Neilson and Dr. David F. Murray. Voucher specimens are in the author's private collection.

Clumps of sedge and cushion plants were counted as individuals. Identifying individuals in tundra vegetation is difficult because of their rhizomatous nature, so each stem coming from the ground was counted (Bliss, 1963). Percentage cover was determined by estimating the areal extent of each species in the quadrat. Percentage cover was also estimated for mosses and lichens, as well as for bare ground. Frequency was computed on the basis of the number of quadrats in which a species occurs in a community and put on a comparable basis with abundance and percentage cover by again establishing classes: I, 0%–10% frequency; II, 10%–25%; III, 25%–50%; IV, 50%–75%; and V, 75%–100%.

Relative abundance, relative frequency, and relative percentage cover were then calculated for all species including mosses and lichens, and were combined to give importance values. These values were divided by three to give relative importance values and are used to represent the importance of a given species in each of the sample sites at 1.5-m intervals across the slopes (Figs. 5, 8, 10, 12).

The depth of the active layer was measured at each sampling site (1.5-m intervals) along the transect to determine rate and extent of thaw under various conditions of plant cover and microtopography. A soil auger 3.2 cm in diameter by 1.5 m long was used to determine thaw depth. The encounter of frozen ground vs. rock could be told by sound. Measurements were made four times at approximately 18-day intervals. Early season measurements are more reliable than those made later in the season, since at greater depths it became increasingly difficult to tell if permafrost had been hit. Rocks were used to mark each auger site so the exact spot could be relocated, but an effort was made not to reuse the same auger hole. The depth was always measured from the surface. The only place where this presented a problem was in the tussock community. In this case, the height of the tussock above the basin was measured and added to the surface, as shown in the middle illustration in Figure 5. Basins were considered to be even with the soil surface, although where frost heave added to the height of the tussock, this may not always have been the case.

SOUTHEAST-FACING SLOPE

Vegetation

The southeast-facing slope is about 914 m wide and has an average gradient of 14°. It is essentially the alb or shelf of the glacial trough and is bound by a ridge 152–213 m high upslope. Meltwater from snow patches, which accumulate in the lee of the ridge, provides moisture through the summer, and solifluction lobes are best developed on this slope (Fig. 4). The vegetation is segregated into the microhabitats provided by the lobes, and sharply delineated communities occur and repeat themselves in predictable patterns. Four major plant

communities were recognized: late snow melt, front, tussock, and dry vegetation (Fig. 3).

Late snow melt community. This comparatively lush community consists of low herbaceous species 5.1-10.2 cm high and contains the greatest number of species of all the communities. Dominant species include *Carex microchaeta*, *Salix pseudopolaris*, and *Artemisia arctica* (Fig. 5). The late snow melt community is restricted to a narrow zone immediately below the fronts (risers) of the lobes. This is a favorable microhabitat, and many species occur in this narrow zone which normally occur farther downslope or in the valleys (Drury, 1962). Three factors account for this: (1) snow accumulates in the lee of the lobes and provides insulation against the desiccating winter wind; (2) there is ample moisture in the spring from melting snow and ground ice; and (3) the soil temperature is higher at the front than elsewhere on the slope because of the higher angle of incidence of solar radiation.

In general, the width of the late snow melt community varies with height of the lobe—the higher the front, the wider the community (Billings and Mark, 1961; Johnson and Billings, 1962). The exception is when the front becomes high enough to enable more snow to accumulate, and this has a deleterious effect on vegetation. If the snow does not melt until late summer, the vegetation does not have enough time to complete its growth cycle

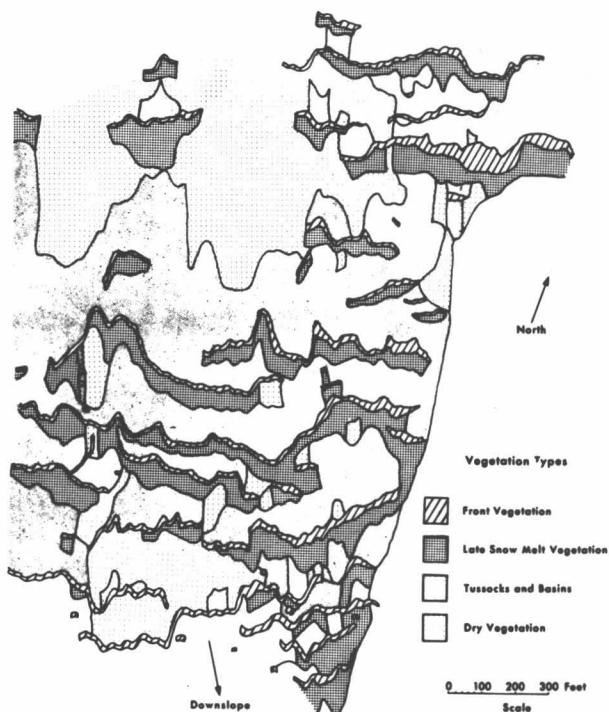


Fig. 3. Major plant communities on southeast-facing slope. Map was constructed with the use of Brunton compass and pacing.



Fig. 4. View of southeast-facing slope looking toward the southwest. Solifluction lobes are best developed on this slope, and those still having snow in their lee are 4.6-6.1 m high. Photograph was taken on July 1, 1967.

and is destroyed. Erosion occurs, and the late snow melt area below the larger lobes becomes bare and rocky.

Front community. Plant cover at the front is similar to the late snow melt community in appearance and in the dominant species (Fig. 5). However, the front vegetation occurs on a slope of 35° - 50° , whereas the late snow melt community has an angle of only 10° - 15° . The narrow strip 0.3-0.6 m wide on either side of the break in slope at the bottom of the front provides the most favorable habitat on the slope, and several species were found to occur exclusively in this zone. These are *Oxyria digyna*, *Petasites frigidus*, and *Saxifraga punctata* (Fig. 5).

Tussock community. This vegetation type occurs on the upper surface of the lobes (tread) and is the most extensive community on the slope, extending 30-91 m upslope from the front community to the late snow-melt community (Fig. 4). Tussocks occasionally extend a few inches down the front, but more often feather out 0.3-0.6 m upslope from the front. This is the sharpest transition on the slope, and the vegetation changes abruptly within this narrow zone. The reason for this change is the rapid improvement in drainage brought about by the higher angle of incidence of the sun's rays at the front, which causes a deeper active layer and more rapid melt (Fig. 5). A few feet upslope under the tussocks, permafrost remains within 0.9 m of the surface throughout the summer, and this impermeable layer maintains near-saturated conditions.

The tussock community is composed of scattered mounds 15.2-61 cm high interspersed by shallow basins, where water stands through much of the season (Raup, 1965). The body of the tussocks consists mainly of mosses (*Sphagnum* spp.). The important vascular species are *Carex microchaeta*, *Salix pseudopolaris*, and *Salix reticulata*. The basins provide a different environment

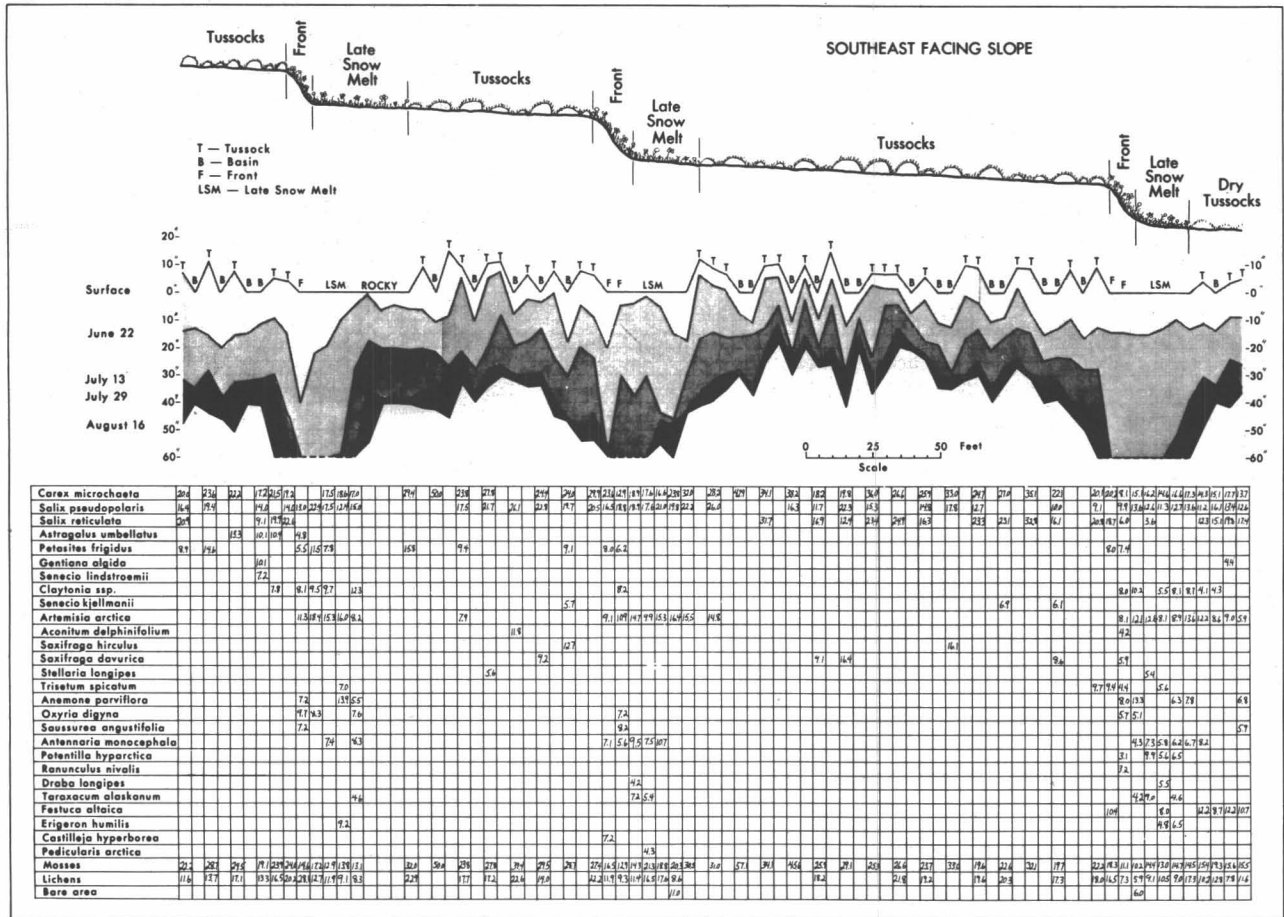


Fig. 5. Southeast-facing slope. Top of illustration shows solifluction lobes with associated plant communities across the slope. The middle illustration gives depth of active layer, and the bottom table gives vegetation composition at 1.5-m intervals across the slope. Notice that active layer is deepest at lobe fronts where it is warmer because of higher angle of incidence. The greater number of species immediately below the fronts is a reflection of the more favorable microhabitat.

from the tussocks and a greater variety of species occurs here: *Senecio kjellmannii*, *S. lindstroemii*, *Saxifraga davurica*, *Aconitum delphinifolium*, *Polemonium acutiflorum*, *Eriophorum triste*, and *Melandrium apetalum*. Many of these occur exclusively in and along the sides of the basins.

The organic layer is 15.2-20.3 cm thick under the tussock community, with an average rooting depth of 51-61 cm, but with many roots extending to 91 cm. This condition is interesting since the active layer does not thaw to this level until late summer (Fig. 5). When the roots hit a flat-lying rock, they often "ball up" on the surface of the rock, but no such phenomenon was observed at permafrost level.

Dry vegetation community. Dry vegetation occurs sporadically on the southeast-facing slope in connection with well-drained rocky sites (Fig. 3). This community type consists of small tussocks 5.1-20.3 cm high and

has the appearance of a regular tussock community that has dried up, except there are no basins. The species are similar to the tussock community with *Carex microchaeta*, *Salix reticulata*, and *Salix pseudopolaris* dominating (Fig. 5). The species that occur in the moist basins of the tussock community, however, are completely absent. Other species, not important in the tussock community, but important here, are *Dryas octopetala* and *Festuca altaica*. The entire surface has a yellowish-green hue owing to the great abundance of lichens (*Cladonia* spp.)

Active Layer

The profiles showing depth to permafrost on the southeast-facing slope are dominated by the presence of the three deep areas (Fig. 5). These coincide with the fronts

of the lobes in every case. There are two principal reasons for this. It is much warmer at the fronts than elsewhere on the slope because of the higher angle of incidence of solar radiation. The average angle of incidence at summer solstice on the lobe fronts is 88° as compared to 65° for the rest of the slope (Fig. 6). This has a great effect on soil-surface temperatures on sunny days. Soil-moisture and temperature cells installed at a depth of 2.54 cm revealed an average 7.5°C higher temperature at the lobe fronts than 15.2 m upslope in the tussock community on sunny days. On other days it averages 1.4°C higher at the lobe front. Therefore, since it is warmer at the lobe fronts, it thaws faster and to a greater depth than elsewhere on the slope.

The second reason for deeper and more rapid thaw at the front is the plant cover. The vegetation here (front and late snow melt communities) consists of low herbaceous species 5.1-10.2 cm high with very little associated mosses to act as insulation. Reciprocally, since the active layer is deeper at the front, it is better drained and provides an environment not conducive to moss growth and accumulation. On the other hand, in the tussock community (Fig. 5) where permafrost is maintained nearer the surface, it is quite moist since water is retained above this impermeable layer. Mosses (*Sphagnum* spp.) accumulate to considerable depth (15.2-61 cm) and provide excellent insulation. Thus, mosses accumulate because of moist conditions engendered by frozen ground; and reciprocally, permafrost is maintained near the surface (50.8-91.4 cm) because of the insulative qualities of the mosses.

The depth to frozen ground across the southeast-facing slope was first sampled on June 22 (Fig. 5). Although the permafrost level is quite uneven, following the surface as it does, the thickness of the thawed layer is comparatively uniform. The insulative effect of the tussocks is reflected in the depth to frozen ground even at this early date. The effects of the higher angle of incidence are not apparent yet, however. This is because more snow accumulates in the lee of the lobes and has not melted, or has melted just a few days previously. In the lee of the upslope and middle lobes in Figure 5 snow melted in the zone immediately below the fronts as of June 22, but part

of the snow patch still remained 3.1 to 6.1 m below the front. As can be seen, the ground was frozen right to the surfaces where the snow had not melted.

The greatest amount of thawing of frozen ground occurred during the period from June 22 to July 13. All of the snow patches melted by the end of the first week in July when the sun was still quite high in the sky. A fairly rapid rate of melting continued from July 13 to July 29, but during the period July 29 to August 16, the rate slowed down considerably. From indications at several sites it is probable that refreezing from the bottom is beginning to occur; certainly thawing in most sites has stopped by the middle of August.

EAST-FACING SLOPE

The east-facing slope has an average gradient of 15° and is the alb of the glacial trough, as is the southeast-facing slope. A ridge upslope, 91-122 m high, allows snow to accumulate and provide meltwater for the slope until the middle of July (Fig. 7). Solifluction lobes are well developed on the east-facing slope, exceeded in size only by those occurring on the southeast-facing slope. The slope is only 305 m wide, however, compared to 914 m for the southeast slope. Stone stripes come one-third the way down the east slope, at which point the lobes begin, but before a series of lobes can develop they reach the steep slope of the glacial trough and eventually collapse as mud flows (Price, 1969).

Vegetation

The vegetation on the east-facing slope is segregated into the same basic communities as that on the southeast-facing slope, but the communities are not as sharply delineated or as distinct. The vegetation analysis indicates that the east-facing slope may be a more severe environment than

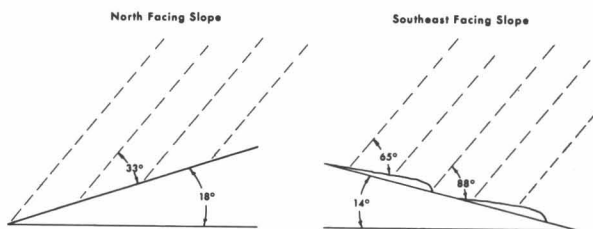


Fig. 6. Angle of incidence of solar radiation for north- and southeast-facing slopes at noon on summer solstice. The calculation was made for $62\frac{1}{2}^\circ\text{N}$ latitude. An average gradient of 37° was used for the lobe fronts on the southeast-facing slope.



Fig. 7. View of east-facing slope looking toward the north. Photograph was taken July 1, 1967. Snow patches on ridge usually remain until about July 20. Average height of solifluction lobes on this slope is 1.0-1.5 m with a maximum height of approximately 2 m.

the southeast-facing slope. For example, some species occur only on the southeast-facing slope (*Oxyria digyna*, *Saxifraga punctata*, *Astragalus umbellatus*, and *Petasites frigidus* (Fig. 8)) and are presumably limited to the southeast-facing slope by habitat preference. On the other hand, some species occur on the east-facing slope (*Cardamine purpurea*, *Arenaria sajanensis*, and *Polygonum viviparum*). Two of these species, *Arenaria sajanensis* and *Polygonum viviparum*, are also important on the southwest- and north-facing slopes, both more severe environments. Thus a gradient of increasing severity appears to occur from the southeast- to the north-facing slopes. Although the entire concept of climax for tundra vegetation has been severely questioned, vegetation is, within limits, a fairly reliable indicator of the local environment (Churchill and Hanson, 1958).

Active Layer

The level of permafrost on the east-facing slope was on the average 25.4 cm deeper when first sampled on June 24

than on the southeast-facing slope (Fig. 8). No snow had accumulated in the lee of the lobes on the east-facing slope on June 18, so the influence of the higher angle of incidence at the lobe fronts showed up on the profile here where it did not on the southeast-facing slope. The active layer is shallowest under the tussock community, as on the southeast-facing slope, but the shallow area below the major front is difficult to explain (Fig. 8). Water issued from under the front at this point, and it remained significantly wetter through the summer than the other fronts. The higher specific heat of water may have acted as a buffering agent.

SOUTHWEST-FACING SLOPE

The southeast- and southwest-facing slopes are separated only by a small stream, but the contrast between them is very great. The southeast-facing slope is the wettest of the four slopes and has well-developed solifluction

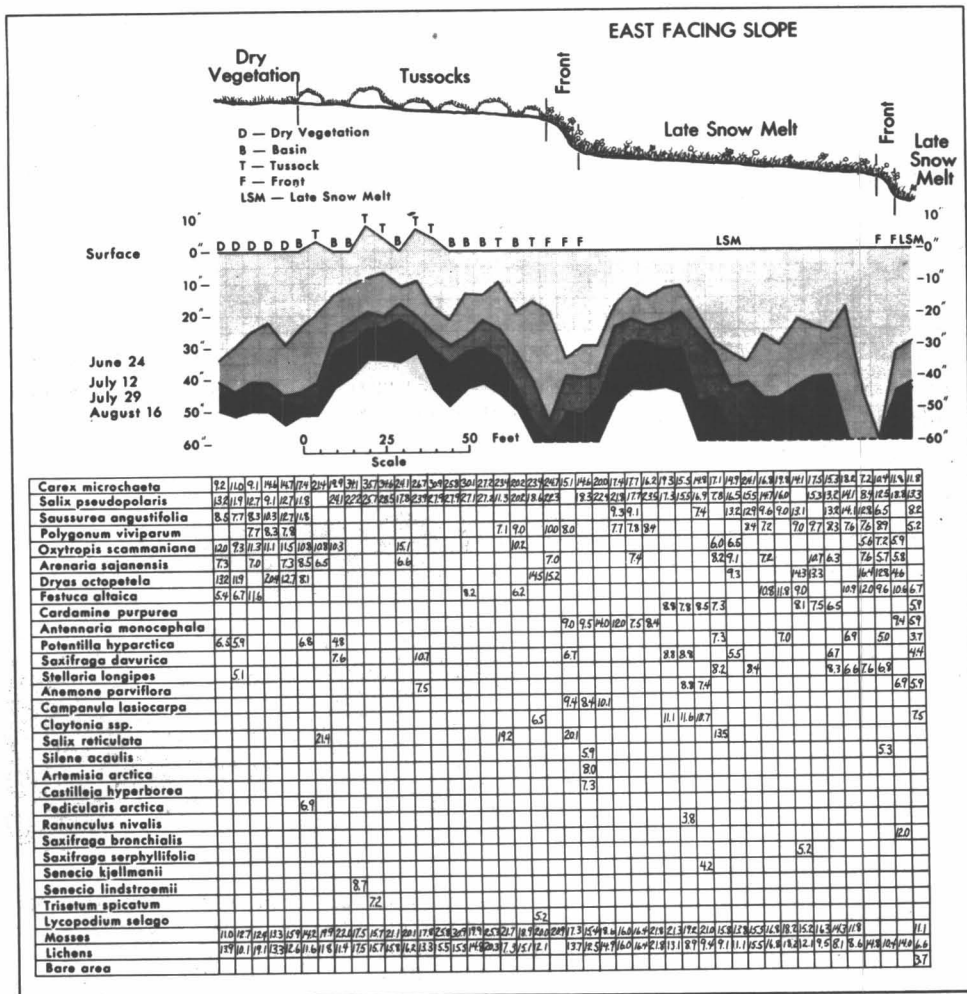


Fig. 8. East-facing slope. Top of illustration shows a cross section for part of slope with solifluction lobes and associated with plant communities. The middle illustration presents depth of active layer at the four designated times during the summer. The bottom table provides vegetational sampling data.

lobes; the southwest-facing slope is the driest and solifluction lobes are virtually absent (Fig. 9). One reason for the xeric quality of this slope is the prevailing northwesterly winter wind (Taylor-Barge, 1969), which sweeps the slope clean of snow, particularly since there are very few microhabitats where snow can accumulate. Snow is an important ecological factor in the tundra owing to meltwater in summer (Billings and Bliss, 1959), and reciprocally, its absence allows the vegetation to be exposed to the desiccating winter wind. Snow accumulates on the ridge above, but mainly on the east and north side, so very little meltwater finds its way down the southwest-facing slope. One narrow strip of meltwater exists on the southwest-facing slope, however, and the only well-developed solifluction lobes on the slope occur along this narrow strip, illustrating rather dramatically the importance of water to the occurrence of such phenomena.

Vegetation

The southwest-facing slope has an average gradient of 17° and is mantled with 1.52 m or more of weathered detritus, consisting largely of pea-sized angular particles (grus). The organic layer is only 5.1-10.2 cm deep, and roots extend down 25.4-50.8 cm. The vegetation on this slope is rather poorly developed because of the xeric nature of the surface. The most important species are *Dryas octopetala* and *Salix reticulata*, though plant cover is thin and continuous. There are very few mosses, but lichens, particularly different species of *Cladonia*, abound and give the slope a general yellowish hue.

The vegetation along the transect is fairly uniform and is typical for the southwest-facing slope (Fig. 10). A short transect taken across one of the solifluction lobes in the narrow snow-melt strip reveals sharply delineated plant communities such as occur on the southeast- and east-facing slopes.

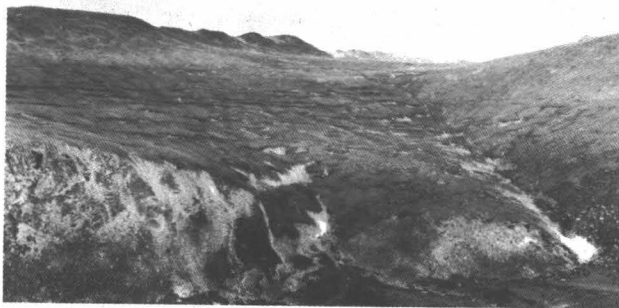


Fig. 9. View of southeast- and southwest-facing slopes. Photograph was taken toward the north and the two slopes are separated only by a small stream. Vegetation and solifluction lobes are well developed on southeast-facing slope, but the southwest-facing slope is quite dry with poorly developed vegetation and solifluction lobes. Reason for both of the above developments is largely the presence or absence of water.

Active Layer

When first sampled, the depth to frozen ground was found to be greater on the southwest-facing slope than on the southeast-facing slope. Moreover, there was less variation in depth (Fig. 10). Both of these facts are accounted for by: (1) the presence of a fairly thin and homogeneous plant cover, (2) very little variation in microtopography, and (3) no areas of snow accumulation. The southwest-facing slope, even in early summer, when most other areas are a saturated morass, is quite dry and well drained. Since water is not present to act as a buffering agent to the same extent, soil temperatures are relatively higher here than on the southeast-facing slope. Thawing continues at a fairly steady rate through the summer on the southwest-facing slope, and the negative effects of microtopography and plant cover are readily visible here, where there are essentially no marked variations across the slope (Fig. 10).

NORTH-FACING SLOPE

This slope has the severest environment of all the study slopes and as a consequence the plant cover is quite impoverished (Fig. 11). The slope has an average gradient of 18° , and the angle of incidence of solar radiation on the slope is low (33°), even at summer solstice (Fig. 6). Mountains to the north and west prevent the sun from shining on the slope during the night hours, and snow patches remain until early July. Where this happens, the plants have only a very short growing season.

Vegetation

The vegetation transect up the north-facing slope reveals only 14 species, about half as many as on the southeast- and east-facing slopes. The plant cover is more sparse and discontinuous, and consistently high importance values are given to bare surface (Fig. 12). *Carex microchaeta* is the most important species; *Salix pseudopolaris* is second, followed by mosses and lichens. The absence of *Salix reticulata* here is noteworthy, since it is a very important species on the other three slopes.

The north-facing slope is mantled with at least 1.5 m or more of weathered detritus and is rockier than the other study slopes. The surface organic layer is very thin (5.1-7.6 cm) compared to the southeast- and east-facing slopes where the layer penetrates 15.2-20.3 cm. In both these respects the north-facing slope is similar to the southwest-facing slope.

Solifluction lobes occur on the north-facing slope, but they are not well developed and there is no apparent genetic relationship with vegetation as may be possible on the southeast- and east-facing slopes (Watt and Jones, 1948; Wilson, 1952). Their formation has been quite clearly due to rock dams, which have retarded the rate of mass

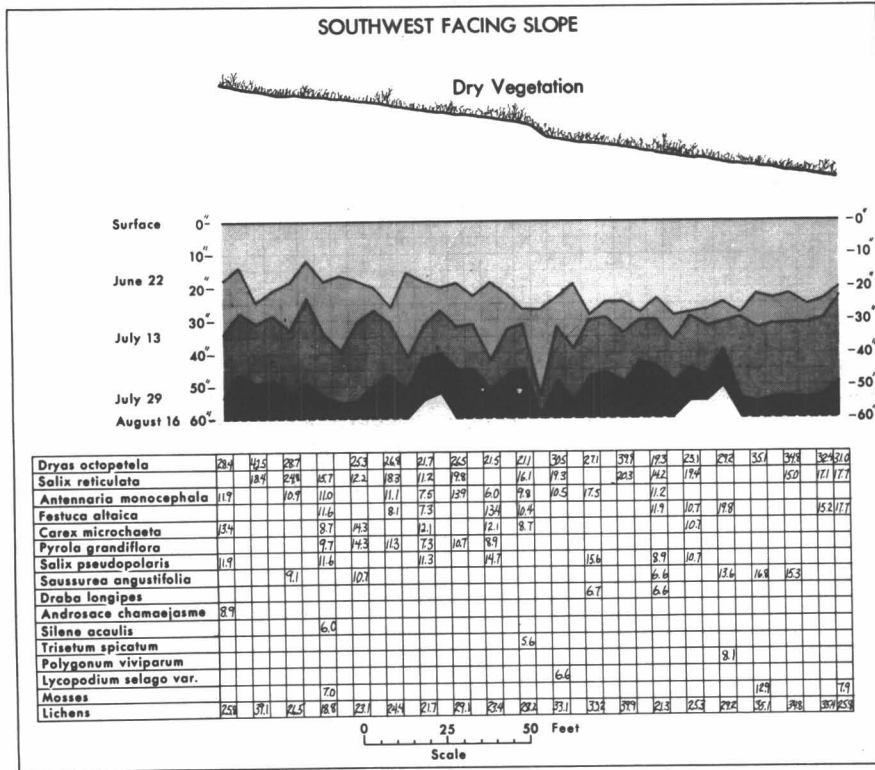


Fig. 10. Southwest-facing slope. Top of illustration shows microtopography and associated plant communities across the slope. The middle illustration gives depth of active layer at 3-m intervals, and the bottom table provides vegetational sampling data.

movement and eventually built up a scarp. The areas immediately below the lobes do not serve as favorable microhabitats because of extreme rockiness and absence of soil.

Active Layer

It was initially thought that the north-facing slope would thaw more slowly than the southeast-facing slope because of the low angle of incidence. This is not the case, however, as can be seen from the transect (Fig. 12).



Fig. 11. View of north-facing slope looking toward the southeast. Slope is rocky with poorly developed soil and vegetation. Solifluction lobes occur singly rather than coalesced and, in general, do not provide favorable microhabitats.

The active layer was deeper here, when first sampled on June 24, than it was on the southeast-facing slope (Fig. 5). The active layer becomes more shallow upslope because of a snow patch where the transect was terminated. The major amount of thawing took place from June 24 to July 12 after the snow patches had disappeared (Fig. 12).

The north-facing slope thaws more quickly and to a greater depth than the southeast-facing slope because of the differences in plant cover. The effect of vegetation on thawing is twofold. (1) The vegetation is sparse and discontinuous on the north-facing slope and provides very little protective insulation, whereas on the southeast-facing slope it is thick and continuous with a large amount of *Sphagnum* spp. mosses. In addition, (2) the soil surface is warmer during the summer on the north-facing slope than on the southeast-facing slope (Price, 1970) because of the higher conductivity of bare soil compared to a thick vegetative mat. The peaty vegetation on the southeast-facing slope has a greater moisture content, and therefore, a higher specific heat. The work of Bouyoucos (1913) indicated that in a natural wet condition, sand and gravel will heat and cool three times more rapidly than peat. Thus, although the sun's rays do not strike the north-facing slope at such a high angle as the southeast-facing slope, they are, nevertheless, more effective in heating the soil surface. Plant cover therefore may be locally more important than exposure in controlling the depth of permafrost. On the southeast-facing slope the

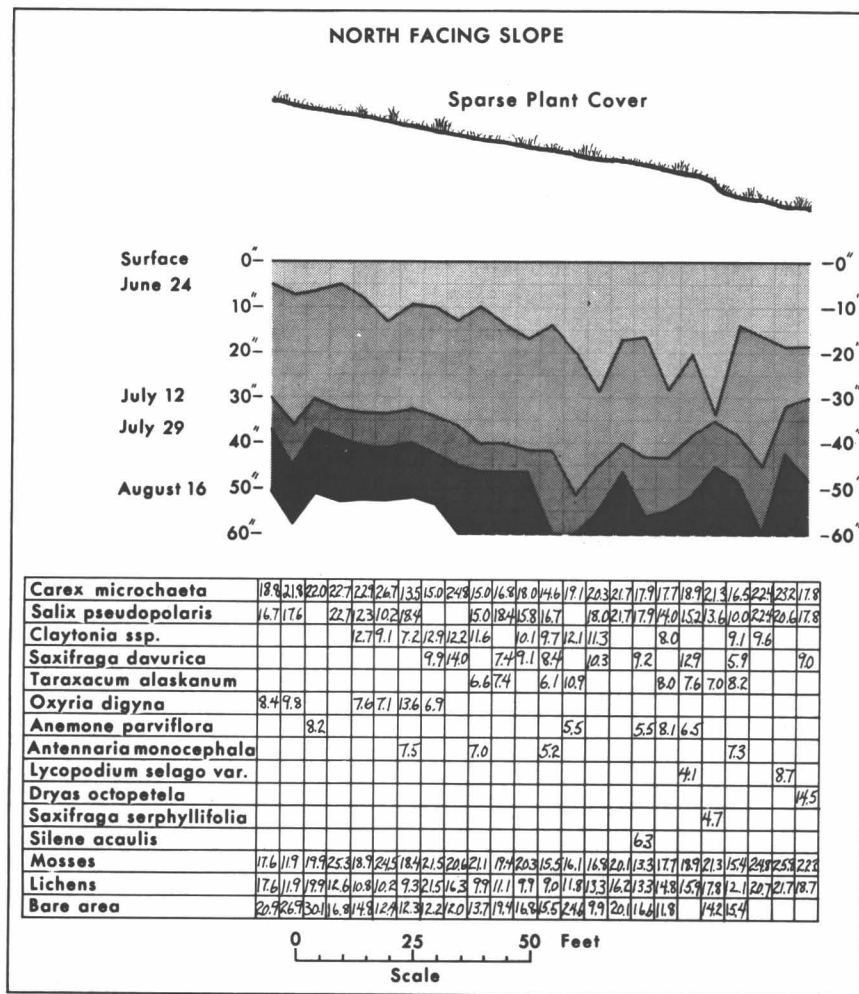


Fig. 12. North-facing slope. Top of illustration shows microtopography and associated plant cover across slope. The middle illustration gives depth of active layer at four designated times, and bottom table provides vegetation sampling data at 1.5-m intervals.

vegetation is better developed, and even though the angle of incidence is much higher, permafrost remains nearer the surface than on the north-facing slope.

Acknowledgments

This research was supported by the Arctic Institute of North America. Excellent logistical support was provided by the Icefield Ranges Research Project, and Mr. Dick Ragle, Dr. J. Peter Johnson, Jr., Mr. Philip Upton, and Dr. Walter Wood were particularly helpful. Mr. Jim Sij, Mr. Charles Volk, and my wife, Nancy, were field assistants. In addition, I would like to thank Dr. C. S. Alexander and Dr. L. C. Bliss for their encouragement and for critically reading the manuscript.

References

Billings, W. D., and Bliss, L. C. (1959) An alpine snowbank environment and its effect on vegetation, plant development and productivity, *Ecology*, 40, 388-397.

Billings, W. D., and Mark, A. F. (1961) Interactions between alpine tundra vegetation and patterned ground in the mountains of southern New Zealand, *Ecology*, 42, 18-31.
 Bliss, L. C. (1956) A comparison of plant development in micro-environments of arctic and alpine tundras, *Ecol. Monogr.*, 26, 303-337.
 Bliss, L. C. (1963) Alpine plant communities of the Presidential Range, New Hampshire, *Ecology*, 44, 678-697.
 Bouyoucos, G. J. (1913) An investigation of soil temperatures and some of the factors influencing it, *Tech. Bull.* 17, Mich. Agr. Coll. Exper. Sta., 196 pp.
 Churchill, E. D., and Hanson, H. C. (1958) The concept of climax in arctic and alpine vegetation, *Bot. Rev.*, 24, 127-191.
 Coleman, E. A. (1964) Instruction manual; MC-300A, soil moisture meter and cells, *Bull. C172-64*, Soiltest, Evanston, Ill., 20 pp.
 Drew, J. V., Tedrow, J. C. F., Shanks, R. E., and Koranda, J. J. (1958) Rate and depth of thaw in arctic soils, *Trans. Am. Geophys. Union*, 39, 697-701.
 Drury, W. H. (1962) Patterned ground and vegetation on southern Bylot Island, Northwest Territories, Canada, *Contrib. Gray Herb.*, 190, 111 pp.
 Hanson, H. C. (1950) Vegetation and soil profiles in some solifluction and mound areas in Alaska, *Ecology*, 31, 606-630.

- Hopkins, D. M., and Sigafoos, R. S. (1951) Frost action and vegetation patterns on Seward Peninsula, Alaska, *Bull. 974-C*, U.S. Geol. Surv., pp. 51-100.
- Hopkins, D. M., Karlstrom, T. N. V., Black, R. F., Williams, J. R., Péwé, T. L., Fernold, A. T., and Muller, E. H. (1955) Permafrost and ground water in Alaska, *Prof. Paper 264-F*, U.S. Geol. Surv., pp. 113-145.
- Johnson, P. L., and Billings, W. D. (1962) The alpine vegetation of the Beartooth Plateau in relation to cryopedogenic processes and patterns, *Ecol. Monogr.*, 32, 105-135.
- Lindsey, A. A. (1953) Notes on some plant communities in the northern Mackenzie Basin, Canada, *Bot. Gaz.*, 155, 44-55.
- Price, L. W. (1969) The collapse of solifluction lobes as a factor in vegetating blockfields, *Arctic*, 22, 395-402.
- Price, L. W. (1970) Morphology and ecology of solifluction lobe development—Ruby Range, Yukon Territory, Ph.D. dissertation, Univ. Illinois, Urbana, 325 pp. (unpubl.).
- Raup, H. M. (1965) The structure and development of turf hummocks in the Mesters Vig District, Northeast Greenland, *Medd. Grøn.*, 1966, 1-112.
- Taylor-Barge, B. (1969) The summer climate of the St. Elias Mountains region, *Res. Paper No. 53*, Arctic Inst. North. Am., 265 pp.
- Watt, A. S., and Jones, E. W. (1948) The ecology of the Cairngorms, Pt. 1; The environment and the altitudinal zonation of the vegetation, *J. Ecol.*, 36, 283-304.
- Williams, P. J. (1957) The direct recording of solifluction movements, *Am. J. Sci.*, 255, 705-714.
- Wilson, W. J. (1952) Vegetation patterns associated with soil movement on Jan Mayen Island, *J. Ecol.*, 40, 249-264.

A Checklist of Vascular Plants

From the Icefield Ranges Research Project Area

James A. Neilson¹

Introduction

The Icefield Ranges Research Project (IRRP) has operated in the vicinity of the St. Elias Mountains since 1961. Increasing interest and research activity in biological subjects have contributed to and developed a need for a checklist of vascular plants for the region. The compilation presented here is the result of two field seasons of collecting in the Shakwak Trench and adjacent Kluane and Ruby Ranges; extensive collections and notes were obtained from the south end of Kluane Lake, the Slims River, the Gladstone Creek drainage area, and at various points between Kluane Lake and Haines Junction (about 35 miles southeast of Kluane Lake). The author's collection has been supplemented by data published by Dr. A. E. Porsild (1951, 1966), by collections and notes by Dr. David Murray, and by miscellaneous collections by various members of the project.

A voucher collection is deposited at the herbarium of the University of Alaska at College, and a duplicate collection is deposited at the herbarium of the National Museum of Canada in Ottawa. Partial collections were given to the herbarium of the U.S. National Museum in Washington, D.C., and to the herbarium of the University of California at Davis.

The Flora

Notes on the species list. The binomials listed here follow those used by Porsild (1951, 1966); and Hultén (1968) for species not cited by Porsild. Those names for which voucher specimens are maintained in the IRRP collection are so marked. The altitude ranges are approximate; for many of the less common species the altitude is known for a single or at most a few collection sites. An attempt is made to suggest the general type of habitat in which the species is most commonly found. Our present state of knowledge, however, is much too fragmentary to suggest the range of habitats for most of the uncommon plants noted in this list.

The notes on the abundance of any species are based on limited data, but the interpretation used indicates the relative probability of locating the species at the same altitudes in similar types of habitat. A plant described here as "abundant" can be found easily and in large numbers in a wide variety of habitats at the altitudes suggested. "Common" describes plants whose frequency is high enough to form easily located stands which, in the local community, are dominants or subdominants with respect to either number or physiognomy. "Occasional" refers to species whose individuals or stands are located at wide intervals; the collector may have to search over a considerable area to encounter the species. "Rare" as used here indicates the plant is localized in one or two small areas, or, if widespread, its frequency is so low that it is represented by only a few scattered individuals over the entire project area.

Much synonymy exists in the nomenclature of plants of Alaska and northern Canada mainly because collections are fragmentary and opinion is divergent on the concept of species. It is hoped that Dr. Eric Hultén's manual, *The Flora of Alaska and Neighboring Territories*, released in 1968, will resolve some of the more difficult nomenclatural problems. It was decided not to include keys to specific binomials at this time because Hultén's new *Flora* has not yet been tested in the field. Anderson's *Flora of Alaska and Adjacent Parts of Canada* (1959) is a useful tool for beginners but for some genera the nomenclature is out of date, or important plants that occur in the Shakwak Trench are omitted. Porsild's "Illustrated flora of the Canadian Arctic Archipelago" (1957) is particularly useful for some of the alpine and most of the tundra elements of the IRRP area. Attention should be called to *A Flora of the Alaskan Arctic Slope*, by Wiggins and Thomas (1962). This too is useful for tundra and alpine species but it is not illustrated, and some of the nomenclature is divergent from more comprehensive works, or it ignores some of the taxonomic problems associated with plants of the Arctic slope. Lastly, Hultén's original "Flora of Alaska and Yukon" (1941-50) is very useful for the professional who needs herbarium documentation.

Plants new or unusual in the flora of the Southwest Yukon. Many individual species are worthy of special

¹ Ecoview Consultants, Homewood, California

note. Indeed, nearly every major collection that has been made in the Kluane Ranges has turned up several species of interest. Probably the most interesting and unexpected plant in the IRRP collection is a new species of wormwood, *Artemisia rupestris* L. ssp. *woodii* Neilson (Neilson, 1968). Its discovery along the edges of the Shakwak Trench represents a disjunct distribution of 3200 miles. The nearest known population of this widespread Eurasian plant is on the Lena River in central Siberia. Apparently the Yukon population (heretofore unknown in North America) is a remnant of a much wider distribution of this wormwood and perhaps indicative of a whole group of plants adapted to a cool dry climate.

Eurotia lanata (Pursh) Moq. (winter fat), another prairie plant common to the great plains and the southwestern deserts, has a disjunct distribution in the Yukon. Two small populations were discovered on the south-facing slopes of the mountain just northwest of the mouth of the Slims River; this is also the site of the original discovery of the *Artemisia*.

South of Kluane on the south-facing slopes of an unnamed mountain overlooking the pass through the Kluane Ranges, by the Dezadeash River, a small alpine composite was collected which has been identified as *Erigeron lanatus*. The nearest known station for this plant is in south-central British Columbia.

The occurrence of *Salix athabascensis* Raup and *Erigeron yukonensis* Rydb. is worthy of note, since these collections are more northerly or westerly extensions of these species within the Yukon itself.

The General Aspect of the Vegetation

No critical analysis of the vegetation of the southwest Yukon has been undertaken so far. Indeed, the flora has not been well enough known to separate ecotypes or to judge the phytogeographical problems inherent in studies of plants occurring in the area embraced by the Icefield Ranges Research Project. When those studies which have been attempted in the past (Drury, 1953; Johnson and Raup, 1964; Porsild, 1951, 1966) are examined closely, the nomenclatural problems to which I alluded earlier confront the student. Problems such as an understanding of species boundaries within the genera *Dryas*, *Potentilla*, *Oxytropis*, *Draba*, *Poa*, *Calamagrostis*, *Carex*, and even *Populus*, to mention only a few, will require additional attention by biosystematists.

On the other hand, the general aspects of the vegetation can be delineated. The discussions of Raup (Johnson and Raup, 1964) paint a general picture and serve as a basis for study. The extensive descriptions by Porsild (1951) which emphasize southeastern Yukon apply only in part to the southwestern Yukon. Nonetheless both Porsild, 1951 and Porsild, 1966 are indispensable references. The descriptions of vegetation supplied by Drury (1953) are very generalized and do not apply locally.

Only a few elements of the central Canadian flora are found in the southwestern Yukon. Many of the meadow and subalpine associations are not represented in the Shakwak Trench even though the aspect and physiognomy are much the same. Elements of the interior British Columbia flora are very common in the major valleys across the base of the St. Elias Mountains, especially in the southern part. They become dominant as one progresses southward along the Alaska Highway southeastward from Kluane Lake or eastward along the Alsek River.

The Phytogeographical Significance of the Yukon Plants

The Shakwak Trench lies along the eastern base of the St. Elias Mountains and hence is in a rain shadow. Annual precipitation approaches a maximum of fifteen inches in the wetter years, and has a bimodal pattern. Two weather systems account for this pattern. In winter the precipitation results from air movement across the St. Elias Mountains from the Gulf of Alaska. Maximum accumulations of snow rarely exceed two feet on the valley floor and winter winds move both dust and snow across the landscape. For vegetation the significant rainfall occurs during June when the Canadian airmass moves westward toward the St. Elias and Rocky Mountains, preventing air movement across the St. Elias Mountains from the Gulf of Alaska. Local summer rainstorms generated in Alaska and continental Canada tend to track westward or southwestward and spend their moisture against the eastern flank of the St. Elias Mountains. July and August are usually warm with occasional periods of light rain.²

The varieties within the flora found along the Shakwak Trench take on an added significance because of the cool, semidesert climate. Continually accumulating evidence points to relict species which were much more widespread on the landscape. The isolated and disjunct occurrences in the southwest Yukon of certain prairie or dry grassland species suggest that a grassland flora was once more extensive than now. Clearly, the climatic pattern has shifted since the Pleistocene, and sufficient moisture permitted the spruce forest to assume dominance almost immediately after the disappearance of the glaciers. Prairie vegetation in modern times is restricted to small isolated areas, principally on dry glacial outwashes, former lake basins, and (at the south end of Kluane Lake) on dead-ice terrain features such as ancient crevasse fillings, kettles, and eskers. Periglacial topography, the accumulation of loess, and modern outwash vegetation types suggest that prairie vegetation could have been well developed in the interglacial periods. Furthermore, the northernmost portion of the Shakwak Trench was apparently free of ice

²Climatic inferences are based on personal communication with several meteorologists who worked in the area. Specific data were obtained from the weather records at Haines Junction.

during the Wisconsin glaciation (Bostock, 1952; Krinsley, 1965; Rampton, 1969). Also, valleys in the Kluane Ranges were relatively free of ice. When Kluane glaciation was at its height, the eastern side of the Shakwak Trench and Ruby Ranges were exposed (Denton and Stuiver, 1967). Ancient Lake Champagne was confined to the southern end of the Shakwak Trench (Kindle, 1952). Ancient Lake Kloo and Lake Alsek are of relatively recent origin (Hughes, *et al.*, 1969). The levels and suggested interconnection with Kluane Lake have been discussed by Bostock (1969). In short, open ground has always been available to support grassland.

This geological sequence indicates that major portions of the Shakwak Trench were free of ice during every critical period. Recent work (G. H. Denton, personal communication) on carbon dating indicates the presence of spruce in the landscape since the Pleistocene. From pollen analysis, Hansen (1953) also indicates that spruce dominated the landscape in the central and northern end of the valley, but the southern end of the Shakwak Trench and the valley of Ancient Lake Champagne had an extensive grassland, at least bordering on the bogs which were sampled. As a result, the present hypothesis can reasonably place prairie vegetation well into the interglacial periods; it was probably dominant then. So far, pollen profile evidence indicates that even during the hypsithermal period of the post-Pleistocene, prairies were restricted to sites similar to those of today, and were interspersed with the dominant spruce forests (Hansen, 1953; Deevey and Flint, 1957; Johnson and Raup, 1964).

The following partial list is of prairie species found along the Shakwak Trench and in southeastern Yukon. Some are more or less disjunct in their distribution; others are widespread and extend into Alaska and Siberia.

Gentiana amarella L.
Artemisia frigida Willd.
Carex atherodes Spreng.
Carex parryana Dew.
Carex filifolia Nutt.
Carex praticola Rydb.
Carex sychnocephala Carey
Carex macloviana d'Urv.
Kobresia myosuroides Hult.
Schizachne purpurascens (Torr.) Swallen
Dentonia intermedia Vasey
Stipa richardsonii Link
Stipa columbiana Macoun
Puccinellia nuttalliana (Schult.) Hitchc.
Poa canbyi (Scribn.) Piper
Poa cusickii Vasey
Poa buckleyana Nash
Agropyron dasystachyum (Hook.) Scribn.

The presence of this array of species, the limited number, and the isolation of unforested sites suitable for prairie vegetation, the disjunct distribution of many species,

the increasing evidence that the spruce forest became dominant almost immediately after the Wisconsin era, the discrepancies in the pollen record, and the fact that the pollen record does not extend beyond the period when Ancient Lake Champagne was at its maximum indicate a reasonable probability that the prairie habitat was widespread and was dominant earlier in geologic time than is currently believed.

References

- Anderson, J. P. (1959) *Flora of Alaska and Adjacent Parts of Canada*, Iowa State Univ. Press, Ames, 543 pp.
- Bostock, H. S. (1952) Geology of northwest Shakwak Valley, Yukon Territory, *Mem. Geol. Surv. Can.*, 267, 54 pp.
- Bostock, H. S. (1969) Kluane Lake, Yukon Territory, Its drainage and allied problems (115 G, and 115 FE) *Geol. Surv. Can., Paper 69-28*, 19 pp.
- Deevey, E. S., and Flint, R. F. (1957) Postglacial hypsithermal interval, *Science*, 125, 182-184.
- *Denton, G. H., and Stuiver, M. (1967) Late Pleistocene glacial stratigraphy and chronology, northeastern St. Elias Mountains, Yukon Territory, Canada, *Bull. Geol. Soc. Am.*, 78, 485-510.
- Drury, W., Jr. (1953) Birds of the St. Elias quadrangle in the southwestern Yukon Territory, *Can. Field-Nat.*, 67, 103-179.
- Hansen, H. P. (1953) Postglacial forests in the Yukon Territory and Alaska, *Am. J. Sci.*, 251, 505-542.
- Hughes, O. L., Campbell, R. B., Muller, J. E., and Wheeler, J. O. (1969) Glacial limits and flow patterns, Yukon Territory south of 65° north latitude, *Geol. Surv. Can., Paper 68-34*, 9 pp.
- Hultén, E. (1941-1950) *Flora of Alaska and Yukon*, Pts. 1-10, Lunds Univ. Årsskr. N.F., Avd. 2, 37, 1-46, 1.
- Hultén, E. (1968) *Flora of Alaska and Neighboring Territories*, Stanford Univ. Press, Stanford, 1008 pp.
- Johnson, F., and Raup, H. M. (1964) Investigations in southwestern Yukon; geo-botanical and archaeological reconnaissance, *Robert S. Peabody Found. Archaeol., Papers*, 6, 198 pp.
- Kindle, E. D. (1952) Dezadeash map-area, Yukon Territory, *Mem. Geol. Surv. Can.*, 268, 68 pp.
- Krinsley, D. B. (1965) Pleistocene geology of the south-west Yukon Territory, Canada, *J. Glaciol.*, 5, 385-397.
- †Neilson, J. A. (1968) New and important additions to the flora of the southwest Yukon Territory, Canada, *Can. Field-Nat.*, 82, 114-119.
- Porsild, A. E. (1951) Botany of southeastern Yukon adjacent to the Canol Road, *Bull. Nat. Mus. Can.*, No. 121, 400 pp.
- Porsild, A. E. (1957) Illustrated flora of the Canadian Arctic Archipelago, *Bull. Nat. Mus. Can.*, No. 146, 209 pp.
- Porsild, A. E. (1966) Contributions to the flora of the southwestern Yukon Territory, *Bull. Nat. Mus. Can.*, No. 216, pp. 1-86.
- Rampton, V. (1969) Pleistocene geology of the Snag-Klutlan area, southwestern Yukon Territory, Canada, Ph.D. dissertation, Univ. Minnesota.
- Wiggins, I. L., and Thomas, J. H. (1962) *A Flora of the Alaskan Arctic Slope*, Univ. Toronto Press, Toronto, 425 pp.

*This article was reprinted in an earlier volume of Icefield Ranges Research Project, Scientific Results.

†This article is reprinted in the present volume.

LIST OF SPECIES

The information in parentheses to the right of each entry is the authority for the existence of the species in the area. (IRRP) indicates specimens in the voucher collection now at the University of Alaska at College; nomenclature for these species is from Hultén (1968). (P 51) and (P 66) indicate species listed by Porsild (1951, 1966), and not found in the voucher series. (Murr) refers to a specimen collected by David Murray but not in the IRRP voucher collection, and (CAN) indicates that there is a specimen in the herbarium of the National Museum of Canada which has not been reported in the literature.

OPHIOGLOSSACEAE		<i>Equisetum variegatum</i> Schleich.	(IRRP)
<i>Botrychium lanceolatum</i> (Gmel.) Ångstr.	(P 66)	Shallow ponds, sandy gravel bars, mossy banks Low elevations (?); common	
Mt. Archibald 3000'; rare			
<i>Botrychium lunaria</i> (L.) Sw.	(IRRP)	LYCOPODIACEAE	
Mesic meadows and dry slopes Up to 5500'; rare		<i>Lycopodium sabinaefolium</i> Willd. var.	(P 66)
<i>Botrychium lunaria</i> (L.) Sw. var.	(P 66)	<i>sitchense</i> (Rupr.) Fern.	
<i>minganense</i> (Vict.) Dole		Vicinity of Mackintosh*	
Near Mackintosh*, rocky slopes among willows Low elevations; rare		SELAGINELLACEAE	
ATHYRIACEAE		<i>Selaginella sibirica</i> (Milde) Hieron.	(P 66)
<i>Cystopteris fragilis</i> (L.) Bernh.	(IRRP)	Rocky slopes on granite	
Mossy banks and rock outcrops Up to 6000'; rare		CUPRESSACEAE	
<i>Cystopteris montana</i> (Lam.) Bernh.	(P 66)	<i>Juniperus communis</i> L. var. <i>montana</i> Ait.	(IRRP)
Mt. Archibald 7000'		Open rocky slopes Low elevations; occasional	
<i>Woodsia ilvensis</i> R. Br.	(P 66)	<i>Juniperus horizontalis</i> Moench	(IRRP)
Tundra on granite; rare		Open rocky slopes Low elevations; occasional	
ASPIDACEAE		PINACEAE	
<i>Dryopteris austriaca</i> (Jacq.) Woyнар	(P 66)	<i>Picea glauca</i> (Moench) Voss var. <i>albertiana</i>	(IRRP)
Mt. Archibald 7000'		(S. Brown) Sarg.	
<i>Dryopteris fragrans</i> (L.) Schott	(IRRP)	Near timberline and dry ridges Middle elevations (?); common	
Rock outcrops and mossy banks Up to 4500' (?); rare		<i>Picea glauca</i> (Moench) Voss var.	(IRRP)
EQUISETACEAE		<i>porsildii</i> Raup	
<i>Equisetum arvense</i> L.	(Murr)	Forms dominate forests of the area Low and middle elevations; abundant	
Moist places Up to 5000'; occasional		SPARGANIACEAE	
<i>Equisetum hiemale</i> L. var.	(IRRP)	<i>Sparganium angustifolium</i> Michx.	(IRRP)
<i>californicum</i> Milde		Shallow ponds Up to 4500'; occasional	
Bogs and wet meadows, stream outwashes Up to timberline; common		<i>Sparganium hyperboreum</i> Laest.	(P 66)
<i>Equisetum palustre</i> L.	(IRRP)	Shallow pools 4600'	
Understory in spruce forests in lowlands or near bogs Up to timberline; common		POTAMOGETONACEAE	
<i>Equisetum scirpoides</i> Michx.	(Murr)	<i>Potamogeton filiformis</i> Pers. var. <i>borealis</i>	(IRRP)
Understory in spruce forests Up to 5000'; common		(Raf.) St. John Shallow mud and water at lake's edge Low elevations; occasional	

<i>Potamogeton pectinatus</i> L.	(P 66)	<i>Calamagrostis canadensis</i> (Michx.) Beauv.	(IRRP)
Sulphur Lake		Wet meadows; Mile 1135	
2100'		Low elevations; occasional	
<i>Potamogeton richardsonii</i> (Benn.) Rydb.	(P 66)	<i>Calamagrostis inexpansa</i> A. Gray	(IRRP)
Sulphur Lake		Slims River floodplain	
2100'		Low elevations; occasional	
JUNCAGINACEAE			
<i>Triglochin palustris</i> L.	(IRRP)	<i>Calamagrostis neglecta</i> (Ehrh.) Gaertn.	(IRRP)
Open sandy areas		Mesic prairies	
Low elevations; common		Low elevations; occasional	
GRAMINEAE			
<i>Alopecurus aequalis</i> Sobol.	(IRRP)	<i>Calamagrostis purpurascens</i> R. Br.	(IRRP)
Muskeg or boggy areas in the open		Mesic prairies and rocky slopes, open or	
Low and middle elevations (?); occasional		partial shade	
<i>Alopecurus alpinus</i> Sm.	(IRRP)	Up to 6000'; common	
Muskeg ponds and wet places		<i>Colpodium vahlianum</i> (Liebm.) Nevski	(P 66)
Up to 4500'; rare		Wet, seepy slopes, Mt. Decoeli	
<i>Alopecurus glaucus</i> Less.	(P 66)	4500' (?); rare (?)	
Alpine stream, Vulcan Creek		<i>Danthonia intermedia</i> Vasey	(P 66)
5400'; rare		Mile 1036 and Vulcan Creek; rare	
<i>Agropyron latiglume</i> (Scrib. & Sm.)	(IRRP)	<i>Deschampsia caespitosa</i> (L.) Beauv.	(IRRP)
Rydb.		Mud flats and sandy gravel bars	
Open slopes and prairies		Low elevations; common	
Up to 6000'; common		<i>Festuca altaica</i> Trin.	(IRRP)
<i>Agropyron sericeum</i> Hitchc.	(IRRP)	Open slopes or meadows to partial shade	
Gravel wash		Up to 6000'; common	
Low elevations		<i>Festuca baffinensis</i> Polunin	(IRRP)
<i>Agropyron subsecundum</i> (Link) Hitchc.	(IRRP)	Mt. Archibald and Kluane Ranges,	
Mesic meadows		moist sites	
Low elevations; occasional to common		Above 5000'; occasional	
<i>Agropyron trachycaulum</i> (Link) Malte	(IRRP)	<i>Festuca brachyphylla</i> Schultes	(IRRP)
Gravel outwash		Open mesic meadows	
Low elevations		Up to 6000'; common	
<i>Agropyron yukonense</i> Scrib. & Merr.	(IRRP)	<i>Festuca rubra</i> L.	(IRRP)
Open prairies, dry sites		Clearings in spruce woods, wet areas	
Low elevations; common to abundant		Low elevations; occasional	
<i>Agrostis scabra</i> Willd.	(IRRP)	<i>Festuca vivipara</i> (L.) SM.	(IRRP)
Mesic meadows		Alpine slopes and tundra	
Low elevations; occasional		Above 4500'; occasional	
<i>Agrohordeum macounii</i> (Vasey) Lepage	(IRRP)	<i>Hierochloë alpina</i> (L.) Beauv.	(IRRP)
Mouth of Bullion Creek		Alpine slopes and tundra	
Low elevations; rare		Above 4500'; occasional	
<i>Arctagrostis latifolia</i> (R. Br.) Grieseb.	(IRRP)	<i>Hierochloë odorata</i> (L.) Beauv.	(IRRP)
Alpine meadows and tundra		Mesic meadows	
Middle to high elevations; occasional		Low elevations; occasional	
<i>Arctophila fulva</i> (Trin.) Anders.	(IRRP)	<i>Hordeum jubatum</i> L.	(IRRP)
Muskeg		Open mesic sites in disturbed places	
Low elevations; rare		Low elevations; abundant	
<i>Bromus inermis</i> Leyss.	(IRRP)	<i>Muhlenbergia richardsonis</i> (Trin.) Rydb.	(IRRP)
Mesic open areas; occasional		Wet meadows	
<i>Bromus pumpellianus</i> Scribn. var.	(P 51)	Low elevations; locally common	
<i>arcticus</i> (Shear) Pors.		<i>Phippsia algida</i> R. Br.	(IRRP)
Mesic open or shrub communities		Alpine meadows, snowflush, north slopes	
Up to timberline; occasional		Above 4500'; occasional	
		<i>Phleum alpinum</i> L.	(IRRP)
		Stream banks, sand bars	
		Up to timberline; occasional	
		to rare	

<i>Poa alpina</i> L.	(IRRP)	<i>Carex atratiformis</i> Britt. ssp. <i>raymondii</i> (Calder) Pors.	(IRRP)
Alpine meadows		Vicinity of Mackintosh*	
Above 4000'; occasional to common			
<i>Poa arctica</i> R. Br.	(IRRP)	<i>Carex atosquama</i> Mack.	(IRRP)
Alpine slopes, meadows, or open sandy places		Subalpine meadows, open woods above 4000'	
Above timberline; occasional to common		Occasional	
<i>Poa arctica</i> ssp. <i>longiculmis</i> Hult.	(IRRP)	<i>Carex bicolor</i> All.	(P 66)
Alpine slopes		Spruce bog near Bear Creek	
<i>Poa canbyi</i> (Scribn.) Piper	(P 66)	<i>Carex capillaris</i> L.	(P 66)
Vicinity of Mackintosh*, mesic meadows		Tundra above Vulcan Creek	
Low elevations		5000'	
<i>Poa fendleriana</i> (Steud.) Vasey	(IRRP)	<i>Carex capillaris</i> L. var. <i>elongata</i>	(IRRP)
Scree and rock rubble, Sheep Mt.*		Olney	
Middle elevations		Muskeg and pond margins	
<i>Poa glauca</i> M. Vahl	(IRRP)	<i>Carex capillaris</i> L. ssp. <i>robustior</i>	(P 66)
Dry meadows or scree, dry slopes		(Lge. ex Drej.) Boecher	
Up to 6000'; occasional		Spruce bog	
<i>Poa interior</i> Rydb.	(IRRP)	Low elevations; rare	
Sandbars		<i>Carex capitata</i> L.	(IRRP)
Low elevations; rare		Sand dunes and beaches, sandy flats,	
<i>Poa nemoralis</i> L.	(IRRP)	south end of Kluane Lake	
Willow-spruce		Low elevations; common on these sites	
Low elevations; rare		<i>Carex circinnata</i> C. A. Mey.	(P 66)
<i>Poa pratensis</i> L.	(IRRP)	Alpine tundra above the Slims River	
Meadows		4800'; rare (?)	
Low and middle elevations (?); occasional		<i>Carex concinna</i> R. Br.	(IRRP)
<i>Poa rupicola</i> Nash	(IRRP)	Open spruce on mossy banks	
Middle and high elevations; occasional		3000'-5000' (?); occasional	
<i>Poa williamsii</i> Nash	(P 66)	<i>Carex consimilis</i> Holm	(IRRP)
<i>Puccinellia borealis</i> Swallen	(IRRP)	Mountains west of Burwash Landing	
Eroded river banks		6000'-7000'; rare (?)	
Low elevations; rare		<i>Carex filifolia</i> Nutt.	(IRRP)
<i>Puccinellia hauptiana</i> Krecz.	(IRRP)	Open prairies, and drier open slopes	
Gravel bars and Slims River flats		Up to 3800'; abundant	
Low elevations; common		<i>Carex franklinii</i> Boott	(P 66)
<i>Puccinellia deschampsoides</i> Th. Sør.	(P 66)	Alsek Pass*	
Slims River flats		<i>Carex garberi</i> Fern. var. <i>bifaria</i> Fern.	(IRRP)
Low elevations; rare		Sandy banks, outwashes	
<i>Puccinellia interior</i> Th. Sør.	(P 66)	Low elevations; occasional	
Mackintosh*, open spruce woods		<i>Carex krausei</i> Boeck.	(IRRP)
Low elevations; rare (?)		Moist washes and sandy banks	
<i>Stipa columbiana</i> Macoun	(P 66)	Low elevations; occasional	
Sulphur Lake		<i>Carex lachenalii</i> Schk.	(IRRP)
Low elevations; rare (?)		Alpine meadows	
<i>Stipa comata</i> Trin. & Rupr.	(IRRP)	Above 5000'; common (?)	
South end of Kluane Lake		<i>Carex macloviana</i> d'Urv.	(IRRP)
Low elevations; rare		Prairies and grasslands	
<i>Trisetum spicatum</i> (L.) Richt.	(IRRP)	Low elevations; occasional	
Tundra		<i>Carex maritima</i> Gunn.	(IRRP)
Above 4500'; occasional		Sandy beaches and bogs	
		Low elevations; occasional	
CYPERACEAE		<i>Carex maritima</i> Gunn. ssp. <i>yukonensis</i>	(IRRP)
<i>Carex aquatilis</i> Wahlenb.	(IRRP)	Pors.	
Marshes, pond borders, wet drains on tundra		Sandy beaches and bogs	
Up to 5000'; common		Low elevations; occasional	

- Carex media* R. Br. (IRRP) Mossy banks in spruce woods, muskeg, and tundra
3500'-6000'; common
- Carex membranacea* Hook. (IRRP) Alpine slopes and stream sides
Above 4500'; common
- Carex microchaeta* Holm (IRRP) Tundra and alpine slopes
Above timberline; abundant
- Carex microglochin* Wahlenb. (IRRP) Sandy beaches, river flats
Low elevations; occasional
- Carex microptera* Mack. (P 66) Disturbed ground between Bear and Pine Creeks
Rare
- Carex obtusata* Liljeb. (IRRP) Thin rocky, or gravelly soil, steep dry slopes, open
Up to 4000'; occasional
- Carex parryana* Dew. (IRRP) Prairies and grasslands
Low elevations; occasional
- Carex podocarpa* R. Br. (IRRP) Alpine meadows, brooks, and tundra drainage courses
Above 5000'; common
- Carex praegracilis* Boott (P 66) Alkaline meadows, vicinity of Mackintosh*
Low elevations; rare
- Carex praticola* Rydb. (IRRP) Prairies and grasslands
Low elevations; occasional
- Carex rupestris* All. (P 66) Alpine slopes and tundra
Above 4000'; rare
- Carex scirpoidea* Michx. (IRRP) Subalpine carex-willow communities near timberline
Above 4000'; occasional to common
- Carex siccata* Dew. (P 51) Open prairies, near Haines Junction
Low elevations
- Carex stans* Drejer (P 66) Bogs in alpine slopes, Mt. Decoeli
- Carex stenophylla* Wahlenb. ssp. (IRRP)
- eleocharis* (Bail.) Hult. Dry hillsides
Low elevations
- Carex stylosa* C. A. Mey. (IRRP) Spruce bogs and pond margins
- Carex supina* Willd. ex Wahlenb. ssp. (IRRP)
- spaniocarpa* (Steud.) Hult. Alpine slopes and open moist sites below timberline
Above 3500'; rare
- Carex vaginata* Tausch. (IRRP) Alpine meadows and bogs below timberline
Above 4000'; rare
- Eleocharis pauciflora* (Lightf.) Link var. (P 66)
suksdorfiana (Beauv.) Svens. Vicinity of Mackintosh*
Low elevations; rare
- Eriophorum angustifolium* Honck. (IRRP) Muskeg and marshes
Up to 5500'; common
- Eriophorum callitrix* Cham. (P 66) Moist places, Bear and Pine Creeks
Low elevations (?)
- Eriophorum russeolum* Fr. (IRRP) Bogs and moist places to 5000'
Up to 5000'; common
- Eriophorum triste* (Th. Fr.) Hadac. (P 66) Wet tundra and alpine slopes
Above timberline; rare
- Eriophorum vaginatum* (L.) (IRRP) ssp. *spissum* (Fern.) Hult. Muskeg and bogs
Below timberline; abundant
- Kobresia myosuroides* (Vill.) (IRRP) Fiori & Paol. Open prairies, scree slopes and dry subalpine slopes
Up to 4500'; common
- Kobresia simpliciuscula* (Wahlenb.) (P 66) Mack. Vicinity of Mackintosh*
- LEMNACEAE
- Lemna minor* L. (P 66) Vicinity of Mackintosh*, quiet pools
Low elevations; occasional
- Lemna trisulca* L. (P 66) Alkaline pond, Sulphur Lake
- JUNCACEAE
- Juncus albescens* (Lge.) Fern. (P 66) Alkaline pond, Sulphur Lake
- Juncus alpinus* Vill. ssp. *rariflorus* (IRRP) Hartm. Sunny pools or marshy areas
Rare
- Juncus balticus* Willd. (IRRP) Bogs, mud flats, mesic prairies
Up to 4500'; common
- Juncus balticus* Willd. var. *alaskanus* (IRRP) (Hult.) Pors. Bogs and mud flats along Slims River
Low elevations; occasional
- Juncus balticus* var. *littoralis* Engelm. (P 66) Bogs, wet places
Low elevations; occasional

- Juncus biglumis* L. (IRRP) IRIDACEAE
Tundra and alpine slopes
Above 4500'; occasional
- Juncus castaneus* Sm. (IRRP)
Outwashes, quiet meanders, and wet sandy
banks
Low elevations; occasional
- Juncus drummondii* E. Mey. (P 66)
Bear Creek Summit*
3000'
- Luzula arcuata* (Wahlenb.) Wahlenb. (IRRP)
Stream side in open snowflush area
Above 4500' (?); rare
- Luzula confusa* Lindeb. (IRRP)
Moist meadows, willow thickets, wet
tundra
Above 5000'; occasional to common
- Luzula nivalis* (Laest.) Beurl. (IRRP)
Alpine meadows
Above 4500'; rare
- Luzula nivalis* var. *latifolia* (Kjellm.) Sam. (P 66)
Moist alpine slopes, Mt. Decoeli
- Luzula parviflora* (Ehrh.) Desv. (IRRP)
Alpine meadows and along water courses
Above 4500'; occasional
- Luzula spicata* (L.) DC. (IRRP)
Willow thickets, and along water courses
3000'-5500'; occasional
- LILIACEAE
- Lloydia serotina* (L.) Rchb. (P 66)
Alpine slopes, Mt. Decoeli
Above 4000'; rare
- Smilacina stellata* (L.) Desf. (IRRP)
Open prairies and sandy slopes
Up to 3800'; occasional
- Streptopus amplexifolius* (L.) DC. var. *americanus* Schultes (P 66)
Alder thickets to alpine meadows
Up to 5000'
- Tofieldia coccinea* Richards. (P 66)
Mountains west of Burwash Landing
6000'-7000'; rare
- Tofieldia pusilla* (Michx.) Pers. (IRRP)
Moist sandy areas, bog margins,
mossy banks
Up to timberline; occasional
- Veratrum eschscholtzii* Gray (P 66)
Mt. Decoeli, among willows along streams,
Dusty Glacier
Rare
- Zygadenus elegans* Pursh (IRRP)
Open prairies, gravel slopes, subalpine
meadows
Up to 4500'; common
- Sisyrinchium angustifolium* Miller (P 66)
Near Mackintosh*
Low elevations; rare
- ORCHIDACEAE
- Cypripedium passerinum* Richards. (IRRP)
Shady bogs in spruce forests, or willow
thickets
Up to 3000'; occasional
- Orchis rotundifolia* Pursh (IRRP)
Spruce forests in open places, mossy
banks
Up to 3500'; occasional to rare
- Lysiella obtusata* (Pursh) Rydb. (IRRP)
Shady bogs in spruce or willows
Up to 3500'; occasional
- Limnorchis dilatata* (Pursh) Rydb. (P 66)
Valley of the Alsek River on silty river
meadow, also alpine meadows
- Limnorchis hyperborea* (L.) Rydb. (IRRP)
Shady bogs in spruce or willows
Up to 3500' (?); occasional
- Corallorrhiza trifida* Chat. (P 51)
Kluane Lake and Duke River
- Goodyera repens* (L.) R. Br. var. *ophiodes* Fern. (P 51)
Kluane Lake (?)
- SALICACEAE
- Populus tacamahacca* Mill. = *P. balsamifera* (IRRP)
Well-drained slopes, outwash fans
Up to 4500'; common
- Populus tremuloides* Michx. (IRRP)
Well-drained slopes, pool margins
Up to 3500' (?); occasional
- Salix alaxensis* (Anders.) Cov. (P 66)
Alpine slopes
Above 5000' (?); occasional
- Salix alaxensis* var. *longistylis* (Rydb.) Schneider (IRRP)
Gravel bars and moist slopes
Up to 3500' (?); occasional
- Salix arbusculoides* Anders. (IRRP)
Well-drained slopes
Up to 4000'; occasional
- Salix arctica* Pall. (IRRP)
Tundra
Above 4500'; occasional
- Salix athabascensis* Raup (IRRP)
Willow thickets, burned-over spruce
forests
Low elevations; rare (?)
- Salix barrattiana* Hook. (IRRP)
Subalpine meadows in willow thickets

- Salix bebbiana* Sarg. (IRRP) POLYGONACEAE
Spruce-willow communities
Low elevations; occasional
- Salix candida* Flügge (P 66)
Calcareous marsh near Mackintosh*
Low elevations; rare
- Salix dodgeana* Rydb. (IRRP)
Alpine slopes
Above 5000'; rare
- Salix glacialis* Anders. (P 66)
Valley of the Alsek River on gravelly
beach
Low elevations; rare
- Salix glauca* L. (IRRP)
Spruce-forest understory and stream sides
Low elevations (?); occasional
- Salix glauca* var. *acutifolia* (IRRP)
Schneider
Ubiquitous
Up to 5000'; abundant
- Salix interior* Rowlee var. *pedicellata* (P 66)
(Anders.) Ball
Roadside near Mackintosh*
Low elevations; rare
- Salix myrtillofolia* Anders. (IRRP)
Meadows and open spruce woods,
where moist
Up to 4000' (?); common
- Salix niphoclada* Rydb. (IRRP)
Meadows
Up to 5000' (?); occasional
- Salix planifolia* Pursh (IRRP)
Muskeg to birch-willow association,
river flats
Up to 5000' (?); occasional
- Salix pseudopolaris* Flod. (IRRP)
Alpine slopes and tundra
Above 5500'; occasional
- Salix reticulata* L. (IRRP)
Bogs, mossy banks, tundra
Up to 6000'; common
- Salix richardsonii* Hook. (IRRP)
Willow-birch association
3500'-6000'; occasional to common
- Salix setchelliana* Ball (IRRP)
Gravel bars and beaches
Low elevations; occasional
- Salix stolonifera* Cov. (P 66)
Mountains west of Burwash Landing
6000'-7000' (?); rare
- BETULACEAE
- Betula glandulosa* Michx. (IRRP)
Mesic meadow borders, subalpine willow-
birch communities
Up to 6000'; common (at high elevations)
- Rumex occidentalis* Wats. (P 51)
Vicinity of Mackintosh*
Damp places
- Rumex utahensis* Rech. (P 51)
Haines Junction; Mile 1016
- Oxyria digyna* (L.) Hill (IRRP)
Snowflush and alpine stream communities
Above 4000'; occasional
- Polygonum bistorta* ssp. *plumosum* (IRRP)
(Small) Hult.
Wet tundra, birch-willow communities
Above 3500'; occasional
- Polygonum viviparum* L. (IRRP)
Wet or mesic open places
2300'-6000'; occasional
- CHENOPODIACEAE
- Chenopodium album* L. (IRRP)
Roadside weed
2300'; occasional
- Chenopodium capitatum* (L.) Aschers. (IRRP)
Weed along roadside, habitations, or
cultivated areas
2300'; occasional
- Chenopodium rubrum* L. var. *humile* (P 66)
(Hook.) Wats.
Wet depressions in alkali meadow,
Mackintosh*
2000'
- Monolepis nuttalliana* (Schultes) Greene (P 66)
Haines Junction
- Suaeda maritima* (L.) Dum. (P 66)
Alkali flats near Mackintosh*
- PORTULACACEAE
- Claytonia bostockii* Pors. (IRRP)
Tundra, birch-willow, and mossy banks
3000'-6000' occasional to common
- Claytonia sarmentosa* C. A. Mey. (IRRP)
Tundra, birch-willow, and mossy banks
?-5000'; occasional
- Claytonia tuberosa* Pall. (IRRP)
Tundra, birch-willow
5000'; rare (?)
- CARYOPHYLLACEAE
- Cerastium arvense* L. (P 66)
Haines Junction
- Stellaria laeta* Richards. (IRRP)
5500'
- Stellaria longipes* Goldie (IRRP)
Many plant communities
2000' to 5500'; common

<i>Stellaria monantha</i> Hult. 8500'	(IRRP)	<i>Anemone multifida</i> Poir.	(IRRP)
<i>Stellaria umbellata</i> Turcz. 6000'; rare	(IRRP)	Open prairies and partial shade of willows	
<i>Arenaria arctica</i> Stev. Kluane Lake	(IRRP)	Low altitudes; common	
<i>Arenaria lateriflora</i> L. Mouth of Gladstone Creek	(IRRP)	<i>Anemone narcissiflora</i> L.	(P 51)
Low altitudes; occasional		Alpine communities	
<i>Arenaria macrocarpa</i> Pursh Tundra above Vulcan Creek	(P 66)	4000'-7000'; occasional	
<i>Arenaria obtusiloba</i> (Rydb.) Fern. Alek Pass*, Mt. Archibald, ridge near Sulphur Lake, west of Kluane Lake	(IRRP)	<i>Anemone parviflora</i> Michx.	(IRRP)
<i>Arenaria rossii</i> R. Br. ssp. <i>elegans</i> (Cham. & Schlecht.) Maguire Mt. Archibald	(P 66)	Ubiquitous in wet places	
<i>Arenaria sajanensis</i> Willd. ex Schlecht. Up to 6000'	(IRRP)	Low to middle altitudes; occasional	
<i>Arenaria uliginosa</i> Schlecht. Southeast end of Kluane Lake	(P 66)	<i>Aquilegia formosa</i> Fisch.	(P 51)
<i>Arenaria verna</i> L. var. <i>pubescens</i> (Cham. & Schlecht.) Fern. Kluane Lake 5000'-7000'	(P 51)	Alek Pass*, willow thickets; rare	
<i>Melandrium apetalum</i> (L.) Fenzl. ssp. <i>attenuatum</i> (Farr) Hara Mt. Decoeli, Mt. Archibald, Sheep Mt.*, Ruby Ranges 4000'-5000'	(IRRP)	<i>Delphinium glaucum</i> S. Wats.	(IRRP)
<i>Silene acaulis</i> L. var. <i>excapa</i> (All.) DC. Kluane and Ruby Ranges 4000'-7000'; occasional	(IRRP)	Moist willow thickets and spruce-willow communities	
<i>Silene menziesii</i> Hook. Haines Junction Low elevations	(P 51)	3000'-4500'; occasional	
<i>Silene repens</i> Patr. Kluane Ranges 4500'	(IRRP)	<i>Ranunculus aquatilis</i> L. var. <i>eradicatus</i> Laest.	(IRRP)
<i>Silene williamsii</i> Britt. Near Mackintosh* Low elevations; occasional	(P 51)	Shallow lakes; occasional	
		<i>Ranunculus circinatus</i> Sibth. var. <i>subrigidus</i> (Drew) Benson	(P 66)
		Lake on Mt. Archibald; rare	
		<i>Ranunculus cymbalaria</i> Pursh	(IRRP)
		Slims River flats, wet mud flats on most streams	
		2600'-3500'; common	
		<i>Ranunculus eschscholtzii</i> Schlecht.	(IRRP)
		Snowflush, or alpine meadow, gravel bars	
		5000'-?; occasional	
		<i>Ranunculus gelidus</i> Karel. & Kiril.	(P 66)
		Mt. Decoeli	
		Alpine; rare	
		<i>Ranunculus nivalis</i> L.	(IRRP)
		Snowflush or alpine meadow	
		Above 4500'; occasional	
		<i>Ranunculus pedatifidus</i> Smith	(IRRP)
		Tundra, alpine streams	
		Above 4500'; rare	
		<i>Ranunculus purshii</i> Richards.	(P 66)
		Pond near Mackintosh*	
		<i>Ranunculus pygmaeus</i> Wahlenb.	(IRRP)
		Snowflush and stream sides	
		Above 4500'; occasional	
		<i>Ranunculus sceleratus</i> L. ssp. <i>multifidus</i> (Nutt.) Hult.	(IRRP)
		Muskeg near vernal pool	
		2600'-?; occasional	
		<i>Ranunculus sulphureus</i> Soland.	(IRRP)
		5000'; rare	
		<i>Pulsatilla ludoviciana</i> (Nutt.) Heller (<i>Anemone patens</i> ssp. <i>multifida</i> Hult.)	(IRRP)
		Meadow and prairie community	
		Low elevations; occasional	

RANUNCULACEAE

PAPAVERACEAE			
<i>Papaver keelei</i> Pors.	(IRRP)	<i>Draba aurea</i> M. Vahl	(P 66)
Tundra		Vicinity of Mackintosh*	
Above 5000'; rare		Low elevations; occasional to common	
<i>Papaver macounii</i> Greene	(P 66)	<i>Draba cinerea</i> Adams	(IRRP)
Tundra		Prairies and dry open slopes	
Above 5000'; occasional		2000'-4500'; occasional	
<i>Papaver radiculatum</i> Rottb. ssp.	(IRRP)	<i>Draba crassifolia</i> Grah.	(IRRP)
<i>occidentale</i> Lundstr.		Snowflashes and scree, Mt. Archibald	
Tundra		Alpine; rare	
Above 4500'; occasional		<i>Draba glabella</i> Pursh	(IRRP)
FUMARIACEAE		Apparently ubiquitous in dry to mesic sites	
<i>Corydalis pauciflora</i> (Steph.) Pers.	(IRRP)	Middle elevations	
Duke River west of Kluane Lake		<i>Draba incerta</i> Payson	(P 66)
Up to 6000'; rare		Mt. Archibald and Mt. Decoeli	
CRUCIFERAE		Alpine (?); rare	
<i>Arabis divaricarpa</i> A. Nels.	(IRRP)	<i>Draba lactea</i> Adams	(IRRP)
Gravel bars and dry sandy areas		Tundra and alpine slopes	
Low elevations; occasional		5000' (?); rare	
<i>Arabis drummondii</i> A. Gray	(P 66)	<i>Draba lanceolata</i> Royle	(IRRP)
Roadsides near Mackintosh*; rare		Open areas, mesic to dry sites	
<i>Arabis hirsuta</i> (L.) Scop. ssp.	(P 66)	Low and middle elevations; occasional	
<i>pyncocarpa</i> (Hopkins) Hult.		<i>Draba longipes</i> Raup	(IRRP)
Weed along roadsides near Mackintosh*; rare		Alpine slopes	
<i>Arabis holboellii</i> Hornem. var	(IRRP)	High elevations (?)	
<i>retrofracta</i> (Grah.) Rydb.		<i>Draba nivalis</i> Liljebl.	(IRRP)
Prairies and gravel bars		Alpine slopes and tundra	
2000'-4500'; common		Above 5000'; occasional	
<i>Arabis lemmonii</i> S. Wats.	(IRRP)	<i>Draba oligosperma</i> Hook.	(IRRP)
Mt. Archibald, alpine slopes,		Scree and dry open slopes	
Nunatak approximately 8 miles east of the terminus of the Kaskawulsh Glacier; rare		?-5500'; occasional	
<i>Braya humilis</i> (C.A. Mey.) Robins.	(IRRP)	<i>Draba palanderiana</i> Kjellm.	(IRRP)
Gravel bars, prairies and disturbed places		Alpine slopes	
2000'-6000'; common		Above 5000'; occasional	
<i>Cardamine bellidifolia</i> L.	(IRRP)	<i>Draba praealta</i> Greene	(P 66)
Alpine scree or snowflush		Vicinity of Makintosh*	
Up to 6000' (?); occasional		Low elevations; occasional	
<i>Cardamine purpurea</i> Cham. & Schlecht.	(IRRP)	<i>Draba stenoloba</i> Ledeb.	(IRRP)
Snowflush, and subalpine communities		Dry open places	
Alpine (?); occasional		Low elevations; rare	
<i>Cardamine umbellata</i> Greene	(P 66)	<i>Draba stenopetala</i> Trautv.	(P 66)
Above 4500' (?)		Tundra and alpine slopes	
<i>Descurainia richardsonii</i> (Sweet) Schulz	(IRRP)	Above 5000'; occasional	
Mesic meadows and wet open bogs		<i>Erysimum cheiranthoides</i> L.	(IRRP)
Low elevations; occasional		Gravel bars and open prairies	
<i>Descurainia sphioides</i> (Fisch.) Schulz	(IRRP)	Low elevations; occasional	
Weed around habitations and disturbed places		<i>Erysimum inconspicuum</i> (S. Wats.) MacMill.	(IRRP)
Low elevations; occasional		Gravel bars and open prairies	
		Low elevations; occasional	
		<i>Erysimum pallasii</i> (Pursh) Fern.	(P 66)
		Mt. Archibald	
		4000'-6000'; rare	
		<i>Eutrema edwardsii</i> R. Br.	(IRRP)
		Tundra and birch-willow communities	
		Above 4000'; occasional	

- Halimolobos mollis* (Hook.) Rollins (P 66)
Vicinity of Mackintosh*
Low elevations (?)
- Lepidium densiflorum* Schrad. (IRRP)
Weedy around habitations
Low elevations; occasional
- Lesquerella arctica* (Richards.) Wats. (P 66)
ssp. purshii (Wats.) Pors.
Open prairies and gravel bars to alpine tundra
- Parrya nudicaulis* (L.) Regel (IRRP)
Tundra, birch-willow, and alpine heath
Above 5500'; occasional
- Rorippa islandica* (Oed.) Borb. var. (IRRP)
microcarpa (Regel) Fern.
Wet meadows
Low elevations; occasional
- Thlaspi arcticum* Pors. (P 66)
Above Vulcan Creek
5600'; rare
- Smelowskia borealis* (Greene) Drury & Rollins (IRRP)
Scree
Above 5000'; rare
- CRASSULACEAE
- Sedum lanceolatum* Torr. (IRRP)
Dry sites
5000'-6000'; rare
- Sedum rosea* ssp. *integrifolium* Hult. (IRRP)
Alpine slopes
Above 4000'; occasional
- SAXIFRAGACEAE
- Chrysoplenium tetrandrum* (Lund) Fries (IRRP)
Sandy alpine depressions in rock outcrops
Above 5000'; occasional
- Chrysoplenium wrightii* Franch. & Sav. (IRRP)
6000'; rare
- Parnassia kotzebuei* Cham. & Schlecht. (IRRP)
Wet sandy places, partial shade
Below timberline rarely; to 5500' common
- Parnassia palustris* L. var. *neogaea* Fern. (IRRP)
Wet sandy places, open to partial shade
Below timberline; common
- Saxifraga adscendens* L. ssp. *oregonensis* (Raf.) Bacigalupi (IRRP)
Mt. Archibald, Kluane Ranges
Up to 6000'; rare
- Saxifraga bronchialis* L. ssp. *funstonii* (Small) Hult. (IRRP)
Alpine slopes or tundra
Above 4000'; occasional
- Saxifraga caespitosa* L. ssp. *monticola* (Small) Pors. (IRRP)
Mt. Archibald and Mt. Decoeli
Above 4000'; rare
- Saxifraga cernua* L. (IRRP)
Snowflush and alpine slopes
Above 4000'; occasional
- Saxifraga davurica* Willd. ssp. *grandipetala* (Engler & Irmsch.) Hult. (IRRP)
Alpine slopes
Above 4500'; occasional
- Saxifraga flagellaris* Willd. (IRRP)
Muskeg, bogs, and tundra
Middle elevations; occasional
- Saxifraga hieracifolia* Waldstr. & Kit. (IRRP)
Muskeg, birch-willow, tundra
Above 3500'; occasional
- Saxifraga hirculus* L. (IRRP)
Muskeg, tundra
Above 3000'; occasional
- Saxifraga lyallii* Engler (P 66)
Mossy slope near Mackintosh*
- Saxifraga oppositifolia* L. (IRRP)
Alpine slopes
Above 5000'; occasional to common
- Saxifraga punctata* L. ssp. *insularis* Hult. (IRRP)
Snowflush and alpine watercourses
Above 4500'; common
- Saxifraga reflexa* Hook. (IRRP)
Alpine slopes; occasional
- Saxifraga serphyllifolia* Pursh (IRRP)
Alpine slopes and dry tundra
Above 5000'; occasional
- Saxifraga tenuis* (Wahlenb.) Sm. (IRRP)
Alpine slopes
Above 4500'; occasional to common
- Saxifraga tricuspidata* Rottb. (IRRP)
- GROSSULARIACEAE
- Ribes hudsonianum* Richards. (IRRP)
Aspen and cottonwood stands in open areas
Low elevations; rare
- Ribes oxycanthoides* L. (IRRP)
Gravel terraces and open prairies near Mackintosh*
Low elevations; occasional
- ROSACEAE
- Chamaerhodos erecta* (L.) Bunge (IRRP)
Prairies and *Artemisia* balds, scree and rocky slopes
Low elevations to 4000'; common
- Dryas alaskensis* Pors. (P 66)
Alpine tundra
7000'
- Dryas crenulata* Juz. (P 66)
Mt. Archibald

- Dryas drummondii* Richards. (IRRP)
Gravel bars and washes subject to occasional flooding
Low elevations; common
- Dryas hookeriana* Juz. (P 66)
Mt. Archibald, alpine slopes
4000'
- Dryas integrifolia* M. Vahl (IRRP)
Tundra
Above 4500'; abundant
- Dryas octopetala* L. (P 66)
Tundra
Above 4500'; occasional
- Dryas punctata* Juz. (P 51)
Tundra
Above timberline
- Dryas sylvatica* (Hult.) Pors. (P 51)
Tundra and openings in spruce forests at low elevations
Low and middle elevations; occasional
- Geum aleppicum* Jacq. var. *strictum* Ait. (P 66)
Near Mackintosh*
- Geum macrophyllum* Willd. ssp. *perincisum* (Rydb.) Hult. (IRRP)
Wet meadows and openings in willow thickets
Low elevations; common
- Fragaria glauca* (S. Wats.) Rydb. (IRRP)
Meadows and mesic prairies
Low elevations; occasional
- Potentilla arguta* Pursh ssp. *convallaria* (Rydb.) Keck (IRRP)
Vicinity of Mackintosh*, mesic prairies
Low elevations; occasional
- Potentilla biflora* Willd. (IRRP)
Alpine slopes and tundra
Above 5000'; occasional
- Potentilla diversifolia* Lehm. var. *glaucophylla* Lehm. (IRRP)
Open gravel terraces and slopes, mesic sites
Low elevations; occasional
- Potentilla fruticosa* L. (IRRP)
Mesic sites, many plant communities
Low to medium elevations; common
- Potentilla furcata* Pors. (IRRP)
Prairies and open slopes
Low elevations; occasional
- Potentilla glabella* Rydb. (P 66)
Vicinity of Mackintosh*
- Potentilla gracilis* Dougl. ssp. *nuttallii* (Lehm.) Keck (IRRP)
Gravel terraces and washes, roadsides
Low elevations; occasional
- Potentilla hyparctica* Malte (IRRP)
Tundra and alpine slopes to wet meadows
Apparently ubiquitous; occasional
- Potentilla multifida* L. (IRRP)
Silver City, at Kluane Lake
Rare
- Potentilla nivea* L. ssp. *fallax* Pors. (IRRP)
Open rocky slopes
3500'-6500'; occasional
- Potentilla nivea* L. ssp. *hookeriana* (Lehm.) Hiit. (P 66)
Open rocky slopes and tundra
Occasional
- Potentilla nivea* L. ssp. *tomentosa* Nilsson-Ehle (IRRP)
Open tundra
Above 4500'; rare
- Potentilla norvegica* L. var. *hirsuta* (Michx.) Lehm. (IRRP)
Open meadows
Low elevations; occasional
- Potentilla pennsylvanica* L. var. *strigosa* Pursh (IRRP)
Roadsides, prairies and open slopes
Low to middle elevations; common
- Potentilla rubricaulis* Lehm. (IRRP)
Rare
- Potentilla uniflora* Ledeb. (IRRP)
Dry tundra
Above 4500'; rare
- Potentilla yukonensis* Hult. (CAN)
Roadsides and open gravel terraces
Low elevations
- Rubus chamaemorus* L. (IRRP)
Aspen woods in open areas
Middle elevations; rare
- LEGUMINOSAE
- Astragalus aboriginum* Richards. (IRRP)
Open sandy areas on gravel outwashes or bars
Up to 5500'; occasional
- Astragalus alpinus* L. (IRRP)
Mesic sites in partial shade of woods
Up to 5000'; occasional to common
- Astragalus americanus* (Hook.) Jones (IRRP)
Open spruce stands
Up to near timberline; occasional to common
- Astragalus eucosmus* Robins. (P 66)
Vicinity of Mackintosh*
Low elevations; rare
- Astragalus linearis* (Rydb.) Pors. (P 66)
Open areas, gravel washes
Up to 4500'
- Astragalus nutzotinensis* Rousseau (IRRP)
Open rocky slopes
Medium elevations; occasional
- Astragalus striatus* Nutt. (IRRP)
Gravel terraces
Low elevations; occasional to common

- Astragalus tananaicus* Hult. (P 66) Low elevations
- Astragalus umbellatus* Bunge (IRRP) Tundra
Above 4500'; occasional
- Astragalus williamsii* Rydb. (IRRP) Mesic sites in open spruce woodland
Low to medium elevations; occasional
- Astragalus yukonis* M. E. Jones (IRRP) Mesic sites on sand bars and gravel slopes
Low elevations; occasional
- Hedysarum alpinum* L. var. *americanum* Michx. (IRRP) Shady to open places in woods and by streams
Low to medium elevations; occasional to common
- Hedysarum mackenzii* Richards. (IRRP) Open gravel bars and outwashes
Low elevations; abundant
- Lupinus arcticus* S. Wats. (IRRP) Widespread
All elevations; common
- Lupinus sericeus* Pursh (P 66) Vicinity of Mackintosh*
Low elevations; rare
- Oxytropis foliolosa* Hook. (IRRP) Willow thickets along streams and gravel bars
Low elevations; occasional
- Oxytropis glutinosa* Pors. (IRRP) Open gravel slopes
Low altitudes; occasional
- Oxytropis gracilis* Nels. (IRRP) Mesic prairie sites
Low elevations; abundant
- Oxytropis huddelsonii* Pors. (IRRP) Mt. Archibald and Mt. Decoeli, Kluane Ranges
Above 4000'; common
- Oxytropis maydelliana* Trautv. (IRRP) Alpine slopes, tundra
Above 5000'; occasional
- Oxytropis pygmaea* (Pall.) Fern (IRRP) Kluane Ranges
Alpine, above 4000'; rare
- Oxytropis retrorsa* Fern. var. *sericea* (T. & G.) Fern. (IRRP) Willow thickets and gravel bars along streams
Low elevations; common
- Oxytropis scammaniana* Hult. (IRRP) Tundra or alpine slopes
Above 5500'; rare
- Oxytropis spicata* (Hook.) Standl. (P 66)
- Oxytropis splendens* Dougl. ex Hook. (IRRP) Prairies and *Artemisia* balds
Low elevations; common
- Oxytropis varians* (Rydb.) Hult. (P 66) Low elevations
- Oxytropis verruculosa* Pors. (P 66) Above 5000'; rare
- Oxytropis viscida* Nutt. (IRRP) Open prairies and rocky slopes
Low elevations; occasional
- Oxytropis viscidula* (Rydb.) Tidestr. ssp. *sulphurea* Pors. (IRRP) Open prairies and rocky slopes
Low and middle elevations; occasional
- LINACEAE
- Linum perenne* L. ssp. *lewisii* (Pursh) Hult. (IRRP) Dry slopes and prairies
Up to 4500'; common
- EMPETRACEAE
- Empetrum nigrum* L. (P 51) Understory of open spruce forest and muskeg
Low to middle elevations; common
- ELAEAGNACEAE
- Shepherdia canadensis* (L.) Nutt. (IRRP) Willow-spruce and open spruce forests
Low elevations; abundant
- Elaeagnus commutata* Bernh. (IRRP) Understory in cottonwood stands on gravel outwashes
Low elevations; common
- ONAGRACEAE
- Epilobium anagallidifolium* Lam. (IRRP) Valley north and above the terminus of the Kaskawulsh Glacier
5500'-6000'
- Epilobium angustifolium* L. (IRRP) Disturbed places, pioneer after fire
Up to 6000'; common
- Epilobium latifolium* L. (IRRP) Gravel bars and disturbed places
Low and middle elevations; common
- Epilobium leptophyllum* Raf. (P 66) Vicinity of Mackintosh*
- HALORAGACEAE
- Myriophyllum exalbescens* Fern. (P 66) Ponds
Low and middle elevations; occasional

<i>Hippurus vulgaris</i> L.	(IRRP)	PRIMULACEAE	
Ponds		<i>Androsace alaskana</i> Cov. & Standl.	(P 66)
Low and middle elevations		Mt. Decoeli	
		4000'; rare	
UMBELLIFERAE		<i>Androsace chamaejasme</i> Host. var. <i>arctica</i>	(IRRP)
<i>Bupleurum americanum</i> C. & R.	(IRRP)	Knuth	
Gravel outwashes, upper Gladstone Creek drainage		Alpine slopes	
4000'; locally common		Above 4000'; occasional	
<i>Coelopleurum gmelini</i> (DC.) Ledeb.	(IRRP)	<i>Androsace septentrionalis</i> L.	(IRRP)
Scree slopes, Alsek Pass*		Rocky slopes in protected places	
3500'; occasional		Above 3000'; occasional	
<i>Conioselinum cnidiifolium</i> (Turcz.) Pors.	(IRRP)	<i>Douglasia gormanii</i> Constance	(IRRP)
Roadside in northern Shakwak Trench		Scree and rocky slopes, subalpine	
Low elevations; occasional		Above 3500'; occasional	
PYROLACEAE		<i>Dodecatheon frigidum</i> Cham. & Schlecht.	(IRRP)
<i>Moneses uniflora</i> (L.) Gray	(IRRP)	Tundra	
Mossy banks near springs in spruce forest		Above 4500'; occasional	
Low and middle elevations; occasional		<i>Primula borealis</i> Duby	(P 66)
<i>Pyrola asarifolia</i> Michx. var. <i>incarnata</i>	(P 51)	Donjek flood plains	
(Fisch.) Fern.		Low elevations (?); rare	
Bogs and wet places in willow stands		<i>Primula sibirica</i> Jacq.	(IRRP)
Low elevations; occasional		Vicinity of Mackintosh* and Christmas Bay,	
<i>Pyrola grandiflora</i> Rad.	(IRRP)	gravel bars	
Bogs, tundra, mossy banks, etc.		Low elevations; rare	
Up to 5500'; common		<i>Primula stricta</i> Hornem.	(P 66)
		Alkaline flat near Mackintosh*	
		Low elevations (?); rare	
ERICACEAE		GENTIANACEAE	
<i>Arctostaphylos rubra</i> (Rehd. & Wils.) Fern.	(IRRP)	<i>Gentiana algida</i> Pall.	(IRRP)
Understory in spruce forests, mossy banks,		Birch-willow or willow-carex communities	
muskeg, subtundra		Above 3000'-5000'; occasional	
Up to 5500'; common		<i>Gentiana amarella</i> L.	(IRRP)
<i>Arctostaphylos uva-ursi</i> (L.) Spreng.	(IRRP)	Mesic prairies	
Mesic areas mainly on burned spruce		Low elevations (?); occasional	
forests and ecotonal to prairies		<i>Gentiana detonsa</i> s. lat.	(IRRP)
Up to 5000'; abundant		Mesic prairies	
<i>Cassiope tetragona</i> (L.) D. Don	(IRRP)	Low elevations; occasional	
Birch-willow and snow beds on north and		<i>Gentiana glauca</i> Pall.	(IRRP)
east tundra slopes		Subalpine and snowflush (?)	
Above 5000'; common		Medium to high elevations; rare	
<i>Ledum groenlandicum</i> Oed.	(IRRP)	<i>Gentiana propinqua</i> Richards.	(IRRP)
Muskeg and open spruce forests		Mesic meadows and moist open areas	
Lower and middle elevations; abundant		Low and middle altitudes; common	
<i>Vaccinium caespitosum</i> Michx.	(P 66)	<i>Gentiana prostrata</i> Haenke	(IRRP)
Vicinity of Mackintosh*		Wet meadows and bogs	
3000'		Low elevations; occasional	
<i>Vaccinium uliginosum</i> L.	(IRRP)	<i>Gentiana tenella</i> Rottb.	(IRRP)
Muskeg, willow-birch and rocky outcrops		Steele Glacier	
on tundra		5000'-6500'; rare	
Above 3000'; abundant		<i>Lomatogonium rotatum</i> (L.) Fr. ssp.	(IRRP)
<i>Vaccinium vitis-idaea</i> L. var. <i>minus</i> Lodd.	(IRRP)	<i>tenuifolium</i> (Grieseb.) Pors.	
Understory in spruce forests and		Bogs and flood plains	
mossy banks		Low elevations; rare	
Low and middle altitudes			

- POLEMONIACEAE**
- Phlox richardsonii* Hook. (IRRP)
Badlands Creek*, alpine tundra,
Steele Glacier
5000'-6000'; rare
- Polemonium acutiflorum* Willd. (IRRP)
Open spruce woods and birch-willow
Above 3500'; occasional
- Polemonium boreale* Adams (IRRP)
Open alpine slopes
Above 5500'; occasional
- Polemonium pulcherrimum* Hook. (IRRP)
Mesic prairies
Low elevations; common
- BORAGINACEAE**
- Eritrichium aretioides* (Cham.) DC. (IRRP)
Tundra
Above 5000'; rare
- Lappula myosotis* Moench (IRRP)
Open slopes
Low to middle elevations; common
- Lappula redowskii* (Hornem.) Greene (P 66)
var. *occidentalis* (S. Wats.) Rydb.
Mackintosh*
Low elevations
- Myosotis alpestris* Schm. ssp. *asiatica* (IRRP)
Vesterg.
Tundra and mossy banks
Above 4000' (?); common
- Mertensia paniculata* (Ait.) G. Don (IRRP)
Spruce forests and willow-spruce
Up to 4500'; common
- SCROPHULARIACEAE**
- Castilleja hyperborea* Pennell (IRRP)
Rocky slopes, scree, and tundra
Above 3500' (?); occasional
- Castilleja muelleri* Pennell (P 51)
Kluane Lake to Donjek River
- Castilleja pallida* (L.) Spreng. ssp. (P 66)
caudata Pennell
Dry open places
- Castilleja raupii* Pennell (P 66)
Silver City, Kluane Lake
Low elevations; rare
- Castilleja unalaschcensis* (Cham. & Schlecht.) (P 66)
Malte
Mackintosh*, Mt. Decoeli, Mt. Archibald
Up to 3500' (?); rare
- Castilleja villosissima* Pennell (P 51)
Bear Creek
Low elevations (?); rare
- Castilleja yukonis* Pennell (IRRP)
Dry open hillsides
Up to 3500'; common
- Euphrasia subarctica* Raup (IRRP)
Springs on sandy soil
Low elevations; rare
- Pedicularis arctica* R. Br. (*P. langsdorffii*) (IRRP)
Tundra
Above 5000'; occasional
- Pedicularis capitata* Adams (IRRP)
Tundra
Above 4500'; occasional
- Pedicularis labradorica* Wirsing (IRRP)
Muskeg and wet open woods
Up to 4500'; occasional
- Pedicularis lanata* Cham. & Schlecht. (IRRP)
Tundra and birch-willow association
Above 4500'; rare
- Pedicularis oederi* M. Vahl (IRRP)
Tundra
Above 4500'; occasional
- Pedicularis sudetica* Willd. (IRRP)
Damp, open, or partially shaded mossy
areas, bogs
Up to 4500'; common
- Pedicularis verticillata* L. (IRRP)
Steele Glacier area
6000'
- Penstemon gormanii* Greene (IRRP)
Dry, open prairies and rocky slopes
Up to 3500'; common
- Penstemon procerus* Dougl. (IRRP)
Mesic meadows
Up to 5000' (?); occasional
- Veronica alpina* L. var. *alterniflora* Fern. (IRRP)
Alpine meadows (?)
Above 3500' (?); occasional
- Veronica alpina* L. var. *unalaschcensis* (IRRP)
Cham. & Schlecht. (*V. wormskjoldii*)
Alpine meadows
Above 4500' (?); occasional
- Veronica americana* Schwein. (P 66)
Near Mackintosh*
Low elevations (?); rare
- Veronica scutellata* L. (IRRP)
Wet meadows and springs
Low elevations; occasional to rare
- LENTIBULARIACEAE**
- Utricularia vulgaris* L. var. *americana* Gray (P 66)
Elsek Lake
Rare
- PLANTAGINACEAE**
- Plantago eriopoda* Torr. (P 66)
Bear Creek and Mackintosh*
Low elevations; occasional (?)

- Plantago septata* Morris (IRRP)
Dry open prairies
Low elevations; common
- RUBIACEAE
- Galium boreale* L. (IRRP)
Mesic habitats in open or low shrub communities
Low and middle elevations; common
- Galium brandegei* Gray (IRRP)
Vernal pools and mudflats
Low elevations; rare
- Galium triflorum* Michx. (P 66)
Mt. Archibald
4000'; rare
- CAPRIFOLIACEAE
- Linnaea borealis* L. var. *americana* (Forbes) Rehd. (IRRP)
Open woods
Up to timberline; common
- ADOXACEAE
- Adoxa moschatellina* L. (P 66)
Alder thickets, Mt. Archibald
Rare
- VALERIANACEAE
- Valeriana capitata* Pall. (IRRP)
Open areas in spruce forests and spruce-willow communities
Up to 4500'; occasional
- Valeriana sitchensis* Bong. (P 66)
Mt. Archibald
4000'; rare
- CAMPANULACEAE
- Campanula lasiocarpa* Cham. (IRRP)
Tundra
Above 5500'; occasional
- Campanula uniflora* L. (IRRP)
Kluane Ranges
4000'-5500'
- COMPOSITAE
- Achillea compacta* Malte (IRRP)
6000'
- Achillea millefolium* L. var. *nigrescens* E. Mey. (IRRP)
Vicarious in nearly all communities
Up to 5500'
- Antennaria alborosea* Pors. (P 66)
Vicinity of Mackintosh*, dry roadsides
Low elevations
- Antennaria elegans* Pors. (P 66)
Bear Creek on gravel terrace
Low elevations
- Antennaria incarnata* Pors. (P 66)
Near Mackintosh*
Low elevations
- Antennaria laingii* Pors. (IRRP)
- Antennaria nitida* Greene (IRRP)
Open dry prairie communities
Low elevations; common
- Antennaria pallida* E. Nels. (P 66)
Near Mackintosh*
- Antennaria philonipha* Pors. (IRRP)
Muskeg and mossy areas
High elevations
- Antennaria pulcherrima* (Hook.) Greene (IRRP)
Vicarious (?)
Low and middle elevations; common
- Antennaria rosea* (Eaton) Greene (IRRP)
Open prairie (?)
Low elevations; occasional
- Antennaria subviscosa* Fern. (P 66)
Near Mackintosh*
- Agoseris aurantiaca* (Hook.) Greene (P 66)
Bear Creek Summit*
Low elevations
- Arnica alpina* (L.) Olin ssp. *angustifolia* (J. Vahl) Maguire (IRRP)
Tundra
High elevations; occasional
- Arnica chamissonis* Less. ssp. *incana* (Gray) Maguire (IRRP)
Mesic prairies
Low elevations; common
- Arnica lessingii* Greene (IRRP)
Tundra, mesic sites
Above 4500'; occasional
- Arnica lonchophylla* Greene ssp. *genuina* Maguire (P 66)
Dry prairies and open woods
Low elevations
- Artemisia alaskana* Rydb. (IRRP)
Open prairies and gravel terraces
Low elevations; rare to occasional
- Artemisia arctica* Less. (IRRP)
Rocky, open slopes or spruce-willow and willow-birch communities
Middle elevations to 5000'; occasional
- Artemisia dracunculus* L. (IRRP)
Open sites, rocky hillsides
Up to 5000'; occasional
- Artemisia frigida* Willd. (IRRP)
Dry open prairies and rocky hillsides
Up to 4500'; abundant

<i>Artemisia hyperborea</i> Rydb.	(IRRP)	<i>Erigeron grandiflorus</i> Hook.	(IRRP)
Rocky slopes on gravel		Open prairies and rocky slopes	
3000'-6000'; abundant		Up to 4500'; occasional	
<i>Artemisia kruhsiana</i> Bess.	(IRRP)	<i>Erigeron lanatus</i> Hook.	(IRRP)
Open gravel outwashes and dry slopes		Alsek Pass*	
Low elevations; common		Scree or rocky slopes; rare	
<i>Artemisia rupestris</i> L. ssp. <i>woodii</i> Neilson	(IRRP)	<i>Erigeron lonchophyllus</i> Hook.	(IRRP)
Open rocky slopes		Roadside at south end of Kluane Lake	
3500'-5000'; locally common		Low elevations; rare	
<i>Artemisia tilesii</i> Ledeb.	(IRRP)	<i>Erigeron purpuratus</i> Greene	(IRRP)
Mesic sites on scree and rocky slopes		Open gravel or rocky slopes	
3500'-5500'; occasional		8500'-9200'; occasional	
<i>Artemisia tilesii</i> Ledeb. var. <i>elatior</i> T. & G.	(IRRP)	<i>Erigeron trifidus</i> (Hook.) Gray	(P 51)
Mesic sites along streams and gravel terraces		<i>Erigeron unalaschkensis</i> (DC.) Vierh.	(P 51)
Low elevations; occasional		Mt. Archibald and Mt. Decoeli	
<i>Artemisia tilesii</i> Ledeb. var. <i>gormanii</i> (?)	(IRRP)	4000'	
(Rydb.) Hult.		<i>Erigeron uniflorus</i> L. ssp. <i>eriocephalus</i>	(IRRP)
Mesic sites on steep slopes in willows,		(Vahl) Cronq.	
scrub		Tundra	
Low elevations; rare		Above 4500'; occasional	
<i>Aster alpinus</i> L. ssp. <i>vierhapperi</i> Onno	(IRRP)	<i>Erigeron yukonensis</i> Rydb.	(IRRP)
Open prairies and meadows		Open prairies	
Low elevations; occasional		Low elevations; common	
<i>Aster junciformis</i> Rydb.	(P 66)	<i>Hieracium gracile</i> Hook.	(P 66)
Near Mackintosh*		Mt. Decoeli	
Low elevations; rare		<i>Petasites frigidus</i> (L.) Fries	(IRRP)
<i>Aster sibiricus</i> L.	(IRRP)	Tundra and birch-willow, muskeg	
Mesic sites in open woods and near bogs		associations	
Middle elevations; occasional		3500'; occasional	
<i>Aster yukonensis</i> Cronq.	(IRRP)	<i>Petasites hyperboreus</i> Rydb.	(P 66)
Mud flats and gravel outwashes, Slims River		Bear Creek Summit*	
Low elevations; locally common		Low elevations	
<i>Crepis elegans</i> Hook.	(IRRP)	<i>Saussurea angustifolia</i> DC.	(IRRP)
Gravel outwashes (?)		Open spruce forests and spruce-willow	
Low elevations; occasional		associations	
<i>Crepis nana</i> Richards.	(IRRP)	Middle elevations; occasional	
Mt. Archibald and Mt. Decoeli, and		<i>Saussurea angustifolia</i> DC. var.	(IRRP)
Kluane Ranges		<i>yukonensis</i> Pors.	
5000'-8500'		Alpine slopes	
<i>Crepis tectorum</i> L.	(P 66)	Above 4000';	
Roadside near Mackintosh*		occasional	
<i>Erigeron acris</i> L. var. <i>asteroides</i>	(IRRP)	<i>Senecio atropurpureus</i> (Ledeb.)	(P 51)
(Andrz.) DC.		Fedtsch.	
Spruce-willow and burned-over spruce forest		Open spruce woods	
Low elevations; occasional		Lower elevations; occasional	
<i>Erigeron acris</i> L. var. <i>elatus</i> Cronq.	(IRRP)	<i>Senecio atropurpureus</i> (Ledeb.) Fedtsch.	(IRRP)
(<i>E. elatus</i>)		var. <i>tomentosus</i> (Kjellm.) Hult.	
Wet shady sites in spruce-willow communities		Tundra	
Low elevations; occasional		Above 4500'; occasional	
<i>Erigeron compositus</i> var. <i>discoideus</i> Gray	(IRRP)	<i>Senecio atropurpureus</i> (Ledeb.) Fedtsch.	(IRRP)
Rocky slopes		var. <i>ulmeri</i> (Steffen) Pors.	
Up to 6000'; rare		Alpine slopes	
<i>Erigeron compositus</i> Pursh var. <i>glabratus</i>	(IRRP)	Above 5000'; occasional	
Macoun		<i>Senecio conterminus</i> Greenm.	(IRRP)
Open rocky slopes		Rocky slopes and tundra	
Up to 6000'; occasional		Middle altitudes; rare	

<i>Senecio cymbalarioides</i> Nutt. var. <i>borealis</i> (T. & G.) Greenm. Open rocky slopes 4000'; occasional	(IRRP)	<i>Senecio resedifolius</i> Less. Tundra Above 4500'	(IRRP)
<i>Senecio indecorus</i> Greene Meadows Low and middle elevations; occasional	(IRRP)	<i>Solidago decumbens</i> Greene var. <i>oreophila</i> (Rydb.) Fern. Many plant communities Low and middle elevations; common	(IRRP)
<i>Senecio lindstroemii</i> (Ostenf.) Pors. Tundra Above 4000'; occasional	(IRRP)	<i>Solidago multiradiata</i> Ait. Open slopes in many communities Middle and high elevations; occasional	(IRRP)
<i>Senecio lugens</i> Richards. Spruce-willow association, open mesic sites Up to 6000'; common	(IRRP)		
<i>Senecio pauperculus</i> Michx. var. <i>thomsenensis</i> (Greenm.) Boiv. Mesic meadows Low elevations; occasional	(IRRP)		

*These are local names, not known to be official. Alsek Pass: region where Alsek River crosses the Kluane Ranges; Badlands Creek: stream north of Burwash Landing; Bear Creek Summit: highest point (elev. 3000 ft.) on Alaska Highway between Bear Creek and Kluane Lake at Mile 1028; Mackintosh: small settlement at Mile 1022 on Alaska Highway; Sheep Mountain: mountain on northwest side of mouth of Slims River.

New and Important Additions to the Flora of the Southwestern Yukon Territory*

James A. Neilson †

Three species normally associated with prairie and subalpine plant communities have been discovered in the Kluane Ranges. Not only have these species been unreported for the Yukon, but their new stations are greatly disjunct from the previously known range of each species.

Hultén (1941-1950), Porsild (1951, 1966) and Johnson and Raup (1964) have suggested the relict nature of prairies in this area. The plants discussed below reinforce the writer's hypothesis that the Shakwak Trench and the adjacent Kluane Ranges to the west provided refugia for plants of prairie and subalpine communities. Today, communities with corresponding species are widespread 1200 to 1500 mi to the south and east. Furthermore, they are now clearly linked with steppe vegetation of Asia. Hultén (1963) reports 60 species occurring in western America which have disjunct ranges centered in the Yukon, and 10 species of Asia or Eurasia which reach the southwestern Yukon Territory. Similarly, Porsild (1951, 1966) indicates 18 prairie and 14 subalpine species whose known distribution in this part of the Yukon is widely disjunct from the northern prairies or Rocky Mountains.

While the glacial history of the Shakwak Trench and the Kluane Ranges before and during the Pleistocene is not yet clear, circumstantial evidence for refugia other than the obvious nunataks can be tentatively put forth. The Shakwak Trench and its major connecting valleys approximately follow the line of separation between the Cordilleran ice cap and the western extension of the Laurentian ice field. Apparently, ice advances from one source were accompanied by at least partial retreat of the other, leaving some portion of the valley or adjacent ranges free of ice.

Today prairie communities are restricted to xeric sites within the boreal forest and form only a small portion of the total vegetation; however, they are common in the central Shakwak Trench.

Erigeron lanatus Hook.

Erigeron lanatus Hook. is a small alpine plant of the Rocky Mountain cordillera. Its range extends from Gunnison Pass in southern Colorado to Waterton Lakes National Park, Banff National Park, Kootenay National Park, Nub Mountain and Windermere in southern British Columbia. Yukon specimens were collected on the north side of Alsek Pass on a steep scree slope, at 4200 ft ele-

vation overlooking the entrance of the Dezadeash River into the Kluane Ranges (137°47' W, 60°46' N). A voucher specimen (Neilson #1307) is deposited in the herbarium at the Natural History Museum in Stockholm, Sweden.

Eurotia lanata (Pursh) Moq.

Eurotia lanata is a plant of dry prairies and rocky desert slopes. It is found in the Great Basin, California, the Mojave Desert, the dry plains of western Texas, the short-grass prairie states, and north to the vicinity of Calgary in central Alberta. It has a close relative, *Eurotia ceratoides*, which is widespread in the xeric portion of Asia.

E. lanata is highly prized as winter forage for domestic sheep throughout its range. The small scattered populations growing at this new station were grazed by the native Dall sheep common in the area. All plants observed arose from heavy crowns, were 8 in. high, and their stems were relatively thin compared to Great Basin material. The long pilose hairs which typically extend over the dense stellate pubescence were more dense and spreading in comparison to herbarium material from other parts of the species' range. In aspect, these plants appear more delicate and woolly than their southern counterparts.

The Yukon populations are 1200 mi from the nearest recorded stands in Alberta (Fig. 1), and were discovered in an open, xeric, gravelly, hillside environment in the Kluane Ranges (Sheep Mountain¹ and the connecting ridge to the west; 138°32'W, 61°02'N, Neilson #1151 and #1238). A portion of #1151 is deposited in the National Herbarium of Canada where there is also an unreported specimen of *Eurotia lanata* collected on July 12, 1944 by H. M. and L. P. Raup (#12412) from one of the more easterly populations on the same hillside.

Artemisia rupestris L.

On the same hillside on which the preceding plant occurred, a widespread Eurasian sagebrush, *Artemisia rupestris*, was discovered. This perennial has not been previously reported from North America. Its nearest known station is on the Lena River drainage in eastern Siberia, a distance of some 3200 mi from the Yukon populations. From the Lena River the species is distributed southward along the Shilka River drainage near Mongolia, then eastward through the mountains of Kirgiz, across the steppes of Kazakhstan and central USSR, to southern Germany and the Swedish offshore islands of Öland and Gotland (Fig. 1).

*This article has previously appeared in *The Canadian Field-Naturalist*, Vol. 82, pp. 114-119 (1968), and is reprinted here with permission.

†Ecoview Consultants, Homewood, California

¹Editor's note: Local name for a mountain on the northwest side of the mouth of Slims River.

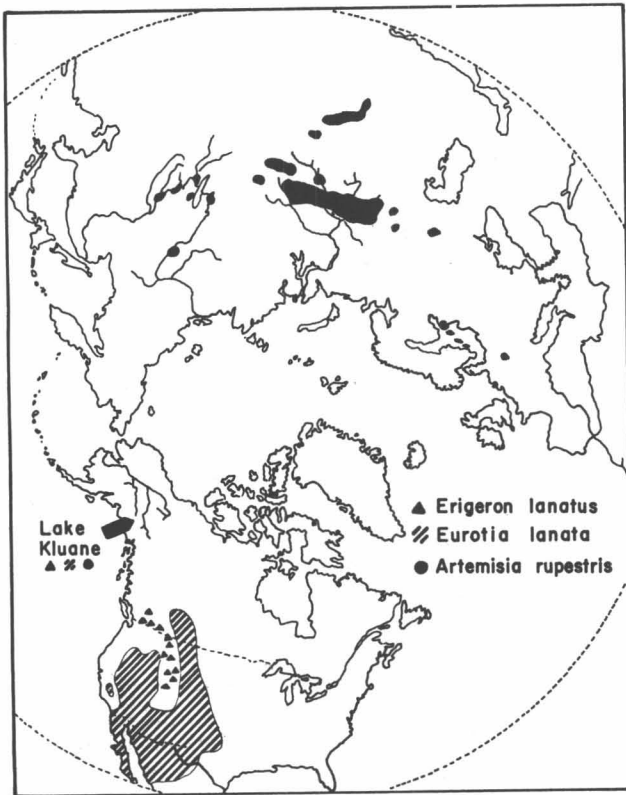


Fig. 1. The known geographical distribution of *Erigeron lanatus* Hook., *Eurotia lanata* (Pursh) Moq., and *Artemisia rupestris* L. in relation to the Yukon populations at Kluane Lake.

This plant has no morphologically similar relative in North America. The habit of the vegetative branches is somewhat reminiscent of *A. frigida* when it suffers from drought, and indeed, it has been mistaken for it (c.f. specimen at the National Herbarium of Canada CAN108195). The sticky, glandular, dark green leaves of *A. rupestris* lack the silvery gray pubescence typical of *A. frigida*. The receptacle is always covered with coarse hairs in *A. rupestris*. This seems to be more reliable as a key character than for *A. frigida* in which receptacle hair is absent in some populations. The habit of the flowering stems and heads might be compared to *A. arctica* or *A. alaskana*. The former is entirely glabrous and the latter is gray pubescent and lacks glands of any kind. The size of the heads of *A. rupestris* is intermediate between the two.

Inasmuch as this species is new to North America a brief description is appropriate.

Artemisia rupestris L. is a caespitose, pungently aromatic, sticky glandular perennial, forming dense, circular, dark-green mats about one to three ft in diameter. Vegetative shoots are decumbent or weakly ascending, one to two in. long. The leaves are dark green, 5 to 10 (15) mm long, once or twice pinnately divided to near the midrib, punctate glandular or with a few simple or branched hairs along the mid-vein. It is always ciliate near the base of the broadly winged petioles.

Fruiting stems are 8 to 25 (30) cm tall, erect, punctate glandular and pubescent with small stellate hairs with occasional long simple or branched hairs. Lower cauline leaves are similar to those on vegetative shoots; median cauline leaves are more spreading, up to 20 mm long, and have thinner, longer lobes. The petioles have narrower wings. The upper leaves are much reduced and become nearly linear; 5 to 20 heads are borne on a narrow raceme. Lower heads are often borne on peduncles 1 to 5 cm long. All heads measure 6 to 9 mm across and 3 to 4 mm high, and are nodding in habit. Florets are sticky glandular and the receptacle is covered with stiff white hairs $\frac{3}{4}$ the length of the floret.

Clearly, the Yukon material should be included with the Eurasiatic *A. rupestris* L. but it does differ in several critical respects. The outer phyllaries are broader with a more rounded apex. These have a broad, scarious, iridescent margin which is lacking or poorly developed in typical *A. rupestris*. More important, the bracts subtending the head are reduced in number—at most four, often none. In the Eurasiatic material there are four to seven which are consistently linear with herbaceous obtuse or acute tips. Those of Yukon plants vary from weakly pinnatifid (rare) to linear (sometimes with a dark scarious tip). In most European material the lobes of the leaves on vegetative shoots are acute and sometimes mucronulate in contrast to the blunt or obtuse condition of those from the Yukon. As far as can be determined from herbarium sheets, neither European nor Asiatic material has the pronounced differences in the habit of vegetative and fruiting shoots apparent in the Yukon plants. Densely spaced leaves and their appressed or slightly spreading habit give the vegetative shoots of Yukon plants a club-shaped appearance. In Eurasiatic material the internode length is slightly longer and leaf habit is loose and much more spreading, therefore similar to the fruiting stems of both groups (Fig. 2).

These differences are sufficiently distinct and uniform to conclude that the Yukon plants represent a geographical race.

Artemisia rupestris L. spp. *woodii* n. ssp.

Una vel, duo bracteae subtentae involucrium vel omnino deficientes lineares vel parum pinnatae saepe ad extremum scariosae. Externa phyllaria lata quarum margines latae, scariosae, iridescentes, fimbriatae interdum ciliatae.

Neilson #1242 collected Aug. 20, 1967. Open prairie on gentle slope (25%), southern exposure, on fine loess soil over schist gravels and scree. Below rock glacier, dry site. 138°32' W, 61°03' N; Sheep Mountain, elevation 3000 ft; Kluane Ranges, vicinity of Kluane Lake, Yukon Territory, Canada.

The plant is named in honor of Dr. Walter A. Wood, pioneer scientific explorer of the St. Elias Mountains, former President of the American Geographical Society, and Director of the Icefield Ranges Research Project of the Arctic Institute of North America.



Fig. 2. *Artemisia rupestris* L. A. Habit sketch of *A. rupestris* L. ssp. *woodii* n. ssp. (x 1). B. Leaf from lower portion of vegetative shoot (x 3). C. Leaf from middle of fruiting stem (x 2¼). D. Morphological variation in bracts and phyllary (top) from head of *A. rupestris woodii* (x 2¼). Lower three types are vegetative, the other two show slight development of a dark scarios margin similar to that of the phyllary. One to four of any types of these may be found subtending a single head. E. Morphological variation in bracts and phyllary (top) from heads of *A. rupestris rupestris* (x 2). Note the narrower dark scarios margin of the phyllary which is sometimes lacking altogether.

The holotype is deposited in the National Herbarium at the Museum of Natural History in Washington, D.C. Iso-types are deposited at the Herbarium of the National Museum of Canada in Ottawa; The Natural History Museum in Stockholm; The Dudley Herbarium at Stanford University in Palo Alto, California; The Herbarium of the University of California at Berkeley, California; and the Gray Herbarium, Harvard University, Cambridge, Massachusetts.

Acknowledgments

I wish to thank Dr. Eric Hultén of the National History Museum, Stockholm, Sweden for his assistance with the taxonomic and distributional details of the *Artemisia*. Dr. A. E. Porsild was kind enough to read the original

manuscript and offer important suggestions. This research was done under the aegis of the Icefield Ranges Research Project of the Arctic Institute of North America.

References

Hultén, E. (1941-1950) Flora of Alaska and the Yukon, Pts. 1-10, Lunds Univ. Årsskr., N. F., Avd. 2, 37, 1-46, 1.
 Hultén, E. (1963) The distributional conditions of the flora of Beringia, in *Pacific Basin Biogeography; A Symposium, 10th Pacific Science Congress, Honolulu, Hawaii, 1961*, edited by J. L. Gressitt, pp. 7-28, Bishop Mus. Press, Honolulu.
 Johnson, F., and Raup, H. M. (1964) Investigations in the southwest Yukon; Geobotanical and archeological reconnaissance, *Papers Robert S. Peabody Found. Archaeol.*, 6, 1-198.
 Porsild, A. E. (1951) Botany of the southeastern Yukon adjacent to the Canal Road, *Bull.* 121, Nat. Mus. Can., 400 pp.
 Porsild, A. E. (1966) Contribution to the flora of the southwestern Yukon Territory, *Bull.* 216, Nat. Mus. Can., 86 pp.

Behavior Study of the Arctic Ground Squirrel,

Citellus parryi plesius

Betsy Jo Lincoln *

ABSTRACT. The locomotion, food, grooming, burrows, and behavior of the Arctic ground squirrel, *Citellus parryi plesius*,¹ were studied at three sites in the region of the Icefield Ranges Research Project during the summers of 1966 and 1967. Studies of food preference were made, and a relative utilization rating was determined for each species of plant found in the squirrels' stomachs. In a study of the squirrel's effect on its environment, it was found that when its burrows and runways were built on steep slopes, they caused considerable erosion.

Introduction

The field work described in this paper was accomplished during the summers of 1966 and 1967. During this period, the locomotion, food, grooming, burrows, and behavior of the Arctic ground squirrel were observed. Although it was impossible to watch the squirrels for long periods at a time, it was possible to determine behavior throughout a day. During the second summer, emphasis was on the food habits of the species as related to the ecology of the area.

The Study Region

Three sites were selected for study in the region of the Icefield Ranges Research Project. One, 250 ft west of the airstrip at Kluane Base Camp, was below timberline at an elevation of 2580 ft. A second, at Kaskawulsh Knoll, was above timberline (elevation, 6200 ft). The third site, near the road between Mile 1054 and nearby Christmas Bay, was selected because it has topography and plant cover typical of the region.

Kluane Base Camp. A plot measuring 60 ft by 135 ft was marked out and divided into 5-yd squares. A map of this grid area was drawn up, showing the locations of the burrow entrances within the plot (Fig. 1). Plants on the plot were identified and grouped into three arbitrary categories of ground cover in addition to trees. The most commonly found are listed in Table 1.

Squirrel burrows were numerous but many were not in use. Mounds associated with the burrows varied from a few inches to as much as 3 ft in height and covered from 2 to 24 ft² of ground. Information from the burrow survey is given in Table 2.

The animals observed here were an adult female and two, or possibly three, young squirrels.

Kaskawulsh Knoll. This site was at the juncture of two arms of the Kaskawulsh Glacier (Plate 1).² Therefore, the population is relatively isolated; it is surrounded by a width of at least two miles of crevassed ice, and to travel down the moraine would require a journey of at least 20 miles. Either journey would be a rigorous one for a squirrel. The area examined extended over approximately 15 acres. The vegetation at this high-altitude site consisted solely of creeping or low alpine plants and grasses, such as cushion pinks and willow. These plants offered little protection from the intense sunlight of midday on a glacier. The number of burrows per unit area here was about the same as at the Kluane site, but there were fewer inactive burrows. Most were on grassy slopes, but some were on rocky ledges overlooking the glacier. Dirt mounds were not as large as those at Kluane.

Squirrels were the predominant animal here, and probably the only mammal that made the area its permanent home. A young squirrel was captured and observed; much of the general behavior described in a later section is based on observation of this squirrel.

Christmas Bay. A plot measuring 100 ft by 550 ft was laid out south of Christmas Bay (a bay at the mouth of Christmas Creek; see Plate 1) near Kluane Hills. This locality was selected for a food study because the terrain and plant life here were thought to be typical for elevations of 2500 to 3000 ft throughout the region. The sample plot crossed a basin between ridges formed by debris deposited in the crevasses of a former glacier. The plot provided a northern slope at one side of the basin and a southern exposure on the opposite side. It was here that plants were systematically collected, identified, and prepared for comparison with the stomach contents of the squirrels examined.

*Mill Lane, Yarmouth Port, Massachusetts

¹Taxonomic authority, A. H. Howell (1938) *North Am. Fauna*, Vol. 56, pp. 1-256; the animal is also known as *Spermophilus undulatus parryi* and *Citellus undulatus* by other workers.

²Plate 1 is a map inside the back cover of this volume.

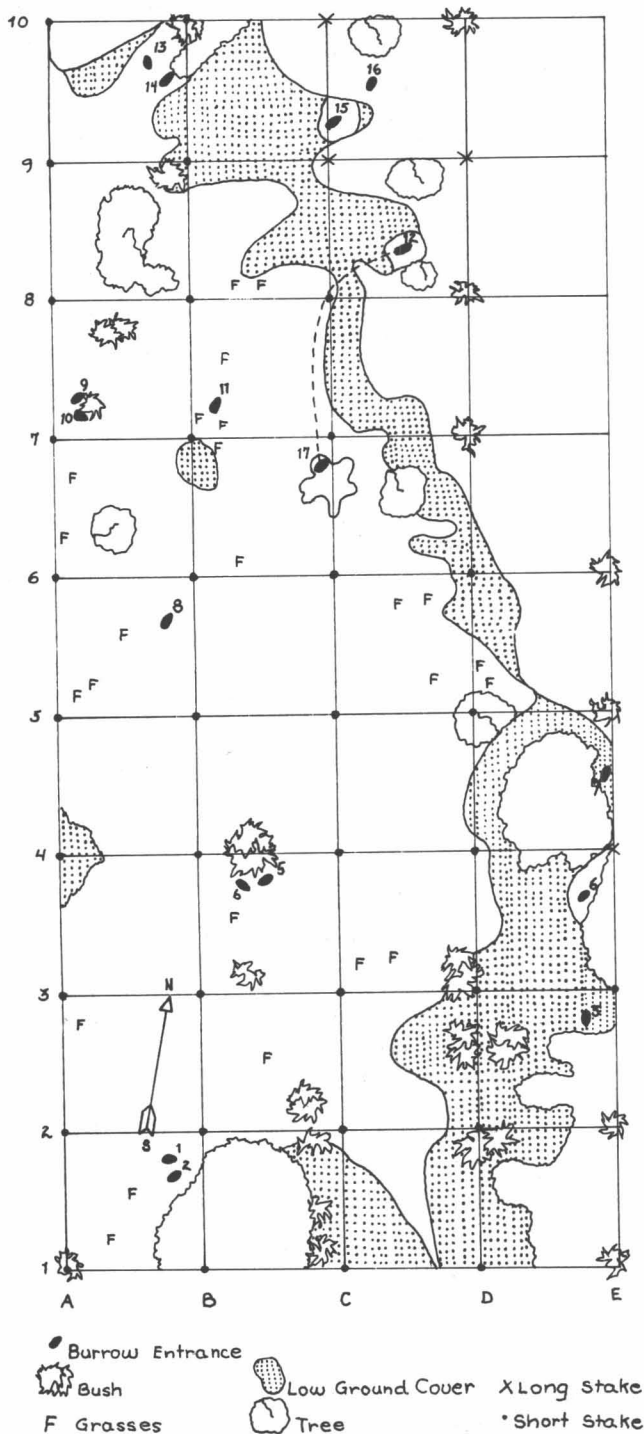


Fig. 1. Map of grid at Kluane Lake Base Camp site.

Seven distinct vegetation stands were identified along a north-south section across the plot (Figs. 2, 3): (1) *Artemisia* bald was common to the southern exposures throughout the area, having a high degree of fidelity. In

these stands there was much bare ground, usually with fine, dusty soil. The squirrels' burrows and runways, when on slopes, were often somewhat eroded; (2) a second stand at the base of the bald was characterized by *Populus*, *Arctostaphylos*, *Rosa*, and *Epilobium*. Squirrel burrows were less evident but present around stump bases or brushy hummocks; (3) beyond these trees was a region predominantly of *Arctostaphylos* and *Shepherdia*. This community type was most common in the Christmas Bay area, and is best described as an ecotone, in that it was a combination of several other types of communities. Squirrel burrows were numerous in this region and a preference was shown for hillocks and old logs.

The floor of the basin had three concentric groups of vegetation, predominantly *Arctostaphylos* but differing in the presence of: (4) *Fragaria*, *Salix*, *Antennaria*, and *Galium*; (5) *Penstemon*; and (6) *Potentilla*. There were no burrows in the flat areas included in stands of 4 and 5 but type 6 was a popular area. The seventh stand was on the northern exposure and was characterized by *Picea*. No squirrel burrows were found there.

Description of the Arctic Ground Squirrel

General. The Arctic ground squirrel is common in all open areas throughout the study region up to an elevation of about 6500 ft or to the vegetation line. It is a ground-dwelling rodent, stockier and somewhat larger than the familiar gray tree squirrel, *Sciurus carolinensis*. Measurements of one specimen were: total length, 320 mm; tail, 92 mm; hind foot, 50 mm; and ear, 5 mm. Its coat is generally reddish to grayish except for the back, which is grayish with white dapples. The tail tends to be black tipped. The individual whose activities were studied at Kaskawulsh Knoll is sketched in Figure 4.

Voice. The Arctic ground squirrel is a vocal animal, having several expressive sounds. Most commonly heard was the alarm call—a loud, carrying chitter, usually of three syllables, sometimes made at precisely regular intervals. In making this call, the mouth is wide open and the teeth bared. A second call, appearing to express anger, is uttered by an alarmed squirrel diving into a burrow, or by a squirrel forcibly held. This is similar to the basic alarm call but longer (that is, more syllables), less piercing, and sometimes trailing off. A third call sounds very like a cricket—a soft chitter. The fourth is a bird-like whistle. The last two were rarely heard, and their behavioral significance is not clear.

Locomotion and posture. The modes of locomotion included (1) an ambling walk (when sniffing around in search of food), (2) a scrambling run (when frightened), and (3) a high leaping run with head and tail held high, sometimes with all four feet springing at once. In modes 2 and 3 the tail is often flicked in a gyrating motion. An extreme of this leaping was observed on two occasions when a squirrel was seen leaping forward for several yards in a semi-standing position on its two hind legs only.

TABLE 1. Plant Species Common in the Vicinity of Kluane Base Camp

Grasses and Forbs	Low ground cover	Shrubs	Trees
<i>Epilobium latifolium</i>	<i>Arctostaphylos uva-ursi</i>	<i>Shepherdia canadensis</i>	<i>Populus balsamifera</i>
<i>Hedysarum mackenzii</i>	<i>Salix uva-ursi</i>	<i>Salix glauca acutifolia</i>	<i>Picea glauca</i>
<i>Potentilla patens</i>	<i>Gaultheria procumbens</i>		
<i>Linum perenne</i>			
<i>Erigeron yukonensis</i>			
<i>Achillea millefolium</i>			
<i>Anemone multifida</i>			
<i>Potentilla arguta</i>			
<i>Lappula redowski</i>			
<i>Carex</i> sp.			
<i>Artemisia frigida</i>			
<i>Poa</i> sp.			

TABLE 2. Burrow Observations at Kluane Study Area

Burrow No.	Mound dimension	Comment
1	4" high; 5' x 4'	Near a bushy area
2	6" high; 4' x 3'	Small hole through sticks lying among bearberry
3	insignificant	Located between two bushes
4	2" high; 2' x 1'	3 and 4 are probably two entrances to the same burrow
5	1' high; 6' x 4'	Very large burrow under roots of willow bush
6	3" high; 1' x 2'	Small burrow between two bushes
7	insignificant	Large entrance; small mound
8,9	3' x 3'	Two entrances with separate mounds
10	insignificant	Small entrance, little-used. Among grasses in center of rise of about 10"
11	3½' x 4'; second mound 6" high; 3' x 3'	One of the largest and most active burrows. Exits from under sticks of willow, recently scratched up. Second mound pushed out beyond willow cover
12,13	not measured (too many bushes in area)	Probably two large entrances to one burrow. Partially filled with sticks, seems to be no longer used
14	6" high; 1½' x 2'	Small but much-used. Under willow sticks
15	insignificant	Probably abandoned; small
16	not measured	Entrance hidden by bearberry; runway to Burrow 11, but not well worn

The squirrel was often seen sitting on some prominent lookout such as a rocky peak, a woodpile, or its own burrow mound. It has several observation postures (Fig. 5): (1) all four feet on the ground; (2) sitting up on its haunches with forepaws hanging at its stomach; (3) same as (2) but with back stiff and straight rather than rounded, and (4) standing up on its hind legs with heels down; a tall, straight bear-like posture.

An interesting behaviorism was observed at the Kluane site when a squirrel was surprised in the runway, away from any burrow. This squirrel ran into a clump of fireweed and leaped as if entering a burrow. After a search,

however, it was found crouched flat in a spot of shade, well camouflaged against the gravel runway.

Sanitation and grooming. In captivity, the squirrel was observed to assume a squatting position both to urinate and to defecate. The caged squirrel reserves a corner of its cage for this purpose. In the field, the squirrel's excrement is apparently confined to a special chamber in a burrow. The scats varied somewhat—as would be expected from the varying diets—but in general were elongate and pellet-like, from 5 to 20 mm in length. Color ranged from almost black to medium brown.

A great deal of the squirrel's time is spent in grooming.

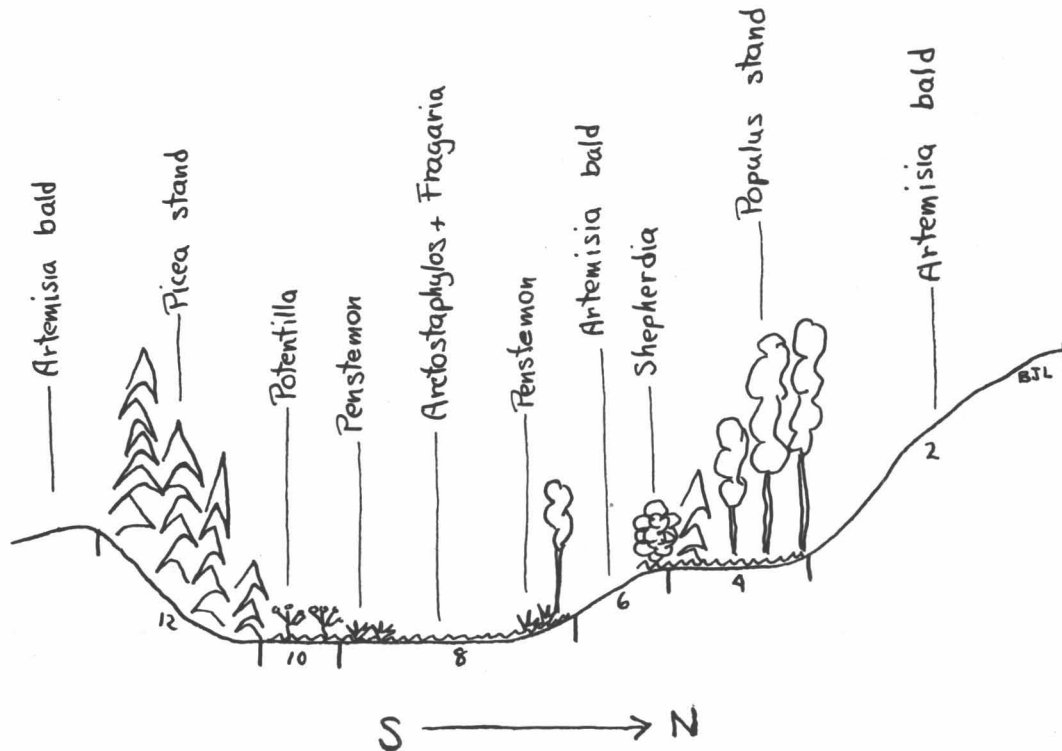


Fig. 2. North-south profile of sample plot at Christmas Bay.

The washing manners are typical of a rodent, consisting of licking and biting in a seated position. The tail, while being groomed, is held between its legs with the forepaws; when washing its sides or back the squirrel frequently topples over, sometimes without interrupting its grooming activity. The washing part of the squirrel's grooming is accompanied by vigorous rolling and scratching in loose soil. On a very hot day, the captive squirrel was observed to dig down to cooler earth to lie down. On the other hand, washing was more frequently terminated by the squirrel stretching out luxuriously to sun itself. While sunning, the squirrel often stretches a good deal; most commonly out flat on its stomach with chin on the ground and feet tucked in, often with forefeet stretched out in front, and sometimes with hind feet also stretched out, soles up behind. The amount of scratching and biting was believed to be an indication of ectoparasites, and indeed, the captive kit was heavily parasitized by mites.

Behavioral Patterns

Kluane Base Camp. Observations at 11:00 hours and 14:00 hours local time showed the greatest amount of activity. Observation at 20:00 hours showed no activity. Activity in the morning and evening consisted primarily of eating, while that at midday showed more playing and sunning.

An intriguing problem was noticed when the author

returned to the base camp on July 25, 1966. There was no sign of the squirrels on the grid itself, while the number of squirrels within the base camp had increased. This seeming population movement or abandonment of burrows was also reported at Christmas Bay, though no evidence of a movement was observed on the knoll. It was originally conjectured that because the glaciers and permafrost were melting, the ground-water level was rising and forcing the squirrels to higher ground, but when a three-foot-deep hole was dug in the center of the grid, no water seeped into it. Perhaps the squirrels are nomadic in general, living in one place only when raising young. The knoll population, however, seemed to have territories. The population dynamics of the squirrel remains an interesting problem for investigators.

Kaskawulsh Knoll. There is a significant difference between the hours of activity of the knoll squirrels and those of the base-camp squirrels. On the knoll, the squirrels were active from 03:00 hours to 10:30 hours and from 14:30 to 20:00 hours. Midday showed practically no activity. This might be explained by the lack of vegetation suitable for protection from exposure to the intense sunlight of midday.

The knoll population was denser and tamer than that at Kluane, and included both young and old squirrels. One female which appeared to be near parturition was seen.

Intraspecific behavior. The size of the functional social unit was not clearly discernible to the author. All

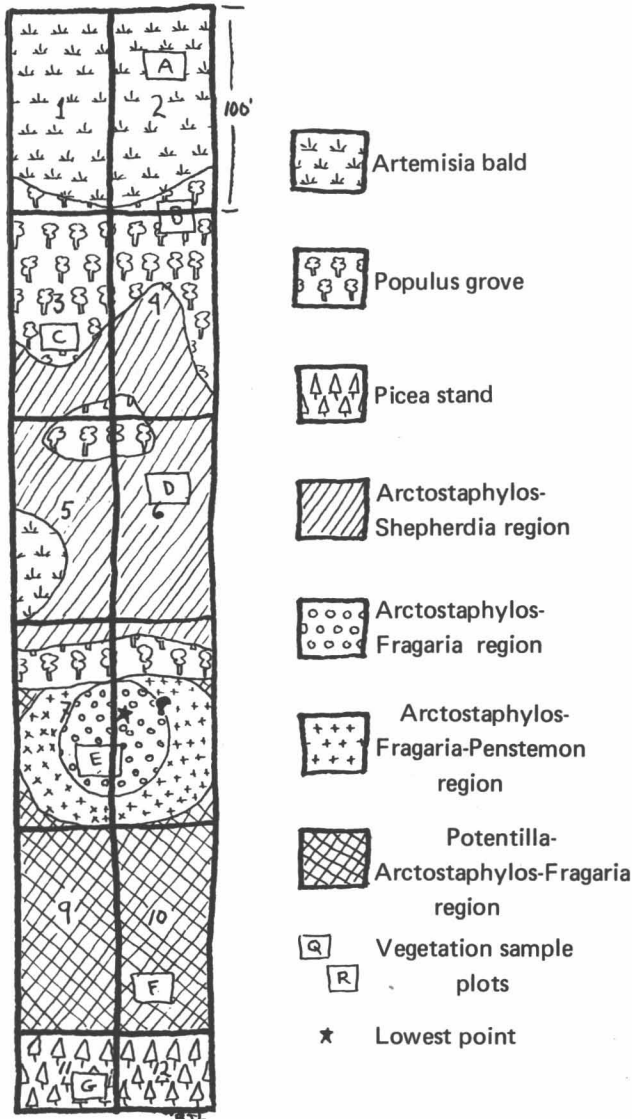


Fig 3. Map of vegetation in sample plot at Christmas Bay.

the squirrels observed seemed to be either single individuals or females with generally two or three kits. The young were frequently observed to play with siblings, but there was no indication of play with other peers. Play consisted of chasing in a sort of hide-and-seek fashion and sometimes rolling over in mock fighting. Several times two kits were seen sitting up facing each other, chittering softly, and touching each other's faces with their forepaws.

Another aspect of intraspecific behavior was territoriality. There was no actual mapping of territories, but the author feels that the following incidents could be considered as evidence of some kind of territoriality among the squirrels. A young squirrel was kept tied outside the tent both on the Kaskawulsh Knoll and at base

camp. On the knoll, there was a large adult female which was seen to use two different burrows within 150 ft of the tent. She frequently came to the tent to be fed. When she discovered the captive kit, she very quietly came up to the kit, struck at it, and ran off. This performance occurred twice on the knoll and seemed to indicate defense of territory by the adult female. No reaction to the kit was observed at the base camp, but the spot where the kit was kept may not have been in a defended territory.

Additional evidence of possible territorial behavior was seen in disputes between free-living individuals on the knoll. Several encounters were observed, apparently between the same two squirrels each time. Starting near the east cairn on the knoll, two adults chased each other, first one chasing and then the other. They made a constant squealing noise most like the second type of call described in the section on voice. When they made contact, they rolled over in a ball, then started off in another direction. A possible explanation is that one squirrel had to cross the territory of the other to get to the tarn to drink; after the chasing incident, on two occasions one squirrel was seen to use a round-about route back to the east cairn after visiting the tarn.

At the base camp there was little indication of territoriality. There seemed to be a great deal of movement and abandonment of old burrows for a new area. Many squirrels frequented the same areas around camp and no fighting was observed.

Interspecific behavior. Observed interaction with other species was limited. Once a magpie was seen to chase off a squirrel to get a piece of bread. The snowshoe-hare population was at an extreme low at this time and provided no competition. At higher altitudes, the pika and hoary marmot offered some competition. Chief predators are the larger birds of prey, wolves, bears, and wolverine. Burrows which had been dug out by a large predator were frequently seen.

Food

The diet of the squirrel was determined by observation of the animals eating in the field, by offering a captive a variety of foods, and by identifying the cheek pouch and



Fig. 4. Sketch of ground squirrel observed at the Kaskawulsh Knoll site.

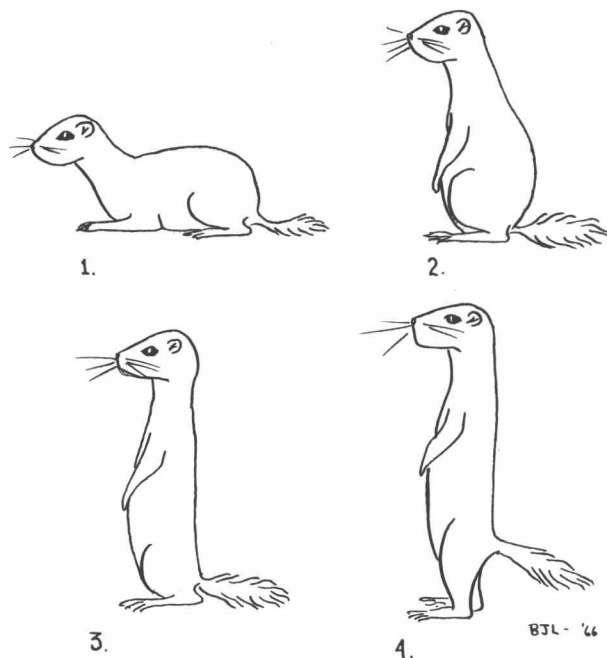


Fig. 5. The four basic observation postures of the ground squirrel.

stomach contents of specimens. The diet of the squirrel was found to be quite varied. Under field conditions, it appeared to prefer more succulent plant parts, such as the blossoms of cushion pinks, willow, and fireweed, and young peavine leaves. Squirrels have also been seen to capture and eat insects.

In order to determine food preference in the "typical habitat," stomach analyses were made and a frequency of occurrence or a relative utilization rating was determined for each species of plant. These utilization ratings were then compared with the availability ratings for these species according to a scheme used by Dudderar (1967).

To determine availability, plant species were given a rating by calculating the area covered by each species. *Arctostaphylos* was by far the most available plant. The relative coverages of the other species are given in Figure 6.

The average volume of the contents of the ten stomachs examined was 15.35 cc. Parts of insects, small seeds, and berry skins were found in the stomachs. One stomach was not full and contained much fatty material. There was a great amount of pollen present in all the stomachs, but this was not identified. The remainder of the contents of the stomachs was finely ground vegetable matter. Slides were made of the vegetable matter, and fragments were identified by comparison with photomicrographs of plant pieces which had been collected for this purpose and processed according to a scheme outlined by Williams (1962). Plant anatomy textbooks by Esau (1960) and Burström and Odhnoff (1964) were also helpful in identifying plant fragments. Figure 7 illustrates the frequency

of occurrence of the plant species represented.

The coverage of a plant species (Fig. 6) was classed as copious (3) if it had a relative value of 50 units or more. The coverage was classed as moderate (2) for a value of 12.5 to 50 units. A value of less than 12.5 units was classed as scarce (1). Three ratings have also been applied to the utilization graph (Fig. 7): frequent (3), moderate (2), and rare (1). Foods were rated as preferred (P) if their availability and utilization numbers coincided; staple (S) if their availability rating was the lower; or as emergency (E) if their utilization rating was the lower. For example, *Arctostaphylos* has copious coverage (3), but it is rarely eaten (1). Thus the utilization rating is lower and it is classified as an emergency food (E). The final list is given in Table 3.

When in captivity and in the area of the research camps, the squirrel was observed to eat a wide variety of food items. A young captive was offered rolled oats, cooked cream of wheat, dried apples, crackers, raisins, and peanut butter, and refused nothing. It would eat small bits of meat, and liked lettuce. This adaptability is probably one reason why the species can live at different altitudes, since the gradation of vegetation with altitude would restrict the range of a more specialized animal.

Drinking was observed quite often. Squirrels on Kaskawulsh Knoll seemed to make daily trips to the tarn to drink; there were several runways which led directly to the water. Drinking was not observed among the squirrels at base camp, but much of the base-camp area was swampy, so a squirrel could drink without making a special trip.

Burrows

A number of burrows were excavated to learn their construction and to get an idea of the habitation behavior of the squirrel. A cluster of burrows between Kluane Lake and the Alaska Highway, a few yards from Silver Creek, was excavated to see if it would reveal a complete burrow system. Four excavated burrow entrances revealed three tunnels, one of which had two entrances, and none of

TABLE 3. Utilization Ratings of Plants Used as Food by the Ground Squirrel

Preferred food	Staple food	Emergency food
<i>Epilobium</i>	<i>Astragalus</i>	<i>Rosa</i>
<i>Artemisia</i>	<i>Achillea</i>	<i>Arctostaphylos</i>
<i>Anemone</i>	<i>Plantago</i>	<i>Shepherdia</i>
<i>Galium</i>	<i>Erigeron</i>	<i>Carex</i>
grasses	<i>Solidago</i>	<i>Fragaria</i>
<i>Penstemon</i>	<i>Antennaria</i>	<i>Picea</i>
		<i>Salix</i>
		<i>Potentilla</i>
		<i>Oxytropis</i>

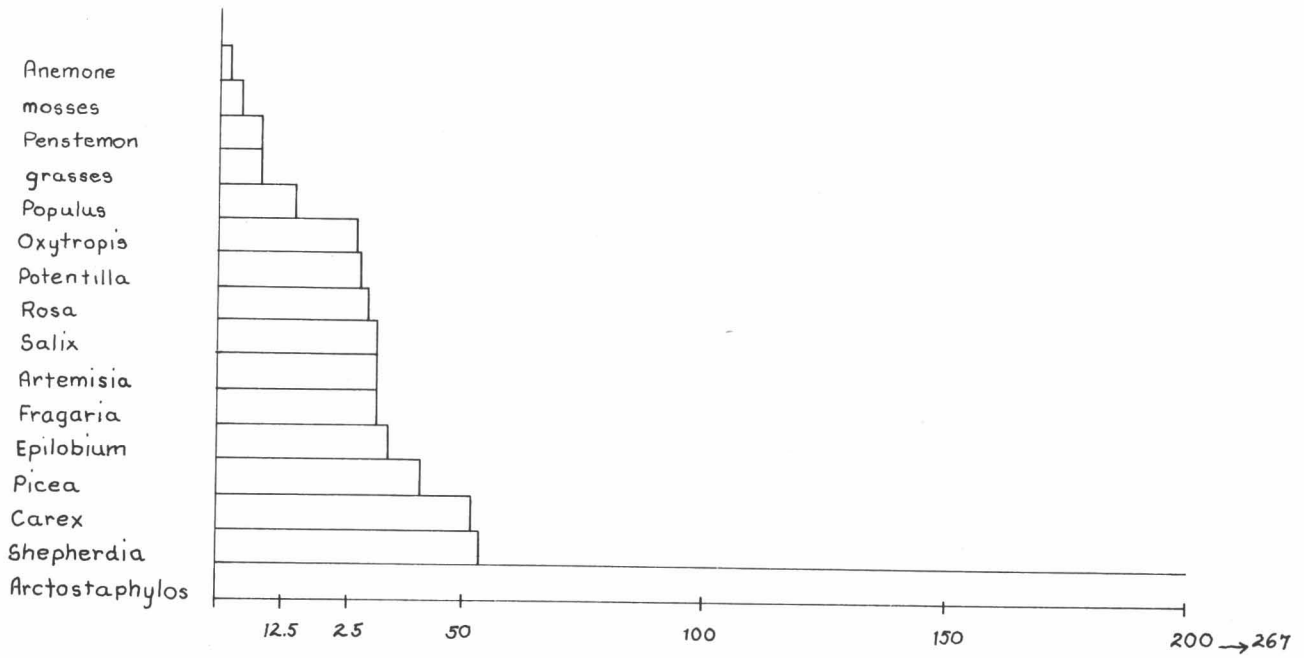


Fig. 6. Graph showing relative coverage of sixteen species of plants in the study plot at Christmas Bay.

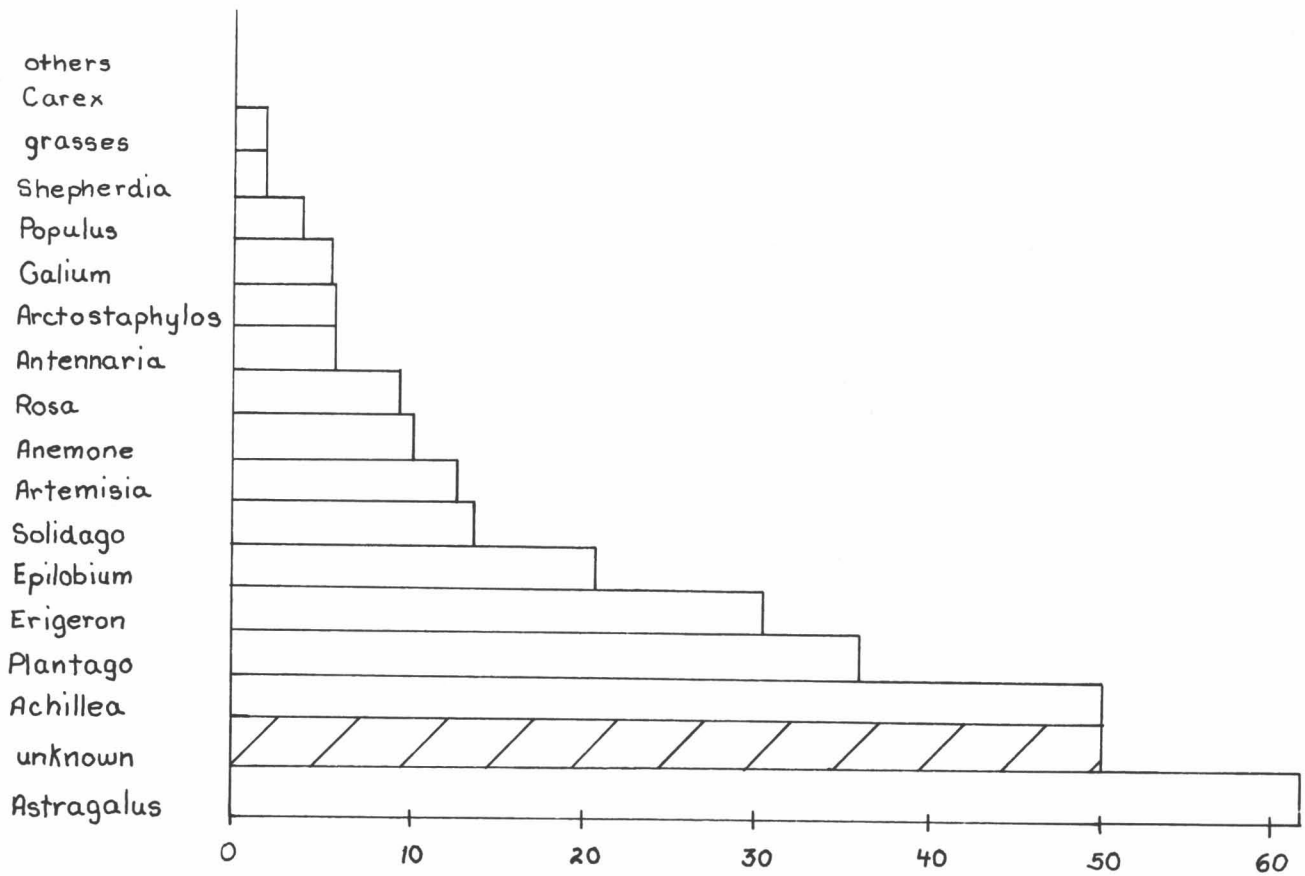


Fig. 7. Graph showing relative frequencies of occurrence of various plant species in stomach samples.

which descended deeper than 18 in. beneath the surface. The first two tunnels excavated met beneath the surface about midway between the entrance where they formed a single tunnel leading down to a small chamber which contained scats (Fig. 8). The other two led to short tunnels (Fig. 9).

In general, the burrows seemed to be shallow. One factor affecting burrow depth may be the permafrost underlying the ground throughout most of the research area. Each burrow entrance was surrounded by a mound of earth, or, if the entrance was protected on one side, the mound was built up on the other. These mounds served both as a protection and as a lookout seat for the squirrels. The entrances were located at the base of a shrub or grass clump, on the slope of a hill, amid rocks, or out in the open ground. There were numerous partial diggings in the area and many of the burrows were connected by surface runways. One especially interesting burrow was observed at the Kaskawulsh tarn. The entrance emerged just above the water level in the bank of the tarn. Earth had been pushed into the water, building up a small platform just above water level at the burrow entrance.

Burrow No. 7 on the Kluane grid (Fig. 1) was dug out and the burrow illustrated in Figure 10 was revealed. The burrow seemed to run just below the sod, the soil of the roof being held by the plants just above. The shortness of the burrow and the two short branches with no chambers, seemed to indicate that this particular burrow was never used for a nest or food storage.

Some indications of nesting material were observed. One squirrel was seen filling its pouches and its mouth with moss and carrying it off, and another was seen taking cloth handkerchiefs into its burrow.

Exactly what comprises the home of the squirrel is still unknown to the author. Possibly a single squirrel, or a single living unit of squirrels, had a burrow system with one main burrow containing the nest, and burrows containing a scat chamber, a food-storage chamber, several short exploratory burrows, and some connection runways throughout its territory. The excavated burrows neither proved nor disproved this idea, and more burrow excavation would be necessary to reveal the habitation behavior of the squirrel.

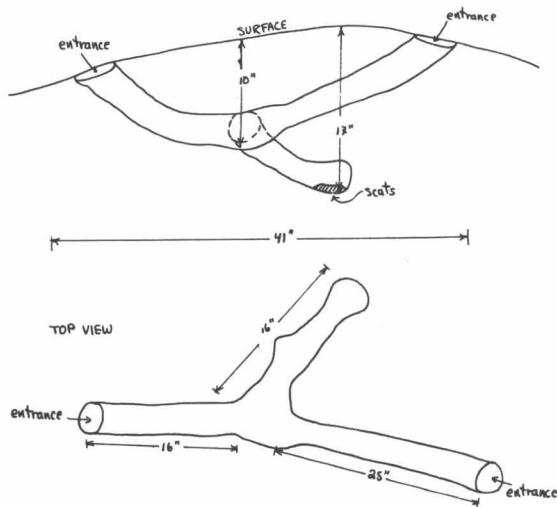


Fig. 8. Burrow with two entrances, excavated at site between Kluane Lake and Alaska Highway, near Silver Creek.

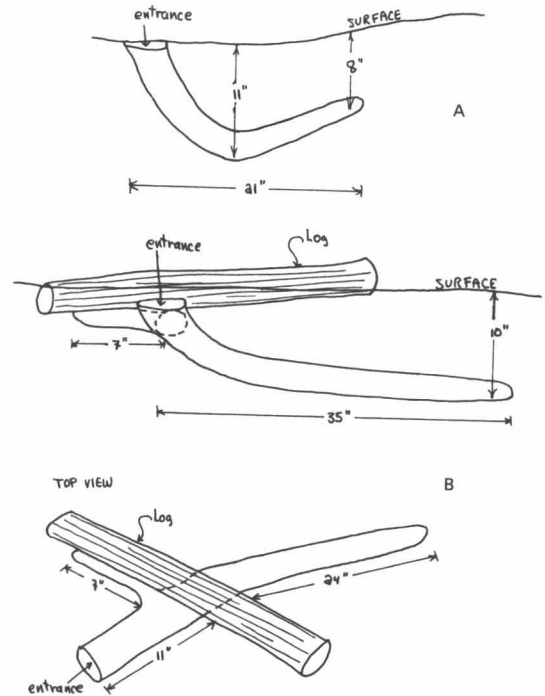


Fig. 9. Short burrows with one entrance each excavated at site between Kluane Lake and Alaska Highway, near Silver Creek.

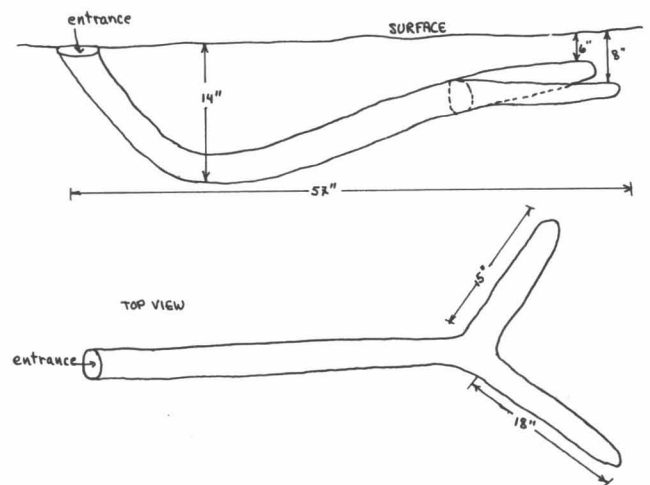


Fig. 10. Diagram of Burrow Seven, excavated on Kluane grid.

The Effect of the Arctic Ground Squirrel on its Environment

A significant effect of the squirrels' burrows on their environment can be seen at Christmas Bay. Here burrows and surface runways were built along the steep canyon walls and were the apparent cause of considerable erosion.

A study was made to determine the erosional effect of the squirrels on the *Artemisia* balds. The observations showed a decrease in the amount of bare ground with increasing distance from the runway, and an increasing number of all plant species with increasing distance. There was little evidence that the plants along these runways had been cropped by the squirrels, though prairie dogs have been observed to do this (King, 1955). Instead, plant growth seemed to be disrupted by the squirrels' digging and running.

Ground squirrels are notorious agricultural pests (Martin, *et al.*, 1951). Since the Yukon is not an agricultural area, however, the Arctic ground squirrel can hardly be regarded as a pest. Tikhomirov (1959) feels they have a positive effect in grassland areas, contributing to a greater variety of plant species. In the author's opinion, the sparsity of vegetation in the *Artemisia* bald is more strongly related to climatic factors than to activities of the ground squirrel.

Conclusions

Necessary to any food-habits study is a knowledge of food availability in relation to use; observations should be obtained throughout the year to get a complete picture. The stomach analysis was crude at best, but it gives a rough estimate of the degree of selectivity at this elevation during the summer, and identifies plant species utilized. The diet of the ground squirrel was found to be quite varied; it is felt that this adaptability is an important factor in the squirrel's ability to live at different altitudes.

It was possible to draw some preliminary conclusions about the squirrel's effect on its environment. When the burrows were built on steep slopes, they were the cause

of considerable erosion. A study of the erosional effect of the squirrels on *Artemisia* balds seemed to show that plant growth was disrupted by the squirrels' digging and running rather than by their feeding on the plants; it was felt that the sparsity of vegetation in the *Artemisia* balds was due more to climatic factors than to the squirrels' activities.

An important result of the work done for this project was the questions raised: (1) How do squirrels hibernate in frozen ground, and when does hibernation begin? What factors stimulate onset of hibernation? (2) What is the habitation behavior of the squirrel? What is the cause of its "migrations"? Does this population movement occur to some extent throughout the species (on the Kaskawulsh Knoll, for example)? (3) What are the population fluctuations of the species? What factors cause them? (4) How did the squirrels come to inhabit the Kaskawulsh Knoll, and is there any movement to or from the knoll now? How is the population on the knoll controlled? (5) Can the same number of squirrels be supported by the same area at several different elevations? When vegetation becomes sparse, do the squirrels become less selective, or does their population thin out proportionately?

References

- Burström, H. G., and Odhnoff, C. (1964) *Vegetative Anatomy of Plants*, Munksgaard, Copenhagen, 149 pp.
- Dudderar, G. R. (1967) A survey of the food habits of the gray squirrel (*Sciurus carolinensis*) in Montgomery County, Virginia, M. Sc. thesis, Virginia Polytech. Inst., Blacksburg (unpubl.).
- Esau, K. (1960) *Anatomy of Seed Plants*, John Wiley and Son, New York, 376 pp.
- King, J. A. (1955) Social behavior, social organization, and population dynamics in a black-tailed prairie dog town in the Black Hills of South Dakota, *Contrib. No. 97*, Lab. Vertebr. Biol., Univ. Michigan.
- Martin, A. C., Zim, H. S., and Nelson, A. L. (1951) *American Wildlife and Plants*, McGraw-Hill, New York, 500 pp.
- Tikhomirov, B. A. (1959) *The Interrelationships of the Animal Life and Vegetational Cover of the Tundra*, Eng. tr. for U.S. Dept. Agricult. by Israel Prog. Sci. Tr., Jerusalem.
- Williams, O. (1962) A technique for studying microtine food habits, *J. Mammal.*, 43, 365-368.

Geomorphic Effect of the Arctic Ground Squirrel in an Alpine Environment*

Larry W. Price †

ABSTRACT. The Arctic Ground Squirrel (*Citellus undulatus*¹) is an important geomorphological agent in the Ruby Range, particularly since its distribution and concentration is highly variable, depending upon the existence of favorable habitats. 320 lbs of material per acre are being excavated annually from a total 53-acre burrowing area (8 tons per acre when calculated for actual area of occurrence) on a southeast-facing slope where solifluction lobes are well developed, while southwest-, east-, and north-facing slopes are little affected. This added denudational component may be important in considerations of valley asymmetry.

Introduction

The presence of burrowing animals are ubiquitous in many alpine and Arctic tundra landscapes, and where they occur in abundance they may have a profound effect on the local ecology. In such extreme environments, the distribution of small animals in any given area is largely controlled by the existence of favorable places to live, and even within this context, there exist microhabitats (Bliss, 1956, pp. 329-335). In the Ruby Range (Fig. 1) the largest burrowing-animal populations occur on south-facing slopes, particularly those with ample microhabitats such as the lee of solifluction lobes (Figs. 2, 3). The concentration of these animals has important ecological and geomorphological implications. This paper is primarily concerned with isolating the geomorphic effect of the Arctic Ground Squirrel (*Citellus undulatus*).

The Ruby Range is located at 61° 23'N, 138° 13'W, about 215 km northwest of Whitehorse (Fig. 1). It is a small intrusive mountain group 130 km long by 65 km wide, oriented northwest-southeast, and situated along the western edge of the Yukon Plateau, in the lee of the towering St. Elias Mountains (highest peak—Mt. Logan 6050 m). The higher peaks of the Ruby Range have an average elevation of 2100 m, and there is a distinct flattening of the uplands which may be an old erosion surface of the Yukon Plateau (Bostock, 1948, p. 72). The area has been considerably dissected by valley glaciation, however, and is quite rugged. The Gulf of Alaska is located only 230 km to the west, but the intervening St. Elias Mountains eliminate direct marine influence, and the Ruby Range has a decidedly continental climatic regime. Tree line occurs at about 1200 m and the combination of latitude, altitude, and continentality gives the Ruby Range a Subarctic alpine tundra environment.

Four slopes formed by the confluence of two ridges were analyzed in detail. These slopes (southeast, southwest, east, and north facing) have the same rock type (biotite granodiorite), similar gradients (14°-18°), and elevations (1675-1980 m). Gross environmental differences are, therefore, largely due to exposure to solar radiation and meltwater from late snow lie. The tundra vegetation is best developed on the southeast-facing slope (Fig. 2), and sequentially less so on the east-, southwest-, and north-facing slopes (Price 1970a). Solifluction lobes also reach their highest development on the southeast-facing slope (Fig. 3), and are increasingly scarce on the east-, north-, and finally the southwest-facing slope, where they are poorly developed or absent.

Local Distribution and Effect of Ground Squirrels

The presence of ground squirrels follows the development of vegetation and solifluction lobes, in that they are most plentiful on the southeast-facing slope and become less so on the southwest-, east-, and north-facing slopes. South-facing slopes are favored habitats due to higher temperatures and better moisture conditions brought about by the higher angle of incidence of solar radiation and a local prevailing northwesterly winter wind which results in snow accumulation on south-facing slopes, providing meltwater through the summer. Within this framework, however, the distribution of ground squirrels is largely controlled by the presence of microhabitats. For example, on the southeast-facing slope their burrows are almost entirely limited to a 15-m zone immediately below the fronts of solifluction lobes (Fig. 2). More favorable conditions exist at the lobe fronts for several reasons: (1) in winter, snow accumulates in the lee of the lobes and provides insulation from extreme cold and the desiccating wind (Pruitt, 1957, pp. 131-138); (2) in summer the lobe fronts experience higher temperatures (11°C on the average) than elsewhere on the slope due to a higher angle of incidence (Price, 1970b, pp. 50-69); (3) because of higher temperatures, the lobe fronts thaw earlier and the active layer penetrates to a greater depth allowing the ground squirrels to begin their activities; (4) vegetation reaches its highest development within the

*This report has previously appeared in *Geografiska Annaler*, Vol. 53 A, pp. 100-106 (1971), and is reprinted here with permission.

†Department of Geography, Portland State University, Portland, Oregon

¹Editor's note: Authority for the name *Citellus undulatus* is *A Field Guide to the Mammals*, by W. H. Burt and R. P. Grossenheider, Houghton Mifflin, Boston (1964), p. 107.



Fig. 1. Location of study area. Stippled pattern represents glaciers.

confines of the microhabitat and provides an ample food supply (Price, 1970a) as well as more stable dens and tunnels due to root structure (Mayer, 1953, p. 342). These favorable conditions are counterbalanced somewhat by active solifluction and the abundance of meltwater in early summer, but apparently neither are severe limiting factors.

Several species of burrowing animals live in the area including the hoary marmot (*Marmota caligata*), the Arctic Ground Squirrel (*Citellus undulatus*), the pika (*Ochotona collaris*), and various species of lemmings, mice and shrews. Of these, ground squirrels have by far the greatest effect. The hoary marmot and pika are both rock dwellers and do not disturb the local area to any great extent, while lemmings, mice, and shrews have small burrow entrances and usually distribute the excavated material inside their burrows. Ground squirrels, on the other hand, are continually bringing material to the surface and usually distribute it downslope.

The impact of ground squirrels on the slope is largely to cause an increase in degradation. They do this directly by (1) breaking away vegetation, (2) creating tunnels in the interior of the lobes which provide channels for meltwater and weaken the interior of the lobes (Fig. 4), (3) changing the density of the consolidated material by bringing it to the surface where it is susceptible to erosion, and (4) actually transporting material downslope in the burrowing process. Indirectly they (1) undermine large rocks at the surface, allowing them to move more quickly by rock creep or even to tumble downslope (Fig. 5); (2) often create circumstances favorable for the development of considerable hydrostatic and/or cryostatic pres-

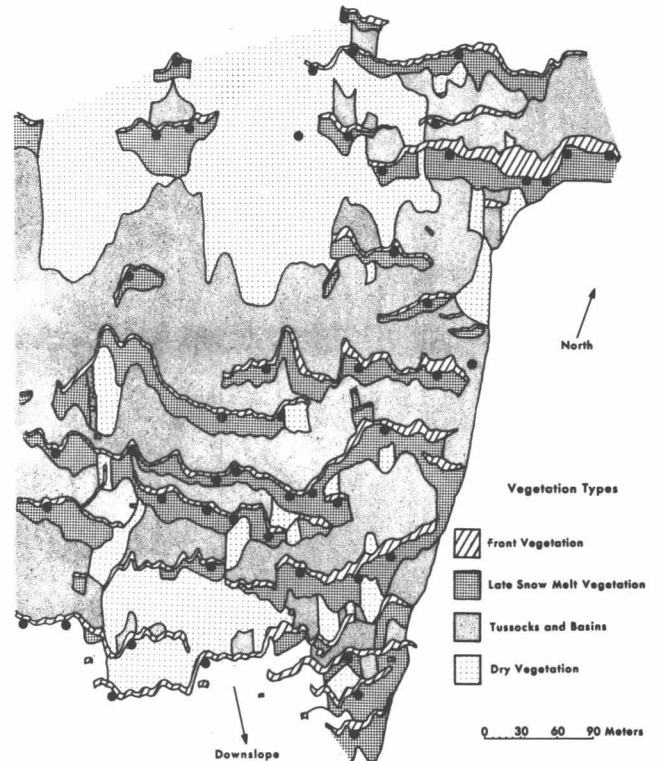


Fig. 2. Distribution of ground squirrel burrowing sites (dots) on southeast-facing slope. Note that they are almost entirely confined to the late snow melt areas immediately below the lobe fronts. The ground squirrels take advantage of this favorable microhabitat where more snow accumulates in winter, and there are higher summer temperature, more rapid thawing, and better developed vegetation.

sure whereby material may be suddenly and forcefully moved downslope (Price, 1970b, pp. 193-208).

Conversely, ground squirrels help stabilize slopes by their body wastes, especially urine. Vegetation is usually darker green and comparatively lush around burrow sites owing to the addition of nitrogen which is deficient in the tundra (Russell, 1940, pp. 269-288). Soil forming processes are slow but ground squirrels do continually mix the material both by bringing fine material to the surface and by taking down bits of vegetation for food and bedding, and this must increase the productivity of the soil just as in middle latitudes (Grinnell, 1923, pp. 1945-1949).

Methods of Study

In order to quantify the impact of ground squirrels on the slope, several projects were undertaken. During the first year I counted burrows along the front of a major solifluction terrace on the southeast-facing slope for a distance of 360 m and found 200 ground squirrel holes and 994 mouse holes. The mouse openings were only 2-3 cm in diameter and very seldom had any loose material downslope from their burrows. They distribute the excavated material inside their dens so the entrances are more difficult to spot. For



Fig. 3. Well-developed solifluction lobes on southeast-facing slope. Photo was taken on July 4, 1967 and lobes with snow in their lee are 4-6 m high. Ground squirrels prefer the lee of the smaller lobes 1-3 m high, where snow melts sooner, allowing the resumption of activities.

this reason their total effect on the slope was much more difficult to quantify, but the 5 to 1 ratio of mouse to ground squirrel holes certainly indicates their potential in weakening the internal structure of the lobes.

Ground squirrels were much fewer in number, but had a greater visible impact on the slope. Their burrow entrances were 7-12 cm in diameter and mounds in all sizes and conditions of activity were present. These small animals are only about 25 cm long and weigh less than 2 lbs (Burt and Grossenheider, 1964, p. 107), but are nevertheless prodigious earth handlers. An excerpt on the activities of the Columbian Ground Squirrel from Washington state by W. T. Shaw (1925, p. 483) indicates their efficiency in this regard:

"Frequently a squirrel would appear at the mouth of one of these holes looking somewhat ruffled, and progressing backwards with his burden of earth. In handling it he would proceed after this fashion. Placing his hind legs firmly and widely apart, he would dig very rapidly with the front feet, packing the loose dirt up under his belly. Then he would kick it back with his hind feet, alternately right and left, quite rapidly, though not so quickly as with the front feet. At this time one would see a shower of earth being shot swiftly to the rear, and the body of the squirrel sink simultaneously into the trough under him, made by this displacement. Not infrequently, after the earth had accumulated into a considerable heap behind him, he would turn and ram through the mound, with his nose plowing the loose dirt ahead, soon emerging with the short stiff hairs of his face bristling with earth particles."

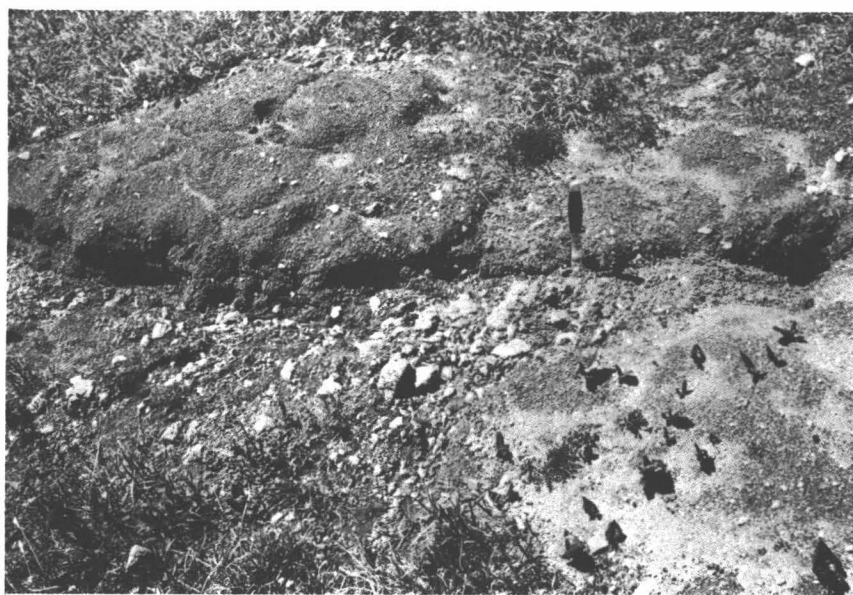


Fig. 4. A ground squirrel burrow that has been dissected by water issuing from the entrance. Tunnels created by ground squirrels provide channels for meltwater and weaken the interior of solifluction lobes. Knife is 20 cm high, and gives scale.



Fig. 5. A ground squirrel burrowing site where several large rocks have been undermined and tumbled downslope. The three rocks to the immediate right of pack (which is 75 cm long) have been recently dislodged. Although too large for ground squirrels to move themselves, they reflect the indirect results of burrowing.

This description could just as easily have been made for the Arctic Ground Squirrel. The question that now arises is, how much material they actually excavate and mound downslope in a year's time.

Several investigators have alluded to the effect of burrowing animals, but few have tried to quantify it. Those who have measured excavated material include: Grinnell (1923, pp. 143-144); Taylor (1935, p. 132); and Thorp (1949, pp. 188-189). Thorp perhaps exemplifies what has been done in this regard although his research was done mainly in plains areas of the United States. The geomorphic effect of burrowing animals is much greater on slopes, since the material is always moved downslope. Thorp's method of calculating the volume of a mound, by assuming it approximates that of a cone, was adopted for my area ($V = \pi r^2 h$) (Thorp, 1949, pp. 188-189). In addition, an attempt was made to isolate current activity in order to ascertain the annual rate of displaced material, as well as to find the total amount.

Burrows were divided into fresh and old on the basis of recent activity; the fresh ones were those appearing to have been formed within at least the last 2 or 3 years, and old burrows were those with little evidence of activity, usually revegetated or with succession beginning on the mound (*Petasides frigidus* was one of the first invaders in mound areas). Where there was recently excavated material on the mound, but it was simply a veneer, it was classified as an old burrow. Even fresh mounds, however, may be partially underlain by older material. For this reason, fresh burrows were considered to have been formed within the last 5 years, rather than 2 or 3 years, an allowance that should compensate for the underlying material. Therefore, the total amount of material measured for fresh burrows can be divided by 5 to get annual displacement of material downslope.

Interpretation of Results

The investigation of the southeast-facing slope during the second field season revealed 53 burrow sites (Fig. 2) with a total of 327 fresh burrows and 963 old burrows. The fresh mounds were measured to contain a total of 805 cu ft of material. Thorp states that 1 cu ft of sandy loam with some gravel will weigh about 100 lbs, so this figure was used to reach a rough estimate of weight of the excavated material (Thorp, 1949, p. 189). The 805 cu ft of fresh material would be 80,500 lbs or 40 tons. If it is assumed that the material was excavated within the last 5 years, a conservative estimate, this yields 161 cu ft or 8 tons per year. The area sampled contains 53 acres, so this amounts to 320 lbs per acre of excavated material. In reality the burrows are concentrated in a narrow zone less than 15 m wide immediately below the lobe fronts (Fig. 2). The actual area affected, then, covers less than one acre which means 8 tons per acre per year excavated by ground squirrels.

The average volume of a mound in the study area was calculated to be 2.46 cu ft. There are 963 old burrows, so this yields a total of 2369 cu ft or 236,900 lbs, or 118 tons of material moved downslope. Projected through time at the current rate of burrowing (8 tons per year) it would have taken 15 years for the ground squirrels to excavate this material. There is a total, therefore, of only 20 years' evidence of ground squirrel activity on the slope.

This brings up a very timely question. Since ground squirrels have certainly lived on the slope longer than 20 years, what has happened to the evidence? The answer seems to lie in the extreme instability of the slope. The solifluction lobes are moving downslope at an average rate of 16 mm/yr and burying the underlying vegetation (Price 1970b, p. 156). The burrow mounds below the

lobe fronts are also being buried as can actually be seen happening at the present time on the slope. Evidence for this occurring in the past was observed while excavating cross sections into selected lobes for collecting C-14 dating samples. The organic layers representing the formerly vegetated surface below the fronts are preserved back into the lobe, but there are occasional breaks or variations in thickness. Some of these involutions may represent former burrows below the lobe fronts which were bare or only thinly vegetated at time of burial (Price, 1970b, pp. 221, and 236). In addition, under sloping conditions the general erosional processes of slope wash and mass movement would probably destroy the burrows beyond recognition within a few years.

Summary

The foregoing has indicated that ground squirrels may have a considerable effect on local areas in the alpine tundra. This is particularly true owing to their highly variable distribution depending upon the existence of favorable conditions. In the study area, ground squirrels are abundant on the south-facing slopes, but absent on the north-facing slopes. Moreover, even within the framework of favorable conditions, they are concentrated in microhabitats, for example, the lee of solifluction lobes.

It can be seen that the presence of ground squirrels gives certain slopes an added component of denudation. From my calculations, 8 tons of material per year are being excavated from a 1-acre area at solifluction lobe fronts on a southeast-facing slope in the Ruby Range. Projected through time this small amount takes on amazing dimensions, and similar circumstances are not difficult to find nearby. This suggests that the presence of burrowing animals is an important consideration in any analysis of slope development, and particularly on a comparative basis, as in valley asymmetry.

Acknowledgments

Financial support was provided by the Arctic Institute of North America and excellent logistical support was provided by the Icefield Ranges Research Project. Particular thanks are due Mr. Richard Ragle, Dr. Walter Wood, Mr. Philip Upton, Dr. Melvin Marcus, and Dr. J. Peter Johnson, for their help and encouragement. Dr. C. S. Alexander, University of Illinois, critically read the manuscript, and Mr. Jim Sij, Mr. Charles Volk, and my wife, Nancy, were field assistants. To all these persons I am extremely grateful.

References

- Bliss, L. C. (1956) A comparison of plant development in micro-environments of arctic and alpine tundras, *Ecol. Monogr.*, 26, 303-337.
- Bostock, H. S. (1948) Physiography of the Canadian Cordillera with special reference to the area north of the fifty-fifth parallel, *Mem. 247*, Geol. Surv. Can., 106 pp.
- Burt, W. H., and Grossenheider, R. P. (1964) *A Field Guide to the Mammals*, Houghton Mifflin, Boston, 284 pp.
- Grinnell, J. (1923) The burrowing rodents of California as agents in soil formation, *J. Mammal.*, 4, 137-149.
- Mayer, W. (1953) A preliminary study of the Barrow Ground Squirrel, *Citellus parryi barrowensis*, *J. Mammal.*, 34, 334-345.
- Price, L. W. (1970) Morphology and ecology of solifluction lobe development—Ruby Range, Yukon Territory, Ph.D. dissertation, Univ. Illinois, Urbana, 325 pp. (unpubl.).
- *Price, L. W. (1971) Vegetation, microphotography, and depth of active layer on different exposures in Subarctic alpine tundra, *Ecology*, 52, 638-647.
- Pruitt, W. D. (1957) Observations on the bioclimate of some taiga mammals, *Arctic*, 10, 131-138.
- Russell, R. S. (1940) Physiological and ecological studies on an arctic vegetation; II, The development of vegetation in relation to nitrogen soil micro organisms on Jan Mayen Island, *J. Ecol.*, 28, 269-288.
- Shaw, W. T. (1925) The Columbian Ground Squirrel as a handler of earth, *Sci. Monthly*, 20, 483-490.
- Taylor, W. P. (1935) Some animal relations to soils, *Ecology*, 16, 127-136.
- Thorp, J. (1949) Effects of certain animals that live in soil, *Sci. Monthly*, 68, 180-191.

*This article is reprinted in the present volume.

Pesticide Residues in Selected Yukon Mammals

Donal W. Halloran* and Arthur M. Pearson †

In the last decade pesticide residues have been found in most eco-systems (Egler, 1964; Woodwell, 1967) including Antarctica (Tatton and Ruzicka, 1967). Furthermore, residues have been detected in air (Antommara, *et al.*, 1967), water (Sparr *et al.*, 1966), soil (Edwards, 1966), and man (Radomski, 1968). Knowing these facts, we were curious to know if pesticide residues might also be present in mammals from the Kluane Game Sanctuary in Southwestern Yukon.

During the summer of 1969 two fat samples from moose (*Alces alces*) and six fat samples from dall sheep (*Ovis dalli*) were obtained when those mammals were collected in connection with a concurrent ecological study of the brown bear (*Ursus arctos*). One fat sample from a wolf pup (*Canis lupus*), accidentally caught and damaged in a bear trap, was also obtained. The fat samples were frozen in capped glass vials for later analysis.

At the close of the field season, the fat samples were shipped by air to Gerald Myrdal at the Department of Agriculture, State of Wisconsin, Madison, for pesticide analysis. The fat was assayed for 13 varieties of chlorinated hydrocarbons and 16 types of organophosphates using a Coleman model 5360 pesticide analyzer following hexane extraction techniques described by the U.S. Department of Health, Education, and Welfare (1969). The sensitivity of the analysis was 0.02 parts per million (ppm) for each of the pesticides.

Pesticide levels above 0.02 ppm were not detected in any of the fat samples from moose or sheep. The wolf

fat contained 0.08 ppm DDT [1,1,1-trichloro-2,2-bis(p-chlorophenyl) ethane] and 0.05 ppm DDE [1,1-dichloro-2,2-bis(p-chlorophenyl) ethylene], a biologically active analog of DDT. We can only speculate as to the origin of the pesticides in the wolf. The wolf may have picked up the pesticides by eating contaminated prey, particularly migratory birds returning from southern latitudes. A possible local source of pesticide contamination might have been from the settlement of Haines Junction, located near the northeast corner of the Kluane Game Sanctuary, where DDT was used to control insects until 1968. While the pesticide levels in this wolf do not suggest toxic conditions, they do document the presence of specific pesticides in another remote habitat.

References

- Antommara, P., Corn, M., and Demaio, L. (1965) Airborne particles in Pittsburgh associated with PIP-DDT, *Science*, **150**, 1476-1479.
- Edwards, C. D. (1966) Insecticide residues in soils, *Residue Rev.*, **13**, 83-132.
- Egler, F. E. (1964) Pesticides in our ecosystem, *Am. Scient.*, **52**, 110-136.
- Radomski, J. L. (1968) Pesticide concentrations in the liver, brain and adipose tissue of terminal hospital patients, *Food Cosmetic Toxicol.*, **6**, 209-220.
- Sparr, B. I., Appleby, W. G., DeVries, D. M., Osmun, J. V., McBride, J. M., and Foster, G. L. (1966) Insecticide residues in waterways from agricultural use, *Advances Chem.*, **60**, 146-162.
- Tatton, J. O'G., and Ruzicka, J. H. A. (1967) Organochloride pesticides in Antarctica, *Nature*, **215**, 346-348.
- U.S. Dept. Health, Educ., Welfare (1969) *Pesticide Analytical Manual*, Vol. 1, §§211.14, 211.15.
- Woodwell, G. M. (1967) Toxic substances and ecological cycles, *Scient. Am.*, **216**, 24-31.

*Department of Botany-Zoology, University of Wisconsin Center System, Marshfield, Wisconsin

†Canadian Wildlife Service, Department of Indian Affairs and Northern Development, Whitehorse, Yukon

ICEFIELD RANGES RESEARCH PROJECT STATIONS

Station No.	Name used in this volume	Names used previously by various authors	Used as:		Type of Surface †
			Camp	Scientific station	
1	Base Station	Kluane, Kluane Camp, Base Camp	+	+	Gravel
2	Terminus Station	Moraine Camp, Terminus	+	+	Gravel (outwash)
3	Kaskawulsh Station A	Kask, Kaskawulsh Camp	+	+	Ice-cored moraine
4	Kaskawulsh Station B	Kask Ice		+	Ice (glacier)
5	Kaskawulsh Station C	Kask Knoll		+	Rock (knoll)
6	Crevasse Camp		+	+	Firn (glacier)
7	Divide Station A	Upper Camp, Glacier Central	+	+	Firn (glacier)
8	Divide Station B	Divide, Meteorological Station	+	+	Firn (glacier)
9	Divide Station C	Divide Cache		+	Rock (nunatak)
10	Divide Station D	Cairn B		+	Snow-covered ridge
11	Seward Station A	Seward	+	+	Rock (nunatak)
12	Seward Station B	Seward Ice		+	Firn (glacier)
13	Lucania Camp		+	+	Firn (glacier)

†Stations on glaciers move with the glacier at a rate varying from a few centimeters to as much as a meter per day. Therefore, locations of stations on glaciers are only approximate.



